DYNAMICS AND STABILITY OF TWO COAXIAL CYLINDRICAL SHELLS CONVEYING FLUID

by

STEVE, SIU PUI CHAN

Under the supervision of Prof. M.P. Paidoussis

A Thesis Submitted to the Faculty of Graduate Studies and Research in Partial Fulfillment of the Requirements for the Degree of Master of Engineering

Department of Mechanical Engineering
McGill University
Montreal, Canada

January, 1984

ABSTRACT

This thesis examines the dynamics and stability of two coaxial, flexible cylindrical shells of circular cross-section conveying fluid inside the inner cylinder and in the annulus between the two cylinders.

Shell motions are described by Flügge's thin-shell equations and Galerkin's method is used in the solution of these equations. The two shells of the system are clamped at both ends. Calculations have been conducted with two flexible shells or with one replaced by an identical rigid cylinder.

In the first part of the thesis, the fluid is assumed to be inviscid and either compressible or incompressible. The analysis of the inviscid aerodynamic forces is based on linearized potential flow theory, and Fourier-transform technique is employed to evaluate these forces. It is found that increasing either the internal or the annular flow can induce buckling instability, followed by coupled-mode flutter. For the systems studied, annular flow renders the system unstable at lower flow velocities than internal flow. It is also found that, with internal flow alone, the instability threshold is not sensitive to whether one or both shells are flexible, whereas with annular flow the system is less stable if both shells are flexible. The effect of compressibility is found to be small.

In the second part of the thesis, fluid viscous effects are partially accounted for by taking into consideration fluid pressurization necessary to overcome pressure drop as well as the surface frictional force associated with viscous mean flow in the inner shell and in the annular region. It is found that with *viscous internal* flow the system becomes more stable, while with *viscous annular* flow, the instability

threshold is lowered, as compared to inviscid flows. Studies on systems subjected to additional uniform pressurization show that the internal fluid pressure has a stabilizing effect on the system; the annular fluid pressure, on the other hand, expedites the precipitation of instability.

SOMMAIRE

Cette thèse traite de la dynamique et de la stabilité d'un système composé de deux coques cylindriques soumises à deux écoulements, l'un à l'intérieur de la coque interne et l'autre dans l'espace annulaire entre les deux coques.

Les déplacements des deux coques, qui sont encastrées aux extrémités, sont décrits par les équations de coques minces de Flügge et leur solution est obtenue par la méthode de Galerkin. Des calculs ont été faits pour les cas de deux coques flexibles ainsi que pour les cas dans lesquels une coque était remplacée par un cylindre rigide de dimensions identiques.

Dans la première partie de la thèse, le fluide est considéré comme non-visqueux, soit compressible, soit incompressible.

L'analyse des forces aérodynamiques non-visqueuses, est basée sur la théorie linéarisée d'écoulements potentiels, et ces forces sont évaluées à l'aide des techniques de transformation de Fourier. On constate que l'augmentation de la vitesse d'écoulement, qu'elle soit interne ou annulaire, peut causer l'instabilité en flambage, suivie par des instabilités oscillatoires (flottement) en modes conjugés. Pour les systèmes en question, l'écoulement annulaire provoque l'instabilité à une vitesse moindre que l'écoulement interne. On a aussi découvert que, avec un écoulement interne seulement, la limite de stabilité n'est pas très sensible au fait que l'une ou les deux coques soit flexible, tandis qu'avec un écoulement annulaire, le système est moins stable lorsque les deux coques sont flexibles. De plus, l'effet de la compressibilité a été déterminé comme étant négligeable.

Dans la deuxième partie de la thèse, on a tenu partiellement compte des effets de la viscosité du fluide en considérant les facteurs de pressurisation du fluide nécessaire pour compenser les pertes de charge ainsi que la force de friction murale, associés à un écoulement visqueux moyeu à l'intérieur de la coque interne et dans l'espace annulaire. Par rapport à des écoulements non-visqueux, les écoulements visqueux rendent le système plus stable lorsque l'écoulement est interne, et moins stable lorsque celui-ci est annulaire. Les études sur des systèmes soumis à une pressurisation uniforme additionnelle révèlent que cette dernière a un effet stabilisant dans le cas du fluide interne et, qu'au contraire, la pressurisation du fluide annulaire accélère l'instabilité.

ACKNOWLEGEMENTS

The author wishes to express his gratitude to his supervisors Prof. M.P. Paidoussis and Prof. A.K. Misra for their attentive guidance, valuable suggestions and persistent encouragement throughout the course of this work.

The help offered by Mr. S.Y. Ang for the preparation of the graphs in this thesis is gratefully acknowledged.

Sincere thanks are also due to Ms. Assunta Cerrone-Mancini for her patience and her excellent job of typing a difficult manuscript.

TABLE OF CONTENTS

NOMENCLATURE

Roman Letters

a	Radius of the inner shell
b	Radius of the outer shell
c	Speed of sound
D_h	Hydraulic diameter
E_i	Young's modulus of the inner-shell material
E_o	Young's modulus of the outer-shell material
f_i	Friction factor for the viscous internal flow
f_o	Friction factor for the viscous annular flow
h_i	Thickness of the inner shell
h_o	Thickness of the outer shell
I_n, K_n	Modified Bessel functions of order n
k_i	$h_i^2/12a^2$
k_o	$h_o^2/12b^2$
L	Length of the flexible portion of the shells
m	Axial mode number
M_i	Mach number of the internal flow
M_o	Mach number of the annular flow
n	Circumferential mode number
P_i	Internal fluid pressure
P_o	Annular fluid pressure
r	Radial coordinate
Re	Reynolds number
t	Time
U_i	Steady internal flow velocity

U_o	Steady annular flow velocity
u_i, v_i, w_i	Axial, circumferential and radial displacements of the inner shell
u_o, v_o, w_o	Axial, circumferential and radial displacements of the outer shell
x	Axial coordinate

Greek Letters

α	Fourier transform variable
δ_{km}	Kronecker delta
ε_i	a/L
ε_o	b/L
ε_r	a/b
η_i	Kinematic viscosity of the internal fluid
η_o	Kinematic viscosity of the annular fluid
θ	Polar coordinate
Λ_i	$E_i h_i/(1-\nu_i^2)$
Λ_o	$E_o h_o/(1-\nu_o^2)$
ν_i	Poisson's ratio of the inner-shell material
ν_o	Poisson's ratio of the outer-shell material
ξ	x/L
ρ_i	Density of the internal fluid
ρ_o	Density of the annular fluid
ρ_{si}	Density of the inner-shell material
ρ_{so}	Density of the outer-shell material
Φ	Velocity potential of flow perturbation
Ψ	Total velocity potential
Ω	Circular frequency of motion

CHAPTER I

INTRODUCTION

1.1 LITERATURE REVIEW

The study of the dynamics of cylindrical structures conveying fluid has received the growing attention of engineers and scientists over the past thirty years or so. Interest was first aroused by the investigation of the wibration of the Trans-Arabian pipeline, by Ashley and Haviland [1]. Since then, numerous studies have been undertaken, contributing to a remarkable development of the subject.

It was found that the effect of internal flow is to reduce the natural frequencies of oscillation at small and moderate flow velocities and, in the case of cantilevered tubes, to damp the free oscillations†. However, at sufficiently high flow velocities, the system can be subjected to fluidelastic instabilities. For simply-supported and clamped-clamped tubes [2,3], buckling (divergence) is observed, in which the tubes buckle, essentially like a column subjected to axial loading. On the other hand, cantilevered tubes develop oscillatory instability (flutter), firstly reported by Benjamin [4,5] and later confirmed both theoretically and experimentally by Gregory and Paidoussis [6,7].

However, the fluidelastic instabilities referred to above rarely materialize in practice, mainly because in most common engineering systems the rigidity of the piping is reasonably large so that the critical flow

---

†Clamped-clamped and pinned-pinned tubes, being gyroscopic conservative systems, do not suffer damping if the flow is inviscid.

velocities at which the systems become unstable are extremely high and seldom encountered [8]. As a result, most of the stability studies deal with fundamental, rather than applied, aspects of the problem. The impetus for conducting such research comes from a desire to understand the intriguing phenomena involved or to investigate a dynamical system of academic importance. On the other hand, one should be aware that there are, indeed, studies with a practical orientation such as those dealing with the commonly encountered problems associated with sub-critical vibrations and vibrations induced by near- and far-field noise conveyed by the mean flow.

In the research described so far, the cylinder was considered as a beam, and only the oscillation in the flexural beam modes was studied. In 1969, Paidoussis and Denise [9] discovered a 'new' flutter phenomenon while experimenting with thin cantilevered tubes conveying low pressure air. They found that, whereas for thick-walled cantilevers, the only instability observed was that in one of the 'beam-type' modes, if the cantilevered tube was short and fairly thin-walled, it could also lose stability by vibrating in the so-called second circumferential 'shell-type' mode. Subsequent experiments showed that this shell-type of flutter instability could also occur in clamped-clamped shells. In a later paper [10], Paidoussis and Denise extended their investigation into the oscillation of thin, circular cylindrical shells conveying fluid, both experimentally and theoretically. Their theory confirmed the possibility of shell-type flutter for cantilevered shells. In the case of clamped-clamped shells, buckling instability followed by coupled-mode flutter was predicted. Their experimental observations are considered to be in good agreement with theory. Similar theoretical results were obtained by Weaver and Unny [11] who examined the case of simply-supported shells.

In parallel to this work with internal flow, there exists a rich literature on the effect of external axial flow on the dynamics and stability of cylindrical shells. This research finds application in the aeronautical field and, accordingly, most of the studies are concerned with flutter in supersonic flow, *e.g.* [12]. Among the numerous outstanding published papers, the work by Dowell and Widnall on the formulation of the generalized aerodynamic forces is particularly worth reviewing [13,14], as their method can easily be adapted for our problem at hand, especially when the fluid is compressible. To deal with the case of subsonic and supersonic flows, Dowell and Widnall developed a method to compute the generalized aerodynamic forces on harmonically oscillating cylindrical shells. By making a Fourier integral transformation of the velocity potential with respect to the streamwise variable, he was able to solve the governing wave equation derived from classical linearized potential flow theory for both subsonic and supersonic flow speeds. In order to make the problem mathematically tractable, the finite flexible cylinder was extended at either end with rigid infinitely long cylinders. This technique enables both the radial and axial boundary conditions to be defined along the complete boundary of the fluid region, so as to make the solution unique.

Similar integral approaches were then utilized by a number of investigators in their studies of flow-induced vibration of cylinders. Shayo and Ellen [16] using the integral transform theory, obtained an expression for the fluid pressure acting on cylindrical pipes containing flowing fluid. From the asymptotic form of the expression for pressure in pipes of large and small length-to-radius ratio, they were able to obtain explicitly the critical flow velocity at divergence in terms of

parameters such as the radius-to-thickness ratio, the longitudinal and circumferential mode numbers, the Mach number, *etc.* In comparison with previously published results, they found that their asymptotic expressions applied within a broad range of the stability parameters and they were able to yield the stability boundaries that would have otherwise required considerable numerical computation to generate.

Kornecki [17], employing a method due to Leipholz and Galerkin's discretization technique, was able to prove the existence of divergence and flutter instability in panels and cylindrical shells in subsonic potential flow. Without resorting to detailed calculation, the proof was done on the basis of a qualitative analysis of the governing equation of motion, in conjunction with the expressions for generalized aerodynamic forces derived by Dowell and Widnall in references [13,14,15]. Paidoussis and Ostoja-Starzewski [18] utilized the integral-transform approach and compared it to other methods in formulating the aerodynamic forces acting on a flexible cylinder with pinned ends, immersed in axial subsonic flow.

In the present study, the inviscid aerodyanmic forces are also derived using the integral transform method. A feature of this integral transform theory, superior to other methods for determining the aerodynamic forces, is that the transform technique, together with Bernoulli's equation for the pressure and the flow boundary conditions, could furnish us with a derivation of the aerodynamic forces resulting from continuous interaction of the flow field and the arbitrary spatial deformation field of the cylinder. However, a difficultly, frequently encountered (and here also), ought to be mentioned: this is the strong implicit frequency dependence of the inverse transform integral involved in the resultant expressions of the generalized aerodynamic forces. One possible simplification is to invoke

the assumption of incompressible flow, in which case the frequency term may be isolated explicitly from the integral expressions. This is, in fact, the procedure taken in most of the calculations in this study.

Another line of work was initiated by attempts to model those internal structures of gas- and water-cooled nuclear reactors where the coolant flows in narrow annuli between coaxial cylinders, one or both of which may be free to vibrate. In most of these studies, the fluid in the annulus is taken to be stationary. The primary interest in these studies is (i) the calculation of the large added (or 'virtual') mass effect resulting from the tremendous accelerations suffered by the fluid in the narrow annular region in the course of vibration, and (ii) the hydrodynamical coupling in the motions of the coaxial cylinders giving rise to sets of in-phase and out-of-phase modes. In what follows, only a few of the papers in the now extensive literature in the field will be discussed.

Krajcinovic [19] examined the free vibration of two infinitely long, coaxial cylinders containing fluid. The added mass was derived from the exact linearized potential flow theory. An approximate formula for the added mass was also derived under the assumption that the fluid is incompressible and its motion confined to the transverse plane. The latter is not only very simple in form but, more importantly, it produces numerical results that are negligibly different from those of the exact formula.

Au-Yang [20] estimated the virtual mass and coupling coefficients of two finite coaxial cylinders of different lengths immersed in a restricted inviscid fluid medium. He found that the axial modes of pinned-pinned cylinders are coupled only if the ratio of their axial mode numbers equals their length ratio. For the uncoupled modes, the cylinders vibrate independently and their frequencies are governed by the virtual mass term only.

Brown and Lieb [21] employed the finite element method to analyze the dynamic behaviour of fluid-coupled coaxial cylinders. The effect of parameter variations on system behaviour, such as cylinder wall thickness, gap width, and boundary conditions was investigated. Moreover, it should be mentioned that the use of the finite element methods [22,23] has become popular nowadays due to its generality and relative ease in incorporating the physical boundary conditions and special geometries of the cylinders.

In the above studies of coaxial cylinders, the fluid is assumed to be inviscid. Although some studies have taken fluid viscosity into account, the role of viscous fluid on structural response has not been extensively investigated. In a paper by Chen, Wambsganss and Jendrzejczyk [24], a closed-form solution for the added mass and damping coefficient is obtained and a series of experiments is performed for a cylindrical rod vibrating in a viscous fluid contained by a rigid, cylindrical shell. Their results show that both the added mass and damping coefficients approach infinity asymptotically as the annular gap width tends to zero.

In another paper by Yeh and Chen [25], the coupled vibrations of two concentric shells separated by a viscous fluid are studied. Employing Flügge's shell equations of motion and the linearized Navier-Stokes equations for the fluid, the natural frequencies, mode shapes and modal damping ratios of the coupled modes are calculated. The modal damping of out-of-phase modes is found to be considerably larger than that of the in-phase modes. Although fluid viscosity contributes significantly to modal damping, its effect on the system natural frequencies is negligibly small in most practical applications.

In yet another paper by Chen [26], a summary is presented of fluid viscous damping for circular cylinders vibrating in stationary fluid, cross

flow and parallel flow. For small amplitude vibrations, the viscous damping terms can be linearized and easily derived; however, if the cylinder motion is large, as is the case in most cross-flow vibrations, complicated flow phenomena, such as boundary layer separation, reverse flow, and vortex formation, render analytical formulation extremely difficult, if not impossible.

In a stationary viscous fluid, the drag force acting on the vibrating cylinder causes viscous damping. However, when the fluid in the annulus is flowing, the drag force will be enhanced and it will become a function of the flow velocity. Due to the difficulty in the analytical formulation of this flow-velocity dependent damping, empirical expressions derived from experimental data are often employed [27,28]. Besides the flow-induced damping, other force components are also brought into play by the flowing fluid. The formation of a boundary layer associated with the mean flow sets up viscous stresses within the fluid which, in turn, impose an axial force on the cylinder surface. The pressure gradient which is required to drive the fluid down the annulus results in a radial force acting on the cylinders. These additional surface loadings would likely influence the stability boundary of the system, since it is well known that cylinders could buckle under the action of lateral pressure or axial compression [29,30]†.

The above brief and selective review of literature is intended to give the reader some idea of the developments in the study of the dynamics of cylindrical structure subjected to external and internal axial flow; no attempt has been made to given an exhaustive list of all the papers in this area. Moreover, vigorous research is being pursued in many other aspects

†In the later part of this thesis, the effects of these external loads, namely the fluid pressurization and the axial frictional force, will be investigated.

of the problem that has not been mentioned and is out of the limited scope of the present work.

1.2 OBJECTIVE AND ORGANIZATION OF THE THESIS

The objective of this thesis is to study the dynamics of two thin concentric cylindrical shells with fluid flowing in the inner shell and in the annular region. The surrounding fluid medium is stationary and its density relatively small. The effect of varying the flow velocity in both inner and annular regions on the stability boundary of the system will be examined. In the first part of the study, the fluid is assumed to be inviscid and the aerodynamic forces are formulated using an integral transform technique based on Dowell's work [13]. The two cylinders have the same length of flexible portion 'clamped' to identical but rigid cylinders of infinite length at both ends. Pressurization and axial surface force caused by a flowing viscous fluid are later incorporated in the analysis. Although this viscous flow model may represent a better approximation of the total hydrodynamical effect of a real fluid flow on the shells, the effort made in the earlier part of the work to obtain inviscid flow results can still be justified: since the effect of fluid viscosity, as approximately taken into account in this thesis, induces a certain set of stress resultants on the shells, the effect of which is to modify but not alter the basic character of the dynamical behaviour of the shells as predicted by inviscid flow theory. This will become obvious in the work presented in Chapter VI.

The structure of this thesis is as follows. In Chapter II, the problem is formulated with Flügge's shell equations and potential flow theory is employed for derivation of the inviscid fluid pressure perturbations.

In Chapter III are presented the methods of solution using Galerkin's technique, and the integral transform approach for obtaining the generalized aerodynamic forces. Attempts to simplify the evaluation of the generalized aerodynamic forces are presented in Chapter IV. Firstly, the method of contour integration is employed but, unfortunately, the scheme is shown to be impracticable. Subsequently, sets of numerically calculated aerodynamic force terms are curve-fitted and represented with much simpler equations for the purpose of interpolation. Reasonably good results are obtained with this method.

In Chapter V are discussed the theoretical results obtained for the case of clamped-clamped shells in annular or internal inviscid flow. Extensive calculations are presented for different geometric configuration (wide and narrow annuli), and with different fluid (air and water) and cylinder materials (rubber and steel).

Chapter VI deals with the effect of fluid viscosity on the dynamics of the system; in particular, the time-averaged (mean) fluid pressurization and the surface frictional force associated with viscous flow are taken into account. Finally, in Chapter VII, general conclusions and some suggestions for future work are presented.

CHAPTER II

FORMULATION OF THE PROBLEM

2.1 THE EQUATIONS OF MOTION

The configuration of the system under consideration is shown in Figure 1. It consists of two infinite coaxial rigid cylindrical shells with a flexible portion of length L. The radius of the inner shell is a and its wall thickness h_i, whilst the corresponding quantities of the outer shell are b and h_o. The material properties of the two shells are densities ρ_{si} and ρ_{so}, Young's moduli E_i and E_o, and Poisson's ratios ν_i and ν_o, where subscripts i and o refer to the inner and outer shell, respectively, throughout this thesis.

The system contains two flows: one in the inner shell and another in the annular space. The two flow velocities are denoted by U_i and U_o and the fluid densities by ρ_i and ρ_o.

Cylindrical coordinates $(x;\theta,r)$ are used, with the x-axis coinciding with the common axis of the two shells. The displacements of the middle surface of the shell from the equilibrium position are $u(x,\theta,t)$, $v(x,\theta,t)$ and $w(x,\theta,t)$ in the axial, circumferential and radial directions, respectively. The fundamental equations of motion are taken to be those developed by Flügge [32], as given below:

$$u_i'' + \frac{1-\nu_i}{2} u_i^{\cdot\cdot} + \frac{1+\nu_i}{2} v_i'^{\cdot} + \nu_i w_i' + k_i \left\{ \frac{1-\nu_i}{2} u_i^{\cdot\cdot} - w_i''' + \frac{1-\nu_i}{2} w_i'^{\cdot\cdot} \right\} = \gamma_i \frac{\partial^2 u_i}{\partial t^2} , \tag{2.1.1}$$

$$\frac{1+\nu_i}{2}u_i'^{\cdot} + v_i^{\cdot\cdot} + \frac{1-\nu_i}{2}v_i'' + w_i^{\cdot} + k_i\left\{\frac{3}{2}(1-\nu_i)v_i'' - \frac{3-\nu_i}{2}w_i'^{\cdot}\right\} = \gamma_i\frac{\partial^2 v_i}{\partial t^2}, \quad (2.1.2)$$

$$\nu_i u_i' + v_i^{\cdot} + w_i + k_i\left\{\frac{1-\nu_i}{2}u_i'^{\cdot\cdot} - u_i''' - \frac{3-\nu_i}{2}v_i''^{\cdot} + \nabla_i^4 w_i + 2w_i^{\cdot\cdot} + w_i\right\}$$

$$= -\gamma_i\left\{\frac{\partial^2 w_i}{\partial t^2} - \frac{q_i}{\rho_{si}h_i}\right\}, \quad (2.1.3)$$

$$u_o'' + \frac{1-\nu_o}{2}u_o^{\cdot\cdot} + \frac{1+\nu_o}{2}v_o'^{\cdot} + \nu_o w_o' + k_o\left\{\frac{1-\nu_o}{2}u_o^{\cdot\cdot} - w_o''' + \frac{1-\nu_o}{2}w_o'^{\cdot\cdot}\right\} = \gamma_o\frac{\partial^2 u_o}{\partial t^2},$$

(2.1.4)

$$\frac{1+\nu_o}{2}u_o'^{\cdot} + v_o^{\cdot\cdot} + \frac{1-\nu_o}{2}v_o'' + w_o^{\cdot} + k_o\left\{\frac{3}{2}(1-\nu_o)v_o'' - \frac{3-\nu_o}{2}w_o'^{\cdot}\right\} = \gamma_o\frac{\partial^2 v_o}{\partial t^2},$$

(2.1.5)

$$\nu_o u_o' + v_o^{\cdot} + w_o + k_o\left\{\frac{1-\nu_o}{2}u_o'^{\cdot\cdot} - u_o''' - \frac{3-\nu_o}{2}v_o''^{\cdot} + \nabla_o^4 w_o + 2w_o^{\cdot\cdot} + w_o\right\}$$

$$= -\gamma_o\left\{\frac{\partial^2 w_o}{\partial t^2} - \frac{q_o}{\rho_{so}h_o}\right\}, \quad (2.1.6)$$

where $(\,)' = a\partial(\,)/\partial x$, $(\,)'' = b\partial(\,)/\partial x$, $(\,)^{\cdot} = \partial(\,)/\partial\theta$, (2.1.6a)

$$k_i = h_i^2/12a^2,\ k_o = h_o^2/12b^2,\ \gamma_i = \rho_{si}a^2(1-\nu_i^2)/E_i,\ \gamma_o = \rho_{so}b^2(1-\nu_o^2)/E_o,$$

$$\nabla_i^2 = a^2\partial^2/\partial x^2 + \partial^2/\partial\theta^2,\ \nabla_o^2 = b^2\partial^2/\partial x^2 + \partial^2/\partial\theta^2 .$$

Here q_i is the radial force component per unit area of the middle surface of the inner shell; it is, therefore, given by the difference between the fluid pressure inside the inner cylinder, P_i, and the pressure in the annulus which we may call the 'annular' pressure P_o. Thus, $q_i = P_i|_{r=a} - P_o|_{r=a}$.

Similarly, $q_o = P_o|_{r=b} - P_e$ is the loading on the outer shell. P_e is the pressure in the region external to the outer cylinder which is assumed to consist of still fluid of negligibly small density.

2.2 DERIVATION OF THE FLUID PRESSURE[†]

Fluids in both the annular region and the inner cylinder are assumed to be inviscid and compressible. Therefore, by virtue of the inviscid assumption, the mean pressure in the shells does not vary with x; moreover, it is assumed that this pressure is the same in the two flow regions and in the surrounding fluid medium. Although the flow is unsteady, it is assumed to be irrotational and isentropic. The effects of fluid pressurization to overcome pressure drop arising from viscous flow will be discussed in Chapter VI.

The irrotational property of the flow is the sufficient condition for the existence of a scalar potential $\Psi(x,\theta,r,t)$ by which the flow velocity can be defined:

$$\vec{V} = \vec{\nabla}\Psi , \qquad (2.2.1)$$

where $\vec{\nabla}$ is the gradient operator.

[†]Since the analysis applies to the flow in both the internal and the annular region, the suffices i and o are omitted for the time being.

The potential, Ψ, consists of two components: a steady part which gives the undisturbed velocity U in the x-direction and an unsteady component $\Phi(x,\theta,r,t)$ which defines the disturbed state. Thus, Ψ can be written as

$$\Psi = Ux + \Phi \ , \tag{2.2.2}$$

and the velocity field of the disturbed flow is given by

$$V_x = U + \frac{\partial \Phi}{\partial x} \ , \ V_\theta = \frac{1}{r}\frac{\partial \Phi}{\partial \theta} \ , \ V_r = \frac{\partial \Phi}{\partial r} \ . \tag{2.2.3}$$

Similarly, the pressure is defined by

$$P = P_o + \bar{P} \ , \tag{2.2.4}$$

where P_o is the steady flow pressure, and $\bar{P}$ is the perturbation pressure that gives rise to the dynamic loadings on the shells.

The fluid pressure and the velocity potential are related by Bernoulli's equation for unsteady flow,

$$\frac{\partial \Phi}{\partial t} + \frac{V^2}{2} + \frac{P}{\rho} = \frac{P_s}{\rho} \ , \tag{2.2.5}$$

where $V^2 = V_x^2 + V_r^2 + V_\theta^2$ and P_s is the stagnation pressure; in view of equation (2.2.3), V^2 may be written as

$$V^2 = U^2 + 2U\frac{\partial \Phi}{\partial x} + (\frac{\partial \Phi}{\partial x})^2 + (\frac{\partial \Phi}{\partial r})^2 + \frac{1}{r^2}(\frac{\partial \Phi}{\partial \theta})^2 \ . \tag{2.2.6}$$

Assuming a sufficiently small disturbance, the above expression may be linearized by dropping the second order terms. Thus,

$$V^2 \simeq U^2 + 2U \frac{\partial \Phi}{\partial x} . \qquad (2.2.7)$$

Also, assuming the validity of Bernoulli's equation for the steady flow,

$$\frac{P_o}{\rho} + \frac{U^2}{2} = \frac{P_s}{\rho} , \qquad (2.2.8)$$

one may obtain the following expression by substituting equations (2.2.7) and (2.2.8) into equation (2.2.5).

$$\bar{P} = -\rho\left(\frac{\partial \Phi}{\partial t} + U \frac{\partial \Phi}{\partial x}\right) . \qquad (2.2.9)$$

By virtue of equation (2.2.9), the inviscid fluid pressure may readily be determined once the velocity potential is found.

2.3 EQUATION GOVERNING THE VELOCITY POTENTIAL

Let us consider the three-dimensional flow equation for an irrotational inviscid unsteady compressible flow

$$\nabla^2 \Psi - \frac{1}{c^2}\left\{\frac{\partial^2 \Psi}{\partial t^2} + \frac{\partial}{\partial t}(\vec{V}\cdot\vec{V}) + \vec{V}\cdot\vec{\nabla}\left(\frac{\vec{V}\cdot\vec{V}}{2}\right)\right\} = 0 \qquad (2.3.1)$$

where Ψ is the velocity potential, $\vec{V}$ is the fluid particle velocity, and c is the speed of sound in the fluid.

A brief derivation of the above equation is given in Appendix N.

From equation (2.2.2), the velocity potential has the form

$$\Psi = Ux + \Phi ,$$

and from equation (2.2.1), the particle velocity is then given by

$$\vec{V} = U\hat{\imath} + \vec{\nabla}\Phi , \tag{2.3.2}$$

with its components in cylindrical coordinates as given in equation (2.2.3), $\hat{\imath}$ being the unit vector in the x-direction.

Substituting equations (2.3.2) and (2.2.2) into equation (2.3.1) and retaining only the linear terms, one obtains, after some manipulation, the linearized wave equation for the perturbation velocity potential, Φ,

$$\nabla^2\Phi - \frac{1}{c^2}\left(\frac{\partial}{\partial t} + U\frac{\partial}{\partial x}\right)^2\Phi = 0 . \tag{2.3.3}$$

Consider now the boundary conditions. The condition of impermeability of the surface of the shell requires that the radial velocity of the fluid particles on the shell surface should match with the instantaneous rate of change of the shell displacement in the radial direction, or, mathematically,

$$V_r = \left.\frac{\partial\Phi}{\partial r}\right|_{\text{at shell surface}} = \frac{\partial w}{\partial t} + U\frac{\partial w}{\partial x} . \tag{2.3.4}$$

In our problem, two regions of fluid will be considered. For the internal region, in view of the above analysis, we have

$$\nabla^2\Phi_i - \frac{1}{c_i^2}\left(\frac{\partial}{\partial t} + U_i \frac{\partial}{\partial x}\right)^2\Phi_i = 0 , \qquad (2.3.5)$$

where Φ_i and U_i are, respectively, the velocity potential and the steady flow velocity inside the inner shell. Equation (2.3.5) is subjected to the boundary condition

$$\left.\frac{\partial\Phi_i}{\partial r}\right|_{r=a} = \frac{\partial w_i}{\partial t} + U_i \frac{\partial w_i}{\partial x} \qquad \text{for } 0 \leq x \leq L ,$$

$$= 0 \qquad \text{for } x < 0 \text{ and } x > L . \qquad (2.3.6)$$

Similarly, the equation governing the velocity potential, Φ_o in the annular region is

$$\nabla^2\Phi_o - \frac{1}{c_o^2}\left(\frac{\partial}{\partial t} + U_o \frac{\partial}{\partial x}\right)^2\Phi_o = 0 , \qquad (2.3.7)$$

with U_o as the steady annular flow velocity; the boundary conditions in this case are

$$\left.\frac{\partial\Phi_o}{\partial r}\right|_{r=a} = \frac{\partial w_i}{\partial t} + U_o \frac{\partial w_i}{\partial x} \qquad \text{for } 0 \leq x \leq L$$

$$= 0 \qquad \text{for } x < 0 \text{ and } x > L . \qquad (2.3.8)$$

and

$$\left.\frac{\partial\Phi_o}{\partial r}\right|_{r=b} = \frac{\partial w_o}{\partial t} + U_o \frac{\partial w_o}{\partial x} \qquad \text{for } 0 \leq x \leq L$$

$$= 0 \qquad \text{for } x < 0 \text{ and } x > L . \qquad (2.3.9)$$

Finally, the boundary conditions at the axial extremities of the cylindrical shells should be specified. If the edges of the shells are

clamped, which is the condition applicable to all calculations in this thesis, there is no displacement or rotation, so that

$$u_i = v_i = w_i = 0 \quad \text{and} \quad \frac{\partial w_i}{\partial x} = 0 \qquad \text{at } x = 0 \text{ and } L$$

and

$$u_o = v_o = w_o = 0 \quad \text{and} \quad \frac{\partial w_o}{\partial x} = 0 \qquad \text{at } x = 0 \text{ and } L \,. \tag{2.3.10}$$

The problem is now completely formulated by the equations of motion of the shells (2.1.1-.6) and the wave equations of the velocity potentials in the internal and annular fluid regions (2.3.5) and (2.3.7), supplemented by the boundary conditions (2.3.6), (2.3.8), (2.3.9) and (2.3.10).

CHAPTER III

METHOD OF SOLUTION

Galerkin's method is employed in the solution of the equations of motion (2.1.1-.6). Accordingly, the displacements u, v and w of the two cylindrical shells are expressed as infinite series of the following form†:

$$u_i(x,\theta,t) = \sum_{m=1}^{\infty} A_{mn} \cos n\theta \, [a\phi_m'(x)] \, e^{i\Omega t} , \qquad (3.0.1)$$

$$v_i(x,\theta,t) = \sum_{m=1}^{\infty} B_{mn} \sin n\theta \, \phi_m(x) \, e^{i\Omega t} , \qquad (3.0.2)$$

$$w_i(x,\theta,t) = \sum_{m=1}^{\infty} C_{mn} \cos n\theta \, \phi_m(x) \, e^{i\Omega t} , \qquad (3.0.3)$$

$$u_o(x,\theta,t) = \sum_{m=1}^{\infty} D_{mn} \cos n\theta \, [b\phi_m'(x)] \, e^{i\Omega t} , \qquad (3.0.4)$$

$$v_o(x,\theta,t) = \sum_{m=1}^{\infty} E_{mn} \sin n\theta \, \phi_m(x) \, e^{i\Omega t} , \qquad (3.0.5)$$

$$w_o(x,\theta,t) = \sum_{m=1}^{\infty} F_{mn} \cos n\theta \, \phi_m(x) \, e^{i\Omega t} , \qquad (3.0.6)$$

here $(\,)'$ stands for $d(\,)/dx$, and A_{mn}, B_{mn}, C_{mn}, D_{mn}, E_{mn} and F_{mn} are constant coefficients; furthermore,

---

†Strictly speaking, the displacements should be expressed as a double series in $\phi_m(x)$ and cos $n\theta$ (or sin $n\theta$). However, due to the orthogonality of the cosine and sine functions, the motions in different circumferential modes will eventually be decoupled. Thus, it would be sufficient to use a single series in $\phi_m(x)$ and a specified circumferential mode.

$$\phi_m(x) = \cosh(\lambda_m \frac{x}{L}) - \cos(\lambda_m \frac{x}{L}) - \sigma_m[\sinh(\lambda_m \frac{x}{L}) - \sin(\lambda_m \frac{x}{L})]$$

are the eigenfunctions of a beam having the same boundary conditions as the shells - in this case, a clamped-clamped beam. The eigenvalues λ_m and the characteristic constants σ_m are given in Appendix A.

The solutions for the perturbed velocity potentials of the two fluid regions are assumed to have the form

$$\Phi_i(x,r,\theta,t) = \psi_{in}(x,r) \cos n\theta \, e^{i\Omega t} , \tag{3.0.7}$$

$$\Phi_o(x,r,\theta,t) = \psi_{on}(x,r) \cos n\theta \, e^{i\Omega t} , \tag{3.0.8}$$

where the terms $\psi_{in}(x,r)$ and $\psi_{on}(x,r)$ would eventually be represented by the inverse Fourier transforms

$$\psi_{in}(x,r) = \frac{1}{2\pi} \int_{-\infty}^{\infty} \psi_{in}^*(\alpha,r) e^{-i\alpha x} \, d\alpha , \tag{3.0.9}$$

$$\psi_{on}(x,r) = \frac{1}{2\pi} \int_{-\infty}^{\infty} \psi_{on}^*(\alpha,r) e^{-i\alpha x} \, d\alpha , \tag{3.0.10}$$

where α is the transformed variable, and the transformed function itself is defined as

$$\psi_{in}^*(\alpha,r) = \int_{-\infty}^{\infty} \psi_{in}(x,r) e^{i\alpha x} \, dx , \tag{3.0.11}$$

$$\psi_{on}^*(\alpha,r) = \int_{-\infty}^{\infty} \psi_{on}(x,r) e^{i\alpha x} \, dx . \tag{3.0.12}$$

3.1 SOLUTION TO THE VELOCITY POTENTIALS OF COMPRESSIBLE FLOW

Let us first consider the fluid region inside the inner cylinder. It may be recalled from Chapter II that the wave equation to be solved is

$$\nabla^2\Phi_i - \frac{1}{c_i^2}\left(\frac{\partial}{\partial t} + U_i \frac{\partial}{\partial x}\right)^2\Phi_i = 0 , \qquad (2.3.5)$$

which, in terms of cylindrical coordinates, may be written as

$$\frac{\partial^2\Phi_i}{\partial r^2} + \frac{1}{r}\frac{\partial\Phi_i}{\partial r} + \frac{1}{r^2}\frac{\partial^2\Phi_i}{\partial\theta^2} + \frac{\partial^2\Phi_i}{\partial x^2} - \frac{1}{c_i^2}\left(\frac{\partial}{\partial t} + U_i \frac{\partial}{\partial x}\right)^2\Phi_i = 0 , \qquad (3.1.1)$$

subject to the boundary condition

$$\left.\frac{\partial\Phi_i}{\partial r}\right|_{r=a} = -\frac{\partial w_i}{\partial t} + U_i \frac{\partial w_i}{\partial x} . \qquad (2.3.6)$$

Upon substituting the assumed solution of Φ_i of equation (3.0.7) into (3.1.1), one obtains

$$\frac{\partial^2\psi_{in}}{\partial r^2} + \frac{1}{r}\frac{\partial\psi_{in}}{\partial r} - \frac{n^2}{r^2}\psi_{in} + \frac{\partial^2\psi_{in}}{\partial x^2} - \frac{1}{c_i^2}\left(-\Omega^2\psi_{in} + 2i\Omega U_i \frac{\partial\psi_{in}}{\partial x} + U_i^2 \frac{\partial^2\psi_{in}}{\partial x^2}\right) = 0 . \qquad (3.1.2)$$

Taking the Fourier transform of equation (3.1.2), yields

$$\frac{\partial^2\psi^*_{in}}{\partial r^2} + \frac{1}{r}\frac{\partial\psi^*_{in}}{\partial r} - \frac{n^2}{r^2}\psi^*_{in} - \alpha^2\psi^*_{in} - \frac{1}{c_i^2}\left(-\Omega^2\psi^*_{in} + 2\Omega\alpha U_i\psi^*_{in} - \alpha^2 U_i^2\psi^*_{in}\right) = 0 , \qquad (3.1.3)$$

where use has been made of the fact that

$$\lim_{x\to\pm\infty} \psi_{in}(x,r) = 0 \quad \text{and} \quad \lim_{x\to\pm\infty} \frac{\partial\psi_{in}(x,r)}{\partial x} = 0 .$$

The above two conditions are justifiable, since both ends of the flexible cylinders are connected to rigid extensions of infinite length; the flow perturbations will become diminishingly small at great distance away from the flexible portion.

Equation (3.1.3) can be written more compactly as

$$\frac{\partial^2\psi^*_{in}}{\partial r^2} + \frac{1}{r}\frac{\partial\psi^*_{in}}{\partial r} - \frac{n^2}{r^2}\psi^*_{in} - \mu_i^2\psi^*_{in} = 0 , \tag{3.1.4}$$

where

$$\mu_i^2 = \alpha^2 - \left[\frac{(\Omega-\alpha U_i)}{c_i}\right]^2 ,$$

or in non-dimensional form

$$\mu_i^2 L^2 = \bar{\alpha}^2 - M_i^2(\bar{\alpha} - \kappa_i)^2 , \tag{3.1.4a}$$

with $\bar{\alpha} = \alpha L$, a dimensionless Fourier transform variable,

$\kappa_i = \frac{\Omega L}{U_i}$, a so-called reduced frequency, and (3.1.4b)

$M_i = \frac{U_i}{c_i}$, the familiar Mach number.

Equation (3.1.4) is, in fact, in the form of a modified Bessel

equation of order n which has a complete solution of

$$\psi^*_{in}(\alpha,r) = C_{n1}(\alpha)I_n(\mu_i r) + C_{n2}(\alpha)K_n(\mu_i r) , \qquad (3.1.5)$$

where $I_n(\mu_i r)$ and $K_n(\mu_i r)$ are the n^{th} order modified Bessel functions of the first and second kind, respectively.

Since $K_n(\mu_i r)$ becomes infinitely large as $r \to 0$, we must have $C_{n2}(\alpha) = 0$ in order that ψ^*_{in}, and hence ψ_{in}, remain finite at $r = 0$. Thus,

$$\psi^*_{in}(\alpha,r) = C_{n1}(\alpha)I_n(\mu_i r) ; \qquad (3.1.6)$$

$C_{n1}(\alpha)$ is then determined from the boundary condition (2.3.6).

Substituting equations (3.0.3) and (3.0.7) into the boundary condition (2.3.6), and taking the Fourier transform, one obtains

$$\left.\frac{\partial \psi^*_{in}(\alpha,r)}{\partial r}\right|_{r=a} = \sum_{m=1}^{\infty} (i\Omega - i\alpha U_i)\phi^*_m(\alpha)C_{mn} , \qquad (3.1.7)$$

where $\phi^*_m(\alpha)$ is the Fourier transform of $\phi_m(x)$, *i.e.*,

$$\phi^*_m(\alpha) = \int_{-\infty}^{\infty} \phi_m(x)e^{i\alpha x}\, dx = \int_0^L \phi_m(x)e^{i\alpha x}\, dx . \qquad (3.1.8)$$

The integration is only carried out from x = 0 to x = L because the shell displacements, being expressed as infinite series in $\phi_m(x)$, vanish beyond the range $o \leq x \leq L$.

Substituting equation (3.1.6) into (3.1.7), and introducing the non-dimensional terms of (3.1.4b), we can then solve for $C_{n1}(\alpha)$, obtaining

$$C_{n1}(\alpha) = \sum_{m=1}^{\infty} \frac{iU_i(\kappa_i-\bar{\alpha})\phi_m^*(\alpha)}{\mu_i L\, I_n'(\mu_i a)} C_{mn} . \qquad (3.1.9)$$

Putting (3.1.9) into (3.1.6), yields

$$\psi_{in}^*(\alpha,r) = \sum_{m=1}^{\infty} \frac{iU_i(\kappa_i-\bar{\alpha})}{\mu_i L} \frac{I_n(\mu_i r)}{I_n'(\mu_i a)} \phi_m^*(\alpha) C_{mn} . \qquad (3.1.10)$$

We shall now proceed in the same manner to determine the velocity potential in the annular region. Realizing that the governing equation (2.3.5) and the assumed form of solution (3.0.7) of the velocity potential have their counterparts for the annular region, one could easily establish the following equation without going through all the detailed derivations:

$$\frac{\partial^2\psi_{on}^*}{\partial r^2} + \frac{1}{r}\frac{\partial\psi_{on}^*}{\partial r} - \frac{n^2}{r^2}\psi_{on}^* - \mu_o^2\psi_{on}^* = 0 , \qquad (3.1.11)$$

where

$$\mu_o^2 L^2 = \bar{\alpha}^2 - M_o^2(\bar{\alpha}-\kappa_o)^2 , \qquad (3.1.11a)$$

with

$$\bar{\alpha} = \alpha L, \ \kappa_o = \frac{\Omega L}{U_o}, \ M_o = \frac{U_o}{c_o} . \qquad (3.1.11b)$$

Similarly to (3.1.4), the solution of equation (3.1.11) is

$$\psi_{on}^*(\alpha,r) = C_{n3}(\alpha)I_n(\mu_o r) + C_{n4}(\alpha)K_n(\mu_o r) , \qquad (3.1.12)$$

where $C_{n3}(\alpha)$ and $C_{n4}(\alpha)$ are determined from boundary conditions (2.3.8) and (2.3.9).

Substituting equations (3.0.6) and (3.0.8) into boundary conditions

(2.3.8) and (2.3.9), one obtains, after Fourier transformation,

$$\left.\frac{\partial \psi^*_{on}(\alpha,r)}{\partial r}\right|_{r=a} = \sum_{m=1}^{\infty} \frac{iU_o(\kappa_o-\bar{\alpha})}{L} \phi^*_m(\alpha)\, C_{mn} \qquad (3.1.13)$$

and

$$\left.\frac{\partial \psi^*_{on}(\alpha,r)}{\partial r}\right|_{r=b} = \sum_{m=1}^{\infty} \frac{iU_o(\kappa_o-\bar{\alpha})}{L} \phi^*_m(\alpha)\, F_{mn} . \qquad (3.1.14)$$

Applying the solution of ψ^*_{on} (3.1.12) to the transformed boundary conditions (3.1.13) and (3.1.14), two simple linear algebraic equations are obtained from which $C_{n3}(\alpha)$ and $C_{n4}(\alpha)$ can easily be determined. The solutions are

$$C_{n3}(\alpha) = \sum_{m=1}^{\infty} \frac{iU_o(\kappa_o-\bar{\alpha})[K'_n(\mu_o a)F_{mn} - K'_n(\mu_o b)C_{mn}]\psi^*_m(\alpha)}{\mu_o L[I'_n(\mu_o b)K'_n(\mu_o a) - I'_n(\mu_o a)K'_n(\mu_o b)]} , \qquad (3.1.15)$$

$$C_{n4}(\alpha) = \sum_{m=1}^{\infty} \frac{iU_o(\kappa_o-\bar{\alpha})[I'_n(\mu_o b)C_{mn} - I'_n(\mu_o a)F_{mn}]\phi^*_m(\alpha)}{\mu_o L[I'_n(\mu_o b)K'_n(\mu_o a) - I'_n(\mu_o a)K'_n(\mu_o b)]} . \qquad (3.1.16)$$

Finally, the rather complicated expression of $\psi^*_{on}(\alpha,r)$ may be obtained by putting equations (3.1.15) and (3.1.16) back into (3.1.12), yielding

$$\psi^*_{on}(\alpha,r) = \sum_{m=1}^{\infty} \frac{iU_o(\kappa_o-\bar{\alpha})}{\mu_o L} \frac{I'_n(\mu_o b)K_n(\mu_o r) - I_n(\mu_o r)K'_n(\mu_o b)}{I'_n(\mu_o b)K'_n(\mu_o a) - I'_n(\mu_o a)K'_n(\mu_o b)} \phi^*_m(\alpha)\, C_{mn}$$

$$+ \frac{iU_o(\kappa_o-\bar{\alpha})}{\mu_o L} \frac{I_n(\mu_o r)K'_n(\mu_o a) - I'_n(\mu_o a)K_n(\mu_o r)}{I'_n(\mu_o b)K'_n(\mu_o a) - I'_n(\mu_o a)K'_n(\mu_o b)} \phi^*_m(\alpha)\, F_{mn} . \qquad (3.1.17)$$

Since the transformed functions (3.1.10) and (3.1.17) are

essentially what is needed later in this chapter to determine the aerodynamic forces, complete explicit expressions for the velocity potentials, Φ_i and Φ_o, will not be given here for conciseness.

3.2 DETERMINATION OF THE INVISCID PERTURBATION PRESSURES

It may be recalled from Chapter II that the inviscid perturbation pressure may be derived from the velocity potential by means of the following equation:

$$\bar{p} = -\rho\left(\frac{\partial \Phi}{\partial t} + U \frac{\partial \Phi}{\partial x}\right) . \tag{2.2.9}$$

Let us first consider the internal region. Equation (3.0.7) is substituted into (2.2.9) and, to be consistent with the form of the other solutions, the perturbation pressure is also assumed to have an oscillatory time-dependence, so that

$$\bar{p}_i(x,r,\theta)e^{i\Omega t} = -\rho_i\left(i\Omega\psi_{in} \cos n\theta\, e^{i\Omega t} + U_i \frac{\partial \psi_{in}}{\partial x} \cos n\theta\, e^{i\Omega t}\right) \tag{3.2.1}$$

It is desirable to define the Fourier transform in terms of the dimensionless variables $\bar{\alpha} = \alpha L$ and $\xi = x/L$; thus,

$$\bar{p}^*(\bar{\alpha},r,\theta) = L \int_{-\infty}^{\infty} \bar{p}(\xi,r,\theta)e^{i\bar{\alpha}\xi}\, d\xi \tag{3.2.2}$$

and the inverse transform

$$\bar{p}(\xi,r,\theta) = \frac{1}{2\pi L} \int_{-\infty}^{\infty} \bar{p}^*(\bar{\alpha},r,\theta)e^{-i\bar{\alpha}\xi}\, d\bar{\alpha} . \tag{3.2.3}$$

Equation (3.2.1) after transformation becomes

$$\bar{p}_i^*(\bar{\alpha},r,\theta) = \frac{-i\rho_i U_i(\kappa_i-\bar{\alpha})}{L} \psi_{in}^*(\bar{\alpha},r) \cos n\theta \ . \tag{3.2.4}$$

Similarly, the transformed perturbation pressure in the annular region is given by

$$\bar{p}_o^*(\bar{\alpha},r,\theta) = \frac{-i\rho_o U_o(\kappa_o-\bar{\alpha})}{L} \psi_{on}^*(\bar{\alpha},r) \cos n\theta \ . \tag{3.2.5}$$

Invoking the assumption that the steady-state pressures in the internal and annular fluids are equal, the net loading on the inner shell arises from the perturbation terms only and is equal to

$$q_i = (\bar{p}_i\big|_{r=a} - \bar{p}_o\big|_{r=a})e^{i\Omega t} \ . \tag{3.2.6}$$

Taking the inverse Fourier transform of (3.2.4) and (3.2.5) and utilizing the expressions of $\psi_{in}^*(\bar{\alpha},r)$ and $\psi_{on}^*(\bar{\alpha},r)$ found in the previous section (equations (3.1.10) and (3.1.17)), equation (3.2.6) can be put in the form

$$q_i = \sum_{m=1}^{\infty} Q_{mn}(\xi) \cos n\theta \ e^{i\Omega t} \ , \tag{3.2.7}$$

where

$$Q_{mn}(\xi) = \frac{\rho_i U_i^2 C_{mn}}{2\pi L^2} \int_{-\infty}^{\infty} \frac{(\kappa_i-\bar{\alpha})^2}{\mu_i L} E_n(\bar{\alpha})\phi_m^*(\bar{\alpha})e^{-i\bar{\alpha}\xi} \, d\bar{\alpha}$$

$$- \frac{\rho_o U_o^2 C_{mn}}{2\pi L^2} \int_{-\infty}^{\infty} \frac{(\kappa_o-\bar{\alpha})^2}{\mu_o L} F_n(\bar{\alpha})\phi_m^*(\bar{\alpha})e^{-i\bar{\alpha}\xi} \, d\bar{\alpha}$$

Continued/

$$- \frac{\rho_o U_o^2 F_{mn}}{2\pi L^2} \int_{-\infty}^{\infty} \frac{(\kappa_o - \bar{\alpha})^2}{\mu_o L} G_n(\bar{\alpha}) \phi_m^*(\bar{\alpha}) e^{-i\bar{\alpha}\xi} \, d\alpha, \tag{3.2.7a}$$

and

$$E_n(\bar{\alpha}) = \frac{I_n(\mu_i a)}{I_n'(\mu_i a)}, \tag{3.2.7b}$$

$$F_n(\bar{\alpha}) = \frac{I_n'(\mu_o b)K_n(\mu_o a) - I_n(\mu_o a)K_n'(\mu_o b)}{I_n'(\mu_o b)K_n'(\mu_o a) - I_n'(\mu_o a)K_n'(\mu_o b)}, \tag{3.2.7c}$$

$$G_n(\bar{\alpha}) = \frac{I_n(\mu_o a)K_n'(\mu_o a) - I_n'(\mu_o a)K_n(\mu_o a)}{I_n'(\mu_o b)K_n'(\mu_o a) - I_n'(\mu_o a)K_n'(\mu_o b)}. \tag{3.2.7d}$$

Equations (3.2.7) and (3.2.7a-d) give explicitly the aerodynamic loadings on the inner shell. Nevertheless, in connection with Galerkin's method used later in the solution of the equations of motion, a more appropriate fluid force term, the so-called generalized aerodynamic force, is required. Accordingly, the amplitudes of these generalized forces, $\bar{Q}_{kmn}$ will be defined here:

$$\bar{Q}_{kmn} = \int_o^L \phi_k(\xi) Q_{mn}(\xi) \, dx$$

$$= L \int_o^1 \phi_k(\xi) Q_{mn}(\xi) \, d\xi, \tag{3.2.8}$$

or non-dimensionally

$$\bar{\bar{Q}}_{kmn} = \frac{\gamma_i}{\rho_{si} h_i L^2} \bar{Q}_{kmn} = \frac{\gamma_i}{\rho_{si} h_i L} \int_o^1 \phi_k(\xi) Q_{mn}(\xi) \, d\xi. \tag{3.2.9}$$

Before proceeding, it is useful to define the following dimensionless quantities:

$$\bar{U}_i = U_i/\upsilon_i \ , \ \bar{U}_o = U_o/\upsilon_o \ , \ \beta_i = (\rho_i a)/(\rho_{si} h_i) \ , \ \beta_o = (\rho_o b)/(\rho_{so} h_o) \ ,$$

$$\varepsilon_i = a/L \ , \ \varepsilon_o = b/L \ , \ \varepsilon_r = a/b \ , \ \upsilon_r = \upsilon_i/\upsilon_o \ , \ \rho_r = \rho_o/\rho_i \ ,$$

$$\bar{C}_{mn} = C_{mn}/L \ , \ \bar{F}_{mn} = F_{mn}/L \ , \tag{3.2.10}$$

where

$$\upsilon_i = \{E_i/[\rho_{si}(1-\nu_i^2)]\}^{\frac{1}{2}} \ , \ \upsilon_o = \{E_o/[\rho_{so}(1-\nu_o^2)]\}^{\frac{1}{2}} \ . \tag{3.2.10a}$$

Then, substituting equations (3.2.7a) into (3.2.9) and utilizing (3.2.10), $\bar{\bar{Q}}_{kmn}$ can be written as

$$\bar{\bar{Q}}_{kmn} = Q'_{kmn}\bar{C}_{mn} + Q''_{kmn}\bar{F}_{mn} \ , \tag{3.2.11}$$

where

$$Q'_{kmn} = \frac{\bar{U}_i^2\beta_i\varepsilon_i}{2\pi} \int_{-\infty}^{\infty} \frac{(\kappa_i-\bar{\alpha})^2}{\mu_i L} E_n(\bar{\alpha})H_{km}(\bar{\alpha}) \, d\bar{\alpha}$$

$$- \frac{\bar{U}_o^2\beta_i\varepsilon_i\rho_r}{2\pi\upsilon_r^2} \int_{-\infty}^{\infty} \frac{(\kappa_o-\bar{\alpha})^2}{\mu_o L} F_n(\bar{\alpha})H_{km}(\bar{\alpha}) \, d\bar{\alpha} \ , \tag{3.2.11a}$$

$$Q''_{kmn} = -\frac{\bar{U}_o^2\beta_i\varepsilon_i\rho_r}{2\pi\upsilon_r^2} \int_{-\infty}^{\infty} \frac{(\kappa_o-\bar{\alpha})^2}{\mu_o L} G_n(\bar{\alpha})H_{km}(\bar{\alpha}) \, d\bar{\alpha} \tag{3.2.11b}$$

and

$$H_{km}(\bar{\alpha}) = \int_0^1 \phi_m(\xi)e^{i\bar{\alpha}\xi} \, d\xi \times \int_0^1 \phi_k(\xi)e^{-i\bar{\alpha}\xi} \, d\xi \ . \tag{3.2.11c}$$

$E_n(\bar{\alpha})$, $F_n(\bar{\alpha})$ and $G_n(\bar{\alpha})$ are as defined in (3.2.7b), (3.2.7c) and (3.2.7d), respectively.

Consider next the pressure acting on the outer cylinder. By assuming the steady-state annular pressure to be equal to the external pressure, the dynamic loading on the outer cylinder is the perturbation pressure in the annular region. Hence,

$$q_o = (\bar{p}_o|_{r=b})e^{i\Omega t} .$$

With the inverse Fourier transform of (3.2.4) and the expression of $\psi^*_{on}(\bar{\alpha},r)$ given by equation (3.1.17), q_o is found to be

$$q_o = \sum_{m=1}^{\infty} R_{mn}(\xi) \cos n\theta \, e^{i\Omega t} , \tag{3.2.12}$$

where

$$R_{mn}(\xi) = \frac{\rho_o U_o^2 C_{mn}}{2\pi L^2} \int_{-\infty}^{\infty} \frac{(\kappa_o-\bar{\alpha})^2}{\mu_o L} L_n(\bar{\alpha})\phi^*_m(\bar{\alpha})e^{-i\bar{\alpha}\xi} \, d\bar{\alpha}$$

$$+ \frac{\rho_o U_o^2 F_{mn}}{2\pi L^2} \int_{-\infty}^{\infty} \frac{(\kappa_o-\bar{\alpha})^2}{\mu_o L} M_n(\bar{\alpha})\phi^*_m(\bar{\alpha})e^{-i\bar{\alpha}\xi} \, d\bar{\alpha} , \tag{3.2.12a}$$

and

$$L_n(\bar{\alpha}) = \frac{I_n'(\mu_o b)K_n(\mu_o b) - I_n(\mu_o b)K_n'(\mu_o b)}{I_n'(\mu_o b)K_n'(\mu_o a) - I_n'(\mu_o a)K_n'(\mu_o b)} , \tag{3.2.12b}$$

$$M_n(\bar{\alpha}) = \frac{I_n(\mu_o b)K_n'(\mu_o a) - I_n'(\mu_o a)K_n(\mu_o b)}{I_n'(\mu_o b)K_n'(\mu_o a) - I_n'(\mu_o a)K_n'(\mu_o b)} . \tag{3.2.12c}$$

The corresponding generalized aerodynamic forces are then given by

$$\bar{R}_{kmn} = L \int_0^1 \phi_k(\xi) R_{mn}(\xi)\, d\xi \,, \tag{3.2.13}$$

and the non-dimensional form is

$$\bar{\bar{R}}_{kmn} = \frac{\gamma_o}{\rho_{so} h_o L^2} \bar{R}_{kmn} = \frac{\gamma_o}{\rho_{so} h_o L} \int_0^1 \phi_k(\xi) R_{mn}(\xi)\, d\xi \,. \tag{3.2.14}$$

Making use of equation (3.2.12a) and the dimensionless terms in (3.2.10), $\bar{\bar{R}}_{kmn}$ can be written as

$$\bar{\bar{R}}_{kmn} = R''_{kmn} \bar{C}_{mn} + R'_{kmn} \bar{F}_{mn} \,, \tag{3.2.15}$$

where

$$R''_{kmn} = \frac{\bar{U}_o^2 \beta_o \varepsilon_o}{2\pi} \int_{-\infty}^{\infty} \frac{(\kappa_o - \bar{\alpha})^2}{\mu_o L} L_n(\bar{\alpha}) H_{km}(\bar{\alpha})\, d\bar{\alpha} \,, \tag{3.2.15a}$$

$$R'_{kmn} = \frac{\bar{U}_o^2 \beta_o \varepsilon_o}{2\pi} \int_{-\infty}^{\infty} \frac{(\kappa_o - \bar{\alpha})^2}{\mu_o L} M_n(\bar{\alpha}) H_{km}(\bar{\alpha})\, d\bar{\alpha} \,, \tag{3.2.15b}$$

with $H_{km}(\bar{\alpha})$, $L_n(\bar{\alpha})$ and $M_n(\bar{\alpha})$ as given in equations (3.2.11c), (3.2.12b) and (3.2.12c), respectively.

The integration in equation (3.2.11c) can be performed analytically and the resultant expression in terms of $\bar{\alpha}$ is given in Appendix B. However, the complexity of the various integrals in the aerodynamic force terms (3.2.11a,b) and (3.2.15a,b) precludes analytical solution. Two methods have been devised to evaluate these integrals, namely, contour integration using the theory of complex variables, and direct numerical integration using the Gaussian quadrature technique. Details on these methods and their feasibility will be discussed in Chapter IV.

3.3 SOLUTIONS TO THE VELOCITY POTENTIALS AND PERTURBATION PRESSURES OF INCOMPRESSIBLE FLOW

Theoretically, the solutions for incompressible flow can be deduced as the limiting cases of the compressible flow results as c, the speed of sound, approaches infinity or, equivalently, as the Mach number, M, tends to zero.

In the text of the previous sections, μ_i and μ_o as defined in (3.1.4a) and (3.1.11a) are the only parameters with Mach number dependence. In the limit as $M_i, M_o \to 0$, μ_i, μ_o will both approach α. Thus, without going through detailed derivations, the solutions for incompressible flow could be obtained by putting α in place of μ_i and μ_o in the appropriate results derived for compressible flow.

For the sake of conciseness, the complete expressions of the velocity potentials and generalized aerodynamic forces for incompressible flow will not be given here because of their similarity to the compressible flow results. The interested reader is referred to Appendix C for details.

An important consequence of the reduction of μ_i and μ_o to α, in the case of incompressible flow, is that the frequency terms involved in the integrals of the generalized aerodynamic forces can now be removed through some simple algebraic manipulations (see Appendix C). This has great advantages in terms of obtaining numerical solutions. This will be elaborated upon in the next section, when solution to the equations of motion is discussed. In the meantime, the resultant expressions will be given of the generalized aerodynamic forces after the integrals are rendered frequency-independent.

(i) For the inner shell, we have

$$\bar{\bar{Q}}_{kmn} = \bar{\Omega}_o^2(q_{kmn}^{C1}\bar{C}_{mn} + q_{kmn}^{F1}\bar{F}_{mn})$$

$$+ \bar{\Omega}_o(q_{kmn}^{C2}\bar{C}_{mn} + q_{kmn}^{F2}\bar{F}_{mn}) + (q_{kmn}^{C3}\bar{C}_{mn} + (q_{kmn}^{F3}\bar{F}_{mn}) , \qquad (3.3.1)$$

where

$$\bar{\Omega}_o = \Omega \times b[\rho_{so}(1-\nu_o^2)/E_o]^{\frac{1}{2}} \qquad (3.3.1a)$$

is another dimensionless form of the frequency, and

$$q_{kmn}^{C1} = \frac{\beta_i\varepsilon_i}{2\pi\varepsilon_o^2 v_r^2}\int_{-\infty}^{\infty}\frac{\hat{E}_n(\bar{\alpha})}{\bar{\alpha}}H_{km}(\bar{\alpha})\,d\bar{\alpha}$$

$$- \frac{\beta_i\varepsilon_i\rho_r}{2\pi\varepsilon_o^2 v_r^2}\int_{-\infty}^{\infty}\frac{\hat{F}_n(\bar{\alpha})}{\bar{\alpha}}H_{km}(\bar{\alpha})\,d\bar{\alpha} , \qquad (3.3.1b)$$

$$q_{kmn}^{F1} = -\frac{\beta_i\varepsilon_i\rho_r}{2\pi\varepsilon_o^2 v_r^2}\int_{-\infty}^{\infty}\frac{\hat{G}_n(\bar{\alpha})}{\bar{\alpha}}H_{km}(\bar{\alpha})\,d\bar{\alpha} , \qquad (3.3.1c)$$

$$q_{kmn}^{C2} = -\frac{\bar{U}_i\beta_i\varepsilon_r}{\pi v_r}\int_{-\infty}^{\infty}\hat{E}_n(\bar{\alpha})H_{km}(\bar{\alpha})\,d\bar{\alpha}$$

$$+ \frac{\bar{U}_o\beta_i\varepsilon_r\rho_r}{\pi v_r^2}\int_{-\infty}^{\infty}\hat{F}_n(\bar{\alpha})H_{km}(\bar{\alpha})\,d\bar{\alpha} , \qquad (3.3.1d)$$

$$q^{F2}_{kmn} = \frac{\bar{U}_o \beta_i \epsilon_r \rho_r}{\pi \upsilon_r^2} \int_{-\infty}^{\infty} \hat{G}_n(\bar{\alpha}) H_{km}(\bar{\alpha})\, d\bar{\alpha} , \tag{3.3.1e}$$

$$q^{C3}_{kmn} = \frac{\bar{U}_i^2 \beta_i \epsilon_i}{2\pi} \int_{-\infty}^{\infty} \bar{\alpha} \hat{E}_n(\bar{\alpha}) H_{km}(\bar{\alpha})\, d\bar{\alpha}$$

$$- \frac{\bar{U}_o^2 \beta_i \epsilon_i \rho_r}{2\pi \upsilon_r^2} \int_{-\infty}^{\infty} \bar{\alpha} \hat{F}_n(\bar{\alpha}) H_{km}(\bar{\alpha})\, d\bar{\alpha} , \tag{3.3.1f}$$

$$q^{F3}_{kmn} = - \frac{\bar{U}_o^2 \beta_i \epsilon_i \rho_r}{2\pi \upsilon_r^2} \int_{-\infty}^{\infty} \bar{\alpha} \hat{G}_n(\bar{\alpha}) H_{km}(\bar{\alpha})\, d\bar{\alpha} , \tag{3.3.1g}$$

and

$$\hat{E}_n(\bar{\alpha}) = \frac{I_n(\alpha a)}{I_n'(\alpha a)} , \tag{3.3.1h}$$

$$\hat{F}_n(\bar{\alpha}) = \frac{I_n'(\alpha b) K_n(\alpha a) - I_n(\alpha a) K_n'(\alpha b)}{I_n'(\alpha b) K_n'(\alpha a) - I_n'(\alpha a) K_n'(\alpha b)} , \tag{3.3.1i}$$

$$\hat{G}_n(\bar{\alpha}) = \frac{I_n(\alpha a) K_n'(\alpha a) - I_n'(\alpha a) K_n(\alpha a)}{I_n'(\alpha b) K_n'(\alpha a) - I_n'(\alpha a) K_n'(\alpha b)} . \tag{3.3.1j}$$

(ii) Similarly, for the outer shell, we have

$$\bar{\bar{R}}_{kmn} = \bar{\Omega}_o^2 (r^{C1}_{kmn} \bar{\bar{C}}_{mn} + r^{F1}_{kmn} \bar{\bar{F}}_{mn}) + \bar{\Omega}_o (r^{C2}_{kmn} \bar{\bar{C}}_{mn} + r^{F2}_{kmn} \bar{\bar{F}}_{mn})$$

$$+ (r^{C2}_{kmn} \bar{\bar{C}}_{mn} + r^{F3}_{kmn} \bar{\bar{F}}_{mn}) , \tag{3.3.2}$$

where

$$r^{C1}_{kmn} = \frac{\beta_o}{2\pi\varepsilon_o} \int_{-\infty}^{\infty} \frac{\hat{L}_n(\bar{\alpha})}{\bar{\alpha}} H_{km}(\bar{\alpha})\, d\bar{\alpha} , \qquad (3.3.2a)$$

$$r^{F1}_{kmn} = \frac{\beta_o}{2\pi\varepsilon_o} \int_{-\infty}^{\infty} \frac{\hat{M}_n(\bar{\alpha})}{\bar{\alpha}} H_{km}(\bar{\alpha})\, d\bar{\alpha} , \qquad (3.3.2b)$$

$$r^{C2}_{kmn} = -\frac{\bar{U}_o\beta_o}{\pi} \int_{-\infty}^{\infty} \hat{L}_n(\bar{\alpha}) H_{km}(\bar{\alpha})\, d\bar{\alpha} , \qquad (3.3.2c)$$

$$r^{F2}_{kmn} = -\frac{\bar{U}_o\beta_o}{\pi} \int_{-\infty}^{\infty} \hat{M}_n(\bar{\alpha}) H_{km}(\bar{\alpha})\, d\bar{\alpha} , \qquad (3.3.2d)$$

$$r^{C3}_{kmn} = \frac{\bar{U}_o^2\beta_o\varepsilon_o}{2\pi} \int_{-\infty}^{\infty} \bar{\alpha}\hat{L}_n(\bar{\alpha}) H_{km}(\bar{\alpha})\, d\bar{\alpha} , \qquad (3.3.2e)$$

$$r^{F3}_{kmn} = \frac{\bar{U}_o^2\beta_o\varepsilon_o}{2\pi} \int_{-\infty}^{\infty} \bar{\alpha}\hat{M}_n(\bar{\alpha}) H_{km}(\bar{\alpha})\, d\bar{\alpha} , \qquad (3.3.2f)$$

and

$$\hat{L}_n(\bar{\alpha}) = \frac{I_n'(\alpha b)K_n(\alpha b) - I_n(\alpha b)K_n'(\alpha b)}{I_n'(\alpha b)K_n'(\alpha a) - I_n'(\alpha a)K_n'(\alpha b)} , \qquad (3.3.2g)$$

$$\hat{M}_n(\bar{\alpha}) = \frac{In(\alpha b)K_n'(\alpha a) - I_n'(\alpha a)K_n(\alpha b)}{I_n'(\alpha b)K_n'(\alpha a) - I_n'(\alpha a)K_n'(\alpha b)} . \qquad (3.3.2h)$$

Separate formulations have also been done for a system with a flexible inner cylinder and a rigid outer cylinder. The corresponding aerodynamic forces for the case of compressible or incompressible flows are given in Appendix D.

3.4 SOLUTION TO THE EQUATIONS OF MOTION

We shall now return to Flügge's shell equations (2.1.1-.6), and express the fluid loads in terms of the displacements. For discussion purposes, let us denote the resultant equations as follows:

$$L_k(u_i, v_i, w_i, u_o, v_o, w_o) = 0, \qquad k = 1, 2, \ldots, 6 ,$$

corresponding to equations (2.1.1-.6).

The series expressions for the displacements (3.0.1-.6) being approximate solutions, would not necessarily satisfy the shell equations (2.1.1-.6) upon substitution; that is, if $\tilde{u}_i$, $\tilde{v}_i$, $\tilde{w}_i$, $\tilde{u}_o$, $\tilde{v}_o$, $\tilde{w}_o$ are the assumed solutions, then we would have, in general

$$L_k(\tilde{u}_i, \tilde{v}_i, \tilde{w}_i, \tilde{u}_o, \tilde{v}_o, \tilde{w}_o) \neq 0 \qquad \text{for} \qquad k = 1, 2, \ldots, 6 .$$

However, according to Galerkin's method, we could impose a requirement that the integration over an arbitrarily chosen range of the expressions $L_k(\tilde{u}_i, \tilde{v}_i, \tilde{w}_i, \tilde{u}_o, \tilde{v}_o, \tilde{w}_o)$, k = 1, 2, ... 6, weighted with the same set of comparison functions employed in the series solutions of the displacements, can be put identically equal to zero, *i.e.*,

$$\int_{x_1}^{x_2} L_k(\tilde{u}_i, \tilde{v}_i, \tilde{w}_i, \tilde{u}_o, \tilde{v}_o, \tilde{w}_o) f_m(x)\, dx = 0 , \qquad (3.4.1)$$

$$k = 1, 2, \ldots, 6 , \qquad m = 1, 2, 3, \ldots$$

where $f_m(x)$ are the weighting functions.

The above procedure will lead to a set of linear algebraic

equations which can be put into matrix-equation form: $[A]\{X\} = \{0\}$.

The eigenfunctions of a beam, $\phi_k(x)$ will be the weighting function for the shell equations (2.1.2-.3) and (2.1.5-.6), whereas their derivatives, $\phi_k'(x)$, will be used to weight equations (2.1.1) and (2.1.4). Following the procedures described earlier, we first substitute equations (3.0.1-.6) into (2.1.1-.6). After multiplying with the weighting functions, the equations are integrated with respect to x between the limits x = 0 and x = L. The shell equations are now identically satisfied. The next step is to non-dimensionalize the resulting equations by making use of the following dimensionless terms as well as some of those from (3.2.10)

$$\bar{A}_{mn} = A_{mn}/L,\ \bar{B}_{mn} = B_{mn}/L,\ \bar{D}_{mn} = D_{mn}/L,\ \bar{E}_{mn} = E_{mn}/L,$$

$$\bar{\Omega}_o = \Omega/\Omega_o,\ \Omega_r = \Omega_i/\Omega_o\ , \qquad (3.4.2)$$

where

$$\Omega_i = (1/a)\{E_i/[\rho_{si}(1-\nu_i^2)]\}^{\frac{1}{2}}\ ,\ \Omega_o = (1/b)\{E_o/[\rho_{so}(1-\nu_o^2)]\}^{\frac{1}{2}}\ . \qquad (3.4.2a)$$

Finally, one obtains the following sets of linear homogeneous algebraic equations:

$$\begin{aligned}
&\sum_{m=1}^{\infty} A^1_{kmn}\bar{A}_{mn} + A^2_{kmn}\bar{B}_{mn} + A^3_{kmn}\bar{C}_{mn} + 0\times\bar{D}_{mn} + 0\times\bar{E}_{mn} + 0\times\bar{F}_{mn} = 0\ ,\\
&\sum_{m=1}^{\infty} A^4_{kmn}\bar{A}_{mn} + A^5_{kmn}\bar{B}_{mn} + A^6_{kmn}\bar{C}_{mn} + 0\times\bar{D}_{mn} + 0\times\bar{E}_{mn} + 0\times\bar{F}_{mn} = 0\ ,\\
&\sum_{m=1}^{\infty} A^7_{kmn}\bar{A}_{mn} + A^8_{kmn}\bar{B}_{mn} + A^9_{kmn}\bar{C}_{mn} + 0\times\bar{D}_{mn} + 0\times\bar{E}_{mn} + Q''_{kmn}\bar{F}_{mn} = 0\ ,\\
&\sum_{m=1}^{\infty} 0\times\bar{A}_{mn} + 0\times\bar{B}_{mn} + 0\times\bar{C}_{mn} + A^{10}_{kmn}\bar{D}_{mn} + A^{11}_{kmn}\bar{E}_{mn} + A^{12}_{kmn}\bar{F}_{mn} = 0\ ,
\end{aligned} \qquad (3.4.3)$$

$$\sum_{m=1}^{\infty} 0\times\bar{A}_{mn} + 0\times\bar{B}_{mn} + 0\times\bar{C}_{mn} + A^{13}_{kmn}\bar{D}_{mn} + A^{14}_{kmn}\bar{E}_{mn} + A^{15}_{kmn}\bar{F}_{mn} = 0 \ ,$$

$$\sum_{m=1}^{\infty} 0\times\bar{A}_{mn} + 0\times\bar{B}_{mn} + R''_{kmn}\bar{C}_{mn} + A^{16}_{kmn}\bar{D}_{mn} + A^{17}_{kmn}\bar{E}_{mn} + A^{18}_{kmn}\bar{F}_{mn} = 0 \ , \quad k = 1, 2, 3, \ldots$$

where

$$A^{1}_{kmn} = \varepsilon_i^2 b_{km} + (\nu_i - 1)(k_i + 1)n^2 a_{km}/2 + a_{km}\bar{\Omega}_o^2/\Omega_r^2 \ , \tag{3.4.4}$$

$$A^{2}_{kmn} = (1+\nu_i)n a_{km}/2 \ , \tag{3.4.5}$$

$$A^{3}_{kmn} = [\nu_i + (\nu_i - 1)k_i n^2/2]a_{km} - k_i\varepsilon_i^2 b_{km} \ , \tag{3.4.6}$$

$$A^{4}_{kmn} = -(1+\nu_i)n\varepsilon_i^2 d_{km}/2 \ , \tag{3.4.7}$$

$$A^{5}_{kmn} = (1+3k_i)(1-\nu_i)\varepsilon_i^2 d_{km}/2 + (\bar{\Omega}_o^2/\Omega_r^2 - n^2)\delta_{km} \ , \tag{3.4.8}$$

$$A^{6}_{kmn} = (3-\nu_i)k_i\varepsilon_i^2 n d_{km}/2 - n\delta_{km} \ , \tag{3.4.9}$$

$$A^{7}_{kmn} = [2\nu_i - k_i(1-\nu_i)n^2]\varepsilon_i^2 d_{km}/2 - \lambda_m^4\varepsilon_i^4 k_i\delta_{km} \ , \tag{3.4.10}$$

$$A^{8}_{kmn} = n\delta_{km} - k_i(3-\nu_i)n\varepsilon_i^2 d_{km}/2 \ , \tag{3.4.11}$$

$$A^{9}_{kmn} = k_i\{[\lambda_m^4\varepsilon_i^4 + (n^2-1)^2]\delta_{km} - 2n^2\varepsilon_i^2 d_{km}\} + (1-\bar{\Omega}_o^2/\Omega_r^2)\delta_{km} + Q'_{kmn} \ , \tag{3.4.12}$$

$$A^{10}_{kmn} = \varepsilon_o^2 b_{km} + (\nu_o - 1)(k_o + 1)n^2 a_{km}/2 + \bar{\Omega}_o^2 a_{km} \ , \tag{3.4.13}$$

$$A^{11}_{kmn} = (1+\nu_o)n a_{km}/2 \ , \tag{3.4.14}$$

$$A^{12}_{kmn} = [\nu_o + (\nu_o - 1)k_o n^2/2]a_{km} - k_o\varepsilon_o^2 b_{km} \ , \tag{3.4.15}$$

$$A^{13}_{kmn} = -(1+\nu_o)n\varepsilon_o^2 d_{km}/2 \ , \tag{3.4.16}$$

$$A^{14}_{kmn} = (1+3k_o)(1-\nu_o)\varepsilon_o^2 d_{km}/2 + (\bar{\Omega}_o^2 - n^2)\delta_{km} \ , \tag{3.4.17}$$

$$A^{15}_{kmn} = (3-\nu_o)k_o\varepsilon_o^2 n d_{km}/2 - n\delta_{km} \ , \tag{3.4.18}$$

$$A^{16}_{kmn} = [2\nu_o - k_o(1-\nu_o)n^2]\varepsilon_o^2 d_{km}/2 - \lambda_m^4\varepsilon_o^4 k_o \delta_{km} \ , \tag{3.4.19}$$

$$A^{17}_{kmn} = n\delta_{km} - k_o(3-\nu_o)n\varepsilon_o^2 d_{km}/2 \ , \tag{3.4.20}$$

$$A^{18}_{kmn} = k_o\{[\lambda_m^4\varepsilon_o^4 + (n^2-1)^2]\delta_{km} - 2n^2\varepsilon_o^2 d_{km}\} + (1-\bar{\Omega}_o^2)\delta_{km} + R'_{kmn} \ , \tag{3.4.21}$$

with

$$a_{km} = L\int_o^L \phi'_k(x)\phi'_m(x)\,dx \ , \tag{3.4.22}$$

$$b_{km} = L^3\int_o^L \phi'_k(x)\phi'''_m(x)\,dx \ , \tag{3.4.23}$$

$$d_{km} = L\int_o^L \phi_k(x)\phi''_m(x)\,dx \ , \text{ and} \tag{3.4.24}$$

$$\delta_{km} = \frac{1}{L}\int_o^L \phi_k(x)\phi_m(x)\,dx \text{ is the Kronecker delta .} \tag{3.4.25}$$

The constants of (3.4.22-.24) are given in Appendix A. Q'_{kmn}, Q''_{kmn}, R'_{kmn}, R''_{kmn} are terms associated with the generalized aerodynamic forces and are given by equations (3.2.11a-b), (3.2.15a-b) for compressible flow and by equations (C.1-.4) of Appendix C for incompressible flow.

Since a solution to the infinite sets of equations (3.4.3) is impossible to obtain, the series solutions (3.0.1-.6) could be truncated, so as to have a finite number of terms. Consequently, only the first three terms of each series are retained (*i.e.* k,m = 1,2,3), assuming that satisfactory convergence would be achieved with the truncated series, at least for the first two modes of the system, and that the results would be reasonable approximations to the exact solutions[†].

The set of equations (3.4.3) are put into matrix form,

$$[A]\{X\} = \{0\} , \tag{3.4.26}$$

where

$$\{X\} = [\bar{A}_{1n}, \bar{A}_{2n}, \bar{A}_{3n}; \bar{B}_{1n}, \ldots; \ldots, \bar{F}_{2n}, \bar{F}_{3n}]^T \tag{3.4.27}$$

is an 18-element column vector, and [A] is an 18x18 matrix the elements of which are the corresponding coefficients of $\bar{A}_{mn}$, $\bar{B}_{mn}$, $\bar{C}_{mn}$, $\bar{D}_{mn}$, $\bar{E}_{mn}$ and $\bar{F}_{mn}$ in (3.4.3). The structure of matrix [A] is shown in Appendix E.

The frequency equation of the system is obtained by setting the determinant of the coefficient matrix [A] in equation (3.4.26) equal to zero; that is,

$$\det [A(\Omega, \bar{U}_i, \bar{U}_o, \text{fluid, material and geometrical properties})] = 0 . \tag{3.4.28}$$

For a given set of fluid and shell parameters and with the flow velocities, $\bar{U}_i$ and $\bar{U}_o$ specified, det[A] would be a function of Ω only.

[†]It has been verified in reference [37] that satisfactorily convergent results can be obtained with a truncated 3-term series.

It should be noted that, in the case of compressible flow the aerodynamic forces are complicated functions of the frequency Ω. Therefore, in order to determine the natural frequencies of the system, an iteration procedure is required in that case. An economical method of obtaining the numerical results will be discussed in Chapter IV.

For incompressible flow, on the other hand, the generalized aerodynamic forces can be rearranged as quadratic functions of the frequency parameter $\bar{\Omega}_0$ (see equations (3.3.1) and (3.3.2)). The matrix equation (3.4.26) can, therefore, be written in the form

$$\bar{\Omega}_0^2[M]\{X\} + \bar{\Omega}_0[C]\{X\} + [K]\{X\} = \{0\} \tag{3.4.29}$$

where $\{X\}$ is as defined in (3.4.27) and the structure of the matrices $[M]$, $[C]$ and $[K]$ is given in Appendix E.

Defining now

$$\{Y\} = \begin{Bmatrix} \{X\} \\ \bar{\Omega}_0\{X\} \end{Bmatrix} , \tag{3.4.30}$$

we can reduce the second-order equation (3.4.29) to a first-order equation, *i.e.*,

$$\begin{bmatrix} [0] & [I] \\ [K] & [C] \end{bmatrix} + \bar{\Omega}_0 \begin{bmatrix} [-I] & [0] \\ [0] & [M] \end{bmatrix} \{Y\} = \{0\} ,$$

or

$$([P] + \bar{\Omega}_0[Q])\{Y\} = \{0\} , \tag{3.4.31}$$

where [I] is the identity matrix.

Thus, the problem for incompressible flow is now reduced to one of solving the eigenvalue equation (3.4.31) which can easily be done using computer library subroutines. In addition to the fact that no iteration procedure is required, the integrals associated with the generalized aerodynamic forces in equations (3.3.7a-g) and (3.3.8a-f) have to be evaluated only once for a particular set of geometric parameters. All these simplifications result in considerable saving in computer time.

CHAPTER IV

METHODS OF EVALUATING THE GENERALIZED AERODYNAMIC FORCES

It has been shown in Chapter III that the generalized aerodynamic force terms involve complicated integrations in the transformed variable $\bar{\alpha}$ that cannot be evaluated analytically. In this Chapter will be presented two methods of calculating the integrals.

The contour integration technique is attempted first. In principle, this method represents an elegant and efficient way of evaluating an integral by making use of the Residue Theorem, but, unfortunately, it has proven impossible to apply it successfully to the problem at hand. Nevertheless, it is considered worthwhile highlighting the progress achieved so far with this method and the difficulties encountered, in the hope that these latter will eventually be overcome. This work is presented in Section 4.1.

The second method is by direct numerical integration and interpolation. The integral is computed numerically using the two-point Gaussian quadrature. Being functions of the reduced frequency, the integrals are calculated with a number of values chosen within the frequency range over which the integration is to be carried out. The results are then curve-fitted and represented by simple interpolation equations. Although this method is rather straightforward and simple in concept, it has certain limitations in terms of its applicability and computational expense, as discussed later in Section 4.2.

4.1 CONTOUR INTEGRATION USING THE THEORY OF COMPLEX VARIABLES[†]

As an example, we consider the second integral, as given in equation (3.2.11a), which is

$$\int_{-\infty}^{\infty} \frac{(\kappa_o-\bar{\alpha})^2}{\mu_o L} F_n(\bar{\alpha}) H_{km}(\bar{\alpha})\, d\bar{\alpha} , \tag{4.1}$$

where

$$F_n(\bar{\alpha}) = \frac{I_n'(\mu_o b)K_n(\mu_o a) - I_n(\mu_o a)K_n'(\mu_o b)}{I_n'(\mu_o b)K_n'(\mu_o a) - I_n'(\mu_o a)K_n'(\mu_o b)} , \tag{3.2.7c}$$

$$H_{km}(\bar{\alpha}) = \int_o^1 \phi_m(\xi) e^{i\bar{\alpha}\xi}\, d\xi \times \int_o^1 \phi_k(\xi) e^{-i\bar{\alpha}\xi}\, d\xi , \tag{3.2.11c}$$

$$\mu_o^2 L^2 = \bar{\alpha}^2 - M_o^2(\bar{\alpha}-\kappa_o)^2 . \tag{3.1.4a}$$

For simplicity and for the purposes of this discussion, we shall assume that $\kappa_o = 0$. The integral may then be written as

$$\int_{-\infty}^{\infty} \frac{|\bar{\alpha}|}{(1-M_o^2)^{\frac{1}{2}}} F_n(|\bar{\alpha}|) H_{km}(\bar{\alpha})\, d\bar{\alpha} = \int_{-\infty}^{\infty} I(\bar{\alpha})\, d\bar{\alpha} , \tag{4.2}$$

where

$$|\bar{\alpha}| = \lim_{\kappa_o \to 0} \frac{[\bar{\alpha}^2 - M_o^2(\bar{\alpha}-\kappa_o)^2]^{\frac{1}{2}}}{(1-M_o^2)^{\frac{1}{2}}} \text{ §} .$$

[†]Basic concepts in the method of evaluating integrals by means of contour integration and the Residue Theorem can be found in references [33,34].

[§]See footnote on following page.

4.1.1 The Poles and Their Residues

Before choosing a contour in the complex-$\bar{\alpha}$ plane, we first locate the singularities of the integrand in (4.2). Since all the terms, other than $F_n'(\bar{\alpha})$, in the integrand $I(\bar{\alpha})$ behave analytically in the entire complex plane of $\bar{\alpha}$, the only singular points are at the zeros of $I_n'(\mu_o b)K_n'(\mu_o a) - I_n'(\mu_o a)K_n'(\mu_o b)$ in the denominator of $F_n'(\bar{\alpha})$. Let us then examine the behaviour of $F_n(\bar{\alpha})$ when the magnitude of $\bar{\alpha}$ is large.

For large $\|x\|$[†] and $0 \leq$ (phase of x) $\leq \pi$, the modified Bessel functions may be approximated as [35]

$$I_n(x) \simeq \frac{e^x}{(2\pi x)^{\frac{1}{2}}} + e^{(n+\frac{1}{2})\pi i} \frac{e^{-x}}{(2\pi x)^{\frac{1}{2}}} , \tag{4.3}$$

$$I_n'(x) = \frac{n}{x} I_n(x) + I_{n+1}(x) \simeq I_{n+1}(x)$$

$$\simeq \frac{e^x}{(2\pi x)^{\frac{1}{2}}} + e^{(n+3/2)\pi i} \frac{e^{-x}}{(2\pi x)^{\frac{1}{2}}} , \tag{4.4}$$

$$K_n(x) \simeq (\frac{\pi}{2x})^{\frac{1}{2}} e^{-x} , \tag{4.5}$$

$$K_n'(x) = \frac{n}{x} K_n(x) - K_{n+1}(x) \simeq -K_{n+1}(x) \simeq -(\frac{\pi}{2x})^{\frac{1}{2}} e^{-x} . \tag{4.6}$$

[†] $\| \ \|$ denotes the magnitude of the complex quantity.

[§] As $\kappa_o \to 0$, the limit is equivalent to squaring $\bar{\alpha}$ and then taking the square root. In the contour integration, $\bar{\alpha}$ is generally complex; if $\bar{\alpha} = Re^{i\theta}$, $|\bar{\alpha}|$ can take on two values: $Re^{i\theta}$ or $Re^{i(\theta+\pi)}$ Note that $|\bar{\alpha}|$ is different from the norm $\|\bar{\alpha}\|$ which is equal to R. To make the function $|\bar{\alpha}|$ single-valued, we dictate that $|\bar{\alpha}| = Re^{i\theta}$ if $\bar{\alpha}$ is in the first quadrant of the complex $\bar{\alpha}$-plane, and $|\bar{\alpha}| = Re^{i(\theta+\pi)}$ or $-Re^{i\theta}$ for $\bar{\alpha}$ belonging to the second quadrant. This notation yields the absolute value of $\bar{\alpha}$, if $\bar{\alpha}$ is real.

Using $\mu_o a = (1-M_o^2)^{\frac{1}{2}}\,\bar{\alpha}\,a/L$ and $\mu_o b = (1-M_o^2)^{\frac{1}{2}}\,\bar{\alpha}\,b/L$ as the arguments in (4.3-.6) and substituting into the expression for $F_n(\bar{\alpha})$, equation (3.2.7c), it can be shown that for large $\bar{\alpha}$, $F_n(\bar{\alpha})$ can be approximated by

$$F_n(\bar{\alpha}) \simeq -\left[\frac{e^{\mu_o(b-a)} + e^{-\mu_o(b-a)}}{e^{\mu_o(b-a)} - e^{-\mu_o(b-a)}}\right]$$

$$= -\coth[\mu_o(b-a)] = -\coth(c\bar{\alpha}) , \qquad (4.7)$$

where

$$c = (1-M_o^2)^{\frac{1}{2}}(b-a)/L . \qquad (4.8)$$

From equation (4.7), we can see that $F_n(\bar{\alpha})$, and therefore $I(\bar{\alpha})$, has singularities at

$$\bar{\alpha} = \frac{r\pi i}{c} , \qquad (4.9)$$

where r is a large enough integer, since at these points $F_n \simeq -\coth(r\pi i) = i\cot(r\pi)$ is not analytical. These singularities are simple poles and the residues can easily be evaluated.

Let $R(\bar{\alpha}_r)$ be the residue at $\bar{\alpha} = \bar{\alpha}_r = r\pi i/c$. It can be shown that

$$R(\bar{\alpha}_r) = \lim_{\bar{\alpha}\to\bar{\alpha}_r} I(\bar{\alpha})(\bar{\alpha}-\bar{\alpha}_r) = \lim_{\bar{\alpha}\to\bar{\alpha}_r} \frac{f(\bar{\alpha})(\bar{\alpha}-\bar{\alpha}_r)}{\sinh(c\bar{\alpha})} , \qquad (4.10)$$

where

$$f(\bar{\alpha}) = -\frac{\bar{\alpha}}{(1-M_o^2)^{\frac{1}{2}}}\cosh(c\bar{\alpha})H_{km}(\bar{\alpha}) .$$

Applying l'Hôpital's Rule, one obtains

$$R(\bar{\alpha}_r) = \lim_{\bar{\alpha}\to\bar{\alpha}_r} \frac{f(\bar{\alpha}) + f'(\bar{\alpha})(\bar{\alpha}-\bar{\alpha}_r)}{c \cosh(c\bar{\alpha})} = \frac{f(\bar{\alpha}_r)}{c \cosh(c\bar{\alpha}_r)}$$

$$= -\frac{ir\pi}{c^2(1-M_0^2)^{\frac{1}{2}}} H_{km}(r\pi i/c) \; . \qquad (4.11)$$

The approximations of the modified Bessel functions (4.3-.6) are valid when the magnitude of the argument is greater than 10. Accordingly, equation (4.7) holds for $\|c\bar{\alpha}\| > 10$. Considering a set of typical parameters, $b/L = 0.06$, $a/L = 0.04$, $M_0 = 0.001$, it is found from (4.8) that $c = 0.02$. Thus, $\|\bar{\alpha}\|$ has to be, at least, of the order of hundreds for (4.7) to hold and, hence, for the foregoing analysis to be applicable.

In addition to the poles, the locations of which are as defined in equation (4.9), $F_n(\bar{\alpha})$ has other singularities situated closer to the origin of the complex $\bar{\alpha}$-plane, where the approximations (4.3-.6) do not hold good. These poles and their residues cannot be determined analytically since the full series expressions have to be used to represent the modified Bessel functions in $F_n(\bar{\alpha})$. Consequently, a computer root-finding subroutine is used to determine the zeros of $I_n'(\mu_0 b)K_n'(\mu_0 a) - I_n'(\mu_0 a)K_n'(\mu_0 b)$ which are, as mentioned before, the singular points of $I(\bar{\alpha})$. To find the residues at these points close to the origin, a 'brute-force' method is utilized. Assuming, initially, the singularities to be simple poles, the residues are given by equation (4.10). After locating the singular point, $\bar{\alpha}_r$, the limiting procedure is carried out numerically; the term $F_n(\bar{\alpha})(\bar{\alpha}-\bar{\alpha}_r)$ is calculated with some values of $\bar{\alpha}$ in the close vicinity of $\bar{\alpha}_r$. The converging result, if it exists, is the residue. Otherwise, the power of $(\bar{\alpha}-\bar{\alpha}_r)$ is raised and the same procedure tried again. In general, the limiting procedure should be applied to the term $F_n(\bar{\alpha})(\bar{\alpha}-\bar{\alpha}_r)^k$, where k is

the lowest power required to obtain a finite converging result. The values of some of the poles and residues found in this way are shown in Table 4.1. Similarly to their 'far away' counterparts, all the numerically found singularities are simple poles and they lie on the imaginary $\bar{\alpha}$-axis.

Finally, another possible candidate as a singular point is the origin of the $\bar{\alpha}$-plane. When $\bar{\alpha} = 0$, the Bessel functions $K_n(\mu_o a)$, $K_n(\mu_o b)$ and their derivatives $K_n'(\mu_o a)$, $K_n'(\mu_o b)$, in the term $F_n(\bar{\alpha})$ as given in

	Poles	Residues
n=1	31.026i	-25.140
	629.955i	-59.526
	4398.232i	-66.669†
n=2	61.905i	-23.676
n=3	92.500i	-21.378

Table 4.1: The poles and residues of the function $F_n(\bar{\alpha})$ (defined in equation (3.2.7c)) in the complex $\bar{\alpha}$-plane; $\kappa_o = 0$, $M_o = 0.001$, $a/L = 1/40$, $b/L = 1/25$.

†It has been shown that $F_n(\bar{\alpha}) \simeq -\coth(c\bar{\alpha})$ when $\|\bar{\alpha}\| >> 1$ and that $F_n(\bar{\alpha})$ has simple poles at $\bar{\alpha} = r\pi i/c$ where r is a large integer. The residues at these poles are

$$\lim_{\bar{\alpha}\to r\pi i/c} F_n(\bar{\alpha})(\bar{\alpha} - \frac{r\pi i}{c}) = \lim - \coth(c\bar{\alpha})(\bar{\alpha} - \frac{r\pi i}{c}) = - 1/c$$

after applying l'Hôpital's rule. For $M_o = 0.001$, $a/L = 1/40$, $b/L = 1/25$, $-1/c = -66.67$. Hence, as one can see, the numerically-determined residue at the 'far away' pole ($\bar{\alpha} = 4398i$) indeed agrees with the theoretical result.

(3.2.7c) are indefinite, since $\mu_o a$ and $\mu_o b$, which are proportional to $\bar{\alpha}$, also vanish. Although an analytical proof is not available, it has been shown numerically that in the limit, as $\bar{\alpha}$ approaches zero, $F_n(\bar{\alpha})$ does indeed converge to a single finite value. Thus, the point $\bar{\alpha} = 0$ may be treated as a singular point with zero residue.

4.1.2. The Contour Integration

We shall choose the contour shown in the diagram below in the complex $\bar{\alpha}$-plane, where X, Y are large real numbers, M is a large integer, and x, y are real variables.

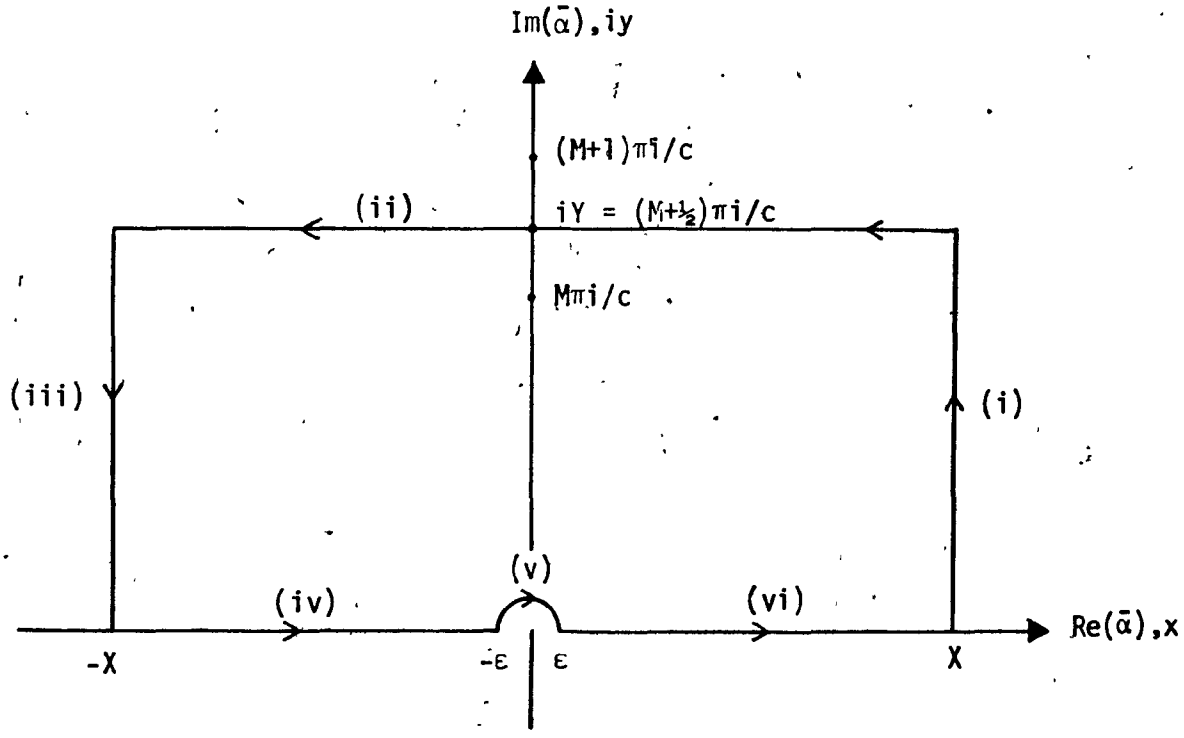

Obviously, the integration along paths (iv)-(vi) is the result we are after. Path (v) is used to avoid the singularity at the origin. By taking X and Y to be large, we can approximate $F_n(\bar{\alpha})$ by - coth($c\bar{\alpha}$) along paths (i), (ii) and (iii). It is shown in Appendix B that $H_{km}(\bar{\alpha})$ can be expressed as

$$H_{km}(\bar{\alpha}) = \frac{1}{(\bar{\alpha}^4-\lambda_m^4)(\bar{\alpha}^4-\lambda_k^4)}[A\bar{\alpha}^2 e^{i\bar{\alpha}} + B\bar{\alpha}e^{i\bar{\alpha}} + Ce^{i\bar{\alpha}} + D\bar{\alpha}^2 e^{-i\bar{\alpha}}$$

$$+ E\bar{\alpha}e^{-i\bar{\alpha}} + Fe^{-i\bar{\alpha}} + G\bar{\alpha}^2 + H\bar{\alpha} + L] \ , \qquad (B.10)$$

where A, B, C, ... *etc.* are given in terms of the beam constants.

Let us carry out the integration along path (i). Along this path, $\bar{\alpha} = X + iy$, $d\bar{\alpha} = idy$, $|\bar{\alpha}| = \bar{\alpha}$. Thus,

$$\int_{(i)} |\bar{\alpha}| F_n(|\bar{\alpha}|) H_{km}(\bar{\alpha})\, d\bar{\alpha} = \int_0^Y - \frac{\bar{\alpha}\coth(c\bar{\alpha})}{(\bar{\alpha}^4-\lambda_m^4)(\bar{\alpha}^4-\lambda_k^4)} [A\bar{\alpha}^2 e^{i\bar{\alpha}} + B\bar{\alpha}e^{i\bar{\alpha}} + Ce^{i\bar{\alpha}}$$

$$+ D\bar{\alpha}^2 e^{-i\bar{\alpha}} + E\bar{\alpha}e^{-i\bar{\alpha}} + Fe^{-i\bar{\alpha}} + G\bar{\alpha}^2 + H\bar{\alpha} + L]\, idy \ .$$

We shall make the following approximation to simplify the integrand further:

$$\coth(c\bar{\alpha}) \cong 1 \qquad (4.12)$$

since $\mathrm{Re}(\bar{\alpha}) = X \gg 1$, and

$$(\bar{\alpha}^4-\lambda_m^4)(\bar{\alpha}^4-\lambda_k^4) \cong \bar{\alpha}^8 \qquad (4.13)$$

since $\|\alpha\| \gg \lambda_m^4$ or λ_k^4 .

Thus, the above integral can be written as,

$$\int_{(i)} |\bar{\alpha}| F_n(|\bar{\alpha}|) H_{km}(\bar{\alpha})\, d\bar{\alpha} \cong \int_0^Y -\left(\frac{Ae^{i\bar{\alpha}}}{\bar{\alpha}^5} + \frac{Be^{i\bar{\alpha}}}{\bar{\alpha}^6} + \frac{Ce^{i\bar{\alpha}}}{\bar{\alpha}^7} + \frac{De^{-i\bar{\alpha}}}{\bar{\alpha}^5} + \frac{Ee^{-i\bar{\alpha}}}{\bar{\alpha}^6}\right.$$

$$\left. + \frac{Fe^{-i\bar{\alpha}}}{\bar{\alpha}^7} + \frac{G}{\bar{\alpha}^5} + \frac{H}{\bar{\alpha}^6} + \frac{L}{\bar{\alpha}^7}\right) i\,dy$$

$$= \int_0^Y -\left[\frac{Ae^{iX}e^{-y}}{(X+iy)^5} + \frac{Be^{iX}e^{-y}}{(X+iy)^6} + \frac{Ce^{iX}e^{-y}}{(X+iy)^7} + \frac{De^{-iX}e^{y}}{(X+iy)^5}\right.$$

$$+ \frac{Ee^{-iX}e^{y}}{(X+iy)^6} + \frac{Fe^{-iX}e^{y}}{(X+iy)^7} + \frac{G}{(X+iy)^5} + \frac{H}{(X+iy)^6}$$

$$\left. + \frac{L}{(X+iy)^7}\right] i\,dy\,. \qquad (4.14)$$

In equation (4.14), terms like $\int_0^Y Ae^{iX}e^{-y}/(X+iy)^5 dy$ or $\int_0^Y G/(X+iy)^5 dy$ would be negligibly small if both X and Y are very large. This may be seen as follows:

$$\left| \int_0^Y \frac{e^{iX}e^{-y}}{(X+iy)^5}\, dy \right| \leq \int_0^Y \frac{|e^{iX}||e^{-y}|}{|(X+iy)^5|}\, dy$$

$$\leq \int_0^Y \frac{|e^{-y}|}{|(X+iy)^5|}\, dy$$

$$= \int_0^Y \frac{e^{-y}}{(X^2+y^2)^{5/2}}\, dy$$

$$< \int_0^Y \frac{dy}{(X^2+y)^{5/2}} = -\frac{2}{3(X^2+y)^{3/2}}\Bigg|_0^Y ,$$

which approaches zero if X and Y are large. Hence, the integral in equation (4.14) can be approximated as

$$\int_{(i)} |\bar{\alpha}|F_n(|\bar{\alpha}|)H_{km}(\bar{\alpha})\, d\bar{\alpha} \cong \int_0^Y -\left[\frac{De^{-iX}e^{y}}{(X+iy)^5} + \frac{Ee^{-iX}e^{y}}{(X+iy)^6} + \frac{Fe^{-iX}e^{y}}{(X+iy)^7}\right]idy \,. \qquad (4.15)$$

Let us now consider the integration along path (iii), whereon $\bar{\alpha} = -X+iy$, $d\bar{\alpha} = idy$, $|\bar{\alpha}| = -\bar{\alpha}$. Thus,

$$\int_{(iii)} |\bar{\alpha}|F_n(|\bar{\alpha}|)H_{km}(\bar{\alpha})\, d\bar{\alpha} \cong \int_Y^0 \frac{\bar{\alpha}\coth(-c\bar{\alpha})}{(\bar{\alpha}^4-\lambda_m^4)(\bar{\alpha}^4-\lambda_k^4)}\left[A\bar{\alpha}^2e^{i\bar{\alpha}} + B\bar{\alpha}e^{i\bar{\alpha}} + Ce^{i\bar{\alpha}}\right.$$

$$\left. + D\bar{\alpha}^2e^{-i\bar{\alpha}} + E\bar{\alpha}e^{-i\bar{\alpha}} + Fe^{-i\bar{\alpha}} + G\bar{\alpha}^2 + H\bar{\alpha} + L\right]idy \,.$$

Invoking the assumptions (4.12), (4.13) and ignoring terms leading to small contributions, it can be shown that

$$\int_{(iii)} |\bar{\alpha}|F_n(|\bar{\alpha}|)H_{km}(\bar{\alpha})\, d\bar{\alpha} \cong \int_0^Y -\left[\frac{De^{iX}e^{y}}{(-X+iy)^5} + \frac{Ee^{iX}e^{y}}{(-X+iy)^6} + \frac{Fe^{iX}e^{y}}{(-X+iy)^7}\right]idy \,. \qquad (4.16)$$

Combining equations (4.15) and (4.16), and choosing $X = 2N\pi$ where N is a large integer so that $e^{-iX} = e^{iX} = 1$, one obtains

$$\int_{(i)\&(iii)} |\bar{\alpha}|F_n(|\bar{\alpha}|)H_{km}(\bar{\alpha})\, d\bar{\alpha} \cong \int_0^Y -\left\{D\left[\frac{e^{y}}{(X+iy)^5} + \frac{e^{y}}{(-X+iy)^5}\right]\right.$$

$$+ E\left[\frac{e^{y}}{(X+iy)^6} + \frac{e^{y}}{(-X+iy)^6}\right]$$

$$\left. + F\left[\frac{e^{y}}{(X+iy)^7} + \frac{e^{y}}{(-X+iy)^7}\right]\right\}idy \,. \qquad (4.17)$$

Proceeding similarly for path (ii), we have

$\bar{\alpha} = x+iY$, $d\bar{\alpha} = dx$, $|\bar{\alpha}| = \bar{\alpha}$ along path in the first quadrant

$|\bar{\alpha}| = -\bar{\alpha}$ along path in the second quadrant.

If Y is chosen to be $(M+\frac{1}{2})\pi/c$, where M is a large but finite integer, then, along path (ii), $F_n(\bar{\alpha})$ can be approximated as follows:

$$F_n(\bar{\alpha}) \cong - \coth [cx + (M+\tfrac{1}{2})\pi i] = - \tanh (cx) . \qquad (4.18)$$

Assumption (4.13) still applies, and so the integral can be written as

$$\int_{(ii)} |\bar{\alpha}| F_n(|\bar{\alpha}|) H_{km}(\bar{\alpha})\, d\bar{\alpha} \cong \int_{-X}^{X} \tanh (cx) \left[\frac{Ae^{-Y}e^{ix}}{(x+iY)^5} + \frac{Be^{-Y}e^{ix}}{(x+iY)^6} + \frac{Ce^{-Y}e^{ix}}{(x+iY)^7}\right.$$

$$+ \frac{De^{Y}e^{-ix}}{(x+iY)^5} + \frac{Ee^{Y}e^{-ix}}{(x+iY)^6} + \frac{Fe^{Y}e^{-ix}}{(x+iY)^7}$$

$$\left. + \frac{G}{(x+iY)^5} + \frac{H}{(x+iY)^6} + \frac{L}{(x+iY)^7}\right] dx . \qquad (4.19)$$

In equation (4.19), terms like $\int_{-X}^{X} \tanh(cx) Ae^{-Y}e^{ix}/(x+iY)^5 dx$ or $\int_{-X}^{X} \tanh(cx) G/(x+iY)^5 dx$ would be insignificant if X and Y are large. For example,

$$\left| \int_{-X}^{X} \frac{\tanh(cx)e^{ix}}{(x+iY)^5}\, dx \right| \leq \int_{-X}^{X} \frac{|\tanh(cx)|\,|e^{ix}|}{|(x+iY)^5|}\, dx$$

continued/

$$\leq \int_{-X}^{X} \frac{dx}{|(x+iY)^5|}$$

$$\leq \int_{-X}^{X} \frac{dx}{(x^2+Y^2)^{5/2}}$$

$$\leq 2 \int_{o}^{X} \frac{dx}{(x+Y^2)^{5/2}}$$

$$= -\frac{4}{3(x+Y^2)^{3/2}}\Bigg|_{o}^{X}$$

tends to vanish if X and Y are large. Hence, an approximation of equation (4.19) would be

$$\int_{(ii)} |\bar{\alpha}| F_n(|\bar{\alpha}|) H_{km}(\bar{\alpha})\, d\bar{\alpha} \cong \int_{-X}^{X} e^{Y} e^{-ix} \tanh(cx) \left[\frac{D}{(x+iY)^5} + \frac{E}{(x+iY)^6} + \frac{F}{(x+iY)^7}\right] dx \,. \tag{4.20}$$

Finally, for path (v), we have

$$\bar{\alpha} = \varepsilon e^{i\theta}, \quad d\bar{\alpha} = i\varepsilon e^{i\theta}\, d\theta \,.$$

Thus,

$$\int_{(v)} |\bar{\alpha}| F_n(|\bar{\alpha}|) H_{km}(\bar{\alpha})\, d\bar{\alpha} = \int_{\pi}^{o} \varepsilon e^{i\theta} F_n(\varepsilon e^{i\theta}) H_{km}(\varepsilon e^{i\theta}) i\varepsilon e^{i\theta}\, d\theta \,.$$

It has been mentioned in Section 4.1.1 that $F_n(\bar{\alpha})$ remains finite as $\bar{\alpha} \to 0$. Hence, one may write

$$|F_n(\varepsilon e^{i\theta}) H_{km}(\varepsilon e^{i\theta})| \leq L \,,$$

where L is a finite number, for arbitrarily small ϵ, and so

$$\int_{(v)} |\bar{\alpha}| F_n(|\bar{\alpha}|) H_{km}(\bar{\alpha})\, d\bar{\alpha} \leq L\epsilon^2 \left| i \int_{\pi}^{0} e^{i2\theta}\, d\theta \right| = 0 .$$

Therefore the integration along path (v) tends to zero as $\epsilon \to 0$.

4.1.3 The Residue Theorem

If the function f(Z) is single-valued and analytic inside and on a simple closed curve C in the complex Z-plane, except at the singularities a, b, c, ... inside C, which have residues given by R_a, R_b, R_c, ..., then the Residue Theorem states that

$$\oint_C f(Z)\, dZ = 2\pi i(R_a + R_b + R_c + \ldots) . \qquad (4.21)$$

In the case at hand, paths (i)-(vi) form a simple closed path enclosing a number of singularities of the integrand given by equation (4.2). Then, according to the Residue Theorem, one has

$$\int_{(i)-(vi)} \frac{|\bar{\alpha}|}{(1-M_o^2)^{\frac{1}{2}}} F_n(|\bar{\alpha}|) H_{km}(\bar{\alpha})\, d\bar{\alpha} = 2\pi i(R_1 + R_2 + \ldots R_N) , \qquad (4.22)$$

where R_1, R_2, ... *etc.* are the residues at the singularities of the integrand. (A discussion on the evaluation of these residues is given in Section 4.1.1 of this Chapter).

Now, the integral of equation (4.2) can equivalently be written as

$$\int_{-\infty}^{\infty} \frac{|\bar{\alpha}|}{(1-M_o^2)^{\frac{1}{2}}} F_n(|\bar{\alpha}|)H_{km}(\bar{\alpha})\, d\bar{\alpha} = \lim_{\substack{X\to\infty \\ \epsilon\to 0}} \int_{(iv),(v),(vi)} \frac{|\bar{\alpha}|}{(1-M_o^2)^{\frac{1}{2}}} F_n(|\bar{\alpha}|)H_{km}(\bar{\alpha})\, d\bar{\alpha} \,. \tag{4.23}$$

Rearranging equation (4.22) and substituting into equation (4.23) yields

$$\int_{-\infty}^{\infty} \frac{|\bar{\alpha}|}{(1-M_o^2)^{\frac{1}{2}}} F_n(|\bar{\alpha}|)H_{km}(\bar{\alpha})\, d\bar{\alpha} = \lim_{X\to\infty} [2\pi i(R_1 + R_2 + \ldots R_N) - \int_{(i),(ii),(iii)} \frac{|\bar{\alpha}|}{(1-M_o^2)^{\frac{1}{2}}} F_n(|\bar{\alpha}|)H_{km}(\bar{\alpha})\, d\bar{\alpha}] \,. \tag{4.24}$$

Substituting (4.17) and (4.20) into (4.24), one obtains,

$$\begin{aligned}\int_{-\infty}^{\infty} \frac{|\bar{\alpha}|}{(1-M_o^2)^{\frac{1}{2}}} F_n(|\bar{\alpha}|)H_{km}(\bar{\alpha})\, d\bar{\alpha} = \lim_{X\to\infty} \Big\{ & 2\pi i(R_1 + R_2 + \ldots R_N) \\ & + \frac{1}{(1-M_o^2)^{\frac{1}{2}}} \int_o^Y \{D[\frac{e^y}{(X+iy)^5} + \frac{e^y}{(-X+iy)^5}] + E[\frac{e^y}{(X+iy)^6} + \frac{e^y}{(-X+iy)^6}] \\ & + F[\frac{e^y}{(X+iy)^7} + \frac{e^y}{(-X+iy)^7}]\}\, idy \\ & - \frac{1}{(1-M_o^2)^{\frac{1}{2}}} \int_{-X}^{X} e^Y e^{-ix\tanh(cx)} [\frac{D}{(x+iY)^5} + \frac{E}{(x+iY)^6} + \frac{F}{(x+iY)^7}]\, dx \Big\} \,.\end{aligned} \tag{4.25}$$

Since Y is only a finite number, in the limit as X approaches infinity, the first integral on the right-hand side of equation (4.25) will eventually vanish. Thus,

$$\int_{-\infty}^{\infty} \frac{|\bar{\alpha}|}{(1-M_o^2)^{\frac{1}{2}}} F_n(|\bar{\alpha}|)H_{km}(\bar{\alpha})\, d\bar{\alpha} = \lim_{X\to\infty}\Big\{ 2\pi i(R_1 + R_2 + \ldots R_N)$$

$$- \frac{1}{(1-M_o^2)^{\frac{1}{2}}} \int_{-X}^{X} e^{Y}e^{-ix}\tanh(cx)\Big[\frac{D}{(x+iY)^5} + \frac{E}{(x+iY)^6} + \frac{F}{(x+iY)^7}\Big]\, dx\Big\}. \tag{4.26}$$

4.1.4. Summary

By means of equation (4.26), the laborious integration of (4.2) is reduced to the evaluation of a number of residues and a much simpler integral†. However, in practice, we would still have trouble in getting the result. For one thing, Y is a large value, of the order of hundreds, for the approximation $F_n(\bar{\alpha}) \cong -\coth(c\bar{\alpha})$ to be valid along the integration contour. The term e^Y associated with the integral on the right-hand side of (4.26) would be formidably large. Terms of equally-large magnitude would also appear in the 'far-away' residues (see equation (4.11) and the expression of $H_{km}(\bar{\alpha})$ in Appendix B). As one can anticipate, these large terms would more or less cancel each other out in the end and give a finite result of the order of tens or hundreds. However, since we are subtracting very large numbers, the error would be as large as the desired answer itself. Besides, the computer may not carry enough significant figures to give any meaningful answers at all.

Moreover, one has to be skeptical about the assumptions and

† In reference [14], Dowell derived the Fourier transform solution for subsonic flow in a cylindrical duct. The integral he evaluated by contour integration was very similar to the first term of equation (3.2.10a). The integration contour was taken to be the real $\bar{\alpha}$-axis and a semi-circle at infinity, enclosing the upper half plane. By assuming that the contribution along the semi-circle vanished in the limit, he was able to express the integral in terms of the sum of the residues only. However, no numerical results were given and the convergence of the expression was not demonstrated - at least not in the published work [14].

simplifications made in arriving at equation (4.26). The enormous factors involved may make a difference if the complete rather than the simplified expressions of certain terms are employed.

4.2 METHOD OF DIRECT NUMERICAL INTEGRATION AND INTERPOLATION

The integrals in the generalized aerodynamic force terms (3.2.11a-b), (3.2.12a) can be evaluated numerically. However, care must be exercised in performing the integration over $\bar{\alpha}$ not to overlook any singularities of the integrand that may lie in the range of integration which, in this case, is along the real $\bar{\alpha}$-axis. Assuming that the numerators of the integrands behave analytically in the entire complex plane of $\bar{\alpha}$, the only singularities are the zeros of the denominators. Thus, the terms to be examined are $\mu_i L$, $\mu_o L$, $I_n'(\mu_i a)$ and $I_n'(\mu_o b)K_n'(\mu_o a) - I_n'(\mu_o a)K_n'(\mu_o b)$; and it should be noted that the simplification $\kappa_i = \kappa_o = 0$ is no longer imposed.

It has been mentioned in Section 4.1.1 that a computer subroutine is used to determine the zeros of $I_n'(\mu_o b)K_n'(\mu_o a) - I_n'(\mu_o a)K_n'(\mu_o b)$. The arguments, $\mu_o a$ and $\mu_o b$ depend on the Mach number M_o, the shell dimensions (a,b,L) and the reduced frequencies κ_o through (3.1.11a). It is impossible to investigate every case within the range of these parameters. Nevertheless, it is found that, for a set of typical values of the parameters, the zeros lie close to the imaginary $\bar{\alpha}$-axis. Thus, it is assumed that the term $I_n'(\mu_o b)K_n'(\mu_o a) - I_n'(\mu_o a)K_n'(\mu_o b)$ presents no complications to the integration along the real $\bar{\alpha}$-axis. There are, of course, the singularities at $\mu_o b = \mu_o a = 0$, but they coincide with the zeros of $\mu_o L$ which will be discussed in the following paragraph.

From equations (3.1.4a) and (3.1.11a), one can easily find the zeros of $\mu_i L$, $\mu_o L$ as follows:

$$\bar{\alpha}_{1,2} = \frac{\kappa_i M_i}{1+M_i} \quad \text{and} \quad -\frac{\kappa_i M_i}{1-M_i}, \quad \text{for} \quad \mu_i L = 0 , \tag{4.27}$$

and

$$\bar{\alpha}_{1,2} = \frac{\kappa_o M_o}{1+M_o} \quad \text{and} \quad -\frac{\kappa_o M_o}{1-M_o}, \quad \text{for} \quad \mu_o L = 0 . \tag{4.28}$$

The roots according to equations (4.27) and (4.28) are located away from the real $\bar{\alpha}$-axis, provided that the reduced frequencies, κ_i and κ_o, have non-zero imaginary parts. However, we are dealing here with clamped-clamped shells which are conservative systems, and the frequencies prior to the onset of instability are indeed real quantities. Thus, it appears that the presence of singularities on the real $\bar{\alpha}$-axis is inevitable. The two singularities are in fact branch points. To deal with this situation, the path of integration should be modified to by-pass the singular points. Accordingly, the appropriate path of integration is as shown in the diagram below.

Finally, the poles of the integrand with the term $E_n(\bar{\alpha}) = I_n(\mu_i a)/I_n'(\mu_i a)$ are the roots of $I_n'(Z)$, where $Z = \mu_i a$, and it is known that all these roots, Z_j, are either imaginary or zero. In terms of $\bar{\alpha}$, we have the poles as

$$\bar{\alpha}_j = -\frac{\kappa_i M_i^2}{1-M_i^2} \pm i \left[\frac{Z_j^2 (L/a)^2}{1-M_i^2} - \left(\frac{\kappa_i M_i}{1-M_i^2}\right)^2 \right]^{\frac{1}{2}} . \tag{4.29}$$

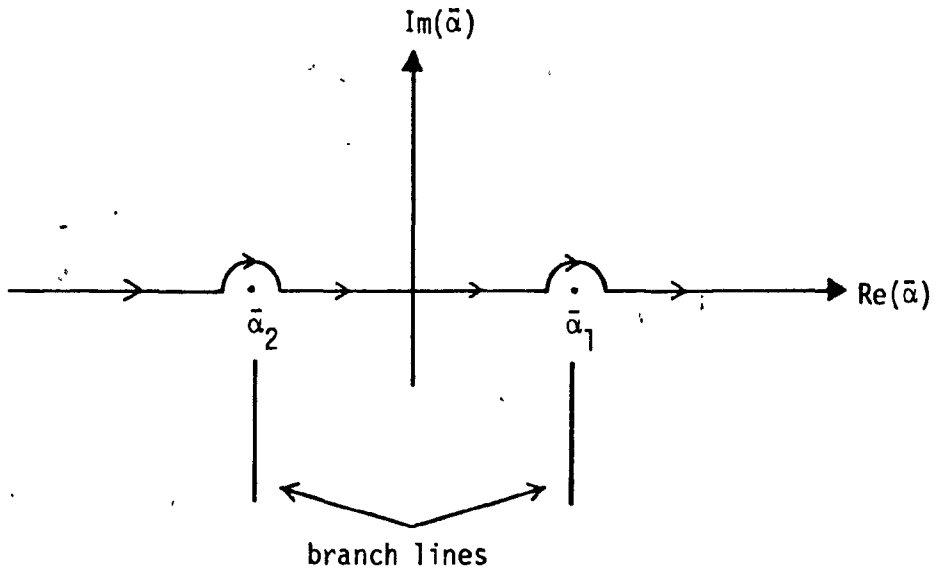

Since Z_j is purely imaginary, then for

$$-\frac{Z_j^2(L/a)^2}{1-M_i^2} > \left(\frac{\kappa_i M_i}{1-M_i^2}\right)^2 \tag{4.30}$$

$\bar{\alpha}_j$ will be complex conjugates. On the other hand, for

$$-\frac{Z_j^2(L/a)^2}{1-M_i^2} < \left(\frac{\kappa_i M_i}{1-M_i^2}\right)^2 \tag{4.31}$$

$\bar{\alpha}_j$ will be real numbers. Thus, again we may have singular points along the real $\bar{\alpha}$-axis. Assuming these singularities to be simple poles, the integration can still be performed by adopting a modified path of integration

as shown in the diagram below.

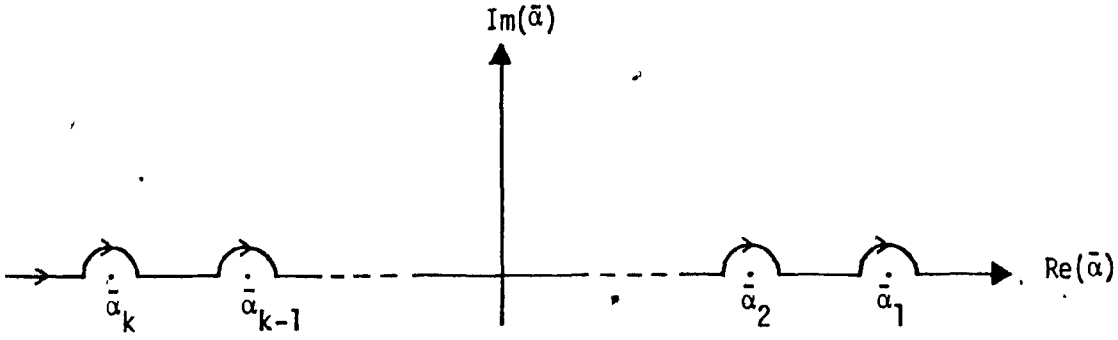

Let us now see how the integration can be accomplished. In the limit, as the small semi-circles 'shrink' to a point, we shall recover the path of integration desired. Thus, we can perform an ordinary numerical integration along the real $\bar{\alpha}$-axis, then add to the result any contribution from the vanishingly small semi-circles. It can be shown that the limit of integrals along the semi-circular arc around the simple poles is given by $-i\pi R$, where R is the residue at the corresponding pole (see [34]). For the branch points associated with $\mu_i L = 0$ or $\mu_o L = 0$, we have to examine them with each individual integral. Let us take the integral in (4.1) as an example. On the semi-circle around the branch point, $\bar{\alpha}_1$ (see Figure on page 59), we have $\bar{\alpha}-\bar{\alpha}_1 = \varepsilon e^{i\theta}$, $d\bar{\alpha} = i\varepsilon e^{i\theta} d\theta$, and $\mu_o L = [(\bar{\alpha}-\bar{\alpha}_1)(\bar{\alpha}-\bar{\alpha}_2)]^{\frac{1}{2}} \cong [\varepsilon e^{i\theta}(\bar{\alpha}_1-\bar{\alpha}_2)]^{\frac{1}{2}}$ as $\varepsilon \to 0$.

The integral around the semi-circle is then given by

$$\int_{\pi}^{0} \frac{(\kappa_o-\bar{\alpha}_1)^2}{[\varepsilon e^{i\theta}(\bar{\alpha}_1-\bar{\alpha}_2)]^{\frac{1}{2}}} F_n(\bar{\alpha}_1) H_{km}(\bar{\alpha}_1) i\varepsilon e^{i\theta} d\theta \ .$$

It has been shown numerically that

$$F_n(\bar{\alpha}_1) = \lim_{\substack{\mu_o a \to 0 \\ \mu_o b \to 0}} F_n(\bar{\alpha}) = N ,$$

where N is a finite number. Hence, the above integral is proportional to $(\varepsilon)^{\frac{1}{2}}$ and vanishes as $\varepsilon \to 0$. Similarly, the integration along the semi-circle round the other singular point $\bar{\alpha}_2$ makes no contribution. Similar analysis can be applied to the other integrals in the generalized force terms.

The direct numerical integration method has been used to calculate the generalized aerodynamic forces for a system consisting of a flexible inner cylindrical shell enclosed by an outer rigid cylinder. The complete expressions for the generalized forces are given in Appendix D. The integrals involved are

$$J_1 = \int_{-\infty}^{\infty} \frac{(\kappa_i - \bar{\alpha})^2}{\mu_i L} E_n(\bar{\alpha}) H_{km}(\bar{\alpha}) \, d\bar{\alpha} , \tag{4.32}$$

$$J_2 = \int_{-\infty}^{\infty} \frac{(\kappa_o - \bar{\alpha})^2}{\mu_o L} F_n(\bar{\alpha}) H_{km}(\bar{\alpha}) \, d\bar{\alpha} . \tag{4.33}$$

For the second integral, J_2, it has been shown that the integration along the semi-circular excursion round the branch points vanishes as its radius approaches zero. Therefore, the numerical integration alone will constitute the complete solution. The first integral, J_1, can have, besides the branch points, a number of simple poles if condition (4.31) is satisfied. However, it turns out that within the range of the reduced frequency κ_i of the systems concerned, it is the condition (4.30) rather

than (4.31) that is applicable[†]. The real $\bar{\alpha}$-axis is, therefore, free of simple poles. Furthermore, it can also be shown that the presence of the branch points makes no contribution. As a result of all the foregoing, the integrals J_1, J_2 can be evaluated by a straightforward numerical integration along the real $\bar{\alpha}$-axis. The two-point Gaussian quadrature is employed to accomplish this integration. Examination of the integrands has shown that their values decrease asymptotically as $\|\bar{\alpha}\|$ becomes large. Thus, the quadrature is applied for $\bar{\alpha}$ in the range (-50,50) using 100 points.

Computation of these integrals on the computer is very expensive. It is recalled from Section 3.4 that for a system with compressible fluid, the frequencies are obtained as the roots of det[A] = 0, using an iteration procedure. Being functions of the reduced frequencies κ_i and κ_0, the integrals have to be calculated for each trial value of the solution. The tremendous amount of computer time required renders the scheme impracticable[§]. To overcome this problem, it was decided that the values of the integrals would be approximated by interpolation. The integrals are calculated exactly for a number of values of the reduced frequencies, chosen evenly within their expected ranges. Interpolation equations are then

---

[†]The smallest non-zero root of $I_n'(Z_j) = 0$ is $Z_1 = 3.045i$ for n = 2. For the two systems that will be considered,

a/L	M_i	expected range of κ_i
0.03861	0.001	$0 \leq \kappa_i < 3000$
1/15	0.025	$0 \leq \kappa_i < 240$

Hence, one can easily check that even with the smallest Z_j, condition (4.31) cannot be satisfied for any κ_i within the above ranges.

[§]For one set of values of κ_i and κ_0, the computation of the integrals given in (4.32, 4.33) for n=2, k,m=1,2,3 requires about 150 execute units (30 sec) in the AMDAHL V7 computer. Supposing that on the average four iterations are required to determine one root, and that to generate one frequency diagram, frequencies of the three axial modes are calculated at 10 different flow velocities, this means that 120 iterations would have to be performed and the computer execute units required can easily exceed the 18,000 mark (*i.e.*, 3,600 sec, or 1 hour).

derived from this data and are used later to approximate the integrals in obtaining the solution of the frequencies. In Figures 3-6, the values of the integrals J_1 and J_2 (equations (4.32, 4.33)) are plotted *versus* the reduced frequencies, and the corresponding interpolation equations are given in Table 1. Surprisingly, the integrals vary 'nicely' with frequency, and the equations have very simple forms. Through the use of these interpolation equations, the computer time required to solve for the frequencies of the system is reduced dramatically†. However, one should note that although a vast amount of saving is achieved in the iteration phase of the algorithm, considerable computer time has to be spent in the derivation of the interpolation equations. So, despite the definite savings, this method of solution is fairly expensive after all.

In principle, this method can become applicable in the post-buckling or the flutter instability regime in which the frequencies are complex. What would be needed then is a two-dimensional interpolation. However, the initial cost of obtaining the data for interpolation is expected to be so immense that utilization of this method would no longer be justified.

†About 10 data points are required to generate the interpolation equations for one case of dynamic analysis and, therefore, the integrals have to be calculated only 10 times, as compared to more than 100 times if the interpolation scheme is not adopted.

CHAPTER V

THEORETICAL RESULTS FOR SYSTEMS SUBJECTED TO INVISCID FLOWS

This Chapter presents the results of an investigation of the free dynamical behaviour, as characterized by the natural frequencies and associated modal shapes, of systems under the effect of inviscid axial flows in the inner shell and the annulus. The behaviour of the system can be influenced by numerous parameters such as the shell thickness/radius ratio, length/radius ratio, the gap width, boundary conditions of the shells, various physical properties of the fluid and shell materials, *etc.* It would be a formidable task to investigate every one of these parameter variations. Hence, this thesis will only deal with the effect of changing what are considered to be the principal parameters: the flow velocities, the gap width, the fluid (air and water), and shell material (rubber and steel). As far as the boundary conditions of the shells are concerned, as mentioned earlier, only the case of clamped-clamped shells will be considered. The fluid is inviscid and it can be compressible or incompressible. The results for incompressible flow will be presented in Section 5.1, followed by the compressible flow results in Section 5.2.

5.1 INCOMPRESSIBLE FLOW RESULTS

This Section presents the results obtained for systems of rubber or steel cylindrical shells subjected to inviscid incompressible flow. The availability of a relatively economical method of solution in this case of incompressible flow (see Section 3.4) enables us to perform extensive calculations and to examine easily the effect of several

parameters on the dynamics of the system. With regard to the shell geometries, two classes of systems are under consideration: the so-called "½-gap system", in which the annular gap width is equal to half the radius of the inner shell (a/b = 2/3), and the "1/10-gap system", in which the gap is one-tenth of the inner radius (a/b = 10/11). The shell and fluid parameters for the two systems are given in Table 5.1.

	Steel Shell		Rubber Shell
	½-gap	1/10-gap	½-gap
a (cm)	6.667	9.091	0.787
b (cm)	10	10	1.180
L (cm)	100	100	20.373
h (mm)	0.50	0.50	0.179
$\varepsilon_i = a/L$	1/15	1/11	0.03861†
$\varepsilon_o = b/L$	1/10	1/10	0.05792
$\varepsilon_r = a/b$	2/3	10/11	2/3
$(h/a) \times 10^3$	7.50	5.50	22.7
$(h/b) \times 10^3$	5.0	5.0	15.1
$\beta_i = (\rho_i a)/(\rho_s h)$	17.09 (water)	23.30 (water)	0.06 (air)
$v_i = \{E_i/[\rho_{si}(1-\nu_i)^2]\}^{\frac{1}{2}}$ (m/s)	5308	5308	36.73
ν_i	0.30	0.30	0.47
$\rho_r = \rho_o/\rho_i$	1.0	1.0	1.0

Table 5.1: The shell and fluid parameters for the ½-gap and 1/10-gap systems.

†For comparison purposes, these rubber shell parameters are the same as those considered by Paidoussis and Denise in [10].

In Section 3.4, it is shown that the assumption of fluid incompressibility results in the reduction of the governing matrix equation into the typical eigenvalue problem of equation (3.4.31). The integrals in the generalized aerodynamic forces are evaluated numerically, but no interpolation is required, since these integrals are independent of the vibration frequency. Equation (3.4.31) is solved using IMSL subroutine EIGZC which gives us the eigenvalues as well as the associated eigenvectors. Detailed information on the computer program is given in Appendix F. The solutions are obtained in the form of a dimensionless eigenfrequency which, for systems with a rigid outer shell, is $\bar{\Omega}_i = \Omega/\Omega_i$, where Ω is the dimensional frequency, Ω_i is as defined in (3.4.2a), and in the case of systems with both shells flexible, it is given by $\bar{\Omega}_o$ as defined in (3.3.1a). The numerical results are presented as frequency diagrams and Argand diagrams (Figures 7-15, 18, 21-24). The modal shapes of a typical system at various flow velocities are shown in Appendix O; a few selected ones from the set are displayed in Figures 16, 17, 19 and 20.

5.1.1 System with a Rigid Outer Shell

5.1.1(a) Effect of the internal flow velocity

Figure 7 shows the frequency diagram for a ½-gap system with a rigid outer shell and a flexible inner one made of rubber. Air is conveyed in the inner shell and the annulus is filled with stagnant air ($\bar{U}_o = 0$). The dimensionless frequencies of the second circumferential ($n = 2$) and first three axial ($m = 1, 2, 3$) modes of the inner shell are plotted against the dimensionless internal flow velocity, $\bar{U}_i$. The more intricate and dynamically interesting portion of the frequency diagram is

shown enlarged in Figure 8.

It can be seen (Figure 7) that increasing $\bar{U}_i$ has the effect of diminishing the frequencies associated with all three modes. Being a conservative system (if material dissipative forces are neglected), the frequencies are real quantities, except in the destabilized state. Referring to Figure 8, it is seen that the frequency of the first axial mode vanishes at point A ($\bar{U}_i = 0.635$), indicating the loss of stability by buckling. Beyond this point, the frequency of this mode becomes purely imaginary (see Argand diagram in Figure 9), but at very slightly higher flow velocity (point B, $\bar{U}_i = 0.638$), it reappears as a real quantity; this corresponds to the point of restabilization of the system. Then at point C ($\bar{U}_i = 0.641$), the loci of the first and second axial modes coalesce. After coalescence, the frequencies become complex conjugate pairs†, as shown in the Argand diagram of Figure 9, which is the characteristic of coupled-mode flutter. The m = 3 mode frequency remains real and decreases with increasing flow until it vanishes at point D ($\bar{U}_i = 0.985$). It should be pointed out that coupled-mode flutter in the first-second-mode combination has reverted to divergence, at $\bar{U}_i = 0.827$ (see Argand diagram of Figure 9), prior to the onset of divergence in the third mode (point D).

Also shown in Figure 7 are the results obtained by Paidoussis and Denise in reference [10] in which a single rubber shell of the same dimensions as the inner shell considered here subjected to an internal flow of air and immersed in an unbounded air medium, was studied. There are certain discrepancies between the two results that are worth mentioning.

---

†In Figures 7, 8 and all subsequent similar figures, the real part of eigenfrequencies when they are complex is omitted to avoid crowding the figures.

According to the results of reference [10], coupled-mode flutter occurs after the buckling of the second axial mode, and the region of brief restabilization that follows the loss of stability of the first axial mode is not predicted. Furthermore, the critical buckling velocity of the third axial mode is much lower than that predicted in the present result. These differences in the prediction of the dynamical behaviour of the system may be due to the different types of solutions used (travelling-wave type solutions were employed in reference [10], whereas the solutions assumed in the present analysis are series of beam eigenfunctions) and the enhanced coupling (hydrodynamic mass) of the fluid in the annulus (although stationary and of small density) of the system under consideration. It is interesting to note that the m = 3 mode frequency locus generated here, which deviates much from that of reference [10] especially at high flow velocity, are in very good agreement with the corresponding results obtained by Pham in reference [37] (also shown in Figure 7). The physical system considered by Pham is identical to the one in reference [10] but, similar to the present study, Pham has also assumed series solutions of beam eigenfunctions†. Despite the similarity in the m = 3 mode behaviour, Pham's results on the dynamics of the m = 1 and m = 2 modes (not shown in Figure 7), on the other hand, agree *qualitatively* with Denise's predictions in reference [10] and, thus, have the same discrepancies with the present results as described earlier. On the other hand, the critical flow velocity in Pham's work agrees better with the results of this analysis; Table 5.2 displays the lowest critical flow velocity for loss of stability

†In [37] and in the present study, calculations were conducted with series of three beam eigenfunctions, the accuracy of third-mode (m=3) eigenfrequencies is likely to be lower than for the first and second modes; this may contribute to the discrepancies with Denise's results in predicting the behaviour of the system in the m = 3 mode.

	Paidoussis & Denise [10]		Pham [37]	Present Work
	$1+k_i = 1$	$1+k_i \neq 1$		
$\bar{U}_i$	0.580	0.594	0.625	0.635

Table 5.2: The lowest critical flow velocities for loss of stability of a clamped-clamped rubber shell subjected to an internal flow of air (a/L = 0.03861, n=2).

of the system as determined in references [10], [37] and by the present analysis. Note that in Paidoussis and Denise's calculations, when k_i (defined in (2.1.6a)) is not neglected as compared to unity in the shell equations ($1+k_i \neq 1$), the critical flow velocity becomes larger.

Numerical results are also obtained for a 1/10-gap system with a rigid outer shell but, in this case, the flexible inner shell is made of steel, and water is used as both the internal and annular fluid ($\bar{U}_o = 0$, $\bar{U}_i$ variable). (In all calculations involving steel shells, the n = 3 circumferential modes are shown, whilst for rubber shells calculations with n = 2 are presented. The reasons for this will be discussed in Section 5.1.4). The frequency diagram of the system is shown in Figure 10. Comparing with Figure 7, it can be seen that the behaviour of the system is qualitatively similar to that of the rubber shell conveying air discussed earlier in this Section. Phenomena such as the buckling of the m = 1 mode, its restabilization and coupled-mode flutter in conjunction with the m = 2 mode are observed. However, unlike the case of the rubber shell with air flow, in which the critical flow velocities for divergence

and restabilization of the m = 1 mode are practically coincident, in this case there is a much larger intervening velocity range between the occurrence of these two phenomena. Furthermore, the critical flow velocities (dimensionally and non-dimensionally) of the steel-water system are much lower. This is reasonable, since the system is subjected to a fluid flow of much higher density (water *vs* air) and the fluid forces are all proportional to fluid density. In addition, the steel-shell system has a narrower annular gap (a/b = 1/10); the effect of gap-width will be discussed in Section 5.1.3.

5.1.1(b) Effect of the annular flow velocity

A typical form of the frequency diagram for this case is shown in Figure 11, for a 1/10-gap system of water-filled cylinders, only the inner one of which is a flexible steel shell. The internal fluid is stationary ($\bar{U}_i = 0$) while the annular flow velocity is varied as shown. The dynamical behaviour of the system at low and medium annular flow velocities is similar to that of the system subjected to an internal flow (Figure 10). The system buckles in the first axial mode at point A, is restabilized at point B and then coalescence of the first and second axial modes leads to coupled-mode flutter at point C. At higher annular flow, the system behaves differently. Point D marks the occurrence of yet another restabilization in which the first and second axial-mode frequencies reappear as two distinct real values (see Argand diagram of Figure 12). Following the restabilization, the first mode frequency drops sharply and vanishes again at point E. Meanwhile, the second mode locus makes a steep climb and coalesces with the third mode locus at F giving rise,

once more, to coupled-mode flutter. All the three axial modes of the system have thus been destabilized, and no restabilization is observed at higher flow velocity. Numerically, the corresponding critical velocities for loss of stability are lower than those in the case of the internal flow (see Table 5.3), showing that the destabilizing effect of the annular flow is more severe than that of the internal flow. However, this

	Critical Flow Velocities	
	U_b	U_f
Internal flow	0.02546	0.03136
Annular flow	0.0136	0.01852

Table 5.3: The lowest buckling and coupled-mode flutter velocities for a steel shell conveying water (b/L = 1/10, a/b = 10/11, n = 3). The subscripts b, f specify, respectively, the critical flow velocities at which the buckling and the coupled-mode flutter instabilities occur.

conclusion is not necessarily true in general, since the magnitude of the destabilizing force (the centrifugal force) depends not only on the flow velocity but also on the dimensions of the cylinders. For systems with a narrow annulus, such as the one under consideration, the annular flow can exert a greater force on the cylinder than the internal fluid flowing at the same velocity does. On the other hand, the reverse may be true if the annulus is relatively wide as compared to the radius of the inner cylinder.

Calculations were also performed for systems subjected to internal and annular flows concurrently. The results are shown in Figure 13, for a 1/10-gap system with a flexible steel inner shell and a rigid outer one. Water flows in both the inner shell and the annulus. The annular flow velocity is kept constant at $\bar{U}_o = 10^{-2}$, while the internal velocity is varied as shown. Table 5.4 compares the critical flow velocities with those obtained for an identical system but with $\bar{U}_o = 0$ (Figure 10). It can be seen that the presence of the constant annular flow has lowered the

Constant annular flow of	Critical internal flow velocities	
	$\bar{U}_b$	$\bar{U}_f$
$\bar{U}_o = 0.0$	0.02546	0.03136
$\bar{U}_o = 0.010$	0.01726	0.02883

Table 5.4: Comparison of the lowest flow velocities for buckling and coupled-mode flutter for steel shells subjected to a constant annular water flow of $\bar{U}_o = 0$ or $\bar{U}_o = 0.010$ and increasing internal flow (b/L = 1/10, a/b = 10/11, n = 3).

critical internal flow velocities, rendering the system less stable. The constant annular flow has also caused a second restabilization of the system followed by coupled-mode flutter of the second and third axial modes - phenomena which have been observed before in systems subjected to annular flow alone ($\bar{U}_i = 0$), but not in the case of varying internal flow ($\bar{U}_o = 0$).

Shown in Figure 14 are the results obtained with an annular velocity

($\bar{U}_o = 2\times10^{-2}$) so high that the first two axial modes are destabilized even when there is no internal flow (the third axial mode is still stable). As the internal velocity increases, a restabilization occurs at point A, which is short-lived, the system buckling again in the m = 1 mode at point B; the m = 2 mode eventually coalesces with the m = 3 mode (point C) inducing couped-mode flutter. This pattern of behaviour is similar to the later part of the frequency diagram in Figure 13 ($\bar{U}_o = 10^{-2}$, $\bar{U}_i$ variable). The above results demonstrate that the destabilizing effects of the internal and annular flow are additive (although not linearly additive).

5.1.2 Systems with Both the Inner and Outer Shells Flexible

5.1.2(a) Effect of the internal flow velocity

Numerical results for a 1/10-gap system of two coaxial flexible shells are shown in Figure 15. The shells are assumed to be made of steel and filled with water. The variation of the frequencies of the lowest six modes with increasing internal flow ($\bar{U}_o = 0$) has been examined. Three of them (open symbols) are associated with azimuthally antisymmetric motions in which the radial displacements of the inner and outer shells are out of phase, while the others (closed symbols) correspond to symmetric motions of the two shells. The members of each of these two groups of modes correspond to the third circumferential (n = 3) and the first three axial modes (m = 1, 2, 3) of the shells. Considering the vibration in stagnant fluids ($\bar{U}_i = \bar{U}_o = 0$), the frequencies of the symmetric modes are about four times greater than those of the corresponding antisymmetric modes.

The behaviour of the antisymmetric modes at low flow velocity is similar to that of the system with a rigid outer shell (*cf.* Figure 10).

Moreover, the corresponding critical flow velocities of the two systems are remarkably close (with the buckling velocities being in fact identical). Probable explanations for this quantitative agreement are the identical shell geometry (both of them are 1/10-gap systems) and the stagnant annular fluid which reduces the dynamical effect of the flexibility of the outer shell to a minimum. [An examination of the modal shapes will clearly demonstrate this latter point (see discussion later in this Section).]

In the low flow regime, all the symmetric modes are relatively stable, except for the symmetric m = 1 mode. The loci of the symmetric m = 1 and the antisymmetric m = 3 modes approach each other but remain just short of coalescence. Then they start to diverge, with the result that the symmetric m = 1 mode frequency finally vanishes.

At higher internal flow velocity, the behaviour of the system is quite unexpected and interesting. The frequencies of the three 'surviving' modes (the other three have lost their stability through buckling or coupled-mode flutter) are initially decreasing functions of the internal flow velocity. However, the frequencies asymptotically level out to some constant values and stay unchanged, despite further increase in the internal velocity. An appropriate explanation for this peculiar behaviour of the system cannot readily be advanced. However, examination of the modal shapes will provide us with a clue, as discussed below.

Figures O.1-O.13 of Appendix O and Figures 16 and 17 show the modal shapes at various internal flow velocity. At very low flow, the axial mode shapes of the system resemble the classical beam mode shapes, and the azimuthal symmetry and antisymmetry of the circumferential mode shapes are illustrated. Figures 16(b),(c) show that the vibration of the outer shell abates substantially and practically stops as the system

becomes unstable by divergence (Figure 16(d)). Because of the absence of a steady annular flow, the only excitation of the annular fluid and, consequently, of the outer shell is caused by the accelerations of the inner shell. As divergence is approached, the vibration frequency of the system is diminished; therefore, the accelerations of the inner shell in that mode and, hence, the fluid accelerations in the annulus tend to zero. As a result, the outer shell becomes decoupled from the inner one and is left undisturbed as the inner shell ceases vibrating at divergence. This explains why divergence in Figures 10 and 15 occurs at the same value of $\bar{U}_i$, whether the outer shell is rigid or flexible, since the outer shell is motionless in both cases.

As the internal flow velocity increases, the three antisymmetric modes are gradually transformed and the system finally ends up with all six symmetric modes (*i.e.* the two shells in all the six modes are vibrating in phase). In the three destabilized modes, the radial displacements of the inner and outer shells are of the same order, whilst the radial displacement of the inner shell in the three stable modes is much smaller than that of the outer one (as an example, see Figure 17(b)). From these observations, one may understand why the frequencies of the stable modes remain sensibly constant: the motions of the inner and outer shells are coupled through the annular fluid, which is stationary in this case. Now if the displacement of the inner shell is small, its influence on the outer shell, transmitted through the annular fluid, will be minimal and, thus, the outer shell will, more or less, vibrate independently at a definite frequency. While this brief survey of the modal shapes, here and in Appendix O, has provided some insight into the dynamical behaviour of the system, the actual cause for the suppression of vibration of the inner

shell (in the stable modes) at high internal flow velocity, resulting in the decoupling of motions of the two shells, is still not known.

5.1.2(b) Effect of the annular flow velocity

A set of typical results is shown in Figure 18, where both cylinders are flexible steel shells filled with water, the gap-width/inner-radius ratio being 1/10. The internal fluid is stationary, and the annular flow velocity is varied as shown. The loci of the lowest six modes (n = 3) of the system will now be discussed. As in the case with varying internal flow, here also three of these modes are antisymmetric modes, while the others are symmetric modes.

The behaviour of the antisymmetric mode loci at low flow velocities resembles that of the system with a rigid outer shell (see Figure 11). Unlike the internal flow results (Figures 10 and 15) in which the lowest buckling velocities of systems with a rigid or flexible outer shell are essentially the same, the instability threshold in this case of annular flow is lowered by the flexibility of the outer shell (see Table 5.5). This is probably due to the fact that the annular flow comes into direct contact, and excites directly, both shells - whereas in the previous case of internal flow, the outer shell could become excited only through indirect inertial coupling with the stagnant annular fluid. The antisymmetric m = 1 mode is the first one to lose stability by buckling at point A. It is restabilized at point B and then coalesces with the antisymmetric m = 2 mode at C, followed by coupled-mode flutter. The system is restabilized again at point D but, before long, the antisymmetric m = 1 mode buckles for the second time at E.

	Flexible shells	
	Inner	Both
Critical internal flow velocity ($\bar{U}_o = 0$)	0.02546	0.02546
Critical annular flow velocity ($\bar{U}_i = 0$)	0.0136	0.00958

Table 5.5: The lowest critical flow velocities for loss of stability of steel shells conveying water, when the inner or both shells are flexible (b/L = 1/10, a/b = 10/11, n = 3).

While the antisymmetric modes suffer all kinds of instabilities, the symmetric modes remain relatively stable with their frequencies declining gradually with increasing flow. One exception is the symmetric m = 1 mode (as in the case of internal flow (Figure 15)) which is 'intercepted' by the antisymmetric m = 2 mode at point F, inducing coupled-mode flutter. However, at higher $\bar{U}_o$ (point G), the involvement of the symmetric m = 1 mode in the flutter instability is terminated when it is replaced by the antisymmetric m = 3 mode. Beyond point G, the gentle-slope locus of the symmetric mode is once again evident. Instabilities associated with the symmetric modes occur at much higher flows. The symmetric m = 1 mode buckles at point H, and is then restabilized at I, but only briefly, before it unites with the symmetric m = 2 mode in coupled-mode flutter (point J). The symmetric m = 3 mode is not involved in any flutter instability; buckling in this mode occurs at point K.

The modal shapes of the system were calculated for various flow

velocities. The results are shown in Appendix O (Figures O.14-O.26) as well as in Figures 19 and 20. It is evident that the modal shapes change dramatically with increasing flow. At zero or low flow velocities, the system possesses classical normal modes with well-defined stationary nodes, which can easily be recognized to correspond to those of the three lowest beam modes. As the velocity is increased, the nodes are no longer stationary, indicating the presence of a travelling wave component (for example, see Figures 19(a)-(c)). Moreover, with increasing flow, and especially prior to or during the occurrence of the instability phenomena, the modal shapes contain components of various axial modes. Different shapes can be displayed depending on which component is dominant. For instance, at (or close to) the buckling flow velocity associated with the antisymmetric m = 1 mode (Figures 20(c),(d)), the modal shape resembles that of a m = 3 mode. Although we designate the frequency curves as the loci of different longitudinal modes (according to the classical mode shapes exhibited at low flow velocities), the development of the curves, in fact, follows the variation of the frequencies rather than the modal shapes which, as mentioned earlier, become combinations of various axial modes as the flow velocity increases, and can no longer be distinctively identified. It should be noted that the above discussion on the modal shapes also applies to the internal flow results presented earlier.

Before ending this section, another set of results worth mentioning is that obtained for a 1/10-gap system of rubber shells which have the same dimensions as a corresponding system of steel shells. The frequency diagram is shown in Figure 21 ($\bar{U}_i = 0$, $\bar{U}_o$ variable). Qualitatively, the dynamics of the system is not affected by the difference in the strength of the shell material (*cf.* Figure 22, presenting results for a 1/10-gap

system of steel shells and n = 2, the same circumferential mode as the rubber-shell system of Figure 21). The same types of phenomena are observed in both systems of steel and rubber shells. However, as expected, the corresponding critical velocities in the case of the rubber shells are much lower (see Table 5.6) due to the small rigidity of the rubber shells

	Critical annular flow velocities				
	Antisymmetric modes		Symmetric modes		
	$\bar{U}_{b1}$	$\bar{U}_{f1,2}$	$\bar{U}_{b1}$	$\bar{U}_{f1,2}$	$\bar{U}_{b3}$
Steel shells	0.0122	0.0181	0.1234	0.1621	0.1976
Rubber shells	0.00399	0.00592	0.0405	0.05305	0.06382

Table 5.6: Comparison of the critical flow velocities of systems of steel or rubber shells conveying water in the annulus ($\bar{U}_i = 0$, b/L = 1/10, a/b = 10/11, n = 2). The subscripts b, f, as before, denote the critical flow velocities at which buckling and coupled-mode flutter instability occurs, respectively. The numerical subscripts refer to the axial modes in which the instabilities occur.

as compared to the ones made of steel.

5.1.3 Effect of Gap-Width Variation

As mentioned at the beginning of Section 5.1, all the systems of coaxial shells under consideration fall into two geometric categories, *viz*, the ½-gap system and the 1/10-gap system. Table 5.7 shows the values of the lowest critical flow velocity for some typical systems in these two

	Flexible steel shells	
	Inner	Both
1/2-gap system	0.0289	0.02057
1/10-gap system	0.0136	0.00958

Table 5.7: The lowest critical flow velocity for loss of stability of systems of steel shells conveying water in annulus of different widths ($\bar{U}_i = 0$, b/L = 1/10, n = 3).

groups subjected to varying annular flow ($\bar{U}_i = 0$). Comparison of the results reveals that the critical flow velocities are lower in the case of the narrow-gap system leading to the conclusion that this system (1/10-gap) is less stable. This outcome is not surprising since, from the physical point of view, the fluid within the highly confined space of the narrow annulus suffers larger accelerations during vibration than in the wider annulus, resulting in greater aerodynamic loadings on the shells. Another factor is the smaller h/a ratio for the 1/10-gap system (see Table 5.1).

5.1.4 Effect of the Circumferential Mode Number n

Due to the decoupling of the circumferential modes in the motion of the cylinders, the vibration of the systems under investigation is confined to one specified circumferential mode at a time. However, the vibration frequencies as well as the critical flow velocities associated with other circumferential modes can be different. In a real situation, a system will

lose its stability at the lowest critical flow velocity, in whatever circumferential mode this velocity corresponds to. Thus, it is of practical interest to conduct our studies of stability on systems vibrating in the circumferential mode for which the critical flow velocity is the minimum. As to which is the 'right' circumferential mode, the answer depends on the type of shell material and the dimensions of the shells.

Presented in Figures 23 and 24 are the vibration frequencies of the first three axial and different circumferential modes of a system in still water ($\bar{U}_i = \bar{U}_o = 0$); the outer shell is rigid. In Figure 23, the results are obtained with an inner shell made of rubber while those of Figure 24 are for a steel inner shell (the two are of different dimensions). It can be seen that the vibration frequency of the first axial mode reaches a minimum in the second circumferential mode for the rubber shell and in the third circumferential mode in the case of the steel shell. Assuming that the mode with the minimum vibration frequency under zero flow condition will also be associated with the first instability (presumably buckling) to be encountered with increasing flow velocity, the appropriate circumferential mode to be considered is the $n = 2$ mode for the rubber shell and the $n = 3$ mode for the steel shell, respectively.

As a matter of fact, in most of the calculations performed with the rubber or steel shells, the appropriate circumferential mode number has been employed. Apart from differences in the values of the vibration frequencies and the corresponding critical velocities, the general behaviour of the shells in different circumferential modes is essentially the same. This is evident from comparison between Figures 18 and 22 which are the frequency diagrams for two coaxial flexible steel shells vibrating in the $n = 3$ and $n = 2$ modes, respectively. Qualitatively, the frequency loci

display similar patterns in both cases.

5.2 COMPRESSIBLE FLOW RESULTS

This Section considers the dynamic response of clamped-clamped shells in the presence of inviscid compressible flow. The shell material is chosen to be either rubber or steel. Air is taken as the flowing internal and annular fluid. Because of the costly computation of the integrals associated with the generalized aerodynamic forces, the outer cylinder is assumed to be rigid, in which case the generalized forces contain only two integral terms to be evaluated (see Appendix D). For the same reason of containing cost, numerical results were obtained only for a limited number of cases. The shell and fluid parameters are the same as those listed in Table 5.1.

It has been shown in Section 3.4 that the natural frequencies of the system are obtained as the roots of equation (3.4.28). The generalized aerodynamic forces are evaluated by the direct numerical integration and interpolation method described in Chapter IV. An IMSL computer subroutine (called ZANLYT) is utilized to determine the roots of equation (3.4.28) for each set of input flow velocities. Detailed information on the computer program are given in Appendix G.

5.2.1 Effect of the Annular Flow Velocity

The results discussed in this Section are obtained for systems subjected to increasing annular flow. Due to certain mathematical complications, the internal fluid is given a small flow velocity of 0.005,

instead of being stationary[†]. The Mach numbers of both the internal and annular flow are assumed to be constant at $M_i = M_o = 0.001$, even though the annular flow is being varied.

Presented in Figure 25 are the results obtained with a ½-gap rubber-shell system (outer shell rigid, $\bar{U}_i = 0.005$, $\bar{U}_o$ variable). The frequencies of all three axial modes of the inner shell decrease with increasing annular flow velocity. The first instability encountered is buckling in the m = 1 mode (at $\bar{U}_o = 0.528$), but the system is restabilized as the flow is increased slightly (at $\bar{U}_o = 0.529$). Stability is then maintained for a very narrow interval of flow velocity, before the first two axial modes coalesce (at $\bar{U}_o = 0.535$). The m = 3 mode eventually buckles at a relatively higher flow velocity. It is assumed that coupled-mode flutter occurs after the coalescence of the two axial modes (m = 1, 2), as is usually the case (for similar gyroscopic conservative systems). However, due to the limitations in the method of evaluating the generalized aerodynamic forces (see Section 4.2), imaginary and complex eigenfrequencies of the system cannot be predicted and, therefore, the existence of coupled-mode flutter instability (and of buckling, for that matter) cannot be positively confirmed.

It is interesting to note that the close proximity of the critical velocities for the first buckling instability (in the m = 1 mode) and its restabilization, as well as that for the coalescence of two modes, is also observed in the same rubber-shell system when it is subjected to an incompressible internal flow of air (see Figure 7). Comparing the lowest

---

[†]If $\bar{U}_i = 0$, the reduced frequency, $\kappa_i = \Omega L/U_i$ involved in the formulation of the generalized aerodynamic forces (see equation (D.1a)) will become infinite.

critical velocities of the two cases (Table 5.8), it can be seen that the annular flow destabilizes the system at lower flow velocity than the

	Critical flow velocities	
	U_b	U_f
Internal flow ($M_i = M_o = 0$)	0.635	0.641
Annular flow ($M_i = M_o = 0.001$)	0.528	0.535

Table 5.8: The lowest buckling and coupled-mode flutter velocities for rubber shell conveying air (b/L = 0.05792, a/b = 2/3, n = 2).

internal flow. Since the compressible flow results are obtained with a low Mach number of 0.001, the effect of fluid compressibility on the stability of the system, if there is any, will be minimal and thus, this shift of stability threshold should mainly be attributed to the difference in flow conditions (annular flow *vs* internal flow). The comparison, therefore, provides us with yet another evidence that the annular flow may indeed be a stronger destabilizing factor than the internal flow. (This has been shown to be true for a 1/10-gap system with a steel shell and incompressible water flow (see Section 5.1.1(b)).)

Also shown in Figure 25 are the results obtained in reference [31] in which, for computational ease, the frequency dependence of the generalized aerodynamic forces was eliminated by equating the frequencies to zero in their evaluation. Obviously, the present results look more reasonable and are probably more accurate, an assessment based on the fact

that here the frequency dependence of the generalized forces has been retained throughout the calculations.

Figure 26 displays the results of a ½-gap system of steel shell subjected to an increasing annular flow of air. Again, the Mach numbers are assumed to be $M_i = M_o = 0.001$ and there is a small internal flow of $\bar{U}_i = 0.005$. The frequencies of all three axial modes of the inner shell decrease with increasing annular flow velocity. These frequencies remain real until they vanish in turn, indicating the onset of buckling (divergence) at sufficiently high flow velocities. Restabilization of the system as well as the coalescence of two axial modes, which invariably occur in all steel-shell systems subjected to water flow (incompressible flow results in Section 5.1), are not observed in this case when the fluid is air. It should be emphasized that although the axial modes are not seen to coalesce when they are stable, they may have done so in their post-buckling state. However, this speculation cannot be verified since, as mentioned earlier, the present method of solution for compressible flow is incapable of accounting for the behaviour of the system in the unstable modes when the eigenfrequencies are either imaginary or complex.

5.2.2 Effect of Fluid Compressibility

Calculations have been performed for the steel shell (the one discussed in the previous section) with different Mach numbers ($M_i = 0.025$, $M_o = 0.500$ as compared to $M_i = M_o = 0.001$ in earlier calculations).

The results are presented in Tables 5.9 and 5.10, together with those obtained with the small Mach numbers ($M_i = M_o = 0.001$). As one can see, the results are very close, the sub-critical vibration frequencies

		Dimensionless' frequency, $\bar{\Omega}_i \times 10^2$					
		n=2, m=1		n=2, m=2		n=2, m=3	
D_i	D_o	M_i=0.001 M_o=0.001	M_i=0.025 M_o=0.500	M_i=0.001 M_o=0.001	M_i=0.025 M_o=0.500	M_i=0.001 M_o=0.001	M_i=0.025 M_o=0.500
0.005	0.2	2.039	2.038	5.263	5.258	9.496	9.482
"	0.4	1.831	1.827	4.984	4.973	9.197	9.173
"	0.6	1.409	1.399	4.483	4.459	8.674	8.632
"	0.8	0.151	0	3.670	3.624	7.885	7.813
"	1.0					6.743	6.618
"	1.2	Buckling		Buckling		5.047	4.817
"	1.4					2.281	1.766

Table 5.9: The vibration frequencies of a steel shell conveying air at different Mach numbers (b/L = 1/10, a/b = 2/3, n = 2).

(Table 5.9) and the buckling velocities (Table 5.10) of the higher Mach number case being about 1-2% lower. Thus, one may conclude that the compressibility of the fluid has a definite but small destabilizing effect on the system. Weak dependence of the stability of the system on the fluid compressibility has also been observed in reference [18]. In view of the minute effect of compressibility of the fluid, the dynamic analysis with compressible flow is not carried on any further.

	Critical annular flow velocity		
	U_{b1}	U_{b2}	U_{b3}
$M_i = 0.001$ $M_o = 0.001$	0.802	1.095	1.471
$M_i = 0.025$ $M_o = 0.500$	0.797	1.084	1.445
% difference	-0.62	-1.00	-1.77

Table 5.10: Comparison of the critical flow velocities for loss of stability of a steel shell conveying air at different Mach numbers (b/L = 1/10, a/b = 2/3, n = 2).

CHAPTER VI

DYNAMICS OF SYSTEMS SUBJECTED TO VISCOUS AXIAL FLOW

The theories and formulations presented in Chapter II apply to systems of two coaxial cylindrical shells coupled by inviscid axial flows in the inner cylinder and the annulus. However, since any real fluid has some viscosity, it would be highly desirable to refine the formulations by incorporating the viscous effect of the fluid. While no ambitious attempt is made to solve the complete three-dimensional equations of motion for the flowing viscous fluid with moving shell boundaries, a modified analysis is adopted to account for certain aspects of the effect of fluid viscosity that are pertinent to the present work; *i.e.*, aspects which are most likely to influence strongly the general dynamics and stability of the system. Accordingly, attention is focused on the influence of fluid pressurization (to overcome pressure drop) and surface frictional force associated with viscous flow.

In this Chapter, the equations of motion of the cylindrical shells are revised to take into consideration the additional mean radial and axial loadings resulting from fluid pressurization and surface frictional forces. The aerodynamic forces arising from the disturbed fluid flow, associated with shell motions, are taken to be the same as those of an inviscid fluid. Thus, the effects of the mean flow and of the perturbation flow field are de-coupled from the outset, rather than through rigorous linearization of the shell and Navier-Stokes equations together. This is deemed to be a sufficiently valid first attempt of taking these effects into account, for the purposes of this study.

Galerkin's method is again employed to solve the resulting equations of motion, and the numerical results are then compared with the case of inviscid flow.

6.1 FORMULATION OF THE PROBLEM

6.1.1 The Equations of Motion

The equations of motion presented in Section 2.1 were derived for an initially stress-free cylindrical shell subjected to motion-related radial loads. In viscous flow, the fluid loadings, as an approximation, are assumed to consist of two parts. The first part consists of the static fluid pressure required to drive the viscous fluid through the cylinders, and the surface frictional force in the axial direction. The second part consists of the inviscid aerodynamic forces which (because they are proportional to the shell deformations, which may be considered to be arbitrarily small) are comparatively smaller than the former components; as a result of this difference in magnitudes, equations (2.1.1-.6) can no longer be utilized.

The reason for this can easily be seen if one considers the two kinds of components as separate loadings. Let us call the large forces, namely the static pressure and the axial frictional force, the *basic loads*. They will induce the *basic stresses* in the shell and produce a configuration of the *basic shell displacements*. Now, the inviscid aerodynamic forces are viewed as *additional loads*. They produce the *additional stresses* and the *additional displacements* which are small as compared to their basic counterparts.[†] What we are looking for are the differential equations

[†]A further distinction between basic and additional loads is that the latter are time-dependent, while the former are not.

governing the additional displacements. In the derivation of these equations, we have to take into account all terms of the same order of magnitude. Obviously, some of these terms are the additional loads and stresses. There is another group of such terms resulting from the fact that the basic loads and stresses are acting on a slightly deformed shell. These terms consist of products of a basic load or stress with an additional displacement or its derivative. Equations (2.1.1-.6) must be modified to include this second group of terms.

To derive the proper equations of motion, we proceed in the following manner. Consider a clamped-clamped cylindrical shell 'pre-stressed' by the following basic loads:

(i) a constant axial force per unit surface area,

$$p_{xI} = B \; , \tag{6.1}$$

(ii) a normal force per unit surface area (*i.e.*, pressure) of the form

$$p_{rI} = -(Cx+D)^{\dagger} \; , \tag{6.2}$$

where x is the streamwise variable; B, C and D are constants; the subscript I denotes quantities pertaining to the basic system.

The stress resultants[§] produced by these loads form the basic stress system. They are found to be:

[†]Reasons for assuming such functional forms for the basic loads will be made clear in the next section.

[§]A stress resultant is the stress force transmitted by a unit length of section on the cut surface of a shell element.

$$N_{\theta I} = -a(Cx+D) , \tag{6.3}$$

$$N_{xI} = -Bx - \frac{(\nu aC-B)}{2} L - \nu aD , \tag{6.4}$$

where $N_{\theta I}$ is the basic hoop stress resultant, and N_{xI} is the basic axial stress resultant; a and L are the radius and length of the cylinder, respectively. Detailed derivations of these stress resultants and basic shell displacements are given in Appendix I.

Now, suppose that the shell is acted upon by additional loads p_x, p_θ, p_r, causing additional displacements u, v and w. The additional stress resultants, moments and shear forces are denoted by N_x, N_θ, $N_{x\theta}$, $N_{\theta x}$, M_x, M_θ, $M_{x\theta}$, $M_{\theta x}$, Q_x and Q_θ[†]. The normal stresses N_x and N_θ are supplementary to the basic stresses of the same kind, so that the total stress resultants are

$$\bar{N}_\theta = N_{\theta I} + N_\theta , \tag{6.5}$$

$$\bar{N}_x = N_{xI} + N_x . \tag{6.6}$$

The next step is to write the six conditions of equilibrium of a *deformed* shell element - three for the forces and three for the moments. The analysis essentially follows that of Flügge [32]. Details are given in Appendix J. However, to give the reader an idea of how this is accomplished, let us consider the contribution of the stress resultant $\bar{N}_x$ to the equilibrium condition of forces in the x-direction.

Diagram 6.1 shows a shell element under the action of the stress

---

[†]For definition of these terms, see reference [32].

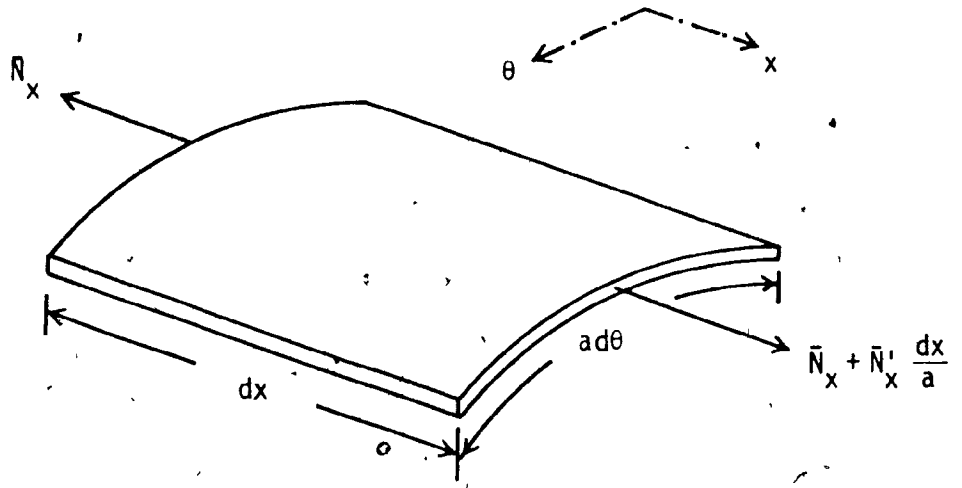

Diagram 6.1

resultants $\bar{N}_x$. The element is shown undeformed for the purpose of illustration. It is, indeed, slightly deformed, so that the force in the x-direction acting on one side of the element is $\bar{N}_x(1+\varepsilon_x)ad\theta$ instead of $\bar{N}_x ad\theta$, where ε_x is the longitudinal strain of the middle surface. Reasons for using ε_x rather than ε_θ, the hoop strain are explained in Flügge's book [32], in which he has given a thorough discussion on the issue of how the stress resultants should be multiplied by the deformed length of the shell element in which it is transmitted. On the opposite side of the shell element, the force is larger by a differential, namely,

$$\frac{\partial}{\partial x}\left[\bar{N}_x(1+\varepsilon_x)ad\theta\right]dx = \left[\bar{N}'_x(1+\varepsilon_x) + \bar{N}_x\varepsilon'_x\right]dxd\theta ,$$

where $(\ )'$ denotes $a\partial(\ )/\partial x$, which makes a contribution to the condition of equilibrium. Putting $\bar{N}_x = N_{xI} + N_x$, $\varepsilon_x = u'/a$ and noting that $N'_{xI} = -ap_{xI}$ in this case (from equations (6.1) and (6.4)), the contribution becomes

$$[-ap_{xI}(\,] + \frac{u'}{a}) + N_x' + N_{xI}\frac{u''}{a}]\, dxd\theta \ ,$$

after neglecting second order terms.

In the above expression, terms belonging to the two different groups mentioned at the beginning of this section can be identified. N_x' is the derivative of an additional stress resultant while $p_{xI}u'/a$, $N_{xI}u''/a$ are products of a basic load or a basic stress resultant with the derivative of an additional displacement, which illustrates the point made earlier.

Contributions from other stress resultants are determined in a similar manner. After obtaining the six conditions of equilibrium, two of them are used to eliminate the transverse shear forces Q_x and Q_θ from the other conditions, yielding a set of four independent equations. Utilizing the constitutive and kinematic relations, the additional stress resultants and moments in the equations can be expressed in terms of the additional displacements and their derivatives. At first sight, it appears that there is one equation too many: four equations for three unknown displacements. However, the redundancy is removed when one of the equations is shown to be an identity, after the stress resultants are expressed in terms of the displacements. In fact, this should come as no surprise, since the condition of equilibrium from which this equation is derived is an immediate consequence of the relation $\tau_{x\theta} = \tau_{\theta x}$[†]. The other three equations then become the three governing differential equations for the additional displacements u, v, and w. The final form of these equations can be found in Appendix J. Two sets of such equations for the two coaxial cylinders

---

[†] $\tau_{x\theta}$ and $\tau_{\theta x}$ are the shear stresses defined in the usual sense.

in our system are given below:

$$u_i'' + \frac{1-\nu_i}{2} u_i'' + \frac{1+\nu_i}{2} v_i'' + \nu_i w_i' + k_i[\frac{1-\nu_i}{2} u_i'' - w_i''' + \frac{1-\nu_i}{2} w_i'''] + q_{i1}u_i''$$

$$+ q_{i2}(v_i' + w_i) + q_{i3}(u_i'' - w_i') = \gamma_i \frac{\partial^2 u_i}{\partial t^2}, \tag{6.7}$$

$$\frac{1+\nu_i}{2} u_i'' + v_i'' + \frac{1-\nu_i}{2} v_i'' + w_i' + k_i[\frac{3}{2}(1-\nu_i)v_i'' - \frac{3-\nu_i}{2} w_i''] + q_{i1}v_i''$$

$$+ q_{i3}(v_i'' + w_i') = \gamma_i \frac{\partial^2 v_i}{\partial t^2}, \tag{6.8}$$

$$\nu_i u_i' + v_i' + w_i + k_i[\frac{1-\nu_i}{2} u_i''' - u_i''' - \frac{3-\nu_i}{2} v_i''' + \nabla_i^4 w_i + 2w_i'' + w_i] - q_{i1}w_i''$$

$$- q_{i3}(u_i' - v_i' + w_i'') = -\gamma_i [\frac{\partial^2 w_i}{\partial t^2} - \frac{q_i}{\rho_{si} h_i}], \tag{6.9}$$

$$u_0'' + \frac{1-\nu_0}{2} u_0'' + \frac{1+\nu_0}{2} v_0'' + \nu_0 w_0' + k_0[\frac{1-\nu_0}{2} u_0'' - w_0''' + \frac{1-\nu_0}{2} w_0'''] + q_{01}u_0''$$

$$+ q_{02}(v_0' + w_0) + q_{03}(u_0'' - w_0') = \gamma_0 \frac{\partial^2 u_0}{\partial t^2}, \tag{6.10}$$

$$\frac{1+\nu_0}{2} u_0'' + v_0'' + \frac{1-\nu_0}{2} v_0'' + w_0' + k_0[\frac{3}{2}(1-\nu_0)v_0'' - \frac{3-\nu_0}{2} w_0'''] + q_{01}v_0''$$

$$+ q_{03}(v_0'' + w_0') = \gamma_0 \frac{\partial^2 v_0}{\partial t^2}, \tag{6.11}$$

$$\nu_o u_o' + v_o^{\cdot} + w_o + k_o\left[\frac{1-\nu_o}{2}u_o'^{\cdot\cdot} - u_o''' - \frac{3-\nu_o}{2}v_o''^{\cdot} + \nabla_o^4 w_o + 2w_o^{\cdot\cdot} + w_o\right]$$

$$- q_{o1}w_o'' - q_{o3}(u_o' - v_o^{\cdot} + w_o^{\cdot\cdot}) = -\gamma_o\left[\frac{\partial^2 w_o}{\partial t^2} - \frac{q_o}{\rho_{so}h_o}\right], \qquad (6.12)$$

where the suffix i denotes the variables and parameters of the inner shell, while those of the outer one are labelled with the suffix o; the operators $(\,)'$, $(\,)''$, $(\,)^{\cdot}$, ∇_i^2, ∇_o^2, and the constants k_i, k_o, γ_i, γ_o are as defined in equation (2.1.6a);

$$q_{i1} = \frac{N_{xIi}}{\Lambda_i}, \quad q_{i2} = \frac{ap_{xIi}}{\Lambda_i}, \quad q_{i3} = \frac{ap_{rIi}}{\Lambda_i}, \qquad (6.13)$$

$$q_{o1} = \frac{N_{xIo}}{\Lambda_o}, \quad q_{o2} = \frac{bp_{xIo}}{\Lambda_o}, \quad q_{o3} = \frac{bp_{rIo}}{\Lambda_o}; \qquad (6.14)$$

$$\Lambda_i = \frac{E_i h_i}{1-\nu_i^2}, \quad \Lambda_o = \frac{E_o h_o}{1-\nu_o^2} \text{ are the extensional rigidities of the two shells,} \qquad (6.14a)$$

$$N_{xIi} = -B_i x - \frac{(\nu_i a C_i - B_i)L}{2} - \nu_i a D_i, \qquad (6.15)$$

$$p_{rIi} = -(C_i x + D_i), \qquad (6.16)$$

$$p_{xIi} = B_i, \qquad (6.17)$$

$$N_{xIo} = -B_o x - \frac{(\nu_o b C_o - B_o)L}{2} - \nu_o b D_o, \qquad (6.18)$$

$$p_{rIo} = -(C_o x + D_o), \qquad (6.19)$$

$$P_{xIo} = B_o \,. \tag{6.20}$$

In the above, p_{xIi}, p_{xIo} and p_{rIi}, p_{rIo} are the axial and radial basic loads acting on the two shells, respectively. N_{xIi}, N_{xIo} are the normal axial basic stress resultants. q_i is the fluid loading on the inner shell due to the perturbation pressure of an inviscid flow. It is, therefore, given by $q_i = \bar{P}_i\big|_{r=a} - \bar{P}_o\big|_{r=a}$, where $\bar{P}_i$ and $\bar{P}_o$ are the perturbation pressures of an inviscid internal and annular flow, respectively. Detailed derivations of these terms have been presented in Chapter III. The corresponding generalized aerodynamic forces are as given in equation (3.3.1) for incompressible flow. Similarly, q_o is the inviscid perturbation pressure on the outer shell. Thus, one has $q_o = \bar{P}_o\big|_{r=b}$ which again has been derived in Chapter III. Equation (3.3.2) defines the corresponding generalized aerodynamic forces for incompressible flow.

6.1.2 Derivation of the Static Fluid Pressure, the Surface Frictional Force and the Basic Loads

From the inviscid flow results, it can be seen that the initial instability of steel-shell systems conveying water generally occurs at such a high flow velocity that if the fluid were viscous, the flow would have been turbulent[†]. Although the critical velocities may be lowered when the fluid viscous effect is taken into account, it is supposed (and later

---

[†]The lowest critical velocity of a ½-gap system of steel shells conveying water (inviscid) in the annulus is approximately $U_o = 0.02$, or dimensionally, $U_o = 106$ m/s. This flow velocity corresponds to a Reynolds number of $Re = 6.30 \times 10^6$ based on the hydraulic diameter.

Its counterpart in the case of a 1/10-gap system is $U_o = 0.01$; the corresponding Reynolds number is $Re = 8.59 \times 10^5$.

Viscous flow in a circular pipe becomes turbulent when the Reynolds number exceeds 2300.

confirmed) that they would still be high enough to be in the turbulent flow regime. Thus, the problem will be formulated under the assumption of a turbulent flow. Of course, the flow is laminar when the velocity is small enough, but since we are more interested in the stability boundary of the system, the error introduced in applying turbulent flow analysis to the sub-critical laminar flow region is tolerable.

In this section, the fluid pressure and the surface frictional force due to a turbulent fully-developed incompressible viscous flow inside a circular cylinder and in the annulus between two coaxial cylinders are derived. The cylinders are assumed to be rigid in this derivation. By means of this static analysis, the basic loads defined in equations (6.16, 6.17) and (6.19,6.20) will be determined.

The schematics of the system is shown in Figure K.1. The flow velocity components in the cylindrical coordinates x, θ, r are $U + u_x$, u_θ and u_r, respectively†; U is the mean velocity in the axial direction while u_x, u_θ, u_r are the fluctuating velocity components of the turbulent flow. Applying the Navier-Stokes equations in the cylindrical coordinates, it may be shown that the time-mean equations may be written as§:

$$\frac{1}{\rho}\frac{\partial P}{\partial x} = -\frac{1}{r}\frac{d}{dr}\left(r\overline{u_x u_r}\right) + \frac{\eta}{r}\frac{d}{dr}\left(r\frac{dU}{dr}\right), \tag{6.21}$$

$$\frac{1}{\rho}\frac{\partial P}{\partial r} = -\frac{1}{r}\frac{d}{dr}\left(r\overline{u_r^2}\right) + \frac{\overline{u_\theta^2}}{r}, \tag{6.22}$$

---

†The analysis applies to both the internal and annular region. Thus, no subscripts are used here to distinguish the variables of one fluid region from the other.

§A derivation of these equations can be found in reference [38].

$$0 = \frac{d}{dr}\left(\overline{u_r u_\theta}\right) + 2\frac{\overline{u_r u_\theta}}{r}, \tag{6.23}$$

where $\bar{(\ )}$ = time mean of ( ); ρ and η are the density and the kinematic viscosity of the fluid, respectively; P is the time-mean pressure.

In the derivation of equations (6.21-.23), the assumption has been made that the flow is fully-developed so that all time-mean quantities, with the exception of the fluid pressure, are independent of the axial coordinate, x. From equations (6.21-.23), one could obtain an expression for the fluid pressure term. Details of the solution of the equations for the internal and annular fluid regions are given in Appendix K. The results are quoted below:

(i) For the internal fluid:

$$P_i(x,r) = -2\frac{\rho_i}{a}U_\tau^2 x - \rho_i\overline{u_{ri}^2} + \rho_i\int_a^r \frac{\overline{u_{\theta i}^2} - \overline{u_{ri}^2}}{r}\,dr + P_i(o,a), \tag{6.24}$$

where U_τ, the so-called stress velocity, is given by

$$U_\tau = \left(-\eta_i \left.\frac{dU_i}{dr}\right|_{r=a}\right)^{\frac{1}{2}}, \tag{6.24a}$$

$$= \left(\frac{\tau_w}{\rho_i}\right)^{\frac{1}{2}}, \tag{6.24b}$$

and

U_i is the mean axial velocity of the internal fluid,

τ_w is the fluid frictional force per unit area on the interior surface of the inner shell,

$P_i(o,a)$ is the internal fluid pressure at the position x=0, r=a,

and the subscript i denotes terms associated with the internal fluid.

(ii) For the annular fluid:

$$P_o(x,r) = -\left(\frac{2b}{b^2-R_m^2}\right)\rho_o U_{\tau b}^2 x - \rho_o \overline{u_{ro}^2} + \rho_o \int_a^r \frac{\overline{u_{\theta o}^2}-\overline{u_{ro}^2}}{r}\,dr + P_o(o,a)\,, \tag{6.25}$$

where

$$U_{\tau b} = \left(-\eta_o \left.\frac{dU_o}{dr}\right|_{r=b}\right)^{\frac{1}{2}}, \tag{6.25a}$$

$$= \left(\frac{\tau_b}{\rho_o}\right)^{\frac{1}{2}}, \tag{6.25b}$$

U_o is the mean axial velocity of the annular fluid ,

τ_b is the fluid frictional force per unit area on the interior surface of the outer shell ,

$P_o(o,a)$ is the annular fluid pressure at the position x=0, r=a ,

R_m is the radius at which the mean velocity U_o is a maximum ,

and the subscript o denotes quantities associated with the annular fluid.

In equation (6.25), R_m cannot be determined analytically, nor is any experimental measurement available. Thus, it will be approximated by its counterpart in the case of laminar flow, which can be found analytically to be

$$R_m = \left[\frac{(b^2-a^2)}{2\ell n(b/a)}\right]^{\frac{1}{2}}. \tag{6.25c}$$

For fully-developed turbulent flows, the frictional forces τ_w, τ_b are constant values and, according to equations (6.24,6.25), the internal and annular pressures are, therefore, linear functions of the x coordinate.

Having determined the fluid pressures, the basic loads on the shells can now be derived.

(i) Basic loads on the inner shell:

The radial basic load is given by

$$p_{rIi} = P_i(x,a) - P_o(x,a) . \tag{6.26}$$

Substituting into equations (6.24,6.25), one obtains

$$p_{rIi} = [-\frac{2\rho_i}{a} U_\tau^2 + (\frac{2b}{b^2-R_m^2}) \rho_o U_{\tau b}^2]x + P_i(o,a) - P_o(o,a) , \tag{6.27}$$

where use has been made of the condition that $\overline{u_{ri}^2}\big|_{r=a} = \overline{u_{ro}^2}\big|_{r=a} = 0$, justification of which lies in the fact that $u_{ri}\big|_{r=a} = u_{ro}\big|_{r=a} = 0$ at all times.

The axial basic load is

$$p_{xIi} = \tau_w + \tau_a , \tag{6.28}$$

where τ_a is the fluid frictional force per unit area on the outer surface of the inner shell. Using equation (6.24b) and defining $U_{\tau a} = (\tau_a/\rho_o)^{\frac{1}{2}}$, equation (6.28) can be written as

$$p_{xIi} = \rho_i U_\tau^2 + \rho_o U_{\tau a}^2 . \tag{6.29}$$

(ii) Basic loads on the outer shell:

The radial basic load is

$$P_{rIo} = P_o(x,b) - P_e \,, \tag{6.30}$$

where P_e is the pressure in the region external to the outer cylinder and is assumed to be equal to the atmospheric pressure, P_{atm}.

Making use of equation (6.25) and realizing that $\overline{u_{ro}^2}\big|_{r=b} = 0$ since $u_{ro}\big|_{r=b} = 0$ at all times, one obtains

$$P_{rIo} = -\left(\frac{2b}{b^2-R_m^2}\right)\rho_o U_{\tau b}^2 x + \rho_o \int_a^b \frac{\overline{u_{\theta o}^2}-\overline{u_{ro}^2}}{r}\,dr + P_o(o,a) - P_{atm} \,. \tag{6.31}$$

The axial basic load is

$$P_{xIo} = \tau_b \,, \tag{6.32}$$

and, from equation (6.25b), one has

$$P_{xIo} = \rho_o U_{\tau b}^2 \,. \tag{6.33}$$

The functional forms of equations (6.27), (6.29), (6.31) and (6.33) are consistent with those of equations (6.16,6.17) and (6.19,6.20), respectively. A one-to-one correspondence leads to the definition of the following terms in equations (6.16,6.17) and (6.19,6.20):

$$B_i = \rho_i U_\tau^2 + \rho_o U_{\tau a}^2 \,, \tag{6.34}$$

$$C_i = \frac{2\rho_i}{a} U_\tau^2 - \left(\frac{2b}{b^2-R_m^2}\right) \rho_o U_{\tau b}^2 , \tag{6.35}$$

$$D_i = P_o(o,a) - P_i(o,a) , \tag{6.36}$$

$$B_o = \rho_o U_{\tau b}^2 , \tag{6.37}$$

$$C_o = \left(\frac{2b}{b^2-R_m^2}\right) \rho_o U_{\tau b}^2 , \tag{6.38}$$

$$D_o = -\rho_o \int_a^b \frac{\overline{u_{\theta o}^2} - \overline{u_{ro}^2}}{r} dr - P_o(o,a) + P_{atm} . \tag{6.39}$$

Equations (6.24,6.25) do not represent a closed form solution of the Navier-Stokes equations. They merely relate the fluid pressures to the frictional forces and the time-mean fluctuating flow velocity components. The equations are of little practical use, unless we know the fluid friction and the time-mean quantities. To this end, we could only rely on experimental data. Differentiating equation (6.24) with respect to x, the internal fluid pressure gradient in the axial direction is given by

$$\frac{\partial P_i}{\partial x} = -\frac{2\rho_i}{a} U_\tau^2 , \tag{6.40}$$

which is constant for a fully-developed turbulent flow. Experiments carried out for circular pipes have shown that the pressure gradient of a fully-developed flow is indeed a constant value. The following formula was suggested [40],

$$\left|\frac{\partial P}{\partial x}\right| = \frac{1}{2}\frac{f\rho}{D_h} U^2 , \tag{6.41}$$

where

ρ is the density of the fluid,

U is the mean axial velocity,

D_h is the hydraulic diameter, defined as four times the ratio of the cross-sectional area of the flow to the perimeter in contact with the fluid,

f is a coefficient known as the friction factor.

By dimensional analysis, it may be shown that the friction factor, f is a function of the Reynolds number, Re[†], and of the relative roughness, k/d of the pipe, where k is the average height of the surface protrusions and d is the pipe diameter. The friction factor may be found graphically from a Moody diagram which is a plot of f *vs* Re for different values of k/d. Alternatively, it may be determined with a number of empirical formulae. A common practice is to use the Colebrook equation [40], which is

$$\frac{1}{(f)^{\frac{1}{2}}} = -2 \log_{10} \left[\frac{k/d}{3.7} + \frac{2.51}{Re(f)^{\frac{1}{2}}}\right] . \tag{6.42}$$

To avoid solving the implicit Colebrook equation, it may be modified as follows [40]:

$$\frac{1}{(f)^{\frac{1}{2}}} = -2 \log_{10} \left[\frac{k/d}{3.7} + \frac{2.51}{Re(f_a)^{\frac{1}{2}}}\right] , \tag{6.43}$$

[†]The Reynolds number is defined as Re = Ud/η.

where f_a is given by the following equation derived by Moody and matches equation (6.42) within ± 5%:

$$f_a = 0.0055 \{1 + [20{,}000 (\frac{k}{d}) + \frac{10^6}{Re}]^{1/3}\} . \quad (6.44)$$

The stress velocities will now be related to the friction factor by comparing the theoretical and empirical formulations of the pressure gradient. For a circular pipe of radius a, the hydraulic diameter is simply $D_h = 2a$ and, comparing equations (6.40) and (6.41), one obtains

$$U_\tau^2 = \frac{1}{8} f_i U_i^2 , \quad (6.45)$$

where the subscript i is supplemented to indicate that the friction factor and mean velocity correspond to the internal flow.

Experiments show that the empirical relations developed for turbulent flow in a pipe of circular cross-section may be applied to non-circular ones and annuli between concentric cylinders if, in place of the diameter of the circle, the hydraulic diameter, D_h, is used whenever applicable [39]. Thus, equation (6.41) holds for the annular flow and one may write

$$\left|\frac{\partial P_o}{\partial x}\right| = \frac{1}{2} \frac{f_o \rho_o}{D_h} U_o^2 , \quad (6.46)$$

where the subscript o is introduced to identify terms associated with the annular flow, and $D_h = 2(b-a)$ is the hydraulic diameter of the annulus.

Another expression for the pressure gradient of the annular flow is,

by differentiating equation (6.25) with respect to x,

$$\frac{\partial P_o}{\partial x} = -\left(\frac{2b}{b^2-R_m^2}\right) \rho_o U_{\tau b}^2 \quad . \tag{6.47}$$

Comparing equations (6.46) and (6.47), one obtains

$$U_{\tau b}^2 = \frac{1}{8} \frac{f_o(b^2-R_m^2)}{b(b-a)} U_o^2 \quad . \tag{6.48}$$

It is shown in Appendix K that the stress velocity $U_{\tau a}$ can be related to $U_{\tau b}$ by the following equation,

$$U_{\tau a}^2 = \frac{b}{a} \frac{(R_m^2-a^2)}{(b^2-R_m^2)} U_{\tau b}^2 \quad . \tag{K.23}$$

Substituting equation (6.48) into equation (K.23), $U_{\tau a}^2$ is found to be

$$U_{\tau a}^2 = \frac{1}{8} \frac{f_o(R_m^2-a^2)}{a(b-a)} U_o^2 \quad . \tag{6.49}$$

By means of equations (6.45), (6.48) and (6.49), most of the terms in the expressions of the basic loads (equations (6.27), (6.29), (6.31) and (6.33)) can be put in terms of the friction factors, the various geometric parameters and the mean flow velocities.

We now turn our attention to the integral term involving the fluctuating velocity components in equation (6.31),

$$\int_a^b \frac{\overline{u_{\theta o}^2}-\overline{u_{ro}^2}}{r} \, dr \quad .$$

To the best of the author's knowledge, experimental data on the fluctuating velocity components of turbulent flow in the annulus between two concentric cylinders are not available. Therefore, the terms $\overline{u_{\theta o}^2}$ and $\overline{u_{ro}^2}$ will be derived from the experimental results of turbulent flow in a circular pipe, which have been obtained by Laufer [38]. Figure 27 displays his measurements of the distributions of $\overline{u_\theta^2}$ and $\overline{u_r^2}$ across a circular pipe of radius a. Details in the derivation of the integral making use of Laufer's measurements are given in Appendix L. The final result is as follows:

$$\int_a^b \frac{\overline{u_{\theta o}^2}-\overline{u_{ro}^2}}{r}\,dr = \left[-0.7864 - \frac{0.56R_m}{(R_m-a)} + \frac{0.5064R_m}{(R_m-a)}\,\ell n\,\left(\frac{R_m}{a}\right) + \frac{0.56R_m^2}{(R_m-a)^2}\,\ell n\,\left(\frac{R_m}{a}\right)\right] \times U_{\tau a}^2 + \left[0.7864 - \frac{0.56R_m}{(b-R_m)} - \frac{0.5064R_m}{(b-R_m)}\,\ell n\,\left(\frac{b}{R_m}\right) + \frac{0.56R_m^2}{(b-R_m)^2}\,\ell n\,\left(\frac{b}{R_m}\right)\right] U_{\tau b}^2 \,. \tag{6.50}$$

Equation (6.50) is a gross approximation of the real situation and its degree of accuracy is not readily assessible; however, fortunately, this integral turns out to be rather insignificant as compared to other terms.

In equation (6.31), the integral is accompanied by, among others, the term $P_o(o,a)$ which is the annular pressure at the upstream end (x=0) of the shells. Assuming that the exit annular pressure at the x = L end is atmospheric†, $P_o(o,a)$ must be large enough to overcome the total pressure drop over the length of the annulus from x = 0 to x = L. Putting x = L,

†This assumption is not as severe as may be thought. If all pressures at exit, in the inner, annular and outer regions are equal, this is dynamically equivalent to the assumption made here.

$r = a$ and $P_o(L,a) = P_{atm}$ in equation (6.25), one has

$$P_o(o,a) = \left(\frac{2b}{b^2-R_m^2}\right) \rho_o U_{\tau b}^2 L + P_{atm} \tag{6.51}$$

$P_o(o,a)$ and the integral as given by equation (6.50) have been evaluated for a 1/10-gap system with a set of typical values of mean flow velocity and friction factor. The result shows that the part of $P_o(o,a)$ due to the pressure drop, *viz*, $[2b\rho_o U_{\tau b}^2 L/(b^2-R_m^2)]$ is much larger than the integral term, their ratio being more than 1000:1. Therefore, any error introduced in the approximation of the integral is easily overwhelmed by the prominent $P_o(o,a)$ term.

Finally, to recapitulate, the internal and annular fluid pressures are as given in equations (6.24,6.25). The basic loads on the inner and outer shells are expressed in equations (6.27), (6.29), (6.31) and (6.33), with the various stress velocities defined in equations (6.45), (6.48) and (6.49). These loadings depend on the mean flow velocities through the use of the friction factor which can be found algebraically by the modified Colebrook equation (6.43).

6.2 SOLUTION TO THE EQUATIONS OF MOTION

Having determined the basic loads in the previous section, the governing equations of motion (6.7-.12) are now completely formulated. Galerkin's method is again employed to solve these equations. The displacements of the two cylindrical shells are assumed to have the same form of series solutions as given in equations (3.0.1-.6), which will be substituted along with equations (3.2.7) and (3.2.12) for q_i and q_o, the

inviscid aerodynamic forces due to flow perturbations, into the governing equations (6.7-.12). In accordance with Galerkin's method, the resulting equations will be multiplied by the appropriate weighting functions ($\phi_k'(x)$ for equations (6.7) and (6.10), $\phi_k(x)$ for equations (6.8,6.9) and (6.11,6.12)) and integrated with respect to x from x = 0 to x = L. To make these equations dimensionless, the following additional dimensionless parameters, as well as some of those from equations (3.2.10) and (3.4.2), are introduced

$$\Gamma_{i1} = -\frac{LB_i}{\Lambda_i}\,,\quad \Gamma_{i2} = \frac{\nu_i}{2}\Gamma_{i4} - \frac{\Gamma_{i1}}{2} + \nu_i\Gamma_{i5}\,,\quad \Gamma_{i3} = -\varepsilon_i\Gamma_{i1}\,,$$

$$\Gamma_{i4} = -\frac{aLC_i}{\Lambda_i}\,,\quad \Gamma_{i5} = -\frac{aD_i}{\Lambda_i}\,,\quad \Gamma_{o1} = -\frac{LB_o}{\Lambda_o}\,,\quad \Gamma_{o2} = \frac{\nu_o}{2}\Gamma_{o4} - \frac{\Gamma_{o1}}{2} + \nu_o\Gamma_{o5}\,,$$

$$\Gamma_{o3} = -\varepsilon_o\Gamma_{o1}\,,\quad \Gamma_{o4} = -\frac{bLC_o}{\Lambda_o}\,,\quad \Gamma_{o5} = -\frac{bD_o}{\Lambda_o}\,, \tag{6.52}$$

where Λ_i, Λ_o are defined in equation (6.14a), and the terms B_i, C_i, D_i, B_o, C_o and D_o are given in equations (6.34-.39).

Finally, one obtains, after some manipulation, the following set of dimensionless algebraic equations:

$$\sum_{m=1}^{\infty} B^1_{kmn}\bar{A}_{mn} + B^2_{kmn}\bar{B}_{mn} + B^3_{kmn}\bar{C}_{mn} + 0\times\bar{D}_{mn} + 0\times\bar{E}_{mn} + 0\times\bar{F}_{mn} = 0\,,$$

$$\sum_{m=1}^{\infty} B^4_{kmn}\bar{A}_{mn} + B^5_{kmn}\bar{B}_{mn} + B^6_{kmn}\bar{C}_{mn} + 0\times\bar{D}_{mn} + 0\times\bar{E}_{mn} + 0\times\bar{F}_{mn} = 0\,, \tag{6.53}$$

$$\sum_{m=1}^{\infty} B^7_{kmn}\bar{A}_{mn} + B^8_{kmn}\bar{B}_{mn} + B^9_{kmn}\bar{C}_{mn} + 0\times\bar{D}_{mn} + 0\times\bar{E}_{mn} + 0''_{kmn}\bar{F}_{mn} = 0\,,$$

$$\sum_{m=1}^{\infty} 0 \times \bar{A}_{mn} + 0 \times \bar{B}_{mn} + 0 \times \bar{C}_{mn} + B^{10}_{kmn}\bar{D}_{mn} + B^{11}_{kmn}\bar{E}_{mn} + B^{12}_{kmn}\bar{F}_{mn} = 0 ,$$

$$\sum_{m=1}^{\infty} 0 \times \bar{A}_{mn} + 0 \times \bar{B}_{mn} + 0 \times \bar{C}_{mn} + B^{13}_{kmn}\bar{D}_{mn} + B^{14}_{kmn}\bar{E}_{mn} + B^{15}_{kmn}\bar{F}_{mn} = 0 , \quad (6.53)$$

$$\sum_{m=1}^{\infty} 0 \times \bar{A}_{mn} + 0 \times \bar{B}_{mn} + R''_{kmn}\bar{C}_{mn} + B^{16}_{kmn}\bar{D}_{mn} + B^{17}_{kmn}\bar{E}_{mn} + B^{18}_{kmn}\bar{F}_{mn} = 0 ,$$

$$k = 1, 2, 3, \ldots$$

where

$$B^{1}_{kmn} = A^{1}_{kmn} + \Gamma_{i1}\varepsilon_i^2 e_{km} + \Gamma_{i2}\varepsilon_i^2 b_{km} - \Gamma_{i4}n^2 g_{km} - \Gamma_{i5}n^2 a_{km} , \quad (6.54)$$

$$B^{2}_{kmn} = A^{2}_{kmn} + \Gamma_{i3}nf_{km}/\varepsilon_i , \quad (6.55)$$

$$B^{3}_{kmn} = A^{3}_{kmn} + \Gamma_{i3}f_{km}/\varepsilon_i - \Gamma_{i4}g_{km} - \Gamma_{i5}a_{km} , \quad (6.56)$$

$$B^{4}_{kmn} = A^{4}_{kmn} , \quad (6.57)$$

$$B^{5}_{kmn} = A^{5}_{kmn} + \Gamma_{i1}\varepsilon_i^2 h_{km} + \Gamma_{i2}\varepsilon_i^2 d_{km} - \Gamma_{i4}n^2 j_{km} - \Gamma_{i5}n^2 \delta_{km} , \quad (6.58)$$

$$B^{6}_{kmn} = A^{6}_{kmn} - \Gamma_{i4}nj_{km} - \Gamma_{i5}n\delta_{km} , \quad (6.59)$$

$$B^{7}_{kmn} = A^{7}_{kmn} - \Gamma_{i4}\varepsilon_i^2 h_{km} - \Gamma_{i5}\varepsilon_i^2 d_{km} , \quad (6.60)$$

$$B^{8}_{kmn} = A^{8}_{kmn} + \Gamma_{i4}nj_{km} + \Gamma_{i5}n\delta_{km} , \quad (6.61)$$

$$B^{9}_{kmn} = A^{9}_{kmn} - \Gamma_{i1}\varepsilon_i^2 h_{km} - \Gamma_{i2}\varepsilon_i^2 d_{km} + \Gamma_{i4} n^2 j_{km} + \Gamma_{i5} n^2 \delta_{km} , \tag{6.62}$$

$$B^{10}_{kmn} = A^{10}_{kmn} + \Gamma_{o1}\varepsilon_o^2 e_{km} + \Gamma_{o2}\varepsilon_o^2 b_{km} - \Gamma_{o4} n^2 g_{km} - \Gamma_{o5} n^2 a_{km} , \tag{6.63}$$

$$B^{11}_{kmn} = A^{11}_{kmn} + \Gamma_{o3} n f_{km}/\varepsilon_o , \tag{6.64}$$

$$B^{12}_{kmn} = A^{12}_{kmn} + \Gamma_{o3} f_{km}/\varepsilon_o - \Gamma_{o4} g_{km} - \Gamma_{o5} a_{km} , \tag{6.65}$$

$$B^{13}_{kmn} = A^{13}_{kmn} , \tag{6.66}$$

$$B^{14}_{kmn} = A^{14}_{kmn} + \Gamma_{o1}\varepsilon_o^2 h_{km} + \Gamma_{o2}\varepsilon_o^2 d_{km} - \Gamma_{o4} n^2 j_{km} - \Gamma_{o5} n^2 \delta_{km} , \tag{6.67}$$

$$B^{15}_{kmn} = A^{15}_{kmn} - \Gamma_{o4} n j_{km} - \Gamma_{o5} n \delta_{km} , \tag{6.68}$$

$$B^{16}_{kmn} = A^{16}_{kmn} - \Gamma_{o4}\varepsilon_o^2 h_{km} - \Gamma_{o5}\varepsilon_o^2 d_{km} , \tag{6.69}$$

$$B^{17}_{kmn} = A^{17}_{kmn} + \Gamma_{o4} n j_{km} + \Gamma_{o5} n \delta_{km} , \tag{6.70}$$

$$B^{18}_{kmn} = A^{18}_{kmn} - \Gamma_{o1}\varepsilon_o^2 h_{km} - \Gamma_{o2}\varepsilon_o^2 d_{km} + \Gamma_{o4} n^2 j_{km} + \Gamma_{o5} n^2 \delta_{km} , \tag{6.71}$$

with

A^{ℓ}_{kmn}, $\ell = 1, 2, \ldots, 18$ defined in equations (3.4.4-.21),

a_{km}, b_{km}, d_{km}, δ_{km} defined in equations (3.4.22-.25),

$$e_{km} = L^2 \int_0^L x\, \phi_k' \, \phi_m''' \, dx \,, \tag{6.72}$$

$$f_{km} = \int_0^L \phi_k' \, \phi_m \, dx \,, \tag{6.73}$$

$$g_{km} = \int_0^L x\, \phi_k' \, \phi_m' \, dx \,, \tag{6.74}$$

$$h_{km} = \int_0^L x\, \phi_k \, \phi_m'' \, dx \,, \tag{6.75}$$

$$j_{km} = \frac{1}{L^2} \int_0^L x\, \phi_k \, \phi_m \, dx \,, \tag{6.76}$$

The constants defined in equations (6.72-.76) are given in Appendix A. The series solutions of the shell displacements given by (3.0.1-.6) are truncated at the third term in each case, on the assumption that satisfactory convergence is thereby attained; equations (6.53) will then become a finite set of equations with k,m = 1,2,3. Since the generalized aerodynamic forces of an incompressible flow are quadratic functions of the dimensionless frequency $\bar{\Omega}_0$ (see Section 3.3), the set of equations in (6.53) can be rearranged as a second-order matrix equation of the form

$$\bar{\Omega}_0^2 [M]\{\ddot{X}\} + \bar{\Omega}_0 [C]\{\dot{X}\} + [K_B]\{X\} = \{0\} \,, \tag{6.77}$$

where {X} is as defined in (3.4.27). The structure of the matrices [M] and [C] is shown in Appendix E; the matrix $[K_B]$ is obtained by replacing the A^{ℓ}_{kmn} elements of the matrix [K] defined in Appendix E by the corresponding B^{ℓ}_{kmn} terms. As discussed in Section 3.4, equation (6.77) can be

reduced to a standard eigenvalue equation of the form

$$([P_B] + \bar{\Omega}_0[Q])\{Y\} = \{0\} , \tag{6.78}$$

where $\{Y\}$ is given by (3.4.30), $[Q]$ is as defined in (3.4.31),

$$[P_B] = \begin{bmatrix} [0] & [I] \\ [K_B] & [C] \end{bmatrix} , \tag{6.78a}$$

and $[I]$ is the identity matrix.

Note that equation (6.78) is the same as the eigenvalue equation (3.4.31) derived for the system with inviscid incompressible flow, except that some elements in one of the matrices (in $[P_B]$) are different. Thus, the computer program developed for the case of inviscid incompressible flow can easily be adapted for use here, with some modifications. Details of the computer program are given in Appendix M.

6.3 THEORETICAL RESULTS

Numerical results were obtained for systems of steel shells with water as the internal and annular fluids. All the shells under consideration have clamped-clamped boundary conditions. For the purpose of comparison, the same geometric configurations as in the case of inviscid flow were studied, namely, the ½-gap system and the 1/10-gap system. The various shell and fluid parameters are as given in Table 5.1.

The effect of varying the internal and annular flow velocities on the dynamics of the system are investigated. The axial frictional force and the static pressure gradient are adjusted at different flow velocities

by making use of the friction factor and the appropriate empirical equations described in Section 6.2. In addition to the basic loads associated with viscous flow, the shells can be subjected to other flow-independent basic loads in the radial and axial directions. Numerical results are obtained for systems in which the fluid is pressurized (in excess of the pressure required to sustain the viscous flow), imposing thereby constant additional radial loads on the shells.

6.3.1 Systems with a Rigid Outer Shell

6.3.1(a) Effect of the viscous annular flow

Figure 28 shows the variation of the dimensionless frequencies of the third circumferential (n=3) and the first three axial (m=1,2,3) modes with increasing annular flow velocity $\bar{U}_0$ for a 1/10-gap system. The internal fluid is stationary and has a constant static pressure of one atmosphere, whilst the flowing annular fluid leaves the x=L end of the annulus at this same pressure of one atmosphere. The annular pressure at other positions along the annulus upstream of the x=L end are higher since, according to equation (6.25), the annular pressure decreases linearly towards the x=L end at a gradient depending on the magnitude of the annular velocity[†]. In the following discussions, fluid flows under such conditions of pressurization (*i.e.* $P_{iL} = P_{oL} = 0$ where P_{iL}, P_{oL} are, respectively, the

[†]It should also be noted that, in this model, the shells are assumed to be clamped to semi-infinite rigid cylinders at both ends. To maintain a viscous flow through the infinitely long channel (from $x = -\infty$ to $x = \infty$ in the inner cylinder or the annulus), it is assumed that there exist infinitely high pressure at the upstream end ($x = -\infty$) and infinitely large suction at the downstream end ($x = \infty$). Strictly speaking, these assumptions are unrealistic. However, in practice, the rigid portion of the cylinders only has to be sufficiently long, so that the flow perturbation will die down to a negligibly small level at the two ends (which is the main purpose of having these rigid end extensions in the first place).

internal and annular gauge pressures at the x=L end (r=a)) are referred to as 'normally' pressurized.

The frequencies associated with all three modes decrease with increasing $\bar{U}_0$ (Figure 28). They remain real until, at sufficiently high flow velocities (points A, B and C), they vanish in turn, indicating the onset of buckling instabilities. The frequencies become imaginary numbers as the velocity increases further. Although it cannot be shown in the frequency diagram (Figure 28), the buckled m=2 mode coalesces with the buckled m=1 mode[†] at a flow velocity $\bar{U}_f$, higher than its buckling velocity, to produce coupled-mode flutter[§]. The behaviour described above is different from that of the same system with inviscid incompressible flow (see Figure 11). The phenomenon of restabilization is not observed here and, quantitatively, the critical velocities associated with viscous flow are lower (see Table 6.1), showing that the stability of the system is weakened. In order to overcome the pressure drop in the viscous annular flow, the annular pressure is greater than the inner one and, therefore, the inner cylinder is being compressed externally. Furthermore, due to the surface frictional force, the inner cylinder is also compressed axially by the reactions from the two clamped ends. Since a radially inward pressure and an axial compressive load are capable of causing buckling of cylinders, the decrease in the critical flow velocities is as anticipated.

Table 6.2 shows the net external pressure and the axial static loads acting on the two ends of the flexible portion of the inner cylinder

---

[†]This coalescence occurs while the two modes lie on the imaginary axis in a complex-frequency Argand diagram.

[§]The frequencies of the combined m=1 and m=2 modes have become complex conjugate pairs but the real part of the complex frequency is not shown in Figure 28, as is the case in all other frequency diagrams.

	Critical annular flow velocities				
	$\bar{U}_{b1}$	$\bar{U}_{b2}$	$\bar{U}_{b3}$	$\bar{U}_{f1,2}$	$\bar{U}_{f2,3}$
Inviscid flow	0.0136	-	-	0.01852	0.02616
Viscous flow	0.00361	0.00832	0.01399	0.01035	-

Table 6.1: Comparison of the critical flow velocities of a 1/10-gap system with a rigid outer shell subjected to inviscid and viscous annular flow. The subscripts b, f specify, respectively, the critical flow velocities at which buckling and coupled-mode flutter instabilities occur. The numeral subscripts refer to the axial modes in which the instabilities occur.

	x=0 end	x=L end
Net external pressure, KN/m^2	1.464×10^2 (3.63×10^1)	0.0 (3.63×10^1)
Axial load, KN/m	-1.658 (-2.97×10^2)	-2.234 (-2.97×10^2)

Table 6.2: The net external pressure and the axial loads at the x=0 and x=L ends of the inner shell at the lowest critical velocity. ( ), critical, axially constant, external pressure and critical axial compression for a shell of the same dimensions without any flow (b/L = 1/10, a/b = 10/11).

when the annular fluid is flowing at the lowest critical velocity ($\bar{U}_{b1}$ = 0.00361). The net pressure is maximum at the x=0 end and decreases linearly with the downstream distance to zero at the other end. The two axial loads

are the reactions of the supports at the ends of the flexible portion. Also shown in Table 6.2 are the critical values of a constant external pressure and of an axial compressive end load[†], the action of either of which would induce buckling of a cylinder with the same dimensions and physical properties as the inner shell in our system but, of course, free of the other aerodynamic loadings[§]. Comparison of these values shows that the average external pressure on the inner shell is of the same order of magnitude as the critical value. Thus, the fluid pressure is probably more important a factor than the axial frictional force in affecting the stability of the system.

Finally, it should be noted that due to the presence of the basic loads, the system is no longer 'purely' conservative. This is reflected in the eigenfrequencies of the system in that they are no longer purely real numbers (as in stable oscillation), imaginary numbers or complex conjugate pairs (as in the post-buckling state or coupled-mode flutter). Instead, one would have, in the stable regime, a complex eigenfrequency with a small, but not quite negligible imaginary part[††].

[†]The values are taken from reference [32].

[§]Furthermore, the ends of this reference cylinder are supported in the tangential and radial directions but are neither restricted in the axial direction nor clamped.

[††]For certain modes, this imaginary part is indeed negative indicating a weak oscillatory instability. However, it should be noted that this is strictly a direct interpretation of the numerical results. With the present scheme of approximating the fluid viscous effects, the system should remain conservative, at least theoretically. Only if a more exact viscous theory had been adopted in which the viscous damping forces are taken into account, then a *positive* imaginary component would have resulted (representing damping of free oscillation). Thus, there is no physical reason for the eigenfrequencies of the present results (in the stable regime) to have an imaginary part, let alone a negative one. However, the very existence of the small imaginary part here probably results from inaccuracies introduced in the mathematical manipulations (in incorporating the basic loads), and they should not be treated in the same footing as the 'true' buckling or flutter instability in which the imaginary part of the eigenfrequencies is very much larger and grows with flow velocity.

The existence of coupled-mode flutter is indicated by pairs of complex eigenfrequencies that resemble complex conjugate pairs but they may, at worst, match only up to the first significant figure. Furthermore, as the frequencies of the two modes that are eventually involved in coupled-mode flutter approach each other, one of them may become complex before the real parts of their eigenfrequencies coincide. Thus, the occurrence of coupled-mode flutter cannot be pin-pointed precisely at a particular flow velocity at which the two modes coalesce, but rather it involves a transition over a small interval of flow velocity, during which the eigenfrequencies of the two modes become complex one after the other. (Hence, the critical flutter velocities, U_f of the viscous flow results displayed in the various Tables are approximate values.)

All these abnormalities should be viewed as due to the accumulative inaccuracies in the process of obtaining the numerical results; they should not be interpreted as new phenomena of the physical system that this mathematical model is intended to represent.

6.3.1(b) Effect of the viscous internal flow

Figure 29 is the frequency diagram for a 1/10-gap system with an internal flow and a quiescent annular fluid; both fluids are normally pressurized[†]. As the internal velocity increases, the frequency of the m=1 mode goes up slightly before it follows a downward trend to vanish at a velocity (point A) that is much higher than its counterpart in the system with an inviscid internal flow (see Table 6.3). The m=1 mode is restabilized at point B and goes on, at higher flow, to produce coupled-mode

[†]That is, it is assumed that $P_{iL} = P_{oL} = 0$.

	Critical internal flow velocities		
	$\bar{U}_{b1}$	$\bar{U}_{b2}$	$\bar{U}_{f1,2}$
Inviscid flow	0.02546	0.04062	0.03136
Viscous flow	0.04136	-	0.0486

Table 6.3: Comparison of the critical velocities of a 1/10-gap system with a rigid outer shell subjected to inviscid and viscous internal flow. The subscripted symbols are similarly interpreted as those in Table 6.1.

flutter with the m=2 mode after their coalescence at C. Both the m=2 and m=3 mode loci start off with a gentle slope. However, unlike the m=2 mode in which the system is eventually destabilized, through coupled-mode flutter, the m=3 mode frequency starts to ascend steadily beyond a certain flow velocity. No instability of any kind is induced in the m=3 mode, up to very high fluid flows.

This unprecedented behaviour of the system may be explained by realizing that the static internal pressure is greater than the annular one because of the viscous internal flow. The net pressure acting on the inner shell is, therefore, in the radially outward direction. It is well established that a cylindrical shell can buckle under the action of an external pressure (radially inward). However, an internal pressure cannot collapse a cylindrical shell, unless it is deformed in the first circumferential mode (n=1, *i.e.* the beam mode) and the length to radius ratio is such that $\ell/a > \pi$ (see [32]).

The tensile hoop stress induced by the internal pressure would,

through the Poisson's effect, tend to shorten the shell. The shrinking process is, of course, restrained by the clamped ends, creating a tensile axial stress within the shell. This is evident from Table 6.4 which shows that the axial load on the x=0 end of the inner cylinder is a tensile force[†] (indicated by the positive sign) when the internal flow is at a moderate velocity of $\bar{U}_i = 0.06$. It is speculated that this axial stress would increase the effective stiffness, so the natural frequencies of the shell would be raised in the same manner as a rope is stiffened when it is

	x=0 end	x=L end
Net internal pressure, kN/m^2	1.791×10^3	0.0
Axial load, kN/m	6.514×10^1	-1.628×10^1

Table 6.4: The net internal pressure and the axial loads at the x=0 and x=L ends of the inner shell when $\bar{U}_i = 0.06$ (b/L = 1/10, a/b = 10/11).

pulled taut[§]. In this respect, the internal pressure can, indeed, be considered as a stabilizing element since the increased stiffness of the shell would enhance its flexural restoring force and, thus, its ability to counteract the destabilizing aerodynamic forces exerted by the fluid flow. The magnitudes of both the internal pressure and the aerodynamic forces increase with the internal velocity, and if it happens that the latter

[†]The surface frictional force produces compressive axial stress over a certain length extending back from the x=L end, masking the tensile stress associated with the internal pressure on that portion of the shell.

[§]The increase in natural frequencies of cylindrical shells with internal pressure is also found in the study of Fung, Sechler and Kaplan [41] on the vibration of thin cylindrical shells under internal pressure.

increases more slowly than the former, then the shell will remain stable with its frequency going up with the flow velocity. This may well explain the strange behaviour of the m=3 mode in this case, as well as the general stabilizing effect of the viscous flow shown in Table 6.3, as compared to inviscid flow.

6.3.2 Systems with Both the Inner and Outer Shells Flexible

6.3.2(a) Effect of the viscous annular flow

Figure 30 shows the results obtained for a 1/10-gap system with normally pressurized fluids. The internal fluid is stationary while the annular flow velocity is varied as shown. The frequency loci of the lowest six modes consisting of three antisymmetric and three symmetric modes are recorded. The behaviour of three of these modes (m=1,2, antisymmetric and m=1, symmetric) are similar to those in the system with a rigid outer shell (*cf.* Figure 28). Their frequencies vanish in turn as the annular velocity increases. However, in this case, coupled-mode flutter occurs after the coalescence of the m=2, antisymmetric and m=1, symmetric modes at a velocity slightly higher than the buckling velocity of the m=1, symmetric mode.

It is interesting to note that the lowest critical velocity is equal to its counterpart in the rigid-outer-shell system (see Table 6.5). With the same annular velocity, the annular pressure and the fluid frictional force acting on the two systems are identical. Therefore, the above result may be interpreted as that the basic loads (fluid pressure and frictional force) are more prominent factors than the flexibility of the outer shell in determining the stability threshold. Moreover, as will be

Critical annular flow velocities	Flexible shells	
	Inner	Both
$\bar{U}_b$	0.00361	0.00361
$\bar{U}_f$	0.01035	0.01307

Table 6.5: Comparison of the lowest buckling and coupled-mode flutter velocities of the systems with a rigid outer shell or both flexible shells subjected to annular flow (b/L = 1/10, a/b = 10/11).

explained later that the annular pressure will not jeopardize the stability of the outer shell (in fact, the outer shell will be strengthened), the failure of the system is mainly due to the collapse of the inner shell under the radial compression. Therefore, the rigidity or flexibility of the outer shell has little effect in this situation.

Frequencies of the other three modes (Figure 30), after being more or less constant in low annular flow, start to increase as the flow becomes moderate. The m=3, antisymmetric-mode frequency, after reaching a maximum level, drops gradually and vanishes at a relatively high flow velocity. On the other hand, the m=2,3 symmetric-mode frequencies continue to increase steadily with the annular flow and remain real quantities, indicating the absence of any instability in these modes. The pattern of behaviour of these two modes has been observed before in the m=3 mode of the system with a rigid outer shell subjected to internal flow (see Figure 29).

The cause of this extraordinarily stable behaviour of the m=3, antisymmetric and m=2,3, symmetric modes cannot be definitely identified.

The following discussion looks at the situation from the physical point of view, whereby a probable explanation is proposed. Let us examine the annular pressure in more detail. The role of the annular pressure is two-fold; it is an external pressure acting on the inner shell but, on the other hand, it is also an internal pressure as far as the outer shell is concerned. Thus, the annular pressure may encourage the destabilization of the inner shell and, in view of the discussion in Section 6.3.1(b), strengthen the outer shell against instability. However, as the motions of the shells are coupled by the annular fluid, we cannot, of course, have one shell destabilized while the other one remains stable. One should address the question of how the annular pressure would affect the stability of the system as a whole. The dynamics of the two shells are interdependent and the ability of each to resist the various destabilizing elements may affect the overall stability of the system. Moreover, in the presence of considerable annular pressure and axial surface force, the modal shapes of the system may become a crucial factor. Although these large loadings can be the primary cause of buckling of the shells, they become critical only if the shells are deformed into a specific mode characteristic of the particular loading (see [30]). Shells with different configurations of deformation may be less (or more) vulnerable under the action of such loads.

In the light of the above discussion, the strange behaviour of the system may be explained. For the modes that remain stable in high annular flow, their modal shapes may be in such a 'favourable' configuration that the inner shell is able to withstand the crushing annular pressure and, through interaction with the stiffened outer shell, the whole system may, indeed, be stabilized or have an exceptionally high critical velocity. The other modes, presumably associated with 'unfavourable' modal shapes

are, therefore, destabilized at much smaller flow. Of course, the validity of the above reasoning has yet to be verified. This may be done with a more thorough examination of the modal shapes or some additional studies focusing on the effect of static radial loads on the stability of the system. However, due to the limited scope of the present work, this will be left as a future task.

Finally, it should be emphasized that, as in the case of inviscid flow, the modal shapes of the system at a high flow velocity are combinations of various axial modes and contain travelling wave components. They can be quite different from the classical normal modes displayed in low fluid flow. Hence, one should not regard the dynamical response in the moderate and high flow regime as the characteristics of the distinctive axial modes of the system, but rather they should be looked upon as the behaviour of certain normal modes of the eigensystem for which the solution is sought.

6.3.2(b) Effect of the viscous internal flow

Calculations are performed for a 1/10-gap system with an internal flow and a quiescent annular fluid. Both fluids are under normally pressurized condition. Figure 31 illustrates the variation of the frequencies of the lowest six modes (three symmetric and three antisymmetric) with increasing internal flow velocity. The $\bar{m}$=1, antisymmetric mode is the first one in which the system buckles; then, at higher flow, the system is restabilized and this mode locus coalesces with that of the m=2, antisymmetric mode to produce coupled-mode flutter. The behaviour of these two modes resembles that of the first two axial modes associated with the system of the same geometry and flow condition but with a rigid outer

shell (see Figure 29). Moreover, the values of the critical flow velocities are not altered by the flexibility of the outer shell, for the same reason as in the case with inviscid internal flow (see Section 5.1.2(a)).

No instability of any type is observed in the other four modes. The frequencies of the m=1,2, symmetric and m=3, antisymmetric modes become more or less constant at high internal flow. This lack of sensitivity to increasing flow was previously observed in systems subjected to inviscid internal flow (see Section 5.1.2(a)). An examination of the modal shapes at high flow velocity has revealed the same kind of dominance of the outer shell vibration (as compared with that of the inner shell) as has been observed in the inviscid flow system. The m=3, symmetric-mode frequency, on the other hand, increases monotonously with the internal velocity. This phenomenon is again not new; it occurs in the m=3 mode of the aforementioned rigid-outer-shell system with viscous internal flow (see Figure 29). Indeed, the same explanation for this dynamical behaviour as proposed in Section 6.3.1(b) can also be applied here.

6.3.3 Effect of Fluid Pressurization

In all the results presented so far, the internal and annular fluids are normally pressurized; that is, they either have a constant static pressure of one atmosphere if the fluid is stagnant or, in the presence of a flow, the fluid is sufficiently pressurized so that the pressure at the downstream end (x=L) of the flexible portion of the shells is maintained at one atmosphere. It would be interesting to examine the effect of changing this condition of fluid pressurization. Theoretical results have been obtained for a 1/10-gap system with an annular flow

($\bar{U}_i = 0$). The internal pressure is kept at one atmosphere, while the annular fluid is excessively pressurized, to the extent that the exit pressure (pressure at the x=L end) is 50 kN/m^2 in excess of one atmosphere[†].

The frequency diagram for this system is shown in Figure 32. Comparing to the system with normally pressurized fluids (Figure 30), one can observe a similar pattern of behaviour, except that the values of the corresponding critical flow velocities are different. Table 6.6 illustrates the differences between the critical flow velocities of the two systems. The increase in the annular pressure has lowered the lowest critical velocity ($\bar{U}_{b1}$, antisymmetric) by more than 40%.

This result provides us with yet another proof that annular pressurization is strongly detrimental to the stability of the system. However, one should note that the highest critical velocity ($\bar{U}_{b3}$, antisymmetric) of the excessively pressurized system is higher. This may be viewed as the manifestation of the other facet of the dual action of the annular pressure, namely, the reinforcement of the outer shell against instability[§] (see Section 6.3.2(a)).

To ascertain the dynamical significance of the internal pressure, additional calculations have been performed for the 1/10-gap system with annular flow ($\bar{U}_i = 0$), but this time the internal fluid also pressurized at 50 kN/m^2 above atmospheric pressure. Since the internal fluid is stationary, this pressure is constant over the entire length of the shell. The flowing annular fluid is pressurized as before so that the exit gauge

---

[†]One atmospheric pressure = 101.3 kN/m^2.

[§]On the other hand, since calculations were conducted with only three comparison functions, the accuracy of the third-mode (or higher mode) results is lower, this may have caused the difference between the two $\bar{U}_{b3}$'s.

Fluid flow and pressurization conditions		Buckling velocities				Coupled-mode flutter velocity
		Antisymmetric modes			Symmetric mode	
Internal	Annular	$\bar{U}_{b1}$	$\bar{U}_{b2}$	$\bar{U}_{b3}$	$\bar{U}_{b1}$	$\bar{U}_f$
stationary $P_{iL}=0.0$	flowing $P_{oL}=0.0$	0.00361	0.00806	0.10995	0.01282	0.01307
stationary $P_{iL}=0.0$	flowing $P_{oL}=50kN/m^2$	0.00211	0.00753	0.11091	0.01263	0.01296

Table 6.6: Comparison of the critical flow velocities of systems with normally pressurized fluids and with excessively pressurized annular fluid (b/L = 1/10, a/b = 10/11).

pressure is maintained at 50 kN/m^2. Figure 33 is the frequency diagram for this system. Table 6.7 compares the critical velocities to those of the system with both fluids normally pressurized. The results show that the presence of the pressurized internal fluid has restored the four lowest critical velocities to almost their original values, *i.e.* the values associated with the case when the fluids have normal pressures. This result may be explained, by considering the fact that the net fluid loadings on the inner shell are the same in both cases. The internal pressure cancels out the constant part of the annular pressure, leaving behind the linearly varying and velocity-dependent portion as the only static fluid loading on the inner shell. In view of its counteraction against the annular pressure, the internal pressure may thus be regarded as a stabilizing agent.

6.3.4 Effect of Gap-Width Variation

To investigate the effect of changing the annular gap width, results are obtained for a ½-gap system of both flexible shells and with an annular flow ($\bar{U}_i = 0$); both the internal and annular fluids are normally pressurized - to be compared with those for the 1/10-gap system discussed in Section 6.3.2(a). The frequency diagram of the system is displayed in Figure 34, and the critical flow velocities are compared with those of the 1/10-gap system under the same fluid flow and pressurization conditions (frequency diagram shown in Figure 30) in Table 6.8. The buckling velocities of the two systems are arranged in increasing order; they do not necessarily correspond to the same mode of vibration. It is evident from the results that the critical flow velocities of the 1/10-gap system are

Fluid flow and pressurization conditions		Buckling velocities				Coupled-mode flutter velocity
		Antisymmetric modes			Symmetric mode	
Internal	Annular	$\bar{U}_{b1}$	$\bar{U}_{b2}$	$\bar{U}_{b3}$	$\bar{U}_{b1}$	$\bar{U}_{f}$
stationary $P_{iL}=0.0$	flowing $P_{oL}=0.0$	0.00361	0.00806	0.10995	0.01282	0.01307
stationary $P_{iL}=50kN/m^2$	flowing $P_{oL}=50kN/m^2$	0.00361	0.00805	0.11133	0.01288	0.01307

Table 6.7: Comparison of the critical flow velocities of systems with normally pressurized fluid and with excessively pressurized fluid in both the internal and annular regions (b/L = 1/10, a/b = 10/11).

	Buckling velocities				Coupled-mode flutter velocity
	$\bar{U}_1$	$\bar{U}_2$	$\bar{U}_3$	$\bar{U}_4$	
1/10-gap system	0.00361	0.00806	0.01282	0.10995	0.01307
1/2-gap system	0.00851	0.01381	0.02162	0.04974	0.02388

Table 6.8: Comparison of the critical flow velocities of a ½-gap system and a 1/10-gap system subjected to viscous annular flow.

lower, indicating that systems with a narrow annulus are more apt to lose stability in increasing annular flow. A similar conclusion was drawn from results obtained with inviscid flow (see Section 5.2.3).

An explanation has already been proposed in Section 5.2.3 that the inviscid aerodynamic loadings due to the perturbed annular flow are relatively larger in narrow-gap systems. In the presence of a viscous flow, the situation is evidently made even worse by the fluid frictional force and fluid pressurization. Table 6.9 shows that, with viscous flow, the lowest critical flow velocity of the 1/10-gap system is 58% lower than that of the ½-gap system, whereas the difference is 53% if the flow is inviscid. The small hydraulic diameter of a narrow annulus reduces the Reynolds number of the annular flow making it 'less turbulent' but, on the other hand, raises the friction factor (according to the Colebrook equation or from the Moody diagram). The surface frictional force and the annular pressure gradient, being proportional to the friction factor and inversely proportional to the hydraulic diameter (see equations (6.48), (6.49), (6.46)) will, therefore, increase accordingly, rendering the system less stable.

Annular flow	Lowest critical flow velocity		% difference
	½-gap system	1/10-gap system	
Inviscid	0.02057	0.00958	-53%
Viscous	0.00851	0.00361	-58%
% difference	-59%	-62%	-

Table 6.9: Difference in the lowest critical flow velocity of a ½-gap system and a 1/10-gap system subjected to inviscid or viscous annular flow.

Interestingly, the percentage difference in the lowest critical flow velocity between inviscid and viscous flow results remains sensibly constant with varying gap (see Table 6.9). Hence, it cannot be argued that non-dimensionally wide annuli make the system less sensitive to viscous effects and hence the use of inviscid flow theory more acceptable.

CHAPTER VII

CONCLUSION

The aim of this thesis has been to study the dynamics and stability of a system of two coaxial cylindrical shells subjected to an internal flow and an annular flow. The two shells under investigation have uniform physical properties and the same length of flexible portions, clamped to rigid extensions at both ends.

In the first part of the thesis (Chapters II-V), the fluid is assumed to be inviscid and either incompressible or compressible. Flügge's shell equations and the linearized potential flow theory were used in formulating the problem. An integral transform technique due to Dowell and Widnall was employed in the derivation of the inviscid aerodynamic forces; subsequently, Galerkin's method was applied to solve for the frequencies of motion of the system.

The case of incompressible flow proved to be computationally fairly easy to analyze. The case of compressible flow, however, posed some difficulties. Two methods were proposed to evaluate the generalized aerodynamic forces due to compressible flow. The first, the method of contour integration, although not very successful, offered scope for some interesting mathematical manipulations and it could serve as an incentive or reference for further investigations into the problem. The second method, the interpolation method, proved to be feasible, but a limitation of the scheme is the considerable amount of computer time required.

In the second part of the thesis (Chapter VI), an attempt was made to account for fluid viscous effects. Flügge's shell equations were

modified to describe a system under the action of lateral pressures and surface axial forces associated with flowing viscous fluid in the internal and annular regions. Due to difficulties in analytical formulation, the viscous damping effect was not considered, and the aerodynamic forces arising from flow perturbation were assumed to be the same as those of an inviscid flow. However, it is well known that conservative systems subjected to viscous damping are stabilized by it, so that the results obtained here are 'conservative' - in the sense that they give the lower bound of instability for real systems.

Three different cases of dynamic analysis were treated, namely, the dynamic stability of the system in (i) inviscid compressible or (ii) inviscid incompressible flow and in (iii) viscous incompressible flow. The effects of parameters such as the internal and annular flow velocities, the gap-width, the fluid and shell material properties and, in the case of viscous flow, the fluid pressurization were studied. The following is a brief summary of the results.

(i) Systems with inviscid compressible or incompressible flows

Let us first discuss the case where the outer shell is rigid. From the incompressible flow results, we have seen that increasing internal or annular flow velocity initially results in reducing the natural frequencies of the system; at sufficiently high flow velocity, the system loses stability by buckling. At higher flow, restabilization takes place, only to be followed by the coalescence of two axial modes, resulting in coupled-mode flutter. It is noteworthy that annular flow (by itself) renders the system unstable at lower flow velocity than internal flow (by itself), even

in the case of a system with large gap-to-radius ratio, indicating that annular flow may have a greater destabilizing effect than internal flow in the inner shell.

Comparing results obtained with different Mach numbers, it has been shown that the effect of compressibility on the dynamics of the system is rather insignificant. By virtue of this observation and due to the computational difficulties in the evaluation of the aerodynamic forces associated with compressible flow, most of the dynamic analysis was subsequently carried out with incompressible flow.

Theoretical results obtained for systems with both shells flexible have shown that with internal flow alone, the instability threshold is not sensitive to whether one (the inner shell) or both shells are flexible; this contrasts to the case of annular flow, where the flexibility of the outer shell makes the system less stable. Furthermore, in systems subjected to internal flow, of the six lowest modes investigated, three were found to remain stable with constant frequencies at high flow velocity. On the other hand, with increasing annular flow, all six modes, sooner or later, become unstable through buckling or coupled-mode flutter. Antisymmetric modes were found to be less stable than symmetric modes.

To investigate the effect of the width of the annular region on the stability boundary, systems of two different geometries, namely the so-called ½-gap system (in which the gap width is equal to half the radius of the inner shell) and the similarly defined 1/10-gap system were considered. In the presence of annular flow, the narrow-gap system was found to be less stable. This phenomenon may be attributed to the greater aerodynamic loadings resulting from the pressure perturbations in the confinement of the narrow annulus.

The dynamics of systems made up of rubber or steel shells of the same dimensions have been studied to investigate the effect of differences in the strength of the shell material. The general behaviour of the two systems is essentially the same, except that the rubber-shell system is much less stable. Fluids of different densities, namely, air and water have been employed in the dynamic analysis. It was found that systems with the more massive fluid (water) lose stability at lower flow velocity, as expected.

(ii) Systems with viscous incompressible flow

A mathematical model was developed to account for the effect of fluid pressurization and the axial surface frictional force associated with viscous flow. It was found that the dynamical behaviour of systems subjected to viscous flows is markedly different from that with inviscid flow in certain respects.

Quantitatively, the instability threshold of systems subjected to viscous internal flow are elevated, whereas systems with viscous annular flow are destabilized at much lower flow velocity, as compared to inviscid flows. Qualitatively, systems in low internal and annular viscous flow exhibit typical patterns of behaviour as observed in the case of inviscid flow. Divergence is always the type of instability encountered first, and flutter occurs by coincidence of two frequencies of the system. Nevertheless, certain variations are observed in the case of annular flow; for example, the onset of coupled-mode flutter is not preceded by a region of brief restabilization as happens in most inviscid flow cases.

The dynamical behaviour of the systems in moderate and high viscous

flow is quite different from that in inviscid flow and is interesting. The frequencies of certain modes remain real and increase continuously with flow velocity. This result indicates that these particular modes are not engaged in any type of instability and, in fact, become more and more stable with increasing flow. This new phenomenon is found to occur in systems with either internal or annular flow.

It is speculated that these quantitative and qualitative differences between inviscid and viscous flow results are primarily caused by the fluid pressurization associated with the viscous flow. The surface frictional force may also play a part, but to a lesser extent. A proposed explanation suggests that the internal pressure required to sustain the viscous internal flow would increase the stiffness of the inner shell, thus, strengthening it against instability. This may explain the increase in the critical velocity of the initial instability and the presence of exceptionally stable modes in systems subjected to viscous internal flow.

The dynamical significance of the annular pressure is more intricate. Apparently, its effects on the stability of the two shells are opposite to each other; the outer shell is reinforced while the inner one is weakened. The resultant behaviour of the system is a compromise of these two opposing effects through the interaction of the shells coupled by the annular fluid, the outcome of which may not be readily predicted. Nevertheless, the theoretical results obtained did provide us with evidence of these counteracting effects of the annular pressure. We have seen, on the one hand, the reduction in the critical velocities of the system when subjected to viscous annular flow and, on the other, the enhancement in the stability of certain modes in such systems with increasing flow. All in all, the annular pressure would be regarded as a destabilizing element, in view of

its effect on the instability threshold. Besides, in all the foregoing it must be borne in mind that, so far, the study has been theoretical and it is still not known whether the dynamical behaviour predicted beyond the first instability could occur in practice. Thus, it is possible that the existence of the increasingly stable modes (or indeed any instabilities after the first one) may be a purely theoretical result.

To investigate further the effect of fluid pressurization, results were obtained for systems in which the annular fluid or both the internal and annular fluids are given a constant static pressure above the minimum pressure level required to overcome the fluid frictional force. The findings are consistent with the observations made earlier that the annular pressure has a destabilizing effect, while the internal pressure contributes positively to the stability of the system.

(iii) General conclusions

In this thesis, a theoretical study has been made of the dynamics of a system of two coaxial cylindrical shells with clamped ends and subjected to internal and annular flows, whereby the existence of buckling and coupled-mode flutter instabilities in such systems is predicted. It has also demonstrated the feasibility of the integral transform technique in formulating the inviscid aerodynamic forces. The analysis has been modified to account for the radial and axial loads due to fluid viscosity; in general, however, this type of loading may arise from other sources, such as physical constraints, thermal expansion or gravitational effects, which, therefore, may easily be incorporated in the present formulation.

It is beyond any doubt that this problem needs supplementary studies

and there is plenty of room for modifications and refinements. In view of the significant difference between the inviscid and viscous flow results, it would be highly desirable and illuminating to verify their correctness experimentally. If the severity of fluid viscous effects is proved to be real, then more refined modelling of the viscous flow should be given high priority in future studies.

In addition to some of the viscous effects, namely the fluid pressurization and the frictional force in the mean flow direction, that have been accounted for in the present work, though in a rudimentary fashion, a more adequate model of the fluid mechanics should also include the effect of the boundary layer for the case of short shells, especially in the annulus, and the viscous damping forces. However, considering the three-dimensional motion of the shells and the complicated flow pattern, the formulation of a rigorous fluid model is not likely to be a simple task. Finally, one may suggest further investigation into the case of clamped-free shells, such as might be used in certain types of sleeve valves and jet (ejector) pumps.

REFERENCES

1. H. Ashley and G. Haviland, "Bending Vibrations of a Pipeline Containing Flowing Fluid", Journal of Applied Mechanics, Vol. 17, 1950, pp. 229-232.

2. F.I. Niordson, "Vibration of a Cylindrical Tube Containing Flowing Fluid", Trans. Royal Inst. Tech. Stockholm, No. 73, 1953.

3. S. Naguleswaran and C.J.H. Williams, "Lateral Vibration of a Pipe Conveying a Fluid", Journal of Mechanical Engineering Science, Vol. 10, 1968, pp. 228-238.

4. T.B. Benjamin, "Dynamics of a System of Articulated Pipes Conveying Fluid - I. Theory", Proceedings of the Royal Society (London), Vol. 261(A), 1961, pp. 457-486.

5. T.B. Benjamin, "Dynamics of a System of Articulated Pipes Conveying Fluid - II. Experiments", Proceedings of the Royal Society (London), Vol. 261(A), 1961, pp. 487-499.

6. R.W. Gregory and M.P. Paidoussis, "Unstable Oscillation of Tubular Cantilevers Conveying Fluid - I. Theory", Proceedings of the Royal Society (London), Vol. 293(A), 1966, pp. 512-527.

7. R.W. Gregory and M.P. Paidoussis, "Unstable Oscillation of Tubular Cantilevers Conveying Fluid - II. Experiments", Proceedings of the Royal Society (London), Vol. 293(A), 1966, pp. 528-542.

8. M.P. Paidoussis, "Flow-Induced Vibrations in Nuclear Reactors and Heat Exchangers - practical experience and state of knowledge", Proccedings of the IAHR/IUTAM Symposium on Practical Experiences with Flow-Induced Vibrations, Springer-Verlag, Berlin, 1980, pp. 1-81.

9. M.P. Paidoussis and J.P. Denise, "Flutter of Cylindrical Shells Conveying Fluid", Journal of Sound and Vibration, Vol. 16, 1971, pp. 459-461.

10. M.P. Paidoussis and J.P. Denise, "Flutter of Thin Cylindrical Shells Conveying Fluid", Journal of Sound and Vibration, Vol. 20, 1972, pp. 9-26.

11. D.S. Weaver and T.E. Unny, "On the Dynamic Stability of Fluid-Conveying Pipes", Journal of Applied Mechanics, Vol. 40, 1973, pp. 48-52.

12. J.W. Miles, "Supersonic Flutter of a Cylindrical Shell. Part I.", Journal of the Aeronautical Sciences, Vol. 24, 1966, pp. 107-118.

13. E.H. Dowell and S.E. Widnall, "Generalized Aerodynamic Forces on an Oscillating Cylindrical Shell: Subsonic and Supersonic Flow", AIAA Journal, Vol. 4, 1966, pp. 607-610.

14. S.E. Widnall and E.H. Dowell, "Aerodynamic Forces on an Oscillating Cylindrical Duct with an Internal Flow", Journal of Sound and Vibration, Vol. 6, 1967, pp. 71-86.

15. E.H. Dowell, "Generalized Aerodynamic Forces on a Flexible Plate Undergoing Transient Motions", Quarterly of Applied Mathematics, Vol. 24, 1967, pp. 331-338.

16. L.K. Shayo and C.H. Ellen, "The Stability of Finite Length Circular Cross-Section Pipes Conveying Inviscid Fluid", Journal of Sound and Vibration, Vol. 37, 1974, pp. 535-545.

17. A. Kornecki, "Static and Dynamic Instability of Panels and Cylindrical Shells in Subsonic Potential Flow", Journal of Sound and Vibration, Vol. 32, 1974, pp. 251-263.

18. M.P. Paidoussis and M. Ostoja-Starzewski, "Dynamics of a Flexible Cylinder in Subsonic Axial Flow", AIAA Journal, Vol. 19, No. 11, 1981, pp. 1467-1475.

19. D. Krajcinovic, "Vibrations of Two Coaxial Cylindrical Shells Containing Fluid", Nuclear Engineering & Design, Vol. 30, 1974, pp. 242-248.

20. M.K. Au-Yang, "Free Vibration of Fluid-Coupled Coaxial Cylindrical Shells of Different Lengths", Journal of Applied Mechanics, Vol. 98, 1976, pp. 480-484.

21. S.J. Brown and B.W. Lieb, "A Comparison of Experimental and Theoretical Vibration Results for Narrow Gap, Fluid-Coupled, Coaxial Flexible Cylinders", Paper No. 80-C2/PVP-104, American Society of Mechanical Engineers, New York, 1980.

22. S.J. Brown and K.H. Hsu, "On the Use of the Finite Element Displacement Method to Solve Solid-Fluid Interaction Vibration Problems", in Fluid Transients and Acoustics in the Power Industry (Ed.: Papadakis and Scarton), American Society of Mechanical Engineers, New York, 1978.

23. H. Chung, P. Turula, T.M. Mulcahy, J.A. Jendrzejczyk, "Analysis of a Cylindrical Shell Vibrating in a Cylindrical Fluid Region", Nuclear Engineering and Design, Vol. 63, 1981, pp. 109-120.

24. S.S. Chen, M.W. Wambsganss, J.A. Jendrzejczyk, "Added Mass and Damping of a Vibrating Rod in Confined Viscous Fluids", Journal of Applied Mechanics, Vol. 98, 1976, pp. 325-329.

25. T.T. Yeh and S.S. Chen, "Dynamics of a Cylindrical Shell System Coupled by Viscous Fluid", Journal of Acoustical Society of America, Vol. 62, No. 2, 1977, pp. 262-270.

26. S.S. Chen, "Fluid Damping for Circular Cylindrical Structures", Nuclear Engineering and Design, Vol. 63, 1981, pp. 81-100.

27. G.I. Taylor, "Analysis of the Swimming of Long and Narrow Animals", Proceedings of the Royal Society (London), Vol. 214, Series A, 1952, pp. 158-183.

28. M.P. Paidoussis, "Dynamics of Cylindrical Structures Subjected to Axial Flow", Journal of Sound and Vibration, Vol. 29, 1973, pp. 365-385.

29. S. Timoshenko, "Theory of Elastic Stability", Engineering Societies Monographs, McGraw-Hill Book Company, New York, 1961.

30. D.O. Brush and B.O. Almroth, "Buckling of Bars, Plates and Shells", McGraw-Hill Book Company, New York, 1975.

31. S.S.P. Chan, "Dynamics of a System of Two Concentric Cylindrical Shells Subjected to Internal and Annular Axial Flow", B.Eng. (Honours) Thesis, Dept. of Mech. Eng., McGill University, August 1981.

32. W. Flügge, "Stresses in Shells", Springer-Verlag, New York Inc., 1967.

33. M.R. Spiegel, "Theory and Problems of Complex Variables", Schaum's Outline Series, McGraw-Hill Book Company, New York, 1964.

34. A. Kyrala, "Applied Functions of a Complex Variable", Wiley-Interscience, John Wiley & Sons, Inc., New York, 1972.

35. N.W. Mclachlan, "Bessel Functions for Engineers", Oxford University Press, London, 1941.

36. G.N. Watson, "A Treatise on the Theory of Bessel Functions", 2nd edition, Cambridge University Press, Cambridge, 1952.

37. T.T. Pham, "Dynamic Stability of Thin Cylindrical Shells Conveying Fluid Under Axial Loads", B.Eng. (Honours) Thesis, Dept. of Mech. Eng., McGill University, August 1980.

38. J. Laufer, "The Structure of Turbulence in Fully Developed Pipe Flow", Natl. Advisory Comm. Aeron., Tech. Note 2954, 1953, NASA.

39. B.S. Massey, "Mechanics of Fluids", 4th edition, Van Nostrand Reinhold, London, 1979.

40. J.W. Murdock, "Fluid Mechanics and its Applications", Houghton Mifflin Company, Boston, 1976.

41. Y.C. Fung, E.E. Sechler, A. Kaplan, "On the Vibration of Thin Cylindrical Shells Under Internal Pressure", Journal of the Aeronautical Sciences, Vol. 24, 1957, pp. 650-660.

42. C.B. Sharma, "Calculation of Integrals Involving Characteristic Beam Functions", Journal of Sound and Vibration, Vol. 56, 1978, pp. 475-480.

43. R.E.D. Bishop and D.C. Johnson, "The Mechanics of Vibration", Cambridge University Press, Cambridge, 1960.

44. A. Ralston and S.W. Wilf, "Mathematical Methods for Digital Computers", Vol. 1, John Wiley & Sons, Inc., New York, 1960.

45. W.L. Frank, "Finding Zeros of Arbitrary Functions", Journal of Association of Computing Mechinery, Vol. 5, 1958, pp. 154-160.

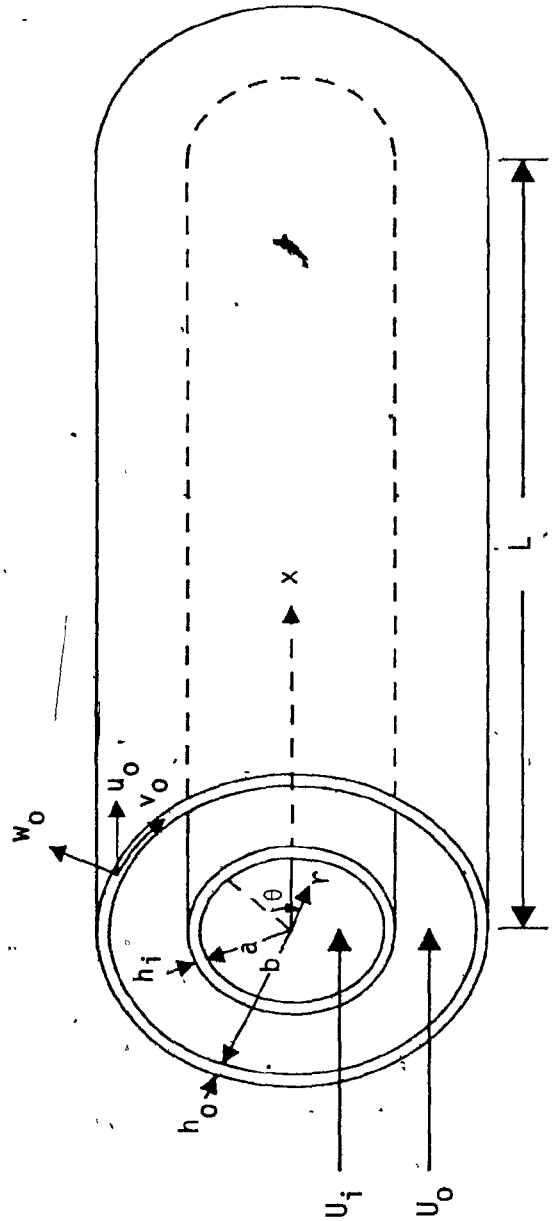

Fig. 1: The system under consideration.

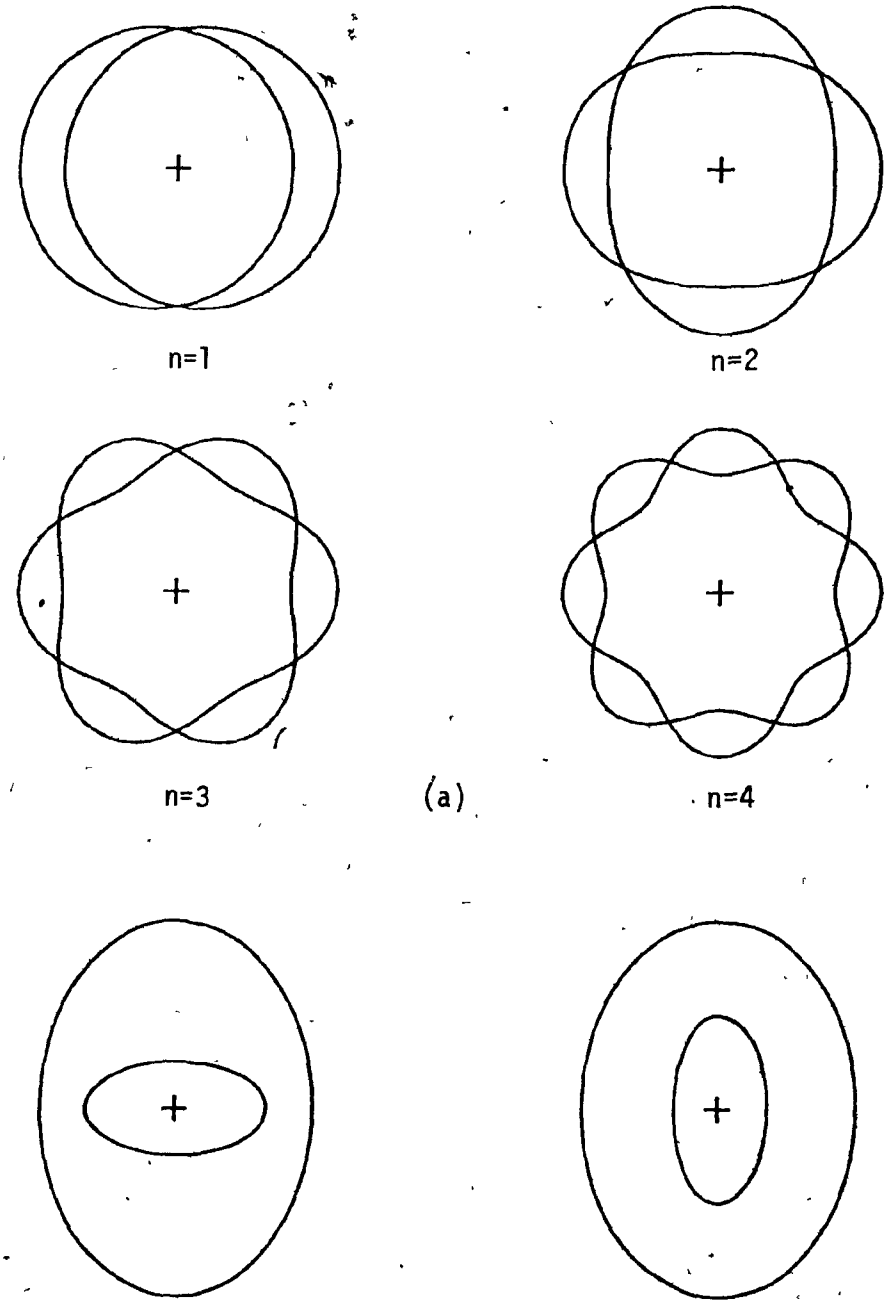

Fig. 2: Various circumferential mode shapes of (a) a single shell, (b) two coaxial shells.

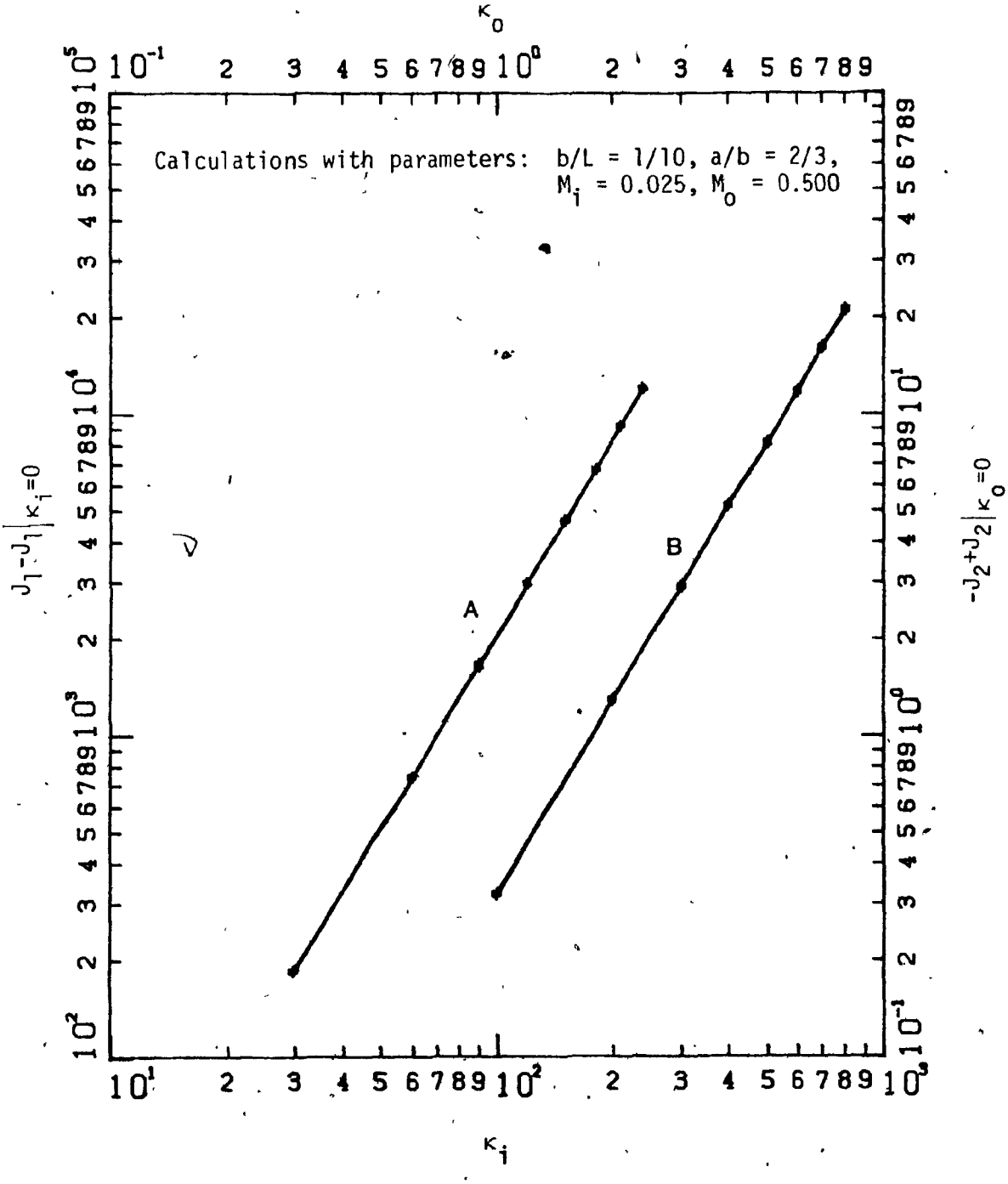

Fig. 3: The integrals J_1 and J_2 of equations (4.32, 4.33) for the generalized aerodynamic forces *versus* the associated reduced frequencies, κ_i and κ_o. Curve A: J_1 (bottom and left-hand scales); curve B: J_2 (top and right-hand scales); in each case, J_1 and J_2 are for $(n,k,m) = (2,1,1)$, $(2,2,2)$ and $(2,3,3)$, sensibly coincident in the scale of this figure.

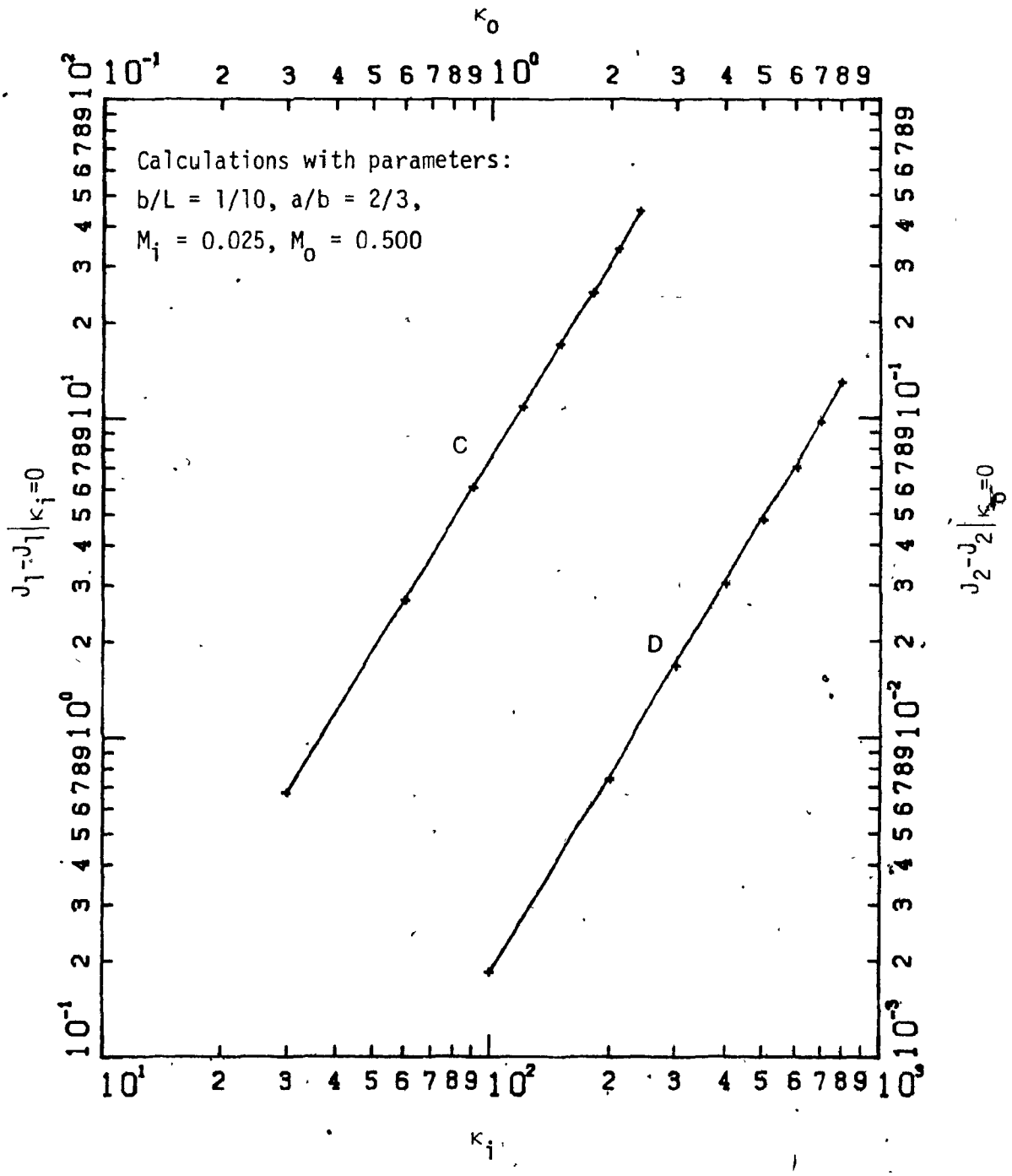

Fig. 4: The integrals J_1 and J_2 of equations (4.32, 4.33) for the generalized aerodynamic forces *versus* the associated reduced frequencies, κ_i and κ_0. Curve C: J_1 (bottom and left-hand scales); curve D: J_2 (top and right-hand scales); in each case, J_1 and J_2 are for (n,k,m) = (2,1,3).

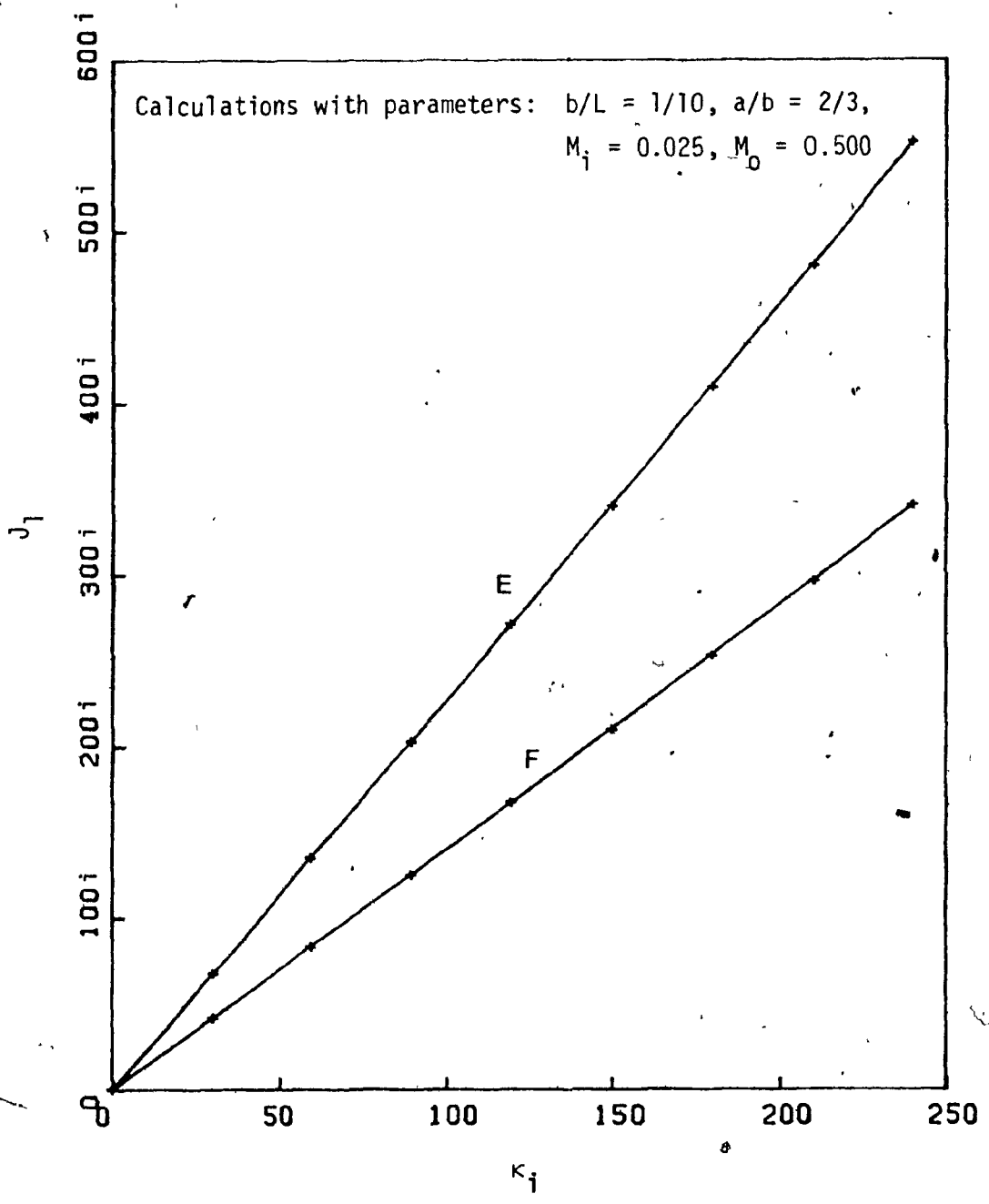

Fig. 5: The integral J_1 of equation (4.32) for the generalized aerodynamic forces *versus* the reduced frequency κ_i. Curve E: J_1 for (n,k,m) = (2,2,3); curve F: J_1 for (n,k,m) = (2,1,2).

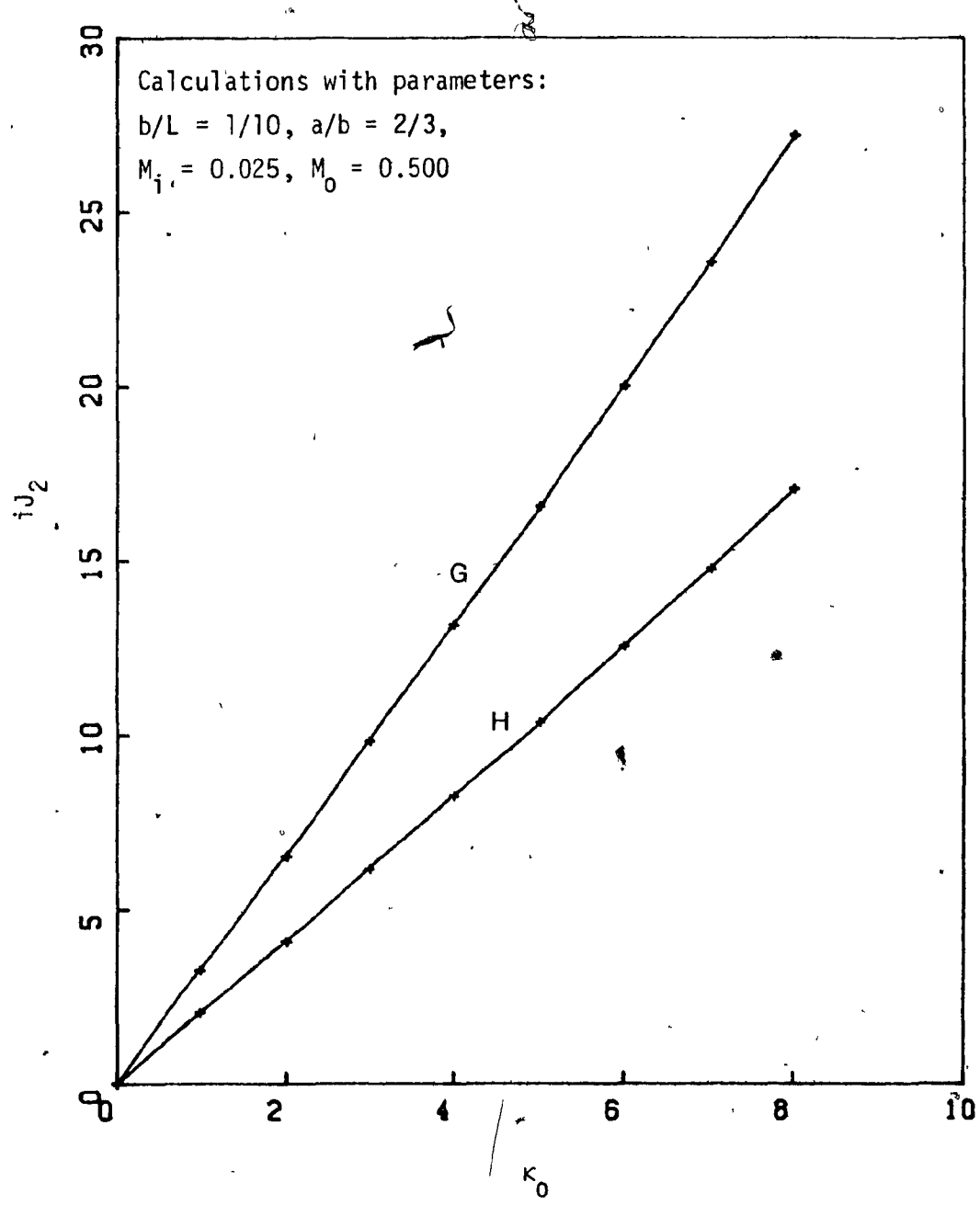

Fig. 6: The integral J_2 of equation (4.33) for the generalized aerodynamic forces *versus* the reduced frequency κ_0. Curve G: iJ_2 for (n,k,m) = (2,2,3); curve H: iJ_2 for (n,k,m) = (2,1,2).

		$J_1 = C_1\kappa_i^p + C_2$				$J_2 = D_1\kappa_o^q + D_2$			
k	m	p	C_1	C_2	Range of κ_i	q	D_1	D_2	Range of κ_o
1	1	2.006	0.204	2.541	(0, 240)	2.001	-0.315	- 3.709	(0, 8)
2	2	2.006	0.202	9.378	(0, 240)	2.011	-0.320	-13.398	(0, 8)
3	3	2.006	0.198	19.713	(0, 240)	2.012	-0.326	-27.298	(0, 8)
1	2	1.000 1.000	1.391i 1.447i	0 - 6.765i	(0, 120) (120, 240)	1.000 1.000	-2.074i -2.224i	0 0.752i	(0, 5) (5, 8)
1	3	2.016	7.063×10^{-4}	- 2.025	(0, 240)	2.046	1.837×10^{-3}	2.956	(0, 8)
2	3	1.000 1.000	2.254i 2.343i	0 -10.621i	(0, 120) (120, 240)	1.000 1.000	-3.311i -3.544i	0 1.163i	(0, 5) (0, 8)

Table 1: Interpolation equations for the integrals J_1 and J_2 of equations (4.32, 4.33) for the generalized aerodynamic forces; n = 2, b/L = 1/10, a/b = 2/3, M_i = 0.025, M_o = 0.500.

Remark: It is assumed that the dimensionless natural frequencies $\bar{\Omega}_i$ of the system (steel shell subjected to air-flow, b/L = 1/10, a/b = 2/3) lie in the range of 9.5×10^{-2} to zero†, as the dimensionless annular flow velocity $\bar{U}_o$ increases from 0.20, whilst the internal flow is kept constant at $\bar{U}_i$ = 0.005. The range of the reduced frequencies may thus be expected to be $0 \leq \kappa_i \leq 240$ and $0 \leq \kappa_o \leq 8$. The Mach numbers are taken to be constant at M_i = 0.025 and M_o = 0.500.

†The upper limit of $\bar{\Omega}_i$ corresponds to the (n=2, m=3)-mode frequency at low annular flow, as given by incompressible flow analysis; $\bar{\Omega}_i$ = 0 corresponds to the threshold of divergence.

Figures 7-24: Inviscid incompressible flow results.

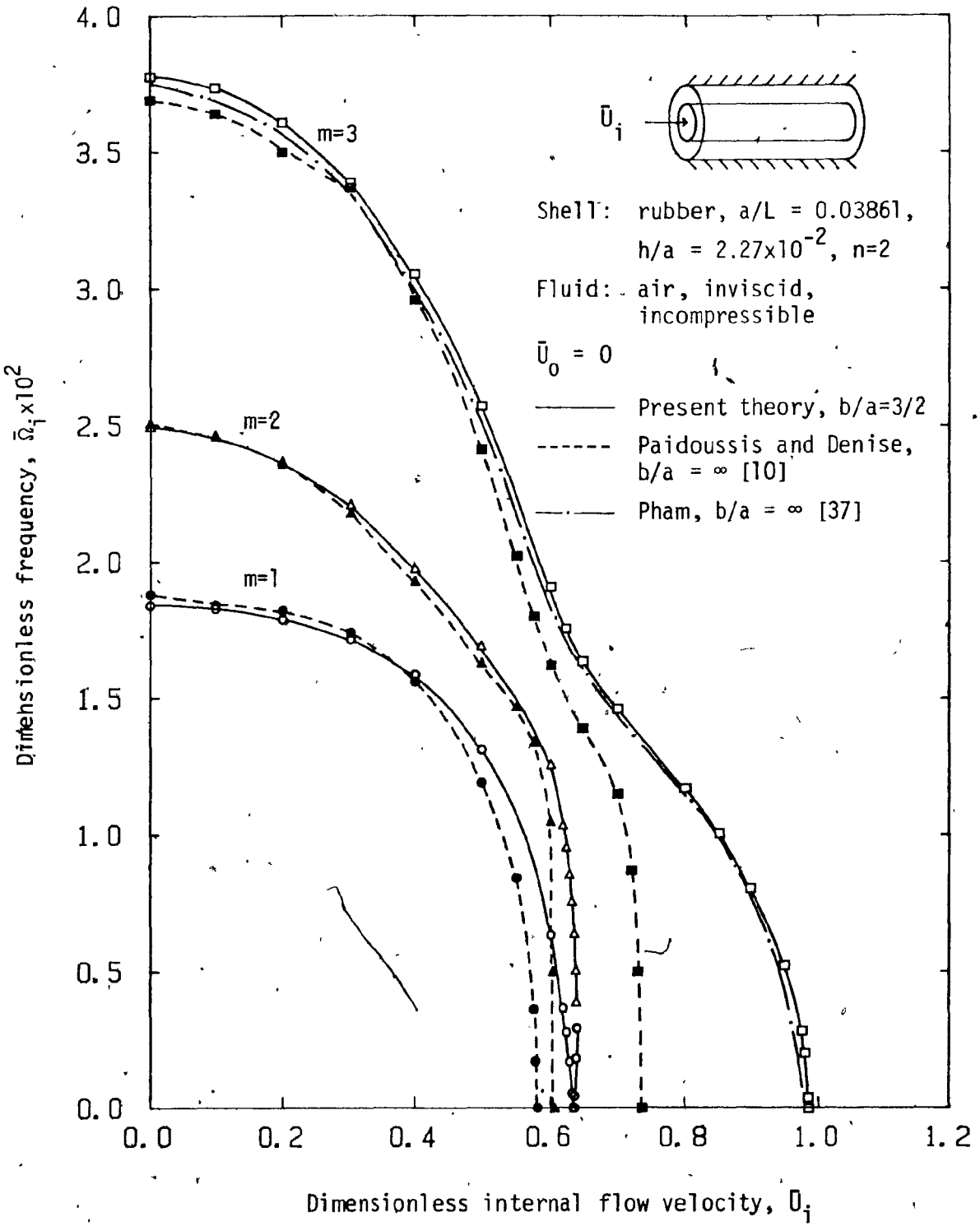

Fig. 7: The real dimensionless eigenfrequencies $\bar{\Omega}_i$ (n=2; m=1,2,3) of the ½-gap rubber-air system as functions of the dimensionless internal flow velocity $\bar{U}_i$; the annular fluid is stagnant and the outer shell rigid.

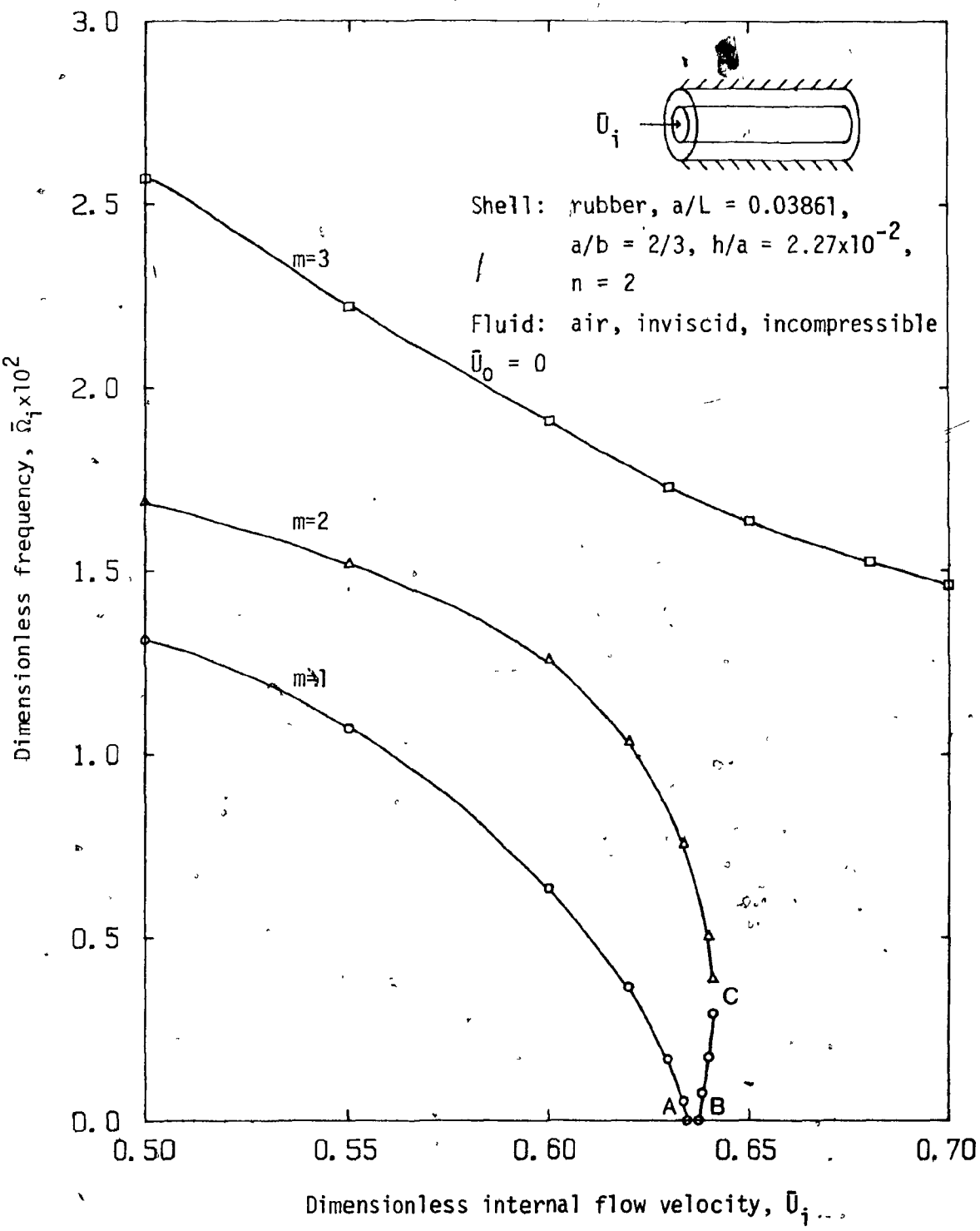

Fig. 8: Enlarged portion of Fig. 7: the real dimensionless eigenfrequencies $\bar{\Omega}_i$ (n=2; m=1,2,3) of the ⅔-gap rubber-air system as functions of the dimensionless internal flow velocity $\bar{U}_i$; the annular fluid is stagnant and the outer shell rigid.

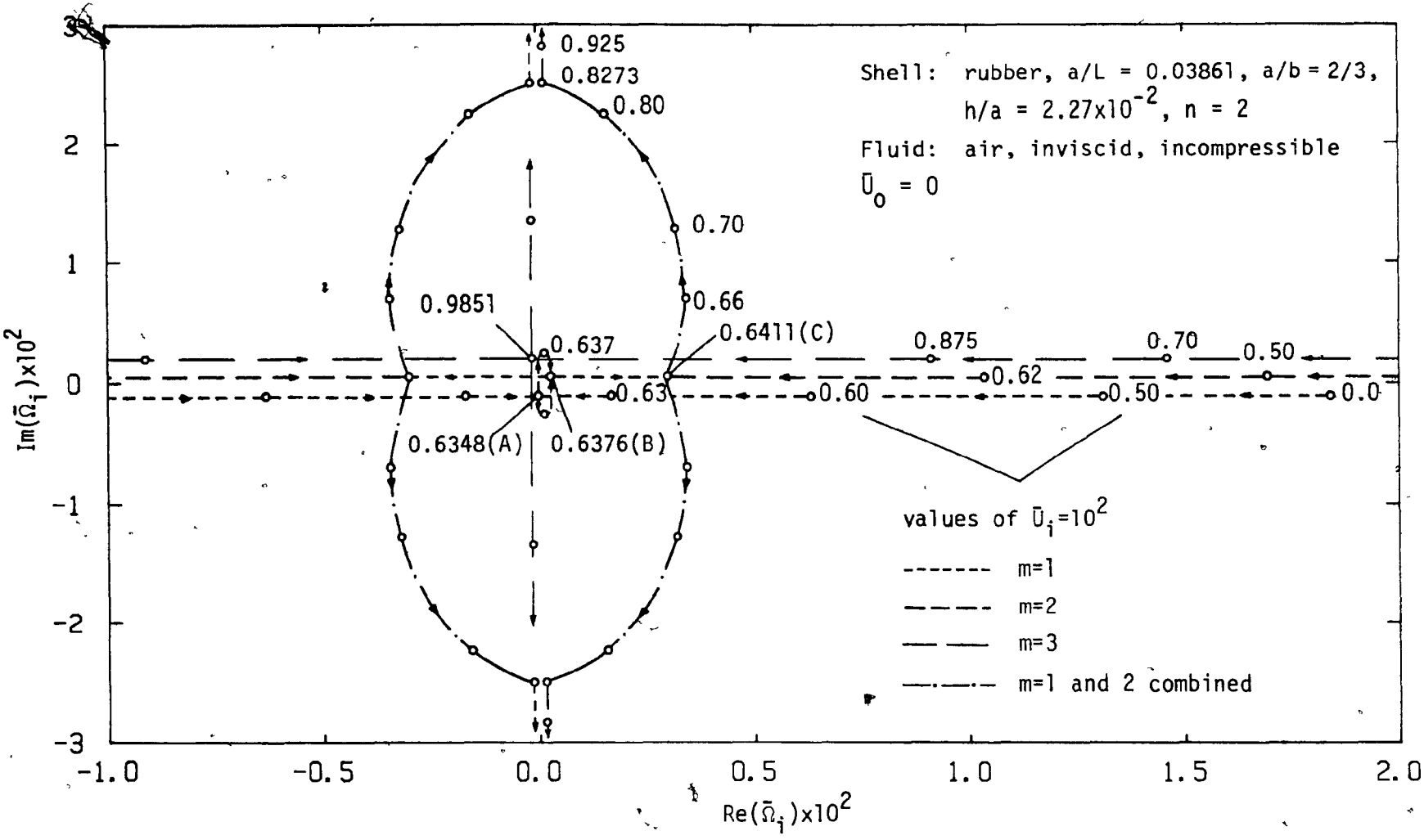

Fig. 9: Argand diagram of the dimensionless eigenfrequencies $\bar{\Omega}_i$ (n=2; m=1,2,3) of the ½-gap rubber-air system as functions of the dimensionless internal flow velocity $\bar{U}_i$; the annular fluid is stagnant and the outer shell rigid. The loci on the $\mathrm{Im}(\bar{\Omega}_i) = 0$ and $\mathrm{Re}(\bar{\Omega}_i) = 0$ axes have been drawn off the axes but parallel to them, for clarity. The letters in parentheses correspond to the points shown in the frequency diagram of Fig. 8.

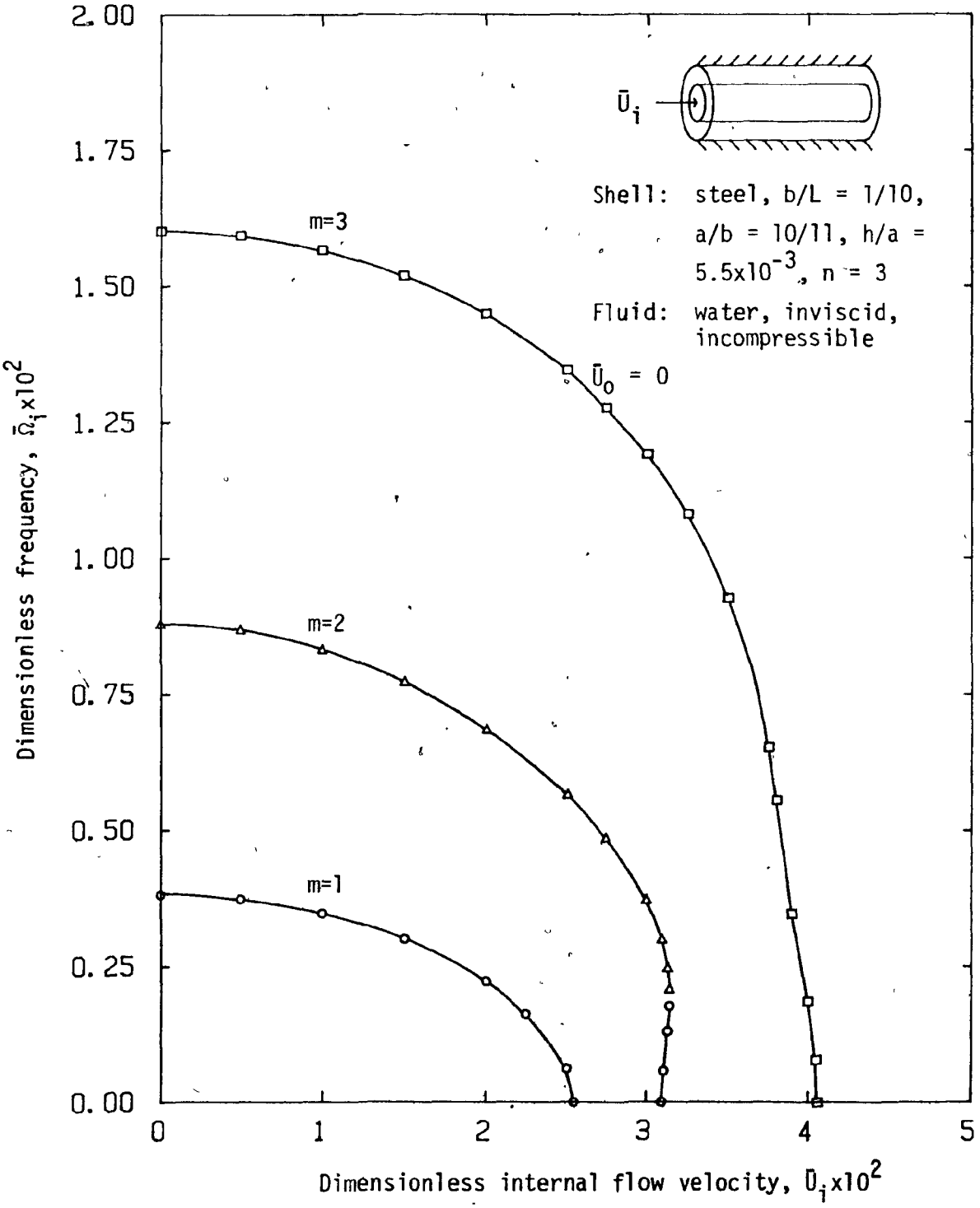

Fig. 10: The real dimensionless eigenfrequencies $\bar{\Omega}_i$ (n=3; m=1,2,3) of the 1/10-gap steel-water system as functions of the dimensionless internal flow velocity $\bar{U}_i$; the annular fluid is stagnant and the outer shell rigid.

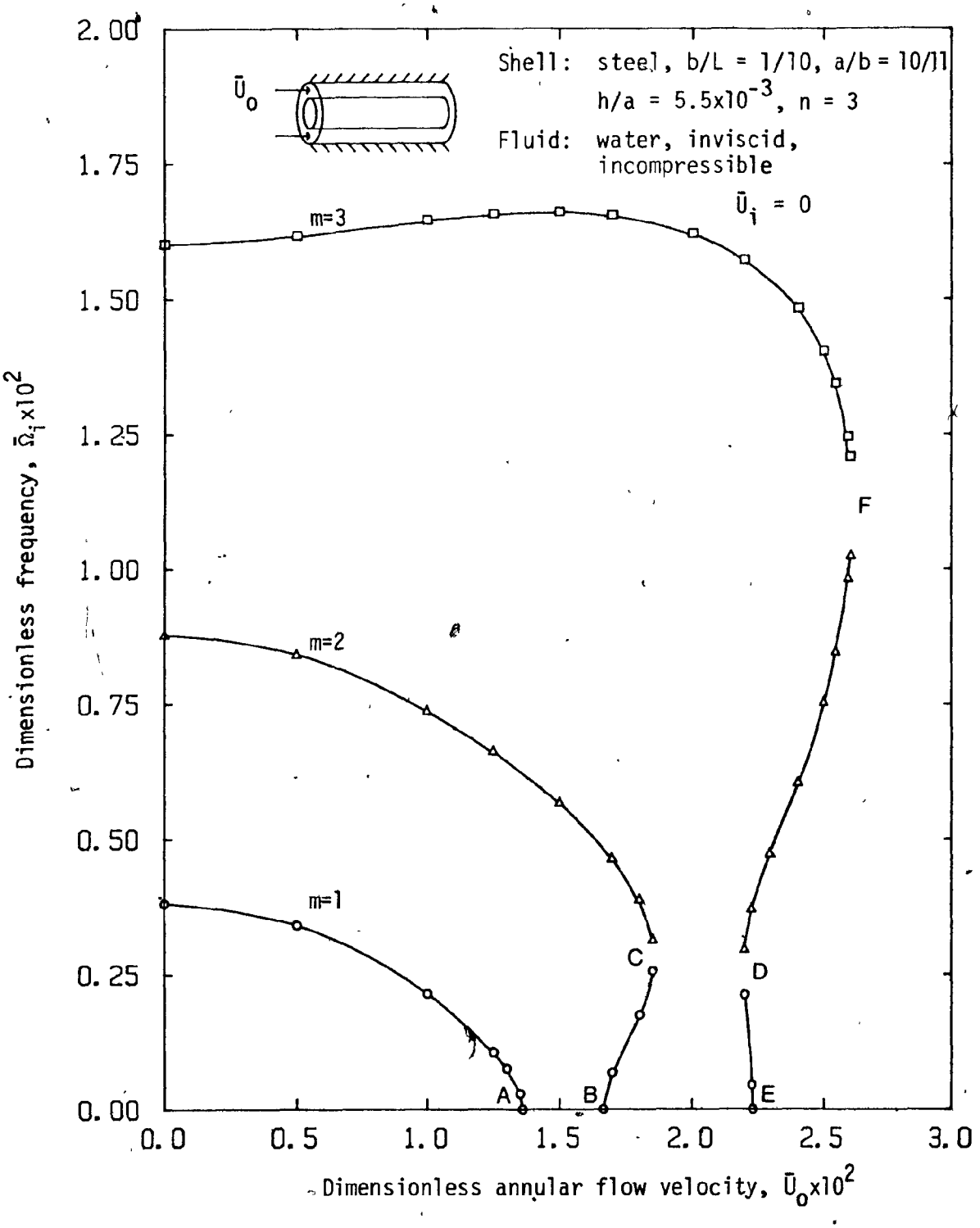

Fig. 11: The real dimensionless eigenfrequencies $\bar{\Omega}_i$ (n=3; m=1,2,3) of the 1/10-gap steel-water system as functions of the dimensionless annular flow velocity $\bar{U}_o$; the fluid in the inner shell is stagnant and the outer shell rigid.

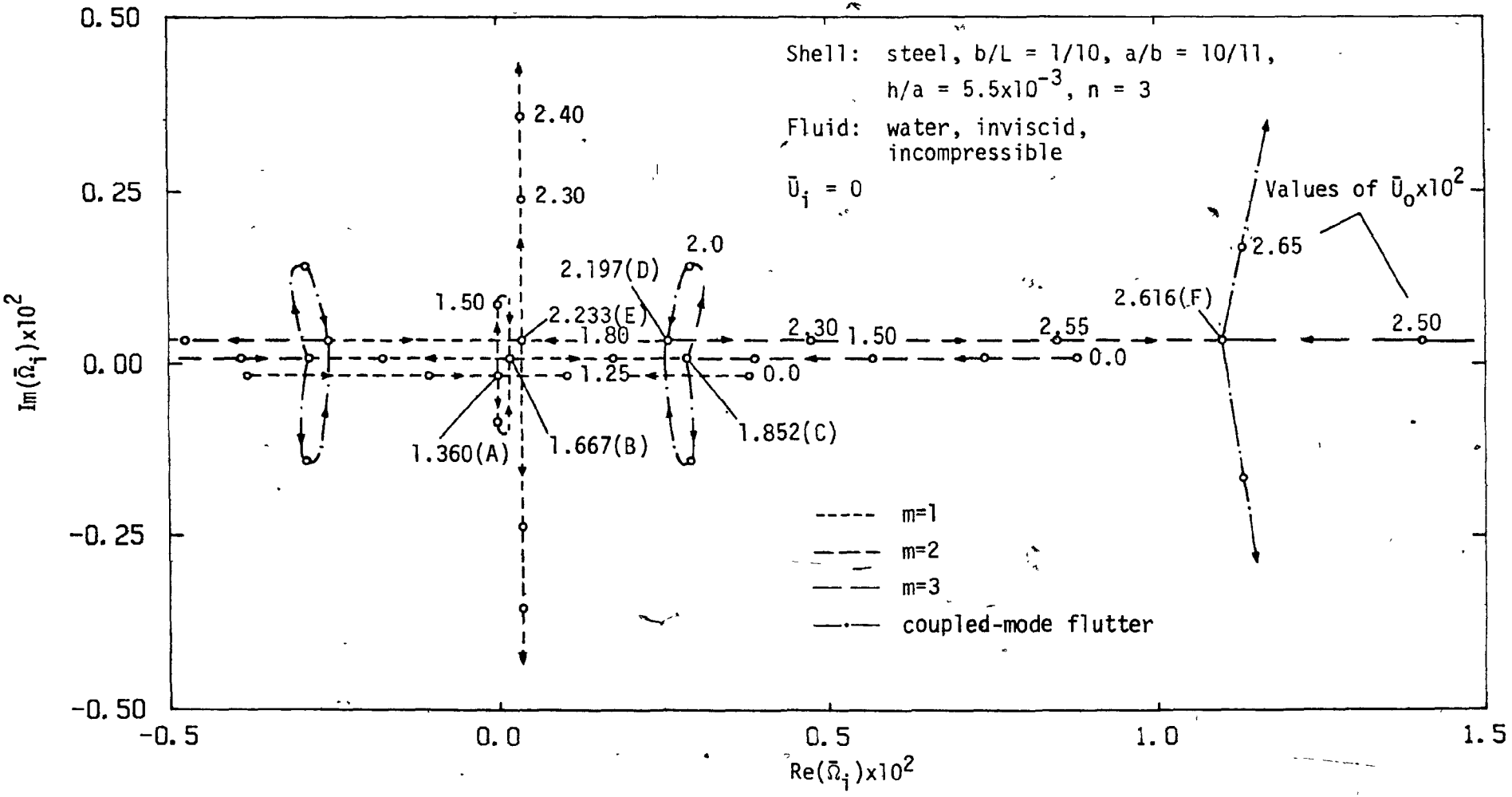

Fig. 12: Argand diagram of the dimensionless eigenfrequencies $\bar{\Omega}_i$ (n=3; m=1,2,3) of the 1/10-gap steel-water system as functions of the dimensionless annular flow velocity $\bar{U}_0$; the fluid in the inner shell is stagnant and the outer shell rigid. The loci on the $\mathrm{Im}(\bar{\Omega}_i) = 0$ and $\mathrm{Re}(\bar{\Omega}_i) = 0$ axes have been drawn off the axes but parallel to them, for clarity. The letters in parentheses correspond to the points shown in the frequency diagram of Fig. 11.

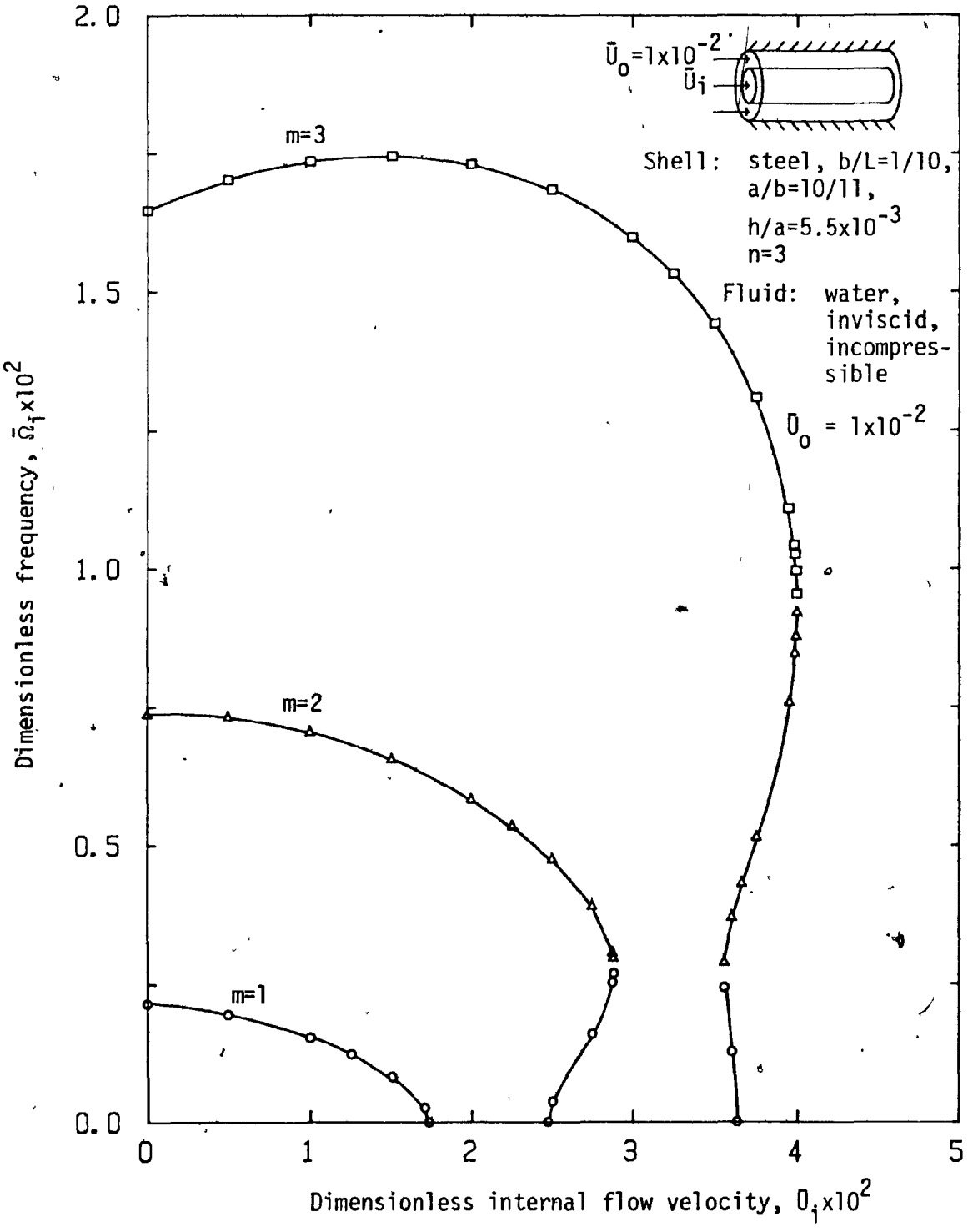

Fig. 13: The real dimensionless eigenfrequencies $\bar{\Omega}_i$ (n=3; m=1,2,3) of the 1/10-gap steel-water system as functions of the dimensionless internal flow velocity $\bar{U}_i$; the outer shell is rigid and the annular flow is constant at $\bar{U}_o = 1 \times 10^{-2}$.

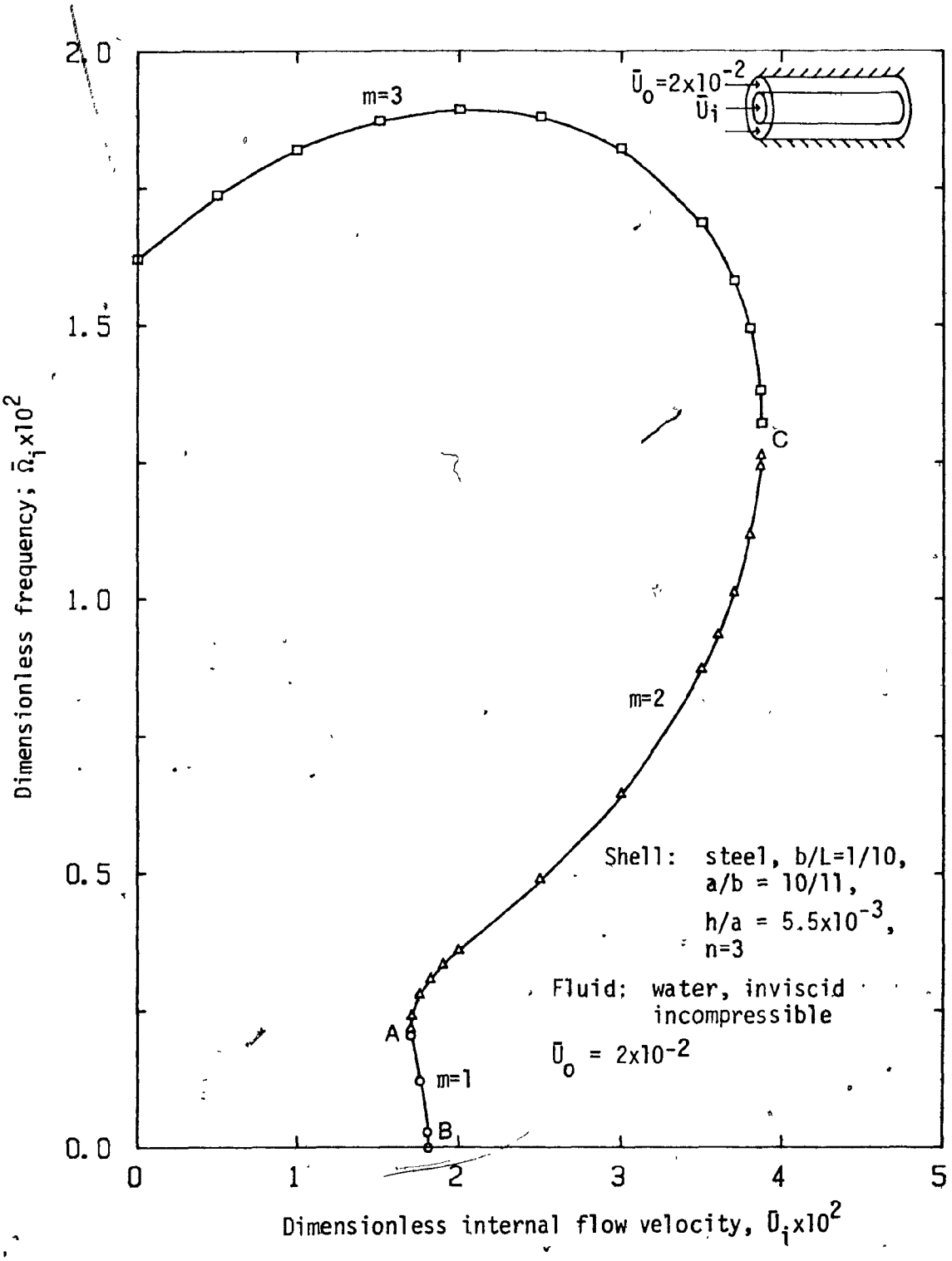

Fig. 14: The real dimensionless eigenfrequencies $\bar{\Omega}_i$ (n=3; m=1,2,3) of the 1/10-gap steel-water system as functions of the dimensionless internal flow velocity $\bar{U}_i$; the outer shell is rigid and the annular flow is constant at $\bar{U}_o = 2\times10^{-2}$.

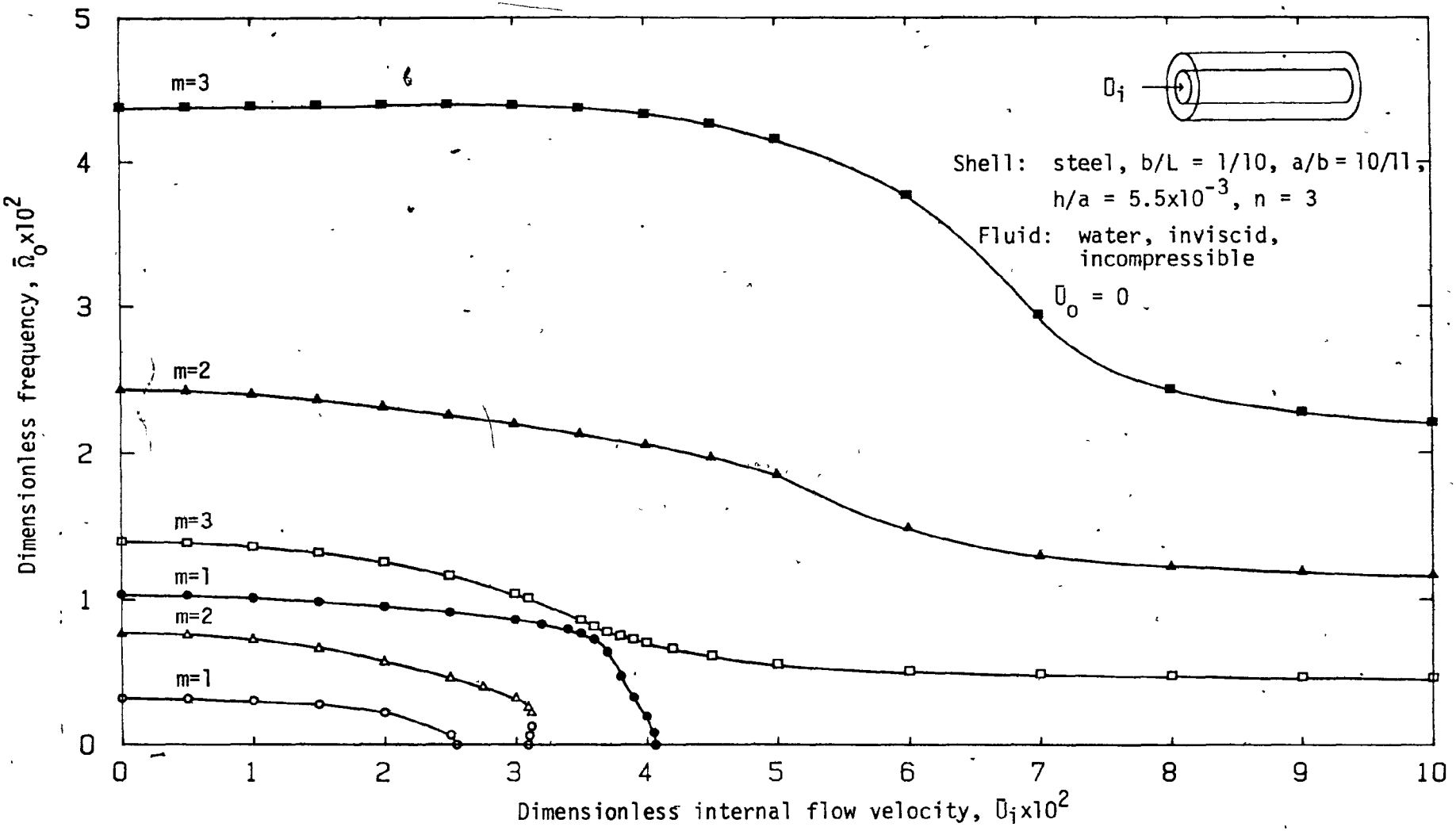

Fig. 15: The real dimensionless eigenfrequencies $\bar{\Omega}_0$ of the 1/10-gap steel-water system as functions of the dimensionless internal flow velocity U_i (n=3; m=1,2,3; open symbols: antisymmetric modes; closed symbols: symmetric modes). Both shells are flexible and the annular fluid is stagnant.

Figures 16, 17: Axial modal shapes of the inner and outer shells of the 1/10-gap steel-water system over half a period.

Shell: steel, b/L = 1/10, a/b = 10/11, both shells flexible

Fluid: water, inviscid, incompressible

$\theta_o = 0$

●	0 period
△	1/10 period†
+	1/5 period
×	3/10 period
◇	2/5 period
▣	1/2 period

†This and the other three small symbols may be indistinct in the Figures because of imperfect duplication.

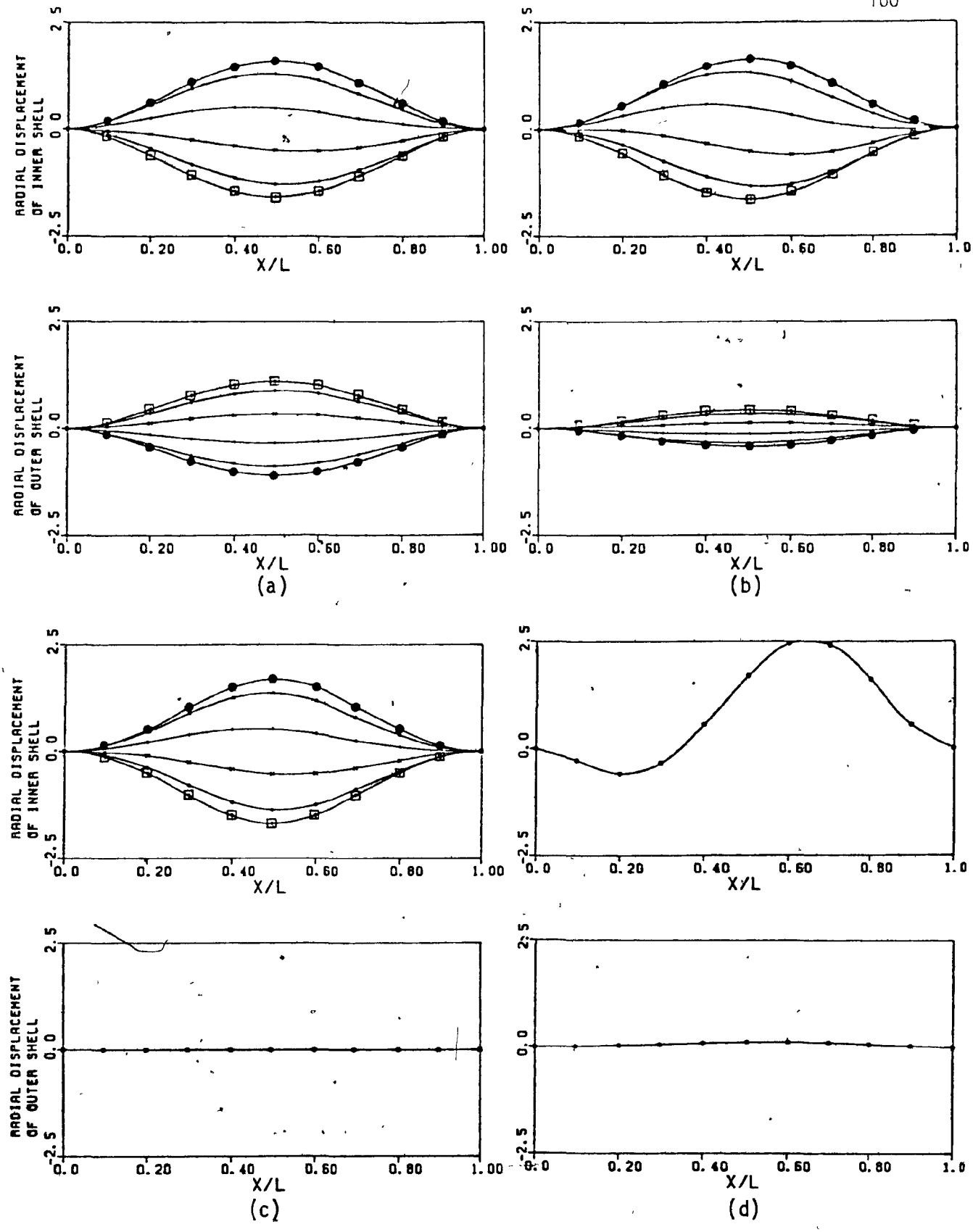

Fig. 16: Axial modal shapes of the inner and outer shells for the n=3, m=1, antisymmetric mode of the 1/10-gap steel-water system of Figure 15, at (a) $\bar{U}_i = 0.010$; (b) $\bar{U}_i = 0.020$, (c) $\bar{U}_i = 0.02530$ (just short of buckling), (d) $\bar{U}_i = 0.030$ (shells have buckled); the annular fluid is stagnant.

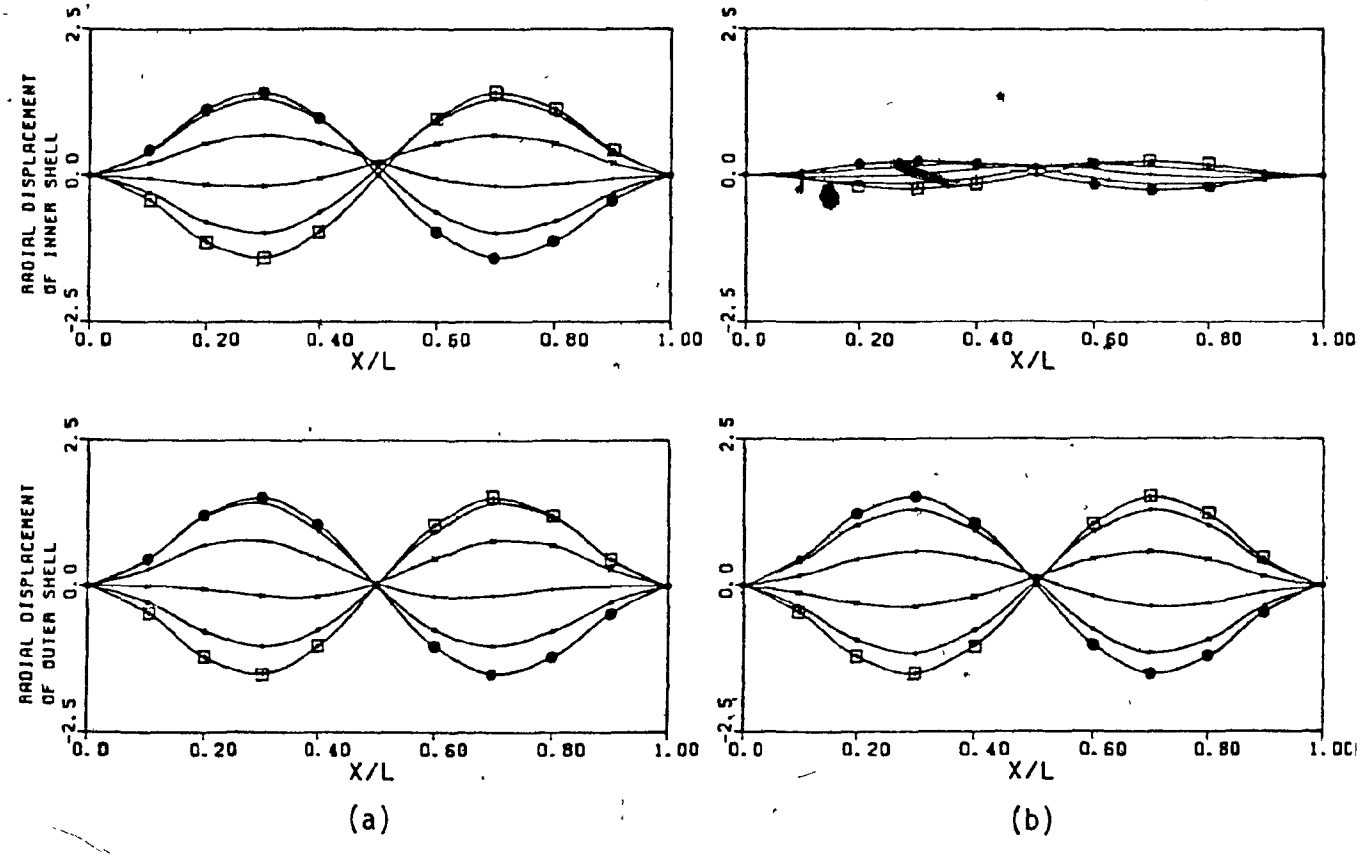

Fig. 17: Axial modal shapes of the inner and outer shells for the n=3, m=2, symmetric mode of the 1/10-gap steel-water system of Figure 15, at (a) $\bar{U}_i$ = 0.010, (b) $\bar{U}_i$ = 0.090 (vibration amplitude of the inner shell is relatively small (*cf.* outer shell) in high internal flow); the annular fluid is stagnant.

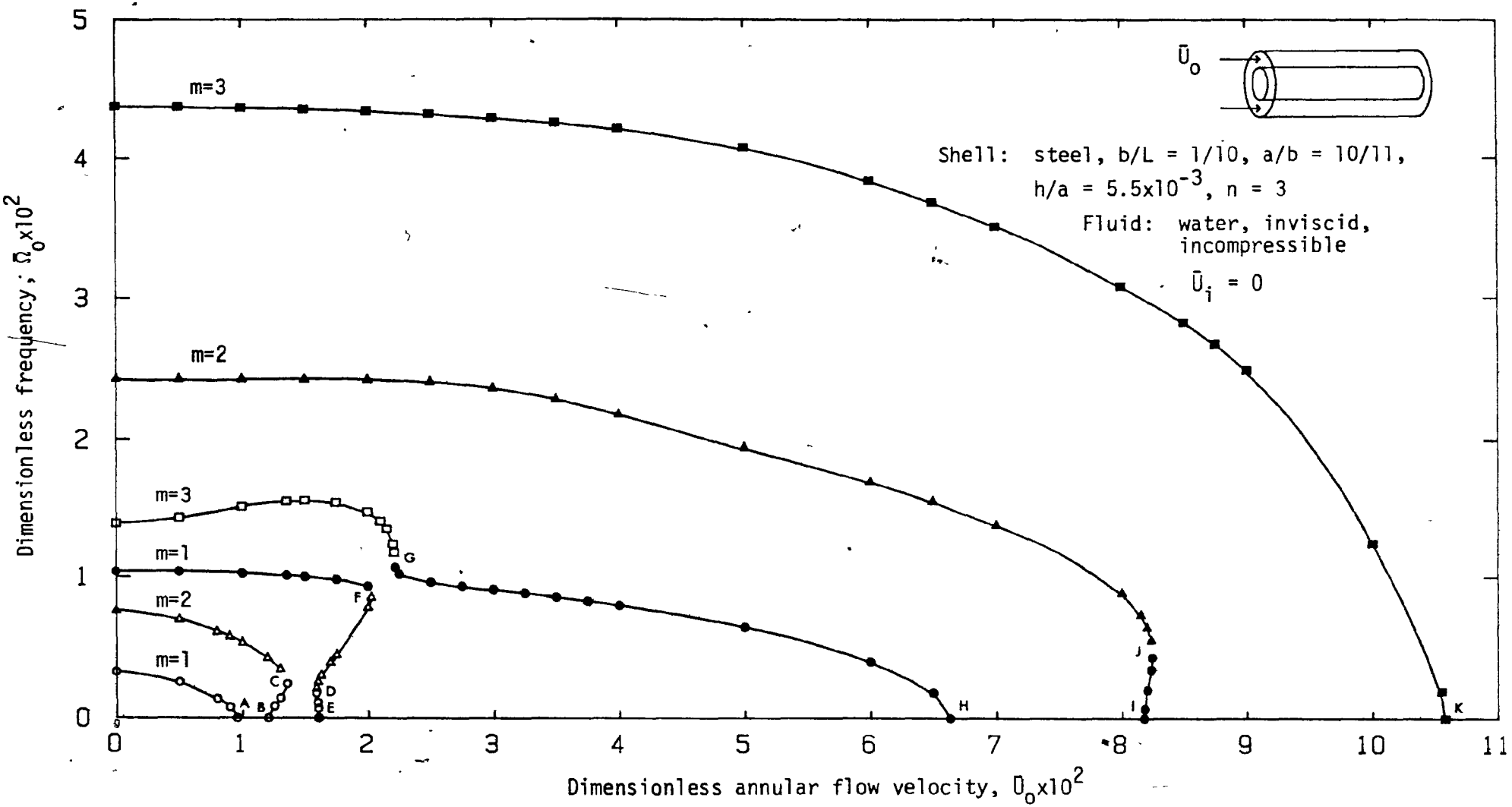

Fig. 18: The real dimensionless eigenfrequencies $\bar{\Omega}_o$ of the 1/10-gap steel-water system as functions of the dimensionless annular flow velocity $\bar{U}_o$ (n=3; m=1,2,3; open symbols: antisymmetric modes; closed symbols: symmetric modes). Both shells are flexible and the fluid in the inner shell is stagnant.

Figures 19, 20: Axial modal shapes of the inner and outer shells of the 1/10-gap steel-water system over half a period.

Shell: steel, b/L = 1/10, a/b = 10/11, both shells flexible

Fluid: water, inviscid, incompressible

$D_i = 0$

●	0 period
△	1/10 period†
+	1/5 period
×	3/10 period
◇	2/5 period
⧈	1/2 period

†This and the other three small symbols may be indistinct in the Figures because of imperfect duplication.

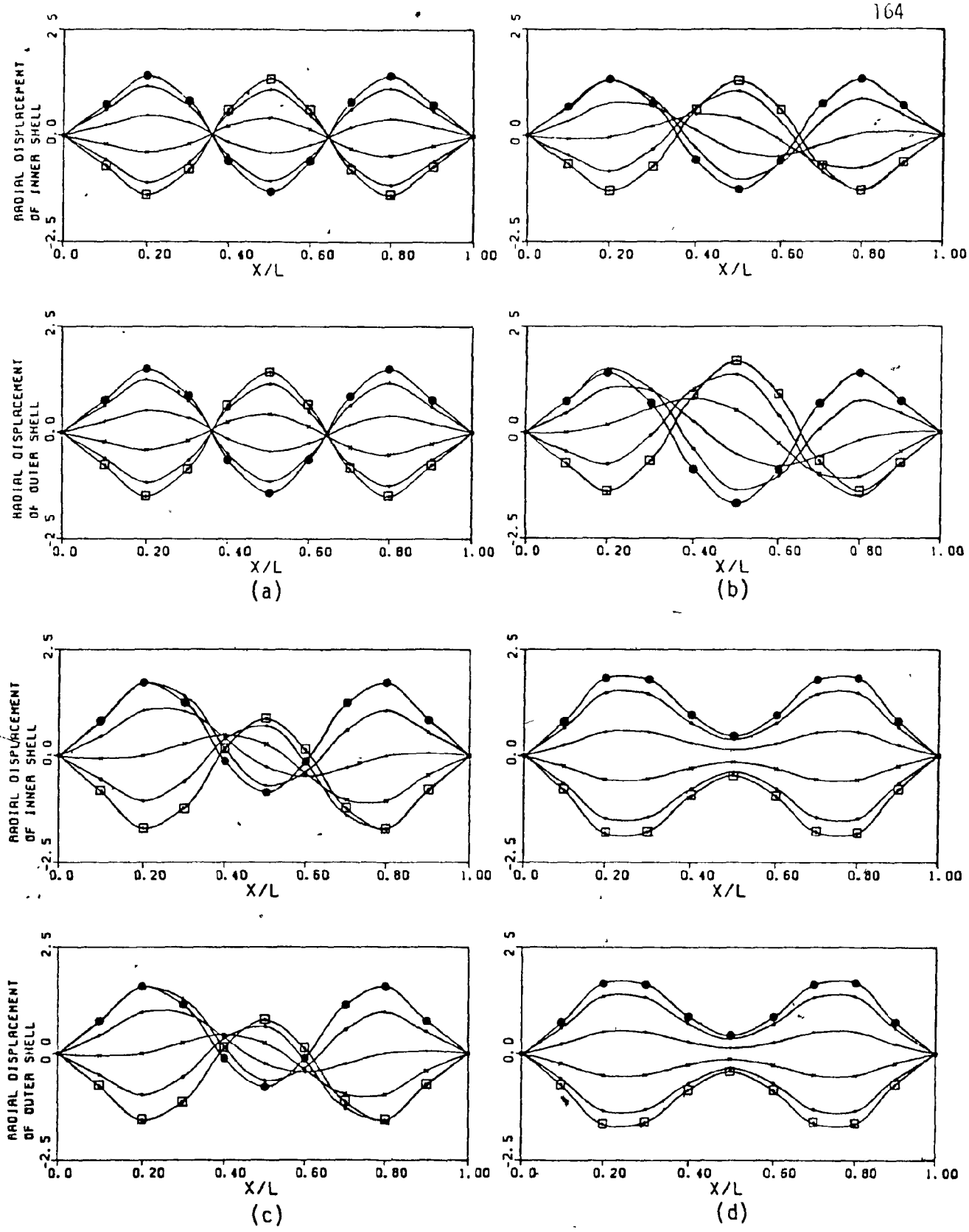

Fig. 19: Axial modal shapes of the inner and outer shells for the n=3, m=3 symmetric mode of the 1/10-gap steel-water system of Figure 16, at (a) $\bar{U}_0 = 0.0050$, (b) $\bar{U}_0 = 0.050$, (c) $\bar{U}_0 = 0.10$, (d) $\bar{U}_0 = 0.10575$; the fluid in the inner shell is stagnant.

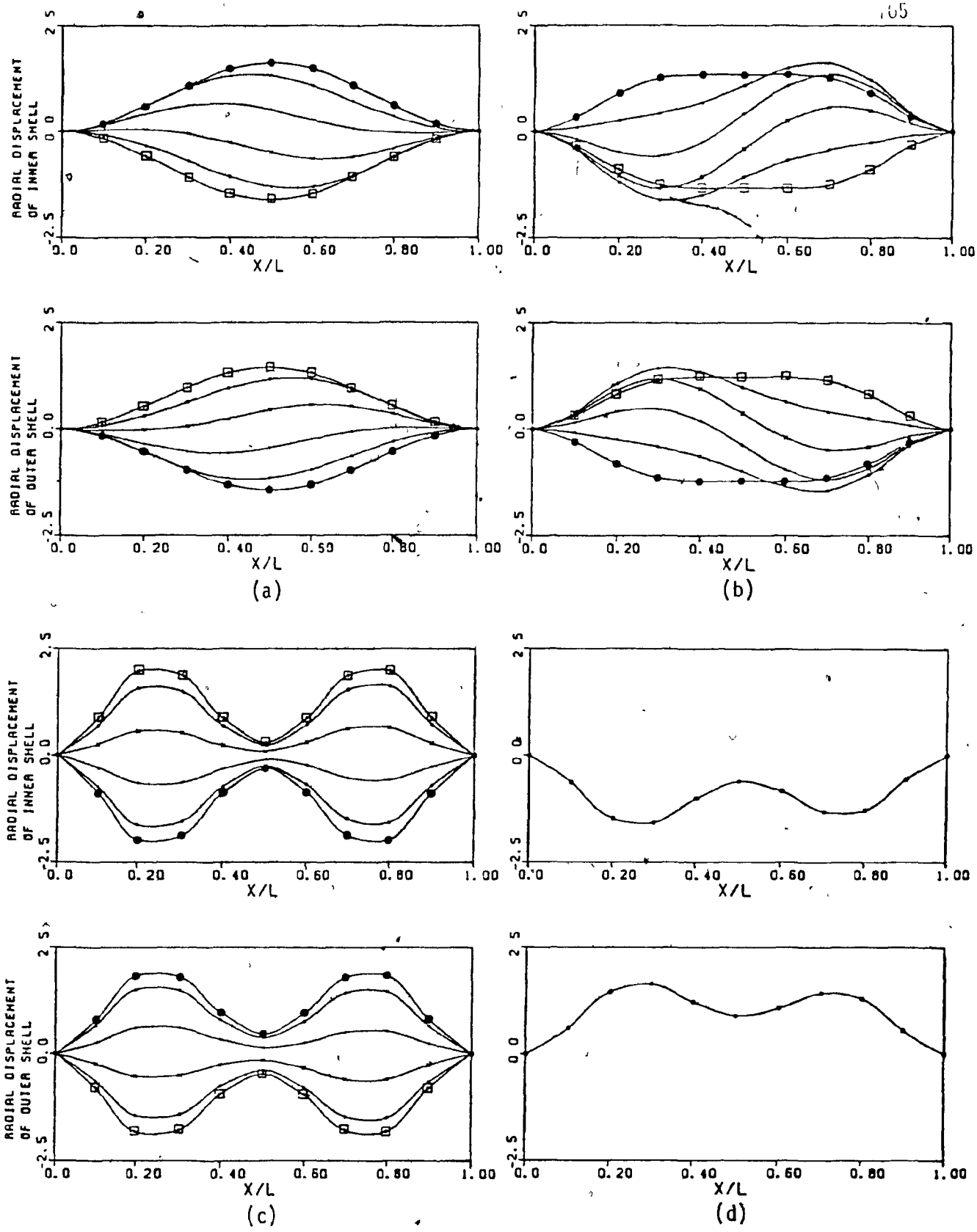

Fig. 20: Axial modal shapes of the inner and outer shells of the n=3, m=1, antisymmetric mode of the 1/10-gap steel-water system of Figure 16, at (a) $\bar{U}_0$ = 0.0050, (b) $\bar{U}_0$ = 0.01355, (c) $\bar{U}_0$ = 0.01602 (just short of buckling), (d) $\bar{U}_0$ = 0.0175 (shells have buckled); the fluid in the inner shell is stagnant.

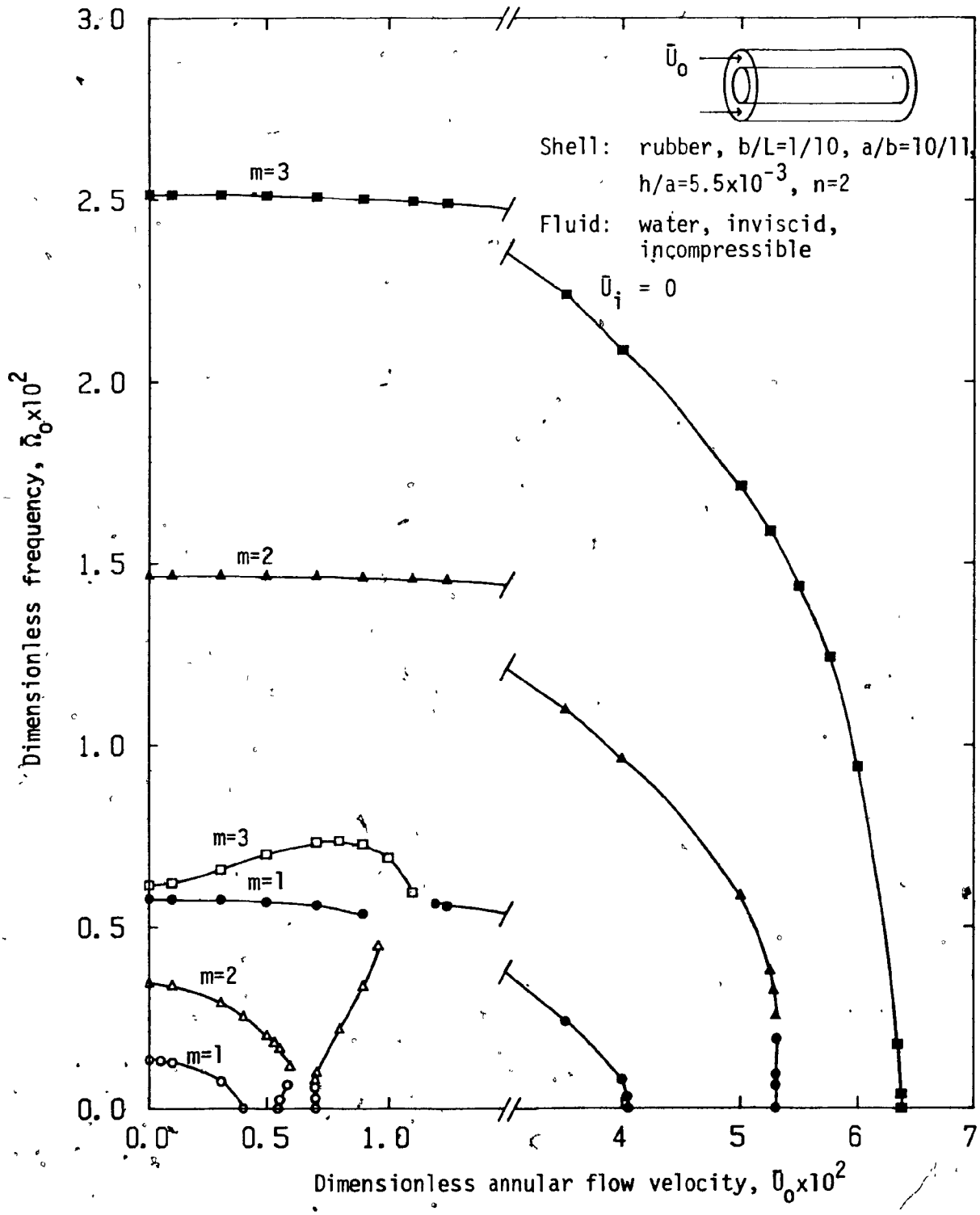

Fig. 21: The real dimensionless eigenfrequencies $\bar{\Omega}_o$ of the 1/10-gap rubber-water system (shell dimensions correspond to those of a steel-shell system) as functions of the dimensionless annular flow velocity $\bar{U}_o$ (n=2; m=1,2,3; open symbols: antisymmetric modes; closed symbols: symmetric modes). Both shells are flexible and the fluid in the inner shell is stagnant.

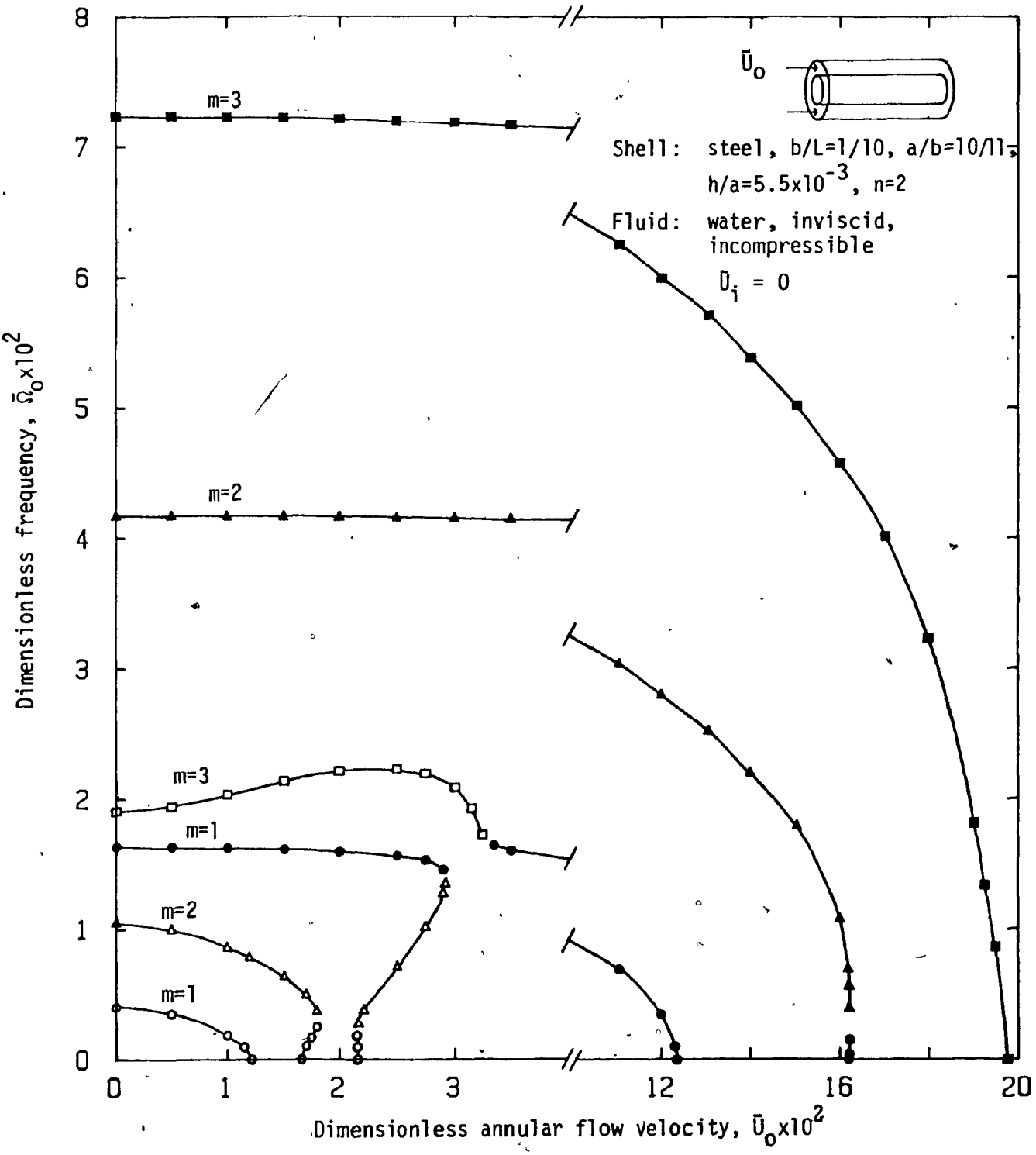

Fig. 22: The real dimensionless eigenfrequencies $\bar{\Omega}_o$ of the 1/10-gap steel-water system as functions of the dimensionless annular flow velocity $\bar{U}_o$ (n=2; m=1,2,3; open symbols: antisymmetric modes; closed symbols: symmetric modes). Both shells are flexible and the fluid in the inner shell is stagnant.

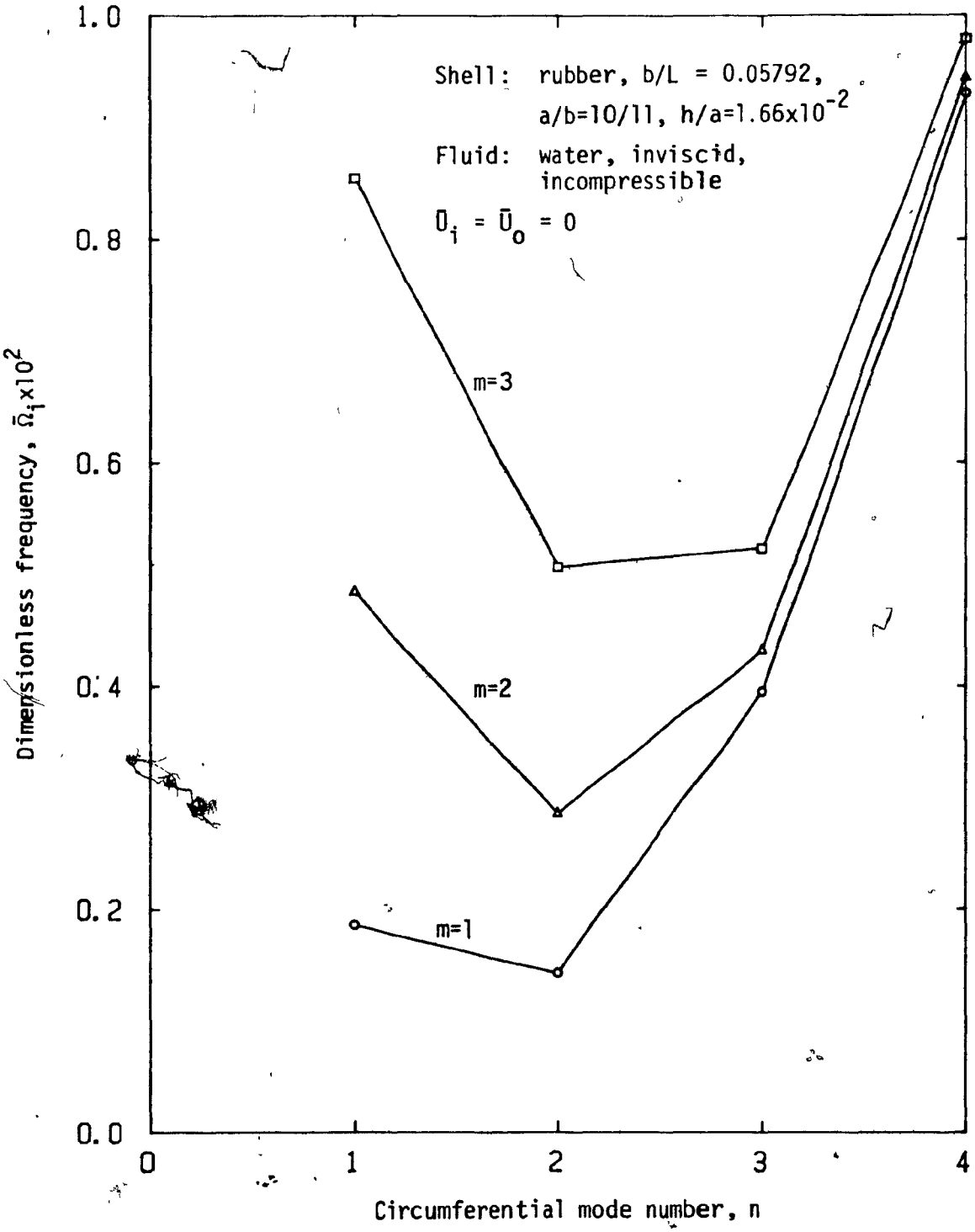

Fig. 23: The dimensionless eigenfrequencies $\bar{\Omega}_i$ (m=1,2,3) of the 1/10-gap rubber-water system at zero internal and annular flows, as functions of the circumferential mode number n; the outer shell is rigid.

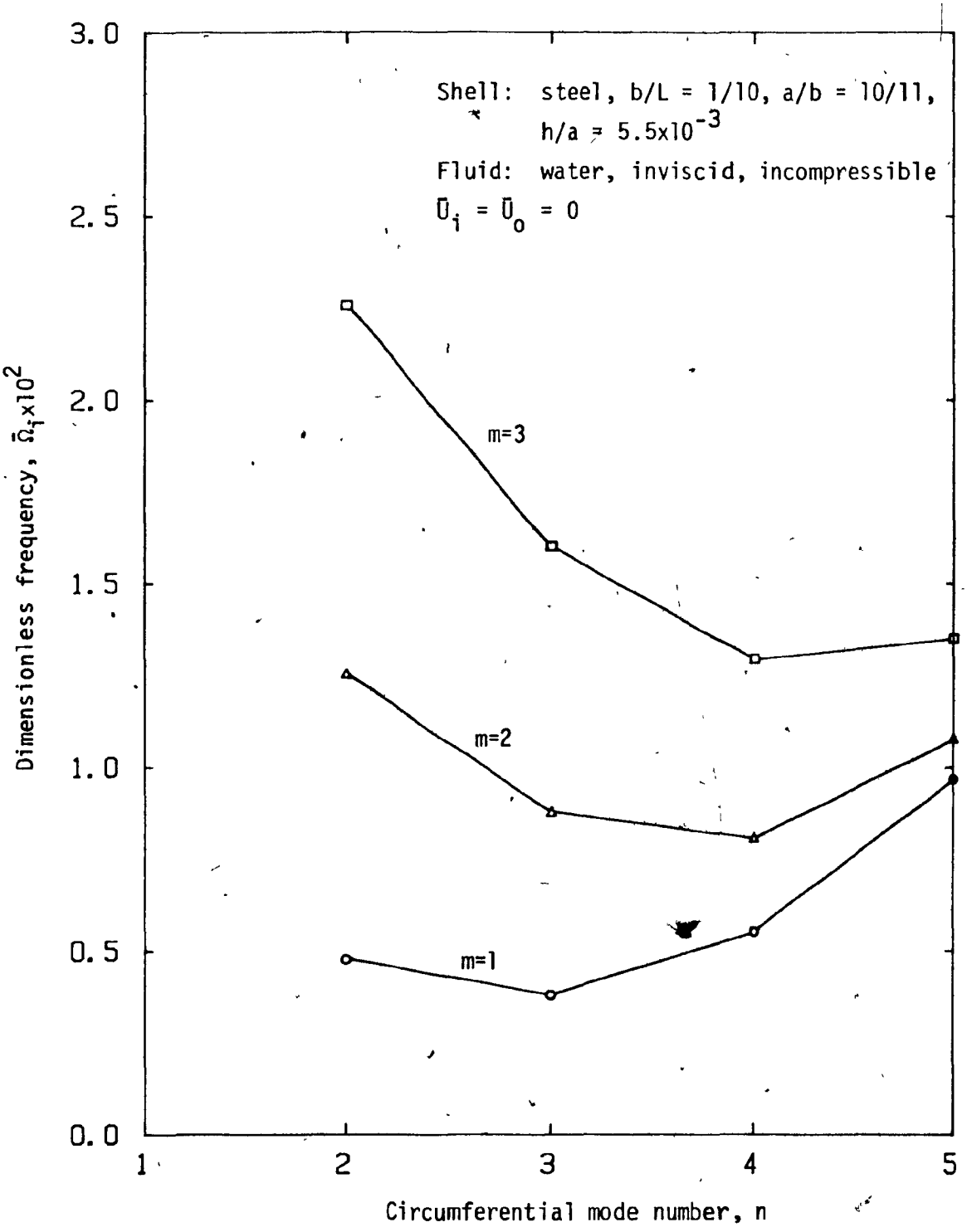

Fig. 24: The dimensionless eigenfrequencies $\bar{\Omega}_i$ (m=1,2,3) of the 1/10-gap steel-water system at zero internal and annular flows, as functions of the circumferential mode number n; the outer shell is rigid.

Figures 25, 26: Inviscid compressible flow results.

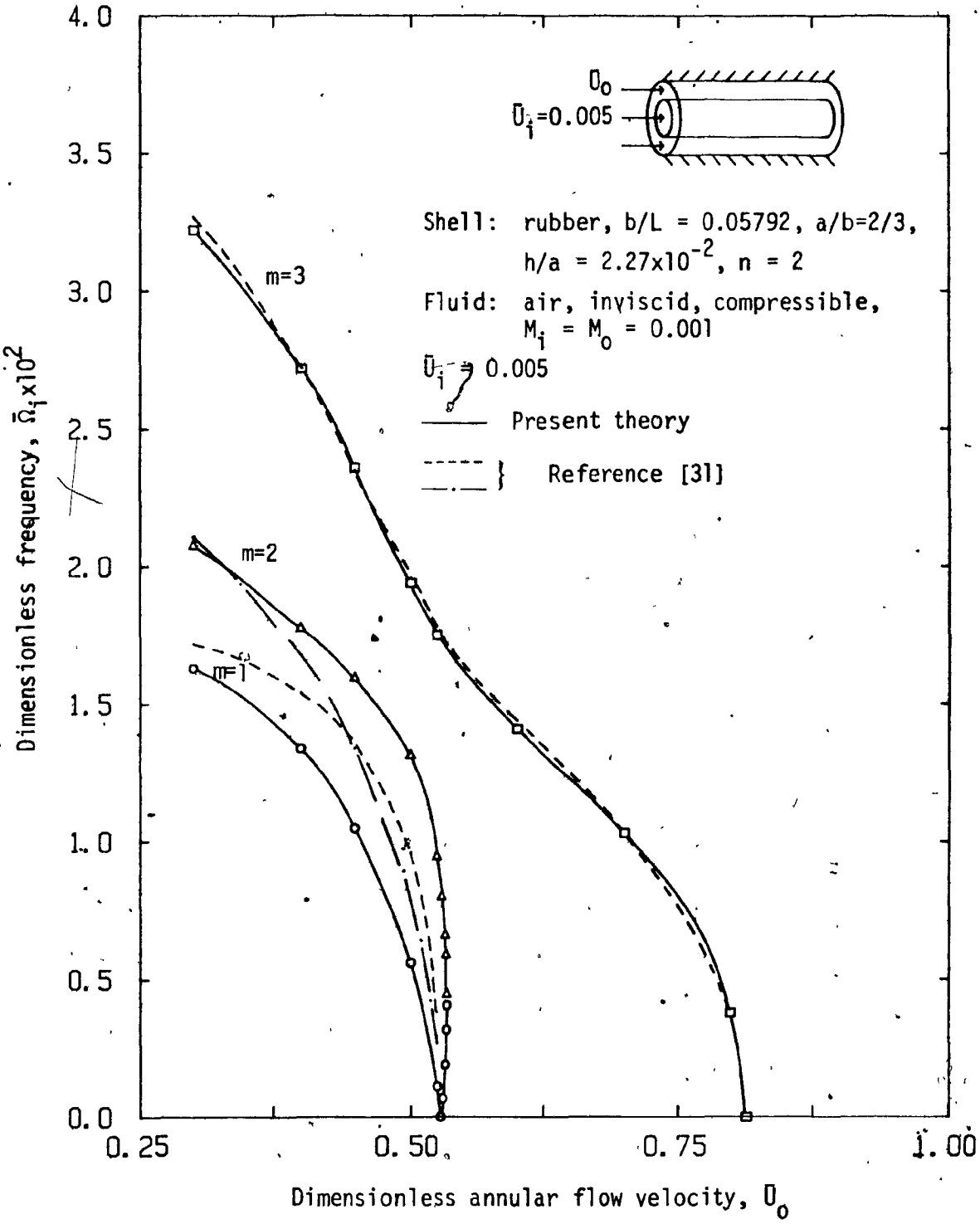

Fig. 25: The real dimensionless eigenfrequencies $\bar{\Omega}_i$ (n=2; m=1,2,3) of the ½-gap rubber-air system conveying *compressible fluids* ($M_i=M_o=0.001$), as functions of the dimensionless annular flow velocity U_o; the internal flow is small and constant at U_i = 0.005, and the outer shell is rigid.

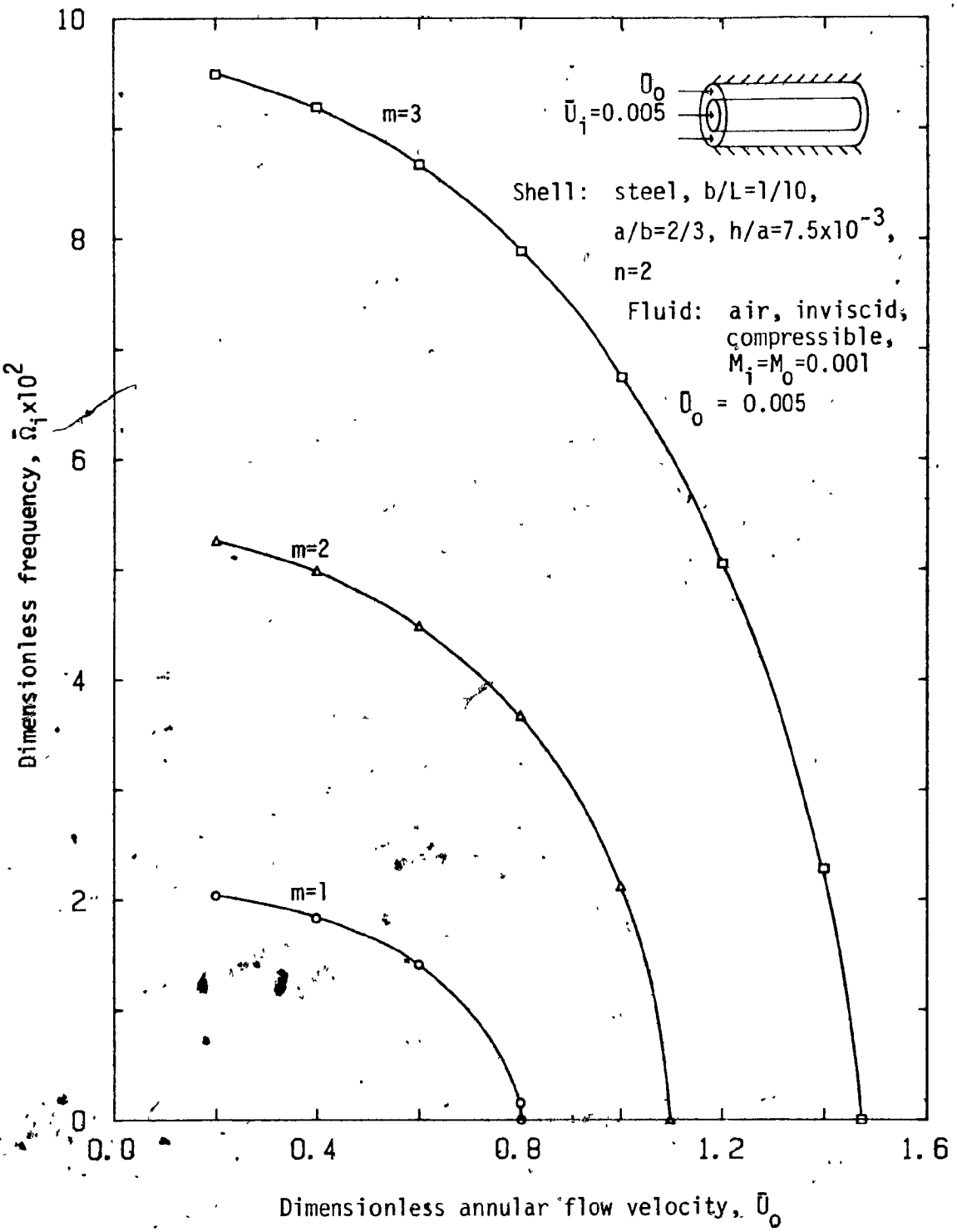

Fig. 26: The real dimensionless eigenfrequencies $\bar{\Omega}_i$ (n=2; m=1,2,3) of the ½-gap steel-air system conveying *compressible fluids* ($M_i=M_o$=0.001), as functions of the dimensionless annular flow velocity $\bar{U}_o$; the internal flow is small and constant at $\bar{U}_i$ = 0.005, and the outer shell is rigid.

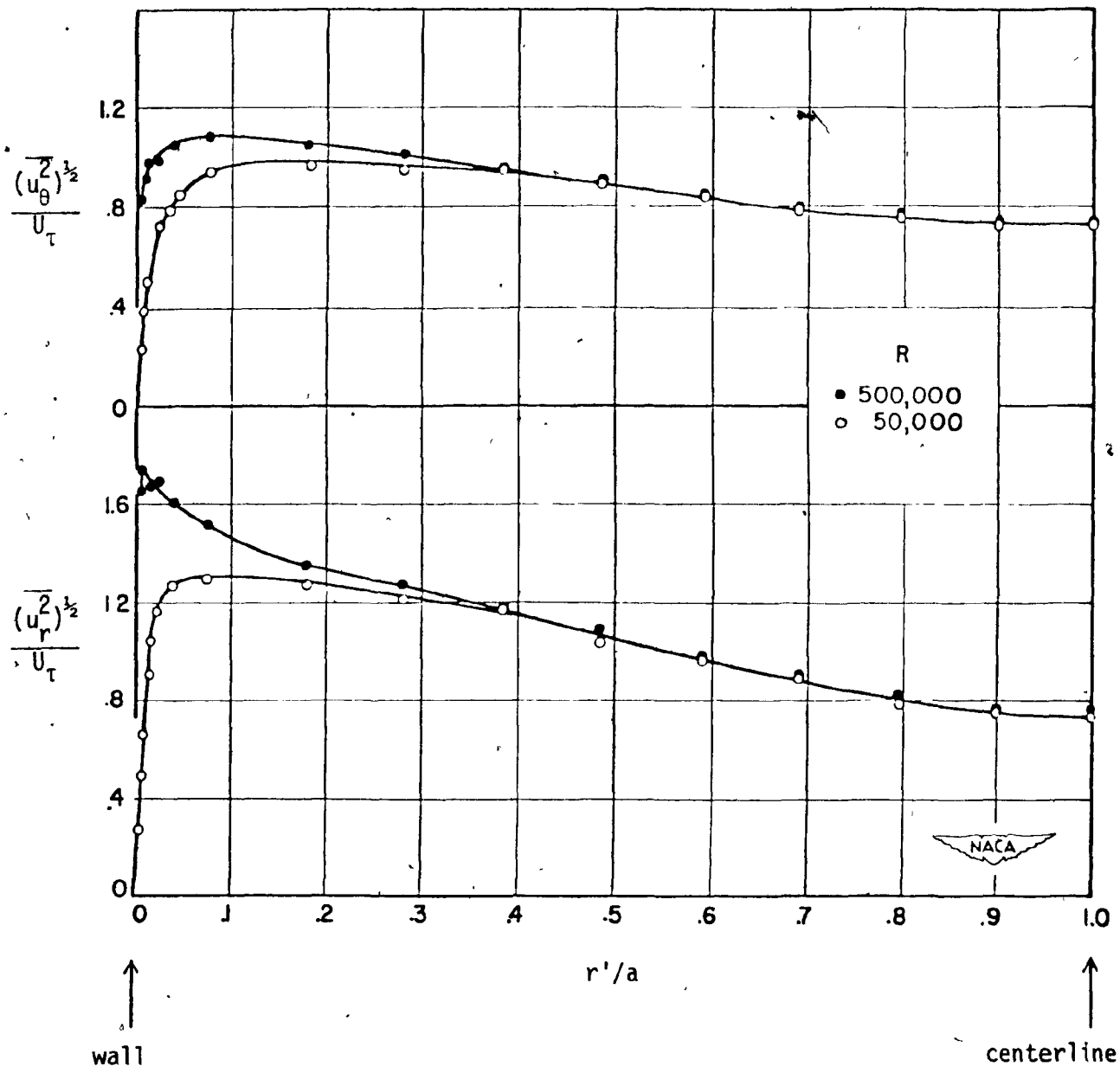

Fig. 27: Distributions of $\overline{u_\theta^2}$ and $\overline{u_r^2}$ across a circular pipe of radius a (from J. Laufer [38]); R is the Reynolds number, U_τ is the shear velocity and r' = a-r.

Figures 28-34: Viscous incompressible flow results.

Remarks: U_f is the flow velocity at which coupled-mode flutter occurs; P_{iL}, P_{oL} are, respectively, the internal and annular gauge pressures at the x=L end.

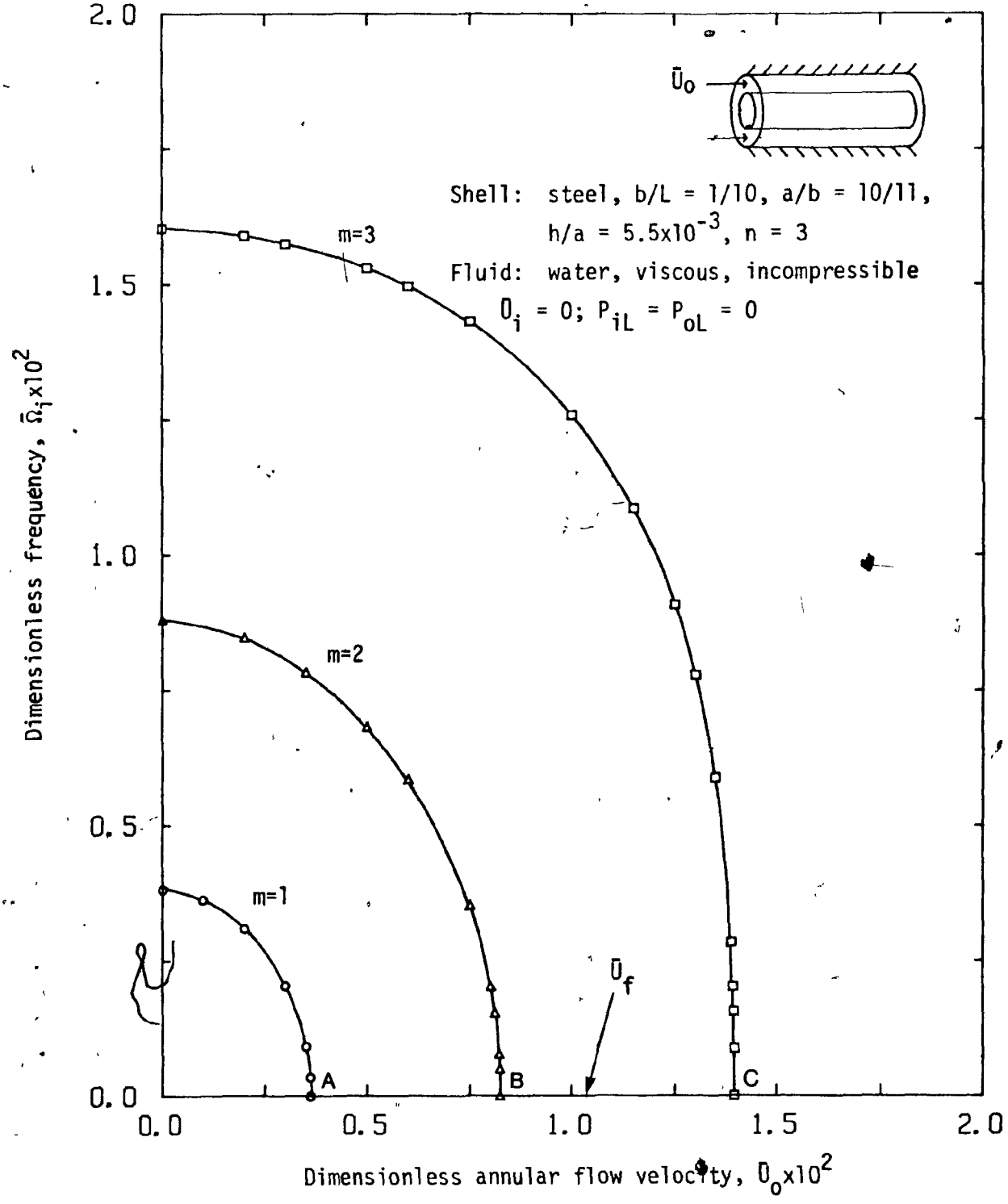

Fig. 28: The real dimensionless eigenfrequencies $\bar{\Omega}_i$ (n=3; m=1,2,3) of the 1/10-gap steel-water system conveying *incompressible viscous fluid*, as functions of the dimensionless annular flow velocity $\bar{U}_0$; the fluid in the inner shell is stagnant and the outer shell rigid.

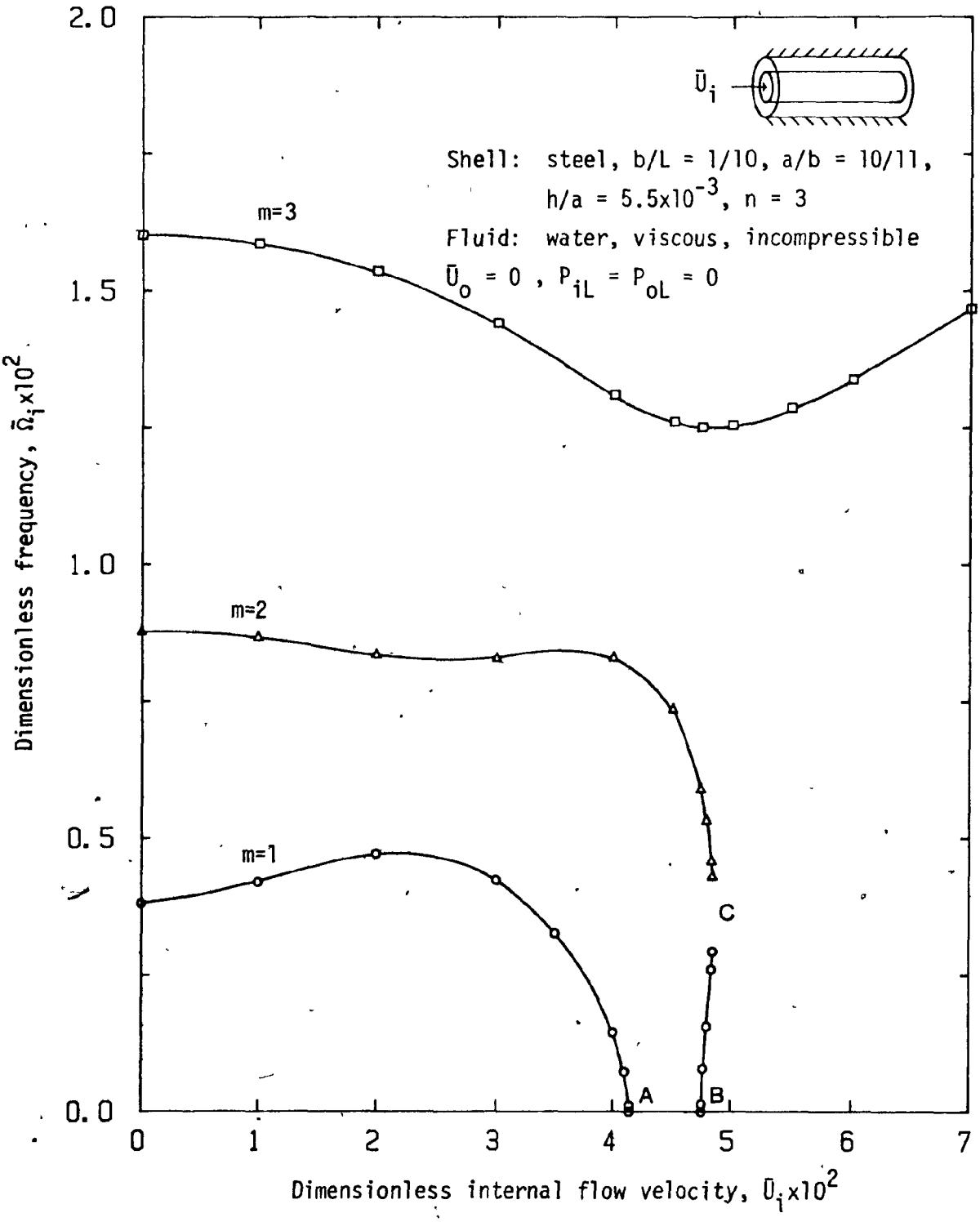

Fig. 29: The real dimensionless eigenfrequencies $\bar{\Omega}_i$ (n=3; m=1,2,3) of the 1/10-gap steel-water system conveying *incompressible viscous fluid*, as functions of the dimensionless internal flow velocity $\bar{U}_i$; the annular fluid is stagnant and the outer shell rigid.

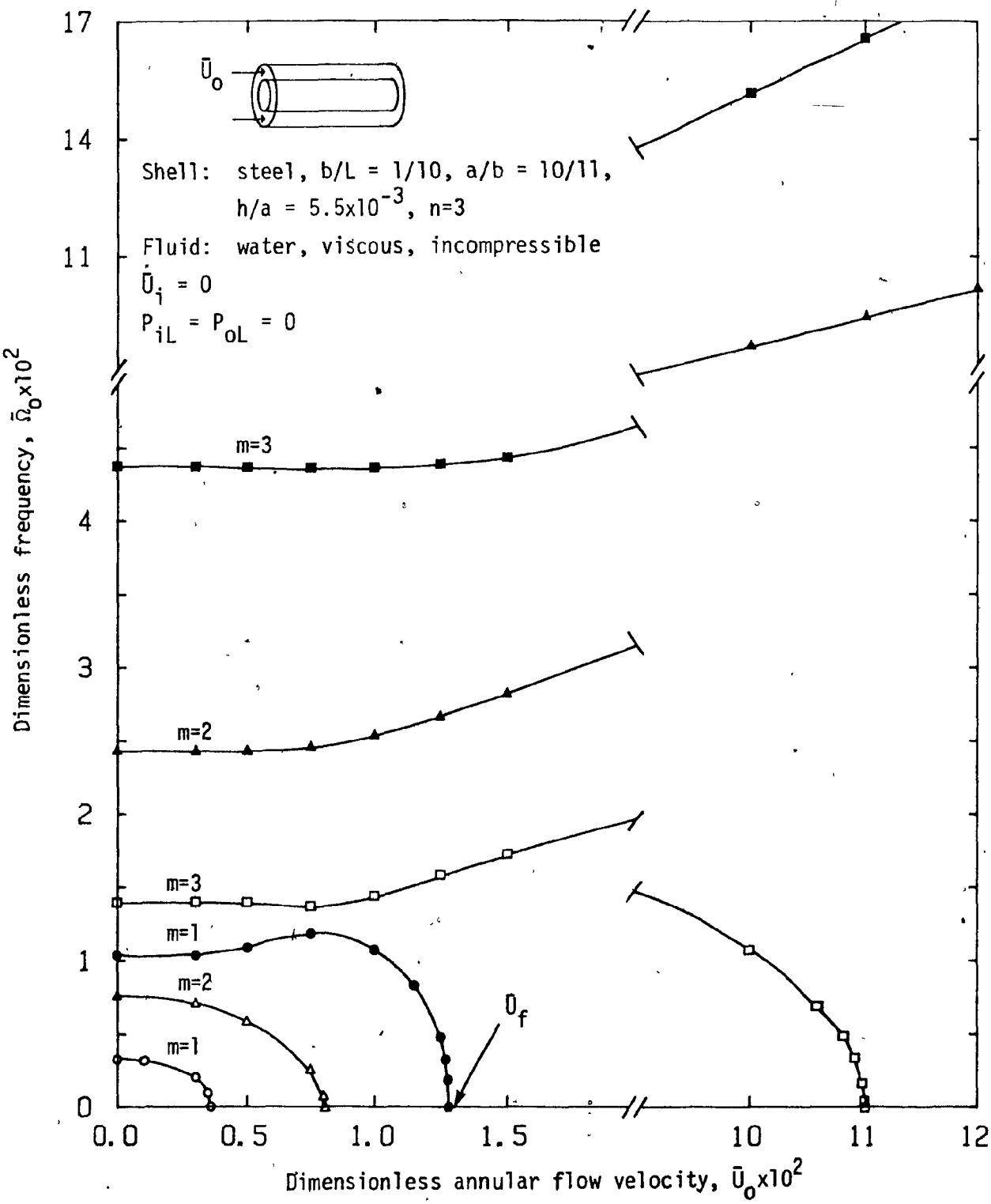

Fig. 30: The real dimensionless eigenfrequencies $\bar{\Omega}_o$ of the 1/10-gap steel-water system conveying *incompressible viscous fluid*, as functions of the dimensionless annular flow velocity U_o (n=3; m=1,2,3; open symbols: antisymmetric modes; closed symbols: symmetric modes). Both shells are flexible and the fluid in the inner shell is stagnant.

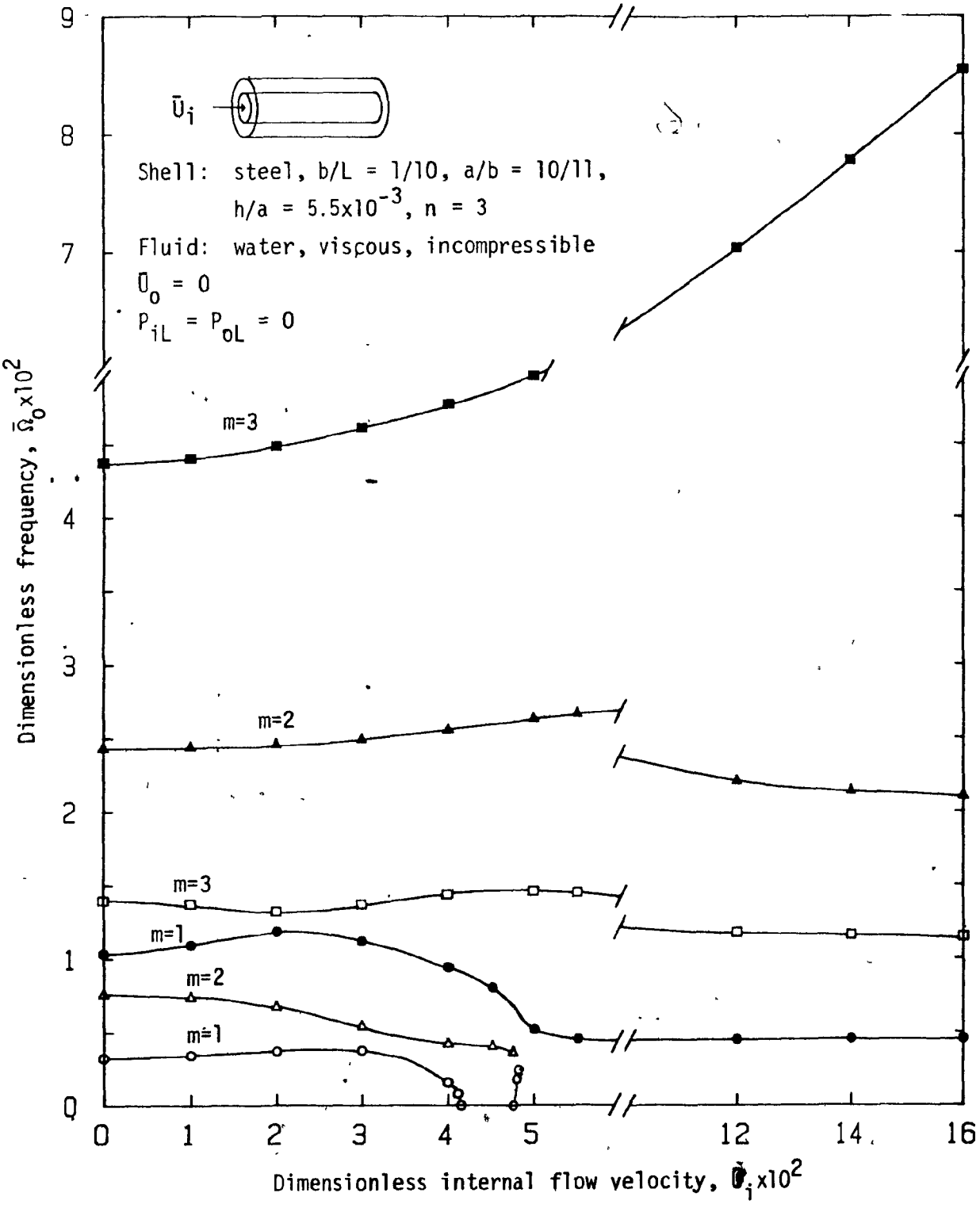

Fig. 31: The real dimensionless eigenfrequencies $\bar{\Omega}_o$ of the 1/10-gap steel-water system conveying *incompressible viscous fluid*, as functions of the dimensionless internal flow velocity $\bar{U}_i$ (n=3; m=1,2,3; open symbols: antisymmetric modes; closed symbols: symmetric modes). Both shells are flexible and the annular fluid is stagnant.

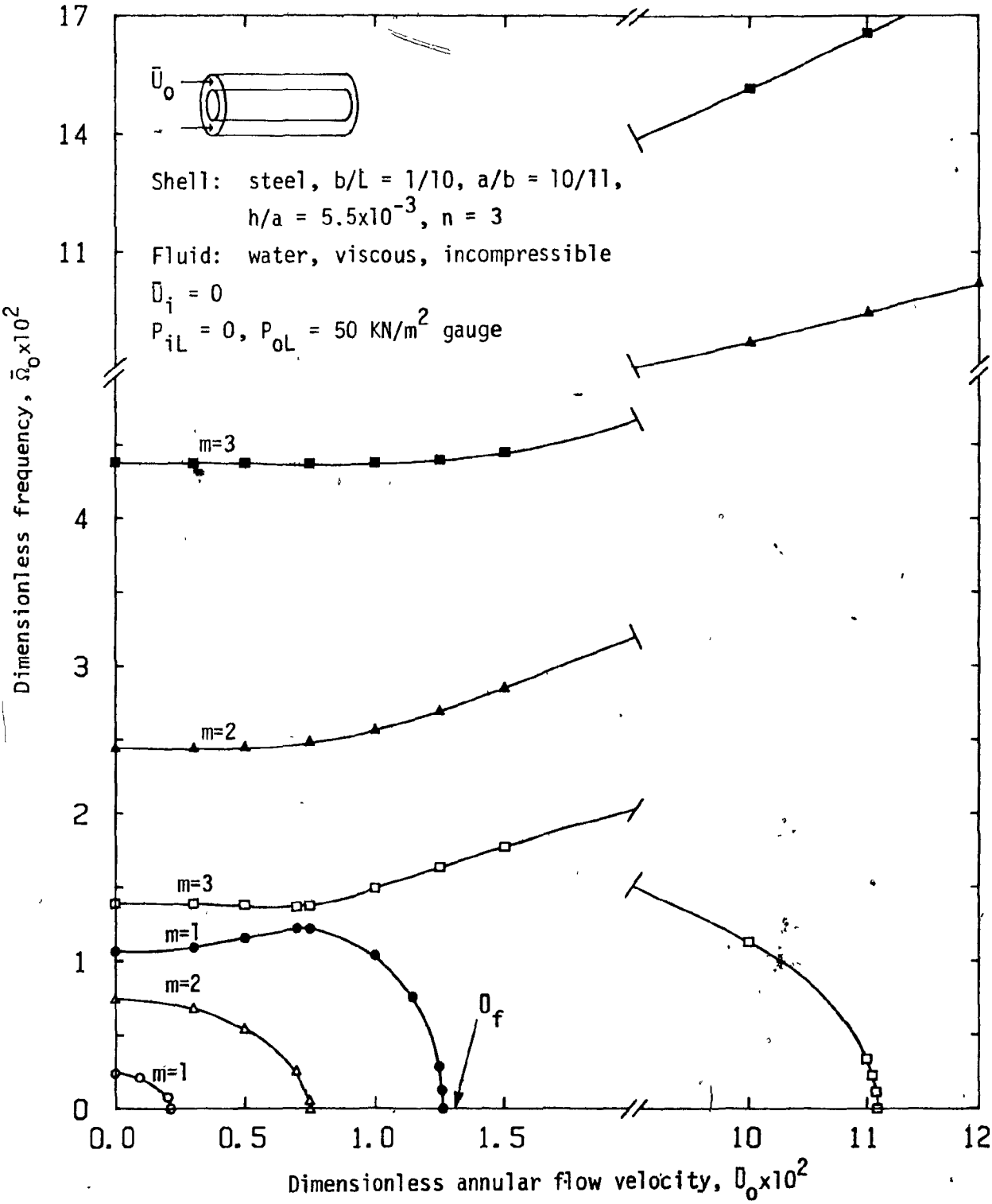

Fig. 32: The real dimensionless eigenfrequencies $\bar{\Omega}_o$ of the 1/10-gap steel-water system conveying *incompressible, viscous, excessively pressurized fluid*, as functions of the dimensionless annular flow velocity U_o (n=3; m=1,2,3; open symbols: antisymmetric modes; closed symbols: symmetric modes). Both shells are flexible, the internal fluid is stagnant and only the annular fluid is pressurized additionally.

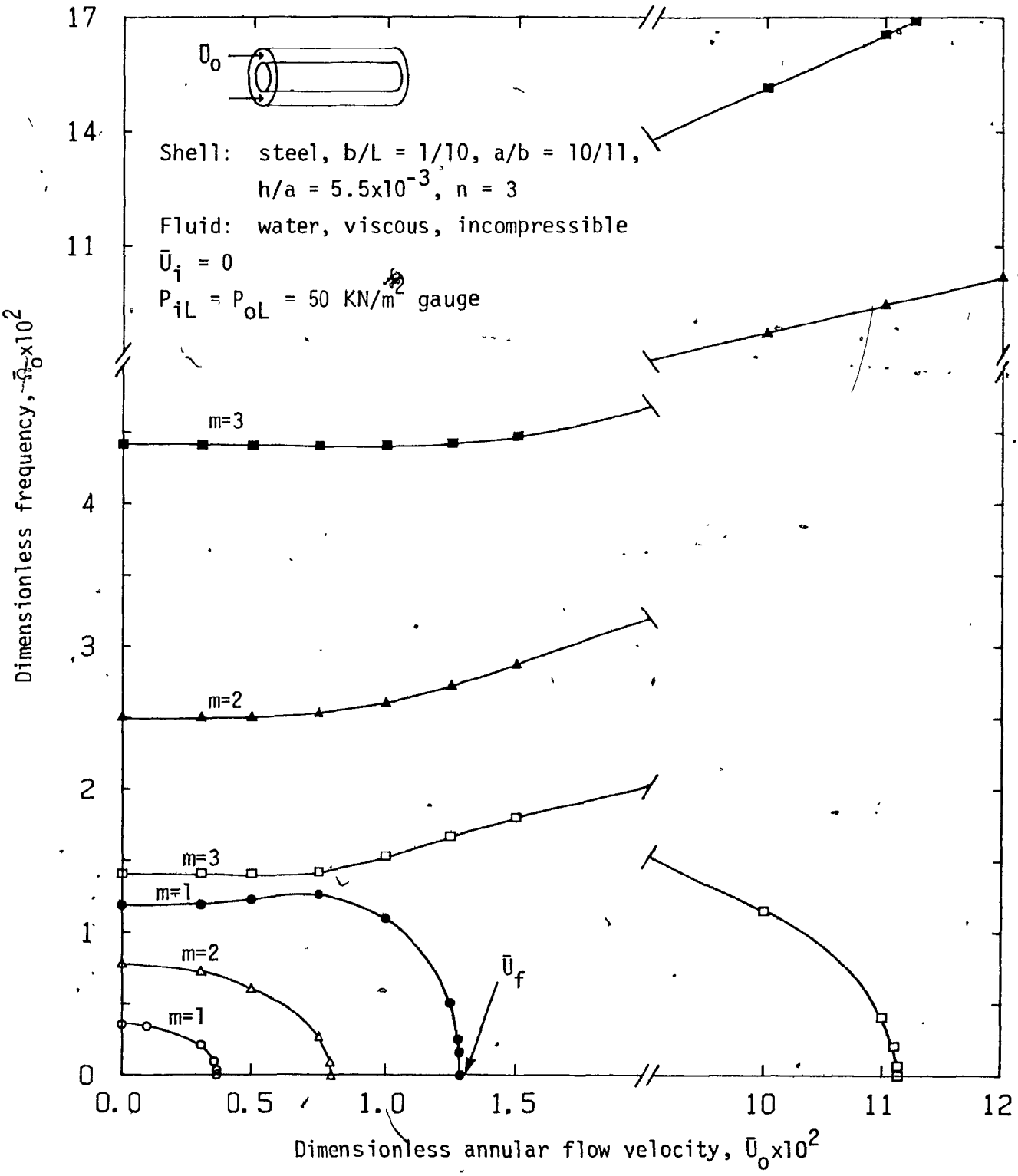

Fig. 33: The real dimensionless eigenfrequencies $\bar{\Omega}_o$ of the 1/10-gap steel-water system conveying *incompressible, viscous, excessively pressurized fluid*, as functions of the dimensionless annular flow velocity $\bar{U}_o$ (n=3; m=1,2,3; open symbols: antisymmetric mode; closed symbols: symmetric modes). Both shells are flexible, the internal fluid is stagnant and both the internal and annular fluids are excessively pressurized.

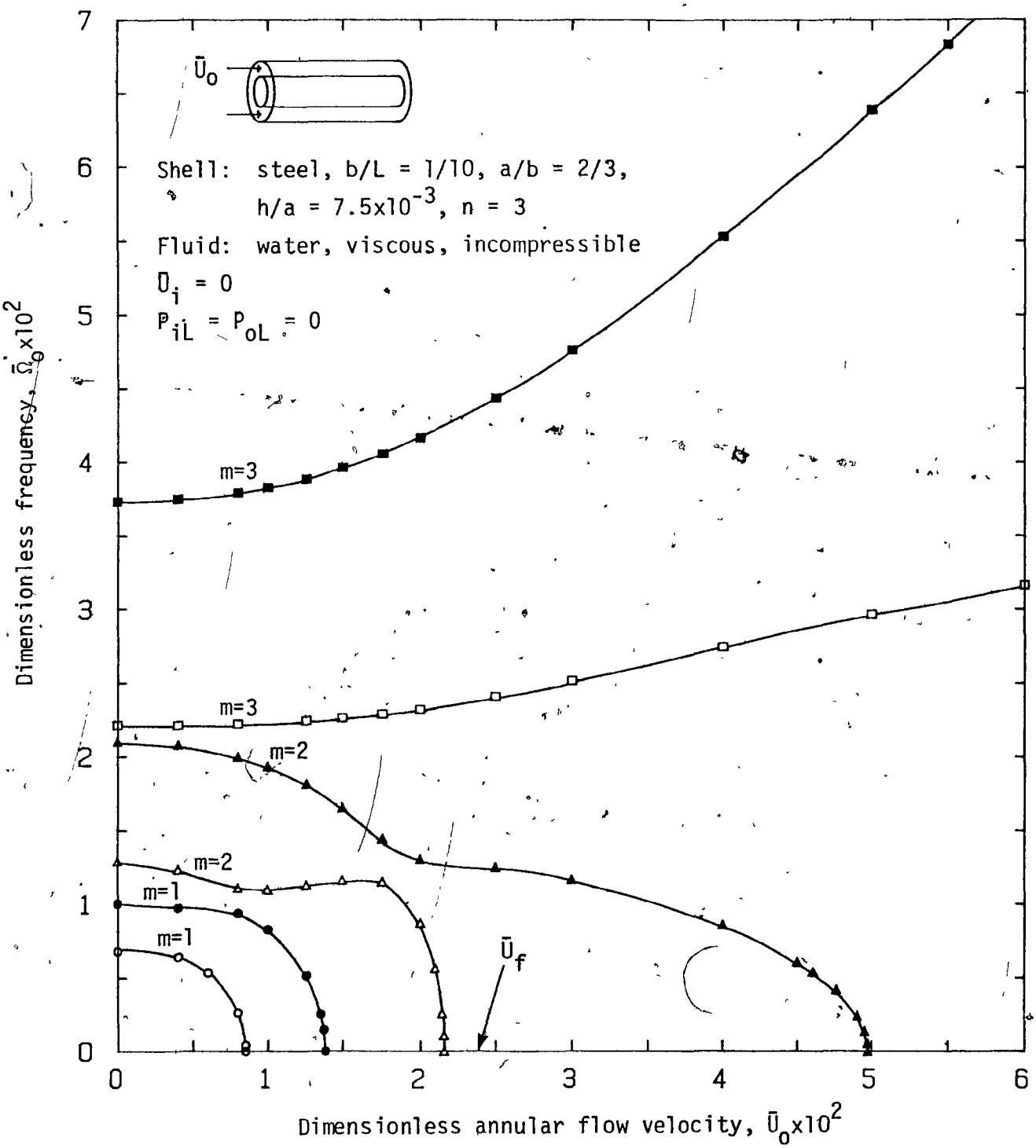

Fig. 34: The real dimensionless eigenfrequencies $\bar{\Omega}_o$ of the ½-gap steel-water system conveying *incompressible viscous fluid*, as functions of the dimensionless annular flow velocity $\bar{U}_o$ (n=3; m=1,2,3; open symbols: antisymmetric modes; closed symbols: symmetric modes). Both shells are flexible and the internal fluid is stagnant.

APPENDIX A

INTEGRALS INVOLVING CHARACTERISTIC BEAM FUNCTION

The constants a_{km}, b_{km}, d_{km}, e_{km}, f_{km}, g_{km}, h_{km} and j_{km} defined in Chapters III and VI can be written in terms of the dimensionlesss variable $\xi = x/L$ as follows:

$$a_{km} = \int_0^1 \frac{d\phi_k}{d\xi} \frac{d\phi_m}{d\xi} d\xi ,$$

$$b_{km} = \int_0^1 \frac{d\phi_k}{d\xi} \frac{d^3\phi_m}{d\xi^3} d\xi ,$$

$$d_{km} = \int_0^1 \phi_k \frac{d^2\phi_m}{d\xi^2} d\xi ,$$

$$e_{km} = \int_0^1 \xi \frac{d\phi_k}{d\xi} \frac{d^3\phi_m}{d\xi^3} d\xi ,$$

$$f_{km} = \int_0^1 \frac{d\phi_k}{d\xi} \phi_m d\xi ,$$

$$g_{km} = \int_0^1 \xi \frac{d\phi_k}{d\xi} \frac{d\phi_m}{d\xi} d\xi ,$$

$$h_{km} = \int_0^1 \xi \phi_k \frac{d^2\phi_m}{d\xi^2} d\xi ,$$

$$j_{km} = \int_0^1 \xi \phi_k \phi_m d\xi ,$$

where ϕ_k and ϕ_m are characteristic functions of a beam. According to the scheme developed by Sharma in reference [42], these integrals can be evaluated using the following general equations. For any functions ϕ_k and ψ_m satisfying the equations $\phi_k^{iv} = \phi_k$ and $\psi_m^{iv} = \psi_m$ where the differentiation is with respect to $\lambda_k \xi$ and $\alpha_m \xi$, respectively, it can be shown that†

$$(\alpha_m^4 - \lambda_k^4)\int_0^1 \phi_k \psi_m \, d\xi = [\alpha_m^3 \psi_m''' \phi_k - \alpha_m^2 \lambda_k \psi_m'' \phi_k' + \alpha_m \lambda_k^2 \psi_m' \phi_k'' - \lambda_k^3 \psi_m \phi_k''']_0^1 , \tag{A.1}$$

$$4\lambda_k \int_0^1 \phi_k^2 \, d\xi = [3\phi_k \phi_k''' + \xi \lambda_k \phi_k^2 - 2\xi \lambda_k \phi_k' \phi_k''' - \phi_k' \phi_k'' + \xi \lambda_k (\phi_k'')^2]_0^1 , \tag{A.2}$$

$$(\alpha_m^4 - \lambda_k^4)\int_0^1 \xi \phi_k \psi_m \, d\xi = [\alpha_m^3 \xi \phi_k \psi_m''' - \alpha_m^2 \lambda_k \xi \phi_k' \psi_m'' + \alpha_m \lambda_k^2 \xi \phi_k'' \psi_m' - \lambda_k^3 \xi \phi_k''' \psi_m + 3\alpha_m^2 \phi_k \psi_m'' + \lambda_k^2 \phi_k'' \psi_m - 2\alpha_m \lambda_k \phi_k' \psi_m']_0^1 - 4\alpha_m^3 \int_0^1 \phi_k \psi_m''' \, d\xi , \tag{A.3}$$

$$8\lambda_k^2 \int_0^1 \xi \phi_k^2 \, d\xi = [6\lambda_k \xi \phi_k \phi_k''' + \lambda_k^2 \xi^2 \phi_k \phi_k - 2\lambda_k \xi \phi_k' \phi_k'' - 2\lambda_k^2 \xi^2 \phi_k' \phi_k''' + \lambda_k^2 \xi^2 \phi_k'' \phi_k'' - 6\phi_k \phi_k'' + 4\phi_k' \phi_k']_0^1 , \tag{A.4}$$

†Equations (A.1,.2) are obtained by Sharma in [42], and equations (A.3,.4) are derived using the same approach.

where primes represent differentiation with respect to the arguments $\lambda_k \xi$ and $\alpha_m \xi$, respectively. By means of equations (A.1-.4), all the above constants (a_{km} - j_{km}) can be determined by replacing ϕ_k and ψ_m with the appropriate beam function or its derivatives. Their values for the case of clamped-clamped beam are listed below:

(1) $$a_{km} = \frac{4\lambda_k^2 \lambda_m^2}{\lambda_k^4 - \lambda_m^4}\left[(-1)^{k+m} + 1\right](\lambda_m \sigma_m - \lambda_k \sigma_k) \quad \text{for } k \neq m ,$$

$$a_{kk} = -\lambda_k \sigma_k (2 - \lambda_k \sigma_k) ,$$

(2) $$b_{km} = 0 \quad \text{for } k \neq m ,$$

$$b_{kk} = -\lambda_k^4 ,$$

(3) $$d_{km} = -a_{km} ,$$

(4) $$e_{km} = -\frac{4(3\lambda_m^4 + \lambda_k^4)\lambda_k^3 \lambda_m^3 \sigma_k \sigma_m}{(\lambda_m^4 - \lambda_k^4)^2}\left[(-1)^{k+m} - 1\right] \quad \text{for } k \neq m ,$$

$$e_{kk} = -\frac{\lambda_k^4}{2} ,$$

(5) $$f_{km} = \frac{4\lambda_k^2 \lambda_m^2}{\lambda_k^4 - \lambda_m^4}\left[(-1)^{k+m} - 1\right] \quad \text{for } k \neq m ,$$

$$f_{kk} = 0 ,$$

(6) $$g_{km} = \frac{(-1)^{k+m} 4 \lambda_k^2 \lambda_m^2 (\lambda_k \sigma_k - \lambda_m \sigma_m)}{(\lambda_m^4 - \lambda_k^4)} - \frac{2(\lambda_m^4 + \lambda_k^4)}{(\lambda_m^4 - \lambda_k^4)} f_{km} \quad \text{for } k \neq m ,$$

$$g_{kk} = \frac{\lambda_k \sigma_k}{2} (\lambda_k \sigma_k - 2) ,$$

(7) $$h_{km} = \frac{(-1)^{k+m} 4 \lambda_k^2 \lambda_m^2 (\lambda_m \sigma_m - \lambda_k \sigma_k)}{(\lambda_m^4 - \lambda_k^4)} + \frac{(3\lambda_m^4 + \lambda_k^4)}{(\lambda_m^4 - \lambda_k^4)} f_{km} \quad \text{for } k \neq m ,$$

$$h_{kk} = \frac{\lambda_k \sigma_k}{2} (2 - \lambda_k \sigma_k) ,$$

(8) $$j_{km} = \frac{16 \lambda_k^3 \lambda_m^3 \sigma_k \sigma_m}{(\lambda_m^4 - \lambda_k^4)^2} [(-1)^{k+m} - 1] \quad \text{for } k \neq m ;$$

$$j_{kk} = \frac{1}{2} ,$$

For a clamped-clamped beam, σ_m is defined as

$$\sigma_m = \frac{\cosh \lambda_m - \cos \lambda_m}{\sinh \lambda_m - \sin \lambda_m} = \frac{\sinh \lambda_m + \sin \lambda_m}{\cosh \lambda_m - \cos \lambda_m} , \qquad (A.5)$$

and the eigenvalues λ_m are the roots of the transcendental equation,

$$\cosh \lambda_m \cos \lambda_m - 1 = 0 . \qquad (A.6)$$

The values of λ_m and σ_m may be found tabulated in reference [43].

APPENDIX B

THE EXPRESSION OF $H_{km}(\bar{\alpha})$

$H_{km}(\bar{\alpha})$ is defined in equations (3.2.11c) as follows:

$$H_{km}(\bar{\alpha}) = \int_0^1 \phi_m(\xi)\, e^{i\bar{\alpha}\xi}\, d\xi \times \int_0^1 \phi_k(\xi)\, e^{-i\bar{\alpha}\xi}\, d\xi \quad ,$$

where $\phi_m(\xi)$ (or $\phi_k(\xi)$) is the characteristic beam function which, in general, has the form

$$\phi_m(\xi) = \cosh \lambda_m \xi - \cos \lambda_m \xi - \sigma_m (\sinh \lambda_m \xi - \sin \lambda_m \xi), \quad \text{(B.1)}$$

and satisfies the equation

$$\phi_m^{iv}(\xi) = \lambda_m^4 \phi_m(\xi) \quad ; \quad \text{(B.2)}$$

the eigenvalues λ_m and the constants σ_m for the clamped-clamped beam are defined in Appendix A, and the differentiation in (B.2) and in all that follows is with respect to ξ.

Let us consider the integral

$$\int_0^1 \phi_m(\xi)\, e^{i\bar{\alpha}\xi}\, d\xi \quad .$$

Using equation (B.2), the integral can be written as

$$\int_0^1 \phi_m(\xi)\, e^{i\bar{\alpha}\xi}\, d\xi = \frac{1}{\lambda_m^4} \int_0^1 \phi_m^{iv}(\xi)\, e^{i\bar{\alpha}\xi}\, d\xi \quad . \tag{B.3}$$

By successive integration by parts, one obtains

$$(\lambda_m^4 - \bar{\alpha}^4) \int_0^1 \phi_m(\xi)\, e^{i\bar{\alpha}\xi}\, d\xi = \Big[\phi_m'''\, e^{i\bar{\alpha}\xi} - i\bar{\alpha}\, \phi_m''\, e^{i\bar{\alpha}\xi} + (i\bar{\alpha})^2 \phi_m'\, e^{i\bar{\alpha}\xi} - (i\bar{\alpha})^3 \phi_m\, e^{i\bar{\alpha}\xi} \Big]_0^1 \quad . \tag{B.4}$$

From equations (B.1), (A.5,.6), the boundary values for a clamped-clamped beam can be shown to be

$$\phi_m(0) = \phi_m(1) = 0 \quad , \quad \phi_m'(0) = \phi_m'(1) = 0 \quad ,$$

$$\phi_m''(0) = 2\lambda_m^2 \quad , \quad \phi_m''(1) = (-1)^{m+1} 2\lambda_m^2 \quad , \tag{B.5}$$

$$\phi_m'''(0) = -2\lambda_m^2 \sigma_m \quad , \quad \phi_m'''(1) = (-1)^{m+1} 2\lambda_m^3 \sigma_m \quad .$$

Substituting equation (B.5) into equation (B.4), yields

$$\int_0^1 \phi_m(\xi)\, e^{i\bar{\alpha}\xi}\, d\xi = \frac{1}{(\lambda_m^4 - \bar{\alpha}^4)} \Big\{ 2\lambda_m^3 \sigma_m \left[(-1)^{m+1} e^{i\bar{\alpha}} + 1 \right] - 2i\bar{\alpha}\lambda_m^2 \left[(-1)^{m+1} e^{i\bar{\alpha}} - 1 \right] \Big\} \quad . \tag{B.6}$$

Replacing m and $\bar{\alpha}$ by k and $-\bar{\alpha}$, respectively, in equation (B.6), one obtains

$$\int_0^1 \phi_k(\xi)\, e^{-i\bar{\alpha}\xi}\, d\xi = \frac{1}{(\lambda_k^4 - \bar{\alpha}^4)} \Big\{ 2\lambda_k^3 \sigma_k \left[(-1)^{k+1} e^{-i\bar{\alpha}} + 1 \right] + 2i\bar{\alpha}\lambda_k^2 \left[(-1)^{k+1} e^{-i\bar{\alpha}} - 1 \right] \Big\} \quad . \tag{B.7}$$

Combining equations (B.6) and (B.7), $H_{km}(\bar{\alpha})$ can be expressed as

$$H_{km}(\bar{\alpha}) = \frac{1}{(\bar{\alpha}^4 - \lambda_m^4)} \left\{ A_m \left[(-1)^{m+1} e^{i\bar{\alpha}} + 1 \right] - B_m \bar{\alpha} \left[(-1)^{m+1} e^{i\bar{\alpha}} - 1 \right] \right\}$$

$$\times \frac{1}{(\bar{\alpha}^4 - \lambda_k^4)} \left\{ A_k \left[(-1)^{k+1} e^{-i\bar{\alpha}} + 1 \right] + B_k \bar{\alpha} \left[(-1)^{k+1} e^{-i\bar{\alpha}} - 1 \right] \right\} , \tag{B.8}$$

where

$$A_m = 2\lambda_m^3 \sigma_m , \qquad B_m = 2i\lambda_m^2 ,$$

$$A_k = 2\lambda_k^3 \sigma_k , \qquad B_k = 2i\lambda_k^2 . \tag{B.9}$$

For the purposes of analysis in Chapter IV, equation (B.8) can be rearranged as follows:

$$H_{km}(\bar{\alpha}) = \frac{1}{(\bar{\alpha}^4 - \lambda_m^4)(\bar{\alpha}^4 - \lambda_k^4)} \left[A\bar{\alpha}^2 e^{i\bar{\alpha}} + B\bar{\alpha} e^{i\bar{\alpha}} + C e^{i\bar{\alpha}} + D\bar{\alpha}^2 e^{-i\bar{\alpha}} \right.$$

$$\left. + E\bar{\alpha} e^{-i\bar{\alpha}} + F e^{-i\bar{\alpha}} + G\bar{\alpha}^2 + H\bar{\alpha} + L \right] , \tag{B.10}$$

where

$$A = B_m B_k (-1)^{m+1} , \quad B = -(A_m B_k + A_k B_m)(-1)^{m+1} ,$$

$$C = A_m A_k (-1)^{m+1} , \quad D = B_m B_k (-1)^{k+1} , \quad E = (A_m B_k + A_k B_m)(-1)^{k+1} ,$$

$$F = A_m A_k (-1)^{k+1} , \quad G = -B_m B_k \left[(-1)^{k+m} + 1 \right] ,$$

$$H = (A_m B_k - A_k B_m) \left[(-1)^{k+m} - 1 \right] , \quad L = A_m A_k \left[(-1)^{k+m} + 1 \right] ,$$

and A_m, A_k, B_m, B_k are defined in equation (B.9).

Equation (B.8) holds for all values of $\bar{\alpha}$ except when $\bar{\alpha}^4 = \lambda_m^4$ or λ_k^4 *i.e.* when

$$\bar{\alpha} = \pm\lambda_m, \pm i\lambda_m, \pm\lambda_k \text{ or } \pm i\lambda_k \quad . \tag{B.11}$$

At these points, the denominator of the integral defined in either equation (B.6) or (B.7) vanishes and so, apparently, the integral will blow up. However, from the physical point of view, as the integrals in (B.6) and (B.7) involve the well-behaved beam eigenfunctions and the exponential function integrated over a finite range of the variable, they should not become infinite for any finite value of $\bar{\alpha}$. Hence, the numerator of the expressions in (B.6) or (B.7) must also be equal to zero when $\bar{\alpha}$ equals to one of the values given in equation (B.11), so that the expressions have a form of 0/0 and their values in the limit can be determined by using l'Hōpital's rule. Accordingly, on applying l'Hōpital's rule to equation (B.6), one may write,

$$\int_0^1 \phi_m(\xi) e^{i\bar{\alpha}\xi} d\xi \Big|_{\bar{\alpha}=\pm\lambda_m, \pm i\lambda_m} = \lim_{\bar{\alpha}\to\pm\lambda_m, \pm i\lambda_m} \left[2i\lambda_m^3 \bar{\sigma}_m (-1)^{m+1} e^{i\bar{\alpha}} + 2\bar{\alpha}\lambda_m^2 (-1)^{m+1} e^{i\bar{\alpha}} - 2i\lambda_m^2 (-1)^{m+1} e^{i\bar{\alpha}} + 2i\lambda_m^2\right] / (-4\bar{\alpha}^3) \quad , \tag{B.12}$$

or explicitly,

$$\int_0^1 \phi_m(\xi) e^{i\lambda_m \xi} d\xi = \left[(-1)^{m+1} e^{i\lambda_m} (i\lambda_m \bar{\sigma}_m + \lambda_m - i) + i\right] / (-2\lambda_m) \quad , \tag{B.13}$$

$$\int_0^1 \phi_m(\xi) e^{-i\lambda_m \xi} d\xi = \left[(-1)^{m+1} e^{-i\lambda_m}(i\lambda_m \bar{\sigma}_m - \lambda_m - i) + i\right]/(2\lambda_m), \quad \text{(B.14)}$$

$$\int_0^1 \phi_m(\xi) e^{-\lambda_m \xi} d\xi = \left[(-1)^{m+1} e^{-\lambda_m}(\lambda_m \bar{\sigma}_m + \lambda_m - 1) + 1\right]/(2\lambda_m), \quad \text{(B.15)}$$

$$\int_0^1 \phi_m(\xi) e^{\lambda_m \xi} d\xi = \left[(-1)^{m+1} e^{\lambda_m}(\lambda_m \bar{\sigma}_m - \lambda_m - 1) + 1\right]/(-2\lambda_m). \quad \text{(B.16)}$$

For the integral in equation (B.7), when $\bar{\alpha} = \pm\lambda_k, \pm i\lambda_k$, the correct expressions can be obtained by replacing the subscript m by k in equations (B.13-.16).

Therefore, $H_{km}(\bar{\alpha})$ is either given by equation (B.8) or, when $\bar{\alpha}$ is one of the values in (B.11), by the appropriate product of (B.6) or (B.7) with one of the equations (B.13-.16) (using subscript m or k whichever is suitable).

APPENDIX C

THE VELOCITY POTENTIALS AND GENERALIZED AERODYNAMIC FORCES DUE TO INCOMPRESSIBLE FLOWS IN SYSTEMS OF TWO FLEXIBLE SHELLS

Solutions to the velocity potentials have the following forms:

(i) for the internal fluid region,

$$\Phi_i(x,r,\theta,t) = \psi_{in}(x,r) \cos n\theta \; e^{i\Omega t} ,$$

where

$$\psi_{in}(x,r) = \frac{1}{2\pi}\int_{-\infty}^{\infty} \psi_{in}^{*}(\alpha,r) e^{-i\alpha x} d\alpha ,$$

and

$$\psi_{in}^{*}(\alpha,r) = \sum_{m=1}^{\infty} \frac{iU_i(\kappa_i-\bar{\alpha})}{\bar{\alpha}} \frac{\hat{I}_n(\alpha r)}{I_n'(\alpha a)} \phi_m^{*}(\bar{\alpha}) C_{mn} ;$$

(ii) for the annular fluid region,

$$\Phi_o(x,r,\theta,t) = \psi_{on}(x,r) \cos n\theta \; e^{i\Omega t} ,$$

where

$$\psi_{on}(x,r) = \frac{1}{2\pi}\int_{-\infty}^{\infty} \psi_{on}^{*}(\alpha,r) e^{-i\alpha x} d\alpha ,$$

and

$$\psi^*_{on}(\alpha,r)=\sum_{m=1}^{\infty}\frac{iU_o(K_o-\bar{\alpha})}{\bar{\alpha}}\frac{I_n'(\alpha b)K_n(\alpha r)-I_n(\alpha r)K_n'(\alpha b)}{I_n'(\alpha b)K_n'(\alpha a)-I_n'(\alpha a)K_n'(\alpha b)}\phi^*_m(\bar{\alpha})C_{mn}$$

$$+\frac{iU_o(K_o-\bar{\alpha})}{\bar{\alpha}}\frac{I_n(\alpha r)K_n'(\alpha a)-I_n'(\alpha a)K_n(\alpha r)}{I_n'(\alpha b)K_n'(\alpha a)-I_n'(\alpha a)K_n'(\alpha b)}\phi^*_m(\bar{\alpha})F_{mn}$$

The generalized aerodynamic forces are given as follows:

(i) for the inner shell,

$$\bar{\bar{Q}}_{kmn}=Q'_{kmn}\bar{C}_{mn}+Q''_{kmn}\bar{F}_{mn}\ ,$$

where

$$Q'_{kmn}=\frac{\bar{U}_i^2\beta_i\varepsilon_i}{2\pi}\int_{-\infty}^{\infty}\frac{(K_i-\bar{\alpha})^2}{\bar{\alpha}}\hat{E}_n(\bar{\alpha})H_{km}(\bar{\alpha})\,d\bar{\alpha}$$

$$+\frac{\bar{U}_o^2\beta_i\varepsilon_i\rho_r}{2\pi v_r^2}\int_{-\infty}^{\infty}\frac{(K_o-\bar{\alpha})^2}{\bar{\alpha}}\hat{F}_n(\bar{\alpha})H_{km}(\bar{\alpha})\,d\bar{\alpha}\ ; \qquad (C.1)$$

$$Q''_{kmn}=-\frac{\bar{U}_o^2\beta_i\varepsilon_i\rho_r}{2\pi v_r^2}\int_{-\infty}^{\infty}\frac{(K_o-\bar{\alpha})^2}{\bar{\alpha}}\hat{G}_n(\bar{\alpha})H_{km}(\bar{\alpha})\,d\bar{\alpha}\ , \qquad (C.2)$$

and $\hat{E}_n(\bar{\alpha})$, $\hat{F}_n(\bar{\alpha})$, $\hat{G}_n(\bar{\alpha})$ and $H_{km}(\bar{\alpha})$ are as defined in equations (3.3.1h), (3.3.1i), (3.3.1j) and (3.2.11c), respectively;

(ii) for the outer shell,

$$\bar{\bar{R}}_{kmn}=R''_{kmn}\bar{C}_{mn}+R'_{kmn}\bar{F}_{mn}\ ,$$

where

$$R''_{kmn} = \frac{\bar{U}_o^2 \beta_o \varepsilon_o}{2\pi} \int_{-\infty}^{\infty} \frac{(\kappa_o - \bar{\alpha})^2}{\bar{\alpha}} \hat{L}_n(\bar{\alpha}) H_{km}(\bar{\alpha}) \, d\bar{\alpha} \quad , \tag{C.3}$$

$$R'_{kmn} = \frac{\bar{U}_o^2 \beta_o \varepsilon_o}{2\pi} \int_{-\infty}^{\infty} \frac{(\kappa_o - \bar{\alpha})^2}{\bar{\alpha}} \hat{M}_n(\bar{\alpha}) H_{km}(\bar{\alpha}) \, d\bar{\alpha} \quad , \tag{C.4}$$

and $\hat{L}_n(\bar{\alpha})$, $\hat{M}_n(\bar{\alpha})$ are given in equations (3.3.2.g), (3.3.2h), respectively.

Note that $\hat{E}_n(\bar{\alpha})$, $\hat{F}_n(\bar{\alpha})$, $\hat{G}_n(\bar{\alpha})$, $\hat{L}_n(\bar{\alpha})$, $\hat{M}_n(\bar{\alpha})$ and $H_{km}(\bar{\alpha})$ are independent of the vibration frequency; hence, the integrals in equations (C.1-.4) can be made frequency-independent, if the terms $(\kappa_i - \bar{\alpha})^2$, $(\kappa_o - \bar{\alpha})^2$ in the integrands are expanded and the reduced frequencies taken 'out of' the integrals.

APPENDIX D

EXPRESSIONS OF THE GENERALIZED AERODYNAMIC FORCES FOR SYSTEMS WITH A RIGID OUTER SHELL

The non-dimensional generalized aerodynamic forces acting on the inner shell are as follows:

(i) for compressible flow,

$$\bar{\bar{Q}}_{kmn} = Q'_{kmn}\,\bar{C}_{mn} \quad , \tag{D.1}$$

where

$$Q'_{kmn} = \frac{\bar{U}_i^2 \beta_i \varepsilon_i}{2\pi} \int_{-\infty}^{\infty} \frac{(K_i - \bar{\alpha})^2}{\mu_i L} E_n(\bar{\alpha}) H_{km}(\bar{\alpha})\, d\bar{\alpha}$$

$$- \frac{\bar{U}_o^2 \beta_i \varepsilon_i \rho_r}{2\pi} \int_{-\infty}^{\infty} \frac{(K_o - \bar{\alpha})^2}{\mu_o L} F_n(\bar{\alpha}) H_{km}(\bar{\alpha})\, d\bar{\alpha} \quad , \tag{D.1a}$$

where $E_n(\bar{\alpha})$, $F_n(\bar{\alpha})$ and $H_{km}(\bar{\alpha})$ are as defined in equations (3.2.7b), (3.2.7c) and (3.2.11c), respectively; all the dimensionless parameters are as given in (3.2.10), except $\bar{U}_o$ which is defined here as

$$\bar{U}_o = \frac{U_o}{v_i} \quad , \tag{D.2}$$

where

$$v_i = \left\{ E_i / \left[\rho_{si} (1 - \nu_i^2) \right] \right\}^{1/2} \quad ;$$

(ii) for incompressible flow,

$$\overline{\overline{Q}}_{kmn} = \left(\bar{\Omega}_i^2 q^1_{kmn} + \bar{\Omega}_i q^2_{kmn} + q^3_{kmn}\right) \bar{C}_{mn} \quad , \tag{D.3}$$

where

$$\bar{\Omega}_i = \Omega \times a\left[\rho_{si}(1-\nu_i^2)/E_i\right]^{1/2} \quad ,$$

$$q^1_{kmn} = \frac{\beta_i}{2\pi\varepsilon_i}\int_{-\infty}^{\infty} \frac{\hat{E}_n(\bar{\alpha})}{\bar{\alpha}} H_{km}(\bar{\alpha})\, d\bar{\alpha}$$

$$- \frac{\beta_i \rho_r}{2\pi\varepsilon_i}\int_{-\infty}^{\infty} \frac{\hat{F}_n(\bar{\alpha})}{\bar{\alpha}} H_{km}(\bar{\alpha})\, d\bar{\alpha} \quad , \tag{D.3a}$$

$$q^2_{kmn} = -\frac{\bar{U}_i \beta_i}{\pi}\int_{-\infty}^{\infty} \hat{E}_n(\bar{\alpha}) H_{km}(\bar{\alpha})\, d\bar{\alpha}$$

$$+ \frac{\bar{U}_o \beta_i \rho_r}{\pi}\int_{-\infty}^{\infty} \hat{F}_n(\bar{\alpha}) H_{km}(\bar{\alpha})\, d\bar{\alpha} \quad , \tag{D.3b}$$

$$q^3_{kmn} = \frac{\bar{U}_i^2 \beta_i \varepsilon_i}{2\pi}\int_{-\infty}^{\infty} \bar{\alpha}\, \hat{E}_n(\bar{\alpha}) H_{km}(\bar{\alpha})\, d\bar{\alpha}$$

$$- \frac{\bar{U}_o^2 \beta_i \varepsilon_i \rho_r}{2\pi}\int_{-\infty}^{\infty} \bar{\alpha}\, \hat{F}_n(\bar{\alpha}) H_{km}(\bar{\alpha})\, d\bar{\alpha} \quad , \tag{D.3c}$$

and $\hat{E}_n(\bar{\alpha})$, $\hat{F}_n(\bar{\alpha})$ are as defined in equations (3.3.1h) and (3.3.1i), respectively.

APPENDIX E

STRUCTURE OF MATRICES [A], [K], [M], [C]

In this Appendix are described in detail the structures of matrix [A] as defined in the matrix equation (3.4.26), and of matrices [K], [M], [C] in the matrix equation (3.4.29). Also given are the structures of their counterparts, denoted by $[A_i]$, $[K_i]$, $[M_i]$ and $[C_i]$, for systems with a rigid outer shell. All the matrices are for the case of k,m = 1,2,3; n = 2 (other values of n may be used).

E.1 Matrix [A]

The structure of this matrix is shown below.

$$
[A] = \begin{array}{c|cccccccccccccccccc}
 & 1 & & & 4 & & & 7 & & & 10 & & & 13 & & & 16 & & \\
1 & A^{1}_{112} & A^{1}_{122} & A^{1}_{132} & A^{2}_{112} & A^{2}_{122} & A^{2}_{132} & A^{3}_{112} & A^{3}_{122} & A^{3}_{132} & 0 & - & - & - & - & - & - & - & 0 \\
 & A^{4}_{112} & A^{4}_{122} & A^{4}_{132} & A^{5}_{112} & A^{5}_{122} & A^{5}_{132} & A^{6}_{112} & A^{6}_{122} & A^{6}_{132} & 1 & & & & & & & & 1 \\
 & A^{7}_{112} & A^{7}_{122} & A^{7}_{132} & A^{8}_{112} & A^{8}_{122} & A^{8}_{132} & A^{9}_{112} & A^{9}_{122} & A^{9}_{132} & 1 & & & & & & & Q''_{112} & Q''_{122} & Q''_{132} \\
4 & A^{1}_{212} & A^{1}_{222} & A^{1}_{232} & A^{2}_{212} & A^{2}_{222} & A^{2}_{232} & A^{3}_{212} & A^{3}_{222} & A^{3}_{232} & 1 & & & & & & & & 1 \\
 & A^{4}_{212} & A^{4}_{222} & A^{4}_{232} & A^{5}_{212} & A^{5}_{222} & A^{5}_{232} & A^{6}_{212} & A^{6}_{222} & A^{6}_{232} & 1 & & & & & & & & 1 \\
 & A^{7}_{212} & A^{7}_{222} & A^{7}_{232} & A^{8}_{212} & A^{8}_{222} & A^{8}_{232} & A^{9}_{212} & A^{9}_{222} & A^{9}_{232} & 1 & & & & & & & Q''_{212} & Q''_{222} & Q''_{232} \\
7 & A^{1}_{312} & A^{1}_{322} & A^{1}_{332} & A^{2}_{312} & A^{2}_{322} & A^{2}_{332} & A^{3}_{312} & A^{3}_{322} & A^{3}_{332} & 1 & & & & & & & & 1 \\
 & A^{4}_{312} & A^{4}_{322} & A^{4}_{332} & A^{5}_{312} & A^{5}_{322} & A^{5}_{332} & A^{6}_{312} & A^{6}_{322} & A^{6}_{332} & 1 & & & & & & & & 1 \\
 & A^{7}_{312} & A^{7}_{322} & A^{7}_{352} & A^{8}_{312} & A^{8}_{322} & A^{8}_{332} & A^{9}_{312} & A^{9}_{322} & A^{9}_{332} & 0 & - & - & - & - & - & Q''_{312} & Q''_{322} & Q''_{332} \\
10 & 0 & - & - & - & - & - & - & - & 0 & A^{10}_{112} & A^{10}_{122} & A^{10}_{132} & A^{11}_{112} & A^{11}_{122} & A^{11}_{132} & A^{13}_{112} & A^{12}_{122} & A^{12}_{132} \\
 & 1 & & & & & & & & 1 & A^{13}_{112} & A^{13}_{122} & A^{13}_{132} & A^{14}_{112} & A^{14}_{122} & A^{14}_{132} & A^{15}_{112} & A^{15}_{122} & A^{15}_{132} \\
 & 1 & & & & & & R''_{112} & R''_{122} & R''_{132} & A^{16}_{112} & A^{16}_{122} & A^{16}_{132} & A^{17}_{112} & A^{17}_{122} & A^{17}_{132} & A^{18}_{112} & A^{18}_{122} & A^{18}_{132} \\
13 & 1 & & & & & & 1 & & & A^{10}_{212} & A^{10}_{222} & A^{10}_{232} & A^{11}_{212} & A^{11}_{222} & A^{11}_{232} & A^{12}_{212} & A^{12}_{222} & A^{12}_{232} \\
 & 1 & & & & & & 1 & & & A^{13}_{212} & A^{13}_{222} & A^{13}_{232} & A^{14}_{212} & A^{14}_{222} & A^{14}_{232} & A^{15}_{212} & A^{15}_{222} & A^{15}_{232} \\
 & 1 & & & & & & R''_{212} & R''_{222} & R''_{232} & A^{16}_{212} & A^{16}_{222} & A^{16}_{232} & A^{17}_{212} & A^{17}_{222} & A^{17}_{232} & A^{18}_{212} & A^{18}_{222} & A^{18}_{232} \\
16 & 1 & & & & & & 1 & & & A^{10}_{312} & A^{10}_{322} & A^{10}_{332} & A^{11}_{312} & A^{11}_{322} & A^{11}_{332} & A^{12}_{312} & A^{12}_{322} & A^{12}_{332} \\
 & 1 & & & & & & 1 & & & A^{13}_{312} & A^{13}_{322} & A^{13}_{332} & A^{14}_{312} & A^{14}_{322} & A^{14}_{332} & A^{15}_{312} & A^{15}_{322} & A^{15}_{332} \\
 & 0 & - & - & - & - & - & R''_{312} & R''_{322} & R''_{332} & A^{16}_{312} & A^{16}_{322} & A^{16}_{332} & A^{17}_{312} & A^{17}_{322} & A^{17}_{332} & A^{18}_{312} & A^{18}_{322} & A^{18}_{332}
\end{array}
$$

A^{ℓ}_{kmn}, Q''_{kmn} and R''_{kmn} ($k,m = 1,2,3$; $n = 2$; $\ell = 1,2, \ldots,18$) are given in equations (3.4.4-.21), (3.2.11b) and (3.2.15a), respectively.

E.1.1 When the outer shell is rigid, the equivalent of matrix [A], denoted by $[A_i]$ has the form

$$[A_i] = \begin{array}{c|ccccccccc} & 1 & & & 4 & & & 7 & & \\ \hline 1 & A^1_{i11} & A^1_{i13} & A^1_{i13} & A^2_{112} & A^2_{122} & A^2_{132} & A^3_{112} & A^3_{122} & A^3_{132} \\ & A^4_{112} & A^4_{122} & A^4_{132} & A^5_{112} & A^5_{122} & A^5_{132} & A^6_{112} & A^6_{122} & A^6_{132} \\ & A^7_{112} & A^7_{122} & A^7_{132} & A^8_{112} & A^8_{122} & A^8_{132} & A^2_{i11} & A^2_{i12} & A^2_{i13} \\ \hline 4 & A^1_{i21} & A^1_{i22} & A^1_{i23} & A^2_{212} & A^2_{222} & A^2_{232} & A^3_{212} & A^3_{222} & A^3_{232} \\ & A^4_{212} & A^4_{222} & A^4_{232} & A^5_{212} & A^5_{222} & A^5_{232} & A^6_{212} & A^6_{222} & A^6_{232} \\ & A^7_{212} & A^7_{222} & A^7_{232} & A^8_{212} & A^8_{222} & A^8_{232} & A^2_{i21} & A^2_{i22} & A^2_{i23} \\ \hline 7 & A^1_{i31} & A^1_{i32} & A^1_{i33} & A^2_{312} & A^2_{322} & A^2_{332} & A^3_{312} & A^3_{322} & A^3_{332} \\ & A^4_{312} & A^4_{322} & A^4_{352} & A^5_{312} & A^5_{322} & A^5_{332} & A^6_{312} & A^6_{322} & A^6_{332} \\ & A^7_{312} & A^7_{322} & A^7_{332} & A^8_{312} & A^8_{322} & A^8_{332} & A^2_{i31} & A^2_{i32} & A^2_{i33} \end{array}$$

A^{ℓ}_{kmn} ($k,m = 1,2,2$; $n = 2$; $\ell = 2,3, \ldots,8$) are given in equations (3.4.5-.11); A^1_{ikm} ($k,m = 1,2,3$) are obtained when the term $\alpha_{km}\bar{\Omega}_o^2/\Omega_r^2$ in A^1_{kmn} as defined in equation (3.4.4) is replaced by $\alpha_{km}\bar{\Omega}_i^2$; similarly, replacing $\delta_{km}\bar{\Omega}_o^2/\Omega_r^2$ by $\delta_{km}\bar{\Omega}_i^2$ in A^9_{kmn} (equation (3.4.12) yields A^2_{ikm} and, finally, the term Q'_{kmn} in A^2_{ikm} is given by equation (D.1a).

E.2 Matrix [K]

Elements of [K] are equal to the corresponding elements of [A], except those specified in the following matrix.

$[K] =$

	1	4	7	10	13	16
1	$K^1_{11}\ K^1_{12}\ K^1_{13}$		$K^2_{11}\ K^2_{12}\ K^2_{13}$			$q^{F3}_{V112}\ q^{F3}_{V122}\ q^{F3}_{V132}$
4	$K^1_{21}\ K^1_{22}\ K^1_{23}$		$K^2_{21}\ K^2_{22}\ K^2_{23}$			$q^{F3}_{V212}\ q^{F3}_{V222}\ q^{F3}_{V232}$
7	$K^1_{31}\ K^1_{32}\ K^1_{33}$		$K^2_{31}\ K^2_{32}\ K^2_{33}$			$q^{F3}_{V312}\ q^{F3}_{V322}\ q^{F3}_{V332}$
10			$r^{C3}_{112}\ r^{C3}_{122}\ r^{C3}_{132}$	$K^3_{11}\ K^3_{12}\ K^3_{13}$		$K^4_{11}\ K^4_{12}\ K^4_{13}$
13			$r^{C3}_{212}\ r^{C3}_{222}\ r^{C3}_{232}$	$K^3_{21}\ K^3_{22}\ K^3_{23}$		$K^4_{21}\ K^4_{22}\ K^4_{23}$
16			$r^{C3}_{312}\ r^{C3}_{322}\ r^{C3}_{332}$	$K^3_{31}\ K^3_{32}\ K^3_{33}$		$K^4_{31}\ K^4_{32}\ K^4_{33}$

q^{F3}_{Vkmn}, r^{C3}_{kmn} are given in equations (3.3.1g), (3.3.2e), respectively, and

$$K^1_{km} = A^1_{kmn} - a_{km}\bar{\Omega}_o^2/\Omega_r^2 \ , \qquad \text{(E.1)}$$

$$K^2_{km} = A^9_{kmn} + \delta_{km}\bar{\Omega}_o^2/\Omega_r^2 - Q'_{kmn} + q^{C3}_{kmn} , \qquad (E.2)$$

$$K^3_{km} = A^{10}_{kmn} - a_{km}\bar{\Omega}_o^2 , \qquad (E.3)$$

$$K^4_{km} = A^{18}_{kmn} + \delta_{km}\bar{\Omega}_o^2 - R'_{kmn} + r^{F3}_{kmn} , \qquad (E.4)$$

where k,m = 1,2,2; n = 2; and q^{C3}_{kmn}, r^{F3}_{kmn} are given in equations (3.3.1f), (3.3.2f), respectively.

E.2.1 When the outer shell is rigid, the equivalent of matrix [K] is denoted by $[K_i]$. Elements of $[K_i]$ are equal to the corresponding elements of $[A_i]$, except those specified in the following matrix.

$$[K_i] = \begin{array}{c|ccc} & 1 & 4 & 7 \\ \hline 1 & K^1_{i11}\ K^1_{i12}\ K^1_{i13} & & K^2_{i11}\ K^2_{i12}\ K^2_{i13} \\ 4 & K^1_{i21}\ K^1_{i22}\ K^1_{i23} & & K^2_{i21}\ K^2_{i22}\ K^2_{i23} \\ 7 & K^1_{i31}\ K^1_{i32}\ K^1_{i33} & & K^2_{i31}\ K^2_{i32}\ K^2_{i33} \end{array}$$

$K^1_{ikm} = K^1_{km}$ (equation (E.1)); K^2_{ikm} can be obtained by replacing the term q^{C3}_{Vkmn} by q^3_{Vkmn} (defined in equation (D.3c)) in K^2_{km} (equation (E.2)).

E.3 Matrix [M]

The structure of this matrix is shown below.

$$[M] = \begin{array}{c|cccccc} & 1 & 4 & 7 & 10 & 13 & 16 \\ 1 & M^1_{11}\ M^1_{12}\ M^1_{13} & 0\ -\ - & -\ -\ - & -\ -\ - & -\ -\ - & -\ -\ 0 \\ & 0 & M^2_{11}\ M^2_{12}\ M^2_{13} & & & & 1 \\ & 1 & & M^3_{11}\ M^3_{12}\ M^3_{13} & & & q^{FI}_{V112}\ q^{FI}_{V122}\ q^{FI}_{V132} \\ 4 & M^1_{21}\ M^1_{22}\ M^1_{23} & & & & & 1 \\ & 1 & M^2_{21}\ M^2_{22}\ M^2_{23} & & & & 1 \\ & 1 & & M^3_{21}\ M^3_{22}\ M^3_{23} & & & q^{FI}_{V212}\ q^{FI}_{V222}\ q^{FI}_{V232} \\ 7 & M^1_{31}\ M^1_{32}\ M^1_{33} & & & & & 1 \\ & 1 & M^2_{31}\ M^2_{32}\ M^2_{33} & & & & 1 \\ & 1 & & M^3_{31}\ M^3_{32}\ M^3_{33} & & & q^{FI}_{V312}\ q^{FI}_{V322}\ q^{FI}_{V332} \\ 10 & 1 & & & a_{11}\ a_{12}\ a_{13} & & 1 \\ & 1 & & & & \delta_{11}\ \delta_{12}\ \delta_{13} & 1 \\ & 1 & & r^{CI}_{112}\ r^{CI}_{122}\ r^{CI}_{132} & & & M^4_{11}\ M^4_{12}\ M^4_{13} \\ 13 & 1 & & & a_{21}\ a_{22}\ a_{23} & & 1 \\ & 1 & & & & \delta_{21}\ \delta_{22}\ \delta_{23} & 1 \\ & 1 & & r^{CI}_{212}\ r^{CI}_{222}\ r^{CI}_{232} & & & M^4_{21}\ M^4_{22}\ M^4_{23} \\ 16 & 1 & & & a_{31}\ a_{32}\ a_{33} & & 1 \\ & 1 & & & & \delta_{31}\ \delta_{32}\ \delta_{33} & 0 \\ & 0\ -\ - & -\ -\ - & r^{CI}_{312}\ r^{CI}_{322}\ r^{CI}_{332} & -\ -\ - & -\ -\ 0 & M^4_{31}\ M^4_{32}\ M^4_{33} \end{array}$$

q^{FI}_{Vkmn}, r^{CI}_{kmn} are given in equations (3.3.1c), (3.3.2a), respectively, and

$$M^1_{km} = a_{km} / \Omega_r^2 \ , \qquad \text{(E.5)}$$

$$M^2_{km} = \delta_{km} / \Omega_r^2 \ , \qquad \text{(E.6)}$$

$$M^3_{km} = M^2_{km} + q^{c1}_{kmn} \quad , \tag{E.7}$$

$$M^4_{km} = \delta_{km} + r^{F1}_{kmn} \quad , \tag{E.8}$$

where k,m = 1,2,3; n = 2; q^{c1}_{kmn}, r^{F1}_{kmn} and α_{km} are given in equations (3.3.1b), (3.3.2b) and (3.4.22), respectively; δ_{km} is the familiar Kronecker delta.

E.3.1 When the outer shell is rigid, the equivalent of matrix [M], denoted by $[M_i]$ has the form

$[M_i] =$

	1			4			7		
1	a_{11}	a_{12}	a_{13}	–	–	–	–	–	0
	1			δ_{11}	δ_{12}	δ_{13}			1
	1						M_{i11}	M_{i12}	M_{i13}
4	a_{21}	a_{22}	a_{23}						1
	1			δ_{21}	δ_{22}	δ_{23}			1
	1						M_{i21}	M_{i22}	M_{i23}
7	a_{31}	a_{32}	a_{33}						1
	1			δ_{31}	δ_{32}	δ_{33}			1
	0	–	–	–	–	–	M_{i31}	M_{i32}	M_{i33}

in which

$$M_{ikm} = \delta_{km} + q^{i}_{kmn} \quad , \tag{E.9}$$

where q^{i}_{kmn} is given in equation (D.3a).

E.4 Matric [C]

The structure of this matrix is shown below.

$$[C] = \begin{array}{c|cccccc} & 1 & 4 & 7 & 10 & 13 & 16 \\ \hline 1 & 0 & & q^{C2}_{112}\ q^{C2}_{122}\ q^{C2}_{132} & & & q^{F2}_{112}\ q^{F2}_{122}\ q^{F2}_{132} \\ 4 & & & q^{C2}_{212}\ q^{C2}_{222}\ q^{C2}_{232} & & & q^{F2}_{212}\ q^{F2}_{222}\ q^{F2}_{232} \\ 7 & & & q^{C2}_{312}\ q^{C2}_{322}\ q^{C2}_{332} & & & q^{F2}_{312}\ q^{F2}_{322}\ q^{F2}_{332} \\ 10 & & & r^{C2}_{112}\ r^{C2}_{122}\ r^{C2}_{132} & & & r^{F2}_{112}\ r^{F2}_{122}\ r^{F2}_{132} \\ 13 & & & r^{C2}_{212}\ r^{C2}_{222}\ r^{C2}_{232} & & & r^{F2}_{212}\ r^{F2}_{222}\ r^{F2}_{232} \\ 16 & 0 & & r^{C2}_{312}\ r^{C2}_{322}\ r^{C2}_{332} & & 0 & r^{F2}_{312}\ r^{F2}_{322}\ r^{F2}_{332} \end{array}$$

q^{C2}_{kmh}, q^{F2}_{kmn}, r^{C2}_{kmn} and r^{F2}_{kmn} (k,m = 1,2,3; n = 2) are given in equations (3.3.1d), (3.3.1e), (3.3.2c) and (3.3.2d), respectively.

E.4.1 When the outer shell is rigid, the equivalent of matrix [C], denoted by $[C_i]$ has the form

$[C_i] =$

	1	4	7
1	O — —	— — —	— — O | q^2_{112} q^2_{122} q^2_{132}
4	| | |		| | q^2_{212} q^2_{222} q^2_{232}
7	| | O — —	— — O	| O q^2_{312} q^2_{322} q^2_{332}

q^2_{kmn} (k,m = 1,2,3; n = 2) is given in equation (D.3b).

APPENDIX F

COMPUTER PROGRAMS FOR THE CASE OF INCOMPRESSIBLE INVISCID FLOW

F.1 PROGRAM FOR SYSTEM WITH A RIGID OUTER SHELL

F.1.1 Function of the Program

The program calculates the dimensionless eigenfrequencies, $\bar{\Omega}_i$, and the associated eigenvectors of a system with a rigid outer shell subjected to internal and annular incompressible inviscid flows. For each set of input data of flow velocities, $\bar{U}_i$, $\bar{U}_o$, the program constructs matrices similar to [P] and [Q] in equation (3.4.31); (the order of the matrices is reduced by half because of the rigidity of the outer shell). The frequencies are then determined as the solutions of a typical eigenvalue equation.

F.1.2 Program Structure

The program is written in Fortran IV language and it has the following structure:

MAIN PROGRAM

SUBROUTINE MKMAT

SUBROUTINE CMAT

SUBROUTINE REDUCE

SUBROUTINE EIGZC.

F.1.3 Description of the Program

The function of each subprogram is summarized as follows:

(1) Subroutine MKMAT constructs the matrices $[M_i]$ and $[K_i]$ as defined in Appendix E. To accomplish this task, the subroutine computes the values of the constants a_{km}, b_{km} and d_{km} using the formulae given in Appendix A. With the flow velocities, $\bar{U}_i$ and $\bar{U}_o$ as input parameters and the computed integrals† which are stored in common block memories, the appropriate generalized aerodynamic force terms ($q^1_{\nu kmn}$, $q^2_{\nu kmn}$ in equations (D.3a) and (D.3c), respectively) are evaluated.

(2) Subroutine CMAT constructs the matrix $[C_i]$ as defined in Appendix E. Essentially, the subroutine calculates the non-zero elements of the matrix, which are given by the generalized aerodynamic force term, $q^2_{\nu kmn}$ (equation (D.3b)), with the input flow velocities and the stored values of the integrals involved.

(3) Subroutine REDUCE constructs the matrices $[P_i]$ and $[Q_i]$ which have the following form:

$$[P_i] = \begin{bmatrix} [0] & [I] \\ [K_i] & [C_i] \end{bmatrix} , \qquad [Q_i] = \begin{bmatrix} -[I] & [0] \\ [0] & [M_i] \end{bmatrix} , \tag{F.1}$$

where [I] is the identity matrix.

The matrices $[P_i]$ and $[Q_i]$ constitute the eigenvalue equation

$$([P_i] + \bar{\omega}_i [Q_i])\{Y_i\} = \{0\} , \tag{F.2}$$

†The computer program for calculating the integrals is described in Appendix H.

where

$$\{Y_i\} = \begin{Bmatrix} \{X_i\} \\ \bar{\Omega}_i \{X_i\} \end{Bmatrix} , \tag{F.2a}$$

and

$$\{X_i\} = [\bar{A}_{1n}, \bar{A}_{2n}, \bar{A}_{3n}; \bar{B}_{1n}, \cdots; \cdots, \bar{C}_{2n}, \bar{C}_{3n}]^T . \tag{F.2b}$$

Equation (F.2) is obtained from the governing second-order matrix equation

$$\bar{\Omega}_i^2 [M_i]\{X_i\} + \bar{\Omega}_i [C_i]\{X_i\} + [K_i]\{X_i\} = \{0\} . \tag{F.3}$$

(4) Subroutine EIGZC is the IMSL subroutine employed to solve the eigenvalue equation (F.2).

All calculations are carried out with double precision. The necessary parameters are defined in the main program. The computed values of the integral terms and the flow velocities are read from the data deck. The output results consist of all eighteen eigenvalues[†] and the upper half segment of the associated eigenvectors $\{Y_i\}$ (in columns) which contains the shell displacement vector $\{X_i\}$. These eigenvectors are normalized by the largest element (*i.e.* the largest element has a magnitude of one). For instance, if $\bar{A}_{1n} = 1$ (and the other elements are small), then this

[†]When three comparison functions are utilized, the governing matrix equation (F.3) is of order nine; however, when this equation is reduced to the eigenvalue equation (F.2), the order is increased to eighteen. The eighteen eigenvalues in the solution consist of nine pairs of double roots corresponding to nine distinctive eigenfrequencies.

eigenvector represents axial displacement in the first axial mode (m=1) and the n^{th} circumferential mode. This same mode of vibration (*i.e.* m=1) can occur in the circumferential direction (when $\bar{B}_{1n} = 1$) or in the radial direction (when $\bar{C}_{1n} = 1$). Similarly, the second and third axial modes (m = 2,3) can be associated with shell displacements in any one of the three directions (together, they account for the *nine* normal modes of the system[†]).

In the eigenvectors associated with the three (or six if both shells are flexible) lowest eigenfrequencies (the loci of which are being studied here), the $\bar{C}_{mn}$ (m = 1,2,3) elements [as well as the $\bar{F}_{mn}$ elements (coefficients associated with the radial displacement of the outer shell) in systems with both shells flexible] are comparatively larger; thus, the vibration of the shell in these modes is mainly in the radial direction. For this reason, the modal shapes displayed in Appendix O and in Figures 16, 17, 19 and 20 are the radial displacements of the shells and they are plotted using the $\bar{C}_{mn}$ and $\bar{F}_{mn}$ elements in the eigenvectors.

Notation used in the computer program, the computer program itself and a sample of the output are given in the following pages.

[†]In systems with both shells flexible, the symmetry and antisymmetry of the vibration of the two shells double the number of eigenfrequencies and normal modes to eighteen.

NOTATION USED IN THE PROGRAM

Notation used in the computer program	Corresponding notation used in the thesis	Definition
C(3)*	σ_k , $k = 1,2,3$	Constants in the characteristic beam functions, defined in equation (A.5) for a clamped-clamped beam.
P(3)*	λ_k , $k = 1,2,3$	Eigenvalues of the characteristic beam equation.
EI*	ε_i	See NOMENCLATURE
NU	ν_i	See NOMENCLATURE
SK	k_i	See NOMENCLATURE
ZI*	β_i	Defined in equation (3.2.10)
UI*	$\bar{U}_i$	Dimensionless internal flow velocity
UO*	$\bar{U}_o$	Dimensionless annular flow velocity
N*	n	Circumferential mode number
MM(9,9)	$[M_i]$	See Appendix E
KK(9,9)	$[K_i]$	See Appendix E
CC(9,9)	$[C_i]$	See Appendix E
AA(18,18)	$[P_i]$	Defined in equation (F.1)
BB(18,18)	$[Q_i]$	Defined in equation (F.1)
Q1(3,3), Q2(3,3), Q3(3,3), Q4(3,3), Q5(3,3), Q6(3,3)		Integral terms in the generalized aerodynamic forces
OMEGA*	$\bar{\Omega}_i$	Dimensionless frequency
A(3,3)*, B(3,3)*, D(3,3)*, DEL(3,3)*	a_{km}, b_{km}, d_{km}, δ_{km}; $k,m = 1,2,3$	Constants defined in equations (3.4.22-.25), respectively)

*Notation with the same definition as in other computer programs.

```
/INFO MVS TI(20) PA(100) R(CENTRAL) CL(20) F(0415) N(STEVE SIU PUI CHAN)
//STEP1 EXEC FORTRAN
//FORT.SYSIN DD *
C*************************************************************************
C      COMPUTER PROGRAM FOR THE CASE OF INCOMPRESSIBLE INVISCID FLOW     *
C      ONLY THE INNER SHELL FLEXIBLE                                     *
C      BOUNDARY CONDITIONS: CLAMPED-CLAMPED                              *
C*************************************************************************
C
C*************************************************************************
C      MAIN PROGRAM                                                      *
C*************************************************************************
      IMPLICIT REAL*8(A-H,O-Z)
      COMPLEX*16 MM(9,9),KK(9,9),CC(9,9),AA(18,18)/324*(0.D0,0.D0)/,
     #BB(18,18)/324*(0.D0,0.D0)/,EIGA(18),EIGB(18),Z(18,18),WK(18,36),
     #OMEGA,Q1(3,3),Q2(3,3),Q3(3,3),Q4(3,3),Q5(3,3),Q6(3,3)
      REAL*8 NU
      COMMON/DATA1/NU,SK,EI,C(3),P(3),N
      COMMON/DATA2/ZI,DR,PI
      COMMON/DATA3/Q1,Q2,Q3,Q4
      COMMON/DATA4/Q5,Q6
      DATA IA/18/,IB/18/,NN/18/,IJOB/2/,IZ/18/
      PI=DARCOS(-1.D0)
      C(1)=0.9825022145762379D0
      C(2)=1.00077731190727D0
      C(3)=0.9999664501254086D0
      P(1)=4.7300407448627D0
      P(2)=7.8532046240958 4D0
      P(3)=10.995607838001 67D0
      EI=1/15.D0
      NU=0.30D0
      SK=(7.50D-3)**2/12
      ZI=1.709D1
      DR=1.D0
      N=2
      DO 3 K=1,3
      DO 3 M=1,3
      READ(5,*) Q1(K,M),Q2(K,M),Q3(K,M),Q4(K,M),Q5(K,M),Q6(K,M)
3     CONTINUE
      UI=0.0D0
      DO 1 L=1,2
      READ(5,*) UO
      CALL MKMAT(UI,UO,MM,KK)
      CALL CMAT(UI,UO,CC)
      CALL REDUCE(MM,KK,CC,AA,BB)
      CALL EIGZC(AA,IA,BB,IB,NN,IJOB,EIGA,EIGB,Z,IZ,WK,INFER,IER)
      PRINT10,UI,UO
10    FORMAT('1','FLOW VELOCITY INSIDE THE INNER CYLINDER=',F8.5/'0','FL
     #OW VELOCITY IN THE ANNULAR REGION=',F8.5)
      PRINT11
11    FORMAT('-','THE FREQUENCIES ARE:')
      DO 20 I=1,18
      OMEGA=-EIGA(I)/EIGB(I)
20    PRINT12,OMEGA
12    FORMAT('0','(',2D24.16,1X,')')
      DO 2 K=1,11,5
      M=K+4
      PRINT21,K,M
```

```
      2    PRINT22,((Z(I,J),J=K,M),I=1,9)
           K=16
           M=18
           PRINT21,K,M
           PRINT23,((Z(I,J),J=16,18),I=1,9)
      21   FORMAT('1','THE ',I2,'-',I2,' EIGENVECTORS')
      22   FORMAT(//5(2X,'(',2D10.3,')')/)
      23   FORMAT(//3(2X,'(',2D10.3,')')/)
      1    CONTINUE
           PRINT100
      100  FORMAT('1')
           STOP
           END
C
C*****************************************************************************
C      SUBROUTINE,MKMAT                                                       *
C*****************************************************************************
           SUBROUTINE MKMAT(UI,UO,MM,KK)
           IMPLICIT REAL*8(A-H,O-Z)
           DIMENSION A(3,3),B(3,3),D(3,3),DEL(3,3)
           COMPLEX*16 MM(9,9),KK(9,9),COE(9,3,3),COEK(3,3,3),Q1(3,3),Q2(3,3),
          #Q3(3,3),Q4(3,3)
           REAL*8 NU
           INTEGER DEL/9*0/,W,V,H
           COMMON/DATA1/NU,SK,EI,C(3),P(3),N
           COMMON/DATA2/ZI,DR,PI
           COMMON/DATA3/Q1,Q2,Q3,Q4
           DO 9 I=1,9
           DO 9 J=1,9
           MM(I,J)=(0.D0,0.D0)
      9    KK(I,J)=(0.D0,0.D0)
           C1=ZI/2/PI/EI
           C2=C1*DR
           DO 3 K=1,3
           DO 3 M=1,3
           IF(K.EQ.M) GO TO 1
           D(K,M)=4*P(K)**2*P(M)**2*((-1)**(K+M)+1)*(C(M)*P(M)-C(K)*P(K))
          C/(P(M)**4-P(K)**4)
           A(K,M)=-D(K,M)
           B(K,M)=0.D0
           GO TO 2
      1    D(K,K)=P(K)*C(K)*(2-P(K)*C(K))
           DEL(K,K)=1
           A(K,K)=-D(K,K)
           B(K,K)=-P(K)**4
      2    COEK(1,K,M)=A(K,M)
           COEK(2,K,M)=DEL(K,M)
      3    COEK(3,K,M)=DEL(K,M)+C1*Q1(K,M)-C2*Q2(K,M)
           C3=UI**2*ZI*EI/2/PI
           C4=UO**2*ZI*EI*DR/2/PI
           DO 4 K=1,3
           DO 4 M=1,3
           COE(1,K,M)=EI**2*B(K,M)+(NU-1)*(SK+1)*N**2*A(K,M)/2
           COE(2,K,M)=-(1+NU)*N*EI**2*D(K,M)/2
           COE(3,K,M)=(P(M)*EI)**4*SK*DEL(K,M)-(2*NU-SK*(1-NU)*N**2)
          C*EI**2*D(K,M)/2
           COE(4,K,M)=(1+NU)*N*A(K,M)/2
           COE(5,K,M)=-N**2*DEL(K,M)+(1+3*SK)*(1-NU)*EI**2*D(K,M)/2
```

```
      COE(6,K,M)=SK*(3-NU)*N*EI**2*D(K,M)/2-N*DEL(K,M)
      COE(7,K,M)=(NU+(NU-1)*SK*N**2/2)*A(K,M)-SK*EI**2*B(K,M)
      COE(8,K,M)=-N*DEL(K,M)+(3-NU)*SK*N*EI**2*D(K,M)/2
 4    COE(9,K,M)=-SK*(((P(M)*EI)**4+(N**2-1)**2)*DEL(K,M)-2*(N*EI)
     #**2*D(K,M))-DEL(K,M)+C3*Q3(K,M)-C4*Q4(K,M)
      K=0
      DO 5 I=1,7,3
      K=K+1
      DO 5 M=1,3
      W=-1
      DO 6 V=1,7,3
      W=W+1
      DO 6 L=1,3
      H=L-1
      KK(I+H,M+V-1)=COE(L+3*W,K,M)
 6    MM(I+H,M+3*H)=COEK(L,K,M)
 5    CONTINUE
      RETURN
      END
C
C*****************************************************************************
C     SUBROUTINE CMAT                                                        *
C*****************************************************************************
      SUBROUTINE CMAT(UI,UO,CC)
      IMPLICIT REAL*8 (A-H,O-Z)
      COMPLEX*16 CC(9,9),Q5,Q6
      COMMON/DATA2/ZI,DR,PI
      COMMON/DATA4/Q5(3,3),Q6(3,3)
      DO 2 I=1,9
      DO 2 J=1,9
 2    CC(I,J)=(0.D0,0.D0)
      C5=UI*ZI/PI
      C6=UO*ZI*DR/PI
      DO 1 K=1,3
      DO 1 M=1,3
      CC(3*K,6+M)=-C5*Q5(K,M)+C6*Q6(K,M)
 1    CONTINUE
      RETURN
      END
C
C*****************************************************************************
C     SUBROUTINE REDUCE                                                      *
C*****************************************************************************
      SUBROUTINE REDUCE(MM,KK,CC,AA,BB)
      COMPLEX*16 AA(18,18),BB(18,18),MM(9,9),KK(9,9),CC(9,9)
      DO 1 I=1,9
      AA(I,I+9)=(1.D0,0.D0)
      BB(I,I)=(-1.D0,0.D0)
 1    CONTINUE
      DO 2 I=1,9
      DO 2 J=1,9
      AA(9+I,J)=KK(I,J)
      AA(9+I,9+J)=CC(I,J)
      BB(9+I,9+J)=MM(I,J)
 2    CONTINUE
      RETURN
      END
//GO.SYSIN DD *
```

```
(0.20851176294837680+00,0.0)
(-0.30762120475931200+00,-0.37294688292169170-15)
(0.25411254691704040+01,0.0)
(-0.36692991168679050+01,-0.22970248156268650-13)
(-0.34806858675265820-06,0.0)
(0.30591657498870500-06,0.21967075683538060-14)
(-0.52440460858342170-17,0.24918099474426780-07)
(0.43689947797445350-15,-0.21886549795518530-07)
(0.17706203843318340-16,0.59218178929270480-04)
(-0.18943318838282500-13,-0.52011993019665230-04)
(-0.11314309528931270-16,-0.69075476143485040+00)
(-0.17266676391454100-14,0.99683597716347380+00)
(0.74742666024552060-03,0.26081370192961110-18)
(-0.39500144127935460-02,-0.13450985452208670-16)
(-0.20249818918769560+01,0.27274972885681900-17)
(0.29173068917767170+01,-0.90932743608901360-13)
(-0.16190977286229220-05,0.89379238473866900-17)
(0.14231921385272310-05,0.27496370677701140-14)
(-0.52440460858342170-17,-0.24918099474426780-07)
(-0.42123115153592250-15,0.21886549795518530-07)
(0.17706203843318340-16,-0.59218178929270480-04)
(0.18911099706362350-13,0.52011993019665230-04)
(-0.11314309528931270-16,0.69075476143485040+00)
(0.17592434939585340-14,-0.99683597716347380+00)
(0.20599875314973050+00,0.0)
(-0.29503362527854530,-0.11926899708807650-14)
(0.93779666704352860+01,0.0)
(-0.13119668620586990+02,-0.17539133799935140-12)
(-0.61991146046507420-05,0.0)
(0.54388272194270470-05,0.12091083492721580-13)
(-0.71344228567178770-17,-0.10623580414975110-06)
(0.13911798718553650-14,0.93341211682407870-07)
(-0.40731024585232080-15,-0.25130886884054030-03)
(0.37050090087408170-12,0.22080043460553180-03)
(0.35623990089511190-16,-0.11200416066562050+01)
(-0.18657659881244350-13,0.15499241097973070+01)
(0.74742666024552060-03,-0.26081370192961110-18)
(-0.39500144127935460-02,-0.12682163892328330-16)
(-0.20249818918769560+01,-0.27274972885681900-17)
(0.29173068917767170+01,-0.90923763384179140-13)
(-0.16190977286229220-05,-0.89379238473866900-17)
(0.14231921385272310-05,0.27758097457178700-14)
(-0.71344228567178770-17,0.10623580414975110-06)
(-0.13709727701451550-14,-0.93341211682407870-07)
(-0.40731024585232080-15,0.25130886884054030-03)
(-0.36935581687677620-12,-0.22080043460553180-03)
(0.35623990089511190-16,0.11200416066562050+01)
(0.18558753232584600-13,-0.15499241097973070+01)
(0.20223284513753740+00,0.0)
(-0.27795379981820400+00,-0.40133636593879220-14)
(0.19712164850415560+02,0.0)
(-0.26362203213149620+02,-0.10538051527827540-11)
(-0.76507423298948460-05,0.0)
(0.67255252195092940-05,0.58867799522011720-13)
0.0100D0
0.0200D0
//
/*
```

FLOW VELOCITY INSIDE THE INNER CYLINDER= 0.0

FLOW VELOCITY IN THE ANNULAR REGION= 0.01000

THE FREQUENCIES ARE:

1	-0.2123376205340491D+01	0.1134075250191070D-15
2	-0.2024170346568848D+01	-0.1036395630552271D-15
3	-0.1372605527039479D+01	0.1723881357169369D-16
4	-0.1218470754438523D+01	0.1003945800709230D-16
5	-0.2063089577813261D+01	0.2331033742517657D-16
6	-0.1276269618852090D+01	0.2624446883744175D-16
7	0.1218470754416870D+01	-0.4099639410633916D-17
8	0.1372605526986162D+01	-0.1203464300796724D-16
9	0.2123376205149902D+01	-0.4396439781570153D-16
10	0.2024170348556970D+01	-0.1173648825501419D-15
11	0.1276269618820544D+01	0.3004997611108115D-16
12	0.2063089577652158D+01	-0.1685933750550093D-16
13	0.2390098321513237D-01	-0.1663231777325393D-15
14	-0.2390100875907252D-01	0.3695684514381265D-16
15	0.1263536460444057D-01	-0.4645914775426644D-16
16	0.4640238712805C36D-02	-0.3395094386559850-16
17	-0.4640241055484637D-02	0.6661875736939458D-16
18	-0.1263537116807588D-01	0.6346935396731792D-17

THE 1- 5 EIGENVECTORS

(0.300D-01 0.993D-16)	(0.265D+00 0.133D-15)	(-0.729D+00 0.173D-16)	(-0.821D+00 0.943D-16)	(0.763D-16 0.846D-04)
(0.109D-15 0.785D-04)	(0.414D-16 0.797D-04)	(-0.254D-16-0.259D-04)	(-0.707D-16-0.364D-04)	(0.254D+00-0.726D-16)
(0.257D+00 0.336D-16)	(0.315D-01 0.353D-15)	(-0.404D+00 0.128D-15)	(0.106D+00 0.149D-16)	(0.168D-15 0.106D-03)
(0.439D-01-0.153D-15)	(-0.494D+00-0.379D-16)	(-0.137D-01 0.815D-16)	(-0.243D-01 0.123D-15)	(-0.799D-16-0.124D-03)
(-0.222D-15-0.160D-03)	(-0.752D-16-0.145D-03)	(0.411D-17 0.418D-05)	(-0.155D-16-0.969D-05)	(-0.485D+00-0.960D-17)
(-0.471D+00-0.704D-17)	(-0.439D-01-0.625D-15)	(-0.811D-01-0.842D-16)	(0.384D-01-0.115D-15)	(-0.283D-15-0.177D-03)
(0.101D-02-0.469D-17)	(-0.111D-01 0.683D-17)	(-0.484D-03 0.189D-17)	(-0.108D-02 0.362D-17)	(-0.142D-16-0.160D-04)
(-0.341D-16-0.245D-04)	(0.458D-17 0.874D-05)	(-0.786D-17-0.801D-05)	(0.509D-17 0.768D-05)	(-0.109D-01 0.219D-16)
(-0.106D-01 0.839D-16)	(-0.957D-03-0.637D-17)	(-0.313D-02 0.227D-16)	(0.178D-02-0.171D-16)	(0.371D-16 0.178D-04)

THE 6-10 EIGENVECTORS

(-0.230D-15-0.136D-03)	(0.821D+00 0.100D-15)	(0.729D+00 0.358D-16)	(-0.800D-01 0.888D-16)	(-0.265D+00 0.120D-15)
(-0.784D+00 0.101D-16)	(0.268D-16-0.364D-04)	(0.241D-16-0.259D-04)	(-0.110D-15 0.785D-04)	(-0.417D-16 0.797D-04)
(-0.197D-16-0.753D-05)	(-0.106D+00-0.352D-16)	(0.404D+00 0.543D-16)	(-0.257D+00-0.326D-16)	(-0.315D-01 0.336D-15)
(-0.165D-17 0.174D-05)	(0.243D-01 0.102D-15)	(0.137D-01 0.663D-16)	(-0.439D-01-0.174D-15)	(0.494D+00-0.274D-16)
(-0.825D-01-0.117D-17)	(0.891D-17-0.969D-05)	(-0.109D-16 0.418D-05)	(0.223D-15-0.160D-03)	(0.736D-16-0.145D-03)
(-0.184D-16-0.736D-05)	(-0.384D-01-0.109D-15)	(0.811D-01-0.269D-16)	(0.471D+00 0.229D-16)	(0.439D-01-0.606D-15)
(-0.472D-17-0.677D-05)	(0.108D-02 0.168D-17)	(0.484D-03 0.133D-17)	(-0.101D-02-0.283D-17)	(0.111D-01-0.820D-17)
(-0.345D-02 0.788D-17)	(-0.534D-17 0.768D-05)	(0.777D-17-0.801D-05)	(0.341D-16-0.245D-04)	(-0.459D-17 0.874D-05)
(0.236D-16 0.110D-04)	(-0.178D-02 0.116D-16)	(0.313D-02-0.256D-16)	(0.106D-01-0.847D-16)	(0.957D-03-0.216D-16)

THE 11-15 EIGENVECTORS

(-0.110D-16-0.136D-03)	(-0.984D-16 0.846D-04)	(0.695D-01 0.305D-15)	(0.695D-01-0.116D-15)	(-0.429D-17 0.407D-01)
(0.784D+00 0.313D-16)	(-0.254D+00-0.100D-15)	(-0.173D-14 0.465D-01)	(-0.310D-15-0.465D-01)	(-0.201D+00 0.283D-16)
(-0.334D-17-0.753D-05)	(-0.220D-15 0.106D-03)	(-0.170D+00 0.718D-16)	(-0.170D+00 0.137D-16)	(-0.114D-14 0.220D-01)
(-0.210D-17 0.174D-05)	(0.966D-16-0.124D-03)	(0.202D-01 0.844D-15)	(0.202D-01-0.883D-16)	(-0.789D-15 0.110D+00)
(0.825D-01 0.234D-16)	(0.485D+00-0.119D-17)	(-0.451D-14 0.116D+00)	(-0.115D-14-0.116D+00)	(-0.504D+00 0.154D-16)
(-0.997D-17-0.736D-05)	(0.376D-15-0.177D-03)	(-0.506D+00 0.103D-15)	(-0.506D+00 0.592D-16)	(-0.344D-14 0.671D-01)
(0.143D-17-0.677D-05)	(0.153D-16-0.160D-04)	(-0.372D-01-0.180D-14)	(-0.872D-01 0.249D-15)	(0.165D-14-0.220D+00)
(0.345D-02-0.747D-17)	(0.109D-01-0.202D-16)	(0.884D-14-0.231D+00)	(0.148D-14 0.231D+00)	(0.100D+01 0.0)
(0.469D-17 0.110D-04)	(-0.428D-16 0.178D-04)	(0.100D+01 0.0)	(0.100D+01 0.0)	(0.697D-14-0.133D+00)

THE 16-18 EIGENVECTORS

(-0.222D+00 0.228D-15)	(-0.222D+00-0.142D-15)	(-0.704D-16-0.407D-01)
(0.445D-15 0.169D-01)	(-0.155D-15-0.169D-01)	(-0.201D+00 0.576D-16)
(0.267D-02-0.132D-14)	(0.267D-02 0.755D-16)	(-0.673D-15-0.220D-01)
(-0.502D+00-0.236D-15)	(-0.502D+00 0.223D-18)	(-0.745D-15-0.110D+00)
(0.117D-14 0.423D-01)	(-0.532D-15-0.423D-01)	(-0.504D+00 0.561D-16)
(0.614D-03-0.385D-14)	(0.614D-03 0.127D-15)	(-0.198D-14-0.671D-01)
(0.100D+01 0.0)	(0.100D+01 0.0)	(0.158D-14 0.220D+00)
(-0.167D-14-0.839D-01)	(0.144D-14 0.839D-01)	(0.100D+01 0.0)
(0.192D-02-0.812D-14)	(0.192D-02-0.942D-16)	(0.381D-14 0.133D+00)

F.2 PROGRAM FOR SYSTEM WITH BOTH SHELLS FLEXIBLE

F.2.1 Function of the Program

The program calculates the dimensionless eigenfrequencies, $\bar{\Omega}_o$, and the associated eigenvectors of a system of two coaxial cylindrical shells subjected to internal and annular incompressible inviscid flows. For each set of input data of flow velocities $\bar{U}_i$, $\bar{U}_o$, the program constructs the matrices [P] and [Q] in equation (3.4.31). The frequencies are then determined as the solutions of this eigenvalue equation (3.4.31).

F.2.2 Program Structure

The program is written in Fortran IV language and it has the following structure:

MAIN PROGRAM
SUBROUTINE PREMAT
SUBROUTINE MKMAT
SUBROUTINE CMAT
SUBROUTINE REDUCE
SUBROUTINE EIGZC.

F.2.3 Description of the Program

The function of each subprogram is summarized as follows:

(1) Subroutine PREMAT fills the matrices [M] and [K] as defined in equation (3.4.29) (the structure of which is shown in Appendix E) with elements that are not dependent on the flow velocities, $\bar{U}_i$ and $\bar{U}_o$. Hence,

this subroutine is called only once in the main program, and the complete construction of the matrices will be achieved by the other subroutine (MKMAT) after each set of flow velocities is read from the data deck.

(2) Subroutine MKMAT completes the construction of the matrices [M] and [K] by supplementing the appropriate elements with the generalized aerodynamic force terms. It calculates the terms q^{C1}_{kmn}, q^{F1}_{kmn}, q^{C3}_{kmn}, q^{F3}_{kmn}, r^{C1}_{kmn}, r^{F1}_{kmn}, r^{C3}_{kmn}, r^{F3}_{kmn} (defined in Section 3.3) with the input flow velocities and the values of the integrals† that have been read and stored in the program.

(3) Subroutine CMAT constructs the matrix [C] as defined in equation (3.4.29) (see Appendix E for the structure of the matrix) by filling in the non-zero elements q^{C2}_{kmn}, q^{F2}_{kmn}, r^{C2}_{kmn}, r^{F2}_{kmn} (defined in Section 3.3).

(4) Subroutine REDUCE constructs the matrices [P] and [Q] in the eigenvalue equation (3.4.31) which is reduced from the second-order matrix equation (3.4.29).

(5) Subroutine EIGZC is the IMSL subroutine employed to solve the eigenvalue equation (3.4.31).

All the necessary parameters are defined in the main program. The output results consist of all thirty-six eigenvalues (when three comparison functions are utilized) and the upper half segment of the associated eigenvectors which contains the shell displacement vector {X} (defined in equation (3.4.27)).

Notation used in the computer program, the computer program itself and a sample of the output are given in the following pages.

---

†The computer program for calculating the integrals is described in Appendix H.

NOTATION USED IN THE PROGRAM

Notation used in the computer program	Corresponding notation used in the thesis	Definition
EI*	ε_i	See NOMENCLATURE
EO*	ε_o	See NOMENCLATURE
ER*	ε_r	See NOMENCLATURE
NI*	ν_i	See NOMENCLATURE
NO*	ν_o	See NOMENCLATURE
SKI*	k_i	See NOMENCLATURE
SKO*	k_o	See NOMENCLATURE
ZO*	β_o	Defined in equation (3.2.10)
OMR*	Ω_r	Defined in equation (3.4.2)
DSR*	ρ_r	Defined in equation (3.2.10)
USR*	υ_r	Defined in equation (3.2.10)
Q(9,3,3), R(6,3,3)		Integral terms in the generalized aerodynamic forces
MM(18,18)	$[M]$	See Appendix E
KK(18,18)	$[K]$	See Appendix E
CC(18,18)	$[C]$	See Appendix E
AA(36,36)	$[\bar{P}]$	Defined by equation (3.4.31)
BB(36,36)	$[Q]$	Defined by equation (3.4.31)

*Notation with the same definition as in other computer programs.

```
/INFO MVS TI(30) PA(100) R(CENTRAL) CL(30) F(0415) N(STEVE SIU PUI CHAN)
//STEP1 EXEC FORTRAN
//FORT.SYSIN DD *
C*************************************************************************
C     COMPUTER PROGRAM FOR THE CASE OF INCOMPRESSIBLE INVISCID FLOW     *
C     BOTH SHELLS FLEXIBLE                                              *
C     BOUNDARY CONDITIONS: CLAMPED-CLAMPED                              *
C*************************************************************************
C
C*************************************************************************
C     MAIN PROGRAM                                                      *
C*************************************************************************
      IMPLICIT REAL*8(A-H,O-Z)
      COMPLEX*16 MM(18,18),KK(18,18),CC(18,18)/324*(0.D0,0.D0)/,
     #AA(36,36)/1296*(0.D0,0.D0)/,BB(36,36)/1296*(0.D0,0.D0)/,EIGA(36),
     #EIGB(36),Z(36,36),WK(36,72),OMEGA,Q(9,3,3),R(6,3,3),CK(2,3,3)
      INTEGER DEL(8,3)
      REAL*8 NI,NO
      COMMON/DATA1/NI,NO,SKI,SKO,C(3),P(3),N
      COMMON/DATA2/EI,EO,ER,OMR
      COMMON/DATA3/ZI,ZO,USR,DSR,PI
      COMMON/DATA4/Q,R
      DATA IA/36/,IB/36/,NN/36/,IJOB/2/,IZ/36/
      PI=DARCOS(-1.D0)
      C(1)=0.98250221457623790D0
      C(2)=1.00077731190727D0
      C(3)=0.99996645012540860D0
      P(1)=4.7300407448627D0
      P(2)=7.853204624095840D0
      P(3)=10.995607838001670D0
      EI=1/15.D0
      EO=0.1D0
      ER=2/3.D0
      NI=0.30D0
      NO=0.30D0
      SKI=(7.50D-3)**2/12
      SKO=SKI*4/9
      OMR=3/2.D0
      ZI=1.709D1
      ZO=ZI/ER
      DSR=1.D0
      USR=1.D0
      N=3
      DO 3 K=1,3
      DO 3 M=1,3
      READ(5,*) (Q(I,K,M),I=1,9),(R(I,K,M),I=1,6)
    3 CONTINUE
      CALL PREMAT(MM,KK,CK,DEL)
      UI=0.0D0
      DO 1 L=1,3
      READ(5,*) UO
C     CALL MKMAT(UI,UO,MM,KK,CK,DEL)
      CALL CMAT(UI,UO,CC)
      CALL REDUCE(MM,KK,CC,AA,BB)
      CALL EIGZC(AA,IA,BB,IB,NN,IJOB,EIGA,EIGB,Z,IZ,WK,INFER,IER)
      PRINT10,UI,UO
   10 FORMAT('1','FLOW VELOCITY INSIDE THE INNER CYLINDER=',F8.5/'0','FL
     #OW VELOCITY IN THE ANNULAR REGION=',F8.5)
```

```
      PRINT11
   11 FORMAT('-','THE FREQUENCIES ARE:')
      DO 20 I=1,36
      OMEGA=-EIGA(I)/EIGB(I)
   20 PRINT12,OMEGA
   12 FORMAT('0','(',2D24.16,1X,')')
      DO 2 K=1,31,5
      M=K+4
      PRINT 21,K,M
    2 PRINT 22,((Z(I,J),J=K,M),I=1,18)
      PRINT 24
      PRINT 23,(Z(I,36),I=1,18)
   21 FORMAT('1','THE ',I2,'-',I2,' EIGENVECTORS')
   22 FORMAT(//5(2X,'(',2D10.3,')')/)
   23 FORMAT(//(2X,'(',2D10.3,')')/)
   24 FORMAT('1','THE ','36',' EIGENVECTOR')
    1 CONTINUE
      PRINT100
  100 FORMAT('1')
      STOP
      END
C
C*****************************************************************************
C     SUBROUTINE PREMAT                                                      *
C*****************************************************************************
      SUBROUTINE PREMAT(MM,KK,CK,DEL)
      IMPLICIT REAL*8(A-H,O-Z)
      DIMENSION A(3,3),B(3,3),D(3,3),DEL(3,3)
      COMPLEX*16 MM(18,18),KK(18,18),COE(9,3,3),COEK(3,3,3),CK(2,3,3)
      REAL*8 NI,NO,NU
      INTEGER DEL,R,Q,W,V,H
      COMMON/DATA1/NI,NO,SKI,SKO,C(3),P(3),N
      COMMON/DATA2/EI,EO,ER,OMR
      DO 9 I=1,18
      DO 9 J=1,18
      MM(I,J)=(0.D0,0.D0)
    9 KK(I,J)=(0.D0,0.D0)
      DO 3 K=1,3
      DO 3 M=1,3
      IF(K.EQ.M) GO TO 1
      D(K,M)=4*P(K)**2*P(M)**2*((-1)**(K+M)+1)*(C(M)*P(M)-C(K)*P(K))
     C/(P(M)**4-P(K)**4)
      A(K,M)=-D(K,M)
      B(K,M)=0.D0
      DEL(K,M)=0
      GO TO 2
    1 D(K,K)=P(K)*C(K)*(2-P(K)*C(K))
      DEL(K,K)=1
      A(K,K)=-D(K,K)
      B(K,K)=-P(K)**4
    2 COEK(1,K,M)=A(K,M)
      COEK(2,K,M)=DEL(K,M)
    3 COEK(3,K,M)=DEL(K,M)
      J=0
      E=EI
      NU=NI
      SK=SKI
   12 DO 4 K=1,3
```

```
      DO 4 M=1,3
      COE(1,K,M)=E**2*B(K,M)+(NU-1)*(SK+1)*N**2*A(K,M)/2
      COE(2,K,M)=-(1+NU)*N*E**2*D(K,M)/2
      COE(3,K,M)=(P(M)*E)**4*SK*DEL(K,M)-(2*NU-SK*(1-NU)*N**2)
     C*E**2*D(K,M)/2
      COE(4,K,M)=(1+NU)*N*A(K,M)/2
      COE(5,K,M)=-N**2*DEL(K,M)+(1+3*SK)*(1-NU)*E**2*D(K,M)/2
      COE(6,K,M)=SK*(3-NU)*N*E**2*D(K,M)/2-N*DEL(K,M)
      COE(7,K,M)=(NU+(NU-1)*SK*N**2/2)*A(K,M)-SK*E**2*B(K,M)
      COE(8,K,M)=-N*DEL(K,M)+(3-NU)*SK*N*E**2*D(K,M)/2
      COE(9,K,M)=-SK*((P(M)*E)**4+(N**2-1)**2)*DEL(K,M)-2*(N*E)
     #**2*D(K,M)-DEL(K,M)
4     CK(J+1,K,M)=COE(9,K,M)
      K=0
      DO 5 I=1,7,3
      K=K+1
      DO 5 M=1,3
      R=I+J*9
      Q=M+J*9
      W=-1
      DO 6 V=1,7,3
      W=W+1
      DO 6 L=1,3
      H=L-1
      KK(R+H,Q+V-1)=COE(L+3*W,K,M)
6     MM(R+H,Q+3*H)=COEK(L,K,M)/(J-(J-1)*OMR**2)
5     CONTINUE
      IF(J.EQ.1) GO TO 8
      J=1
      E=EO
      NU=NO
      SK=SKO
      GO TO 12
8     CONTINUE
      RETURN
      END
C
C*****************************************************************
C     SUBROUTINE MKMAT                                           *
C*****************************************************************
      SUBROUTINE MKMAT(UI,UO,MM,KK,CK,DEL)
      IMPLICIT REAL*8(A-H,O-Z)
      COMPLEX*16 MM(18,18),KK(18,18),CK(2,3,3),Q(9,3,3),R(6,3,3)
      INTEGER DEL(3,3)
      COMMON/DATA2/EI,EO,ER,OMR
      COMMON/DATA3/ZI,ZO,USR,DSR,PI
      COMMON/DATA4/Q,R
      Q1=ZI*EI/2/PI/EO**2/USR**2
      Q2=Q1*DSR
      Q3=UI**2*ZI*EI/2/PI
      Q4=UO**2*ZI*EI*DSR/2/PI/USR**2
      R1=ZO/2/PI/EO
      R2=UO**2*ZO*EO/2/PI
      K=0
      DO 1 I=3,9,3
      K=K+1
      N=I+9
      DO 1 M=1,3
```

```
      L=M+6
      J=L+9
      KK(I,L)=CK(1,K,M)+Q3*Q(3,K,M)-Q4*Q(6,K,M)
      KK(I,J)=-Q4*Q(9,K,M)
      MM(I,L)=DEL(K,M)/OMR**2+Q1*Q(2,K,M)-Q2*Q(5,K,M)
      MM(I,J)=-Q2*Q(8,K,M)
      KK(N,J)=CK(2,K,M)+R2*R(6,K,M)
      KK(N,L)=R2*R(3,K,M)
      MM(N,J)=DEL(K,M)+R1*R(5,K,M)
      MM(N,L)=R1*R(2,K,M)
    1 CONTINUE
      RETURN
      END
C
C*************************************************************************
C     SUBROUTINE CMAT                                                    *
C*************************************************************************
      SUBROUTINE CMAT(UI,UO,CC)
      IMPLICIT REAL*8(A-H,O-Z)
      COMPLEX*16 CC(18,18),Q(9,3,3),R(6,3,3)
      COMMON/DATA2/EI,EO,ER,OMR
      COMMON/DATA3/ZI,ZO,USR,DSR,PI
      COMMON/DATA4/Q,R
      Q5=UI*ZI*ER/PI/USR
      Q6=UO*ZI*ER*DSR/PI/USR**2
      R3=UO*ZO/PI
      DO 1 K=1,3
      I=3*K
      II=I+9
      DO 1 M=1,3
      J=M+6
      JJ=J+9
      CC(I,J)=-Q5*Q(1,K,M)+Q6*Q(4,K,M)
      CC(I,JJ)=Q6*Q(7,K,M)
      CC(II,J)=-R3*R(1,K,M)
      CC(II,JJ)=-R3*R(4,K,M)
    1 CONTINUE
      RETURN
      END
C
C*************************************************************************
C     SUBROUTINE REDUCE                                                  *
C*************************************************************************
      SUBROUTINE REDUCE(MM,KK,CC,AA,BB)
      COMPLEX*16 AA(36,36),BB(36,36),MM(18,18),KK(18,18),CC(18,18)
      DO 1 I=1,18
      AA(I,I+18)=(1.D0,0.D0)
      BB(I,I)=(-1.D0,0.D0)
    1 CONTINUE
      DO 2 I=1,18
      DO 2 J=1,18
      AA(18+I,J)=KK(I,J)
      AA(18+I,18+J)=CC(I,J)
      BB(18+I,18+J)=MM(I,J)
    2 CONTINUE
      RETURN
      END
//GO.SYSIN DD *
```

```
(-0.2890189487239503D-06,0.D0)
(0.1393110690919361D+00,0.D0)
(0.1705368800527476D+01,0.D0)
(0.2660289319962818D-06,-0.1868688691154308D-15)
(-0.1655069832604356D+00,0.2553490443000322D-16)
(-0.2011334753979894D+01,0.7037229509394624D-15)
(-0.9638445477451997D-07,0.8504345526911056D-16)
(0.1345369717709292D+00,-0.1096626859724626D-16)
(0.1617822735858261D+01,-0.6992446468493798D-15)
(0.6425630324137880D-07,-0.3188811674447007D-15)
(-0.8969131451391969D-01,0.1319368907332701D-16)
(-0.1078548490571852D+01,0.1065609002297195D-13)
(-0.3486206040141913D-06,0.8475480650180876D-16)
(0.2479776423190240D+00,-0.4258588140151997D-17)
(0.3006692439684595D+01,-0.2582502009977377D-14)
(-0.7595545043302750D-17,-0.4635193666396506D+00)
(-0.3493985561308399D-17,0.2071083591670780D-07)
(0.1280325901621925D-16,0.4922197501411912D-04)
(0.5270091996945850D-15,0.5467118674964745D+00)
(-0.5615031471458955D-16,-0.1905137052050897D-07)
(-0.4856623623462007D-14,-0.4527659901670027D-04)
(-0.2252352362098623D-15,-0.4398371058593326D+00)
(0.2220811692905043D-16,0.6861123644586984D-08)
(0.2057632409073206D-14,0.1630086329031229D-04)
(0.1032870802265429D-14,0.2932247372394789D+00)
(-0.3664548376597598D-16,-0.4574082436428917D-08)
(-0.3485457623269350D-13,-0.1086724219316598D-04)
(-0.2849982099649656D-15,-0.8173033283886056D+00)
(0.5874640554172223D-17,0.2494759283287686D-07)
(0.8303797447904569D-14,0.5928706632459122D-04)
(-0.1344171251251656D-05,0.5982278243355582D-17)
(0.2502530206638508D-03,0.1742202535041026D-18)
(-0.1356451885410314D+01,0.1766665033111523D-17)
(0.1237397299804226D-05,0.3473654502034835D-15)
(-0.7935232932433042D-03,-0.4605728693621104D-16)
(0.1602751337687827D+01,-0.7012345353758176D-14)
(-0.4488287222369220D-06,-0.1194086173060520D-15)
(0.1213610613484465D-02,0.1993221837259288D-16)
(-0.1294065917592288D+01,0.8421263593472302D-15)
(0.2992191481303737D-06,-0.1208065036565199D-14)
(-0.8090737423177347D-03,0.2574232636227161D-16)
(0.8627106117282512D+00,0.4680161105943991D-13)
(-0.1621789093104325D-05,0.2883057296116006D-15)
(0.1416325814646316D-02,-0.4345392348774801D-17)
(-0.2397943421026591D+01,-0.1093022614720827D-13)
(-0.7595545043302750D-17,0.4635193666396506D+00)
(-0.3493985561308399D-17,-0.2071083591670780D-07)
(0.1280325901621925D-16,-0.4922197501411912D-04)
(-0.5091037977393918D-15,-0.5467118674964745D+00)
(0.6448962380635904D-16,0.1905137052050897D-07)
(0.4829960346888875D-14,0.4527659901670027D-04)
(0.2108446751248950D-15,0.4398371058593326D+00)
(-0.2903050398912725D-16,-0.6861123644586984D-08)
(-0.2040348373702852D-14,-0.1630086329031229D-04)
(-0.1023277094875441D-14,-0.2932247372394789D+00)
(0.4119374180602675D-16,0.4574082436428917D-08)
(0.3484305354244643D-13,0.1086724219316598D-04)
(0.2582365005513510D-15,0.8173033283886056D+00)
```

```
(-0.1838680512807832D-16,-0.2494759283287686D-07)
(-0.8265608003926213D-14,-0.5928706632459122D-04)
(-0.5161242089028442D-05,0.D0)
(0.1384569070761792D+00,0.D0)
(0.6336100528081735D+01,0.D0)
(0.4742426007811891D-05,-0.4818511456360506D-14)
(-0.1628769399841652D+00,0.3257762812199737D-15)
(-0.7391909319082398D+01,0.1092025624732897D-12)
(-0.1689795578036776D-05,0.1624031691193301D-14)
(0.1305297403181802D+00,-0.1263836221171813D-15)
(0.5850023413154393D+01,-0.3017532498852721D-13)
(0.1126530385384463D-05,-0.9256074504610996D-14)
(-0.8701982687876826D-01,0.2755793083122359D-15)
(-0.3900015608769352D+01,0.3587646479927868D-12)
(-0.6202053519409924D-05,0.2149085773894211D-14)
(0.2432885745425819D+00,-0.7323709577007043D-16)
(0.1101160144439360D+02,-0.7771596143757799D-13)
(0.2409414777298159D-16,-0.7581629515661440D+00)
(-0.4805380404083589D-17,-0.8825507255690017D-07)
(-0.2745673612882188D-15,-0.2087817271474474D-03)
(0.4643306945629120D-14,0.8816097069169224D+00)
(-0.4062208095643473D-15,0.8120960680877015D-07)
(-0.6616415426105696D-13,0.1921099564877068D-03)
(-0.1813913592696576D-14,-0.6944200929033301D+00)
(0.1649206766410976D-15,-0.2933618814561975D-07)
(0.2273036281986111D-13,-0.6938213052369398D-04)
(-0.1941261711255243D-14,0.4629467286022191D+00)
(0.2134587139883961D-16,0.1955745877342013D-07)
(0.7949576834740758D-13,0.4625475368015035D-04)
(0.4618730526777892D-15,-0.1312006276181646D+01)
(-0.4824145207274254D-17,-0.1063832605888907D-06)
(-0.1930285867759761D-13,-0.2516538706680979D-03)
(-0.1344171251251656D-05,-0.5982278243355582D-17)
(0.2502530206638508D-03,-0.1742202535041026D-18)
(-0.1356451885410314D+01,-0.1766665033111523D-17)
(0.1237397299804226D-05,0.3615397570688440D-15)
(-0.7935232932433042D-03,-0.4564326211814969D-16)
(0.1602751337687827D+01,-0.7007942715180164D-14)
(-0.4488287222369220D-06,-0.1308830571001824D-15)
(0.1213610613484465D-02,0.1959554475870905D-16)
(-0.1294065917592288D+01,0.8383017296742668D-15)
(0.2992191481303737D-06,-0.1200415410035790D-14)
(-0.8090737423177347D-03,0.2596677543819464D-16)
(0.8627106117282512D+00,0.4680416081255523D-13)
(-0.1621789093104325D-05,0.2670875828605982D-15)
(0.1416325814646316D-02,-0.4965773073882907D-17)
(-0.2397943421026591D+01,-0.1093692141246031D-13)
(0.2409414777298159D-16,0.7581629515661440D+00)
(-0.4805380404083589D-17,0.8825507255690017D-07)
(-0.2745673612882188D-15,0.2087817271474474D-03)
(-0.4699412319131075D-14,-0.8816097069169224D+00)
(0.4174864361437056D-15,-0.8120960680877015D-07)
(0.6680671497692505D-13,-0.1921099564877068D-03)
(0.1858194438397101D-14,0.6944200929033301D+00)
(-0.1739024653326135D-15,0.2933618814561975D-07)
(-0.2324154026033169D-13,0.6938213052369398D-04)
(0.1911741147454861D-14,-0.4629467286022191D+00)
(-0.1535801227115792D-16,-0.1955745877342013D-07)
```

```
(-0.7915498338709353D-13,-0.4625475368015035D-04)
(-0.3783418634799955D-15,0.1312006276181646D+01)
(-0.1198468035562802D-16,0.1063832605888907D-06)
(0.1834456601645112D-13,0.2516538706680979D-03)
(-0.6350909698057574D-05,0.D0)
(0.1371499215948725D+00,0.D0)
(0.1345434890848073D+02,0.D0)
(0.5846857252439295D-05,-0.1003111748921954D-13)
(-0.1590275057634876D+00,0.8854564896880767D-15)
(-0.1544550853220029D+02,0.9570184411235733D-13)
(-0.2122252939652193D-05,0.4256181940899100D-14)
(0.1246957944011807D+00,-0.3653442490327280D-15)
(0.1191935721661525D+02,-0.4948711463825588D-13)
(0.1414835292498975D-05,-0.7665569597592951D-14)
(-0.8313052960078406D-01,0.2952735865352885D-15)
(-0.7946238144409769D+01,0.2523139066604228D-12)
(-0.7663818970663815D-05,0.2065239511601115D-14)
(0.2364358402185395D+00,-0.9302239810137137D-16)
(0.2288662767446464D+02,-0.6152691229559147D-13)
0.00500D0
0.04230D0
0.04710D0
//
/*
```

FLOW VELOCITY INSIDE THE INNER CYLINDER= 0.0

FLOW VELOCITY IN THE ANNULAR REGION= 0.00500

THE FREQUENCIES ARE:

1	0.4632025390869821D+01	-0.7540624543385773D-16
2	0.4534000203841366D+01	0.2825972308457638D-15
3	-0.4632025391064961D+01	-0.1826338525720512D-15
4	-0.4534000203857790D+01	0.2866630429560404D-15
5	-0.4572470349473905D+01	-0.1507040790915518D-16
6	0.4572470349315959D+01	0.1322726613155116D-16
7	0.3184758959671109D+01	0.1980782419458146D-14
8	0.2697145391843522D+01	0.2368981134643626D-16
9	0.2865365408851199D+01	0.2477401708921561D-16
10	0.3036539282043769D+01	0.1326575353735453D-14
11	0.3094649098722099D+01	-0.3127921267187664D-16
12	0.2758946832025150D+01	0.9053077852508906D-16
13	0.2058660144020186D+01	0.1968477337075247D-14
14	0.1827680680142453D+01	-0.2835023706190689D-14
15	0.1914404425856356D+01	-0.2195509392447805D-17
16	-0.2697145391852973D+01	0.1935300533676549D-16
17	-0.2865365408875639D+01	0.8619403831400292D-17
18	-0.3184758959983582D+01	0.1849207555485385D-14
19	-0.3036539282068609D+01	0.1328905105652901D-14
20	-0.2758946832039339D+01	0.2043515680972547D-15
21	-0.3094649099001660D+01	-0.1526511239845838D-15
22	-0.2058860144109278D+01	0.1926407012661779D-14
23	-0.1827680680177027D+01	-0.2624999146818311D-14
24	-0.1914404425910665D+01	-0.1924456856018302D-17
25	-0.3742295312875725D-01	0.7674169093087012D-17
26	0.3742291509292948D-01	0.5360948475302432D-16
27	-0.2241423484680733D-01	-0.2598486043845191D-16
28	-0.2063303865212113D-01	-0.7182629257700436D-16
29	-0.1268867018971075D-01	0.2605809572194121D-17
30	-0.9919889778393766D-02	-0.3493044144897999D-17
31	-0.6461718519224954D-02	0.1199541402398791D-16
32	0.2241421098892045D-01	0.3550294609460232D-16
33	0.2063301786633041D-01	-0.1172845565984935D-16
34	0.1268866194163319D-01	0.2637146891448066D-16
35	0.6461715778658426D-02	0.3017362352210029D-17
36	0.9919887834934167D-02	0.2177715207455339D-17

THE 1- 5 EIGENVECTORS

(0.229D-03-0.804D-16)	(-0.754D-01-0.333D-16)	(-0.229D-03-0.890D-16)	(0.754D-01-0.374D-16)	(-0.151D-16 0.990D-05)
(0.311D-16 0.125D-04)	(0.669D-18 0.105D-04)	(-0.310D-16 0.126D-04)	(-0.856D-18 0.105D-04)	(0.742D-01-0.694D-18)
(-0.745D-01 0.305D-17)	(-0.862D-02-0.256D-15)	(0.745D-01-0.170D-17)	(0.862D-02-0.289D-15)	(-0.376D-15 0.149D-04)
(-0.222D-01 0.237D-15)	(0.221D+00 0.186D-16)	(0.222D-01 0.260D-15)	(-0.221D+00 0.173D-16)	(-0.656D-16-0.255D-04)
(-0.945D-16-0.381D-04)	(-0.193D-17-0.303D-04)	(0.942D-16-0.382D-04)	(0.283D-17-0.302D-04)	(-0.219D+00 0.620D-18)
(0.216D+00-0.712D-17)	(0.225D-01 0.738D-15)	(-0.216D+00-0.318D-17)	(-0.225D-01 0.837D-15)	(0.109D-14-0.416D-04)
(-0.625D-03 0.560D-17)	(0.630D-02 0.795D-18)	(0.625D-03 0.861D-17)	(-0.630D-02 0.298D-18)	(-0.166D-17-0.260D-05)
(-0.105D-16-0.422D-05)	(0.617D-19 0.738D-06)	(0.104D-16-0.423D-05)	(-0.499D-19 0.737D-06)	(-0.621D-02-0.347D-17)
(0.608D-02 0.138D-16)	(0.641D-03 0.211D-16)	(-0.608D-02-0.141D-16)	(-0.641D-03 0.233D-16)	(0.228D-16 0.193D-05)
(0.230D-05-0.371D-18)	(-0.101D-03-0.390D-18)	(-0.230D-05-0.461D-18)	(0.101D-03-0.439D-18)	(0.876D-17 0.319D-07)
(0.171D-18 0.519D-07)	(0.432D-19-0.693D-08)	(-0.169D-18 0.520D-07)	(-0.429D-19-0.690D-08)	(0.968D-04-0.215D-18)
(-0.932D-04 0.409D-18)	(-0.112D-04 0.133D-18)	(0.932D-04 0.226D-18)	(0.112D-04-0.245D-19)	(-0.128D-16-0.224D-07)
(-0.510D-04 0.102D-17)	(0.547D-03 0.782D-18)	(0.510D-04 0.147D-17)	(-0.547D-03 0.972D-18)	(-0.321D-16-0.186D-06)
(-0.945D-18-0.287D-06)	(-0.232D-18 0.374D-07)	(0.933D-18-0.288D-06)	(0.230D-18 0.372D-07)	(-0.527D-03 0.114D-17)
(0.498D-03-0.870D-18)	(0.559D-04 0.886D-18)	(-0.498D-03 0.492D-19)	(-0.559D-04 0.170D-17)	(0.364D-16 0.119D-06)
(-0.199D-03 0.140D-17)	(0.209D-02-0.132D-19)	(0.199D-03 0.334D-17)	(-0.209D-02 0.480D-18)	(-0.226D-17-0.729D-06)
(-0.382D-17-0.116D-05)	(-0.867D-18 0.140D-06)	(0.377D-17-0.116D-05)	(0.859D-18 0.139D-06)	(-0.203D-02 0.473D-17)
(0.195D-02-0.177D-17)	(0.214D-03 0.551D-17)	(-0.195D-02 0.163D-17)	(-0.214D-03 0.871D-17)	(0.794D-17 0.440D-06)

THE 6-10 EIGENVECTORS

(-0.495D-16 0.991D-05)	(0.165D-02-0.435D-16)	(0.371D+00-0.446D-16)	(0.349D+00-0.336D-16)	(0.599D-02 0.365D-16)
(-0.742D-01 0.458D-18)	(-0.519D-17-0.289D-05)	(-0.730D-17-0.352D-05)	(-0.200D-18-0.262D-05)	(-0.102D-16 0.447D-06)
(-0.304D-15 0.149D-04)	(0.391D-02 0.120D-15)	(-0.489D-01-0.183D-15)	(0.201D+00-0.320D-15)	(0.120D-02 0.314D-15)
(0.569D-16-0.255D-04)	(0.204D-03 0.727D-16)	(0.730D-02-0.158D-15)	(0.374D-02-0.160D-15)	(-0.266D-02 0.503D-16)
(0.219D+00-0.854D-18)	(0.891D-17 0.199D-05)	(0.862D-17-0.629D-06)	(-0.119D-16 0.319D-06)	(0.360D-16-0.191D-06)
(0.898D-15-0.416D-04)	(-0.190D-02-0.356D-15)	(-0.120D-01 0.533D-15)	(0.252D-01 0.705D-15)	(-0.149D-03-0.955D-15)
(0.795D-18-0.260D-05)	(-0.368D-03-0.706D-16)	(0.413D-03-0.428D-17)	(0.190D-03-0.434D-17)	(0.455D-02 0.355D-17)
(0.621D-02 0.346D-17)	(0.654D-18-0.342D-05)	(0.119D-17 0.755D-06)	(-0.194D-17-0.926D-06)	(0.106D-17 0.377D-06)
(0.337D-16 0.192D-05)	(0.401D-02-0.116D-16)	(-0.684D-03 0.137D-16)	(0.181D-02 0.228D-16)	(0.412D-03-0.953D-18)
(0.560D-17 0.320D-07)	(-0.134D-01 0.194D-14)	(0.521D-04 0.396D-18)	(0.182D-03-0.585D-17)	(-0.118D+00-0.372D-15)
(-0.968D-04 0.263D-18)	(-0.210D-17 0.258D-04)	(0.182D-18 0.109D-06)	(-0.585D-18-0.188D-06)	(-0.173D-17 0.260D-04)
(-0.643D-17-0.223D-07)	(-0.114D+00-0.256D-15)	(-0.119D-03 0.132D-17)	(0.299D-03-0.311D-17)	(-0.140D-01-0.338D-15)
(-0.179D-16-0.186D-06)	(-0.292D-01-0.519D-14)	(-0.196D-03-0.148D-17)	(-0.245D-03 0.214D-16)	(0.329D+00 0.156D-15)
(0.527D-03-0.124D-17)	(0.545D-17-0.789D-04)	(-0.334D-18-0.211D-06)	(0.134D-17 0.439D-06)	(0.597D-17-0.708D-04)
(0.127D-16 0.118D-06)	(0.314D+00 0.986D-16)	(0.188D-03-0.753D-18)	(-0.587D-03-0.163D-17)	(0.292D-01 0.190D-14)
(0.568D-18-0.730D-06)	(-0.973D-03-0.177D-15)	(0.129D-03-0.142D-17)	(0.569D-04-0.893D-18)	(0.113D-01 0.520D-17)
(0.203D-02-0.482D-17)	(0.359D-18-0.181D-04)	(0.367D-18 0.165D-06)	(-0.732D-18-0.196D-06)	(0.651D-18 0.637D-05)
(0.115D-16 0.438D-06)	(0.104D-01-0.397D-17)	(-0.212D-03 0.496D-17)	(0.400D-03 0.574D-17)	(0.994D-03 0.575D-16)

THE 11-15 EIGENVECTORS

(-0.131D-14-0.134D-05)	(0.233D-13-0.132D-04)	(0.915D-04 0.814D-16)	(-0.238D-03 0.459D-16)	(0.256D-16 0.482D-06)
(0.439D-02-0.149D-15)	(0.362D+00 0.215D-16)	(-0.172D-16 0.454D-06)	(-0.570D-17-0.298D-06)	(-0.559D-03-0.293D-16)
(-0.209D-14 0.145D-05)	(0.290D-14-0.812D-06)	(-0.513D-03 0.115D-16)	(0.218D-03 0.133D-15)	(-0.596D-16-0.430D-06)
(0.294D-17 0.140D-05)	(0.401D-15 0.119D-06)	(-0.129D-03-0.919D-16)	(-0.265D-03-0.182D-16)	(0.940D-17 0.477D-06)
(-0.233D-02-0.221D-18)	(0.247D-01 0.154D-15)	(0.268D-16 0.587D-06)	(0.576D-17-0.498D-06)	(-0.857D-03-0.159D-15)
(0.404D-15-0.504D-06)	(0.876D-15-0.500D-06)	(-0.791D-03-0.584D-15)	(0.417D-03-0.780D-15)	(-0.604D-16-0.761D-06)
(0.230D-16-0.232D-05)	(0.133D-16-0.673D-06)	(0.320D-03-0.540D-16)	(0.653D-03-0.305D-16)	(-0.247D-16-0.115D-05)
(0.432D-02-0.804D-17)	(0.135D-02 0.101D-16)	(0.888D-18-0.135D-05)	(-0.166D-19 0.122D-05)	(0.205D-02 0.168D-17)
(0.370D-16 0.128D-05)	(0.583D-16 0.110D-05)	(0.177D-02 0.320D-16)	(-0.999D-03-0.252D-16)	(-0.270D-16 0.178D-05)
(-0.662D-15 0.276D-04)	(-0.334D-15-0.716D-07)	(0.486D+00-0.202D-14)	(0.547D+00-0.868D-15)	(-0.260D-13-0.670D-04)
(-0.113D+00 0.320D-17)	(0.307D-03-0.684D-17)	(0.643D-17-0.128D-04)	(-0.149D-16-0.179D-04)	(0.522D+00-0.448D-16)
(-0.725D-15 0.348D-04)	(-0.271D-15 0.141D-06)	(0.269D+00 0.191D-14)	(-0.705D-01-0.314D-14)	(-0.426D-15-0.373D-05)
(0.149D-14-0.604D-04)	(-0.493D-15 0.261D-06)	(0.137D-01-0.349D-14)	(0.243D-01-0.219D-14)	(-0.802D-15 0.125D-05)
(0.323D+00-0.396D-18)	(-0.637D-03-0.494D-17)	(0.315D-17 0.309D-05)	(0.520D-18-0.713D-05)	(0.826D-01-0.119D-15)
(0.174D-14-0.874D-04)	(0.184D-14-0.246D-06)	(0.811D-01 0.303D-14)	(-0.385D-01 0.463D-15)	(-0.130D-14-0.544D-05)
(0.519D-16-0.117D-04)	(-0.107D-16-0.142D-06)	(0.762D-03-0.128D-15)	(-0.163D-02-0.737D-16)	(-0.592D-16-0.743D-05)
(0.109D-01-0.739D-17)	(0.421D-03 0.707D-17)	(0.761D-18-0.888D-05)	(0.142D-18 0.849D-05)	(0.518D-02 0.240D-17)
(0.761D-16 0.132D-04)	(0.806D-16 0.240D-06)	(0.460D-02 0.122D-15)	(-0.261D-02-0.148D-16)	(-0.522D-16 0.122D-04)

THE 16-20 EIGENVECTORS

(-0.371D+00-0.790D-16)	(-0.349D+00 0.662D-17)	(-0.165D-02-0.778D-16)	(-0.599D-02 0.825D-16)	(-0.460D-13-0.132D-04)
(0.340D-16-0.352D-05)	(0.280D-16-0.262D-05)	(0.947D-17-0.290D-05)	(-0.602D-17 0.445D-06)	(-0.362D+00-0.160D-14)
(0.489D-01-0.300D-15)	(-0.201D+00 0.263D-16)	(-0.391D-02 0.165D-16)	(-0.120D-02-0.253D-16)	(-0.143D-14-0.814D-06)
(-0.730D-02-0.275D-15)	(-0.374D-02 0.129D-15)	(-0.204D-03 0.793D-16)	(0.266D-02-0.195D-15)	(0.186D-14 0.119D-06)
(-0.104D-15-0.629D-06)	(-0.781D-16 0.320D-06)	(-0.252D-16 0.200D-05)	(0.148D-16-0.190D-06)	(-0.247D-01-0.303D-14)
(0.120D-01 0.751D-15)	(-0.252D-01-0.237D-15)	(0.190D-02-0.102D-15)	(0.149D-03 0.217D-15)	(-0.133D-13-0.501D-06)
(-0.413D-03-0.815D-17)	(-0.190D-03 0.421D-17)	(0.368D-03-0.658D-16)	(-0.455D-02-0.344D-17)	(0.246D-16-0.673D-06)
(-0.382D-17 0.756D-06)	(-0.413D-16-0.927D-06)	(-0.114D-17-0.342D-05)	(0.344D-18 0.375D-06)	(-0.135D-02-0.969D-16)
(0.684D-03 0.232D-16)	(-0.131D-02-0.102D-16)	(-0.401D-02-0.196D-17)	(-0.412D-03 0.332D-16)	(-0.240D-15 0.110D-05)
(-0.521D-04-0.711D-18)	(-0.182D-03-0.579D-17)	(0.134D-01 0.182D-14)	(0.118D+00-0.367D-15)	(-0.896D-15-0.714D-07)
(0.453D-18 0.110D-06)	(0.800D-18-0.189D-06)	(0.196D-17 0.258D-04)	(0.190D-17 0.260D-04)	(-0.307D-03 0.531D-16)
(0.119D-03 0.113D-17)	(-0.299D-03 0.298D-19)	(0.114D+00-0.248D-15)	(0.140D-01-0.379D-15)	(-0.384D-14 0.142D-06)
(0.196D-03-0.534D-17)	(0.245D-03 0.212D-16)	(0.292D-01-0.487D-14)	(-0.329D+00 0.151D-15)	(-0.700D-15 0.261D-06)
(-0.162D-17-0.211D-06)	(-0.204D-17 0.440D-06)	(-0.505D-17-0.790D-04)	(-0.706D-17-0.708D-04)	(0.637D-03-0.716D-15)
(-0.188D-03 0.987D-17)	(0.587D-03-0.413D-17)	(-0.314D+00 0.893D-16)	(-0.292D-01 0.198D-14)	(0.113D-13-0.246D-06)
(-0.129D-03-0.289D-17)	(-0.569D-04 0.210D-17)	(0.973D-03-0.166D-15)	(-0.113D-01 0.299D-17)	(-0.134D-16-0.142D-06)
(-0.125D-17 0.165D-06)	(-0.821D-19-0.196D-06)	(-0.519D-18-0.181D-04)	(-0.256D-18 0.637D-05)	(-0.421D-03-0.391D-16)
(0.212D-03 0.648D-17)	(-0.400D-03-0.229D-17)	(-0.104D-01 0.518D-18)	(-0.994D-03 0.712D-16)	(0.245D-15 0.241D-06)

THE 21-25 EIGENVECTORS

(-0.618D-15-0.133D-05)	(-0.915D-04-0.141D-14)	(0.238D-03-0.652D-15)	(0.411D-16 0.482D-06)	(0.103D-01-0.660D-15)
(-0.439D-02-0.208D-15)	(0.490D-15 0.455D-06)	(0.449D-15-0.298D-06)	(0.559D-03-0.565D-16)	(0.555D-15-0.595D-02)
(-0.708D-16 0.146D-05)	(0.513D-03 0.684D-14)	(-0.218D-03 0.301D-14)	(-0.140D-16-0.431D-06)	(-0.572D-01 0.523D-14)
(0.655D-15 0.140D-05)	(0.129D-03 0.488D-14)	(0.265D-03 0.251D-14)	(0.308D-15 0.477D-06)	(0.192D-02 0.535D-14)
(0.233D-02 0.916D-16)	(-0.184D-14 0.588D-06)	(-0.130D-14-0.498D-06)	(0.857D-03 0.455D-16)	(0.137D-15-0.198D-01)
(-0.182D-14-0.506D-06)	(0.791D-03-0.144D-13)	(-0.417D-03-0.702D-14)	(-0.136D-14-0.762D-06)	(-0.208D+00 0.821D-14)
(-0.203D-18-0.231D-05)	(-0.320D-03 0.117D-15)	(-0.653D-03 0.604D-16)	(0.323D-16-0.115D-05)	(-0.485D-02 0.925D-16)
(-0.432D-02-0.518D-17)	(-0.485D-16-0.135D-05)	(-0.314D-16 0.122D-05)	(-0.205D-02 0.908D-17)	(-0.236D-15 0.592D-01)
(-0.194D-15 0.129D-05)	(-0.177D-02-0.504D-15)	(0.999D-03-0.309D-15)	(-0.703D-16 0.178D-05)	(0.619D+00 0.669D-15)
(0.128D-14 0.276D-04)	(-0.486D+00-0.262D-14)	(-0.547D+00-0.167D-14)	(-0.926D-17-0.670D-04)	(0.294D-01 0.146D-15)
(0.113D+00 0.175D-16)	(-0.324D-16-0.128D-04)	(-0.464D-16-0.179D-04)	(-0.522D+00 0.466D-16)	(-0.249D-16-0.143D-01)
(0.440D-14 0.348D-04)	(-0.269D+00 0.584D-14)	(0.705D-01 0.366D-15)	(0.337D-15-0.373D-05)	(-0.755D-01 0.211D-15)
(-0.133D-14-0.603D-04)	(-0.137D-01-0.121D-14)	(-0.243D-01-0.681D-15)	(0.169D-14 0.125D-05)	(0.843D-02-0.328D-15)
(-0.323D+00-0.128D-16)	(-0.297D-15 0.309D-05)	(-0.219D-15-0.714D-05)	(-0.825D-01-0.163D-16)	(-0.247D-16-0.539D-01)
(-0.116D-13-0.875D-04)	(-0.811D-01-0.879D-14)	(0.385D-01-0.819D-14)	(-0.127D-14-0.545D-05)	(-0.337D+00 0.377D-15)
(-0.410D-16-0.117D-04)	(-0.762D-03-0.512D-17)	(-0.163D-02-0.128D-17)	(0.620D-16-0.742D-05)	(-0.221D-01 0.512D-16)
(-0.109D-01-0.438D-17)	(-0.205D-16-0.889D-05)	(-0.123D-16 0.849D-05)	(-0.518D-02 0.934D-17)	(0.145D-16 0.160D+00)
(-0.386D-15 0.132D-04)	(-0.460D-02-0.393D-15)	(0.261D-02-0.353D-15)	(-0.882D-16 0.122D-04)	(0.100D+01 0.0)

THE 26-30 EIGENVECTORS

(0.103D-01 0.352D-15)	(0.153D-01 0.541D-15)	(0.101D-14-0.118D-01)	(-0.894D-15-0.162D-01)	(-0.105D+00 0.166D-14)
(0.636D-15 0.595D-02)	(0.865D-15 0.547D-02)	(-0.807D-01-0.143D-14)	(-0.101D+00 0.189D-15)	(0.111D-14-0.559D-02)
(-0.572D-01 0.463D-14)	(-0.923D-01 0.955D-14)	(-0.230D-14 0.272D-01)	(-0.170D-14-0.117D-01)	(0.909D-03 0.624D-14)
(0.192D-02 0.175D-14)	(-0.121D-02 0.419D-14)	(0.120D-14-0.229D-01)	(-0.277D-14-0.580D-01)	(-0.334D+00 0.593D-15)
(-0.152D-15 0.198D-01)	(0.669D-15 0.182D-01)	(-0.269D+00-0.435D-14)	(-0.335D+00 0.163D-15)	(0.434D-14-0.186D-01)
(-0.208D+00 0.105D-13)	(-0.337D+00 0.165D-13)	(-0.122D-13 0.990D-01)	(-0.235D-14-0.431D-01)	(0.990D-03 0.154D-13)
(-0.485D-02-0.495D-16)	(0.506D-02-0.101D-15)	(-0.924D-15 0.682D-01)	(0.699D-14 0.174D+00)	(0.100D+01 0.0)
(-0.872D-15-0.592D-01)	(-0.872D-15-0.544D-01)	(0.803D+00 0.118D-13)	(0.100D+01 0.0)	(-0.948D-14 0.556D-01)
(0.619D+00 0.134D-14)	(0.100D+01 0.0)	(0.504D-13-0.294D+00)	(-0.853D-14 0.128D+00)	(-0.149D-02 0.157D-14)
(0.294D-01 0.151D-15)	(-0.123D-01 0.461D-15)	(0.889D-17-0.898D-02)	(-0.339D-15 0.131D-01)	(-0.754D-01-0.125D-15)
(0.562D-16 0.143D-01)	(0.403D-17 0.390D-01)	(-0.895D-01-0.441D-16)	(0.277D-01 0.156D-16)	(0.783D-15-0.379D-02)
(-0.755D-01 0.313D-15)	(0.152D-01 0.380D-15)	(0.889D-16+0.129D-01)	(-0.128D-14 0.387D-02)	(0.601D-03 0.107D-14)
(0.843D-02 0.410D-15)	(-0.236D-01 0.767D-15)	(0.107D-16-0.463D-01)	(-0.230D-14 0.494D-01)	(-0.256D+00 0.551D-15)
(0.304D-15 0.539D-01)	(-0.105D-15 0.147D+00)	(-0.336D+00 0.723D-16)	(0.104D+00-0.995D-16)	(0.299D-14-0.142D-01)
(-0.337D+00 0.112D-15)	(0.674D-01 0.541D-15)	(0.527D-15-0.584D-01)	(-0.566D-14 0.180D-01)	(-0.107D-02 0.379D-14)
(-0.221D-01-0.143D-15)	(0.699D-01 0.105D-15)	(0.330D-15 0.139D+00)	(0.636D-14-0.148D+00)	(0.766D+00 0.263D-16)
(-0.885D-15-0.160D+00)	(0.370D-16-0.436D+00)	(0.100D+01 0.0)	(-0.310D+00 0.315D-16)	(-0.861D-14 0.424D-01)
(0.100D+01 0.0)	(-0.200D+00-0.110D-14)	(-0.279D-15 0.174D+00)	(0.161D-13-0.539D-01)	(0.557D-02-0.102D-13)

THE 31-35 EIGENVECTORS

(0.842D-01 0.225D-14)	(0.153D-01 0.121D-15)	(-0.608D-15 0.118D-01)	(0.198D-15 0.162D-01)	(0.842D-01 0.142D-15)
(-0.430D-14 0.139D-01)	(0.101D-14-0.547D-02)	(-0.807D-01-0.860D-15)	(-0.101D+00-0.201D-15)	(-0.329D-14-0.139D-01)
(-0.155D-02-0.955D-14)	(-0.923D-01 0.808D-14)	(0.229D-14-0.272D-01)	(0.344D-14 0.117D-01)	(-0.155D-02-0.571D-14)
(0.267D+00 0.741D-14)	(-0.121D-02 0.550D-14)	(-0.108D-14 0.229D-01)	(0.223D-15 0.580D-01)	(0.267D+00 0.143D-14)
(-0.788D-14 0.464D-01)	(0.218D-14-0.182D-01)	(-0.269D+00-0.262D-14)	(-0.335D+00 0.143D-15)	(0.241D-14-0.464D-01)
(-0.379D-02-0.223D-13)	(-0.337D+00 0.210D-13)	(0.476D-14-0.990D-01)	(0.907D-14 0.431D-01)	(-0.379D-02-0.149D-13)
(-0.800D+00-0.176D-13)	(0.506D-02 0.442D-16)	(0.109D-14-0.682D-01)	(-0.769D-15-0.174D+00)	(-0.800D+00-0.379D-14)
(0.272D-13-0.138D+00)	(-0.309D-14 0.544D-01)	(0.803D+00 0.923D-14)	(0.100D+01 0.0)	(0.850D-14 0.138D+00)
(0.101D-01 0.309D-13)	(0.100D+01 0.0)	(-0.355D-13 0.294D+00)	(-0.108D-13-0.128D+00)	(0.101D-01 0.514D-14)
(-0.984D-01 0.170D-14)	(-0.123D-01 0.848D-15)	(-0.707D-17 0.898D-02)	(-0.427D-15-0.131D-01)	(-0.984D-01 0.531D-15)
(-0.915D-15-0.844D-02)	(-0.309D-15-0.390D-01)	(-0.895D-01 0.354D-16)	(0.277D-01-0.330D-15)	(-0.234D-15 0.844D-02)
(0.117D-02-0.687D-14)	(0.152D-01-0.708D-15)	(-0.745D-15 0.129D-01)	(0.137D-14-0.387D-02)	(0.117D-02-0.321D-14)
(-0.334D+00-0.731D-15)	(-0.236D-01 0.119D-14)	(-0.135D-15 0.463D-01)	(-0.413D-15-0.494D-01)	(-0.334D+00-0.566D-15)
(-0.306D-14-0.317D-01)	(-0.143D-14-0.147D+00)	(-0.336D+00 0.987D-16)	(0.104D+00-0.119D-14)	(-0.704D-15 0.317D-01)
(0.314D-03-0.309D-13)	(0.674D-01-0.471D-14)	(-0.285D-14 0.584D-01)	(0.564D-14-0.180D-01)	(0.314D-03-0.153D-13)
(0.100D+01 0.0)	(0.699D-01-0.105D-14)	(-0.469D-15-0.139D+00)	(0.200D-14 0.148D+00)	(0.100D+01 0.0)
(-0.816D-14 0.943D-01)	(0.395D-14 0.436D+00)	(0.100D+01 0.0)	(-0.310D+00 0.350D-14)	(0.167D-14-0.943D-01)
(0.220D-02 0.925D-13)	(-0.200D+00 0.150D-13)	(0.980D-14-0.174D+00)	(-0.175D-13 0.539D-01)	(0.220D-02 0.451D-13)

THE 36 EIGENVECTOR

(-0.105D+00-0.123D-14)
(0.339D-15 0.559D-02)
(0.909D-03 0.673D-14)
(-0.334D+00 0.126D-13)
(-0.531D-15 0.186D-01)
(0.990D-03 0.181D-15)
(0.100D+01 0.0)
(0.624D-14-0.556D-01)
(-0.149D-02 0.312D-13)
(-0.754D-01-0.510D-15)
(0.103D-14 0.379D-02)
(0.601D-03 0.161D-15)
(-0.256D+00-0.174D-14)
(0.455D-14 0.142D-01)
(-0.107D-02-0.105D-14)
(0.766D+00 0.783D-14)
(-0.130D-13-0.424D-01)
(0.557D-02 0.326D-14)

APPENDIX G

COMPUTER PROGRAM FOR THE CASE OF COMPRESSIBLE INVISCID FLOW

G.1 FUNCTION OF THE PROGRAM

The program calculates the dimensionless eigenfrequencies, $\bar{\Omega}_i$, and the associated eigenvectors of a system with a rigid outer shell subjected to internal and annular compressible inviscid flows. For each set of input data of flow velocities, $\bar{U}_i$, $\bar{U}_o$, the program constructs the matrix $[A_i]$, as given in Appendix E. The frequencies are then determined as the zeros of the determinant of the matrix $[A_i]$.

G.2 PROGRAM STRUCTURE

The program is written in Fortran IV language and it has the following structure:

MAIN PROGRAM

SUBROUTINE MATRIX

SUBROUTINE AERO

SUBROUTINE MAT1

COMPLEX FUNCTION DET

COMPLEX FUNCTION F

SUBROUTINE ZANLYT

SUBROUTINE LEQT1C.

G.3 DESCRIPTION OF THE PROGRAM

The function of each subprogram is summarized as follows:

(1) Subroutine MATRIX fills in the elements of matrix $[A_i]$ that are not dependent on the flow velocities and the vibration frequency. Hence, this subroutine is called only once in the main program, and the complete construction of the matrix will be left to the other subroutines, for each set of input flow velocities and for each trial value of the frequency in the iterative procedure of the solution.

(2) Subroutine AERO calculates the generalized aerodynamic forces, Q'_{kmh}, as defined in equation (D.1a), with the input flow velocities and the integral terms approximated with the aid of interpolation equations (as functions of frequency).

(3) Subroutine MAT1 completes the construction of matrix $[A_i]$ by putting in the generalized aerodynamic forces, calculated in subroutine AERO, and the other frequency-dependent terms.

(4) Complex function DET evaluates the determinant of a matrix by means of the Gauss-Jordan reduction method†.

(5) Complex function F defines the function for which the zeros are sought. Therefore, in this case it is the determinant of matrix $[A_i]$. For each trial value of the frequency, the subroutines AERO and MAT1 are called upon to complete the construction of matrix $[A_i]$. The determinant of the matrix is then calculated by the function subprogram DET and its value is assigned to F.

(6) Subroutine ZANLYT is the IMSL subroutine used to find the zeros of the complex function F which, of course, has been defined as the

---

†For details of the method, see reference [44].

determinant of matrix $[A_i]$. The computer method used by ZANLYT is based on the quadratic fit of deflation†.

(7) Subroutine LEQT1C is another IMSL subroutine. Its function is to solve a set of linear algebraic equations which can be put into the matrix form,

$$[L]\{X\} = \{B\} \quad , \tag{G.1}$$

where $[L]$ is a constant matrix, $\{B\}$ is a constant column vector and $\{X\}$ is the unknown vector to be determined.

LEQT1C is employed to find the corresponding eigenvector of the system after each frequency is evaluated. To do so, matrix $[A_i]$ is constructed with the determined value of the frequency. $[A_i]$ is the coefficient matrix in the following matrix equation

$$[A_i]\{X_i\} = \{0\} \quad , \tag{G.2}$$

where $\{X_i\}$ is defined in equation (G.1b); it is this $\{X_i\}$ that we like to determine. One of the elements of $\{X_i\}$, the i^{th} element, say, is assigned the value of unity. The order of $[A_i]$ is then reduced by one by deleting the last row and taking out the i^{th} column which becomes the negative of the column vector $\{B\}$ appearing in equation (G.1). The 'reduced' $[A_i]$ is the matrix $[L]$, and $\{X_i\}$ with the absence of the i^{th} element becomes the unknown vector $\{X\}$. Subroutine LEQT1C is then used to solve equation (G.1), and the eigenvector is obtained by substituting back the unit

---

†For details of the method, see reference [45].

i^{th} element into the now determined vector $\{X\}$.

All calculations are carried out with double precision. The necessary parameters are defined in the main program. After specifying the initial guesses and the number of zeros to be determined, the main program calls upon subroutine ZANLYT to find the eigenfrequencies as the zeros of the determinant of $[A_i]$. On completion of the task, control is transferred back to the main program which in turn calls subroutine LEQT1C to solve for the corresponding eigenvectors.

Notation used in the computer program, the computer program itself and a sample of the output are given in the following pages.

A modified version of the computer program has been developed to determine the critical buckling velocities of the system. The program structure and the computation procedures are basically the same as those of the program described above. The essential difference is that, in the modified version, one of the flow velocities ($\bar{U}_i$ or $\bar{U}_o$) becomes the unknown variable (the other flow velocity has to be a known constant) instead of the vibration frequency which is assigned to be zero, its value at the onset of the buckling instability. The computer program and a sample of the output are given at the end of this Appendix.

NOTATION USED IN THE PROGRAM

Notation used in the computer program	Corresponding notation used in the thesis	Definition
E	ε_i	See NOMENCLATURE
NU	ν_i	See NOMENCLATURE
SK	k_i	See NOMENCLATURE
DR	ρ_r	Defined in equation (3.2.10)
AA(9,9)	$[A_i]$	See Appendix E
QB(3,3)	Q'_{kmn} , $k,m=1,2,3$	Generalized aerodynamic forces defined in equation (D.1a)
MI*	M_i	See NOMENCLATURE
MO*	M_o	See NOMENCLATURE
KI*	κ_i	Reduced frequency defined in equation (3.1.4b)
KO*	κ_o	Reduced frequency defined in equation (3.1.11b)
AAA(9,9)		Dummy matrix used in place of AA(9,9) in algorithms in which the matrix is eventually destroyed (*e.g.* in complex function DET)
B(8)	$\{B\}$	On return from subroutine LEQTIC, B(8) contains the solution of {X}
AP(8,8)	$[L]$	Defined by equation (G.1)
X(M), M = 1,2,...		On entry to subroutine ZANLYT, X(M) contains the initial guesses; on return, X(M) contains the the determined eigen-frequencies

*Notation with the same definition as in other computer programs.

```
/INFO MVS TI(20) PA(50) R(CENTRAL) CL(20) F(0415)
//STEP1 EXEC FORTRAN
//FORT.SYSIN DD *
C*****************************************************************
C     COMPUTER PROGRAM FOR THE CASE OF COMPRESSIBLE INVISCID FLOW      *
C     VERSION FOR DETERMINING THE EIGENFREQUENCIES AS A FUNCTION OF    *
C     THE FLOW VELOCITIES                                              *
C     ONLY THE INNER SHELL FLEXIBLE                                    *
C     BOUNDARY CONDITIONS: CLAMPED-CLAMPED                             *
C*****************************************************************
C
C*****************************************************************
C     MAIN PROGRAM                                                     *
C*****************************************************************
      IMPLICIT REAL*8(A-H,O-Z)
      COMPLEX*16 F,X(3),AAA(9,9),AP(8,8),B(8),WA(8),UNIT,QB(3,3)
      REAL*8 NU
      INTEGER INFER(3)
      EXTERNAL F
      COMMON/DATA1/NU,SK,E,C(3),P(3),N
      COMMON/DATA2/ZI,DR
      COMMON/DATA3/UI,UO
      COMMON/AREA1/AAA
      DATA EPS/1.D-12/,NSIG/5/,NGUESS/1/,ITMAX/20/,II/1/,NN/8/,IA/
     #8/,MM/1/,IB/8/,IJOB/0/,UNIT/(1.D0,0.D0)/
      C(1)=0.98250221457623790D0
      C(2)=1.00077731190727D0
      C(3)=0.9999664501254086D0
      P(1)=4.7300407448627D0
      P(2)=7.85320462409584D0
      P(3)=10.99560783800167D0
      E=0.06667D0
      NU=0.30D0
      SK=(7.50D-3)**2/12
      ZI=2.212D-2
      DR=1.D0
      N=2
      UI=0.005D0
      CALL MATRIX
      DO 14 L=1,2
      READ(5,*) UO
      PRINT10,UI,UO
   10 FORMAT('1','FLOW VELOCITY INSIDE THE INNER CYLINDER=',F7.4/
     #'0','FLOW VELOCITY IN THE ANNULAR REGION=',F7.4)
      DO 14 M=2,2
      NK=M-2
      READ(5,*) X(1)
      CALL ZANLYT(F,EPS,NSIG,NK,NGUESS,II,X,ITMAX,INFER,IER)
      CALL AERO(UI,UO,X(1),QB)
      CALL MAT1(X(1),QB,AAA)
      DO 4 J=1,8
    4 B(J)=-AAA(J,6+M)
      DO 5 I=1,8
      DO 5 J=1,6
    5 AP(I,J)=AAA(I,J)
      K=7
      DO 6 I=1,3
      IF(I.EQ.M) GO TO 6
```

```
      DO 8 J=1,8
    8 AP(J,K)=AAA(J,6+I)
      K=K+1
    6 CONTINUE
      CALL LEQT1C(AP,NN,IA,B,MM,IB,IJOB,WA,IER)
      PRINT20,X(1)
   20 FORMAT('-','THE MODAL SHAPE CORRESPONDING TO THE FREQUENCY, ','(',
     #2D24.16,1X,')'/)
      IF(M.EQ.3) GO TO 12
      K=5+M
      J=6+M
      PRINT11,(B(I),I=1,K)
   11 FORMAT(' ','(',2D24.16,1X,')')
      PRINT11,UNIT
      PRINT11,(B(I),I=J,8)
      GO TO 13
   12 PRINT11,(B(I),I=1,8)
      PRINT11,UNIT
   13 CONTINUE
      PRINT15,INFER(1)
   15 FORMAT('0','NO. OF ITERATIONS REQUIRED=',I3/)
   14 CONTINUE
      PRINT30
   30 FORMAT('1')
      STOP
      END
C
C*****************************************************************************
C     SUBROUTINE MATRIX                                                      *
C*****************************************************************************
      SUBROUTINE MATRIX
      IMPLICIT REAL*8(A-Z)
      COMPLEX*16 AA(9,9),COE(9,3,3)
      INTEGER DEL(3,3),K,M,J,N,R,Q,I,W,V,L,H
      DIMENSION A(3,3),B(3,3),D(3,3)
      COMMON/DATA1/ NU,SK,E,C(3),P(3),N
      COMMON/AREA/AA,A,DEL
      DO 3 K=1,3
      DO 3 M=1,3
      IF(K.EQ.M) GO TO 1
      D(K,M)=4*P(K)**2*P(M)**2*((-1)**(K+M)+1)*(C(M)*P(M)-C(K)*P(K))
     C/(P(M)**4-P(K)**4)
      A(K,M)=-D(K,M)
      B(K,M)=0.D0
      DEL(K,M)=0
      GO TO 3
    1 D(K,K)=P(K)*C(K)*(2-P(K)*C(K))
      DEL(K,K)=1
      A(K,K)=-D(K,K)
      B(K,K)=-P(K)**4
    3 CONTINUE
      DO 4 K=1,3
      DO 4 M=1,3
      COE(1,K,M)=E**2*B(K,M)+(NU-1)*(SK+1)*N**2*A(K,M)/2
      COE(2,K,M)=-(1+NU)*N*E**2*D(K,M)/2
      COE(3,K,M)=(P(M)*E)**4*SK*DEL(K,M)-(2*NU-SK*(1-NU)*N**2)
     C*E**2*D(K,M)/2
      COE(4,K,M)=(1+NU)*N*A(K,M)/2
```

```
      COE(5,K,M)=-N**2*DEL(K,M)+(1+3*SK)*(1-NU)*E**2*D(K,M)/2
      COE(6,K,M)=SK*(3-NU)*N*E**2*D(K,M)/2-N*DEL(K,M)
      COE(7,K,M)=(NU+(NU-1)*SK*N**2/2)*A(K,M)-SK*E**2*B(K,M)
      COE(8,K,M)=-N*DEL(K,M)+(3-NU)*SK*N*E**2*D(K,M)/2
    4 COE(9,K,M)=-SK*(((P(M)*E)**4+(N**2-1)**2)*DEL(K,M)-2*(N*E)
     C**2*D(K,M))-DEL(K,M)
      K=0
      DO 5 I=1,7,3
      K=K+1
      DO 5 M=1,3
      R=I
      Q=M
      W=-1
      DO 5 V=1,7,3
      W=W+1
      DO 5 L=1,3
      H=L-1
      AA(R+H,Q+V-1)=COE(L+3*W,K,M)
    5 CONTINUE
      RETURN
      END
C
C*****************************************************************
C     COMPLEX FUNCTION F                                         *
C*****************************************************************
      COMPLEX FUNCTION F*16(OMI)
      IMPLICIT REAL*8(A-Z)
      COMPLEX*16 OMI,RES,QB(3,3),AAA(9,9),DET
      INTEGER L(9),M(9)
      COMMON/DATA3/UI,UO
      COMMON/AREA1/AAA
      CALL AERO(UI,UO,OMI,QB)
      CALL MAT1(OMI,QB,AAA)
      F=DET(AAA,L,M,9)
      RETURN
      END
C
C*****************************************************************
C     SUBROUTINE MAT1                                            *
C*****************************************************************
      SUBROUTINE MAT1(OMI,QB,AAA)
      IMPLICIT REAL*8(A-Z)
      COMPLEX*16 AA(9,9),AAA(9,9),OMI,QB(3,3),COEK(3,3,3),OMIS
      INTEGER I,J,K,M,H,L,DEL(3,3)
      COMMON/AREA/AA,A(3,3),DEL
      DO 1 I=1,9
      DO 1 J=1,9
    1 AAA(I,J)=AA(I,J)
      OMIS=OMI**2
      DO 2 K=1,3
      DO 2 M=1,3
      COEK(1,K,M)=A(K,M)*OMIS
      COEK(2,K,M)=DEL(K,M)*OMIS
    2 COEK(3,K,M)=DEL(K,M)*OMIS+QB(K,M)
      K=0
      DO 3 I=1,7,3
      K=K+1
      DO 3 M=1,3
```

```
      DO 3 L=1,3
      H=L-1
      AAA(I+H,M+3*H)=AAA(I+H,M+3*H)+COEK(L,K,M)
    3 CONTINUE
      RETURN
      END
C
C*****************************************************************
C     SUBROUTINE AERO                                           *
C*****************************************************************
      SUBROUTINE AERO(UI,UO,OMI,QB)
      IMPLICIT REAL*8(A-Z)
      COMPLEX*16 OMI,QB(3,3),I,DCONJG
      INTEGER K,KK,M,N,J,IER
      DIMENSION U(1),S(1)
      COMMON/DATA2/ZI,DR
      I=(0.D0,1.D0)
      PI=3.14159265358979D0
      EI=0.06667D0
      EO=0.10D0
      KI=OMI/UI/EI
      KO=KI*UI/UO
      C1=UI**2*ZI*EI/2/PI
      C2=UO**2*ZI*EI*DR/2/PI
      IF(KO.LT.0.D0) KO=-KO
      IF(KI.LT.0.D0) KI=-KI
      QB(1,1)=C1*(0.204113*KI**2.0063334+2.5411463)-C2*(-0.3150215*KO**2
     #.0108154-3.7093031)
      QB(2,2)=C1*(0.201741*KI**2.006218+9.3781204)-C2*(-0.320331*KO**2.0
     #113876-13.397501)
      QB(3,3)=C1*(0.198179*KI**2.0060497+19.712729)-C2*(-0.325959*KO**2.
     #0119743-27.297784)
      IF(KI.GT.120.D0) GO TO 10
      QB(1,2)=C1*1.3906222*KI*I
      QB(2,3)=C1*2.254498*KI*I
      GO TO 20
   10 QB(1,2)=C1*(166.87467+1.4465174*(KI-120))*I
      QB(2,3)=C1*(270.53976+2.3426566*(KI-120))*I
   20 IF(KO.GT.5.D0) GO TO 30
      QB(1,2)=QB(1,2)-C2*(-2.0736718*KO*I)
      QB(2,3)=QB(2,3)-C2*(-3.3113042*KO*I)
      GO TO 40
   30 QB(1,2)=QB(1,2)-C2*(-10.368359-2.224116*(KO-5))*I
      QB(2,3)=QB(2,3)-C2*(-16.556521-3.5440903*(KO-5))*I
   40 QB(1,3)=C1*(7.06283D-4*KI**2.0157489-2.0249953)-C2*(1.8367D-3*KO**
     #2.046171+2.9557921)
      DO 2 K=1,2
      KK=K+1
      DO 2 M=KK,3
    2 QB(M,K)=DCONJG(QB(K,M))
      RETURN
      END
C
C*****************************************************************
C     COMPLEX FUNCTION DET                                      *
C*****************************************************************
      COMPLEX FUNCTION DET*16(A,L,M,N)
      DIMENSION A(N,N),L(N),M(N)
```

```
      COMPLEX*16 A,PIVOT,HOLD
      INTEGER END,ROW,COL,PIVROW,PIVCOL
      END=N-1
      DET=(1.D0,0.D0)
      DO 10 I=1,N
      L(I)=I
   10 M(I)=I
      DO 100 LMNT=1,END
      PIVOT=(0.D0,0.D0)
      DO 20 I=LMNT,N
      ROW=L(I)
      DO 20 J=LMNT,N
      COL=M(J)
      IF(CDABS(PIVOT).GE.CDABS(A(ROW,COL))) GO TO 20
      PIVROW=I
      PIVCOL=J
      PIVOT=A(ROW,COL)
   20 CONTINUE
      IF(PIVROW.EQ.LMNT) GO TO 22
      DET=-DET
      KEEP=L(PIVROW)
      L(PIVROW)=L(LMNT)
      L(LMNT)=KEEP
   22 IF(PIVCOL.EQ.LMNT) GO TO 26
      DET=-DET
      KEEP=M(PIVCOL)
      M(PIVCOL)=M(LMNT)
      M(LMNT)=KEEP
   26 DET=DET*PIVOT
      IF(CDABS(PIVOT).EQ.0.D0) GO TO 333
      JAUG=LMNT+1
      PIVROW=L(LMNT)
      PIVCOL=M(LMNT)
      DO 100 I=JAUG,N
      ROW=L(I)
      HOLD=A(ROW,PIVCOL)/PIVOT
      DO 100 J=JAUG,N
      COL=M(J)
  100 A(ROW,COL)=A(ROW,COL)-HOLD*A(PIVROW,COL)
      DET=DET*A(ROW,COL)
  333 RETURN
      END
//GO.SYSIN DD *
0.8D0
(3.60D-2,0.D0)
1.0D0
(6.63D-2,0.D0)
//
/*
```

```
FLOW VELOCITY INSIDE THE INNER CYLINDER= 0.0050
FLOW VELOCITY IN THE ANNULAR REGION= 0.8000

THE MODAL SHAPE CORRESPONDING TO THE FREQUENCY, (  0.3624286479477561D-01  0.0 )

(  0.0                          0.2746844213795535D-01 )
( -0.2015515002667089D+00       0.0                    )
(  0.0                          0.7694469574644208D-02 )
(  0.0                          0.6863262302143966D-01 )
( -0.5045377560354591D+00       0.0                    )
(  0.0                          0.2390950358483722D-01 )
(  0.0                         -0.1369359301181663D+00 )
(  0.1000000000000000D+01       0.0                    )
(  0.0                         -0.4769670754313472D-01 )

NO. OF ITERATIONS REQUIRED=  5



FLOW VELOCITY INSIDE THE INNER CYLINDER= 0.0050
FLOW VELOCITY IN THE ANNULAR REGION= 1.0000

THE MODAL SHAPE CORRESPONDING TO THE FREQUENCY, (  0.6618481289207645D-01  0.0 )

(  0.0                          0.2888600409688247D+00 )
( -0.2022147342575488D+00       0.0                    )
(  0.0                         -0.1190242663167368D+01 )
(  0.0                         -0.3094762703179601D+00 )
( -0.5049615895023536D+00       0.0                    )
(  0.0                         -0.3539449221432670D+01 )
(  0.0                          0.6381768778136536D+00 )
(  0.1000000000000000D+01       0.0                    )
(  0.0                          0.6992853998832567D+01 )

NO. OF ITERATIONS REQUIRED=  5
```

```
/INFO MVS TI(20) PA(50) R(CENTRAL) CL(20) F(0415) N(STEVE SIU PUI CHAN)
//STEP1 EXEC FORTRAN
//FORT.SYSIN DD *
C*************************************************************************
C     COMPUTER PROGRAM FOR THE CASE OF COMPRESSIBLE INVISCID FLOW       *
C     VERSION FOR DETERMINING THE BUCKLING FLOW VELOCITY                *
C     ONLY THE INNER SHELL FLEXIBLE                                     *
C     BOUNDARY CONDITIONS: CLAMPED-CLAMPED                              *
C*************************************************************************
C
C*************************************************************************
C     MAIN PROGRAM                                                      *
C*************************************************************************
      IMPLICIT REAL*8(A-H,O-Z)
      COMPLEX*16 F,X(3),QB(3,3),OMI,AAA(9,9),AP(8,8),B(8),WA(8),UNIT
      REAL*8 NU
      INTEGER I,J,N,K,M,INFER(3),NSIG,NK,NGUESS,ITMAX,IER
      EXTERNAL F
      COMMON/DATA1/NU,SK,E,C(3),P(3),N
      COMMON/DATA2/ZI,DR
      COMMON/DATA3/UI
      DATA EPS/1.D-12/,NSIG/5/,NGUESS/1/,II/1/,ITMAX/15/,OMI/(0.D0,0.D0)
     #/,UNIT/(1.D0,0.D0)/,II/1/,NN/8/,IA/8/,MM/1/,IB/8/,IJOB/0/
      C(1)=0.98250221457623790D0
      C(2)=1.00077731190727D0
      C(3)=0.99996645012540860D0
      P(1)=4.7300407448627D0
      P(2)=7.8532046240958 4D0
      P(3)=10.995607838001670D0
      E=0.06667D0
      NU=0.30D0
      SK=(7.50D-3)**2/12
      ZI=2.212D-2
      DR=1.D0
      N=2
      UI=0.005D0
      X(1)=(0.76D0,0.D0)
      X(2)=(1.10D0,0.D0)
      X(3)=(1.44D0,0.D0)
      CALL MATRIX
      PRINT10,UI
  10  FORMAT('1','FLOW VELOCITY INSIDE THE INNER CYLINDER=',F7.4)
      DO 1 M=1,3
      NK=M-1
      CALL ZANLYT(F,EPS,NSIG,NK,NGUESS,II,X,ITMAX,INFER,IER)
      PRINT12,X(M)
  12  FORMAT('-','ANNULAR FLOW VELOCITY AT THE ONSET OF THE BUCKLING INS
     #TABILITY=(',2D24.16,1X,')')
      CALL AERO(UI,X(M),QB)
      CALL MAT1(QB,AAA)
      DO 4 J=1,8
  4   B(J)=-AAA(J,6+M)
      DO 5 I=1,8
      DO 5 J=1,6
  5   AP(I,J)=AAA(I,J)
      K=7
      DO 6 I=1,3
      IF(I.EQ.M) GO TO 6
```

```
      DO 8 J=1,8
    8 AP(J,K)=AAA(J,6+I)
      K=K+1
    6 CONTINUE
      CALL LEQT1C(AP,NN,IA,B,MM,IB,IJOB,WA,IER)
      PRINT15
   15 FORMAT('0','THE CORRESPONDING MODAL SHAPE')
      IF(M.EQ.3) GO TO 16
      K=5+M
      J=6+M
      PRINT17,(B(I),I=1,K)
   17 FORMAT(' ','(',2D24.16,1X,')')
      PRINT17,UNIT
      PRINT17,(B(I),I=J,8)
      GO TO 18
   16 PRINT17,(B(I),I=1,8)
      PRINT17,UNIT
   18 CONTINUE
      PRINT30,INFER(M)
   30 FORMAT('0','NO. OF ITERATIONS REQUIRED=',I3//)
    1 CONTINUE
      PRINT20
   20 FORMAT('1')
      STOP
      END
C
C*****************************************************************************
C     SUBROUTINE MATRIX                                                      *
C*****************************************************************************
      SUBROUTINE MATRIX
      IMPLICIT REAL*8(A-Z)
      COMPLEX*16 AA(9,9),COE(9,3,3)
      INTEGER DEL(3,3),K,M,J,N,R,Q,I,W,V,L,H
      DIMENSION A(3,3),B(3,3),D(3,3)
      COMMON/DATA1/ NU,SK,E,C(3),P(3),N
      COMMON/AREA/AA,A,DEL
      DO 3 K=1,3
      DO 3 M=1,3
      IF(K.EQ.M) GO TO 1
      D(K,M)=4*P(K)**2*P(M)**2*((-1)**(K+M)+1)*(C(M)*P(M)-C(K)*P(K))
     C/(P(M)**4-P(K)**4)
      A(K,M)=-D(K,M)
      B(K,M)=0.D0
      DEL(K,M)=0
      GO TO 3
    1 D(K,K)=P(K)*C(K)*(2-P(K)*C(K))
      DEL(K,K)=1
      A(K,K)=-D(K,K)
      B(K,K)=-P(K)**4
    3 CONTINUE
      DO 4 K=1,3
      DO 4 M=1,3
      COE(1,K,M)=E**2*B(K,M)+(NU-1)*(SK+1)*N**2*A(K,M)/2
      COE(2,K,M)=-(1+NU)*N*E**2*D(K,M)/2
      COE(3,K,M)=(P(M)*E)**4*SK*DEL(K,M)-(2*NU-SK*(1-NU)*N**2)
     C*E**2*D(K,M)/2
      COE(4,K,M)=(1+NU)*N*A(K,M)/2
      COE(5,K,M)=-N**2*DEL(K,M)+(1+3*SK)*(1-NU)*E**2*D(K,M)/2
```

```
      COE(6,K,M)=SK*(3-NU)*N*E**2*D(K,M)/2-N*DEL(K,M)
      COE(7,K,M)=(NU+(NU-1)*SK*N**2/2)*A(K,M)-SK*E**2*B(K,M)
      COE(8,K,M)=-N*DEL(K,M)+(3-NU)*SK*N*E**2*D(K,M)/2
    4 COE(9,K,M)=-SK*(((P(M)*E)**4+(N**2-1)**2)*DEL(K,M)-2*(N*E)
     C**2*D(K,M))-DEL(K,M)
      K=0
      DO 5 I=1,7,3
      K=K+1
      DO 5 M=1,3
      R=I
      Q=M
      W=-1
      DO 5 V=1,7,3
      W=W+1
      DO 5 L=1,3
      H=L-1
      AA(R+H,Q+V-1)=COE(L+3*W,K,M)
    5 CONTINUE
      RETURN
      END
C
C*************************************************************************
C     COMPLEX FUNCTION F                                                 *
C*************************************************************************
      COMPLEX FUNCTION F*16(UO)
      IMPLICIT REAL*8(A-Z)
      COMPLEX*16 QB(3,3),AAA(9,9),DET,UO
      INTEGER L(9),M(9)
      COMMON/DATA3/UI
      CALL AERO(UI,UO,QB)
      CALL MAT1(QB,AAA)
      F=DET(AAA,L,M,9)
      RETURN
      END
C
C*************************************************************************
C     SUBROUTINE MAT1                                                    *
C*************************************************************************
      SUBROUTINE MAT1(QB,AAA)
      IMPLICIT REAL*8(A-Z)
      COMPLEX*16 AA(9,9),AAA(9,9),QB(3,3),COEK(3,3,3),OMIS
      INTEGER I,J,K,M,H,L,DEL(3,3)
      COMMON/AREA/AA,A(3,3),DEL
      DO 1 I=1,9
      DO 1 J=1,9
    1 AAA(I,J)=AA(I,J)
      K=0
      DO 3 I=1,7,3
      K=K+1
      DO 3 M=1,3
      AAA(I+2,M+6)=AAA(I+2,M+6)+QB(K,M)
    3 CONTINUE
      RETURN
      END
C
C*************************************************************************
C     SUBROUTINE AERO                                                    *
C*************************************************************************
```

```
      SUBROUTINE AERO(UI,UO,QB)
      IMPLICIT REAL*8(A-Z)
      COMPLEX*16 QB(3,3),I,DCONJG,UO,C1,C2
      INTEGER K,KK,M,N,J,IER
      COMMON/DATA2/ZI,DR
      I=(0.D0,1.D0)
      PI=3.14159265358979D0
      EI=0.06667D0
      EO=0.1D0
      C1=UI**2*ZI*EI/2/PI
      C2=UO**2*ZI*EI*DR/2/PI
      QB(1,1)=C1*2.5411463+C2*3.7093031
      QB(2,2)=C1*9.3781204+C2*13.397501
      QB(3,3)=C1*19.712729+C2*27.297784
      QB(1,2)=C1*0.5923156D-4+C2*0.5889203D-4
      QB(2,3)=-C1*0.25136556D-3-C2*0.25000252D-3
      QB(1,3)=-C1*2.0249953-C2*2.9557921
      DO 2 K=1,2
      KK=K+1
      DO 2 M=KK,3
    2 QB(M,K)=DCONJG(QB(K,M))
      RETURN
      END
C
C*****************************************************************************
C     COMPLEX FUNCTION DET                                                    *
C*****************************************************************************
      COMPLEX FUNCTION DET*16(A,L,M,N)
      DIMENSION A(N,N),L(N),M(N)
      COMPLEX*16 A,PIVOT,HOLD
      INTEGER END,ROW,COL,PIVROW,PIVCOL
      END=N-1
      DET=(1.D0,0.D0)
      DO 10 I=1,N
      L(I)=I
   10 M(I)=I
      DO 100 LMNT=1,END
      PIVOT=(0.D0,0.D0)
      DO 20 I=LMNT,N
      ROW=L(I)
      DO 20 J=LMNT,N
      COL=M(J)
      IF(CDABS(PIVOT).GE.CDABS(A(ROW,COL))) GO TO 20
      PIVROW=I
      PIVCOL=J
      PIVOT=A(ROW,COL)
   20 CONTINUE
      IF(PIVROW.EQ.LMNT) GO TO 22
      DET=-DET
      KEEP=L(PIVROW)
      L(PIVROW)=L(LMNT)
      L(LMNT)=KEEP
   22 IF(PIVCOL.EQ.LMNT) GO TO 26
      DET=-DET
      KEEP=M(PIVCOL)
      M(PIVCOL)=M(LMNT)
      M(LMNT)=KEEP
   26 DET=DET*PIVOT
```

```
      IF(CDABS(PIVOT).EQ.0.DO) GO TO 333
      JAUG=LMNT+1
      PIVROW=L(LMNT)
      PIVCOL=M(LMNT)
      DO 100 I=JAUG,N
      ROW=L(I)
      HOLD=A(ROW,PIVCOL)/PIVOT
      DO 100 J=JAUG,N
      COL=M(J)
  100 A(ROW,COL)=A(ROW,COL)-HOLD*A(PIVROW,COL)
      DET=DET*A(ROW,COL)
  333 RETURN
      END
//GO.SYSIN DD *
//
/*
```

FLOW VELOCITY INSIDE THE INNER CYLINDER= 0.0050

ANNULAR FLOW VELOCITY AT THE ONSET OF THE BUCKLING INSTABILITY=(0.797474705653753 4D+00 0.0)

THE CORRESPONDING MODAL SHAPE

-0.2242640713286370D+00	0.0
-0.1234853322683816D-05	0.0
0.1031473460568863D-01	0.0
-0.5016420648667892D+00	0.0
-0.3094407766175331D-05	0.0
0.2337724873366698D-01	0.0
0.1000000000000000D+01	0.0
0.6135358377697671D-05	0.0
-0.4309725440001237D-01	0.0

NO. OF ITERATIONS REQUIRED= 5

ANNULAR FLOW VELOCITY AT THE ONSET OF THE BUCKLING INSTABILITY=(0.108397115187039 3D+01 0.0)

THE CORRESPONDING MODAL SHAPE

0.1017264368755151D-04	0.0
-0.2012683280527782D+00	0.0
0.1194699504451688D-05	0.0
0.2410223736964490D-04	0.0
-0.5043564818354629D+00	0.0
0.3912660347540870D-05	0.0
-0.4807750451435739D-04	0.0
0.1000000000000000D+01	0.0
-0.7888499305342922D-05	0.0

NO. OF ITERATIONS REQUIRED= 5

ANNULAR FLOW VELOCITY AT THE ONSET OF THE BUCKLING INSTABILITY=(0.144482594721395 3D+01 0.0)

THE CORRESPONDING MODAL SHAPE

-0.1775175616130500D+00	0.0
-0.6411975724564302D-05	0.0
-0.1665000362389234D+00	0.0
-0.5386622017962799D+00	0.0
-0.1606771941282780-04	0.0
-0.5039479549966401D+00	0.0
0.1077035895259266D+01	0.0
0.3185764761367373D-04	0.0
0.1000000000C000C0D+01	0.0

NO. OF ITERATIONS REQUIRED= 5

APPENDIX H

COMPUTER PROGRAM FOR THE EVALUATION OF THE INTEGRALS OF THE GENERALIZED AERODYNAMIC FORCES

H.1 FUNCTION OF THE PROGRAM

The program evaluates the integrals in the expressions of the generalized aerodynamic forces by numerical integration. The forms of the integrals in the cases of compressible and incompressible flow are somewhat different. Hence, the program is slightly modified accordingly as the fluid is compressible or not. Nevertheless, the program structure and the computation procedures in the different versions of the program are essentially the same.

H.2 PROGRAM STRUCTURE

The program is written in Fortran IV language and it has the following structure:

MAIN PROGRAM

COMPLEX FUNCTION H

COMPLEX FUNCTION IN

COMPLEX FUNCTION KN

DOUBLE PRECISION FUNCTION R

DOUBLE PRECISION FUNCTION F

DOUBLE PRECISION FUNCTION FA.

H.3 DESCRIPTION OF THE PROGRAM

The functions of the subprograms are summarized as follows:

(1) Complex function H evaluates the term $H_{km}(\bar{\alpha})$, which appears in the integrands, according to the expressions given in Appendix B.

(2) Complex functions IN and KN are used to calculate the modified Bessel functions of the first and second kind, In and Kn, according to the expressions given in Section H.4. Functions R, F and FA are function subprograms called upon by IN and KN.

H.3.1 Version for the Case of Incompressible Flow

After defining the necessary parameters, the numerical integrations are performed in the main program using the two-point Gaussian scheme† with 100 points in the range (-50.0, 50.0) of the variable $\bar{\alpha}$. The complex function H and the subprograms for Bessel functions are called upon in the evaluation of the integrands at these 100 chosen values of $\bar{\alpha}$. The integrals to be evaluated are given in equations (3.3.1b-.1g), (3.3.2a-.2f) for systems with both shells flexible, and in equations (D.3a-.3c) for systems with a rigid outer shell. Separate programs are written for the two types of systems. They are shown in pages H.7-H.23 with a sample of the output.

H.3.2 Version for the Case of Compressible Flow

After defining the necessary parameters including the Mach numbers, M_i and M_o, the numerical integrations are performed in the main program

†For details of the scheme, see reference [44].

using the two-point Gaussian scheme with 100 points in the range (-50.0, 50.0) of the variable $\tilde{\alpha}$. The integrals to be evaluated are given in equations (D.1a). Since these integrals are frequency-dependent, the values of the reduced frequencies, K_i and K_o, have to be specified. By means of a DO-loop, the integrals can be calculated for the desired number of times with the reduced frequencies incremented after each repetition of the loop. This feature allows us to generate the data required to derive the interpolation equations which will then be used to approximate the integrals as a function of the reduced frequencies. The computer program and a sample of the output are given in pages H.24-H.29.

All calculations are carried out with double precision.

H.4 EXPRESSIONS UTILIZED FOR THE BESSEL FUNCTIONS

The evaluation of the Bessel functions is based on the following identities†.

(i) Modified Bessel function of the first kind

In this case, we have

$$I_n(x) = \sum_{k=0}^{\infty} \frac{x^{2k+n}}{2^{2k+n}\, k!\, \Gamma(n+k+1)} \qquad (H.1)$$

For $\|x\| \geq 20$ and $0 \leq (\text{phase of } x) \leq \pi$, I_n is approximated by

†Quoted from reference [35].

$$I_n(x) \simeq \frac{e^x}{(2\pi x)^{1/2}}\left[1 - \frac{(4n^2-1^2)}{1!\,8x} + \frac{(4n^2-1^2)(4n^2-3^2)}{2!\,(8x)^2} + \cdots\right]$$

$$+ e^{(n+1/2)\pi i}\frac{e^{-x}}{(2\pi x)^{1/2}}\left[1 + \frac{(4n^2-1^2)}{1!\,8x} + \frac{(4n^2-1^2)(4n^2-3^2)}{2!\,(8x)^2} + \cdots\right]. \tag{H.2}$$

For $\|x\| \geq 20$ and $-\pi < (\text{phase of } x) \leq 0$, I_n is approximated by

$$I_n(x) \simeq \frac{e^x}{(2\pi x)^{1/2}}\left[1 - \frac{(4n^2-1^2)}{1!\,8x} + \frac{(4n^2-1^2)(4n^2-3^2)}{2!\,(8x)^2} + \cdots\right]$$

$$+ e^{-(n+1/2)\pi i}\frac{e^{-x}}{(2\pi x)^{1/2}}\left[1 + \frac{(4n^2-1^2)}{1!\,8x} + \frac{(4n^2-1^2)(4n^2-3^2)}{2!\,(8x)^2} + \cdots\right]. \tag{H.3}$$

The derivative of $I_n(x)$ with respect to its argument is evaluated by using

$$xI_n'(x) = nI_n(x) + xI_{n+1}(x). \tag{H.4}$$

(ii) Modified Bessel function of the second kind

In this case, we have

$$K_n(x) = \frac{1}{2}\sum_{k=0}^{n-1}\frac{(-1)^k(n-k-1)!}{k!}\left(\frac{2}{x}\right)^{n-2k}$$

$$+ (-1)^{n+1}\sum_{k=0}^{\infty}\frac{x^{n+2k}}{2^{n+2k}\,k!\,(n+k)!}\left\{\log\frac{x}{2} - \frac{1}{2}\left[\psi(k+1) + \psi(n+k+1)\right]\right\}, \tag{H.5}$$

where

$$\psi(k+1) = \left(1 + \frac{1}{2} + \frac{1}{3} + \cdots + \frac{1}{k}\right) - \gamma \,, \qquad \psi(1) = -\gamma \,,$$

$$\psi(n+k+1) = \left(1 + \frac{1}{2} + \frac{1}{3} + \cdots + \frac{1}{n+k}\right) - \gamma \,,$$

$$\gamma = \lim_{n\to\infty} \left(1 + \frac{1}{2} + \frac{1}{3} + \cdots + \frac{1}{n} - \log n\right)$$

$$= 0.5772 \ldots \,.$$

For $\|x\| \geq 15$,

$$K_n(x) \simeq \left(\frac{\pi}{2x}\right)^{1/2} e^{-x} \left[1 + \frac{(4n^2-1^2)}{8x} + \frac{(4n^2-1^2)(4n^2-3^2)}{2!\,(8x)^2} + \cdots\right] .$$

The derivative of $K_n(x)$ with respect to its argument is evaluated by using

$$x K_n'(x) = n K_n(x) - x K_{n+1}(x) \,. \qquad \text{(H.7)}$$

NOTATION USED IN THE PROGRAMS

Notation used in the computer programs	Corresponding notation used in the thesis	Definition
IN(X,N)	$I_n(x)$	Modified Bessel function of the first kind
KN(X,N)	$K_n(x)$	Modified Bessel function of the second kind
INP(X)	$I_n'(x)$	Derivative of I_n
KNP(X)	$K_n'(x)$	Derivative of K_n
EN(V.I.F.)	$\hat{E}_n(\bar{\alpha})$	Defined in equation (3.3.1h)
EN(V.C.F.)	$E_n(\bar{\alpha})$	Defined in equation (3.2.7b)
FN(V.I.F.)	$\hat{F}_n(\bar{\alpha})$	Defined in equation (3.3.1i)
FN(V.C.F.)	$F_n(\bar{\alpha})$	Defined in equation (3.2.7c)
GN	$\hat{G}_n(\bar{\alpha})$	Defined in equation (3.3.1j)
LN	$\hat{L}_n(\bar{\alpha})$	Defined in equation (3.3.2g)
MN	$\hat{M}_n(\bar{\alpha})$	Defined in equation (3.3.2h)
HKM	$H_{km}(\bar{\alpha})$	Defined in equation (3.2.11c)
Q(9,3,3), R(6,3,3)†		Integrals in the generalized aerodynamic forces for system with both shells flexible subjected to incompressible flow
Q1, Q2, Q3, Q4, Q5, Q6		Integrals in the generalized aerodynamic forces for system with a rigid outer shell subjected to incompressible flow.
I1, I2		Integrals in the generalized aerodynamic forces for system with a rigid outer shell subjected to compressible flow.

(V.I.F.) - In versions for incompressible flow
(V.C.F.) - In version for compressible flow

†In output, they are denoted by Q1, Q2, ..., Q9 and R1, R2, ..., R6.

```
/INFO MVS TI(40) PA(100) R(MUSIC) CL(20) N(STEVE SIU PUI CHAN)
//STEP1 EXEC FORTRAN
//FORT.SYSIN DD *
C*****************************************************************
C     COMPUTER PROGRAM FOR CALCULATING THE INTEGRALS IN THE GENERALIZED*
C     AERODYNAMIC FORCES                                          *
C     VERSION FOR INCOMPRESSIBLE FLUID                            *
C     ONLY THE INNER SHELL FLEXIBLE                               *
C*****************************************************************
C
C*****************************************************************
C     MAIN PROGRAM                                                *
C*****************************************************************
      IMPLICIT COMPLEX*16(A-Z)
      REAL*8 C(3),P(3),PI,GAMA,EI,EO,X1,X2,D
      INTEGER N,K,M,I
      COMMON PI,GAMA
      COMMON/DATA1/C,P
      INP(Y)=N*IN(Y,N)/Y+IN(Y,N+1)
      KNP(Y)=N*KN(Y,N)/Y-KN(Y,N+1)
      PI=3.14159265358979D0
      GAMA=0.57721566490116l8D0
      C(1)=0.98250221457623 79D0
      C(2)=1.00077731190727D0
      C(3)=0.9999664501254086D0
      P(1)=4.7300407448627D0
      P(2)=7.85320462409584D0
      P(3)=10.99560783800167D0
      EI=1/15.D0
      EO=0.10D0
      N=3
      D=2.D0
      DO 2 K=1,3
      DO 2 M=1,3
      X1=-50.D0+D/2*(1-DSQRT(1/3.D0))
      X2=-50.D0+D/2*(1+DSQRT(1/3.D0))
      Q1=(0.D0,0.D0)
      Q2=Q1
      Q3=Q2
      Q4=Q3
      Q5=Q4
      Q6=Q5
      DO 1 I=1,98
      EIX=X1*EI
      EOX=X1*EO
      INIX=IN(EIX,N)
      INOX=IN(EOX,N)
      KNIX=KN(EIX,N)
      KNOX=KN(EOX,N)
      INPIX=INP(EIX)
      INPOX=INP(EOX)
      KNPIX=KNP(EIX)
      KNPOX=KNP(EOX)
      DEM=INPOX*KNPIX-INPIX*KNPOX
      EN=INIX/INPIX
      FN=(INPOX*KNIX-INIX*KNPOX)/DEM
      HKM=H(X1,K,M)
      QG1=EN*HKM
```

```
      QG2=FN*HKM
      Q1=Q1+QG1/X1
      Q2=Q2+QG2/X1
      Q3=Q3+QG1*X1
      Q4=Q4+QG2*X1
      Q5=Q5+QG1
      Q6=Q6+QG2
      X1=X1+D
      IF(I.EQ.49) X1=X2
    1 CONTINUE
      PRINT10,N,K,M
   10 FORMAT('-','N=',I1,' K=',I1,' M=',I1)
      PRINT11,Q1
      PRINT12,Q2
      PRINT13,Q3
      PRINT14,Q4
      PRINT15,Q5
      PRINT16,Q6
    2 CONTINUE
      PRINT40
   11 FORMAT('0','Q1=(',2D24.16,1X,')')
   12 FORMAT('0','Q2=(',2D24.16,1X,')')
   13 FORMAT('0','Q3=(',2D24.16,1X,')')
   14 FORMAT('0','Q4=(',2D24.16,1X,')')
   15 FORMAT('0','Q5=(',2D24.16,1X,')')
   16 FORMAT('0','Q6=(',2D24.16,1X,')')
   40 FORMAT('1')
      STOP
      END
C
C*****************************************************************************
C     COMPLEX FUNCTION H                                                      *
C*****************************************************************************
      COMPLEX FUNCTION H*16(AB,K,M)
      IMPLICIT COMPLEX*16(A-Z)
      REAL*8 AB,C(3),P(3),AB1
      INTEGER K,M,J,M1
      COMMON/DATA1/C,P
      H=(1.D0,0.D0)
      I=(0.D0,1.D0)
      AB1=AB
      M1=M
      DO 1 J=1,2
      IF(DABS(AB).EQ.M1) GO TO 10
      A=2*C(M1)*P(M1)**3
      B=I*2*P(M1)**2
      E1=(-1)**(M1+1)*CDEXP(I*AB1)+1
      E2=E1-2
      IM=(A*E1-B*AB1*E2)/(AB1**4-P(M1)**4)
      GO TO 11
   10 IF(J.EQ.2) GO TO 20
      IM=((I*C(M1)*P(M1)**3-I*P(M1)**2+AB*P(M1)**2)*(-1)**(M1+1)*
     #CDEXP(I*AB)+I*P(M1)**2)/(-2*AB**3)
      GO TO 11
   20 IM=((-I*C(M1)*P(M1)**3+I*P(M1)**2+AB*P(M1)**2)*(-1)**(M1+1)*
     #CDEXP(-I*AB)-I*2*P(M1)**2)/(-2*AB**3)
   11 H=H*IM
      M1=K
```

```
      AB1=-AB
    1 CONTINUE
      RETURN
      END
C
C*****************************************************************************
C     SUBPROGRAMS FOR CALCULATING THE BESSEL FUNCTIONS                        *
C*****************************************************************************
      COMPLEX FUNCTION IN*16(X,N)
      IMPLICIT REAL*8(A-Z)
      COMPLEX*16 W,X,Y,Z,T,T1,T2,T3,T4,I,DCMPLX,DCONJG
      INTEGER K,N
      COMMON PI,GAMA
      I=(0.D0,1.D0)
      IF(CDABS(X).GE.20.D0) GO TO 10
      IN=(0.D0,0.D0)
      K=0
   11 T=(X/2)**(2*K)/FA(K)/FA(N+K)
      IF(CDABS(T).LT.1.D-12) GO TO 12
      IN=IN+T
      K=K+1
      GO TO 11
   12 IN=(X/2)**N*IN
      RETURN
   10 T1=(4*N**2-1)/8/X
      T2=T1*(4*N**2-9)/16/X
      T3=CDEXP(X)/CDSQRT(2*PI*X)
      T4=CDEXP(-X)/CDSQRT(2*PI*X)
      Y=X-DCONJG(X)
      Z=DCMPLX(0.D0,CDABS(Y))
      W=Y+Z
      IF(CDABS(Y).EQ.0.D0) GO TO 14
      IF(CDABS(W).EQ.0.D0) GO TO 13
   14 IN=T3*(1-T1+T2)+(-1)**N*I*T4*(1+T1+T2)
      RETURN
   13 IN=T3*(1-T1+T2)+(-1)**(N+1)*I*T4*(1+T1+T2)
      RETURN
      END
C
      COMPLEX FUNCTION KN*16(X,N)
      IMPLICIT REAL*8(A-Z)
      COMPLEX*16 X,KN1,T,T1,T2,T3
      INTEGER N,M,K,I
      COMMON PI,GAMA
      IF(CDABS(X).GE.15.D0) GO TO 40
      IF(N.EQ.0) GO TO 46
      KN=FA(N-1)*(2/X)**N
      IF(N.EQ.1) GO TO 45
      M=N-1
      DO 41 I=1,M
   41 KN=KN+(-1)**I*FA(N-I-1)/FA(I)*(2/X)**(N-2*I)
   45 KN=KN/2
      GO TO 47
   46 KN=(0.D0,0.D0)
   47 KN1=(0.D0,0.D0)
      K=0
   43 T=(X/2)**(N+2*K)/FA(K)/FA(N+K)*(CDLOG(X/2)-(F(K+1)+F(N+K+1))/2)
      IF(CDABS(T).LT.1.D-12) GO TO 42
```

```
      KN1=KN1+T
      K=K+1
      GO TO 43
   42 KN=KN+KN1*(-1)**(N+1)
      RETURN
   40 T1=(4*N**2-1)/8/X
      T2=T1*(4*N**2-9)/16/X
      T3=CDEXP(-X)*CDSQRT(PI/2/X)
      KN=T3*(1+T1+T2)
      RETURN
      END
C
      DOUBLE PRECISION FUNCTION R(K)
      IMPLICIT REAL*8(A-Z)
      INTEGER K,I
      R=0.D0
      DO 40 I=1,K
   40 R=R+1.D0/I
      RETURN
      END
C
      DOUBLE PRECISION FUNCTION F(K)
      IMPLICIT REAL*8(A-Z)
      INTEGER K
      COMMON PI,GAMA
      IF(K.EQ.1) GO TO 50
      F=R(K-1)-GAMA
      RETURN
   50 F=-GAMA
      RETURN
      END
C
      DOUBLE PRECISION FUNCTION FA(K)
      IMPLICIT REAL*8(A-Z)
      INTEGER K,L
      FA=1.D0
      L=1
   21 FA=FA*L
      IF(L.GE.K) GO TO 22
      L=L+1
      GO TO 21
   22 CONTINUE
      RETURN
      END
//GO.SYSIN DD *
//
/*
```

N=3 K=1 M=1

Q1=(0.1393110690919361D+00 0.0)

Q2=(-0.1655069832604356D+00 0.2553490443000322D-16)

Q3=(0.1705368800527476D+01 0.0)

Q4=(-0.2011334753979894D+01 0.7037229509394624D-15)

Q5=(-0.2890189487239503D-06 0.0)

Q6=(0.2660289319962818D-06 -0.1868688691154308D-15)

N=3 K=1 M=2

Q1=(-0.3493985561308399D-17 0.2071083591670780D-07)

Q2=(-0.5615031471458955D-16 -0.1905137052050897D-07)

Q3=(0.1280325901621925D-16 0.4922197501411912D-04)

Q4=(-0.4856623623462007D-14 -0.4527659901670027D-04)

Q5=(-0.7595545043302750D-17 -0.4635193666396506D+00)

Q6=(0.5270091996945850D-15 0.5467118674964745D+00)

N=3 K=1 M=3

Q1=(0.2502530206638508D-03 0.1742202535041026D-18)

Q2=(-0.7935232932433042D-03 -0.4605728693621104D-16)

Q3=(-0.1356451885410314D+01 0.1766665033111523D-17)

Q4=(0.1602751337687827D+01 -0.7012345353758176D-14)

Q5=(-0.1344171251251656D-05 0.5982278243355582D-17)

Q6=(0.1237397299804226D-05 0.3473654502034835D-15)

N=3 K=2 M=1

Q1=(-0.3493985561308399D-17 -0.2071083591670780D-07)

Q2=(0.6448962380635904D-16 0.1905137052050897D-07)

Q3=(0.1280325901621925D-16 -0.4922197501411912D-04)

Q4=(0.4829960346888875D-14 0.4527659901670027D-04)

Q5=(-0.7595545043302750D-17 0.4635193666396506D+00)

```
Q6=( -0.5091037977393918D-15 -0.5467118674964745D+00 )

N=3 K=2 M=2

Q1=(  0.1384569070761792D+00  0.0                    )

Q2=( -0.1628769399841652D+00  0.3257762812199737D-15 )

Q3=(  0.6336100528081735D+01  0.0                    )

Q4=( -0.7391909319082398D+01  0.1092025624732897D-12 )

Q5=( -0.5161242089028442D-05  0.0                    )

Q6=(  0.4742426007811891D-05 -0.4818511456360506D-14 )

N=3 K=2 M=3

Q1=( -0.4805380404083589D-17 -0.8825507255690017D-07 )

Q2=( -0.4062208095643473D-15  0.8120960680877015D-07 )

Q3=( -0.2745673612882188D-15 -0.2087817271474474D-03 )

Q4=( -0.6616415426105696D-13  0.1921099564877068D-03 )

Q5=(  0.2409414777298159D-16 -0.7581629515661440D+00 )

Q6=(  0.4643306945629120D-14  0.8816097069169224D+00 )

N=3 K=3 M=1

Q1=(  0.2502530206638508D-03 -0.1742202535041026D-18 )

Q2=( -0.7935232932433042D-03 -0.4564326211814969D-16 )

Q3=( -0.1356451885410314D+01 -0.1766665033111523D-17 )

Q4=(  0.1602751337687827D+01 -0.7007942715180164D-14 )

Q5=( -0.1344171251251656D-05 -0.5982278243355582D-17 )

Q6=(  0.1237397299804226D-05  0.3615397570688440D-15 )

N=3 K=3 M=2

Q1=( -0.4805380404083589D-17  0.8825507255690017D-07 )

Q2=(  0.4174864361437056D-15 -0.8120960680877015D-07 )

Q3=( -0.2745673612882188D-15  0.2087817271474474D-03 )

Q4=(  0.6680671497692505D-13 -0.1921099564877068D-03 )
```

```
Q5=(  0.2409414777298159D-16  0.7581629515661440D+00 )
Q6=( -0.4699412319131075D-14 -0.8816097069169224D+00 )

N=3 K=3 M=3
Q1=(  0.1371499215948725D+00  0.0                    )
Q2=( -0.1590275057634876D+00  0.8854564896880767D-15 )
Q3=(  0.1345434890848073D+02  0.0                    )
Q4=( -0.1544550853220029D+02  0.9570184411235733D-13 )
Q5=( -0.6350909698057574D-05  0.0                    )
Q6=(  0.5846857252439295D-05 -0.1003111748921954D-13 )
```

```
//ME15INTE JOB (ME15,104,040,0200,0000,20,,1),'STEVE SIU PUI CHAN'
//STEP1 EXEC FORTRAN
//FORT.SYSIN DD *
C*************************************************************************
C     COMPUTER PROGRAM FOR CALCULATING THE INTEGRALS IN THE GENERALIZED*
C     AERODYNAMIC FORCES                                                *
C     VERSION FOR INCOMPRESSIBLE FLUID                                  *
C     BOTH SHELLS FLEXIBLE                                              *
C*************************************************************************
C
C*************************************************************************
C     MAIN PROGRAM                                                      *
C*************************************************************************
      IMPLICIT COMPLEX*16(A-Z)
      REAL*8 C(3),P(3),PI,GAMA,EI,EO,X1,X2,D
      INTEGER N,K,M,I
      DIMENSION Q(9,3,3),R(6,3,3)
      COMMON PI,GAMA
      COMMON/DATA1/C,P
      DATA Q/81*(0.D0,0.D0)/,R/54*(0.D0,0.D0)/
      INP(Y)=N*IN(Y,N)/Y+IN(Y,N+1)
      KNP(Y)=N*KN(Y,N)/Y-KN(Y,N+1)
      PI=3.14159265358979D0
      GAMA=0.5772156649011618D0
      C(1)=0.9825022145762379D0
      C(2)=1.00077731190727D0
      C(3)=0.9999664501254086D0
      P(1)=4.7300407448627D0
      P(2)=7.85320462409584D0
      P(3)=10.99560783800167D0
      EI=1/11.D0
      EO=0.100D0
      N=3
      D=2.D0
      DO 2 K=1,3
      DO 2 M=1,3
      X1=-50.D0+D/2*(1-DSQRT(1/3.D0))
      X2=-50.D0+D/2*(1+DSQRT(1/3.D0))
      DO 1 I=1,98
      EIX=X1*EI
      EOX=X1*EO
      INIX=IN(EIX,N)
      INOX=IN(EOX,N)
      KNIX=KN(EIX,N)
      KNOX=KN(EOX,N)
      INPIX=INP(EIX)
      INPOX=INP(EOX)
      KNPIX=KNP(EIX)
      KNPOX=KNP(EOX)
      DEM=INPOX*KNPIX-INPIX*KNPOX
      EN=INIX/INPIX
      FN=(INPOX*KNIX-INIX*KNPOX)/DEM
      GN=(INIX*KNPIX-INPIX*KNIX)/DEM
      LN=(INPOX*KNOX-INOX*KNPOX)/DEM
      MN=(INOX*KNPIX-INPIX*KNOX)/DEM
      HKM=H(X1,K,M)
      Q1=EN*HKM
      Q2=FN*HKM
```

```
      Q3=GN*HKM
      R1=LN*HKM
      R2=MN*HKM
      Q(1,K,M)=Q(1,K,M)+Q1
      Q(2,K,M)=Q(2,K,M)+Q1/X1
      Q(3,K,M)=Q(3,K,M)+Q1*X1
      Q(4,K,M)=Q(4,K,M)+Q2
      Q(5,K,M)=Q(5,K,M)+Q2/X1
      Q(6,K,M)=Q(6,K,M)+Q2*X1
      Q(7,K,M)=Q(7,K,M)+Q3
      Q(8,K,M)=Q(8,K,M)+Q3/X1
      Q(9,K,M)=Q(9,K,M)+Q3*X1
      R(1,K,M)=R(1,K,M)+R1
      R(2,K,M)=R(2,K,M)+R1/X1
      R(3,K,M)=R(3,K,M)+R1*X1
      R(4,K,M)=R(4,K,M)+R2
      R(5,K,M)=R(5,K,M)+R2/X1
      R(6,K,M)=R(6,K,M)+R2*X1
      X1=X1+D
      IF(I.EQ.49) X1=X2
1     CONTINUE
      PRINT10,N,K,M
10    FORMAT('-','N=',I1,' K=',I1,' M=',I1)
      DO 3 I=1,9
3     PRINT11,I,Q(I,K,M)
11    FORMAT('0','Q',I1,'=(',2D24.16,1X,')')
      DO 4 I=1,6
4     PRINT12,I,R(I,K,M)
12    FORMAT('0','R',I1,'=(',2D24.16,1X,')')
2     CONTINUE
      PRINT40
40    FORMAT('1')
      STOP
      END
C
C*****************************************************************************
C     COMPLEX FUNCTION H                                                      *
C*****************************************************************************
      COMPLEX FUNCTION H*16(AB,K,M)
      IMPLICIT COMPLEX*16(A-Z)
      REAL*8 AB,C(3),P(3),AB1
      INTEGER K,M,J,M1
      COMMON/DATA1/C,P
      H=(1.D0,0.D0)
      I=(0.D0,1.D0)
      AB1=AB
      M1=M
      DO 1 J=1,2
      IF(DABS(AB).EQ.M1) GO TO 10
      A=2*C(M1)*P(M1)**3
      B=I*2*P(M1)**2
      E1=(-1)**(M1+1)*CDEXP(I*AB1)+1
      E2=E1-2
      IM=(A*E1-B*AB1*E2)/(AB1**4-P(M1)**4)
      GO TO 11
10    IF(J.EQ.2) GO TO 20
      IM=((I*C(M1)*P(M1)**3-I*P(M1)**2+AB*P(M1)**2)*(-1)**(M1+1)*
     #CDEXP(I*AB)+I*P(M1)**2)/(-2*AB**3)
```

```
      GO TO 11
   20 IM=((-I*C(M1)*P(M1)**3+I*P(M1)**2+AB*P(M1)**2)*(-1)**(M1+1)*
     #CDEXP(-I*AB)-I*2*P(M1)**2)/(-2*AB**3)
   11 H=H*IM
      M1=K
      AB1=-AB
    1 CONTINUE
      RETURN
      END
C
C*********************************************************************
C     SUBPROGRAMS FOR CALCULATING THE BESSEL FUNCTIONS              *
C*********************************************************************
      COMPLEX FUNCTION IN*16(X,N)
      IMPLICIT REAL*8(A-Z)
      COMPLEX*16 W,X,Y,Z,T,T1,T2,T3,T4,I,DCMPLX,DCONJG
      INTEGER K,N
      COMMON PI,GAMA
      I=(0.D0,1.D0)
      IF(CDABS(X).GE.20.D0) GO TO 10
      IN=(0.D0,0.D0)
      K=0
   11 T=(X/2)**(2*K)/FA(K)/FA(N+K)
      IF(CDABS(T).LT.1.D-12) GO TO 12
      IN=IN+T
      K=K+1
      GO TO 11
   12 IN=(X/2)**N*IN
      RETURN
   10 T1=(4*N**2-1)/8/X
      T2=T1*(4*N**2-9)/16/X
      T3=CDEXP(X)/CDSQRT(2*PI*X)
      T4=CDEXP(-X)/CDSQRT(2*PI*X)
      Y=X-DCONJG(X)
      Z=DCMPLX(0.D0,CDABS(Y))
      W=Y+Z
      IF(CDABS(Y).EQ.0.D0) GO TO 14
      IF(CDABS(W).EQ.0.D0) GO TO 13
   14 IN=T3*(1-T1+T2)+(-1)**N*I*T4*(1+T1+T2)
      RETURN
   13 IN=T3*(1-T1+T2)+(-1)**(N+1)*I*T4*(1+T1+T2)
      RETURN
      END
C
      COMPLEX FUNCTION KN*16(X,N)
      IMPLICIT REAL*8(A-Z)
      COMPLEX*16 X,KN1,T,T1,T2,T3
      INTEGER N,M,K,I
      COMMON PI,GAMA
      IF(CDABS(X).GE.15.D0) GO TO 40
      IF(N.EQ.0) GO TO 46
      KN=FA(N-1)*(2/X)**N
      IF(N.EQ.1) GO TO 45
      M=N-1
      DO 41 I=1,M
   41 KN=KN+(-1)**I*FA(N-I-1)/FA(I)*(2/X)**(N-2*I)
   45 KN=KN/2
      GO TO 47
```

```
   46  KN=(0.D0,0.D0)
   47  KN1=(0.D0,0.D0)
       K=0
   43  T=(X/2)**(N+2*K)/FA(K)/FA(N+K)*(CDLOG(X/2)-(F(K+1)+F(N+K+1))/2)
       IF(CDABS(T).LT.1.D-12) GO TO 42
       KN1=KN1+T
       K=K+1
       GO TO 43
   42  KN=KN+KN1*(-1)**(N+1)
       RETURN
   40  T1=(4*N**2-1)/8/X
       T2=T1*(4*N**2-9)/16/X
       T3=CDEXP(-X)*CDSQRT(PI/2/X)
       KN=T3*(1+T1+T2)
       RETURN
       END
C
       DOUBLE PRECISION FUNCTION R(K)
       IMPLICIT REAL*8(A-Z)
       INTEGER K,I
       R=0.D0
       DO 40 I=1,K
   40  R=R+1.D0/I
       RETURN
       END
C
       DOUBLE PRECISION FUNCTION F(K)
       IMPLICIT REAL*8(A-Z)
       INTEGER K
       COMMON PI,GAMA
       IF(K.EQ.1) GO TO 50
       F=R(K-1)-GAMA
       RETURN
   50  F=-GAMA
       RETURN
       END
C
       DOUBLE PRECISION FUNCTION FA(K)
       IMPLICIT REAL*8(A-Z)
       INTEGER K,L
       FA=1.D0
       L=1
   21  FA=FA*L
       IF(L.GE.K) GO TO 22
       L=L+1
       GO TO 21
   22  CONTINUE
       RETURN
       END
//GO.SYSIN DD *
//
/*
```

N=3 K=1 M=1

Q1=(-0.3280206164830202D-06 0.0)

Q2=(0.1896062132537650D+00 0.0)

Q3=(0.2312184916463780D+01 0.0)

Q4=(0.6190663329733319D-06 0.9114964994383228D-15)

Q5=(-0.6759592315814779D+00 0.6040495708646455D-15)

Q6=(-0.8122943495441742D+01 -0.1783665717388016D-12)

Q7=(-0.5949173465983090D-06 0.2730464022728906D-17)

Q8=(0.7138061018030161D+00 -0.5147728870668369D-15)

Q9=(0.8569145764091334D+01 0.1145911243714064D-12)

R1=(0.5408339515794209D-06 0.4252013678016080D-15)

R2=(-0.6489146380026265D+00 0.4649481588998984D-15)

R3=(-0.7790132512812177D+01 -0.1342991415052941D-12)

R4=(-0.6771914051714807D-06 0.2336123706823247D-15)

R5=(0.7435324606622264D+00 -0.3953589880319306D-15)

R6=(0.8934416806883038D+01 0.8421966111077975D-13)

N=3 K=1 M=2

Q1=(-0.1029541159227697D-16 -0.6285111159652311D+00)

Q2=(-0.4766713517681613D-17 0.2348738759364798D-07)

Q3=(0.1628817143484548D-16 0.5581861620806592D-04)

Q4=(-0.8161994647154542D-15 0.2207959405904953D+01)

Q5=(-0.9633476396856025D-15 -0.4420631811524404D-07)

Q6=(0.3248617160053225D-12 -0.1050433756703668D-03)

Q7=(-0.7896814912951367D-15 -0.2329277443221273D+01)

Q8=(0.8166325603169927D-15 0.4244661030438371D-07)

Q9=(-0.1947442668883681D-12 0.1008576980023068D-03)

R1=(0.8289664281683351D-14 0.2117524948383588D+01)

R2=(-0.9792191731388415D-15 -0.3858782759559040D-07)

```
R3=( -0.7733679049467813D-13 -0.9168881635822351D-04 )
R4=( -0.6766979859523874D-14 -0.2428534253154542D+01 )
R5=(  0.7903454115827526D-15  0.4835465234972159D-07 )
R6=(  0.7284915850159565D-13  0.1149004051113856D-03 )

N=3 K=1 M=3
Q1=( -0.1525785682687179D-05  0.8129588219495467D-17 )
Q2=(  0.6318529334634996D-03  0.2371590276574419D-18 )
Q3=( -0.1842035225332608D+01  0.2469456692931669D-17 )
Q4=(  0.2881073360038401D-05  0.3146543647328196D-13 )
Q5=( -0.6372597942142652D-02 -0.1397338347729216D-14 )
Q6=(  0.6485864327386988D+01 -0.1082602378816420D-11 )
Q7=( -0.2769121159207947D-05 -0.2196590551975507D-13 )
Q8=(  0.7017078876918594D-02  0.1049768623391913D-14 )
Q9=( -0.6844252009758827D+01  0.7285050198337377D-12 )
R1=( -0.2517382871767113D-05  0.2502434899182478D-13 )
R2=( -0.6379162615243331D-02 -0.1052366471568723D-14 )
R3=(  0.6222047281603371D+01 -0.9163929289836358D-12 )
R4=( -0.3151609586744456D-05 -0.1717996837028040D-13 )
R5=(  0.7027982593785703D-02  0.7838016151482439D-15 )
R6=( -0.7133930243991075D+01  0.6068625400795199D-12 )

N=3 K=2 M=1
Q1=( -0.1029541159227697D-16  0.6285111159652311D+00 )
Q2=( -0.4766713517681613D-17 -0.2348738759364798D-07 )
Q3=(  0.1628817143484548D-16 -0.5581861620806592D-04 )
Q4=(  0.8884379566400543D-15 -0.2207959405904953D+01 )
Q5=(  0.9976375229975989D-15  0.4420631811524404D-07 )
Q6=( -0.3249472677089020D-12  0.1050433756703668D-03 )
Q7=(  0.7134810718936100D-15  0.2329277443221273D+01 )
```

```
Q8=( -0.852864065138355D-15 -0.4244661030438371D-07 )
Q9=(  0.1948324113980102D-12 -0.1008576980023068D-03 )
R1=( -0.8220391173136591D-14 -0.2117524948383588D+01 )
R2=(  0.1012156904794655D-14  0.3858782759559040D-07 )
R3=(  0.7725665912227731D-13  0.9168881635822351D-04 )
R4=(  0.6687525215708392D-14  0.2428534253154542D+01 )
R5=( -0.8280645177715693D-15 -0.4835465234972159D-07 )
R6=( -0.7275519458967751D-13 -0.1149004051113856D-03 )

N=3 K=2 M=2
Q1=( -0.5845163463897832D-05  0.0                    )
Q2=(  0.1874795661657285D+00  0.0                    )
Q3=(  0.8541245969912896D+01  0.0                    )
Q4=(  0.1094831275117628D-04 -0.9403806651428478D-13 )
Q5=( -0.6551227020549533D+00  0.3629635273343210D-14 )
Q6=( -0.2934937066445356D+02  0.3409919784229403D-11 )
Q7=( -0.1049698053587602D-04  0.6488410355947742D-13 )
Q8=(  0.6908633621273766D+00 -0.2663248619134660D-14 )
Q9=(  0.3091333379178624D+02 -0.2319704810248190D-11 )
R1=(  0.9542709579259302D-05 -0.1156875277383343D-12 )
R2=( -0.6280576019341661D+00  0.3825841999713141D-14 )
R3=( -0.2810303071981653D+02  0.4465622672323831D-11 )
R4=( -0.1197471004215592D-04  0.7849958137573403D-13 )
R5=(  0.7205530776322418D+00 -0.2734317652635607D-14 )
R6=(  0.3227826606765166D+02 -0.2991284808234241D-11 )

N=3 K=2 M=3
Q1=(  0.3245031071165055D-16 -0.1020380446668096D+01 )
Q2=( -0.6494989735391820D-17 -0.1001263295044486D-06 )
Q3=( -0.3708457815126825D-15 -0.2368581614173008D-03 )
```

```
Q4=(  0.5827035508300584D-13  0.3481847626998819D+01 )
Q5=( -0.1049759241826247D-14  0.1887126541802776D-06 )
Q6=( -0.2935986399221754D-11  0.4463713138848790D-03 )
Q7=( -0.3608184921736982D-13 -0.3665667574609826D+01 )
Q8=(  0.6106639506547822D-15 -0.1812772250460474D-06 )
Q9=(  0.1863968377723573D-11 -0.4287704796688965D-03 )
R1=(  0.5785951407214072D-14  0.3332425067828181D+01 )
R2=(  0.4249815393813545D-15  0.1647974772513057D-06 )
R3=( -0.9243694423341424D-12  0.3897913450954734D-03 )
R4=( -0.3007502803462137D-15 -0.3829206018116956D+01 )
R5=( -0.4151863472895973D-15 -0.2064264201705002D-06 )
R6=(  0.5116057671682966D-12 -0.4882696959283045D-03 )

N=3 K=3 M=1
Q1=( -0.1525785682687179D-05 -0.8129588219495467D-17 )
Q2=(  0.6318529334634996D-03 -0.2371590276574419D-18 )
Q3=( -0.1842035225332608D+01 -0.2469456692931669D-17 )
Q4=(  0.2881073360038401D-05  0.3152308191943916D-13 )
Q5=( -0.6372597942142652D-02 -0.1395647285094802D-14 )
Q6=(  0.6485864327386988D+01 -0.1082583167229549D-11 )
Q7=( -0.2769121159207947D-05 -0.2202675498652739D-13 )
Q8=(  0.7017078876918594D-02  0.1047982834621040D-14 )
Q9=( -0.6844252009758827D+01  0.7284846121116094D-12 )
R1=(  0.2517382871767113D-05  0.2507966668889053D-13 )
R2=( -0.6379162615243331D-02 -0.1050743027231568D-14 )
R3=(  0.6222047281603371D+01 -0.9163743765089733D-12 )
R4=( -0.3151609586744456D-05 -0.1724337492465774D-13 )
R5=(  0.7027982593785703D-02  0.7819415002230843D-15 )
R6=( -0.7133930243991075D+01  0.6068414002957997D-12 )
```

```
N=3 K=3 M=2
Q1=(  0.3245031071165055D-16  0.1020380446668096D+01 )
Q2=( -0.6494989735391820D-17  0.1001263295044486D-06 )
Q3=( -0.3708457815126825D-15  0.2368581614173008D-03 )
Q4=( -0.5849237066104017D-13 -0.3481847626998819D+01 )
Q5=(  0.1094816421191028D-14 -0.1887126541802776D-06 )
Q6=(  0.2938548715885774D-11 -0.4463713138848790D-03 )
Q7=(  0.3631563021553369D-13  0.3665667574609826D+01 )
Q8=( -0.6581554102431736D-15  0.1812772250460474D-06 )
Q9=( -0.1866668515549782D-11  0.4287704796688965D-03 )
R1=( -0.5998479587362754D-14 -0.3332425067828181D+01 )
R2=( -0.3818074852101207D-15 -0.1647974772513057D-06 )
R3=(  0.9268241130852384D-12 -0.3897913450954734D-03 )
R4=(  0.5449175538252418D-15  0.3829206018116956D+01 )
R5=(  0.3656306024357804D-15  0.2064264201705002D-06 )
R6=( -0.5144238698130742D-12  0.4882696959283045D-03 )

N=3 K=3 M=3
Q1=( -0.7209652058832401D-05  0.0                    )
Q2=(  0.1842879810863270D+00  0.0                    )
Q3=(  0.1797966673170376D+02  0.0                    )
Q4=(  0.1361799752242200D-04  0.1967468088413858D-12 )
Q5=( -0.6253330262705698D+00 -0.8825999633830738D-14 )
Q6=( -0.5977549941567372D+02 -0.5833364557530585D-11 )
Q7=( -0.1309009494198558D-04 -0.1421976233591080D-12 )
Q8=(  0.6580636959632403D+00  0.6694176618350606D-14 )
Q9=(  0.6280648449464918D+02  0.4027927694837117D-11 )
R1=(  0.1190008631203729D-04  0.1697832081055174D-12 )
R2=( -0.5982397236030192D+00 -0.7144912928212175D-14 )
R3=( -0.5709680408604452D+02 -0.5400575466090407D-11 )
```

R4=(-0.1489682485360829D-04 -0.1208661458018139D-12)

R5=(0.6876998626623333D+00 0.5367088152614521D-14)

R6=(0.6573090386110939D+02 0.3671070834977743D-11)

```
/INFO MVS TI(50) PA(150) R(MUSIC) CL(20) N(STEVE SIU PUI CHAN)
//STEP1 EXEC FORTRAN
//FORT.SYSIN DD *
C*************************************************************************
C     COMPUTER PROGRAM FOR CALCULATING THE INTEGRALS IN THE GRNERALIZED*
C     AERODYNAMIC FORCES AS A FUNCTION OF THE REDUCED FREQUENCIES      *
C     VERSION FOR COMPRESSIBLE FLUID                                   *
C     ONLY THE INNER SHELL FLEXIBLE                                    *
C*************************************************************************
C
C*************************************************************************
C     MAIN PROGRAM                                                     *
C*************************************************************************
      IMPLICIT COMPLEX*16(A-Z)
      REAL*8 C(3),P(3),PI,GAMA,EI,EO,MI,MO,X1,X2,D
      INTEGER I,N,L,K,M
      COMMON PI,GAMA
      COMMON/DATA1/C,P
      INP(Y)=N*IN(Y,N)/Y+IN(Y,N+1)
      KNP(Y)=N*KN(Y,N)/Y-KN(Y,N+1)
      PI=3.14159265358979D0
      GAMA=0.5772156649011618D0
      C(1)=0.982502214576237 9D0
      C(2)=1.00077731190727D0
      C(3)=0.9999664501254086D0
      P(1)=4.7300407448627D0
      P(2)=7.8532046240958 4D0
      P(3)=10.99560783800167D0
      EI=0.03861D0
      EO=0.05792D0
      MI=0.025D0
      MO=0.500D0
      N=2
      D=2.D0
      KI=(120.D0,0.D0)
      KO=(4.D0,0.D0)
      DO 3 L=1,1
      PRINT30,KI,KO
   30 FORMAT('1','VALUES OF THE INTEGRALS IN THE AERODYNAMIC FORCE TERMS
     # WITH KI=','(',2D12.4,1X,')'/' ',60X,'KO=','(',2D12.4,1X,')')
      DO 2 K=1,3
      DO 2 M=1,3
      X1=-50.D0+D/2*(1-DSQRT(1/3.D0))
      X2=-50.D0+D/2*(1+DSQRT(1/3.D0))
      I1=(0.D0,0.D0)
      I2=I1
      DO 1 I=1,98
      MIL=CDSQRT(X1**2-MI**2*(X1-KI)**2)
      MOL=CDSQRT(X1**2-MO**2*(X1-KO)**2)
      MIA=EI*MIL
      MOA=EI*MOL
      MOB=EO*MOL
      INOA=IN(MOA,N)
      KNOA=KN(MOA,N)
      INPOA=INP(MOA)
      INPOB=INP(MOB)
      KNPOA=KNP(MOA)
      KNPOB=KNP(MOB)
```

```
      DEM=INPOB*KNPOA-INPOA*KNPOB
      EN=IN(MIA,N)/INP(MIA)
      FN=(INPOB*KNOA-KNPOB*INOA)/DEM
      HKM=H(X1,K,M)
      IG1=(KI-X1)**2*EN*HKM/MIL
      IG2=(KO-X1)**2*FN*HKM/MOL
      I1=I1+IG1
      I2=I2+IG2
      X1=X1+D
      IF(I.EQ.49) X1=X2
    1 CONTINUE
      PRINT10,N,K,M
   10 FORMAT('-','N=',I1,' K=',I1,' M=',I1)
      PRINT11,I1
   11 FORMAT('0','I1=(',2D24.16,1X,')')
      PRINT12,I2
   12 FORMAT('0','I2=(',2D24.16,1X,')')
    2 CONTINUE
      KI=KI+30.D0
      KO=KO+1.D0
    3 CONTINUE
      PRINT40
   40 FORMAT('1')
      STOP
      END
C
C*********************************************************************
C     COMPLEX FUNCTION H                                             *
C*********************************************************************
      COMPLEX FUNCTION H*16(AB,K,M)
      IMPLICIT COMPLEX*16(A-Z)
      REAL*8 AB,C(3),P(3),AB1
      INTEGER K,M,J,M1
      COMMON/DATA1/C,P
      H=(1.D0,0.D0)
      I=(0.D0,1.D0)
      AB1=AB
      M1=M
      DO 1 J=1,2
      IF(DABS(AB).EQ.M1) GO TO 10
      A=2*C(M1)*P(M1)**3
      B=I*2*P(M1)**2
      E1=(-1)**(M1+1)*CDEXP(I*AB1)+1
      E2=E1-2
      IM=(A*E1-B*AB1*E2)/(AB1**4-P(M1)**4)
      GO TO 11
   10 IF(J.EQ.2) GO TO 20
      IM=((I*C(M1)*P(M1)**3-I*P(M1)**2+AB*P(M1)**2)*(-1)**(M1+1)*
     #CDEXP(I*AB)+I*P(M1)**2)/(-2*AB**3)
      GO TO 11
   20 IM=((-I*C(M1)*P(M1)**3+I*P(M1)**2+AB*P(M1)**2)*(-1)**(M1+1)*
     #CDEXP(-I*AB)-I*2*P(M1)**2)/(-2*AB**3)
   11 H=H*IM
      M1=K
      AB1=-AB
    1 CONTINUE
      RETURN
      END
```

```
C
C*************************************************************************
C     SUBPROGRAMS FOR CALCULATING THE BESSEL FUNCTIONS                   *
C*************************************************************************
      COMPLEX FUNCTION IN*16(X,N)
      IMPLICIT REAL*8(A-Z)
      COMPLEX*16 W,X,Y,Z,T,T1,T2,T3,T4,I,DCMPLX,DCONJG
      INTEGER K,N
      COMMON PI,GAMA
      I=(0.D0,1.D0)
      IF(CDABS(X).GE.20.D0) GO TO 10
      IN=(0.D0,0.D0)
      K=0
   11 T=(X/2)**(2*K)/FA(K)/FA(N+K)
      IF(CDABS(T).LT.1.D-12) GO TO 12
      IN=IN+T
      K=K+1
      GO TO 11
   12 IN=(X/2)**N*IN
      RETURN
   10 T1=(4*N**2-1)/8/X
      T2=T1*(4*N**2-9)/16/X
      T3=CDEXP(X)/CDSQRT(2*PI*X)
      T4=CDEXP(-X)/CDSQRT(2*PI*X)
      Y=X-DCONJG(X)
      Z=DCMPLX(0.D0,CDABS(Y))
      W=Y+Z
      IF(CDABS(Y).EQ.0.D0) GO TO 14
      IF(CDABS(W).EQ.0.D0) GO TO 13
   14 IN=T3*(1-T1+T2)+(-1)**N*I*T4*(1+T1+T2)
      RETURN
   13 IN=T3*(1-T1+T2)+(-1)**(N+1)*I*T4*(1+T1+T2)
      RETURN
      END
C
      COMPLEX FUNCTION KN*16(X,N)
      IMPLICIT REAL*8(A-Z)
      COMPLEX*16 X,KN1,T,T1,T2,T3
      INTEGER N,M,K,I
      COMMON PI,GAMA
      IF(CDABS(X).GE.15.D0) GO TO 40
      IF(N.EQ.0) GO TO 46
      KN=FA(N-1)*(2/X)**N
      IF(N.EQ.1) GO TO 45
      M=N-1
      DO 41 I=1,M
   41 KN=KN+(-1)**I*FA(N-I-1)/FA(I)*(2/X)**(N-2*I)
   45 KN=KN/2
      GO TO 47
   46 KN=(0.D0,0.D0)
   47 KN1=(0.D0,0.D0)
      K=0
   43 T=(X/2)**(N+2*K)/FA(K)/FA(N+K)*(CDLOG(X/2)-(F(K+1)+F(N+K+1))/2)
      IF(CDABS(T).LT.1.D-12) GO TO 42
      KN1=KN1+T
      K=K+1
      GO TO 43
   42 KN=KN+KN1*(-1)**(N+1)
```

```
      RETURN
   40 T1=(4*N**2-1)/8/X
      T2=T1*(4*N**2-9)/16/X
      T3=CDEXP(-X)*CDSQRT(PI/2/X)
      KN=T3*(1+T1+T2)
      RETURN
      END
C
      DOUBLE PRECISION FUNCTION R(K)
      IMPLICIT REAL*8(A-Z)
      INTEGER K,I
      R=0.DO
      DO 40 I=1,K
   40 R=R+1.DO/I
      RETURN
      END
C
      DOUBLE PRECISION FUNCTION F(K)
      IMPLICIT REAL*8(A-Z)
      INTEGER K
      COMMON PI,GAMA
      IF(K.EQ.1) GO TO 50
      F=R(K-1)-GAMA
      RETURN
   50 F=-GAMA
      RETURN
      END
C
      DOUBLE PRECISION FUNCTION FA(K)
      IMPLICIT REAL*8(A-Z)
      INTEGER K,L
      FA=1.DO
      L=1
   21 FA=FA*L
      IF(L.GE.K) GO TO 22
      L=L+1
      GO TO 21
   22 CONTINUE
      RETURN
      END
//GO.SYSIN DD *
//
/*
```

```
VALUES OF THE INTEGRALS IN THE AERODYNAMIC FORCE TERMS WITH
KI=( 0.120D+03   0.0     )
KO=( 0.400D+01   0.0     )

N=2 K=1 M=1

I1=(  0.1747463702802756D+04   0.0                          )

I2=( -0.5106817927871355D+01   0.2499615828904897D-15 )

N=2 K=1 M=2

I1=( -0.4214632248946571D-13   0.9706904778349672D+02 )

I2=( -0.1270884192684148D-15 -0.4816399999889064D+01 )

N=2 K=1 M=3

I1=(  0.9197218252565925D+00   0.9330412921776054D-15 )

I2=(  0.1757419826634989D+01   0.1438228070904065D-15 )

N=2 K=2 M=1

I1=( -0.4214632248946571D-13 -0.9706904778349672D+02 )

I2=(  0.8333601494085540D-16   0.4816399999889064D+01 )

N=2 K=2 M=2

I1=(  0.1744289969225194D+04   0.0                          )

I2=( -0.1104771980665259D+02   0.4223035437760120D-16 )

N=2 K=2 M=3

I1=( -0.6568687782005721D-13   0.1592341119332808D+03 )

I2=(  0.7408134104155985D-15 -0.7859838757346369D+01 )

N=2 K=3 M=1

I1=(  0.9197218252565925D+00 -0.9330412921776054D-15 )

I2=(  0.1757419826634989D+01   0.3139512588133328D-16 )

N=2 K=3 M=2
```

```
I1=( -0.656868778200572ID-13 -0.159234111933280 8D+03 )

I2=(  0.668173950317501 1D-15  0.785983875734636 9D+01 )

N=2 K=3 M=3

I1=(  0.173940116830568 4D+04  0.0                    )

I2=( -0.200452697683559 6D+02  0.310332121771903 8D-16 )
```

APPENDIX I

DERIVATION OF THE BASIC STRESSES AND THE BASIC SHELL DISPLACEMENTS DUE TO STEADY-STATE LOADING

In this Appendix will be derived the stresses and the displacements of a circular cylindrical shell subjected to the following static loads:

(i) a constant axial force per unit surface area,

$$p_{xI} = B, \tag{I.1}$$

(ii) a radially normal pressure of the form

$$p_{rI} = -(Cx + D), \tag{I.2}$$

where x is the lengthwise variable; B, C and D are constants.

The results will be used as the basic stress system and the basic shell displacements (denoted by subscript I) in the derivation of the equations of motion for the same cylindrical shell 'pre-stressed' by the above loadings. The configuration of the shell is shown in Figure I.1.

The ends of the shell are assumed to be clamped. p_o and p_L are the axial reactions per unit circumference at the two supported ends.

Assuming the bending and twisting moments to be negligibly small, the conditions of equilibrium of an infinitesimal shell element lead to the following equations†,

---

†For detailed derivation of equations (I.3-I.5), see reference [32].

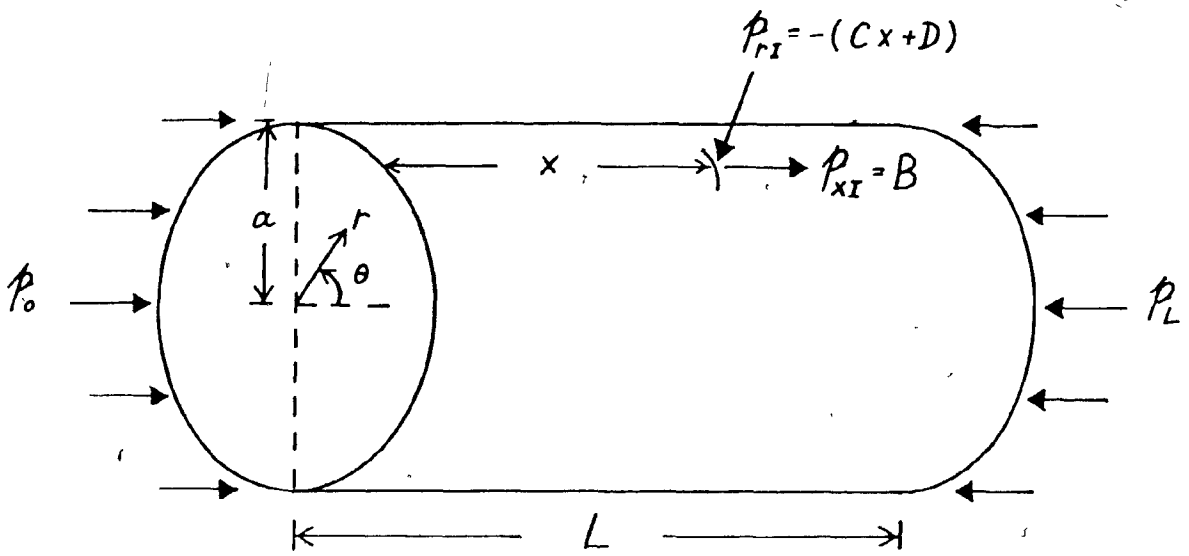

Fig. I.1

$$N_{\theta I} = p_{rI}\, a \quad , \tag{I.3}$$

$$\frac{\partial N_{x\theta I}}{\partial x} = -\frac{1}{a}\,\frac{\partial N_{\theta I}}{\partial \theta} \quad , \tag{I.4}$$

$$\frac{\partial N_{xI}}{\partial x} = -p_{xI} - \frac{1}{a}\,\frac{\partial N_{x\theta I}}{\partial \theta} \quad , \tag{I.5}$$

where $N_{\theta I}$ is the hoop stress resultant, N_{xI} is the axial stress resultant, and $N_{x\theta I}$ is the shear stress resultant. The orientations of the various stress resultants are shown in Figure J.1. Since p_{rI} is a function of x only (equation (I.2)), $N_{\theta I}$ as given in equation (I.3) will be independent of θ; therefore, $\partial N_{\theta I}/\partial\theta = 0$ and equation (I.4) becomes

$$\frac{\partial N_{x\theta I}}{\partial x} = 0 \quad . \tag{I.6}$$

Integrating equations (I.6) and (I.5), one obtains

$$N_{x\theta I} = f_1(\theta) \quad , \tag{I.7}$$

$$N_{xI} = -\int_0^x \left(p_{xI} + \frac{1}{a} \frac{\partial N_{x\theta I}}{\partial \theta} \right) dx + f_2(\theta) \quad , \tag{I.8}$$

where $f_1(\theta)$ and $f_2(\theta)$ are functions of θ.

Since the loading is axisymmetric, $N_{x\theta I}$ and N_{xI} are independent of θ; thus, $\partial N_{x\theta I}/\partial\theta = 0$ and $f_1(\theta) = C_1$, a constant; similarly, $f_2(\theta) = C_2$, another constant. Equations (I.7) and (I.8) can then be written as

$$N_{x\theta I} = C_1 \quad , \tag{I.9}$$

$$N_{xI} = -\int_0^x p_{xI} \, dx + C_2 \quad . \tag{I.10}$$

Applying the boundary conditions, at x = 0, $N_{x\theta I} = 0$ and $N_{xI} = -p_o$ †, to equations (I.9) and (I.10), yields

$$C_1 = 0 \quad , \tag{I.11}$$

$$C_2 = -p_o \quad . \tag{I.12}$$

---

†If p_o is positive in the direction shown in Figure I.1, the axial stress, $N_{xI}(x=0)$ is a compressive stress; this explains the use of the negative sign.

Substituting equations (I.1), (I.2), (I.11) and (I.12) into equations (I.3), (I.9) and (I.10), the basic stress system of the shell is found to be

$$N_{\theta I} = -a(\bar{C}x + D) \quad , \tag{I.13}$$

$$N_{x\theta I} = 0 \quad , \tag{I.14}$$

$$N_{xI} = -\int_0^x B\, dx - P_0$$

$$= -Bx - P_0 \quad . \tag{I.15}$$

Let us now determine the displacements of the shell. From the constitutive equations and the kinematic relations of the strains and displacements, one obtains the following equations†,

$$\varepsilon_{xI} = \frac{\partial u_I}{\partial x} = \frac{1}{Eh}(N_{xI} - \nu N_{\theta I}) \quad , \tag{I.16}$$

$$\gamma_{x\theta I} = \frac{\partial v_I}{\partial x} + \frac{1}{a}\frac{\partial u_I}{\partial \theta} = \frac{2(1+\nu)}{Eh} N_{x\theta I} \quad , \tag{I.17}$$

$$\varepsilon_{\theta I} = \frac{w_I}{a} + \frac{1}{a}\frac{\partial v_I}{\partial \theta} = \frac{1}{Eh}(N_{\theta I} - \nu N_{xI}) \quad , \tag{I.18}$$

where h is the thickness of the shell; E and ν are the familiar elastic modulus and Poisson's ratio; $\varepsilon_{\theta I}$, $\gamma_{x\theta I}$ and ε_{xI} are the hoop, shear and longitudinal strains, respectively; u_I, v_I and w_I are the basic shell

†Equations III-19 of Flügge [32], p. 130.

displacements in the axial, circumferential and radial directions, respectively. Due to symmetry, u_I , v_I , w_I are independent of θ , and since $N_{x\theta I} = 0$, equations (I.16-.18) can be simplified to

$$\frac{du_I}{dx} = \frac{1}{Eh}(N_{xI} - \nu N_{\theta I}) , \tag{I.19}$$

$$\frac{dv_I}{dx} = 0 , \tag{I.20}$$

$$\frac{w_I}{a} = \frac{1}{Eh}(N_{\theta I} - \nu N_{xI}) . \tag{I.21}$$

Substituting equations (I.13), (I.15) into (I.19-.21) and integrating, yields

$$u_I = \frac{1}{Eh}\left[\frac{(\nu aC - B)}{2}x^2 + (\nu aD - p_o)x\right] + u_I|_{x=0} , \tag{I.22}$$

$$v_I = A , \tag{I.23}$$

$$w_I = \frac{a}{Eh}[(\nu B - aC)x + \nu p_o - aD] , \tag{I.24}$$

where A is a constant.

From the boundary conditions of the displacements which are

$$u_I = v_I = w_I = 0 \quad \text{and} \quad \frac{\partial w_I}{\partial x} = 0$$

at x = 0,L for clamped-ends, A can easily be shown to be zero. To determine the other unknowns, $u_I|_{x=0}$ and p_o , only two boundary conditions

are needed; so it seems that there are too many boundary conditions and that they cannot all be satisfied; thus, we have to make a choice. Since the axial stresses at the two ends ($N_{xI}|_{x=0} = -p_o$, $N_{xI}|_{x=L} = -p_L$) are non-zero, it is probably more reasonable to assume that the u_I displacement is restrained there, and to say that the boundary conditions for w_I can be fulfilled by the small bending moments that we have neglected. Thus, putting $u_I = 0$ for $x=0$ and $x=L$ in equation (I.22), one obtains,

$$u_I|_{x=0} = 0 \ , \tag{I.25}$$

$$p_o = \frac{(\nu aC - B)}{2} L + \nu aD \ . \tag{I.26}$$

Substituting equations (I.25), (I.26) into (I.22), (I.24), the solution of the basic shell displacements is,

$$u_I = \frac{1}{Eh}\left[\frac{(\nu aC - B)}{2} x^2 - \frac{(\nu aC - B)}{2} L x\right] \ , \tag{I.27}$$

$$v_I = 0 \ , \tag{I.28}$$

$$w_I = \frac{a}{Eh}\left[(\nu B - aC)x + \nu\frac{(\nu aC - B)}{2} L + \nu^2 aD - aD\right] . \tag{I.29}$$

Substituting equation (I.26) into equation (I.15), the basic stress system can then be written as

$$N_{\theta I} = -a(Cx + D) \ , \tag{I.13}$$

$$N_{x\theta I} = 0 \ , \tag{I.14}$$

$$N_{xI} = -Bx - \frac{(\nu aC - B)L}{2} - \nu aD \ . \tag{I.30}$$

APPENDIX J

DERIVATION OF THE EQUATIONS OF MOTION OF A PRE-STRESSED CIRCULAR CYLINDRICAL SHELL

In this Appendix will be derived the equations of motion of a circular cylindrical shell pre-stressed by the following static loads:

(i) a constant axial force per unit surface area,

$$p_{xI} = B \ ,$$

(ii) a radially normal pressure of the form

$$p_{rI} = -(Cx + D) \ ,$$

where x is the lengthwise variable; B, C and D are constants.

These are the basic loads (as indicated by the subscript I) which produce the basic stress system $(N_{xI}, N_{\theta I})$, as derived in Appendix I. The configuration of the shell is shown in Figure I.1 (Appendix I). The ends of the shell are assumed to be clamped.

When the shell is acted upon by the additional loads, p_x , p_θ, p_r, additional displacements u , v , w and additional stress resultants, moments and shear forces are induced, denoted by N_x , N_θ , $N_{x\theta}$, $N_{\theta x}$, M_x, M_θ , $M_{x\theta}$, $M_{\theta x}$, Q_x, Q_θ[†]. Figure J.1 shows an infinitesimal shell element

---

† N_x , N_θ are the normal stress resultants,
$N_{x\theta}$, $N_{\theta x}$ are the shear stress resultants,
M_x , M_θ are the bending moments (per unit length)
$M_{x\theta}$, $M_{\theta x}$ are the twisting moments (per unit length)
Q_x , Q_θ are the transverse shear forces (per unit length).

under the action of the various external loads and the internal stress resultants and moments. The element is shown undeformed for the purpose

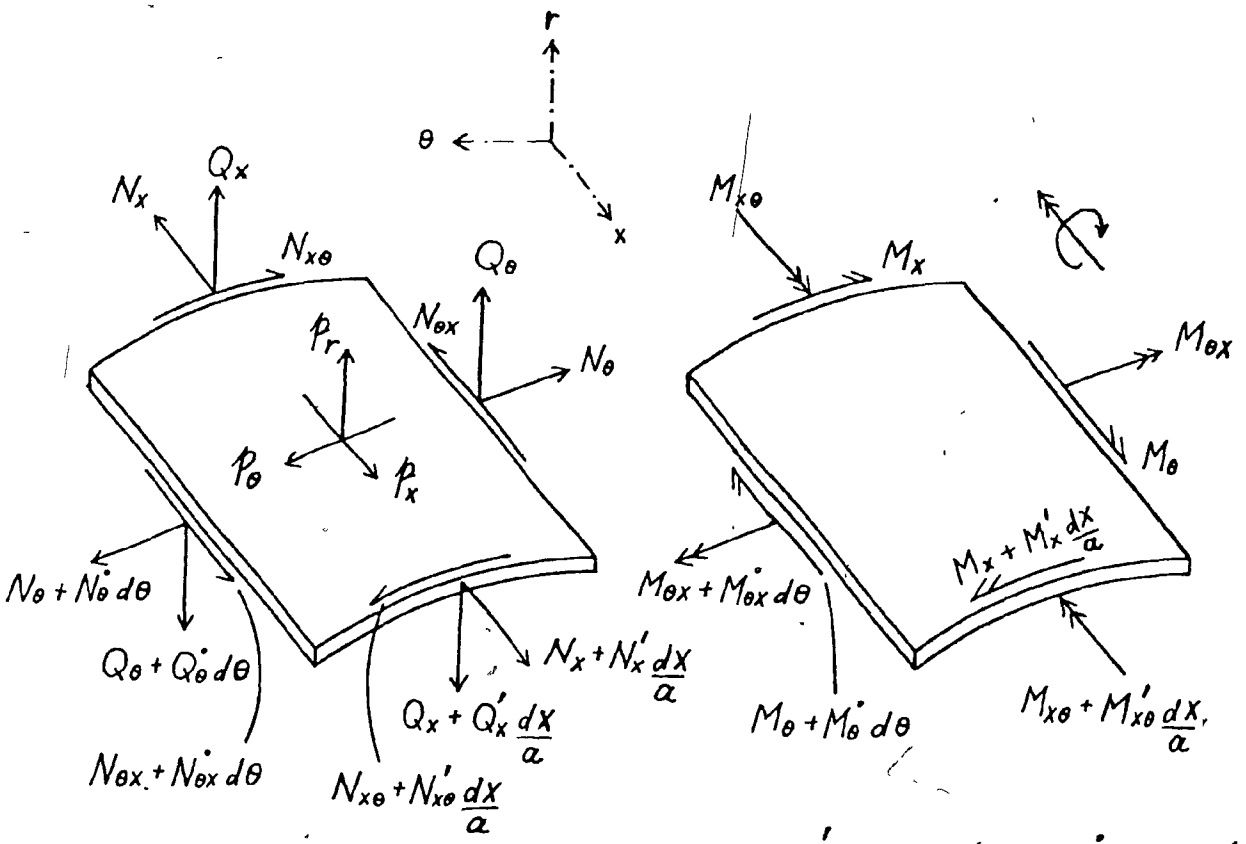

Fig. J.1 $( )' = a\,\partial( )/\partial x$, $( )^{\cdot} = \partial( )/\partial\theta$

of illustration, and only the additional loads, stresses and moments are depicted, for the sake of clarity of the figure; the total forces and moments are, indeed, made up of both the basic and the additional components. Thus, the total axial and radial loads are

$$\bar{p}_x = p_{xI} + p_x \quad , \tag{J.1}$$

$$\bar{p}_r = p_{rI} + p_r \quad , \tag{J.2}$$

and the total axial and hoop stress resultants are

$$\bar{N}_x = N_{xI} + N_x \ , \tag{J.3}$$

$$\bar{N}_\theta = N_{\theta I} + N_\theta \ , \tag{J.4}$$

where N_{xI} and $N_{\theta I}$ are given in equations (I.30) and (I.13), respectively. Other forces and moments consist solely of the additional components, since their basic counterparts are non-existent in this system.

The quantities $\bar{N}_x, \bar{N}_\theta, \ldots, M_\theta, \ldots, Q_x$ are forces (and moments) per unit length of certain line elements. Since we are interested in products of the basic forces p_{xI}, N_{xI}, ..., with such quantities as ε_x or ε_θ (the longitudinal or hoop strain), we must decide to which length the stress resultants should be referred, *i.e.* whether to the original length of the line element or to its length after deformation. The issue is not as simple as it might appear; a detailed discussion on the subject can be found in reference [32]. The following convention (used by Flügge in [32]) regarding the multiplication of the stress resultants with the deformed lengths of the shell element is adopted. Accordingly, the stress resultant must be multiplied by the magnitude of the *deformed reference vector* to give the force per unti length of the *undeformed* line element. The undeformed and deformed reference vectors associated with the shell element are shown in Figures J.2(a) and (b). As an example, let us find the total normal force acting on the side a-b of the deformed shell element (Figure J.2(b)). The normal stress resultant on side a-b is $\bar{N}_x$ and the magnitude of the reference vector in the same direction as $\bar{N}_x$ is

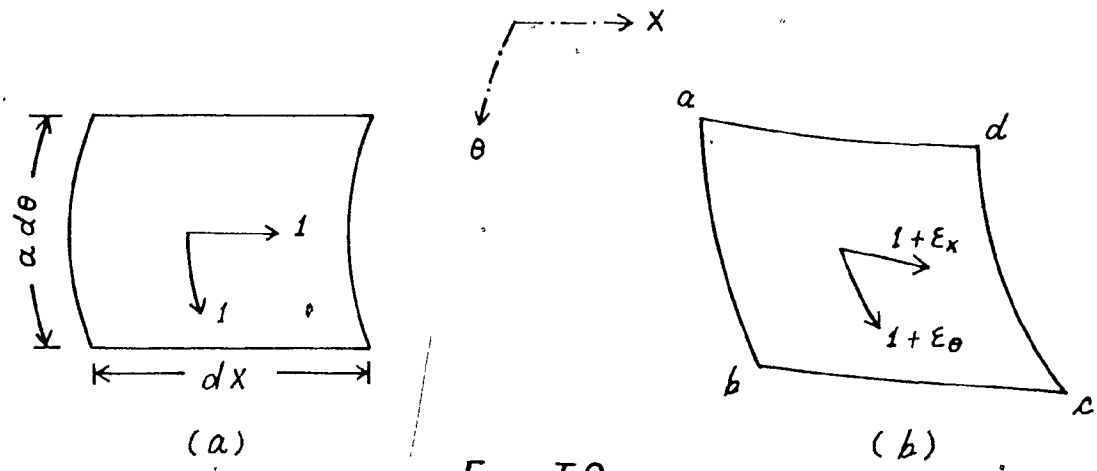

Fig. J.2

$(1 + \varepsilon_x)$. Thus, according to the above convention, the normal force per unit length of the undeformed line element $a\,d\theta$ is given by $\bar{N}_x(1+\varepsilon_x)$ and hence, the total normal force on side a-b is $N_x(1+\varepsilon_x)a\,d\theta$. The forces acting in other directions or along other sides of the shell element can be determined in a similar manner.

Let us now write the six conditions for the equilibrium of the shell element shown in Figure J.1.

J.1 EQUILIBRIUM OF FORCES IN THE x DIRECTION

J.1.1 Contribution from $\bar{N}_x$

As shown above, the force in the x-direction on one side of the element is $\bar{N}_x(1+\varepsilon_x)a\,d\theta$. On the opposite side, the force is larger by the differential

$$\frac{\partial}{\partial x}\left[\bar{N}_x(1+\varepsilon_x)\,a\,d\theta\right]dx = \left[\bar{N}_x'(1+\varepsilon_x)+\bar{N}_x\varepsilon_x'\right]dx\,d\theta$$

which makes a contribution to the condition of equilibrium. Putting $\bar{N}_x = N_{xI} + N_x$, $\varepsilon_x = u'/a$ [†] and noting that $N_{xI}' = -a p_{xI}$ in this case (from equations (I.30) and (I.1)), this contribution becomes, neglecting second order terms,

$$\left[-a p_{xI}\left(1+\frac{u'}{a}\right) + N_x' + N_{xI}\frac{u''}{a}\right]dx\,d\theta \ .$$

J.1.2 Contribution from $N_{\theta x}$

Since $N_{\theta x}$ is a 'small' additional stress resultant, the shearing force on the side dx of the element is $N_{\theta x}\,dx$; use of the deformed line element will only introduce second-order terms. The shearing force on the other side is larger by a differential, yielding the contribution

$$\frac{\partial}{\partial\theta}\left(N_{\theta x}\,dx\right)d\theta = N_{\theta x}'\,dx\,d\theta \ .$$

J.1.3 Contribution from $\bar{N}_\theta$

The normal force on the side dx of the element is $\bar{N}_\theta(1+\varepsilon_\theta)\,dx$. It makes an angle of u'/a with the θ direction (see Figure J.3) and therefore has a component $\bar{N}_\theta(1+\varepsilon_\theta)\,dx\,u'/a$ in the x direction. On the opposite side, the component is larger by a differential. Thus, the contribution to the condition of equilibrium is

---

[†] For the definition of the strains, see reference [32].

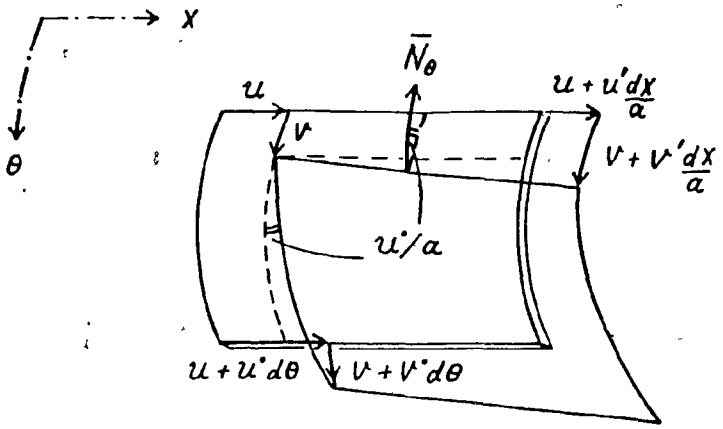

Fig. J. 3

$$\frac{\partial}{\partial\theta}\left[\bar{N}_\theta(1+\varepsilon_\theta)dx\frac{u^{\cdot}}{a}\right]d\theta \ .$$

Neglecting ε_θ compared to 1 and using equations (J.4) and (I.3), the first-order approximation of the contribution is

$$p_{rI}\ddot{u}\,dx\,d\theta \ .$$

J.1.4 Contribution from the External Load $\bar{p}_x$

The total surface area of the deformed shell element is $(1+\varepsilon_x)dx(1+\varepsilon_\theta)a\,d\theta$; therefore, the contribution from the external load is

$$\bar{p}_x(1+\varepsilon_x)dx(1+\varepsilon_\theta)a\,d\theta \ .$$

Putting $\varepsilon_x = u'/a$, $\varepsilon_\theta = (v^{\cdot}+w)/a$ and using equation (J.1), the contribution

can be written as

$$\left[p_{xI} \left(1 + \frac{u' + v^{\cdot} + w}{a} \right) + p_x \right] a \, dx \, d\theta \, .$$

J.1.5 Contribution from the External Load $\bar{p}_r$

Due to the w displacement, the shell element is slightly tilted (see Figure J.4), and the external force has a component

$$-\bar{p}_r (1 + \varepsilon_x) dx (1 + \varepsilon_\theta) a \, d\theta \frac{w'}{a}$$

in the x direction. Retaining only the first-order terms, the contribution

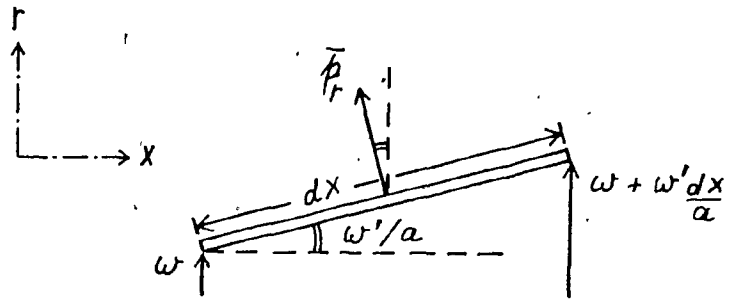

Fig. J.4

becomes

$$-p_{rI} w' dx \, d\theta \, .$$

J.1.6 Contribution from all Components Together

Collecting all the terms and rearranging, the first condition of

equilibrium may be written as

$$N_x' + N_{\theta x}^{\cdot} + N_{xI}\frac{\ddot{u}}{a} + p_{xI}(\dot{v}+\omega) + p_{rI}(\ddot{u}-\omega') + p_x a = 0 \ . \qquad (J.5)$$

J.2 EQUILIBRIUM OF FORCES IN THE θ DIRECTION.

J.2.1 Contribution from $N_{x\theta}$

$N_{x\theta}$ is a small additional stress and its contribution can easily be found to be

$$N_{x\theta}' \, dx \, d\theta \ .$$

J.2.2 Contribution from Q_θ

The shearing forces Q_θ on the sides dx of the element make an angle of $d\theta$ with each other (see Figure J.5) and therefore have a

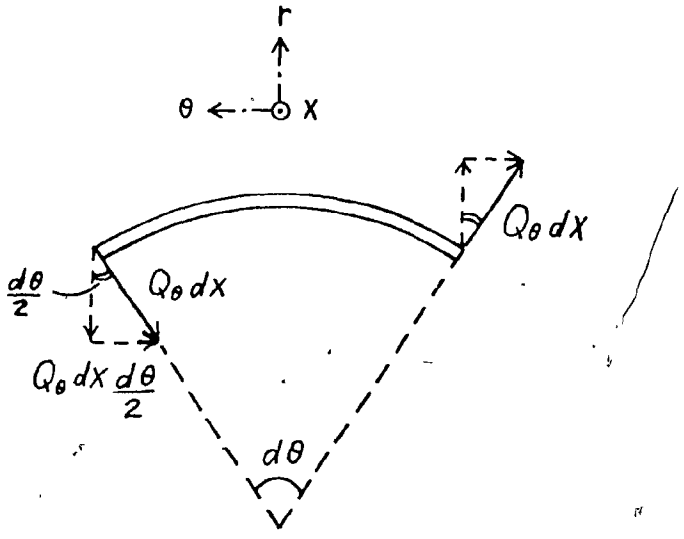

Fig. J.5

resultant of

$$-Q_\theta \, dx \, d\theta$$

in the θ direction.

J.2.3 Contribution from $\bar{N}_x$

The force $\bar{N}_x(1+\varepsilon_x)a\,d\theta$ makes an angle of v'/a with the x direction (see Figure J.6) and therefore has a component $\bar{N}_x(1+\varepsilon_x)a\,d\theta \cdot v'/a$ in the θ

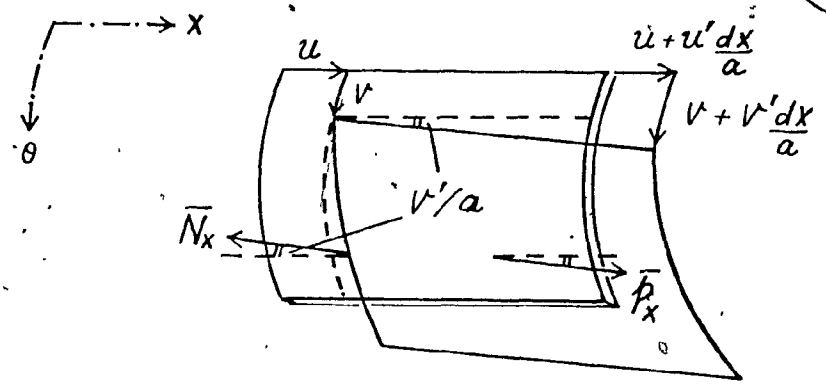

Fig. J.6

direction. The differential increment of this component

$$\frac{\partial}{\partial x}\left[\bar{N}_x(1+\varepsilon_x)a\,d\theta\,\frac{v'}{a}\right]dx$$

on the opposite side of the element contributes to the condition of equilibrium. Dropping the second-order terms, the contribution is

$$\left[-\bar{p}_{x1}v' + N_{x1}\frac{v''}{a}\right]dx\,d\theta\ .$$

J.2.4 Contribution from $\bar{N}_\theta$

The contribution from the force $\bar{N}_\theta(1+\varepsilon_\theta)dx$ is quite straightforward; it is

$$\frac{\partial}{\partial\theta}\left[\bar{N}_\theta(1+\varepsilon_\theta)\,dx\right]d\theta = \left[N_\theta^{\cdot} + p_{rI}(v''+w')\right]dx\,d\theta$$

after making use of equation (I.3).

J.2.5 Contribution from the External Load $\bar{p}_x$

The external load $\bar{p}_x$ makes an angle of v'/a with the x direction (see Figure J.6). Thus, its contribution in the θ direction is

$$\bar{p}_x(1+\varepsilon_x)dx\,(1+\varepsilon_\theta)a\,d\theta\,\frac{v'}{a} = p_{xI}\,v'dx\,d\theta$$

to the first order.

J.2.6 Contribution from the External Load p_θ

p_θ is an additional load, and its contribution is simply

$$p_\theta\,a\,dx\,d\theta\,.$$

The difference in the surface area of the undeformed and deformed shell element, when multiplied to p_θ, will only give rise to second-order terms.

J.2.7 Contribution from all Components Together

We are now ready to collect the terms and to write the equation for the second condition of equilibrium, as follows:

$$N_\theta^{\cdot} + N_{x\theta}' - Q_\theta + N_{xI}\frac{v''}{a} + p_{rI}(v'' + w^{\cdot}) + p_\theta a = 0 \quad . \tag{J.6}$$

J.3 EQUILIBRIUM OF FORCES IN THE r DIRECTION

J.3.1 Contribution from Q_θ and Q_x

The transverse shear forces Q_θ and Q_x are small additional forces. Their contributions are the differential increments

$$-Q_\theta^{\cdot}\, dx\, d\theta - Q_x'\, dx\, d\theta \quad .$$

J.3.2 Contribution from $\bar{N}_x$

Because of the w displacement, the force $\bar{N}_x(1+\varepsilon_x)a\,d\theta$ at one side of the element makes an angle of w'/a with the x direction (see Figure J.7) and therefore has a component $-\bar{N}_x(1+\varepsilon_x)a\,d\theta\, w'/a$ in the r direction. At the

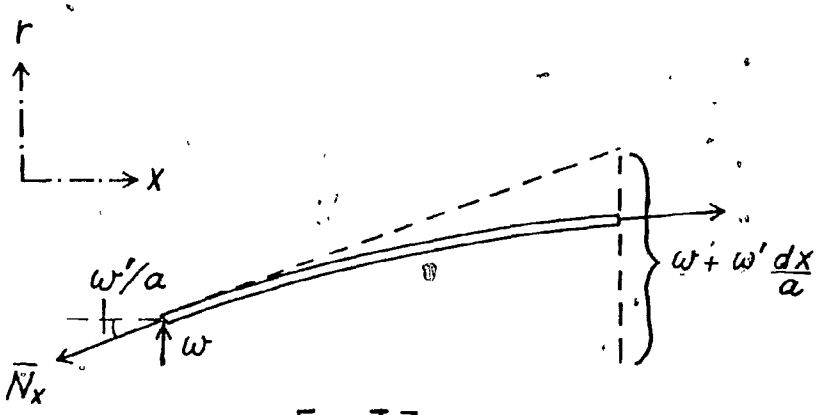

Fig. J.7

opposite side this component is larger by a differential and the contribution to our equation is

$$\frac{\partial}{\partial x}\left[\bar{N}_x(1+\varepsilon_x)\,a\,d\theta\,\frac{w'}{a}\right]dx = \left(N_{xI}\frac{w''}{a} - p_{xI}w'\right)dx\,d\theta\,.$$

J.3.3 Contribution from $\bar{N}_\theta$

Due to the displacements v and w, the force $\bar{N}_\theta(1+\varepsilon_\theta)dx$ at one side of the element makes an angle of $(d\theta/2 + v/a + w'/a)$ with the θ direction (see Figure J.8(a), (b), (c)) and therefore has a component of

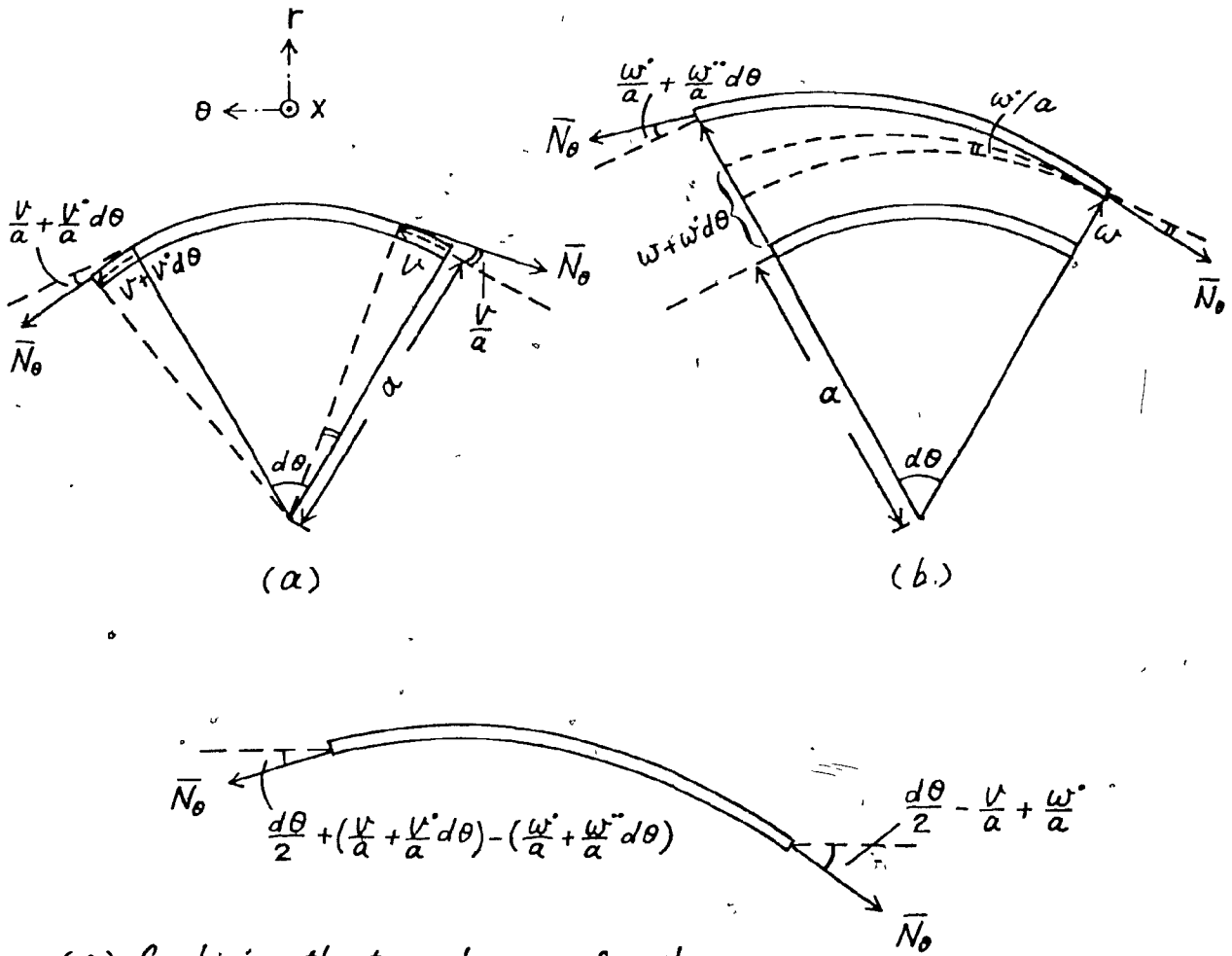

Fig. J.8

$-\bar{N}_\theta(1+\varepsilon_\theta)dx(d\theta/2+v/a+\omega'/a)$ in the r direction. At the opposite side of the element, the angle between the force $\bar{N}_\theta(1+\varepsilon_\theta)dx$† and the x direction becomes $[d\theta/2+(v/a+v'd\theta/a)-(\omega/a+\omega'd\theta/a)]$ (see Figure J.8(a), (b), (c)). Note that the sense of the angle deviations caused by displacements v and ω has been reversed. Thus, the component in the r direction is $-\bar{N}_\theta(1+\varepsilon_\theta)dx\cdot[d\theta/2+(v/a+v'd\theta/a)+(\omega'/a+\omega''d\theta/a)]$; and the total contribution to the condition of equilibrium is,

$$-\bar{N}_\theta(1+\varepsilon_\theta)dx\left(\frac{d\theta}{2}-\frac{v}{a}+\frac{\omega'}{a}\right)-\bar{N}_\theta(1+\varepsilon_\theta)dx\left[\frac{d\theta}{2}+\left(\frac{v}{a}+\frac{v'}{a}d\theta\right)+\left(\frac{\omega'}{a}+\frac{\omega''}{a}d\theta\right)\right]$$

$$=-\bar{N}_\theta(1+\varepsilon_\theta)dx\left(1+\frac{v'-\omega''}{a}\right)d\theta$$

which simplifies to

$$-\left[N_\theta+N_{\theta I}\left(1+\frac{2v'+\omega-\omega''}{a}\right)\right]dx\,d\theta\ ,$$

when terms of second or higher order are neglected.

J.3.4 Contribution from the External Load $\bar{p}_x$

The inclination of the shell element caused by the displacement w sets the external load $\bar{p}_x(1+\varepsilon_x)dx(1+\varepsilon_\theta)a\,d\theta$ at an angle of ω'/a to the x direction (see Figure J.9). Thus, the contribution from the load $\bar{p}_x$ is the component

$$\bar{p}_x(1+\varepsilon_x)dx(1+\varepsilon_\theta)a\,d\theta\frac{\omega'}{a}=p_{xI}\,\omega'dx\,d\theta\ .$$

---

†The differential change of the force $\bar{N}_\theta(1+\varepsilon_\theta)dx$ has been neglected since it will only lead to second-order terms.

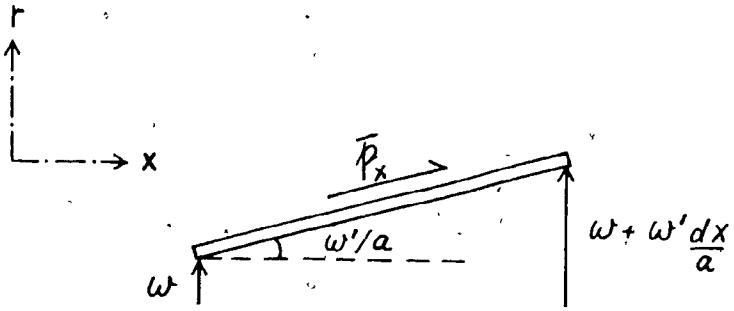

Fig. J.9

J.3.5 Contribution from the External Load $\bar{p}_r$

This last contribution to our equation is simply

$$\bar{p}_r (1+\varepsilon_x) dx (1+\varepsilon_\theta) a\, d\theta$$

$$= p_{rI} \left(1 + \frac{u' + v^{\cdot} + w}{a}\right) a\, dx\, d\theta + p_r a\, dx\, d\theta$$

J.3.6 Contribution from all Components Together

We may now write the third condition of equilibrium as

$$Q_\theta^{\cdot} + Q_x' + N_\theta - N_{xI} \frac{w''}{a} - p_{rI}(u' - v^{\cdot} + w^{\cdot\cdot}) - p_r a = 0 \quad . \qquad (J.7)$$

J.4 EQUILIBRIUM OF MOMENTS IN THE x DIRECTION

The conditions for the moment equilibrium are much easier to obtain since none of the basic stresses (N_{xI} and $N_{\theta I}$) produces moments with respect to the axes in the x , θ and r directions.

Let us equate the moments about an axis coinciding with the vector p_x shown in Figure J.1. The contributions include the increments of the

bending moment M_θ and the twisting moment $M_{x\theta}$, and the couple formed by the two forces $Q_\theta dx$. The condition of equilibrium is, therefore,

$$M_\theta^{\cdot} + M_{x\theta}' - a Q_\theta = 0 \tag{J.8}$$

J.5 EQUILIBRIUM OF MOMENTS IN THE θ DIRECTION

The condition for the moments having the vector p_θ as an axis is quite similar to the case in the x direction. Here the bending moment M_x, the twisting moment $M_{\theta x}$ and the transverse shear force Q_x are involved. The equation for the equilibrium of moments can easily be shown to be

$$M_x' + M_{\theta x}^{\cdot} - a Q_x = 0 \tag{J.9}$$

J.6 EQUILIBRIUM OF MOMENTS IN THE r DIRECTION

This last condition of equilibrium contains moments about a radius of the shell (or equivalently, vector p_r). The obvious contributions are the two couples formed by the forces $N_{x\theta} a d\theta$ and $N_{\theta x} dx$, respectively. Not to be omitted is the resultant of the two twisting moments $M_{\theta x} dx$ including the angle $d\theta$. One has, therefore, the equation

$$a N_{x\theta} - a N_{\theta x} + M_{\theta x}^{\cdot} = 0 \tag{J.10}$$

J.7 THE EQUATIONS OF MOTION

Eliminating the transverse forces Q_x and Q_θ from equations (J.5-.10), one obtains a set of four equations:

$$a N_{x\theta} - a N_{\theta x} + M_{\theta x} = 0 \quad , \tag{J.10}$$

$$a N_x' + a N_{\theta x}^{\cdot} + N_{xI} u'' + a p_{xI}(v^{\cdot} + w) + a p_{rI}(u^{\cdot\cdot} - w') + p_x a^2 = 0 \quad , \tag{J.11}$$

$$a N_\theta^{\cdot} + a N_{x\theta}' - M_\theta^{\cdot} - M_{x\theta}' + N_{xI} v'' + a p_{rI}(v^{\cdot\cdot} + w^{\cdot}) + p_\theta a^2 = 0 \quad , \tag{J.12}$$

$$M_\theta^{\cdot\cdot} + M_{x\theta}^{\prime\cdot} + M_{\theta x}^{\prime\cdot} + M_x'' + a N_\theta - N_{xI} w'' - a p_{rI}(u' - v^{\cdot} + w^{\cdot\cdot}) - p_r a^2 = 0 \quad . \tag{J.13}$$

The additional stress resultants and moments in equations (J.10-.13) may now be expressed in terms of the additional displacements u, v, w and their derivatives by making use of the constitutive and kinematic relations†. In doing so, one may find that equation (J.10) is just an identity and the other three become the differential equations for u, v and w. They may be written as follows:

$$u'' + \frac{1-\nu}{2} u^{\cdot\cdot} + \frac{1+\nu}{2} v^{\prime\cdot} + \nu w' + k\left(\frac{1-\nu}{2} u^{\cdot\cdot} - w''' + \frac{1-\nu}{2} w^{\prime\cdot\cdot}\right) + q_1 u'' + q_2(v^{\cdot} + w) + q_3(u^{\cdot\cdot} - w') + \frac{p_x a^2}{\Lambda} = 0 \quad , \tag{J.14}$$

$$\frac{1+\nu}{2} u^{\prime\cdot} + v^{\cdot\cdot} + \frac{1-\nu}{2} v'' + w^{\cdot} + k\left(\frac{3}{2}(1-\nu)v'' - \frac{3-\nu}{2} w^{\prime\prime\cdot}\right) + q_1 v'' + q_3(v^{\cdot\cdot} + w^{\cdot}) + \frac{p_\theta a^2}{\Lambda} = 0 \quad , \tag{J.15}$$

†See equations (V-9a,h) of reference [32], p. 214.

$$\nu u' + v^{\cdot} + w + k\left(\frac{1-\nu}{2}u^{\cdot\cdot} - u''' - \frac{3-\nu}{2}v''^{\cdot} + w^{IV} + 2w''^{\cdot\cdot} + w^{\cdot\cdot\cdot\cdot}\right.$$

$$\left. + 2w^{\cdot\cdot} + w\right) - q_1 w'' - q_3(u' - v^{\cdot} + w^{\cdot\cdot}) - \frac{p_r a^2}{\Lambda} = 0 \quad , \qquad (J.16)$$

where

$$k = \frac{h^2}{12\,a^2} \quad , \qquad \Lambda = \frac{Eh}{1-\nu^2} \quad ,$$

$$q_1 = \frac{N_{xI}}{\Lambda} \quad , \qquad q_2 = \frac{a\,p_{xI}}{\Lambda} \quad , \qquad q_3 = \frac{a\,p_{rI}}{\Lambda} \quad ,$$

and N_{xI} , p_{xI} and p_{rI} are given in equations (I.30), (I.1) and (I.2), respectively.

If the pre-stressed shell is subjected to additional radial load only and is free to vibrate, the forces p_x and p_θ become the inertial forces and p_r consists of both the inertial force and the radial load. Thus, one may write

$$p_x = -\rho_s h \frac{\partial^2 u}{\partial t^2} \quad , \qquad (J.17)$$

$$p_\theta = -\rho_s h \frac{\partial^2 v}{\partial t^2} \quad , \qquad (J.18)$$

$$p_r = -\rho_s h \frac{\partial^2 w}{\partial t^2} + q_e \quad , \qquad (J.19)$$

where $\rho_s h$ is the material density per unit surface area of the shell and q_e is the external radial force. The equations of motion of the cylindrical

shell can then be obtained by substituting the following terms into equations (J.14-.16),

$$\frac{p_x a^2}{\Lambda} = -\gamma \frac{\partial^2 u}{\partial t^2} \quad , \tag{J.20}$$

$$\frac{p_\theta a^2}{\Lambda} = -\gamma \frac{\partial^2 v}{\partial t^2} \quad , \tag{J.21}$$

$$\frac{p_r a^2}{\Lambda} = -\gamma \left(\frac{\partial^2 w}{\partial t^2} - \frac{q_e}{\rho_s h} \right) \quad , \tag{J.22}$$

where

$$\gamma = \rho_s a^2 (1 - \nu^2) / E \quad .$$

APPENDIX K

DERIVATION OF THE STATIC FLUID PRESSURES OF FULLY-DEVELOPED TURBULENT FLOWS IN THE INTERNAL AND ANNULAR FLUID REGIONS

In this Appendix will be derived the time-mean fluid pressure of a fully-developed turbulent incompressible flow inside a circular cylinder and in the annulus between two coaxial cylinders.

The schematics of the system is shown in Figure K.1. The time-mean Navier-Stokes equations for the flows in the two fluid regions can be shown

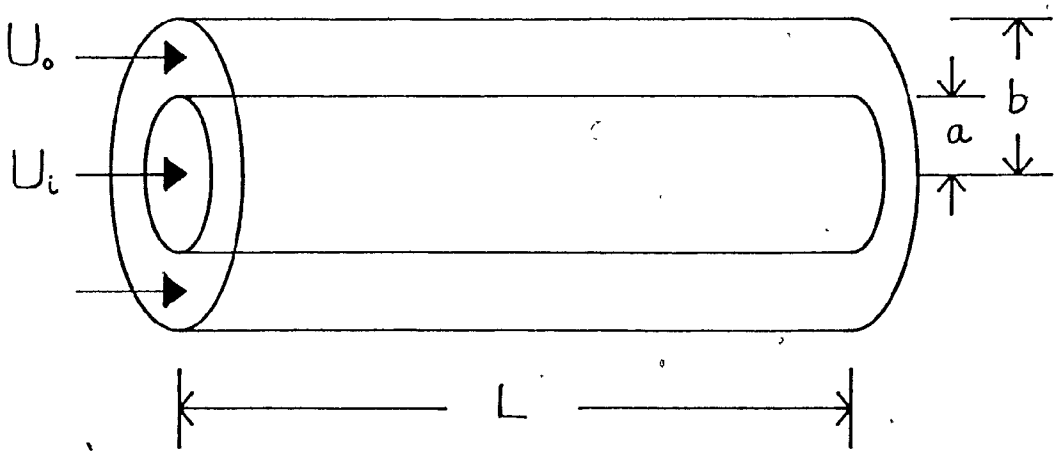

Fig. K.1

to be, in cylindrical coordinates [38]:

$$\frac{1}{\rho}\frac{\partial P}{\partial x} = -\frac{1}{r}\frac{d}{dr}(r\overline{u_x u_r}) + \frac{\eta}{r}\frac{d}{dr}\left(r\frac{dU}{dr}\right) \quad , \tag{K.1}$$

$$\frac{1}{\rho}\frac{\partial P}{\partial r} = -\frac{1}{r}\frac{d}{dr}(r\overline{u_r^2}) + \frac{\overline{u_\theta^2}}{r} \quad , \tag{K.2}$$

$$0 = \frac{d}{dr}(\overline{u_r u_\theta}) + 2\frac{\overline{u_r u_\theta}}{r} \quad , \tag{K.3}$$

where $\overline{(\ )}$ = time-mean of ( ); ρ and η are the density and the kinematic viscosity of the fluid, respectively; is the time-mean pressure; is the time-mean axial flow velocity and u_x , u_θ , u_r are the fluctuating flow velocity components in the x , θ and r directions, respectively.

By virtue of the assumption that the flow is fully-developed, all time-mean quantities, with the exception of the fluid pressure, are independent of x. It should be emphasized once again that equations (K.1-.3) apply to both the internal and annular fluid regions.

K.1 DERIVATION OF THE INTERNAL FLUID PRESSURE

Let us now derive the fluid pressure of the internal flow from equations (K.1-.3). For the sake of brevity, the subscript i, generally used to denote terms associated with the internal flow, will be suppressed for the time being.

Integrating equation (K.3), one has

$$\overline{u_r u_\theta} = \frac{C}{r^2} \quad ,$$

where C is a constant. At $r = a$, $\overline{u_r u_\theta} = 0$ since the velocity fluctuations u_r and u_θ at the solid boundary $r = a$ are zero at all times. This implies that $C = 0$, and thus

$$\overline{u_r u_\theta} = 0$$

everywhere. Since all the time-mean quantities are independent of x, equation (K.2) shows that $\partial P/\partial r$ is independent of x; therefore, $\partial P/\partial x$ is

independent of r†. Thus, equation (K.1) can be integrated to yield

$$\frac{r^2}{2\rho}\frac{\partial P}{\partial x} = -r\,\overline{u_x u_r} + \eta r \frac{dU}{dr} + A(x) \,, \tag{K.4}$$

where $A(x)$ is a function of x. Similarly, integrating equation (K.2),

$$\frac{P}{\rho} = -\overline{u_r^2} + \int_a^r \frac{\overline{u_\theta^2} - \overline{u_r^2}}{r}\,dr + B(x) \,, \tag{K.5}$$

where $B(x)$ is another function of x.

$A(x)$ and $B(x)$ are to be determined by the boundary conditions. At r = 0, one has $dU/dr = 0$ and $\overline{u_x u_r} = 0$. The mean flow is assumed to be axisymmetric, therefore, the first condition is justified. The vanishing of the correlation between u_x and u_r needs a little elaboration. Near the wall of the pipe, the mean flow gradient dU/dr is large. When a fluid particle moves away from the wall with a negative u_r, it will be entering a faster-moving part of the stream and will decrease locally the velocity in the x direction resulting in a negative u_x (see Figure K.2). Conversely, if the fluid particle moves towards the wall (positive u_r), it is transposed from a faster-moving part of the stream to a slower part and will, thus, accelerate the latter (positive u_x). Hence, $u_x u_r$ is always positive and the correlation is particularly strong near the wall.

---

† $\partial P/\partial r$ is independent of x; this implies

$$0 = \frac{\partial}{\partial x}\left(\frac{\partial P}{\partial r}\right) = \frac{\partial^2 P}{\partial x\,\partial r} = \frac{\partial}{\partial r}\left(\frac{\partial P}{\partial x}\right) \,.$$

Hence $\partial P/\partial x$ is independent of r.

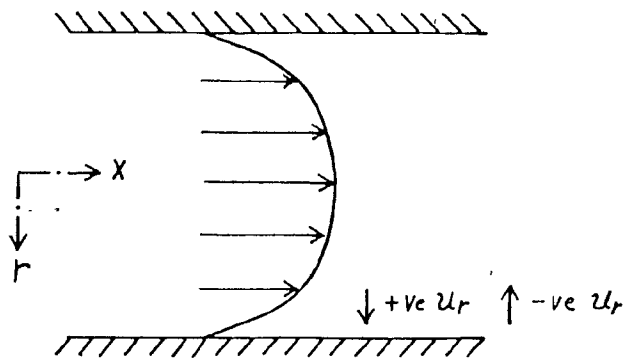

Fig. K.2

Towards the center, dU/dr is small (the mean velocity profile for turbulent flow in a pipe is fairly flat as shown in Figure K.2), the correlation is much less pronounced and practically vanishes at the center where $dU/dr = 0$. Without a dominant mean velocity gradient, the velocity fluctuations assume random independent variations at the center of the pipe and their correlation will be zero there.

At the boundary r = a, one has $\overline{u_x u_r} = \overline{u_r^2} = 0$ because the velocity vanishes at the wall. The quantity U_τ, called the shear velocity will be defined as

$$U_\tau^2 = -\eta \left.\frac{dU}{dr}\right|_{r=a} , \qquad (K.6)$$

and is related to τ_ω, the fluid viscous force per unit area on the inner surface of the pipe, by

$$U_\tau^2 = \frac{\tau_\omega}{\rho} . \qquad (K.7)$$

Applying the conditions at r = 0, equation (K.4) demands that A(x) = 0; and from the conditions at r = a and equation (K.6), one may write

$$\frac{1}{\rho}\frac{\partial P}{\partial x} = -\frac{2}{a}U_\tau^2 \quad . \tag{K.8}$$

Integrating equation (K.8), one obtains

$$\frac{P}{\rho} = -\frac{2}{a}U_\tau^2 x + C(r) \quad , \tag{K.9}$$

where C(r) is a function of r.

Comparing equations (K.5) and (K.9), one has

$$B(x) = -\frac{2}{a}U_\tau^2 x \quad ,$$

and

$$C(r) = -\overline{u_r^2} + \int_a^r \frac{\overline{u_\theta^2} - \overline{u_r^2}}{r}\,dr + C_1 \quad ,$$

where C_1 is a constant.

Thus, the pressure distribution is given by

$$\frac{P(x,r)}{\rho} = -\frac{2}{a}U_\tau^2 x - \overline{u_r^2} + \int_a^r \frac{\overline{u_\theta^2} - \overline{u_r^2}}{r}\,dr + C_1 \quad . \tag{K.10}$$

Putting x = 0, r = a in equation (K.10), yields

$$C_1 = \frac{P(0,a)}{\rho} \quad . \tag{K.11}$$

Substituting equation (K.11) into equation (K.10) and putting in the subscript i, the pressure distribution in the internal fluid region can be written as

$$P_i(x,r) = -\frac{2\rho_i}{a} U_\tau^2 x - \rho_i \overline{u_{ri}^2} + \rho_i \int_a^r \frac{\overline{u_{\theta i}^2} - \overline{u_{ri}^2}}{r}\, dr + P_i(o,a) \quad , \qquad (K.12)$$

where

$$U_\tau^2 = -\eta_i \left.\frac{dU_i}{dr}\right|_{r=a} \quad , \qquad (K.12a)$$

$$= \frac{\tau_w}{\rho_i} \quad . \qquad (K.12b)$$

K.2 DERIVATION OF THE ANNULAR FLUID PRESSURE

Similar solution procedures may now be applied to the annular fluid region. Again the subscript o will be omitted while the details of the derivation are being worked out.

Integrating equation (K.3) and applying the condition that at $r = a,b$; $\overline{u_r u_\theta} = o$ will lead to the conclusion

$$\overline{u_r u_\theta} = o$$

everywhere. Integrating equations (K.1, K.2) yields equations of the same form as (K.4, K.5), respectively. The 'new' A(x) and B(x) will again be determined using the boundary conditions.

Assuming that R_m is the radius at which the mean annular velocity

is a maximum, one has

$$\frac{dU}{dr} = 0 \quad \text{and} \quad \overline{u_x u_r} = 0 \quad \text{at} \quad r = R_m \ ; \tag{K.13}$$

the correlation $\overline{u_x u_r}$ vanishes for the same reason as given in Section K.1. The other boundary conditions are

$$\overline{u_x u_r} = \overline{u_r^2} = 0 \ , \quad \eta \frac{dU}{dr} = U_{\tau a}^2 = \frac{\tau_a}{\rho} \quad \text{at} \quad r = a \ , \tag{K.14}$$

$$\overline{u_x u_r} = \overline{u_r^2} = 0 \ , \quad \eta \frac{dU}{dr} = -U_{\tau b}^2 = -\frac{\tau_b}{\rho} \quad \text{at} \quad r = b^{\dagger} \ , \tag{K.15}$$

where τ_a and τ_b are the fluid frictional forces per unit area of the pipe surface exposed to the annular flow at r = a and r = b, respectively. Applying condition (K.13) to equation (K.4), one obtains,

$$A(x) = \frac{R_m^2}{2\rho} \frac{\partial P}{\partial x} \ . \tag{K.16}$$

Substituting equation (K.16) into equation (K.4) and applying the condition at r = b (equation (K.15)), yields

$$\frac{1}{2\rho} \frac{\partial P}{\partial x} \left(\frac{b^2 - R_m^2}{b} \right) = - U_{\tau b}^2 \ . \tag{K.17}$$

Integrating equation (K.17),

---

†The mean flow velocity gradient dU/dr has different signs at the two boundaries, r=a and r=b, since the mean flow *increases* from zero at r=a, reaches a maximum and *decreases* back to zero at r=b.

$$\frac{P}{\rho} = -\left(\frac{2b}{b^2-R_m^2}\right) U_{\tau b}^2 x + C(r) \quad , \tag{K.18}$$

where C(r) is a function of r.

Comparing equations (K.5) and (K.18), one may deduce

$$B(x) = -\left(\frac{2b}{b^2-R_m^2}\right) U_{\tau b}^2 x \quad ,$$

$$C(r) = -\overline{u_r^2} + \int_a^r \frac{\overline{u_\theta^2} - \overline{u_r^2}}{r}\, dr + C_1 \quad ,$$

where C_1 is a constant. Thus, equation (K.18) becomes

$$\frac{P(x,r)}{\rho} = -\left(\frac{2b}{b^2-R_m^2}\right) U_{\tau b}^2 x - \overline{u_r^2} + \int_a^r \frac{\overline{u_\theta^2} - \overline{u_r^2}}{r}\, dr + C_1 \quad . \tag{K.19}$$

Putting x = 0, r = a into equation (K.19), C_1 is found to be $P(o,a)/\rho$. Reverting to the use of subscript o, equation (K.19) may be modified to give the pressure distribution in the annular fluid region,

$$P_o(x,r) = -\left(\frac{2b}{b^2-R_m^2}\right) \rho_o U_{\tau b}^2 x - \rho_o \overline{u_{ro}^2} + \rho_o \int_a^r \frac{\overline{u_{\theta o}^2} - \overline{u_{ro}^2}}{r}\, dr + P_o(o,a), \tag{K.20}$$

where

$$U_{\tau b}^2 = -\eta_o \left.\frac{dU_o}{dr}\right|_{r=b} \quad , \tag{K.20a}$$

$$= \frac{\tau_b}{\rho_o} \quad . \tag{K.20b}$$

Finally, let us find the relation between the fluid frictional forces τ_a and τ_b exerted by the annular flow on the walls of the inner and outer cylinders, respectively. Recall that equation (K.17), *i.e.*,

$$\frac{1}{2\rho}\frac{\partial P}{\partial X}\left(\frac{b^2 - R_m^2}{b}\right) = -U_{\tau b}^2$$

or, equivalently,

$$\frac{1}{2\rho}\frac{\partial P}{\partial X} = -\left(\frac{b}{b^2 - R_m^2}\right)U_{\tau b}^2 \tag{K.21}$$

has been obtained by applying the boundary conditions at r=b (equation (K.15)) to equation (K.4). On the other hand, it is equally valid to apply the conditions at r=a (equation (K.14)) to equation (K.4) to obtain

$$\frac{1}{2\rho}\frac{\partial P}{\partial X} = \left(\frac{a}{a^2 - R_m^2}\right)U_{\tau a}^2 \quad . \tag{K.22}$$

For equations (K.21) and (K.22) to be equivalent, one must have

$$\left(\frac{b}{b^2 - R_m^2}\right)U_{\tau b}^2 = \left(\frac{a}{R_m^2 - a^2}\right)U_{\tau a}^2 \quad ,$$

or

$$U_{\tau a}^2 = \frac{b}{a}\frac{(R_m^2 - a^2)}{(b^2 - R_m^2)}U_{\tau b}^2 \quad . \tag{K.23}$$

Since $U_{\tau a}^2 = \tau_a/\rho$ and $U_{\tau b}^2 = \tau_b/\rho$ by definition, equation (K.23) may be

rewritten as

$$\tau_a = \frac{b}{a} \frac{(R_m^2 - a^2)}{(b^2 - R_m^2)} \tau_b \quad . \tag{K.24}$$

The relation between τ_a and τ_b has also been derived more rigorously by considering the equilibrium of axial forces acting on a control volume in the annular fluid region, and making use of equation (K.17). The result is found to be the same as equation (K.24).

APPENDIX L

EVALUATION OF THE INTEGRAL $\int_a^b [(\overline{u_{\theta o}^2} - \overline{u_{ro}^2})/r]dr$

In this Appendix will be given the details in the evaluation of the integral

$$\int_a^b \frac{\overline{u_{\theta o}^2} - \overline{u_{ro}^2}}{r} dr$$

appearing in equation (6.31). Due to the lack of experimental data on the fluctuating velocity components of turbulent flow *in the annulus* between two coaxial cylinders, the terms $\overline{u_{\theta o}^2}$ and $\overline{u_{ro}^2}$ will be derived from experimental results of turbulent flow in a *circular pipe* obtained by Laufer [38]. Figure 27 shows his measurements on the distributions of $\overline{u_\theta^2}$ and $\overline{u_r^2}$ across a circular pipe of radius a. Except for a small portion near the pipe wall (r=a), the distributions may be approximated by the following equations:

$$\frac{(\overline{u_\theta^2})^{1/2}}{U_\tau} = 1.533 - 0.900\frac{(a-r)}{a}, \qquad 0 \leq r \leq a \tag{L.1}$$

$$\frac{(\overline{u_r^2})^{1/2}}{U_\tau} = 1.133 - 0.500\frac{(a-r)}{a}, \qquad 0 \leq r \leq a \tag{L.2}$$

where U_τ is the shear velocity defined as $U_\tau^2 = \tau_\omega/\rho$; τ_ω is the fluid viscous force per unit area on the inner surface of the pipe. Using equations (L.1) and (L.2), one can easily show that

$$\overline{u_\theta^2} - \overline{u_r^2} = 0.400 \frac{r}{a}\left(1.266 + 1.400 \frac{r}{a}\right) U_\tau^2 \quad , \qquad 0 \le r \le a \tag{L.3}$$

It is obvious from equations (L.1) and (L.2) that the distributions of $\overline{u_\theta^2}$ and $\overline{u_r^2}$ depend on the radius as well as the shear velocity. In view of the fact that the shear velocities at the two solid boundaries of the annular region are different ($U_{\tau a}$ at r=a, $U_{\tau b}$ at r=b), the distributions of $\overline{u_{\theta o}^2}$ and $\overline{u_{ro}^2}$ in the annulus will be approximated in the following manner. The annulus is divided into two parts at $r = R_m$, the radius at which the mean annular velocity is maximum. The $\overline{u_{\theta o}^2}$ and $\overline{u_{ro}^2}$ distributions over the region from r=a to $r = R_m$ are taken to be the same as those for a circular pipe of radius $(R_m - a)$ with a shear velocity of $U_{\tau a}$ at the wall. Similarly, the distributions over the other portion (from $r = R_m$ to r = b) are approximated by their counterparts for a circular pipe of radius $(b - R_m)$ and with a shear velocity of $U_{\tau b}$. According to the above scheme and making use of equation (L.3), the term $(\overline{u_{\theta o}^2} - \overline{u_{ro}^2})$ may be expressed as follows:

$$\overline{u_{\theta o}^2} - \overline{u_{ro}^2} = 0.400 \frac{(R_m - r)}{(R_m - a)}\left[1.266 + 1.400 \frac{(R_m - r)}{(R_m - a)}\right] U_{\tau a}^2 \qquad \text{for} \quad a \le r < R_m$$

$$= 0.400 \frac{(r - R_m)}{(b - R_m)}\left[1.266 + 1.400 \frac{(r - R_m)}{(b - R_m)}\right] U_{\tau b}^2 \qquad \text{for} \quad R_m < r \le b \, . \tag{L.4}$$

Thus, the integral under consideration may be written as

$$\int_a^b \frac{\overline{u_{\theta o}^2} - \overline{u_{ro}^2}}{r} \, dr = \int_a^{R_m} \frac{0.400 (R_m - r)}{r \, (R_m - a)}\left[1.266 + 1.400 \frac{(R_m - r)}{(R_m - a)}\right] U_{\tau a}^2 \, dr$$

$$+ \int_{R_m}^b \frac{0.400 (r - R_m)}{r \, (b - R_m)}\left[1.266 + 1.400 \frac{(r - R_m)}{(b - R_m)}\right] U_{\tau b}^2 \, dr \, .$$

After some manipulations, one may obtain

$$\int_a^b \frac{\overline{u_{\theta 0}^2} - \overline{u_{r0}^2}}{r}\, dr = \left[-0.7864 - \frac{0.5600\, R_m}{(R_m - a)} + \frac{0.5064\, R_m}{(R_m - a)} \ln\left(\frac{R_m}{a}\right) + \frac{0.5600\, R_m^2}{(R_m - a)^2} \ln\left(\frac{R_m}{a}\right)\right] U_{\tau a}^2$$

$$+ \left[0.7864 - \frac{0.5600\, R_m}{(b - R_m)} - \frac{0.5064\, R_m}{(b - R_m)} \ln\left(\frac{b}{R_m}\right) + \frac{0.5600\, R_m^2}{(b - R_m)^2} \ln\left(\frac{b}{R_m}\right)\right] U_{\tau b}^2 \,. \tag{L.5}$$

It should be emphasized that the result as given in equation (L.5) is only an approximation of the integral. Other possible schemes of evaluation may be devised; however, until appropriate experimental data for the annular region become available, one has to be satisfied with the approximate result, and hope that it is not too far off from the exact solution.

APPENDIX M

COMPUTER PROGRAMS FOR THE CASE OF INCOMPRESSIBLE VISCOUS FLOW

M.1 PROGRAM FOR SYSTEM WITH A RIGID OUTER SHELL

M.1.1 Function of the Program

The program calculates the dimensionless eigenfrequencies, $\bar{\Omega}_i$, and the associated eigenvectors of a system with a rigid outer shell subjected to internal and annular incompressible viscous flows. For each set of input data of flow velocities, $\bar{U}_i$, $\bar{U}_o$, the program constructs the matrices $[P_{Bi}]$ and $[Q_i]$ involved in the eigenvalue equation

$$\left([P_{Bi}] + \bar{\Omega}_i [Q_i]\right)\{Y_i\} = \{0\} \quad , \tag{M.1}$$

where $\{Y_i\}$ is defined in equation (F.1a); matrices $[P_{Bi}]$ and $[Q_i]$ will be defined later. The frequencies are then determined as the solutions of this eigenvalue equation.

M.1.2 Program Structure

The program is written in Fortran IV language and it has the following structure:

MAIN PROGRAM

SUBROUTINE CONT

SUBROUTINE PREMAT

SUBROUTINE MKMAT

SUBROUTINE CMAT

SUBROUTINE REDUCE

SUBROUTINE EIGZC.

M.1.3 Description of the Program

The function of each subprogram is summarized as follows:

(1) Subroutine CONT evaluates the constants a_{km}, b_{km}, ..., h_{km}, j_{km} according to the formulae given in Appendix A.

(2) Subroutine PREMAT calculates the flow-independent terms in the elements of the matrices $[M_i]$ and $[K_{Bl}]$ involved in the equation

$$\bar{\Omega}_i^2 [M_i]\{X_i\} + \bar{\Omega}_i [C_i]\{X_i\} + [K_{Bl}]\{X_i\} = \{0\} \quad . \qquad (M.2)$$

Equation (M.2) is the governing matrix equation for systems with a rigid outer shell subjected to incompressible viscous flows, which can be derived similarly to equation (6.77). The matrices $[M_i]$ and $[C_i]$ are shown in Appendix E; $\{X_i\}$ is defined in equation (F.2b); the structure of matrix $[K_{Bi}]$ is the same as that of matrix $[K_i]$ (see Appendix E), except that all the A^l_{kmn} terms are replaced by the corresponding B^l_{kmn} terms defined in equations (6.54-.62).

(3) Subroutine MKMAT completes the construction of matrices $[M_i]$ and $[K_{Bl}]$ by filling in the flow-dependent terms which include the generalized aerodynamic forces (q^1_{kmn}, q^2_{kmn} in equations (D.3a) and (D.3c), respectively) and terms associated with the fluid frictional forces and fluid pressurization due to the viscous flows (Γ_{i1}, Γ_{i2}, ..., Γ_{i5} defined in equation (6.52)). The former terms are obtained with the input data of

flow velocities and the computed values of the integrals involved, while the latter quantities are evaluated through the use of the friction factors which are determined with equations (6.43) and (6.44) for each set of input flow velocities.

(4) Subroutine CMAT constructs the matrix $[C_i]$ by evaluating the generalized aerodynamic force, q^2_{kmn} (which gives rise to the only non-zero elements of the matrix) as defined in equation (D.3b).

(5) Subroutine REDUCE constructs the matrices $[P_{Bi}]$ and $[Q_i]$ which have the following form:

$$[P_{Bi}] = \begin{bmatrix} [0] & [I] \\ [K_{Bi}] & [C_i] \end{bmatrix}, \qquad [Q_i] = \begin{bmatrix} -[I] & [0] \\ [0] & [M_i] \end{bmatrix}, \tag{M.3}$$

where $[I]$ is the identity matrix. Matrices $[P_{Bi}]$ and $[Q_i]$ appear in the eigenvalue equation (M.1) which is reduced from the governing second-order matrix equation (M.2).

(6) Subroutine EIGZC is the IMSL subroutine employed to solve the eigenvalue equation (M.1).

All calculations are carried out with double precision. The necessary parameters are defined in the main program. The flow velocities and the computed values of the integrals involved in the generalized aerodynamic forces are read from the data deck. The output results consist of all eighteen eigenvalues and the upper half segment of the associated eigenvectors which contains the shell displacement vector $\{X_i\}$.

Notation used in the computer program, the computer program iteself and a sample of the output are given in the following pages.

NOTATION USED IN THE PROGRAM

Notation used in the computer program	Corresponding notation used in the thesis	Definition
RMS*	R_m^2/b^2	R_m defined in equation (6.25c)
NU	ν_i	See NOMENCLATURE
SK	k_i	See NOMENCLATURE
DEN*	ρ_i $(=\rho_o)$	See NOMENCLATURE
DDI*	$\rho_i a/\Lambda_i$	See NOMENCLATURE
VIS*	η_i/ρ_i $(=\eta_o/\rho_o)$	Dynamical viscosity
Q1(3,3), Q2(3,3), Q3(3,3), Q4(3,3), Q5(3,3), Q6(3,3)		Integral terms in the generalized aerodynamic forces
MM(9,9)	$[M_i]$	See Appendix E
KK(9,9)	$[K_{Bi}]$	See equation (M.2)
CC(9,9)	$[C_i]$	See Appendix E
AA(9,9)	$[P_{Bi}]$	Defined in equation (M.3)
BB(9,9)	$[Q_i]$	Defined in equation (M.3)
PPI*	$P_i(o,a)$	Static internal fluid pressure at x=0, r=a
PPO*	$P_o(o,a)$	Static annular fluid pressure at x=0, r=a
PO, PL	p_o, p_L	The axial reactions per unit circumference at the x=0 and x=L ends of the inner cylinder, respectively (see Appendix I)
SE(3,3)*, SF(3,3)*, G(3,3*), H(3,3)*, SJ(3,3)*	e_{km}, f_{km}, g_{km}, h_{km}, j_{km}; $k,m=1,2,3$	Constants defined in equations (6.72-.76)
SU*	v_i $(=v_o)$	Defined in equation (3.2.10a)

Notation used in the computer program	Corresponding notation used in the thesis	Definition
UIM*, UOM*	U_i , U_o	The dimensional internal and annular flow velocities, respectively
RR*	k/d	Relative roughness of the shell surface (see Section 6.1.2)
RI*, RO*		Reynolds numbers of the internal and annular flows, respectively
FI*, FO*	f_i , f_o	Friction factors of the internal and annular flows, respectively
UTS*, UTAS*, UTBS*	U_τ^2 , $U_{\tau a}^2$, $U_{\tau b}^2$	The various stress velocities (see Section 6.1.2)
BB, CC, DD	B_i , C_i , D_i	Defined in equations (6.34-.36), respectively
GM1, GM2, GM3, GM4, GM5	Γ_{i1} , Γ_{i2} , Γ_{i3} , Γ_{i4} , Γ_{i5}	Defined in equation (6.52)

*Notation with the same definition as in other computer programs.

```
/INFO MVS TI(30) R(MUSIC) CL(20) N(STEVE SIU PUI CHAN)
//STEP1 EXEC FORTRAN
//FORT.SYSIN DD *
C*************************************************************************
C     COMPUTER PROGRAM FOR THE CASE OF INCOMPRESSIBLE VISCOUS FLOW      *
C     ONLY THE INNER SHELL FLEXIBLE                                     *
C     BOUNDARY CONDITIONS: CLAMPED-CLAMPED                              *
C*************************************************************************
C
C*************************************************************************
C     MAIN PROGRAM                                                      *
C*************************************************************************
      IMPLICIT REAL*8(A-H,O-Z)
      COMPLEX*16 MM(9,9),KK(9,9),CC(9,9),AA(18,18)/324*(0.D0,0.D0)/,
     #BB(18,18)/324*(0.D0,0.D0)/,EIGA(18),EIGB(18),Z(18,18),WK(18,36),
     #OMEGA,Q1(3,3),Q2(3,3),Q3(3,3),Q4(3,3),Q5(3,3),Q6(3,3)
      REAL*8 NU
      COMMON/DATA1/NU,SK,EI,EO,ER,C(3),P(3),N
      COMMON/DATA2/ZI,DR,PI
      COMMON/DATA3/Q1,Q2
      COMMON/DATA4/Q3,Q4
      COMMON/DATA5/Q5,Q6
      COMMON/DATA6/PPI,PPO,PO,PL,RMS,DEN,DDI,VIS
      DATA IA/18/,IB/18/,NN/18/,IJOB/2/,IZ/18/
      PI=DARCOS(-1.D0)
      C(1)=0.9825022145762379D0
      C(2)=1.000777731190727D0
      C(3)=0.9999664501254086D0
      P(1)=4.7300407448627D0
      P(2)=7.853204624095 84D0
      P(3)=10.995607838001 67D0
      EI=1/11.D0
      EO=0.1D0
      ER=10/11.D0
      RMS=(1-ER**2)/2/DLOG(1/ER)
      NU=0.30D0
      SK=(5.50D-3)**2/12
      ZI=2.330D1
      DR=1.D0
      N=3
      DEN=998.6D0
      DDI=8.261D-7
      VIS=1.1216D-6
      DO 3 K=1,3
      DO 3 M=1,3
      READ(5,*) Q1(K,M),Q2(K,M),Q3(K,M),Q4(K,M),Q5(K,M),Q6(K,M)
    3 CONTINUE
      CALL CONT(C,P)
      CALL PREMAT(MM,KK)
      UO=0.0D0
      DO 1 L=1,3
      READ(5,*) UI
      CALL MKMAT(UI,UO,MM,KK)
      CALL CMAT(UI,UO,CC)
      CALL REDUCE(MM,KK,CC,AA,BB)
      CALL EIGZC(AA,IA,BB,IB,NN,IJOB,EIGA,EIGB,Z,IZ,WK,INFER,IER)
      PRINT10,UI,UO
   10 FORMAT('1','FLOW VELOCITY INSIDE THE INNER CYLINDER=',F8.5/'0','FL
```

```
     #OW VELOCITY IN THE ANNULAR REGION=',F8.5)
      PRINT13,PPO
   13 FORMAT('-','GAUGE PRESSURE AT THE UPSTREAM END OF THE CYLINDERS IN
     # THE ANNULAR FLUID REGION=',D24.16,' N/M**2')
      PRINT14,PPI
   14 FORMAT('0',52X,'IN THE INNER FLUID REGION=',D24.16,' N/M**2')
      PRINT15,PO,PL
   15 FORMAT('-','AXIAL COMPRESSIVE LOAD ACTING ON THE X=0 END OF THE IN
     #NER CYLINDER=',D24.16,' N/M'/'0',37X,'X=L END',22X,'=',D24.16,' N/
     #M')
      PRINT11
   11 FORMAT('-','THE FREQUENCIES ARE:')
      DO 20 I=1,18
      OMEGA=-EIGA(I)/EIGB(I)
   20 PRINT12,OMEGA
   12 FORMAT('0','(',2D24.16,1X,')')
      DO 2 K=1,11,5
      M=K+4
      PRINT21,K,M
    2 PRINT22,((Z(I,J),J=K,M),I=1,9)
      K=16
      M=18
      PRINT21,K,M
      PRINT23,((Z(I,J),J=16,18),I=1,9)
   21 FORMAT('1','THE ',I2,'-',I2,' EIGENVECTORS')
   22 FORMAT(//5(2X,'(',2D10.3,')')/)
   23 FORMAT(//3(2X,'(',2D10.3,')')/)
    1 CONTINUE
      PRINT100
  100 FORMAT('1')
      STOP
      END
C
C*****************************************************************************
C     SUBROUTINE CONT                                                        *
C*****************************************************************************
      SUBROUTINE CONT(C,P)
      IMPLICIT REAL*8(A-H,O-Z)
      DIMENSION A(3,3),B(3,3),C(3),D(3,3),SE(3,3),SF(3,3),G(3,3),H(3,3),
     #SJ(3,3),SL(3,3),DEL(3,3),P(3)
      INTEGER DEL
      COMMON/CON1/A,B,D,DEL
      COMMON/CON2/SE,SF,G,H,SJ,SL
      DO 3 K=1,3
      DO 3 M=1,3
      IF(K.EQ.M) GO TO 1
      DEM=P(M)**4-P(K)**4
      PC=P(M)*C(M)-P(K)*C(K)
      PWR=(-1)**(K+M)
      PMKS=P(M)**2*P(K)**2
      A(K,M)=-4*PMKS*(PWR+1)*PC/DEM
      B(K,M)=0.D0
      D(K,M)=-A(K,M)
      SE(K,M)=4*(3*P(M)**4+P(K)**4)*PMKS*P(M)*P(K)*(1-PWR)/DEM**2
      SF(K,M)=4*PMKS*(1-PWR)/DEM
      G(K,M)=-4*PWR*PMKS*PC/DEM-2*(P(M)**4+P(K)**4)*SF(K,M)/DEM
      SL(K,M)=-SF(K,M)
      H(K,M)=4*PWR*PMKS*PC/DEM-(3*P(M)**4+P(K)**4)*SL(K,M)/DEM
```

```
      SJ(K,M)=16*PMKS*P(M)*P(K)*C(M)*C(K)*(PWR-1)/DEM**2
      DEL(K,M)=0
      GO TO 3
    1 A(K,K)=P(K)*C(K)*(P(K)*C(K)-2)
      B(K,K)=-P(K)**4
      D(K,K)=-A(K,K)
      SE(K,K)=-B(K,K)/2
      SF(K,K)=0.D0
      G(K,K)=A(K,K)/2
      H(K,K)=-G(K,K)
      SJ(K,K)=0.5D0
      SL(K,K)=0.D0
      DEL(K,K)=1
    3 CONTINUE
      RETURN
      END
C
C*****************************************************************
C     SUBROUTINE PREMAT                                          *
C*****************************************************************
      SUBROUTINE PREMAT(MM,KK)
      IMPLICIT REAL*8(A-H,O-Z)
      DIMENSION A(3,3),B(3,3),D(3,3),DEL(3,3),COEM(3,3,3),COE(9,3,3)
      COMPLEX*16 MM(9,9),KK(9,9),Q1(3,3),Q2(3,3)
      REAL*8 NU
      INTEGER DEL,H
      COMMON/DATA1/NU,SK,EI,EO,ER,C(3),P(3),N
      COMMON/DATA2/ZI,DR,PI
      COMMON/DATA3/Q1,Q2
      COMMON/CON1/A,B,D,DEL
      COMMON/COEF/COE
      DO 9 I=1,9
      DO 9 J=1,9
      MM(I,J)=(0.D0,0.D0)
    9 KK(I,J)=(0.D0,0.D0)
      C1=ZI/2/PI/EI
      C2=C1*DR
      DO 3 K=1,3
      DO 3 M=1,3
      COEM(1,K,M)=A(K,M)
      COEM(2,K,M)=DEL(K,M)
    3 COEM(3,K,M)=DEL(K,M)+C1*Q1(K,M)-C2*Q2(K,M)
      DO 4 K=1,3
      DO 4 M=1,3
      COE(1,K,M)=EI**2*B(K,M)+(NU-1)*(SK+1)*N**2*A(K,M)/2
      COE(2,K,M)=-(1+NU)*N*EI**2*D(K,M)/2
      COE(3,K,M)=(P(M)*EI)**4*SK*DEL(K,M)-(2*NU-SK*(1-NU)*N**2)
     C*EI**2*D(K,M)/2
      COE(4,K,M)=(1+NU)*N*A(K,M)/2
      COE(5,K,M)=-N**2*DEL(K,M)+(1+3*SK)*(1-NU)*EI**2*D(K,M)/2
      COE(6,K,M)=SK*(3-NU)*N*EI**2*D(K,M)/2-N*DEL(K,M)
      COE(7,K,M)=(NU+(NU-1)*SK*N**2/2)*A(K,M)-SK*EI**2*B(K,M)
      COE(8,K,M)=-N*DEL(K,M)+(3-NU)*SK*N*EI**2*D(K,M)/2
    4 COE(9,K,M)=-SK*(((P(M)*EI)**4+(N**2-1)**2)*DEL(K,M)-2*(N*EI)
     #**2*D(K,M))-DEL(K,M)
      K=0
      DO 5 I=1,7,3
      K=K+1
```

```
      DO 5 M=1,3
      DO 5 L=1,3
      H=L-1
      MM(I+H,M+3*H)=COEM(L,K,M)
    5 CONTINUE
      RETURN
      END
C
C ***************************************************************************
C     SUBROUTINE MKMAT                                                      *
C***************************************************************************
      SUBROUTINE MKMAT(UI,UO,MM,KK)
      IMPLICIT REAL*8(A-H,O-Z)
      COMPLEX*16 MM(9,9),KK(9,9),Q3(3,3),Q4(3,3),CCOE(9,3,3)
      INTEGER DEL(3,3),W,V,HH
      REAL*8 NU
      DIMENSION A(3,3),B(3,3),D(3,3),SE(3,3),SF(3,3),G(3,3),H(3,3),
     #SJ(3,3),SL(3,3),COE(9,3,3)
      COMMON/DATA1/NU,SK,EI,EO,ER,C(3),P(3),N
      COMMON/DATA2/ZI,DR,PI
      COMMON/DATA4/Q3,Q4
      COMMON/DATA6/PPI,PPO,PO,PL,RMS,DEN,DDI,VIS
      COMMON/CON1/A,B,D,DEL
      COMMON/CON2/SE,SF,G,H,SJ,SL
      COMMON/COEF/COE
      FA(RR,RE)=DSQRT(0.0055*(1+(20000*RR+1.D6/RE)**(1./3.)))
      F(RR,RE)=1/(-4*DLOG10(RR/3.7+2.51/RE/FA(RR,RE)))**2
      SU=5.3082D3
      UOM=UO*SU
      UIM=UI*SU
      RR=0.D0
      RO=UOM*2*(EO-EI)/VIS
      RI=UIM*2*EI/VIS
      IF(RI.EQ.0.D0) GO TO 10
      FI=F(RR,RI)
      GO TO 11
   10 FI=0.D0
   11 IF(RO.EQ.0.D0) GO TO 12
      FO=F(RR,RO)
      GO TO 13
   12 FO=0.D0
   13 PPI=DEN*FI*UIM**2/EI
      PPO=DEN*FO*UOM**2/(EO-EI)
      UTBS=(1-RMS)/2/(1-ER)*FO*UOM**2
      UTAS=(RMS-ER**2)/2/ER/(1-ER)*FO*UOM**2
      UTS=FI*UIM**2/2
      BB=UTS+UTAS
      CC=2*UTS/EI-2*UTBS/EO/(1-RMS)
      DD=(PPO-PPI)/DEN
      GM1=-BB*DDI/EI
      GM2=-(NU*CC*DDI+GM1)/2-NU*DD*DDI
      GM3=BB*DDI
      GM4=-CC*DDI
      GM5=-DD*DDI
      C3=UI**2*ZI*EI/2/PI
      C4=UO**2*ZI*EI*DR/2/PI
      PO=((NU*EI*CC-BB)/2+NU*EI*DD)*DEN
      PL=((NU*EI*CC+BB)/2+NU*EI*DD)*DEN
```

```
      DO 4 K=1,3
      DO 4 M=1,3
      CCOE(1,K,M)=COE(1,K,M)+GM1*EI**2*SE(K,M)+GM2*EI**2*B(K,M)-GM4*N**
     #2*G(K,M)-GM5*N**2*A(K,M)
      CCOE(2,K,M)=COE(2,K,M)
      CCOE(3,K,M)=COE(3,K,M)+GM4*EI**2*H(K,M)+GM5*EI**2*D(K,M)
      CCOE(4,K,M)=COE(4,K,M)+GM3*N/EI*SF(K,M)
      CCOE(5,K,M)=COE(5,K,M)+GM1*EI**2*H(K,M)+GM2*EI**2*D(K,M)-GM4*N**
     #2*SJ(K,M)-GM5*N**2*DEL(K,M)
      CCOE(6,K,M)=COE(6,K,M)-GM4*N*SJ(K,M)-GM5*N*DEL(K,M)
      CCOE(7,K,M)=COE(7,K,M)+GM3/EI*SF(K,M)-GM4*G(K,M)-GM5*A(K,M)
      CCOE(8,K,M)=COE(8,K,M)-GM4*N*SJ(K,M)-GM5*N*DEL(K,M)
4     CCOE(9,K,M)=COE(9,K,M)+GM1*EI**2*H(K,M)+GM2*EI**2*D(K,M)-GM4*N**2*
     #SJ(K,M)-GM5*N**2*DEL(K,M)+C3*Q3(K,M)-C4*Q4(K,M)
      K=0
      DO 5 I=1,7,3
      K=K+1
      DO 5 M=1,3
      W=-1
      DO 5 V=1,7,3
      W=W+1
      DO 5 L=1,3
      HH=L-1
      KK(I+HH,M+V-1)=CCOE(L+3*W,K,M)
5     CONTINUE
      RETURN
      END
C
C*****************************************************************************
C     SUBROUTINE CMAT                                                        *
C*****************************************************************************
      SUBROUTINE CMAT(UI,UO,CC)
      IMPLICIT REAL*8 (A-H,O-Z)
      COMPLEX*16 CC(9,9),Q5,Q6
      COMMON/DATA2/ZI,DR,PI
      COMMON/DATA5/Q5(3,3),Q6(3,3)
      DO 2 I=1,9
      DO 2 J=1,9
2     CC(I,J)=(0.D0,0.D0)
      C5=UI*ZI/PI
      C6=UO*ZI*DR/PI
      DO 1 K=1,3
      DO 1 M=1,3
      CC(3*K,6+M)=-C5*Q5(K,M)+C6*Q6(K,M)
1     CONTINUE
      RETURN
      END
C
C*****************************************************************************
C     SUBROUTINE REDUCE                                                      *
C*****************************************************************************
      SUBROUTINE REDUCE(MM,KK,CC,AA,BB)
      COMPLEX*16 AA(18,18),BB(18,18),MM(9,9),KK(9,9),CC(9,9)
      DO 1 I=1,9
      AA(I,I+9)=(1.D0,0.D0)
      BB(I,I)=(-1.D0,0.D0)
1     CONTINUE
      DO 2 I=1,9
```

```
      DO 2 J=1,9
      AA(9+I,J)=KK(I,J)
      AA(9+I,9+J)=CC(I,J)
      BB(9+I,9+J)=MM(I,J)
    2 CONTINUE
      RETURN
      END
//GO.SYSIN DD *
(0.189606213253765OD+00,0.D0)
(-0.6759592315814779D+00,0.6040495708646455D-15)
(0.2312184916463780D+01,0.D0)
(-0.8122943495441742D+01,-0.1783665717388016D-12)
(-0.3280206164830202D-06,0.D0)
(0.6190663329733319D-06,0.9114964994383228D-15)
(-0.4766713517681613D-17,0.2348738759364798D-07)
(-0.9633476396856025D-15,-0.4420631811524404D-07)
(0.1628817143484548D-16,0.5581861620806592D-04)
(0.3248617160053225D-12,-0.1050433756703668D-03)
(-0.1029541159227697D-16,-0.6285111159652311D+00)
(-0.8161994647154542D-15,0.2207959405904953D+01)
(0.6318529334634996D-03,0.2371590276574419D-18)
(-0.6372597942142652D-02,-0.1397338347729216D-14)
(-0.1842035225332608D+01,0.2469456692931669D-17)
(0.6485864327386988D+01,-0.1082602378816420D-11)
(-0.1525785682687179D-05,0.8129588219495467D-17)
(0.2881073360038401D-05,0.3146543647328196D-13)
(-0.4766713517681613D-17,-0.2348738759364798D-07)
(0.9976375229975989D-15,0.4420631811524404D-07)
(0.1628817143484548D-16,-0.5581861620806592D-04)
(-0.3249472677089020D-12,0.1050433756703668D-03)
(-0.1029541159227697D-16,0.6285111159652311D+00)
(0.8884379566400543D-15,-0.2207959405904953D+01)
(0.1874795661657285D+00,0.D0)
(-0.6551227020549533D+00,0.3629635273343210D-14)
(0.8541245969912896D+01,0.D0)
(-0.2934937066445356D+02,0.3409919784229403D-11)
(-0.5845163463897832D-05,0.D0)
(0.1094831275117628D-04,-0.9403806651428478D-13)
(-0.6494989735391820D-17,-0.1001263295044486D-06)
(-0.1049759241826247D-14,0.1887126541802776D-06)
(-0.3708457815126825D-15,-0.2368581614173008D-03)
(-0.2935986399221754D-11,0.4463713138848790D-03)
(0.3245031071165055D-16,-0.1020380446668096D+01)
(0.5827035508300584D-13,0.3481847626998819D+01)
(0.6318529334634996D-03,-0.2371590276574419D-18)
(-0.6372597942142652D-02,-0.1395647285094802D-14)
(-0.1842035225332608D+01,-0.2469456692931669D-17)
(0.6485864327386988D+01,-0.1082583167229549D-11)
(-0.1525785682687179D-05,-0.8129588219495467D-17)
(0.2881073360038401D-05,0.3152308191943916D-13)
(-0.6494989735391820D-17,0.1001263295044486D-06)
(0.1094816421191028D-14,-0.1887126541802776D-06)
(-0.3708457815126825D-15,0.2368581614173008D-03)
(0.2938548715885774D-11,-0.4463713138848790D-03)
(0.3245031071165055D-16,0.1020380446668096D+01)
(-0.5849237066104017D-13,-0.3481847626998819D+01)
(0.1842879810863270D+00,0.D0)
(-0.6253330262705698D+00,-0.8825999633830738D-14)
```

```
(0.1797966673170376D+02,0.D0)
(-0.5977549941567372D+02,-0.5833364557530585D-11)
(-0.7209652058832401D-05,0.D0)
(0.1361799752242200D-04,0,1967468088413858D-12)
0.04100D0
0.05000D0
0.06000D0
//
/*
```

FLOW VELOCITY INSIDE THE INNER CYLINDER= 0.04100

FLOW VELOCITY IN THE ANNULAR REGION= 0.0

GAUGE PRESSURE AT THE UPSTREAM END OF THE CYLINDERS IN THE ANNULAR FLUID REGION= 0.0 N/M**2

IN THE INNER FLUID REGION= 0.8808780733525616D+06 N/M**2

AXIAL COMPRESSIVE LOAD ACTING ON THE X=0 END OF THE INNER CYLINDER= -0.3203192994009315D+05 N/M

X=L END = 0.8007982485023292D+04 N/M

THE FREQUENCIES ARE:

(-0.3144919800711159D+01 0.1727727493924256D-08)
(-0.3021194071833964D+01 -0.7854080199365140D-09)
(-0.3069750459379013D+01 -0.1284391765180942D-08)
(-0.2014141227328058D+01 -0.1216327202383280D-10)
(-0.1818423609899859D+01 0.3946118751818450D-09)
(0.3144919800551305D+01 0.1727726367306285D-08)
(0.3021194071817564D+01 -0.7854074661372771D-09)
(0.3069750459237169D+01 -0.1284390881222627D-08)
(0.2014141227288077D+01 -0.1216327677400487D-10)
(0.1818423609884807D+01 0.3946117284261491D-09)
(0.1891449826964575D+01 0.3872280745490673D-09)
(-0.1891449826987257D+01 0.3872282006785136D-09)
(-0.1297511990118048D-01 0.2831288137627006D-04)
(-0.8227846742884967D-02 0.9135657269354116D-05)
(0.1297470924757517D-01 0.2831339969070351D-04)
(0.8227772486752800D-02 0.9137420664546391D-05)
(0.7288453766548101D-03 -0.3744677454690443D-04)
(-0.7284772901804052D-03 -0.3745343957721765D-04)

THE 1- 5 EIGENVECTORS

(0.956D-02 0.402D-07)	(0.118D+00-0.458D-08)	(0.458D-03 0.170D-04)	(-0.496D+00 0.300D-11)	(-0.550D+00-0.119D-09)
(0.291D-03 0.179D-04)	(-0.426D-03 0.164D-04)	(0.114D+00 0.680D-08)	(-0.141D-02-0.729D-05)	(0.543D-03-0.101D-04)
(0.115D+00 0.212D-08)	(0.138D-01-0.722D-07)	(-0.211D-03 0.231D-04)	(-0.276D+00 0.252D-07)	(0.724D-01 0.220D-07)
(0.304D-01-0.123D-06)	(-0.331D+00 0.860D-10)	(-0.130D-02-0.381D-04)	(-0.113D-01 0.426D-08)	(-0.206D-01-0.214D-08)
(-0.785D-03-0.540D-04)	(0.118D-02-0.451D-04)	(-0.326D+00 0.136D-09)	(-0.185D-03 0.149D-05)	(0.650D-04-0.338D-05)
(-0.318D+00-0.175D-09)	(-0.307D-01 0.184D-06)	(0.595D-03-0.595D-04)	(-0.687D-01-0.627D-09)	(0.333D-01 0.935D-08)
(0.285D-03-0.133D-07)	(-0.301D-02 0.191D-07)	(-0.118D-04-0.553D-05)	(-0.166D-03-0.841D-08)	(-0.370D-03 0.371D-08)
(-0.715D-05-0.916D-05)	(0.108D-04 0.418D-05)	(-0.298D-02 0.365D-07)	(-0.318D-05-0.433D-05)	(0.126D-05 0.405D-05)
(-0.293D-02 0.208D-07)	(-0.274D-03-0.311D-07)	(0.548D-05 0.835D-05)	(-0.110D-02 0.145D-07)	(0.621D-03-0.619D-08)

THE 6-10 EIGENVECTORS

(-0.956D-02 0.482D-07)	(-0.118D+00-0.458D-08)	(-0.458D-03 0.170D-04)	(0.496D+00 0.300D-11)	(0.550D+00-0.119D-09)
(-0.291D-03 0.179D-04)	(0.426D-03 0.164D-04)	(-0.114D+00 0.680D-08)	(0.141D-02-0.729D-05)	(-0.543D-03-0.101D-04)
(-0.115D+00 0.212D-08)	(-0.138D-01-0.722D-07)	(0.211D-03 0.231D-04)	(0.276D+00 0.252D-07)	(-0.724D-01 0.220D-07)
(-0.304D-01-0.123D-06)	(0.331D+00 0.860D-10)	(0.130D-02-0.381D-04)	(0.113D-01 0.426D-08)	(0.206D-01-0.214D-08)
(0.785D-03-0.540D-04)	(-0.118D-02-0.451D-04)	(0.326D+00 0.136D-09)	(0.185D-03 0.149D-05)	(-0.650D-04-0.338D-05)
(0.318D+00-0.175D-09)	(0.307D-01 0.184D-06)	(-0.595D-03-0.595D-04)	(0.687D-01-0.627D-09)	(-0.333D-01 0.935D-08)
(-0.285D-03-0.133D-07)	(0.301D-02 0.191D-07)	(0.118D-04-0.553D-05)	(0.166D-03-0.841D-08)	(0.370D-03 0.371D-08)
(0.715D-05-0.916D-05)	(-0.108D-04 0.418D-05)	(0.298D-02 0.365D-07)	(0.318D-05-0.433D-05)	(-0.126D-05 0.405D-05)
(0.293D-02 0.208D-07)	(0.274D-03-0.311D-07)	(-0.548D-05 0.835D-05)	(0.110D-02 0.145D-07)	(-0.621D-03-0.619D-08)

THE 11-15 EIGENVECTORS

(-0.617D-03-0.380D-04)	(0.617D-03-0.380D-04)	(0.565D-01-0.459D-01)	(-0.945D-01 0.145D-01)	(-0.218D-01 0.634D-01)
(0.529D+00-0.108D-09)	(-0.529D+00-0.108D-09)	(-0.346D-01-0.948D-01)	(0.238D-01 0.184D-01)	(-0.927D-01-0.929D-05)
(-0.135D-02-0.215D-05)	(0.135D-02-0.215D-05)	(-0.805D-01 0.542D-03)	(-0.185D-01-0.478D-01)	(-0.250D-01-0.698D-01)
(0.166D-05 0.519D-06)	(-0.166D-05 0.519D-06)	(0.108D+00-0.153D+00)	(-0.334D+00 0.521D-03)	(-0.978D-01 0.142D+00)
(0.699D-01-0.159D-07)	(-0.699D-01-0.159D-07)	(-0.126D+00-0.343D+00)	(0.863D-01 0.668D-01)	(-0.336D+00 0.108D-05)
(-0.372D-03-0.258D-05)	(0.372D-03-0.258D-05)	(-0.338D+00 0.406D-03)	(-0.819D-01-0.201D+00)	(-0.106D+00-0.292D+00)
(0.331D-06-0.337D-05)	(-0.331D-06-0.337D-05)	(-0.320D+00 0.457D+00)	(0.100D+01 0.0)	(0.293D+00-0.421D+00)
(0.119D-02 0.299D-07)	(-0.119D-02 0.299D-07)	(0.374D+00 0.102D+01)	(-0.257D+00-0.199D+00)	(0.100D+01 0.0)
(-0.627D-05 0.575D-05)	(0.627D-05 0.575D-05)	(0.100D+01 0.0)	(0.245D+00 0.596D+00)	(0.316D+00 0.864D+00)

THE 16-18 EIGENVECTORS

(-0.945D-01-0.145D-01)	(-0.117D-02-0.255D-01)	(-0.117D-02 0.255D-01)
(0.238D-01-0.184D-01)	(-0.927D-01 0.278D-05)	(-0.927D-01-0.278D-05)
(-0.185D-01 0.478D-01)	(0.479D-01-0.216D-01)	(0.479D-01-0.216D-01)
(-0.334D+00-0.521D-03)	(0.442D-01-0.635D-01)	(0.442D-01 0.635D-01)
(0.863D-01-0.668D-01)	(-0.336D+00-0.348D-06)	(-0.336D+00 0.348D-06)
(-0.819D-01 0.201D+00)	(0.202D+00 0.903D-01)	(0.202D+00-0.903D-01)
(0.100D+01 0.0)	(-0.134D+00 0.189D+00)	(-0.134D+00-0.189D+00)
(-0.257D+00 0.199D+00)	(0.100D+01 0.0)	(0.100D+01 0.0)
(0.245D+00-0.596D+00)	(-0.599D+00-0.267D+00)	(-0.599D+00 0.267D+00)

M.2 PROGRAM FOR SYSTEM WITH BOTH SHELLS FLEXIBLE

M.2.1 Function of the Program

The program calculates the dimensionless eigenfrequencies, $\bar{\Omega}_o$, and the associated eigenvectors of a system of two coaxial cylindrical shells subjected to internal and annular incompressible viscous flows. For each set of input data of flow velocities $\bar{U}_i$, $\bar{U}_o$, the program constructs the matrices $[P_B]$ and $[Q]$ in the eigenvalue equation (6.78). The frequencies are then determined as the solutions of this eigenvalue equation.

M.2.2 Program Structure

The program is written in Fortran IV language. Its structure is the same as that of the program written for a system with a rigid outer shell as described in Section (M.1), involving the sequence MAIN PROGRAM, SUBROUTINE CONT, SUBROUTINE PREMAT, SUBROUTINE MKMAT, SUBROUTINE CMAT, SUBROUTINE REDUCE, SUBROUTINE EIGZC.

M.2.3 Description of the Program

The function of each subprogram is summarized as follows:

(1) Subroutine CONT evaluates the constants a_{km}, b_{km}, ..., h_{km}, j_{km} according to the formulae given in Appendix A.

(2) Subroutine PREMAT calculates the flow-independent terms in the elements of the matrices $[M]$ and $[K_B]$ in the matrix equation (6.77). The structure of matrix $[M]$ is shown in Appendix E and matrix $[K_B]$ can be obtained by replacing the A^{ℓ}_{kmn} terms in the matrix $[K]$ (shown in

Appendix E) by the corresponding B^{l}_{kmn} terms defined in equations (6.54-.71).

(3) Subroutine MKMAT completes the construction of matrices $[M]$ and $[K_B]$ by filling in the flow-dependent terms. These include (i) the generalized aerodynamic forces (q^{C1}_{kmn}, q^{F1}_{kmn}, q^{C3}_{kmn}, q^{F3}_{kmn}, r^{C1}_{kmn}, r^{F1}_{kmn}, r^{C3}_{kmn}, r^{F3}_{kmn}, as defined in Section 3.3), which are evaluated with the input data of flow velocities and computed values of the integrals involved, and (ii) terms associated with the fluid frictional forces and fluid pressurization (Γ_{i1}, Γ_{i2}, ..., Γ_{i5}, Γ_{o1}, ..., Γ_{o5}, defined in equation (6.52)) which also depend on the flow velocities as well as the friction factors found using equations (6.43) and (6.44).

(4) Subroutine CMAT constructs the matrix $[C]$ in the matrix equation (6.77) (The structure of $[C]$ is shown in Appendix E). The terms to be calculated are the generalized aerodynamic forces q^{C2}_{kmn}, q^{F2}_{kmn}, r^{C2}_{kmn}, r^{F2}_{kmn}, as defined in Section 3.3.

(5) Subroutine REDUCE constructs the matrices $[P_B]$ and $[Q]$, as defined in equations (6.78a) and (3.4.31), respectively.

(6) Subroutine EIGZC is the IMSL subroutine employed to solve the eigenvalue equation (6.78).

All the necessary parameters are defined in the main program. The flow velocities and the computed values of the integrals involved in the generalized aerodynamic forces are read from the data deck. The output results consist of all thirty-six eigenvalues and the upper half segment of the associated eigenvectors which contains the shell displacement vector $\{X\}$ (defined in equation (3.4.27)).

Notation used in the computer program, the computer program itself and a sample of the output are given in the following pages.

NOTATION USED IN THE PROGRAM

Notation used in the computer program	Corresponding notation used in the thesis	Definition
DDO	$\rho_o b/\Lambda_o$	See NOMENCLATURE
CA, CB		Coefficients associated with $U^2_{\tau a}$ and $U^2_{\tau b}$ on the right-hand side of equation (6.50), respectively
Q(9,3,3), R(6,3,3)		Integral terms in the generalized aerodynamic forces
MM(18,18)	$[M]$	See Appendix E
KK(18,18)	$[K_\theta]$	See equation (6.77)
CC(18,18)	$[C]$	See Appendix E
AA(36,36)	$[P_\beta]$	Defined in equation (6.78a)
BB(36,36)	$[Q]$	Defined in equation (3.4.31)
PO(I), PL(I); I = 1,2		The axial reactions per unit circumference at the x=0 and x=L ends of the inner (I=1) and outer (I=2) cylinders
BI, CI, DI	B_i, C_i, D_i	Defined in equations (6.34-.36), respectively
BO, CO, DO	B_o, C_o, D_o	Defined in equations (6.37-6.39), respectively

```
/INFO MVS TI(30) R(MUSIC) CL(30) N(STEVE SIU PUI CHAN)
//STEP1 EXEC FORTRAN
//FORT.SYSIN DD *
C*************************************************************************
C      COMPUTER PROGRAM FOR THE CASE OF INCOMPRESSIBLE VISCOUS FLOW      *
C      BOTH SHELLS FLEXIBLE                                              *
C      BOUNDARY CONDITIONS: CLAMPED-CLAMPED                              *
C*************************************************************************
C
C*************************************************************************
C      MAIN PROGRAM                                                      *
C*************************************************************************
       IMPLICIT REAL*8(A-H,O-Z)
       COMPLEX*16 MM(18,18),KK(18,18),CC(18,18)/324*(0.D0,0.D0)/,
      #AA(36,36)/1296*(0.D0,0.D0)/,BB(36,36)/1296*(0.D0,0.D0)/,EIGA(36),
      #EIGB(36),Z(36,36),WK(36,72),OMEGA,Q(9,3,3),R(6,3,3),CK(2,3,3)
       INTEGER DEL(3,3)
       REAL*8 NI,NO
       COMMON/DATA1/NI,NO,SKI,SKO,C(3),P(3),N
       COMMON/DATA2/EI,EO,ER,OMR
       COMMON/DATA3/ZI,ZO,USR,DSR,PI
       COMMON/DATA4/Q,R
       COMMON/DATA5/PPI,PPO,PO(2),PL(2),RMS,DEN,DDI,DDO,VIS,CA,CB
       DATA IA/36/,IB/36/,NN/36/,IJOB/2/,IZ/36/
       PI=DARCOS(-1.D0)
       C(1)=0.9825022145762379D0
       C(2)=1.00077731190727D0
       C(3)=0.9999664501254086D0
       P(1)=4.7300407448627D0
       P(2)=7.85320462409584D0
       P(3)=10.99560783800167D0
       EI=1/11.D0
       EO=0.1D0
       ER=10/11.D0
       RMS=(1-ER**2)/2/DLOG(1/ER)
       NI=0.30D0
       NO=0.30D0
       SKI=(5.50D-3)**2/12
       SKO=SKI*100/121
       OMR=11/10.D0
       ZI=2.330D1
       ZO=ZI/ER
       DSR=1.D0
       USR=1.D0
       N=3
       DEN=998.6D0
       DDI=8.261D-7
       DDO=DDI/ER
       VIS=1.1216D-6
       RM=DSQRT(RMS)
       RMA=RM/(RM-ER)
       LRA=DLOG(RM/ER)
       RMB=RM/(1-RM)
       LRB=DLOG(1/RM)
       CA=-0.7864D0-0.56*RMA+0.5064*RMA*LRA+0.56*RMA**2*LRA
       CB=0.7864D0-0.56*RMB-0.5064*RMB*LRB+0.56*RMB**2*LRB
       DO 3 K=1,3
       DO 3 M=1,3
```

```
      READ(5,*) (Q(I,K,M),I=1,9),(R(I,K,M),I=1,6)
    3 CONTINUE
      CALL CONT(C,P)
      CALL PREMAT(MM,KK)
      UI=0.0D0
      DO 1 L=1,3
      READ(5,*) UO
      CALL MKMAT(UI,UO,MM,KK)
      CALL CMAT(UI,UO,CC)
      CALL REDUCE(MM,KK,CC,AA,BB)
      CALL EIGZC(AA,IA,BB,IB,NN,IJOB,EIGA,EIGB,Z,IZ,WK,INFER,IER)
      PRINT10,UI,UO
   10 FORMAT('1','FLOW VELOCITY INSIDE THE INNER CYLINDER=',F8.5/'0','FL
     #OW VELOCITY IN THE ANNULAR REGION=',F8.5)
      PRINT13,PPO
   13 FORMAT('-','GAUGE PRESSURE AT THE UPSTREAM END OF THE CYLINDERS IN
     # THE ANNULAR FLUID REGION=',D24.16,' N/M**2')
      PRINT14,PPI
   14 FORMAT('0',52X,'IN THE INNER FLUID REGION=',D24.16,'N/M**2')
      PRINT15,PO(2),PL(2),PO(1),PL(1)
   15 FORMAT('-','AXIAL COMPRESSIVE LOAD ACTING ON THE X=0 END OF THE OU
     #TER CYLINDER=',D24.16,' N/M'/'0',37X,'X=L END',22X,'=',D24.16,' N/
     #M'/'-','AXIAL COMPRESSIVE LOAD ACTING ON THE X=0 END OF THE INNER
     #CYLINDER=',D24.16,' N/M'/'0',37X,'X=L END',22X,'=',D24.16,' N/M')
      PRINT11
   11 FORMAT('-','THE FREQUENCIES ARE:')
      DO 20 I=1,36
      OMEGA=-EIGA(I)/EIGB(I)
   20 PRINT12,OMEGA
   12 FORMAT('0','(',2D24.16,1X,')')
      DO 2 K=1,31,5
      M=K+4
      PRINT 21,K,M
    2 PRINT 22,((Z(I,J),J=K,M),I=1,18)
      PRINT 24
      PRINT 23,(Z(I,36),I=1,18)
   21 FORMAT('1','THE ',I2,'-',I2,' EIGENVECTORS')
   22 FORMAT(//5(2X,'(',2D10.3,')')/)
   23 FORMAT(//(2X,'(',2D10.3,')')/)
   24 FORMAT('1','THE ','36',' EIGENVECTOR')
    1 CONTINUE
      PRINT100
  100 FORMAT('1')
      STOP
      END
C
C*************************************************************************
C     SUBROUTINE CONT                                                    *
C*************************************************************************
      SUBROUTINE CONT(C,P)
      IMPLICIT REAL*8(A-H,O-Z)
      DIMENSION A(3,3),B(3,3),C(3),D(3,3),SE(3,3),SF(3,3),G(3,3),H(3,3),
     #SJ(3,3),SL(3,3),DEL(3,3),P(3)
      INTEGER DEL
      COMMON/CON1/A,B,D,DEL
      COMMON/CON2/SE,SF,G,H,SJ,SL
      DO 3 K=1,3
      DO 3 M=1,3
```

```
      IF(K.EQ.M) GO TO 1
      DEM=P(M)**4-P(K)**4
      PC=P(M)*C(M)-P(K)*C(K)
      PWR=(-1)**(K+M)
      PMKS=P(M)**2*P(K)**2
      A(K,M)=-4*PMKS*(PWR+1)*PC/DEM
      B(K,M)=0.D0
      D(K,M)=-A(K,M)
      SE(K,M)=4*(3*P(M)**4+P(K)**4)*PMKS*P(M)*P(K)*(1-PWR)/DEM**2
      SF(K,M)=4*PMKS*(1-PWR)/DEM
      G(K,M)=-4*PWR*PMKS*PC/DEM-2*(P(M)**4+P(K)**4)*SF(K,M)/DEM
      SL(K,M)=-SF(K,M)
      H(K,M)=4*PWR*PMKS*PC/DEM-(3*P(M)**4+P(K)**4)*SL(K,M)/DEM
      SJ(K,M)=16*PMKS*P(M)*P(K)*C(M)*C(K)*(PWR-1)/DEM**2
      DEL(K,M)=0
      GO TO 3
1     A(K,K)=P(K)*C(K)*(P(K)*C(K)-2)
      B(K,K)=-P(K)**4
      D(K,K)=-A(K,K)
      SE(K,K)=-B(K,K)/2
      SF(K,K)=0.D0
      G(K,K)=A(K,K)/2
      H(K,K)=-G(K,K)
      SJ(K,K)=0.5D0
      SL(K,K)=0.D0
      DEL(K,K)=1
3     CONTINUE
      RETURN
      END
C
C*****************************************************************************
C     SUBROUTINE PREMAT                                                      *
C*****************************************************************************
      SUBROUTINE PREMAT(MM,KK)
      IMPLICIT REAL*8(A-H,O-Z)
      DIMENSION A(3,3),B(3,3),D(3,3),DEL(3,3),COEM(3,3,3),COE(2,9,3,3)
      COMPLEX*16 MM(18,18),KK(18,18)
      REAL*8 NI,NO,NU
      INTEGER DEL,R,Q,W,V,H
      COMMON/DATA1/NI,NO,SKI,SKO,C(3),P(3),N
      COMMON/DATA2/EI,EO,ER,OMR
      COMMON/CON1/A,B,D,DEL
      COMMON/COEF/COE
      DO 9 I=1,18
      DO 9 J=1,18
      MM(I,J)=(0.D0,0.D0)
9     KK(I,J)=(0.D0,0.D0)
      DO 3 K=1,3
      DO 3 M=1,3
      COEM(1,K,M)=A(K,M)
      COEM(2,K,M)=DEL(K,M)
3     COEM(3,K,M)=DEL(K,M)
      J=0
      E=EI
      NU=NI
      SK=SKI
12    JJ=J+1
      DO 4 K=1,3
```

```
      DO 4 M=1,3
      COE(JJ,1,K,M)=E**2*B(K,M)+(NU-1)*(SK+1)*N**2*A(K,M)/2
      COE(JJ,2,K,M)=-(1+NU)*N*E**2*D(K,M)/2
      COE(JJ,3,K,M)=(P(M)*E)**4*SK*DEL(K,M)-(2*NU-SK*(1-NU)*N**2)
     C*E**2*D(K,M)/2
      COE(JJ,4,K,M)=(1+NU)*N*A(K,M)/2
      COE(JJ,5,K,M)=-N**2*DEL(K,M)+(1+3*SK)*(1-NU)*E**2*D(K,M)/2
      COE(JJ,6,K,M)=SK*(3-NU)*N*E**2*D(K,M)/2-N*DEL(K,M)
      COE(JJ,7,K,M)=(NU+(NU-1)*SK*N**2/2)*A(K,M)-SK*E**2*B(K,M)
      COE(JJ,8,K,M)=-N*DEL(K,M)+(3-NU)*SK*N*E**2*D(K,M)/2
 4    COE(JJ,9,K,M)=-SK*(((P(M)*E)**4+(N**2-1)**2)*DEL(K,M)-2*(N*E)
     #**2*D(K,M))-DEL(K,M)
      K=0
      DO 5 I=1,7,3
      K=K+1
      DO 5 M=1,3
      R=I+J*9
      Q=M+J*9
      DO 6 L=1,3
      H=L-1
 6    MM(R+H,Q+3*H)=COEM(L,K,M)/(J-(J-1)*OMR**2)
 5    CONTINUE
      IF(J.EQ.1) GO TO 8
      J=1
      E=EO
      NU=NO
      SK=SKO
      GO TO 12
 8    CONTINUE
      RETURN
      END
C
C*****************************************************************************
C     SUBROUTINE MKMAT                                                        *
C*****************************************************************************
      SUBROUTINE MKMAT(UI,UO,MM,KK)
      IMPLICIT REAL*8(A-H,O-Z)
      COMPLEX*16 MM(18,18),KK(18,18),CK(2,3,3),Q(9,3,3),R(6,3,3)
      INTEGER DEL(3,3),W,V,HH
      REAL*8 NU,NI,NO
      DIMENSION A(3,3),B(3,3),D(3,3),SE(3,3),SF(3,3),G(3,3),H(3,3),
     #SJ(3,3),SL(3,3),COE(2,9,3,3),CCOE(9,3,3)
      COMMON/DATA1/NI,NO,SKI,SKO,C(3),P(3),N
      COMMON/DATA2/EI,EO,ER,OMR
      COMMON/DATA3/ZI,ZO,USR,DSR,PI
      COMMON/DATA4/Q,R
      COMMON/DATA5/PPI,PPO,PO(2),PL(2),RMS,DEN,DDI,DDO,VIS,CA,CB
      COMMON/CON1/A,B,D,DEL
      COMMON/CON2/SE,SF,G,H,SJ,SL
      COMMON/COEF/COE
      FA(RR,RE)=DSQRT(0.0055*(1+(20000*RR+1.D6/RE)**(1./3.)))
      F(RR,RE)=1/(-4*DLOG10(RR/3.7+2.51/RE/FA(RR,RE)))**2
      SU=5.3082D3
      UOM=UO*SU
      UIM=UI*SU
      RR=0.D0
      RO=UOM*2*(EO-EI)/VIS
      RI=UIM*2*EI/VIS
```

```
      IF(RI.EQ.0.D0) GO TO 10
      FI=F(RR,RI)
      GO TO 11
   10 FI=0.D0
   11 IF(RO.EQ.0.D0) GO TO 12
      FO=F(RR,RO)
      GO TO 13
   12 FO=0.D0
   13 PPI=DEN*FI*UIM**2/EI+0.5D5
      PPO=DEN*FO*UOM**2/(EO-EI)+0.5D5
      UTBS=(1-RMS)/2/(1-ER)*FO*UOM**2
      UTAS=(RMS-ER**2)/2/ER/(1-ER)*FO*UOM**2
      UTS=FI*UIM**2/2
      BI=UTS+UTAS
      CI=2*UTS/EI-2*UTBS/EO/(1-RMS)
      DI=(PPO-PPI)/DEN
      BO=UTBS
      CO=2*UTBS/EO/(1-RMS)
      DO=-(CA*UTAS+CB*UTBS)-PPO/DEN
      J=0
      E=EI
      NU=NI
      BB=BI
      CC=CI
      DD=DI
      BD=DDI
   14 GM1=-BB*BD/E
      GM2=-(NU*CC*BD+GM1)/2-NU*DD*BD
      GM3=BB*BD
      GM4=-CC*BD
      GM5=-DD*BD
      JJ=J+1
      PO(JJ)=((NU*E*CC-BB)/2+NU*E*DD)*DEN
      PL(JJ)=((NU*E*CC+BB)/2+NU*E*DD)*DEN
      DO 4 K=1,3
      DO 4 M=1,3
      CCOE(1,K,M)=COE(JJ,1,K,M)+GM1*E**2*SE(K,M)+GM2*E**2*B(K,M)-GM4*N**
     #2*G(K,M)-GM5*N**2*A(K,M)
      CCOE(2,K,M)=COE(JJ,2,K,M)
      CCOE(3,K,M)=COE(JJ,3,K,M)+GM4*E**2*H(K,M)+GM5*E**2*D(K,M)
      CCOE(4,K,M)=COE(JJ,4,K,M)+GM3*N/E*SF(K,M)
      CCOE(5,K,M)=COE(JJ,5,K,M)+GM1*E**2*H(K,M)+GM2*E**2*D(K,M)-GM4*N**
     #2*SJ(K,M)-GM5*N**2*DEL(K,M)
      CCOE(6,K,M)=COE(JJ,6,K,M)-GM4*N*SJ(K,M)-GM5*N*DEL(K,M)
      CCOE(7,K,M)=COE(JJ,7,K,M)+GM3/E*SF(K,M)-GM4*G(K,M)-GM5*A(K,M)
      CCOE(8,K,M)=COE(JJ,8,K,M)-GM4*N*SJ(K,M)-GM5*N*DEL(K,M)
      CCOE(9,K,M)=COE(JJ,9,K,M)+GM1*E**2*H(K,M)+GM2*E**2*D(K,M)-GM4*N**2
     #*SJ(K,M)-GM5*N**2*DEL(K,M)
    4 CK(JJ,K,M)=CCOE(9,K,M)
      K=0
      DO 5 I=1,7,3
      K=K+1
      DO 5 M=1,3
      IR=I+J*9
      IQ=M+J*9
      W=-1
      DO 6 V=1,7,3
      W=W+1
```

```
      DO 6 L=1,3
      HH=L-1
    6 KK(IR+HH,IQ+V-1)=CCOE(L+3*W,K,M)
    5 CONTINUE
      IF(J.EQ.1) GO TO 8
      J=1
      E=EO
      NU=NO
      BB=BO
      CC=CO
      DD=DO
      BD=DDO
      GO TO 14
    8 Q1=ZI*EI/2/PI/EO**2/USR**2
      Q2=Q1*DSR
      Q3=UI**2*ZI*EI/2/PI
      Q4=UO**2*ZI*EI*DSR/2/PI/USR**2
      R1=ZO/2/PI/EO
      R2=UO**2*ZO*EO/2/PI
      K=0
      DO 1 I=3,9,3
      K=K+1
      N=I+9
      DO 1 M=1,3
      L=M+6
      J=L+9
      KK(I,L)=CK(1,K,M)+Q3*Q(3,K,M)-Q4*Q(6,K,M)
      KK(I,J)=-Q4*Q(9,K,M)
      MM(I,L)=DEL(K,M)/OMR**2+Q1*Q(2,K,M)-Q2*Q(5,K,M)
      MM(I,J)=-Q2*Q(8,K,M)
      KK(N,J)=CK(2,K,M)+R2*R(6,K,M)
      KK(N,L)=R2*R(3,K,M)
      MM(N,J)=DEL(K,M)+R1*R(5,K,M)
      MM(N,L)=R1*R(2,K,M)
    1 CONTINUE
      RETURN
      END
C
C*****************************************************************************
C     SUBROUTINE CMAT                                                        *
C*****************************************************************************
      SUBROUTINE CMAT(UI,UO,CC)
      IMPLICIT REAL*8(A-H,O-Z)
      COMPLEX*16 CC(18,18),Q(9,3,3),R(6,3,3)
      COMMON/DATA2/EI,EO,ER,OMR
      COMMON/DATA3/ZI,ZO,USR,DSR,PI
      COMMON/DATA4/Q,R
      Q5=UI*ZI*ER/PI/USR
      Q6=UO*ZI*ER*DSR/PI/USR**2
      R3=UO*ZO/PI
      DO 1 K=1,3
      I=3*K
      II=I+9
      DO 1 M=1,3
      J=M+6
      JJ=J+9
      CC(I,J)=-Q5*Q(1,K,M)+Q6*Q(4,K,M)
      CC(I,JJ)=Q6*Q(7,K,M)
```

```
      CC(II,J)=-R3*R(1,K,M)
      CC(II,JJ)=-R3*R(4,K,M)
    1 CONTINUE
      RETURN
      END
C
C*****************************************************************************
C     SUBROUTINE REDUCE                                                      *
C*****************************************************************************
      SUBROUTINE REDUCE(MM,KK,CC,AA,BB)
      COMPLEX*16 AA(36,36),BB(36,36),MM(18,18),KK(18,18),CC(18,18)
      DO 1 I=1,18
      AA(I,I+18)=(1.D0,0.D0)
      BB(I,I)=(-1.D0,0.D0)
    1 CONTINUE
      DO 2 I=1,18
      DO 2 J=1,18
      AA(18+I,J)=KK(I,J)
      AA(18+I,18+J)=CC(I,J)
      BB(18+I,18+J)=MM(I,J)
    2 CONTINUE
      RETURN
      END
//GO.SYSIN DD *
(-0.3280206164830202D-06,0.D0)
(0.1896062132537650D+00,0.D0)
(0.2312184916463780D+01,0.D0)
(0.6190663329733319D-06,0.9114964994383228D-15)
(-0.6759592315814779D+00,0.6040495708646455D-15)
(-0.8122943495441742D+01,-0.1783665717388016D-12)
(-0.5949173465983090D-06,0.2730464022728906D-17)
(0.7138061018030161D+00,-0.514772887066836 9D-15)
(0.8569145764091334D+01,0.1145911243714064D-12)
(0.5408339515794209D-06,0.4252013678016080D-15)
(-0.6489146380026265D+00,0.4649481588998984D-15)
(-0.7790132512812177D+01,-0.1342991415052941D-12)
(-0.6771914051714807D-06,0.2336123706823247D-15)
(0.7435324606622264D+00,-0.3953589880319306D-15)
(0.8934416806883038D+01,0.8421966111077975D-13)
(-0.1029541159227697D-16,-0.6285111159652311D+00)
(-0.4766713517681613D-17,0.2348738759364798D-07)
(0.1628817143484548D-16,0.5581861620806592D-04)
(-0.8161994647154542D-15,0.2207959405904953D+01)
(-0.9633476396856025D-15,-0.4420631811524404D-07)
(0.3248617160053225D-12,-0.1050433756703668D-03)
(-0.7896814912951367D-15,-0.2329277443221273D+01)
(0.8166325603169927D-15,0.4244661030438371D-07)
(-0.1947442668883681D-12,0.1008576980023068D-03)
(0.8289664281683351D-14,0.2117524948383588D+01)
(-0.9792191731388415D-15,-0.3858782759559040D-07)
(-0.7733679049467813D-13,-0.9168881635822351D-04)
(-0.6766979859523874D-14,-0.2428534253154542D+01)
(0.7903454115827526D-15,0.4835465234972159D-07)
(0.7284915850159565D-13,0.1149004051113856D-03)
(-0.1525785682687179D-05,0.8129588219495467D-17)
(0.6318529334634996D-03,0.2371590276574419D-18)
(-0.1842035225332608D+01,0.2469456692931669D-17)
(0.2881073360038401D-05,0.3146543647328196D-13)
```

(-0.6372597942142652D-02,-0.1397338347729216D-14)
(0.6485864327386988D+01,-0.1082602378816420D-11)
(-0.2769121159207947D-05,-0.2196590551975507D-13)
(0.7017078876918594D-02,0.1049768623391913D-14)
(-0.6844252009758827D+01,0.7285050198337377D-12)
(0.2517382871767113D-05,0.2502434899182478D-13)
(-0.6379162615243331D-02,-0.1052366471568723D-14)
(0.6222047281603371D+01,-0.9163929289836358D-12)
(-0.3151609586744456D-05,-0.1717996837028040D-13)
(0.7027982593785703D-02,0.7838016151482439D-15)
(-0.7133930243991075D+01,0.6068625400795199D-12)
(-0.1029541159227697D-16,0.6285111159652311D+00)
(-0.4766713517681613D-17,-0.2348738759364798D-07)
(0.1628817143484548D-16,-0.5581861620806592D-04)
(0.8884379566400543D-15,-0.2207959405904953D+01)
(0.9976375229975989D-15,0.4420631811524404D-07)
(-0.3249472677089020D-12,0.1050433756703668D-03)
(0.7134810718936100D-15,0.2329277443221273D+01)
(-0.8528640651383555D-15,-0.4244661030438371D-07)
(0.1948324113980102D-12,-0.1008576980023068D-03)
(-0.8220391173136591D-14,-0.2117524948383588D+01)
(0.1012156904794655D-14,0.3858782759559040D-07)
(0.7725665912227731D-13,0.9168881635822351D-04)
(0.6687525215708392D-14,0.2428534253154542D+01)
(-0.8280645177715693D-15,-0.4835465234972159D-07)
(-0.7275519458967751D-13,-0.1149004051113856D-03)
(-0.5845163463897832D-05,0.D0)
(0.1874795661657285D+00,0.D0)
(0.8541245969912896D+01,0.D0)
(0.1094831275117628D-04,-0.9403806651428478D-13)
(-0.6551227020549533D+00,0.3629635273343210D-14)
(-0.2934937066445356D+02,0.3409919784229403D-11)
(-0.1049698053587602D-04,0.6488410355947742D-13)
(0.6908633621273766D+00,-0.2663248619134660D-14)
(0.3091333379178624D+02,-0.2319704810248190D-11)
(0.9542709579259302D-05,-0.1156875277383343D-12)
(-0.6280576019341661D+00,0.3825841999713141D-14)
(-0.2810303071981653D+02,0.4465622672323831D-11)
(-0.1197471004215592D-04,0.7849958137573403D-13)
(0.7205530776322418D+00,-0.2734317652635607D-14)
(0.3227826606765166D+02,-0.2991284808234241D-11)
(0.3245031071165055D-16,-0.1020380446668096D+01)
(-0.6494989735391820D-17,-0.1001263295044486D-06)
(-0.3708457815126825D-15,-0.2368581614173008D-03)
(0.5827035508300584D-13,0.3481847626998819D+01)
(-0.1049759241826247D-14,0.1887126541802776D-06)
(-0.2935986399221754D-11,0.4463713138848790D-03)
(-0.3608184921736982D-13,-0.3665667574609826D+01)
(0.6106639506547822D-15,-0.1812772250460474D-06)
(0.1863968377723573D-11,-0.4287704796688965D-03)
(0.5785951407214072D-14,0.3332425067828181D+01)
(0.4249815393813545D-15,0.1647974772513057D-06)
(-0.9243694423341424D-12,0.3897913450954734D-03)
(-0.3007502803462137D-15,-0.3829206018116956D+01)
(0.4151863472895973D-15,-0.2064264201705002D-06)
(0.5116057671682966D-12,-0.4882696959283045D-03)
(-0.1525785682687179D-05,-0.8129588219495467D-17)
(0.6318529334634996D-03,-0.2371590276574419D-18)

```
(-0.1842035225332608D+01,-0.2469456692931669D-17)
(0.2881073360038401D-05,0.3152308191943916D-13)
(-0.6372597942142652D-02,-0.1395647285094802D-14)
(0.6485864327386988D+01,-0.1082583167229549D-11)
(-0.2769121159207947D-05,-0.2202675498652739D-13)
(0.7017078876918594D-02,0.1047982834621040D-14)
(-0.6844252009758827D+01,0.7284846121116094D-12)
(0.2517382871767113D-05,0.2507966668889053D-13)
(-0.6379162615243331D-02,-0.1050743027231568D-14)
(0.6222047281603371D+01,-0.9163743765089733D-12)
(-0.3151609586744456D-05,-0.1724337492465774D-13)
(0.7027982593785703D-02,0.7819415002230843D-15)
(-0.7133930243991075D+01,0.6068414002957997D-12)
(0.3245031071165055D-16,0.1020380446668096D+01)
(-0.6494989735391820D-17,0.1001263295044486D-06)
(-0.3708457815126825D-15,0.2368581614173008D-03)
(-0.5849237066104017D-13,-0.3481847626998819D+01)
(0.1094816421191028D-14,-0.1887126541802776D-06)
(0.2938548715885774D-11,-0.4463713138848790D-03)
(0.3631563021553369D-13,0.3665667574609826D+01)
(-0.6581554102431736D-15,0.1812772250460474D-06)
(-0.1866668515549782D-11,0.4287704796688965D-03)
(-0.5998479587362754D-14,-0.3332425067828181D+01)
(-0.3818074852101207D-15,-0.1647974772513057D-06)
(0.9268241130852384D-12,-0.3897913450954734D-03)
(0.5449175538252418D-15,0.3829206018116956D+01)
(0.3656306024357804D-15,0.2064264201705002D-06)
(-0.5144238698130742D-12,0.4882696959283045D-03)
(-0.7209652058832401D-05,0.D0)
(0.1842879810863270D+00,0.D0)
(0.1797966673170376D+02,0.D0)
(0.1361799752242200D-04,0.1967468088413858D-12)
(-0.6253330262705698D+00,-0.8825999633830738D-14)
(-0.5977549941567372D+02,-0.5833364557530585D-11)
(-0.1309009494198558D-04,-0.1421976233591080D-12)
(0.6580636959632403D+00,0.6694176618350606D-14)
(0.6280648449464918D+02,0.4027927694837117D-11)
(0.1190008631203729D-04,0.1697832081055174D-12)
(-0.5982397236030192D+00,-0.7144912928212175D-14)
(-0.5709680408604452D+02,-0.5400575466090407D-11)
(-0.1489682485360829D-04,-0.1208661458018139D-12)
(0.6876998626623333D+00,0.5367088152614521D-14)
(0.6573090386110939D+02,0.3671070834977743D-11)
0.00500D0
0.01000D0
0.01500D0
//
/*
```

FLOW VELOCITY INSIDE THE INNER CYLINDER= 0.0

FLOW VELOCITY IN THE ANNULAR REGION= 0.00300

GAUGE PRESSURE AT THE UPSTREAM END OF THE CYLINDERS IN THE ANNULAR FLUID REGION= 0.154210[illegible]572671590+06 N/M**2

IN THE INNER FLUID REGION= 0.0 N/M**2

AXIAL COMPRESSIVE LOAD ACTING ON THE X=0 END OF THE OUTER CYLINDER= -0.296163026448790D+04 N/M

X=L END = -0.249512261869315D+04 N/M

AXIAL COMPRESSIVE LOAD ACTING ON THE X=0 END OF THE INNER CYLINDER= 0.254389640594663D+04 N/M

X=L END = 0.302547120478197D+04 N/M

THE FREQUENCIES ARE:

(-0.346794896549998D+01 0.624804487442112D-11)
(-0.333346503507211OD+01 -0.199922307576455D-11)
(-0.338621028070783D+01 -0.186098033286530D-11)
(-0.318378071078310D+01 0.544928570149022D-11)
(-0.303532498115360D+01 -0.515081375540490D-11)
(-0.309353372848385OD+01 -0.110975663422574D-10)
(-0.221558261219931D+01 0.254330932743275D-12)
(-0.182779333449842D+01 0.263218164672319D-10)
(-0.199978484842488D+01 -0.796015884165285D-11)
(-0.205891221666480D+01 -0.547227387432072D-12)
(-0.208026923510595D+01 -0.811930784349292D-11)
(-0.191449522579294D+01 0.258889282308683D-10)
(0.346794896944022D+01 0.621381206615557D-11)
(0.333346503506677OD+01 -0.200358125624854D-11)
(0.338621028065346D+01 -0.182947618289166D-11)
(0.318378071065893D+01 0.544678550528847D-11)
(0.303532498114655D+01 -0.516240293834680D-11)
(0.309353372840862D+01 -0.110722181352532D-10)

```
(  0.221558261218591 3D+01   0.254110723134495 9D-12 )
(  0.182779333446881 7D+01  -0.263092911093706 9D-10 )
(  0.199978484842006 7D+01  -0.794308254919338 4D-11 )
(  0.205891221663975 0D+01  -0.558292067486402 8D-12 )
(  0.208026923509785 7D+01  -0.810229511935814 5D-11 )
(  0.191449522577788 8D+01   0.258690568594325 3D-10 )
(  0.437974575264576 0D-01   0.105456640771663 0D-07 )
( -0.437974667258665 0D-01   0.105468010956047 2D-07 )
( -0.244908948335760 5D-01  -0.729107353602772 3D-07 )
(  0.244908888198106 0D-01  -0.729098663897755 0D-07 )
( -0.138979783507136 4D-01   0.220316821295738 5D-06 )
( -0.109549503160139 4D-01  -0.167746300437623 7D-06 )
(  0.138979562801445 8D-01   0.220315857069217 8D-06 )
(  0.109549497261201 5D-01  -0.167746326619157 3D-06 )
( -0.682702999971677 6D-02   0.262458451926227 2D-06 )
( -0.485842468949730 7D-09   0.244747154781557 6D-02 )
(  0.682702532207670 2D-02   0.262460294972157 8D-06 )
( -0.484579098852412 6D-09  -0.244797693335315 6D-02 )
```

THE 1- 5 EIGENVECTORS

(0.843D-02-0.946D-09)	(0.106D+00 0.168D-09)	(-0.459D-04 0.316D-05)	(-0.864D-03-0.548D-09)	(-0.741D-02 0.207D-09)
(-0.284D-04 0.325D-05)	(0.456D-04 0.309D-05)	(0.102D+00-0.118D-09)	(-0.249D-05-0.195D-05)	(0.203D-05 0.153D-06)
(0.103D+00-0.431D-10)	(0.124D-01 0.165D-08)	(0.229D-04 0.427D-05)	(-0.629D-02 0.619D-10)	(-0.896D-03-0.188D-09)
(0.276D-01 0.260D-08)	(-0.300D+00 0.178D-12)	(0.137D-03-0.718D-05)	(-0.133D-02 0.176D-08)	(0.164D-01-0.610D-09)
(0.797D-04-0.990D-05)	(-0.129D-03-0.857D-05)	(-0.295D+00 0.163D-12)	(0.673D-05 0.481D-05)	(-0.409D-05-0.329D-06)
(-0.288D+00-0.518D-12)	(-0.279D-01-0.425D-08)	(-0.650D-04-0.111D-04)	(0.137D-01-0.589D-10)	(0.142D-02 0.346D-09)
(0.781D-03 0.322D-09)	(-0.877D-02-0.435D-09)	(0.396D-05-0.118D-05)	(0.692D-03-0.263D-09)	(-0.818D-02 0.306D-09)
(0.226D-05-0.186D-05)	(-0.377D-05 0.618D-06)	(-0.851D-02-0.804D-09)	(-0.184D-05-0.169D-05)	(0.314D-05 0.204D-06)
(-0.813D-02-0.425D-09)	(-0.813D-03 0.631D-09)	(-0.187D-05 0.133D-05)	(-0.746D-02 0.289D-09)	(-0.726D-03-0.321D-09)
(0.197D-03-0.936D-11)	(0.328D-02 0.590D-10)	(-0.723D-06 0.242D-06)	(0.134D-01 0.192D-08)	(0.118D+00-0.366D-09)
(-0.388D-06 0.457D-06)	(0.206D-05-0.248D-06)	(0.307D-02 0.234D-09)	(0.290D-04 0.702D-05)	(-0.457D-04 0.703D-05)
(0.293D-02 0.182D-09)	(0.368D-03-0.497D-09)	(0.147D-05-0.650D-06)	(0.114D+00 0.101D-09)	(0.140D-01-0.328D-08)
(0.953D-03 0.175D-09)	(-0.113D-01-0.531D-09)	(0.376D-06-0.126D-05)	(0.292D-01-0.514D-08)	(-0.329D+00 0.559D-12)
(0.154D-05-0.166D-05)	(-0.694D-05 0.836D-06)	(-0.107D-01-0.852D-09)	(-0.795D-04-0.214D-04)	(0.127D-03-0.192D-04)
(-0.987D-02-0.613D-09)	(-0.102D-02 0.153D-08)	(-0.470D-05 0.208D-05)	(-0.314D+00-0.538D-12)	(-0.292D-01 0.818D-08)
(0.665D-03 0.245D-09)	(-0.753D-02-0.354D-09)	(0.338D-05-0.930D-06)	(0.898D-03-0.755D-09)	(-0.104D-01 0.105D-08)
(0.192D-05-0.145D-05)	(-0.325D-05 0.469D-06)	(-0.729D-02-0.641D-09)	(-0.240D-05-0.486D-05)	(0.399D-05 0.178D-05)
(-0.693D-02-0.320D-09)	(-0.699D-03 0.521D-09)	(-0.163D-05 0.103D-05)	(-0.962D-02 0.105D-08)	(-0.914D-03-0.152D-08)

THE 6-10 EIGENVECTORS

(-0.329D-05-0.105D-05)	(-0.451D+00-0.663D-13)	(0.287D-02-0.290D-09)	(-0.500D+00 0.198D-11)	(0.203D-01-0.208D-08)
(-0.672D-02 0.418D-09)	(0.143D-03-0.124D-05)	(-0.341D-06-0.489D-06)	(-0.575D-04-0.170D-05)	(0.283D-04 0.732D-05)
(0.580D-06 0.411D-06)	(-0.253D+00-0.477D-09)	(-0.111D-02 0.241D-10)	(0.651D-01-0.411D-09)	(0.148D-02 0.196D-08)
(0.935D-05 0.276D-05)	(-0.101D-01-0.813D-10)	(0.697D-03-0.470D-10)	(-0.184D-01 0.453D-10)	(0.990D-03-0.356D-10)
(0.153D-01-0.968D-09)	(0.184D-04 0.257D-06)	(-0.256D-06-0.371D-06)	(-0.677D-05-0.563D-06)	(0.423D-05 0.134D-05)
(-0.898D-06-0.850D-06)	(-0.619D-01 0.140D-10)	(-0.122D-02 0.535D-10)	(0.296D-01-0.174D-09)	(0.164D-02 0.499D-09)
(-0.328D-05-0.113D-05)	(-0.472D-03 0.160D-09)	(-0.122D-02 0.727D-10)	(-0.102D-02-0.796D-10)	(-0.547D-03-0.127D-09)
(-0.788D-02 0.561D-09)	(0.962D-06-0.741D-06)	(0.444D-06 0.667D-06)	(-0.428D-06 0.673D-06)	(-0.871D-06-0.707D-06)
(0.155D-05 0.689D-06)	(-0.295D-02-0.278D-09)	(0.192D-02-0.956D-10)	(0.160D-02 0.115D-09)	(-0.342D-02 0.238D-09)
(0.460D-04 0.746D-05)	(-0.308D-02-0.278D-09)	(-0.547D+00-0.788D-11)	(-0.817D-02-0.143D-08)	(-0.486D+00 0.129D-12)
(0.113D+00 0.313D-09)	(0.383D-07-0.408D-06)	(0.575D-04-0.497D-05)	(-0.367D-05 0.100D-05)	(-0.142D-03-0.352D-05)
(-0.229D-04 0.953D-05)	(-0.291D-02-0.269D-09)	(0.706D-01 0.111D-08)	(-0.251D-02-0.754D-09)	(-0.269D+00 0.127D-08)
(-0.136D-03-0.162D-04)	(0.248D-03-0.811D-10)	(-0.243D-01-0.136D-09)	(0.209D-03-0.533D-11)	(-0.138D-01 0.264D-09)
(-0.323D+00 0.116D-11)	(-0.551D-06 0.274D-06)	(0.810D-05-0.199D-05)	(-0.394D-06-0.784D-07)	(-0.224D-04 0.849D-06)
(0.642D-04-0.239D-04)	(0.545D-03 0.147D-10)	(0.386D-01 0.575D-09)	(-0.136D-02-0.272D-09)	(-0.812D-01-0.332D-10)
(-0.421D-05-0.312D-05)	(-0.398D-03 0.102D-09)	(-0.154D-02 0.246D-09)	(-0.863D-03-0.635D-10)	(-0.691D-03-0.505D-09)
(-0.101D-01 0.196D-08)	(0.802D-06-0.510D-06)	(0.562D-06 0.236D-05)	(-0.370D-06 0.435D-06)	(-0.118D-05-0.245D-05)
(0.199D-05 0.369D-05)	(-0.248D-02-0.183D-09)	(0.245D-02-0.379D-09)	(0.132D-02 0.872D-10)	(-0.435D-02 0.872D-09)

THE 11-15 EIGENVECTORS

(-0.534D-04-0.668D-05)	(0.687D-05 0.348D-05)	(-0.843D-02-0.943D-09)	(-0.106D+00 0.167D-09)	(0.459D-04 0.316D-05)
(-0.481D+00 0.187D-11)	(0.449D-02-0.553D-09)	(0.284D-04 0.324D-05)	(-0.456D-04 0.310D-05)	(-0.102D+00-0.118D-09)
(-0.138D-03-0.408D-06)	(-0.145D-05-0.960D-06)	(-0.103D+00-0.429D-10)	(-0.124D-01 0.164D-08)	(-0.229D-04 0.425D-05)
(0.454D-06 0.840D-07)	(0.327D-06 0.443D-06)	(-0.276D-01 0.259D-08)	(0.300D+00 0.181D-12)	(-0.137D-03-0.721D-05)
(-0.625D-01 0.319D-09)	(0.244D-02-0.333D-09)	(-0.797D-04-0.985D-05)	(0.129D-03-0.860D-05)	(0.295D+00 0.160D-12)
(-0.375D-04-0.468D-06)	(-0.149D-05-0.797D-06)	(0.288D+00-0.513D-12)	(0.279D-01-0.424D-08)	(0.650D-04-0.111D-04)
(0.794D-07-0.577D-06)	(-0.950D-07-0.615D-06)	(-0.781D-03 0.322D-09)	(0.877D-02-0.436D-09)	(-0.396D-05-0.118D-05)
(-0.325D-02-0.602D-09)	(-0.385D-02 0.528D-09)	(-0.226D-05-0.185D-05)	(0.377D-05 0.620D-06)	(0.851D-02-0.803D-09)
(-0.207D-05 0.102D-05)	(0.202D-05 0.975D-06)	(0.813D-02-0.423D-09)	(0.813D-03 0.627D-09)	(0.187D-05 0.132D-05)
(-0.275D-04 0.643D-05)	(0.581D-04-0.186D-04)	(-0.197D-03-0.980D-11)	(-0.328D-02 0.596D-10)	(0.723D-06 0.243D-06)
(-0.349D-02 0.118D-08)	(-0.522D+00-0.707D-11)	(0.388D-06 0.454D-06)	(-0.206D-05-0.249D-06)	(-0.307D-02 0.235D-09)
(-0.162D-04 0.427D-05)	(0.139D-03-0.104D-05)	(-0.293D-02 0.181D-09)	(-0.368D-03-0.494D-09)	(-0.147D-05-0.646D-06)
(-0.811D-06 0.410D-06)	(0.450D-07 0.337D-06)	(-0.953D-03 0.176D-09)	(0.113D-01-0.531D-09)	(-0.376D-05-0.126D-05)
(0.105D-02 0.493D-09)	(-0.827D-01-0.971D-09)	(-0.154D-05-0.165D-05)	(0.694D-05 0.839D-06)	(0.107D-01-0.852D-09)
(-0.410D-05 0.964D-06)	(0.460D-04-0.151D-05)	(0.987D-02-0.609D-09)	(0.102D-02 0.152D-08)	(0.470D-05 0.207D-05)
(0.506D-07-0.389D-06)	(-0.135D-06-0.204D-05)	(-0.685D-03 0.245D-09)	(0.753D-02-0.355D-09)	(-0.338D-05-0.933D-06)
(-0.273D-02-0.512D-09)	(-0.487D-02 0.181D-08)	(-0.192D-05-0.144D-05)	(0.325D-05 0.471D-06)	(0.729D-02-0.640D-09)
(-0.183D-05 0.731D-06)	(0.258D-05 0.338D-05)	(0.693D-02-0.317D-09)	(0.699D-03 0.517D-09)	(0.163D-05 0.102D-05)

THE 16-20 EIGENVECTORS

(0.864D-03-0.548D-09)	(0.741D-02 0.209D-09)	(0.329D-05-0.105D-05)	(0.451D+00-0.164D-12)	(-0.287D-02-0.289D-09)
(0.249D-05-0.194D-05)	(-0.203D-05 0.155D-06)	(0.672D-02 0.417D-09)	(-0.143D-03-0.123D-05)	(0.341D-06-0.488D-06)
(0.629D-02 0.609D-10)	(0.896D-03-0.186D-09)	(-0.580D-06 0.406D-06)	(0.253D+00-0.476D-09)	(0.111D-02 0.240D-10)
(0.133D-02 0.176D-08)	(-0.164D-01-0.612D-09)	(-0.935D-05 0.276D-05)	(0.101D-01-0.818D-10)	(-0.697D-03-0.471D-10)
(-0.673D-05 0.478D-05)	(0.409D-05-0.332D-06)	(-0.153D-01-0.965D-09)	(-0.184D-04 0.256D-06)	(0.256D-06-0.370D-06)
(-0.137D-01-0.574D-10)	(-0.142D-02 0.342D-09)	(0.898D-06-0.840D-06)	(0.619D-01 0.147D-10)	(0.122D-02 0.534D-10)
(-0.692D-03-0.264D-09)	(0.818D-02 0.307D-09)	(0.328D-05-0.114D-05)	(0.472D-03 0.161D-09)	(0.122D-02 0.728D-10)
(0.184D-05-0.168D-05)	(-0.314D-05 0.206D-06)	(0.788D-02 0.561D-09)	(-0.962D-06-0.738D-06)	(-0.444D-06 0.666D-06)
(0.746D-02-0.287D-09)	(0.726D-03-0.318D-09)	(-0.155D-05 0.682D-06)	(0.295D-02-0.277D-09)	(-0.192D-02-0.951D-10)
(-0.134D-01 0.192D-08)	(-0.118D+00-0.363D-09)	(-0.460D-04 0.746D-05)	(0.308D-02-0.276D-09)	(0.547D+00-0.791D-11)
(-0.290D-04 0.701D-05)	(0.457D-04 0.704D-05)	(-0.113D+00 0.313D-09)	(-0.383D-07-0.406D-06)	(-0.575D-04-0.497D-05)
(-0.114D+00 0.101D-09)	(-0.140D-01-0.328D-08)	(0.229D-04 0.951D-05)	(0.291D-02-0.268D-09)	(-0.706D-01 0.111D-08)
(-0.292D-01-0.514D-08)	(0.329D+00 0.534D-12)	(0.136D-03-0.162D-04)	(-0.248D-03-0.810D-10)	(-0.243D-01-0.136D-09)
(0.795D-04-0.214D-04)	(-0.127D-03-0.192D-04)	(0.323D+00 0.116D-11)	(0.551D-06 0.272D-06)	(-0.810D-05-0.198D-05)
(0.314D+00-0.534D-12)	(0.292D-01 0.817D-08)	(-0.642D-04-0.239D-04)	(-0.545D-03 0.146D-10)	(-0.386D-01 0.574D-09)
(-0.898D-03-0.755D-09)	(0.104D-01 0.105D-08)	(0.421D-05-0.312D-05)	(0.398D-03 0.102D-09)	(0.154D-02 0.246D-09)
(0.240D-05-0.485D-05)	(-0.399D-05 0.178D-05)	(0.101D-01 0.195D-08)	(-0.802D-06-0.508D-06)	(-0.562D-06 0.236D-05)
(0.962D-02 0.104D-08)	(0.914D-03-0.152D-08)	(-0.199D-05 0.368D-05)	(0.248D-02-0.182D-09)	(-0.245D-02-0.379D-09)

THE 21-25 EIGENVECTORS

(0.500D+00 0.185D-11)	(-0.203D-01-0.207D-08)	(0.534D-04-0.666D-05)	(-0.687D-05 0.347D-05)	(0.234D-01 0.144D-05)
(0.575D-04-0.170D-05)	(-0.283D-04 0.728D-05)	(0.481D+00 0.188D-11)	(-0.449D-02-0.551D-09)	(0.752D-05 0.184D-02)
(-0.651D-01-0.410D-09)	(-0.148D-02 0.195D-08)	(0.138D-03-0.405D-06)	(0.145D-05-0.957D-06)	(-0.740D-01 0.971D-05)
(0.184D-01 0.450D-10)	(-0.990D-03-0.352D-10)	(-0.454D-06 0.850D-07)	(-0.327D-06 0.443D-06)	(0.382D-02 0.147D-04)
(0.677D-05-0.562D-06)	(-0.423D-05 0.134D-05)	(0.625D-01 0.318D-09)	(-0.244D-02-0.331D-09)	(0.212D-04 0.665D-02)
(-0.296D-01-0.173D-09)	(-0.164D-02 0.497D-09)	(0.375D-04-0.466D-06)	(0.149D-05-0.794D-06)	(-0.311D+00 0.411D-04)
(0.102D-02-0.797D-10)	(0.547D-03-0.128D-09)	(-0.794D-07-0.578D-06)	(0.950D-07-0.615D-06)	(-0.899D-02-0.442D-04)
(0.428D-06 0.672D-06)	(0.871D-06-0.703D-06)	(0.325D-02-0.600D-09)	(0.385D-02 0.526D-09)	(-0.628D-04-0.198D-01)
(-0.160D-02 0.114D-09)	(0.342D-02 0.237D-09)	(0.207D-05 0.102D-05)	(-0.202D-05 0.971D-06)	(0.923D+00-0.122D-03)
(0.817D-02-0.142D-08)	(0.486D+00 0.104D-12)	(0.275D-04 0.640D-05)	(-0.581D-04-0.186D-04)	(0.284D-01 0.207D-04)
(0.367D-05 0.999D-06)	(0.142D-03-0.351D-05)	(0.349D-02 0.118D-08)	(0.522D+00-0.706D-11)	(-0.216D-03 0.296D-02)
(0.251D-02-0.752D-09)	(0.269D+00 0.127D-08)	(0.162D-04 0.425D-05)	(-0.139D-03-0.104D-05)	(-0.755D-01-0.263D-06)
(-0.209D-03-0.493D-11)	(0.138D-01 0.264D-09)	(0.811D-06 0.409D-06)	(-0.450D-07 0.338D-06)	(0.492D-02 0.701D-04)
(0.394D-06-0.782D-07)	(0.224D-04 0.848D-06)	(-0.105D-02 0.491D-09)	(0.827D-01-0.970D-09)	(-0.804D-03 0.111D-01)
(0.136D-02-0.272D-09)	(0.812D-01-0.333D-10)	(0.410D-05 0.959D-06)	(-0.460D-04-0.151D-05)	(-0.337D+00-0.221D-06)
(0.863D-03-0.635D-10)	(0.691D-03-0.505D-09)	(-0.506D-07-0.389D-06)	(0.135D-06-0.204D-05)	(-0.116D-01-0.210D-03)
(0.370D-06 0.433D-06)	(0.118D-05-0.244D-05)	(0.273D-02-0.511D-09)	(0.487D-02 0.181D-08)	(0.239D-02-0.331D-01)
(-0.132D-02 0.869D-10)	(0.435D-02 0.871D-09)	(0.183D-05 0.728D-06)	(-0.258D-05 0.337D-05)	(0.100D+01 0.0)

THE 26-30 EIGENVECTORS

(0.234D-01-0.144D-05)	(-0.231D-03-0.806D-03)	(-0.231D-03 0.806D-03)	(0.180D-01 0.433D-02)	(-0.771D-01 0.391D-03)
(0.752D-05-0.184D-02)	(-0.831D-01 0.106D-03)	(-0.831D-01-0.106D-03)	(-0.289D-02-0.361D-01)	(0.309D-02-0.523D-02)
(-0.740D-01-0.971D-05)	(0.652D-03-0.285D-02)	(0.652D-03 0.285D-02)	(-0.800D-01-0.513D-04)	(0.244D-02 0.780D-03)
(0.362D-02-0.147D-04)	(-0.121D-03-0.555D-02)	(-0.121D-03 0.555D-02)	(-0.202D-01 0.144D-01)	(-0.255D+00 0.209D-02)
(0.212D-04-0.665D-02)	(-0.301D+00 0.382D-03)	(-0.301D+00-0.382D-03)	(-0.105D-01-0.131D+00)	(0.112D-01-0.190D-01)
(-0.311D+00-0.411D-04)	(0.274D-02-0.120D-01)	(0.274D-02 0.120D-01)	(-0.337D+00-0.383D-04)	(0.711D-02 0.331D-02)
(-0.899D-02 0.442D-04)	(0.340D-03 0.167D-01)	(0.340D-03-0.167D-01)	(0.630D-01-0.431D-01)	(0.763D+00-0.628D-02)
(-0.628D-04 0.198D-01)	(0.896D+00-0.114D-02)	(0.896D+00 0.114D-02)	(0.312D-01 0.390D+00)	(-0.333D-01 0.565D-01)
(0.923D+00 0.122D-03)	(-0.813D-02 0.358D-01)	(-0.813D-02-0.358D-01)	(0.100D+01 0.0)	(-0.191D-01-0.984D-02)
(0.284D-01-0.270D-04)	(-0.569D-03-0.319D-02)	(-0.569D-03 0.319D-02)	(-0.334D-01 0.445D-02)	(-0.978D-01 0.202D-03)
(-0.216D-03-0.296D-02)	(-0.895D-01-0.173D-07)	(-0.895D-01 0.173D-07)	(-0.456D-02 0.533D-02)	(-0.421D-03 0.696D-03)
(-0.755D-01 0.263D-06)	(-0.194D-03-0.244D-03)	(-0.194D-03 0.244D-03)	(0.486D-01-0.439D-03)	(-0.565D-03-0.559D-03)
(0.492D-02-0.701D-04)	(-0.217D-02-0.112D-01)	(-0.217D-02 0.112D-01)	(-0.548D-01 0.147D-01)	(-0.334D+00 0.767D-05)
(-0.804D-03-0.111D-01)	(-0.336D+00-0.164D-08)	(-0.336D+00 0.164D-08)	(-0.172D-01 0.200D-01)	(-0.158D-02 0.262D-02)
(-0.337D+00 0.221D-06)	(-0.896D-03-0.125D-02)	(-0.896D-03 0.125D-02)	(0.216D+00-0.175D-02)	(-0.742D-02-0.250D-02)
(-0.116D-01 0.210D-03)	(0.649D-02 0.335D-01)	(0.649D-02-0.335D-01)	(0.162D+00-0.438D-01)	(0.100D+01 0.0)
(0.239D-02 0.331D-01)	(0.100D+01 0.0)	(0.100D+01 0.0)	(0.510D-01-0.596D-01)	(0.470D-02-0.778D-02)
(0.100D+01 0.0)	(0.268D-02 0.382D-02)	(0.268D-02-0.382D-02)	(-0.642D+00 0.505D-02)	(0.252D-01 0.741D-02)

THE 31-35 EIGENVECTORS

(0.180D-01-0.433D-02)	(-0.771D-01-0.391D-03)	(-0.677D-02-0.427D-01)	(-0.100D+00 0.764D-09)	(-0.677D-02 0.427D-01)
(-0.289D-02 0.361D-01)	(0.309D-02 0.523D-02)	(-0.927D-01 0.341D-06)	(-0.853D-02 0.908D-08)	(-0.927D-01-0.341D-06)
(-0.800D-01 0.513D-04)	(0.244D-02-0.780D-03)	(-0.148D-02-0.987D-02)	(0.529D-03-0.251D-08)	(-0.148D-02 0.987D-02)
(-0.202D-01-0.144D-01)	(-0.255D+00-0.209D-02)	(-0.241D-01-0.153D+00)	(-0.334D+00 0.275D-10)	(-0.241D-01 0.153D+00)
(-0.105D-01 0.131D+00)	(0.112D-01 0.190D-01)	(-0.336D+00 0.252D-07)	(-0.309D-01 0.329D-07)	(-0.336D+00-0.252D-07)
(-0.337D+00 0.383D-04)	(0.711D-02-0.331D-02)	(-0.654D-02-0.434D-01)	(-0.190D-02-0.106D-07)	(-0.654D-02 0.434D-01)
(0.630D-01 0.431D-01)	(0.763D+00 0.628D-02)	(0.721D-01 0.457D+00)	(0.100D+01 0.0)	(0.721D-01-0.457D+00)
(0.312D-01-0.390D+00)	(-0.333D-01-0.565D-01)	(0.100D+01 0.0)	(0.920D-01-0.979D-07)	(0.100D+01 0.0)
(0.100D+01 0.0)	(-0.191D-01 0.984D-02)	(0.196D-01 0.130D+00)	(0.828D-02 0.313D-07)	(0.196D-01-0.130D+00)
(-0.334D-01-0.445D-02)	(-0.978D-01-0.202D-03)	(-0.180D-01-0.255D-01)	(-0.985D-02 0.187D-08)	(-0.180D-01 0.255D-01)
(-0.456D-02-0.533D-02)	(-0.421D-03-0.696D-03)	(0.423D-01-0.133D-02)	(0.232D-02-0.433D-08)	(0.423D-01 0.133D-02)
(0.486D-01 0.439D-03)	(-0.565D-03 0.559D-03)	(-0.607D-04 0.716D-02)	(0.686D-04 0.172D-08)	(-0.607D-04-0.716D-02)
(-0.548D-01-0.147D-01)	(-0.334D+00-0.767D-05)	(-0.615D-01-0.781D-01)	(-0.335D-01 0.846D-08)	(-0.615D-01 0.781D-01)
(-0.172D-01-0.200D-01)	(-0.158D-02-0.262D-02)	(0.159D+00-0.499D-02)	(0.872D-02-0.163D-07)	(0.159D+00 0.499D-02)
(0.216D+00 0.175D-02)	(-0.742D-02 0.250D-02)	(-0.117D-02 0.309D-01)	(-0.185D-03 0.780D-08)	(-0.117D-02-0.309D-01)
(0.162D+00 0.438D-01)	(0.100D+01 0.0)	(0.184D+00 0.233D+00)	(0.100D+00-0.254D-07)	(0.184D+00-0.233D+00)
(0.510D-01 0.596D-01)	(0.470D-02 0.778D-02)	(-0.472D+00 0.149D-01)	(-0.259D-01 0.484D-07)	(-0.472D+00-0.149D-01)
(-0.642D+00-0.505D-02)	(0.252D-01-0.741D-02)	(0.406D-02-0.908D-01)	(0.862D-03-0.232D-07)	(0.406D-02 0.908D-01)

THE 36 EIGENVECTOR

(-0.100D+00-0.432D-09)
(-0.211D-03 0.111D-07)
(0.808D-03 0.142D-08)
(-0.334D+00-0.155D-10)
(-0.764D-03 0.403D-07)
(-0.731D-03 0.598D-08)
(0.100D+01 0.0)
(0.227D-02-0.120D-06)
(0.480D-02-0.177D-07)
(-0.864D-02 0.378D-09)
(-0.204D-02-0.508D-08)
(-0.208D-04-0.773D-09)
(-0.295D-01 0.351D-09)
(-0.768D-02 0.191D-07)
(-0.525D-03-0.345D-08)
(0.882D-01-0.102D-08)
(0.228D-01 0.568D-07)
(0.183D-02 0.102D-07)

APPENDIX N

DERIVATION OF THE THREE-DIMENSIONAL UNSTEADY COMPRESSIBLE FLOW EQUATION

In this Appendix will be derived the exact unsteady compressible flow equation governing an inviscid, irrotational and isentropic flow.

We shall start with the two basic equations in fluid dynamics. First, the continuity equation which arises from the conservation of mass is

$$\frac{\partial \rho}{\partial t} + \vec{V}\cdot\vec{\nabla}\rho + \rho\vec{\nabla}\cdot\vec{V} = 0 , \qquad (N.1)$$

where ρ is the density of the fluid and $\vec{V}$ is the fluid particle velocity. Second, the equation of conservation of momentum, from which the equations of motion of the fluid may be obtained,

$$\frac{\partial \vec{V}}{\partial t} + (\vec{V}\cdot\vec{\nabla})\vec{V} = -\frac{1}{\rho}\vec{\nabla}P , \qquad (N.2)$$

where P is the fluid pressure.

For irrotational flow, one has $\vec{\nabla}\times\vec{V} = 0$. This condition ensures the existence of a scalar velocity potential, Ψ , such that

$$\vec{V} = \vec{\nabla}\Psi . \qquad (N.3)$$

Substituting equation (N.3) into (N.2) and using the identity†,

†A proof of the identity is given at the end of this Appendix.

$$2(\vec{V}\cdot\vec{\nabla})\vec{V} = \vec{\nabla}(\vec{V}\cdot\vec{V}) - 2\vec{V}\times(\vec{\nabla}\times\vec{V}) = \vec{\nabla}(\vec{V}\cdot\vec{V}) \tag{N.4}$$

for irrotational flow, since $\vec{\nabla}\times\vec{V} = o$, one may obtain the equation,

$$\frac{\partial}{\partial t}(\vec{\nabla}\Psi) + \vec{\nabla}\left(\frac{\vec{V}\cdot\vec{V}}{2}\right) = -\frac{1}{\rho}\vec{\nabla}P \,. \tag{N.5}$$

Equation (N.5), in fact, represents three different equations,

$$\frac{\partial}{\partial t}\left(\frac{\partial\Psi}{\partial x_i}\right) + \frac{\partial}{\partial x_i}\left(\frac{\vec{V}\cdot\vec{V}}{2}\right) = -\frac{1}{\rho}\frac{\partial P}{\partial x_i} \,, \qquad i = 1,2,3 \tag{N.6}$$

where x_i ; $i = 1,2,3$ are the Cartesian coordinates of the system corresponding to x, y and z. Multiplying each equation in (N.6) by the corresponding differential, dx_i , and summing them up, one obtains

$$\frac{\partial}{\partial t}\left(\frac{\partial\Psi}{\partial x_i}\,dx_i\right) + \frac{\partial}{\partial x_i}\left(\frac{\vec{V}\cdot\vec{V}}{2}\right)dx_i = -\frac{1}{\rho}\frac{\partial P}{\partial x_i}\,dx_i \,, \tag{N.7}$$

where the repeated index in i indicates summation. Noting that

$$\frac{\partial\Psi}{\partial x_i}\,dx_i = d\Psi \,,$$

$$\frac{\partial}{\partial x_i}\left(\frac{\vec{V}\cdot\vec{V}}{2}\right)dx_i = d\left(\frac{\vec{V}\cdot\vec{V}}{2}\right) \,,$$

$$\frac{\partial P}{\partial x_i}\,dx_i = dP \,,$$

equation (N.7) may be written as

$$\frac{\partial}{\partial t}\left(d\Psi\right) + d\left(\frac{\vec{V}\cdot\vec{V}}{2}\right) = -\frac{1}{\rho}dP \ . \tag{N.8}$$

Integrating equation (N.8) yields

$$\frac{\partial \Psi}{\partial t} + \frac{\vec{V}\cdot\vec{V}}{2} + \int\frac{dP}{\rho} = f(t) \ , \tag{N.9}$$

where f(t) is the result of integration and may be 'absorbed' in the velocity potential Ψ . Indeed, equation (N.9) is the so-called unsteady Bernoulli's equation.

Taking the partial derivative, with respect to time, of equation (N.9), one obtains

$$\frac{\partial}{\partial t}\int\frac{dP}{\rho} = -\frac{\partial}{\partial t}\left(\frac{\partial \Psi}{\partial t} + \frac{\vec{V}\cdot\vec{V}}{2}\right) \ . \tag{N.10}$$

For an isentropic process, the pressure and density are related by

$$\frac{P}{\rho^{\gamma}} = k \ , \tag{N.11}$$

where k is a constant. Using equation (N.11), it can easily be shown that

$$\int\frac{dP}{\rho} = \frac{\gamma}{\gamma-1}k\rho^{\gamma-1} \ ; \tag{N.12}$$

thus

$$\frac{\partial}{\partial t}\int\frac{dP}{\rho} = \gamma k\rho^{\gamma-2}\frac{\partial \rho}{\partial t} = \frac{\gamma P}{\rho^2}\frac{\partial \rho}{\partial t} = \frac{c^2}{\rho}\frac{\partial \rho}{\partial t} \ , \tag{N.13}$$

where

$$c = \left(\frac{dP}{d\rho}\right)^{1/2}_{\text{isentropic}} = \left(\frac{\gamma P}{\rho}\right)^{1/2} \tag{N.13a}$$

is the local sound speed. Substituting equation (N.13) into equation (N.10), one obtains,

$$\frac{1}{\rho}\frac{\partial \rho}{\partial t} = -\frac{1}{c^2}\frac{\partial}{\partial t}\left(\frac{\partial \Psi}{\partial t} + \frac{\vec{V}\cdot\vec{V}}{2}\right) . \tag{N.14}$$

Applying the gradient operator to equation (N.9), and making use of equations (N.12), (N.11), (N.13a) and (N.3), one can show that

$$\frac{c^2}{\rho}\vec{\nabla}\rho = -\left[\frac{\partial}{\partial t}(\vec{\nabla}\Psi) + \vec{\nabla}\left(\frac{\vec{V}\cdot\vec{V}}{2}\right)\right] = -\left[\frac{\partial \vec{V}}{\partial t} + \vec{\nabla}\left(\frac{\vec{V}\cdot\vec{V}}{2}\right)\right] . \tag{N.15}$$

Taking the scalar product with $\vec{V}$ on both sides of equation (N.15) leads to

$$\frac{\vec{V}\cdot\vec{\nabla}\rho}{\rho} = -\frac{1}{c^2}\left[\frac{\partial}{\partial t}\left(\frac{\vec{V}\cdot\vec{V}}{2}\right) + \vec{V}\cdot\vec{\nabla}\left(\frac{\vec{V}\cdot\vec{V}}{2}\right)\right] . \tag{N.16}$$

Finally, substituting equations (N.14) and (N.16) into the continuity equation (N.1) and noting that $\vec{\nabla}\cdot\vec{V} = \vec{\nabla}\cdot(\vec{\nabla}\Psi) = \nabla^2\Psi$, one obtains

$$\nabla^2\Psi - \frac{1}{c^2}\left[\frac{\partial^2\Psi}{\partial t^2} + \frac{\partial}{\partial t}(\vec{V}\cdot\vec{V}) + \vec{V}\cdot\vec{\nabla}\left(\frac{\vec{V}\cdot\vec{V}}{2}\right)\right] = 0 \tag{N.17}$$

which is the three-dimensional unsteady compressible flow equation.

The proof of the identity (N.4) can be achieved very efficiently using Tensor Analysis. In tensor notation, one may write

where ( ),j is the covariant derivative, and summation is over repeated covariant and contravariant indices. Thus,

$$2(\vec{V}\cdot\vec{\nabla})\vec{V} = 2V_{i,j}V^j$$

$$= 2V_{j,i}V^j - 2V_{j,i}V^j + 2V_{i,j}V^j$$

$$= 2V_{j,i}V^j - 2(\delta_i^m\delta_j^n - \delta_j^m\delta_i^n)V_{n,m}V^j$$

$$= (V^jV_j)_{,i} - 2\varepsilon_{ijl}\varepsilon^{lmn}V_{n,m}V^j$$

$$= \nabla(\vec{V}\cdot\vec{V}) - 2\vec{V}\times(\vec{\nabla}\times\vec{V})$$

in vectorial form, where δ_i^m, δ_j^n, *etc.* are the Kronecker deltas; ε_{ijl} and ε^{lmn} are the covariant and contravariant permutation symbols, respectively.

APPENDIX O

AXIAL MODAL SHAPES OF THE SYSTEM AT DIFFERENT FLOW VELOCITIES

This Appendix presents the axial modal shapes over half a period for the six lowest modes (n=3, m=1,2,3, antisymmetric and n=3, m=1,2,3, symmetric) of the 1/10-gap steel-water system:

Shell: steel, b/L = 1/10, a/b = 10/11, h/a = 5.5×10^{-3}, both shells flexible

Fluid: water, inviscid, incompressible

Figures O.1-O.13: Axial modal shapes at different internal flow velocities $\bar{U}_i$; the annular fluid stagnant (corresponding frequency diagram shown in Figure 15).

Figures O.14-O.26: Axial modal shapes at different annular flow velocities $\bar{U}_o$; the internal fluid stagnant (corresponding frequency diagram shown in Figure 18).

● 0 period

△ 1/10 period

\+ 1/5 period

× 3/10 period

◇ 2/5 period

⧈ 1/2 period

Remark: If the symbols in the graphs of the two shells are in the same order, the radial displacements of the shells are in phase; on the other hand, if the order of the symbols in one graph is the reverse of the other, the shells are vibrating out of phase. The four smaller symbols may be indistinct in the Figures because of imperfect duplication.

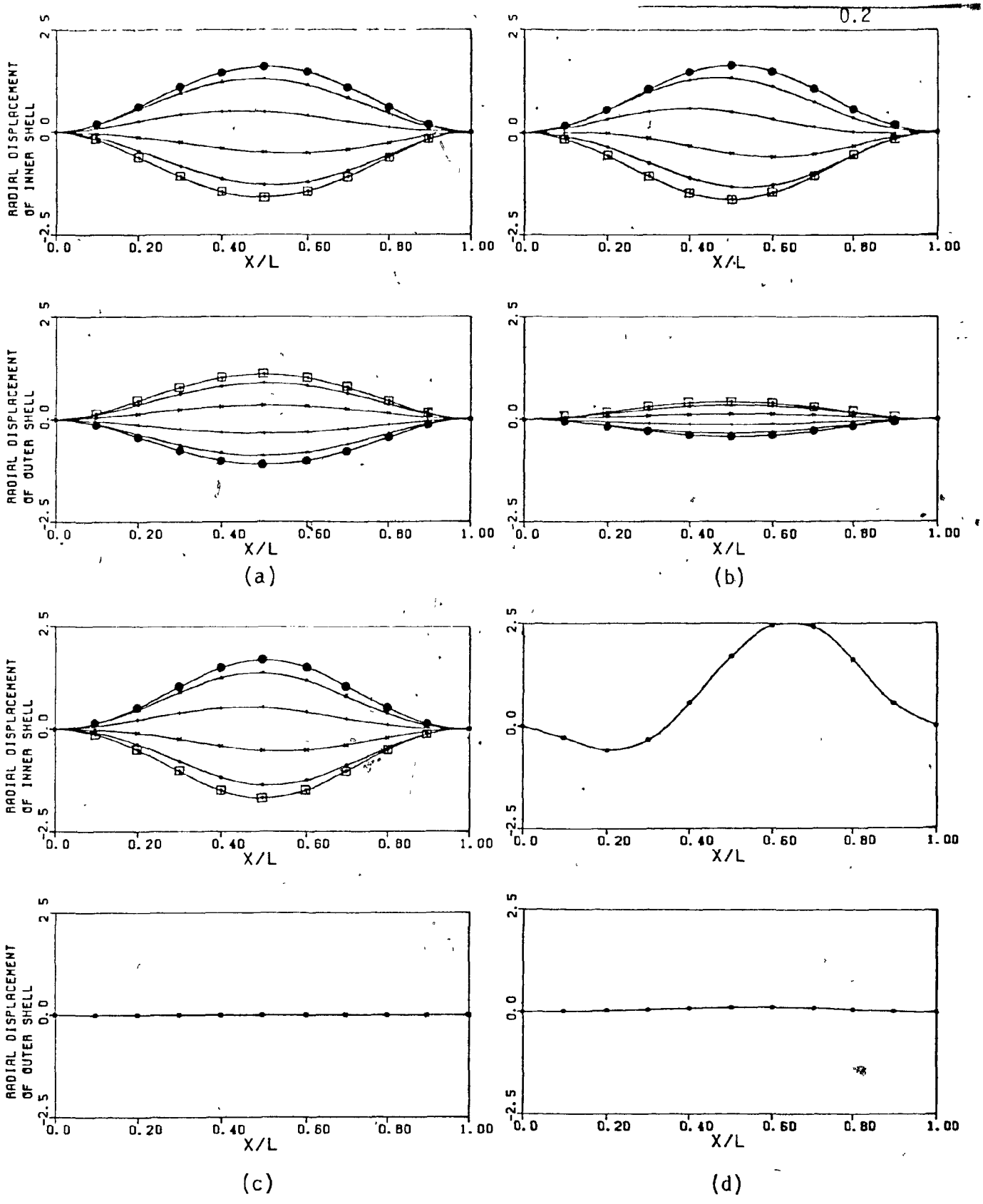

Fig. 0.1: Axial modal shapes of the inner and outer shells for the n=3, m=1, antisymmetric mode of the 1/10-gap steel-water system of Figure 15, at (a) $\bar{U}_i = 0.010$, (b) $\bar{U}_i = 0.020$, (c) $\bar{U}_i = 0.02530$ (just short of buckling), (d) $\bar{U}_i = 0.030$ (shells have buckled).

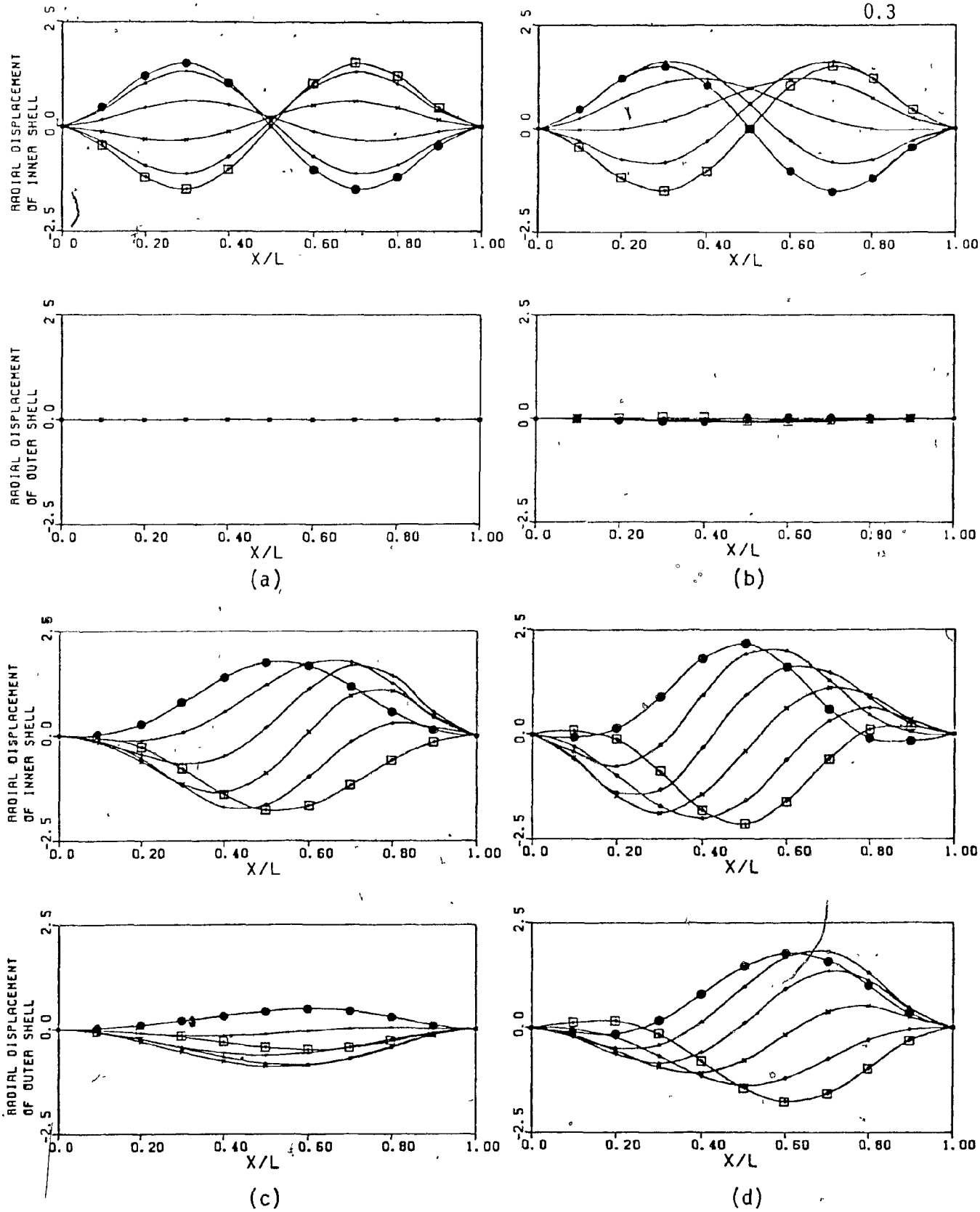

Fig. 0.2: Axial modal shapes of the inner and outer shells for the n=3, m=1, antisymmetric mode of the 1/10-gap steel-water system of Figure 15, at (a) Ω_i = 0.03092 (just after restabilization), (b) Ω_i = 0.03125 (prior to coupled-mode fluttering with the m=2, antisymmetric mode), (c) Ω_i = 0.0350 (whilst fluttering), (d) Ω_i = 0.050 (whilst fluttering).

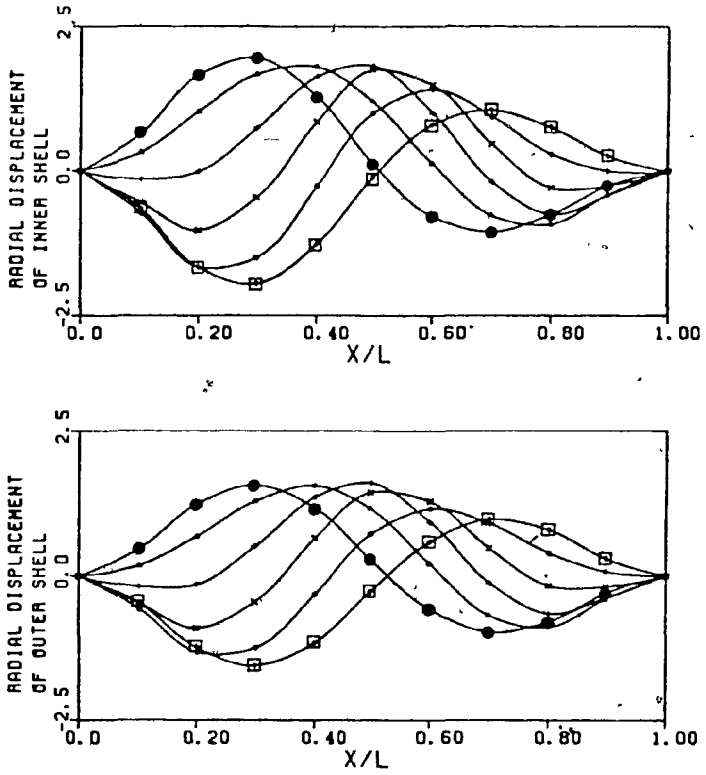

(a)

Fig. 0.3: Axial modal shapes of the inner and outer shells for the n=3, m=1, antisymmetric mode of the 1/10-gap steel-water system of Figure 15, at (a) $\bar{U}_i$ = 0.090 (whilst fluttering).

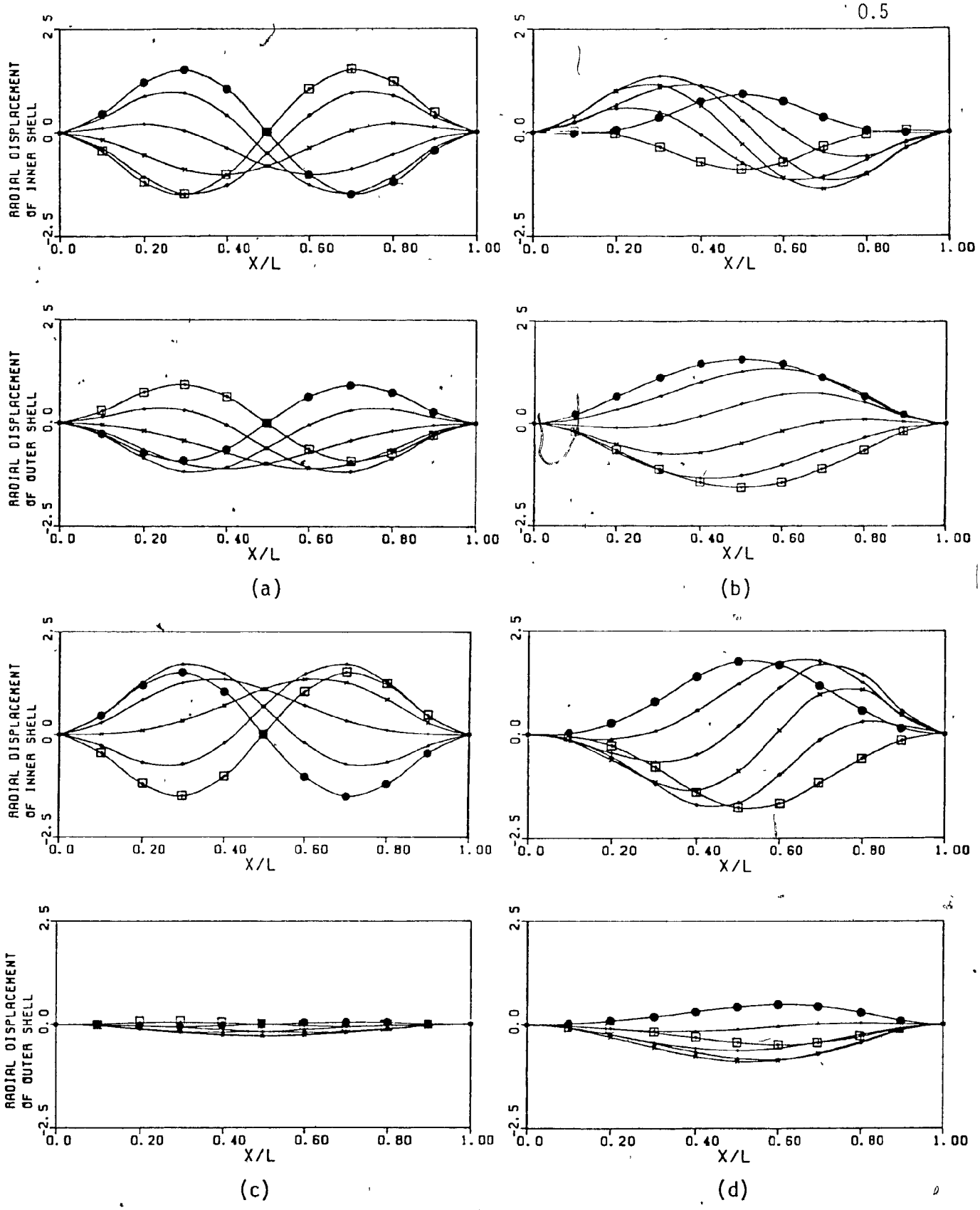

Fig. 0.4: Axial modal shapes of the inner and outer shells for the n=3, m=2, antisymmetric mode of the 1/10-gap steel-water system of Figure 15, at (a) $\bar{U}_i = 0.010$, (b) $\bar{U}_i = 0.020$, (c) $\bar{U}_i = 0.03125$ (prior to coupled-mode fluttering with the m=1, antisymmetric mode), (d) $\bar{U}_i = 0.0350$ (whilst fluttering).

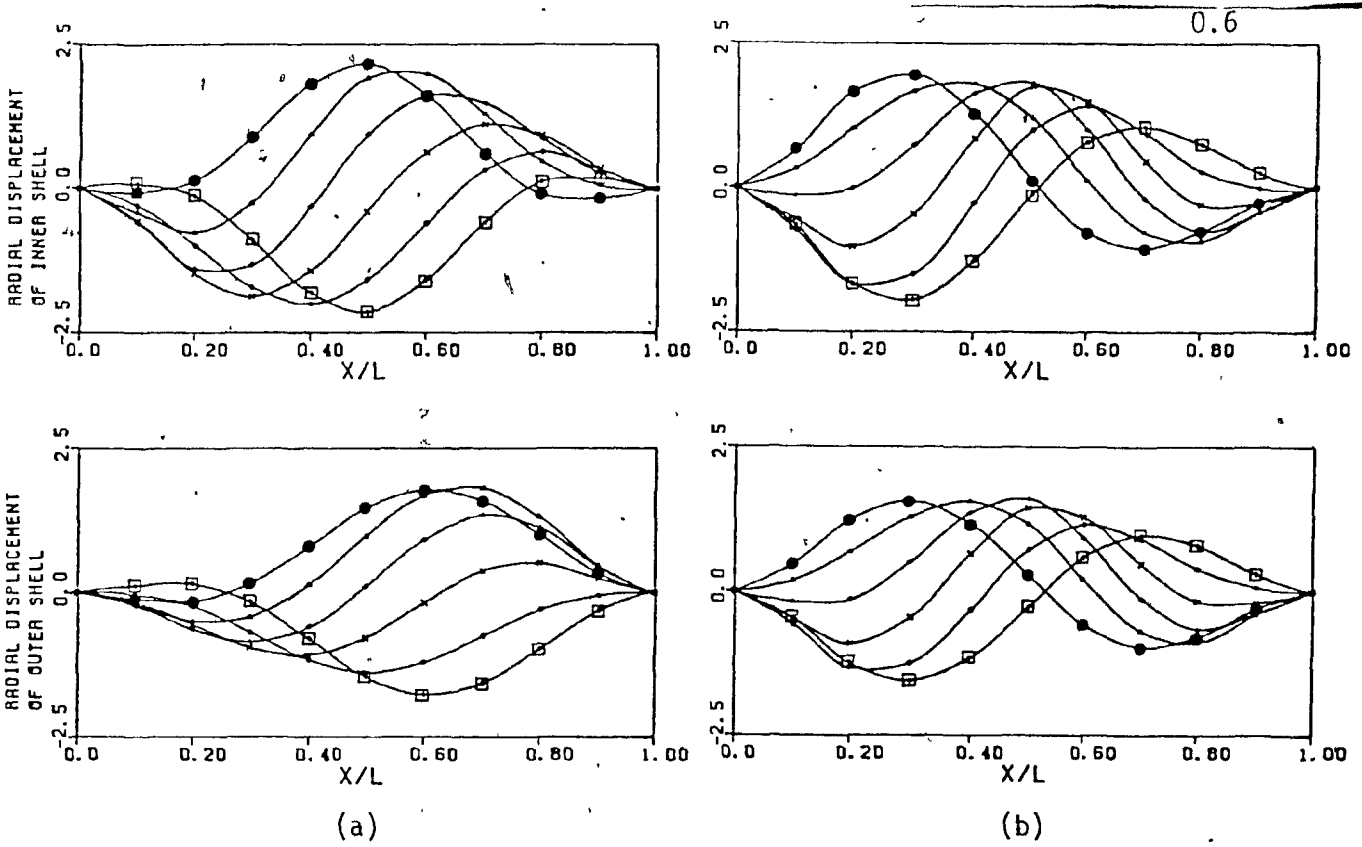

Fig. 0.5: Axial modal shapes of the inner and outer shells for the n=3, m=2, antisymmetric mode for the 1/10-gap steel-water system of Figure 15, at (a) $\bar{U}_i$ = 0.050 (whilst fluttering), (b) $\bar{U}_i$ = 0.090 (whilst fluttering).

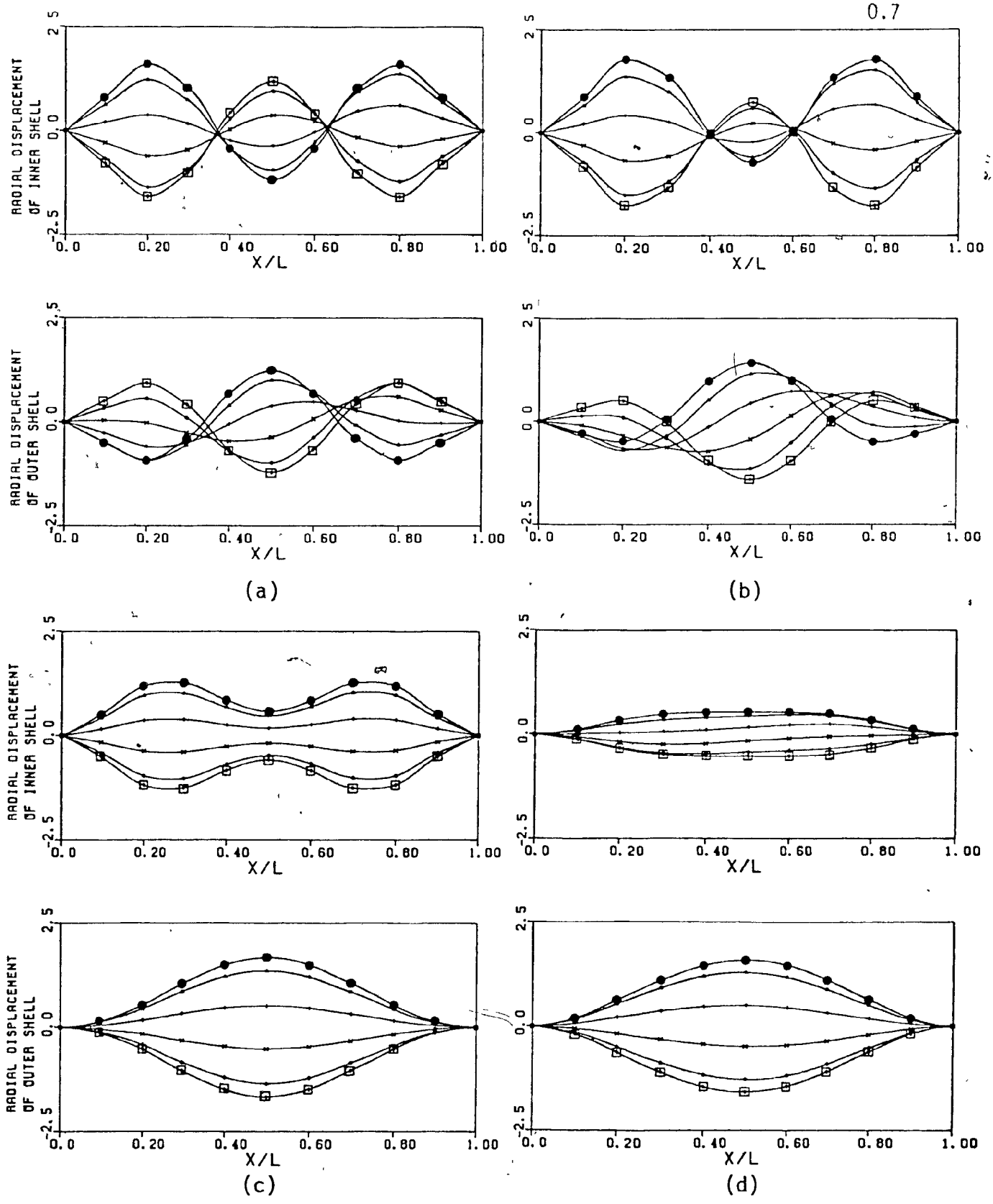

Fig. 0.6: Axial modal shapes of the inner and outer shells for the n=3, m=3, antisymmetric mode of the 1/10-gap steel-water system of Figure 15, at (a) $\bar{\Omega}_i$ = 0.010, (b) $\bar{\Omega}_i$ = 0.020, (c) $\bar{\Omega}_i$ = 0.03650 (when the frequencies of the m=1, symmetric and the m=3, antisymmetric modes are closest to each other), (d) $\bar{\Omega}_i$ = 0.050 (modal shape resembles that of the m=1, symmetric mode).

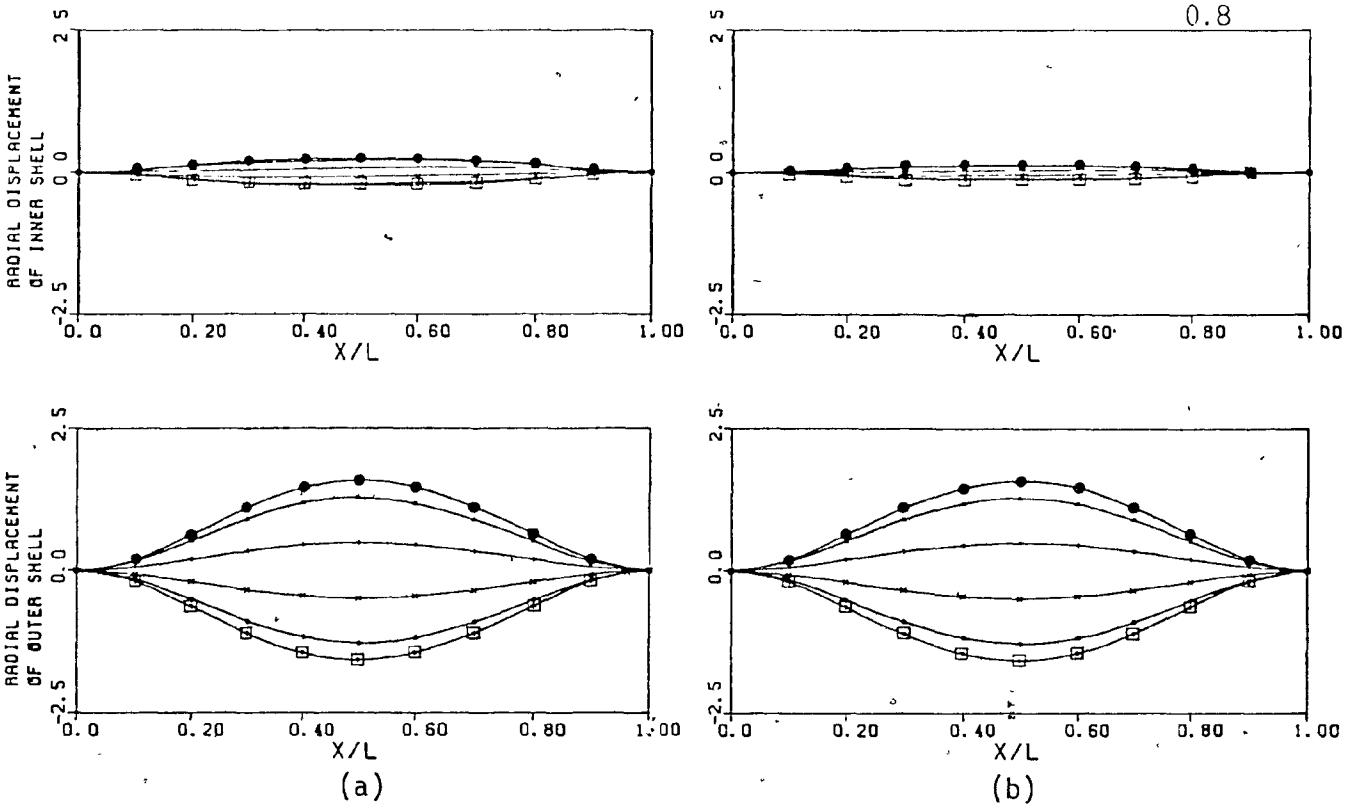

Fig. 0.7: Axial modal shapes of the inner and outer shells for the n=3, m=3, antisymmetric mode of the 1/10-gap steel-water system of Figure 15, at (a) $\bar{U}_i$ = 0.070, at (b) $\bar{U}_i$ = 0.090 (vibration amplitude of the inner shell is relatively small (*cf.* outer shell) in high internal flow).

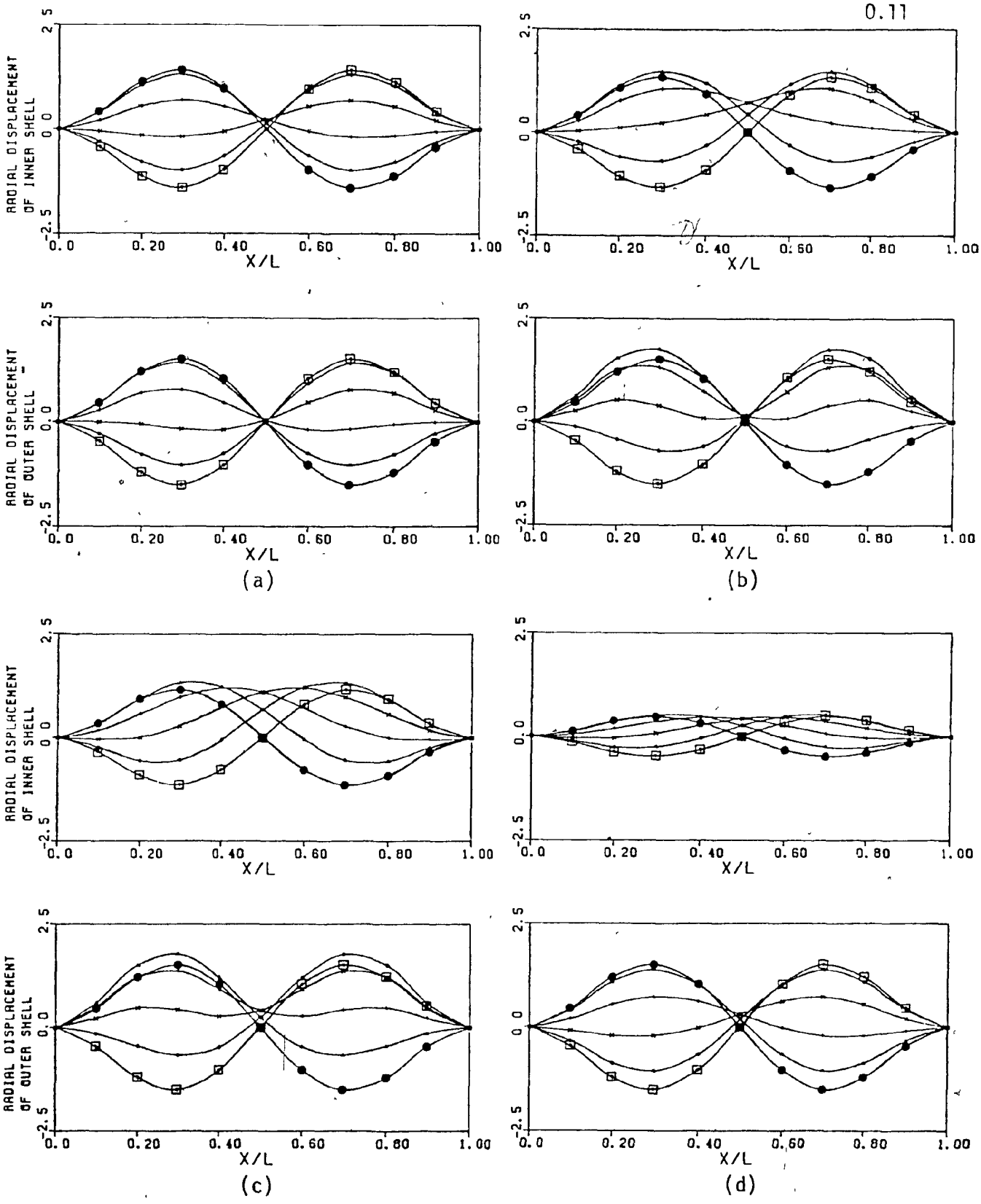

Fig. 0.10: Axial modal shapes of the inner and outer shells for the n=3, m=2, symmetric mode of the 1/10-gap steel-water system of Figure 15, at (a) $\bar{U}_i$ = 0.010, (b) $\bar{U}_i$ = 0.030, (c) $\bar{U}_i$ = 0.050, (d) $\bar{U}_i$ = 0.070.

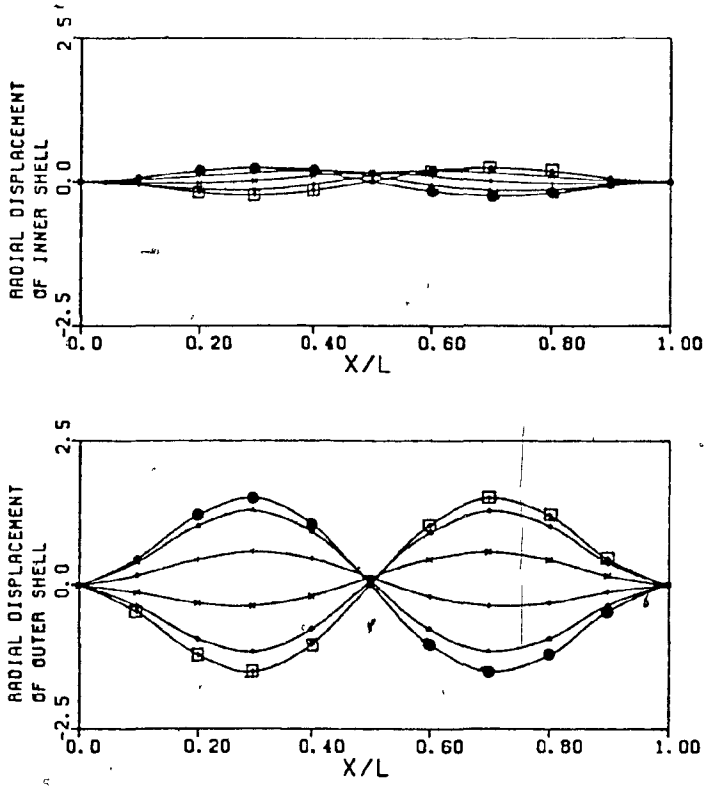

(a)

Fig. 0.11: Axial modal shapes of the inner and outer shells for the n=3, m=2, symmetric mode of the 1/10-gap steel-water system of Figure 15, at (a) $\bar{U}_i$ = 0.090 (vibration amplitude of the inner shell is relatively small (*cf.* outer shell) in high internal flow).

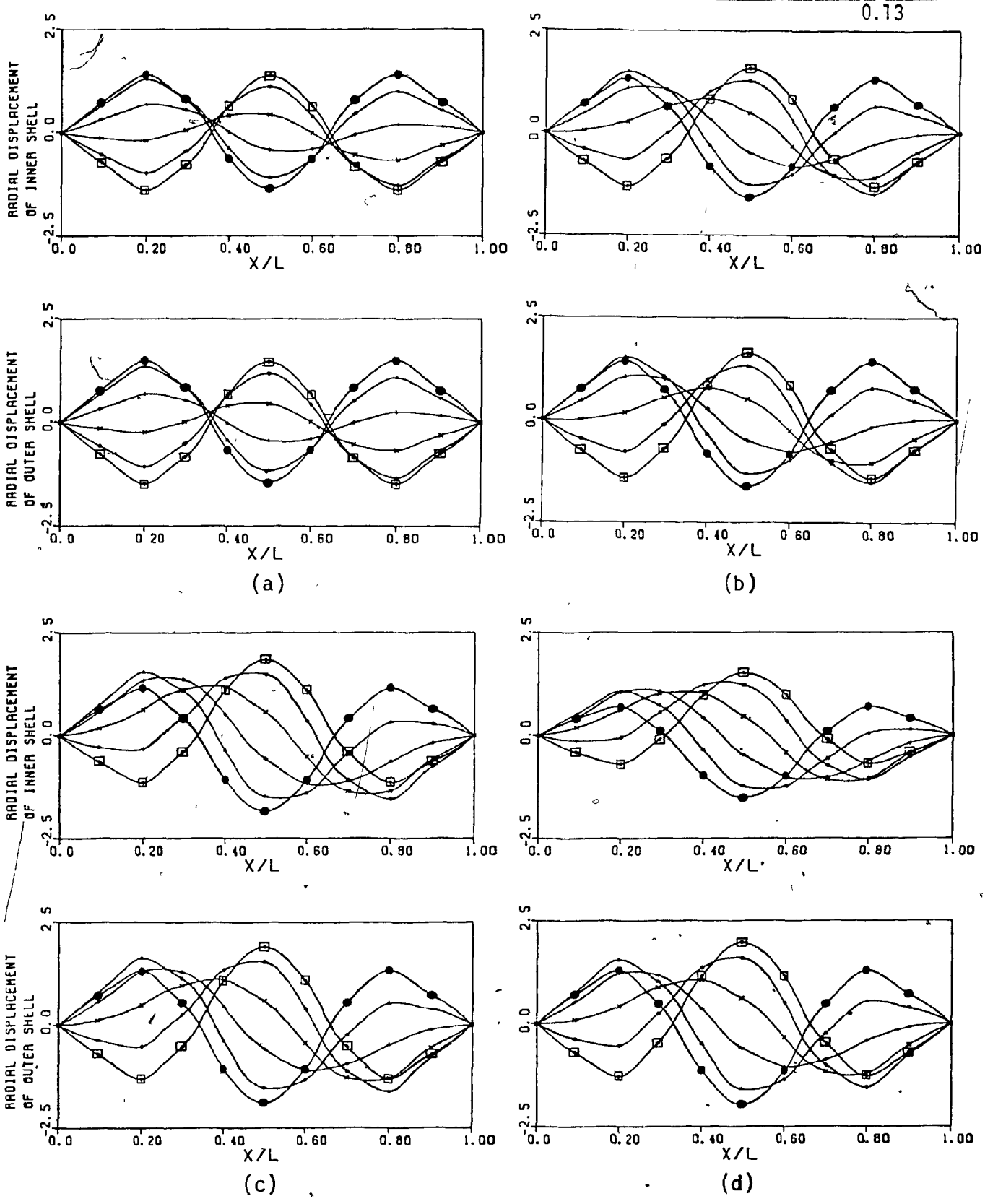

Fig. 0.12: Axial modal shapes of the inner and outer shells for the n=3, m=3, symmetric mode of the 1/10-gap steel-water system of Figure 15, at (a) $\bar{U}_i = 0.010$, (b) $\bar{U}_i = 0.030$, (c) $\bar{U}_i = 0.050$, (d) $\bar{U}_i = 0.070$.

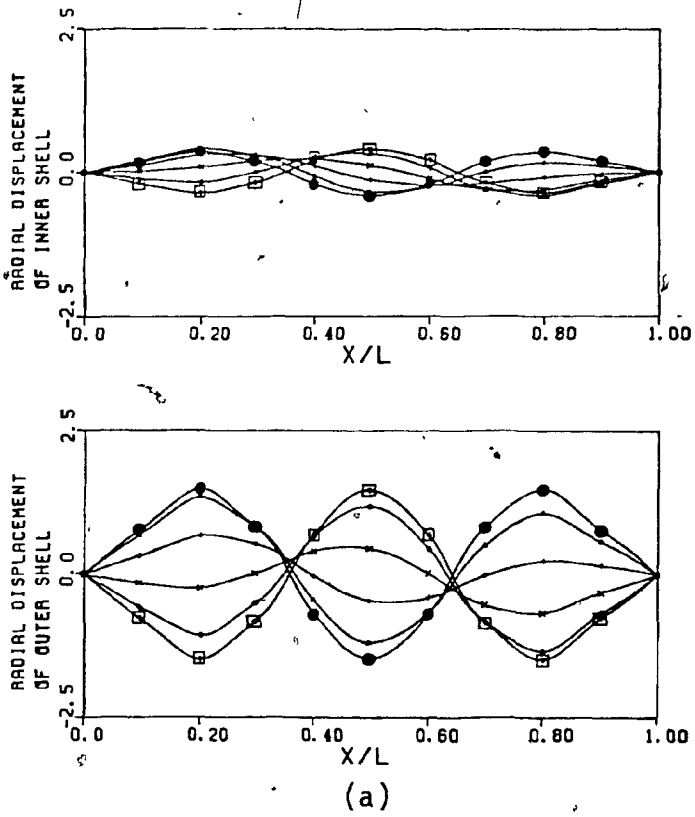

(a)

Fig. 0.13: Axial modal shapes of the inner and outer shells for the n=3, m=3, symmetric mode of the 1/10-gap steel-water system of Figure 15, at (a) U_i = 0.090 (vibration amplitude of the inner shell is relatively small (*cf.* outer shell) in high internal flow).

Figures 0.14-0.26: Axial modal shapes at different annular flow velocities $\bar{U}_0$; the internal fluid stagnant (corresponding frequency diagram shown in Figure 18).

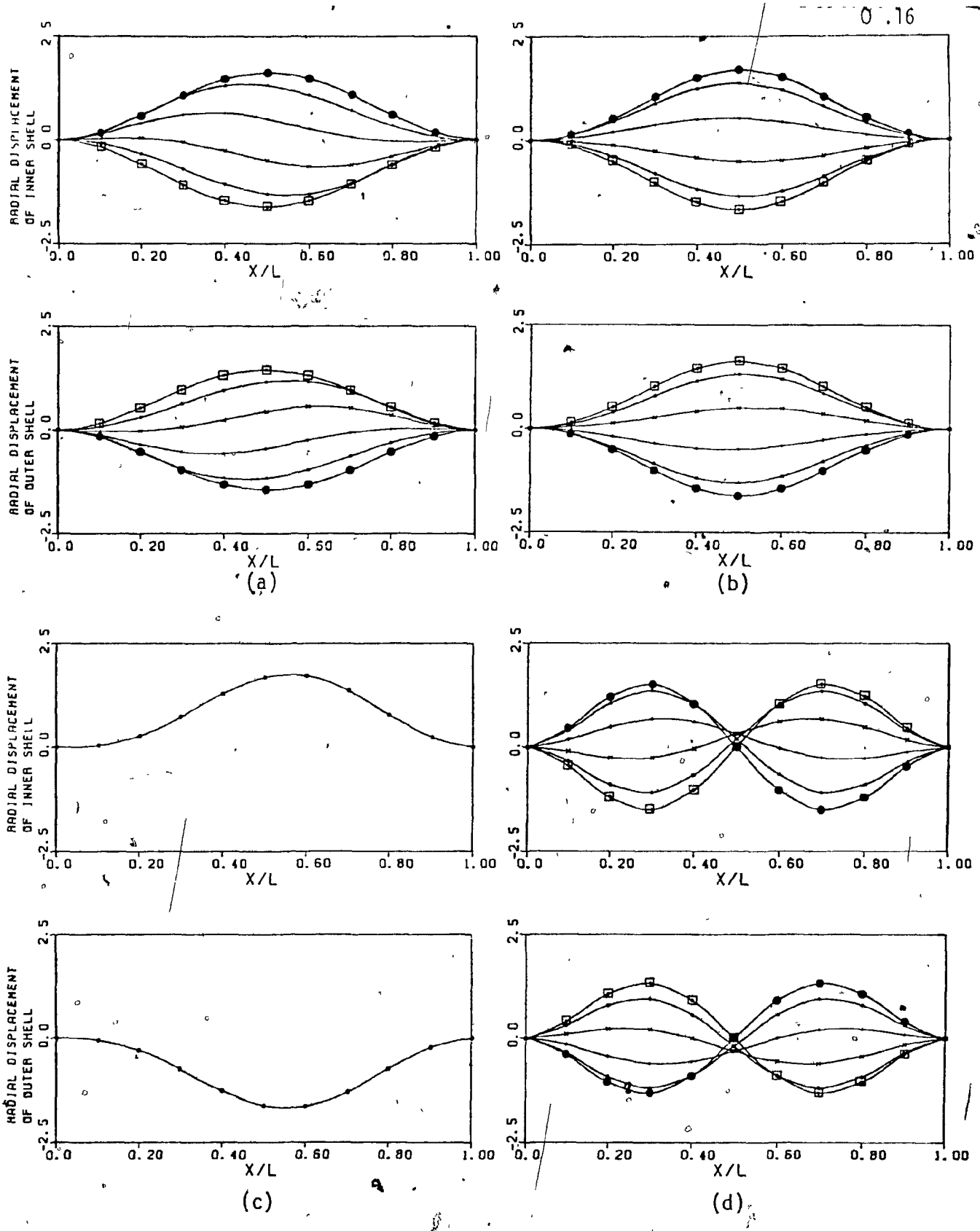

Fig. 0.14: Axial modal shapes of the inner and outer shells for the n=3, m=1, antisymmetric mode of the 1/10-gap steel-water system of Figure 18, at (a) $\bar{D}_0 = 0.0050$, (b) $\bar{D}_0 = 0.00957$ (just short of buckling (point A of Figure 18)), (c) $\bar{D}_0 = 0.010$ (shells have buckled), (d) $\bar{D}_0 = 0.01205$ (immediately after the first restabilization (point B)).

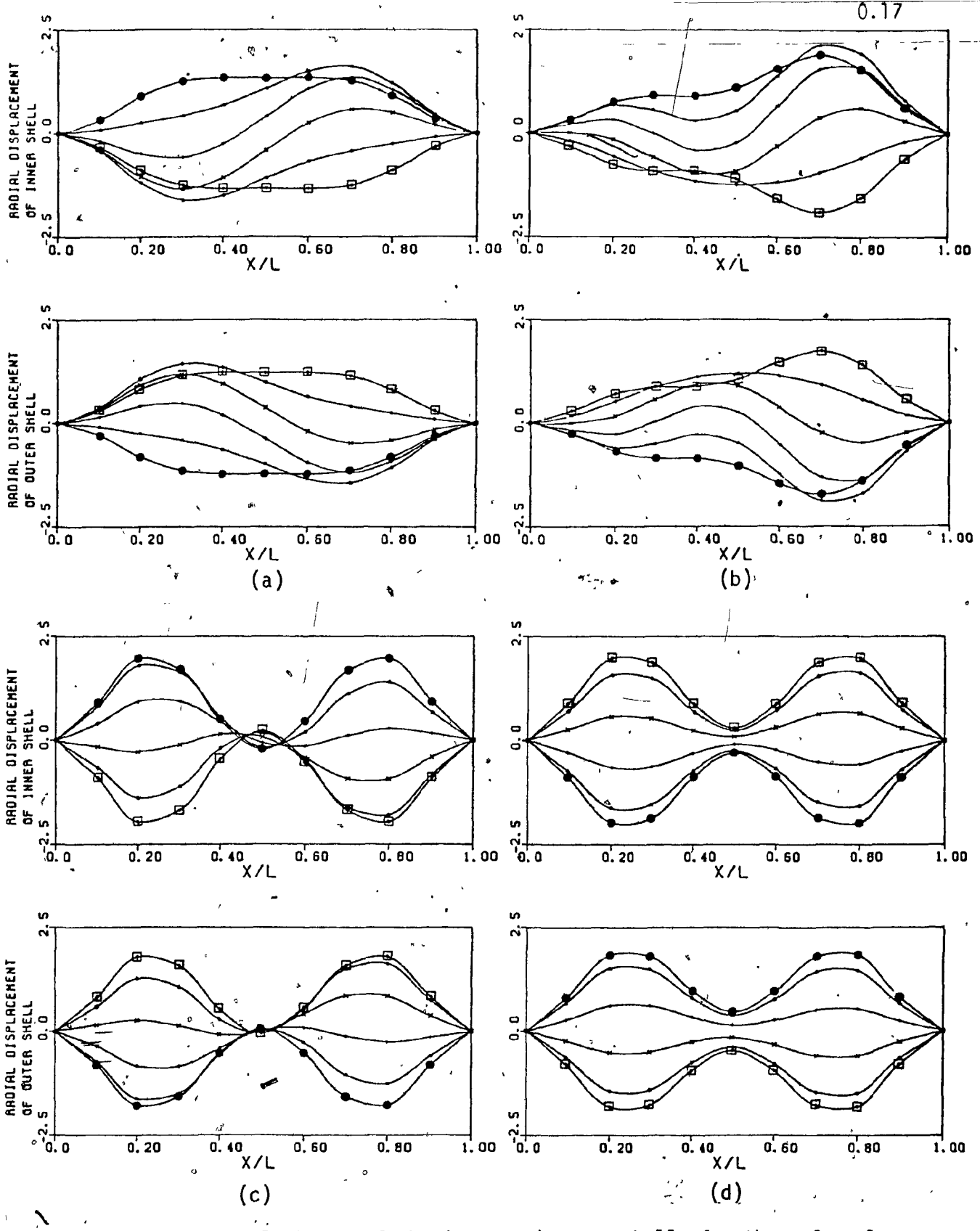

Fig. 0.15: Axial modal shapes of the inner and outer shells for the n=3, m=1, antisymmetric mode of the 1/10-gap steel-water system of Figure 18, at (a) $\bar{U}_0$ = 0.01355 (prior to coupled-mode fluttering with the m=2, antisymmetric mode (point C of Figure 18)), (b) $\bar{U}_0$ = 0.0150 (whilst fluttering), (c) $\bar{U}_0$ = 0.01587 (immediately after the second restabilization (point D)), (d) $\bar{U}_0$ = 0.01602 (just short of buckling (point E)).

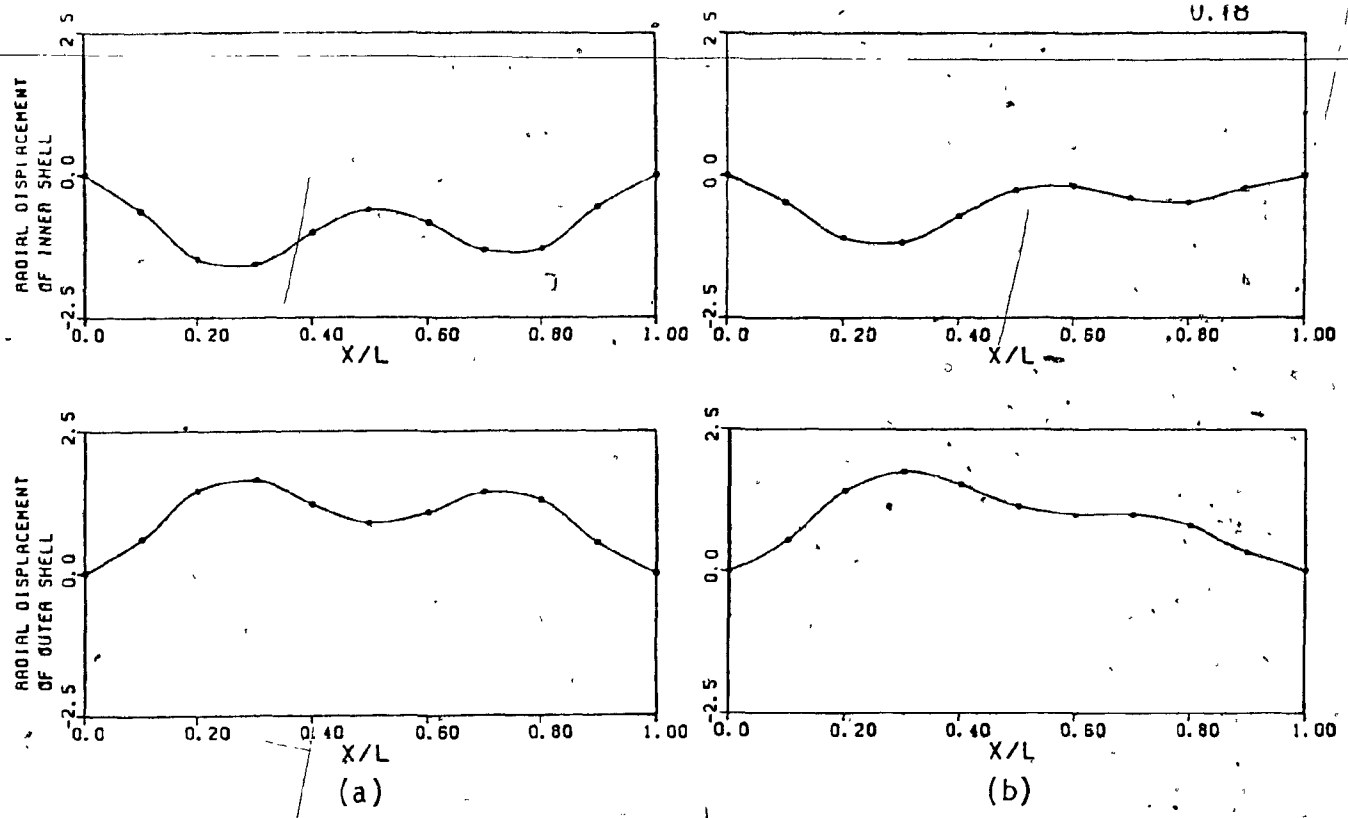

Fig. 0.16: Axial modal shapes of the inner and outer shells for the n=3, m=1, antisymmetric mode of the 1/10-gap steel-water system of Figure 18, at (a) $\bar{U}_0$ = 0.0175 (shells have buckled), (b) $\bar{U}_0$ = 0.030 (shells have buckled).

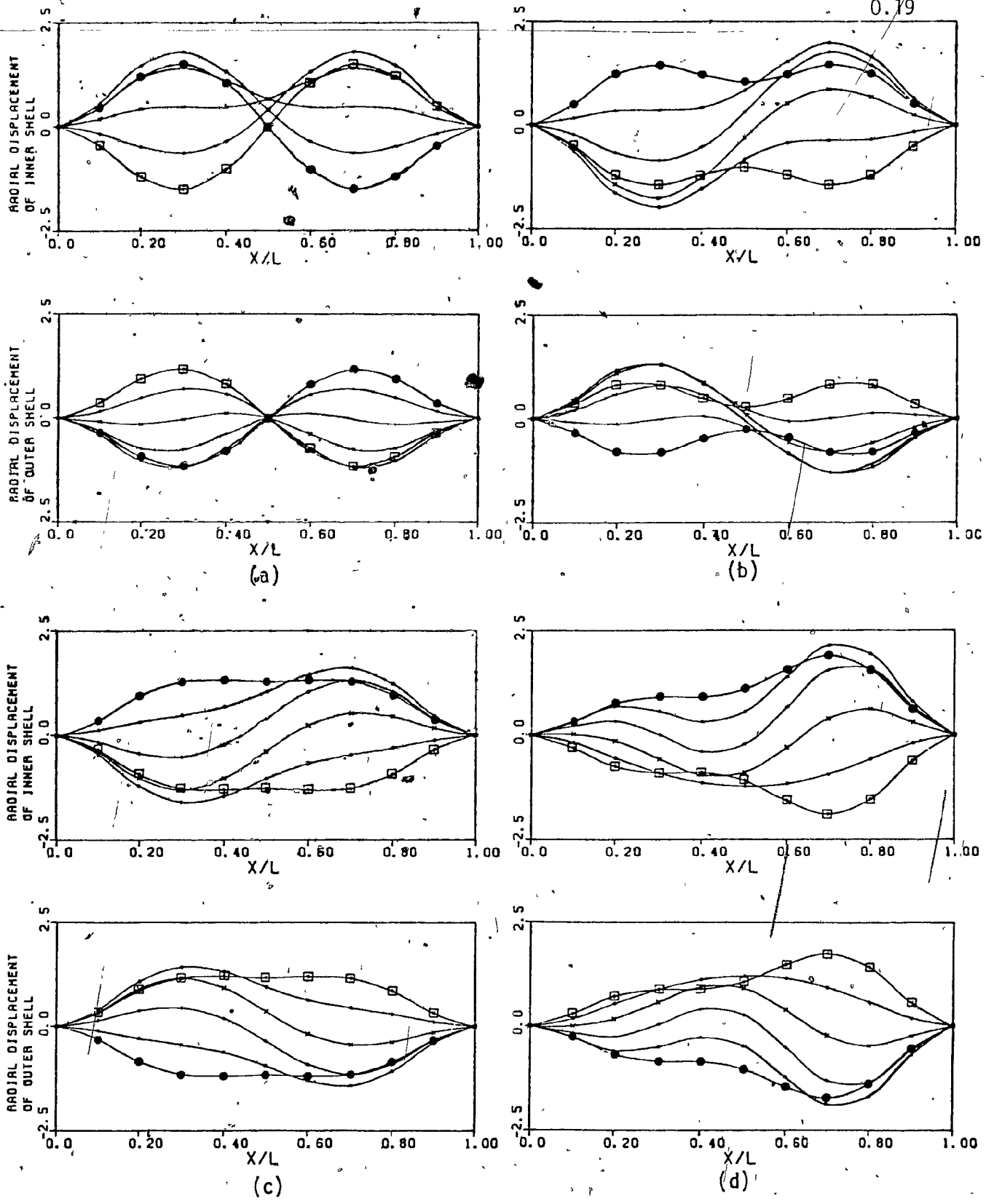

Fig. 0.17: Axial modal shapes of the inner and outer shells for the n=3, m=2, antisymmetric mode of the 1/10-gap steel-water system of Figure 18, at (a) $\bar{U}_0 = 0.0050$, (b) $\bar{U}_0 = 0.0080$, (c) $\bar{U}_0 = 0.01355$ (prior to coupled-mode fluttering with the m=1, antisymmetric mode (point C of Figure 18)), (d) $\bar{U}_0 = 0.0150$ (whilst fluttering).

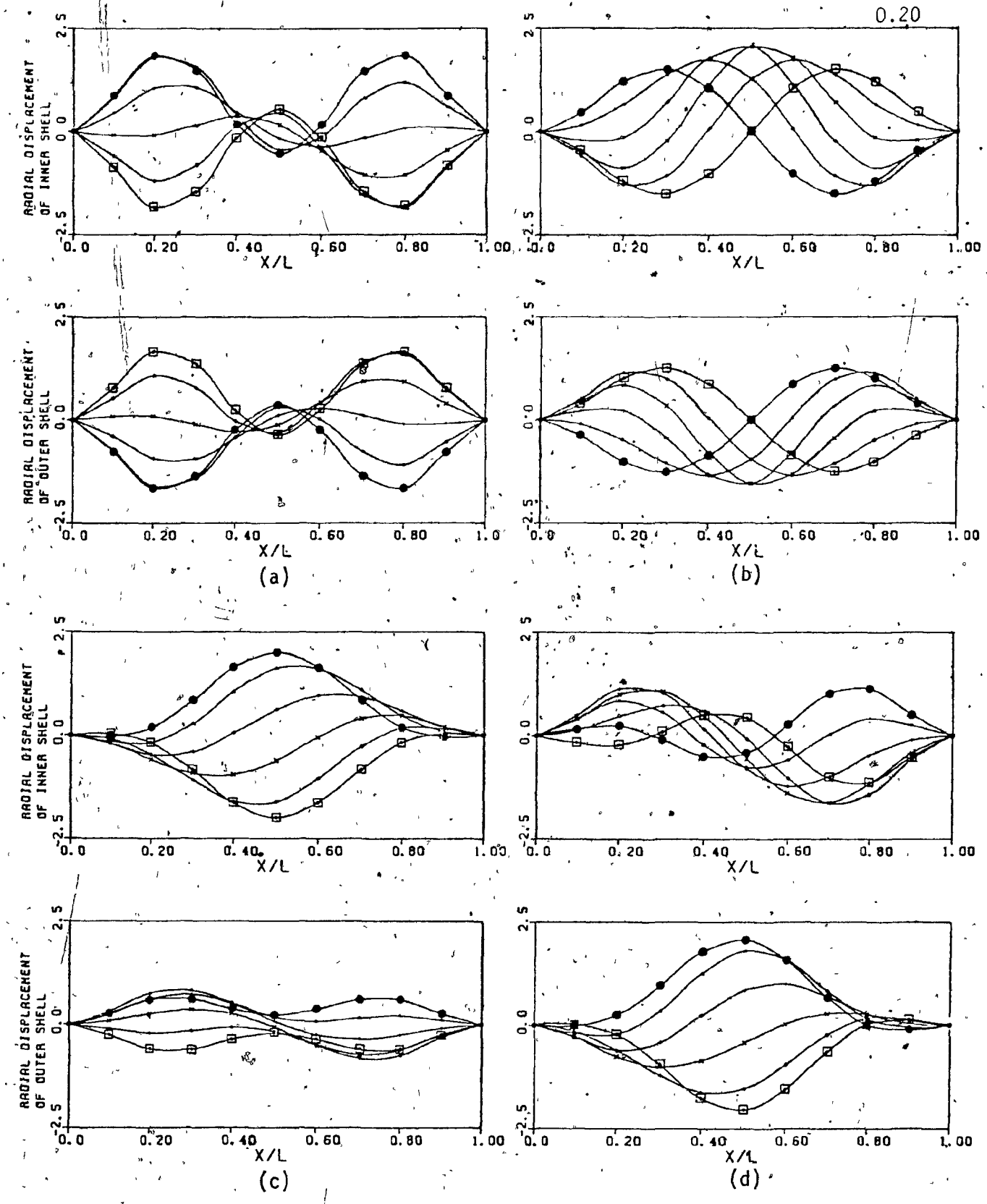

Fig. 0.18: Axial modal shapes of the inner and outer shells for the n=3, m=2, antisymmetric mode of the 1/10-gap steel-water system of Figure 18, at (a) $\bar{U}_0 = 0.01587$ (immediately after restabilization (point D of Figure 18)), (b) $\bar{U}_0 = 0.0175$, (c) $\bar{U}_0 = 0.02027$ (prior to coupled-mode fluttering with the m=1, symmetric mode (point F)), (d) $\bar{U}_0 = 0.0225$ (just before the m=1, symmetric mode is replaced by the m=3, antisymmetric mode in the coupled-mode flutter with the m=2, antisymmetric mdoe (point G)).

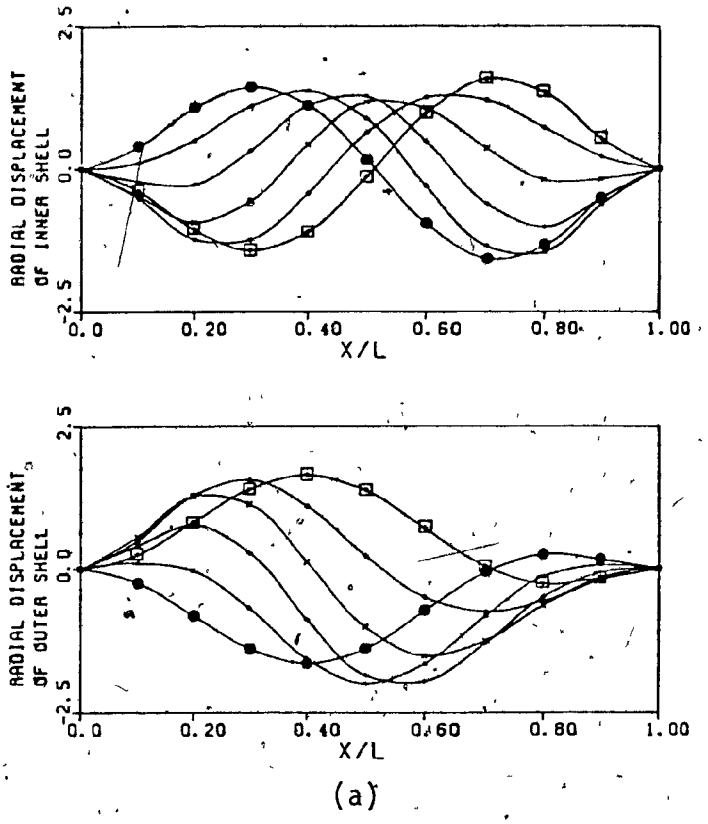

(a)

Fig. 0.19: Axial modal shapes of the inner and outer shells for the n=3, m=2, antisymmetric mode of the 1/10-gap steel-water system of Figure 18, at (a) $\bar{U}_0 = -0.030$ (engaging in coupled-mode flutter with the m=3, antisymmetric mode).

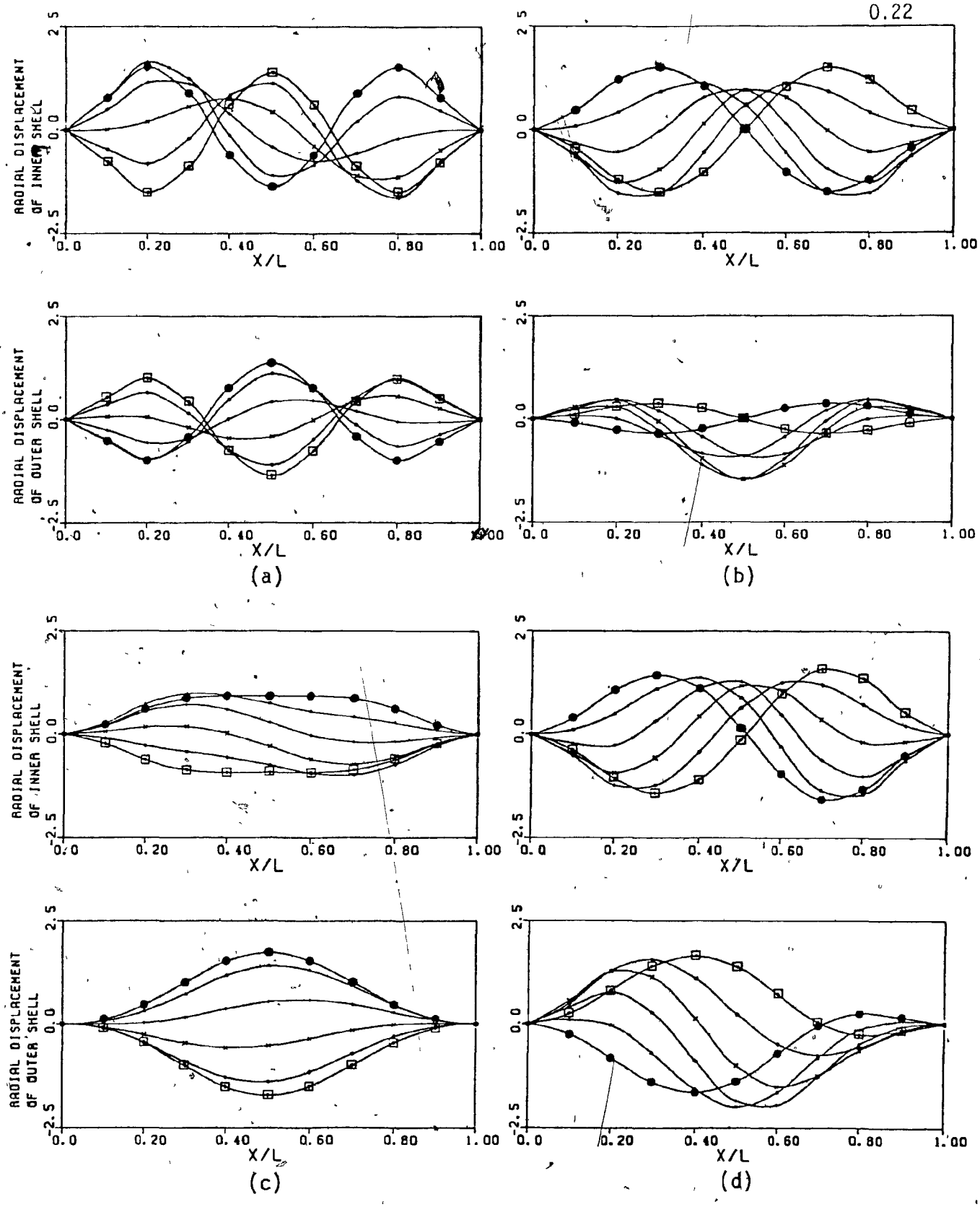

Fig. 0.20: Axial modal shapes of the inner and outer shells for the n=3, m=3, antisymmetric mode of the 1/10-gap steel-water system of Figure 18, at (a) $\bar{U}_0 = 0.0050$, (b) $\bar{U}_0 = 0.0150$, (c) $\bar{U}_0 = 0.0225$ (prior to coupled-mode fluttering with the m=2, antisymmetric mode (point G of Figure 18)), (d) $\bar{U}_0 = 0.030$ (whilst fluttering).

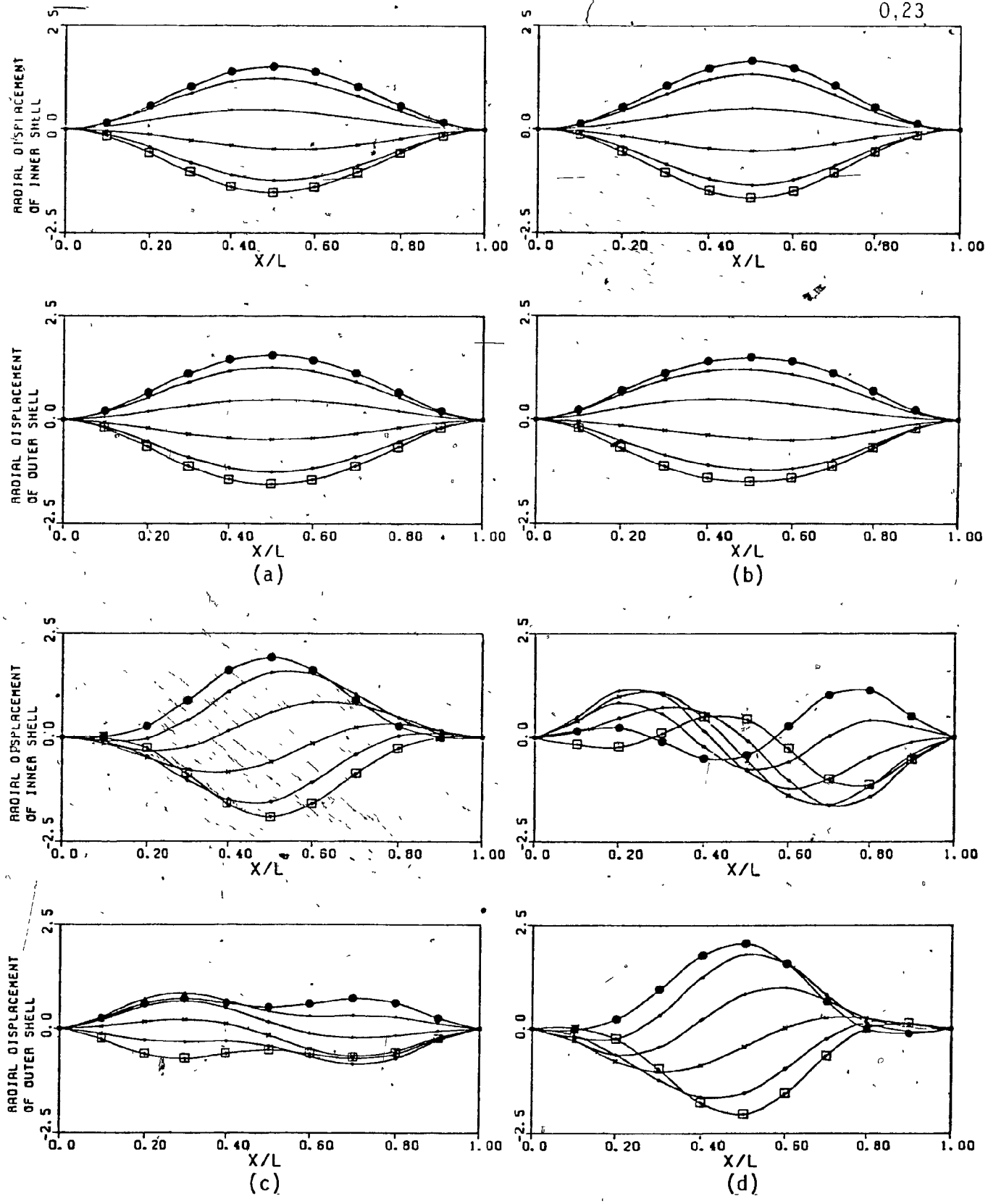

Fig. 0.21: Axial modal shapes of the inner and outer shells for the n=3, m=1, symmetric mode of the 1/10-gap steel-water system of Figure 18, at (a) $\bar{U}_0 = 0.0050$, (b) $\bar{U}_0 = 0.0150$, (c) $\bar{U}_0 = 0.02027$ (prior to coupled-mode fluttering with the m=2, antisymmetric mode (point F of Figure 18)), (d) $\bar{U}_0 = 0.0225$ (just before the m=1, symmetric mode is replaced by the m=3, antisymmetric mode in the coupled-mode flutter with the m=2, antisymmetric mode (point G)).

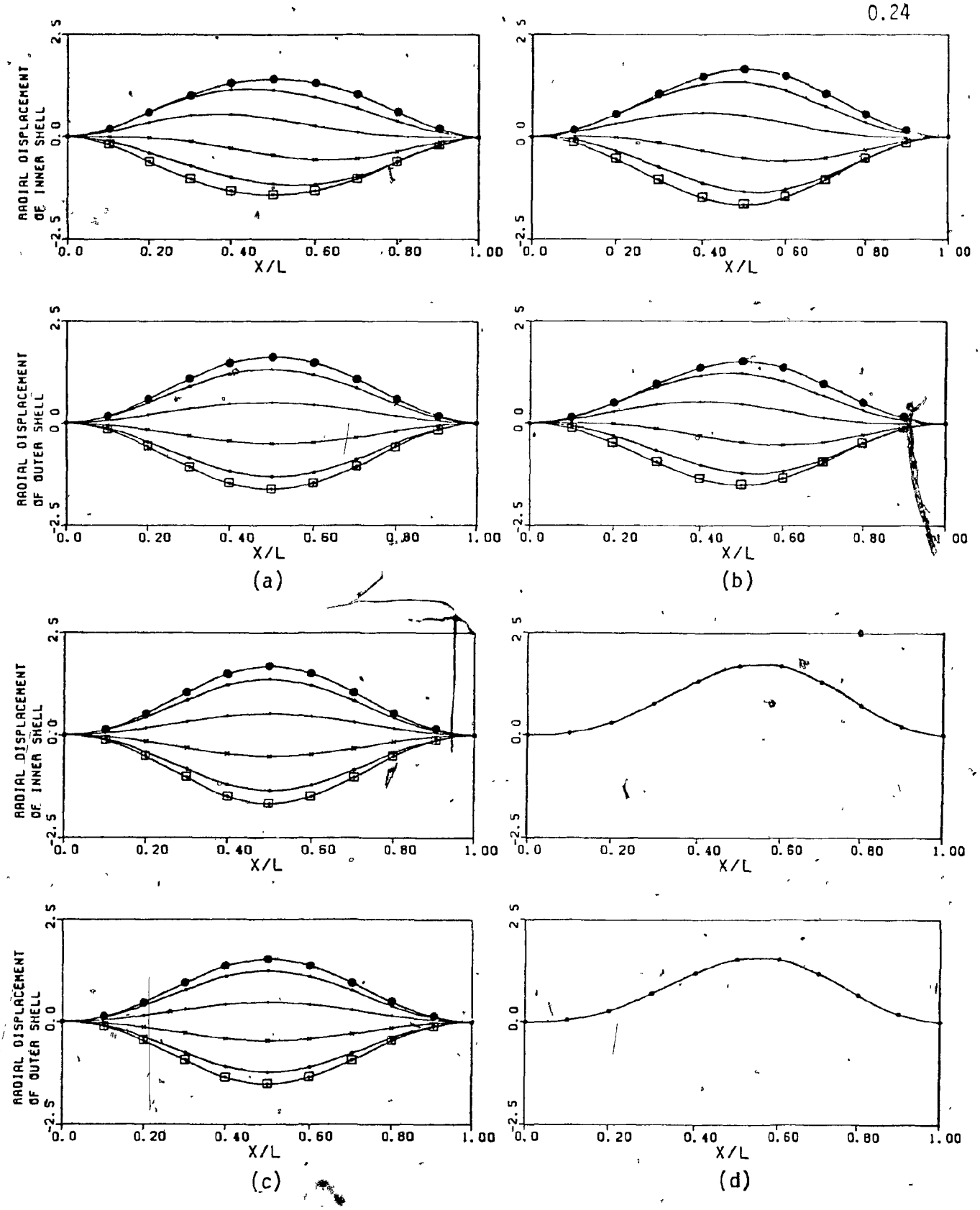

Fig. 0.22: Axial modal shapes of the inner and outer shells for the n=3, m=1, symmetric mode of the 1/10-gap steel-water system of Figure 18, at (a) $\bar{U}_0 = 0.0250$ (after restabilizing from coupled-mode flutter), (b) $\bar{U}_0 = 0.060$, (c) $\bar{U}_0 = 0.0663$ (just short of buckling (point H of Figure 18)), (d) $\bar{U}_0 = 0.070$ (shells have buckled).

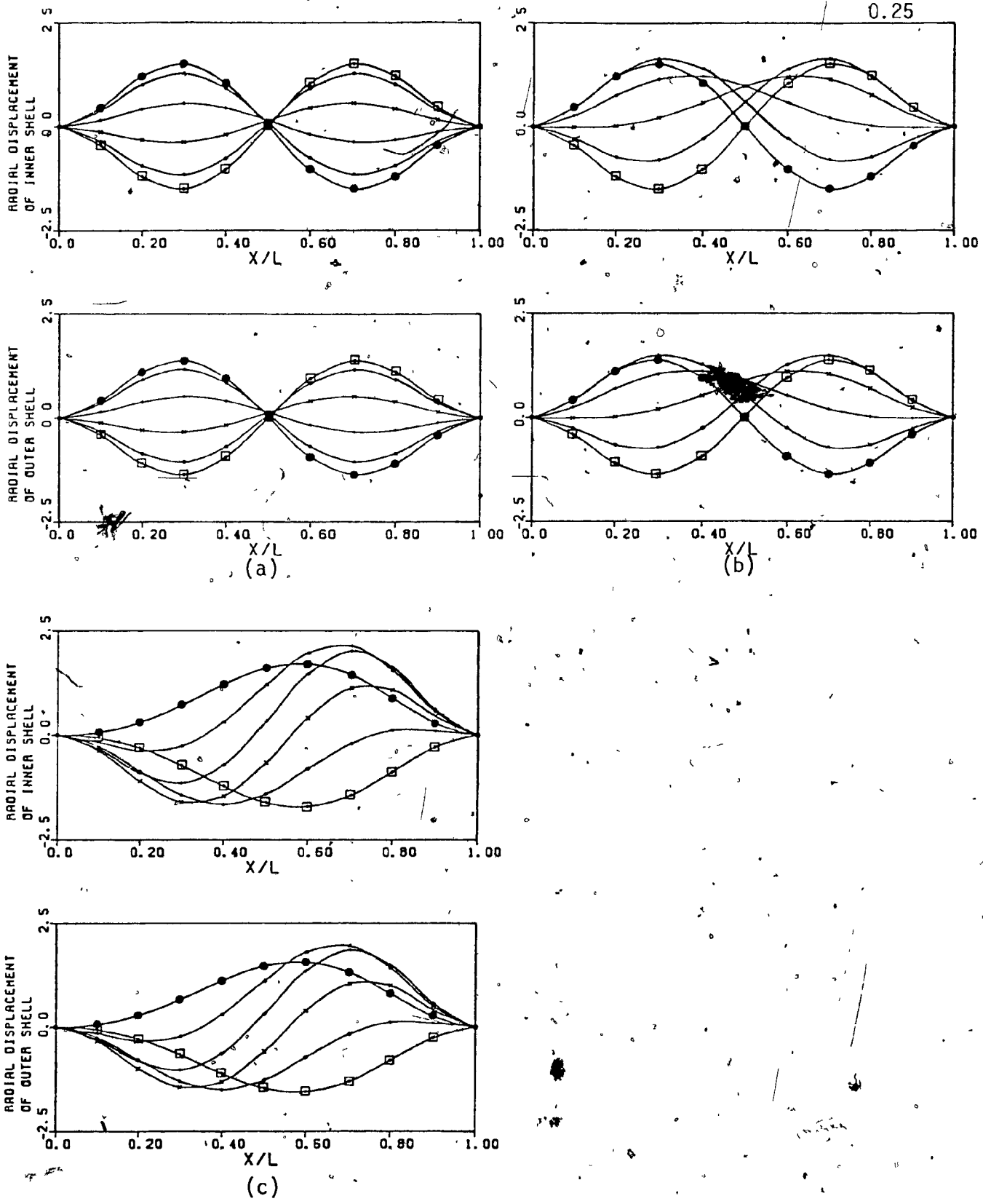

Fig. 0.23: Axial modal shapes of the inner and outer shells for the n=3, m=1, symmetric mode of the 1/10-gap steel-water system of Figure 18, at (a) $\bar{U}_0$ = 0.08175 (immediately after restabilization (point I of Figure 18)), (b) $\bar{U}_0$ = 0.0824 (prior to coupled-mode fluttering with the m=2, symmetric mode (point J)), (c) $\bar{U}_0$ = 0.0850 (whilst fluttering).

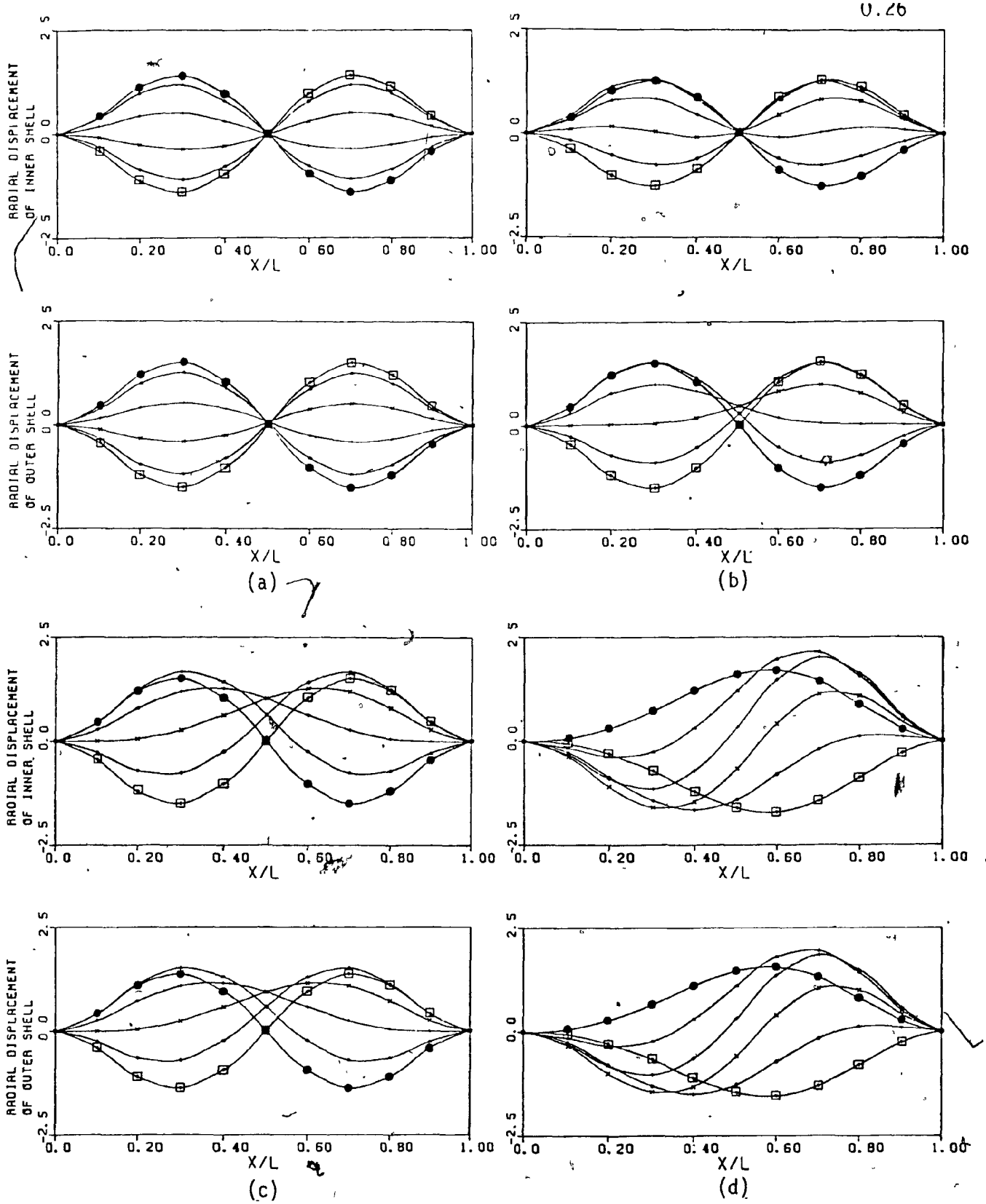

Fig. 0.24: Axial modal shapes of the inner and outer shells for the n=3, m=2, symmetric mode of the 1/10-gap steel-water system of Figure 18, at (a) $\bar{U}_0 = 0.0050$, (b) $\bar{U}_0 = 0.040$, (c) $\bar{U}_0 = 0.0824$ (prior to coupled-mode fluttering with the m=1, symmetric mode (point J of Figure 18)), (d) $\bar{U}_0 = 0.0850$ (whilst fluttering).

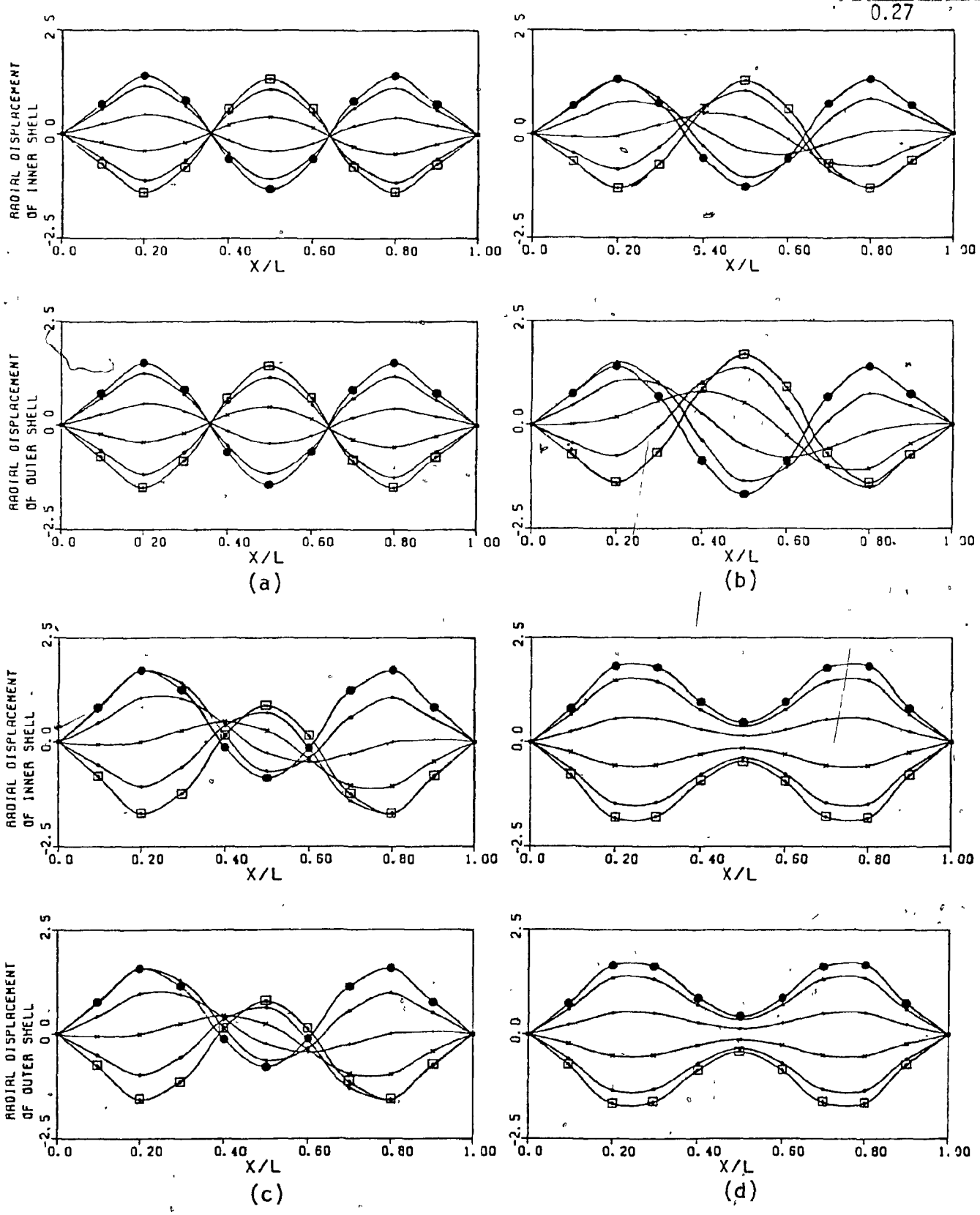

Fig. 0.25: Axial modal shapes of the inner and outer shells for the n=3, m=3, symmetric mode of the 1/10-gap steel-water system of Figure 18, at (a) $\bar{U}_0 = 0.0050$, (b) $\bar{U}_0 = 0.050$, (c) $\bar{U}_0 = 0.10$, (d) $\bar{U}_0 = 0.10575$ (just short of buckling (point K of Figure 18)).

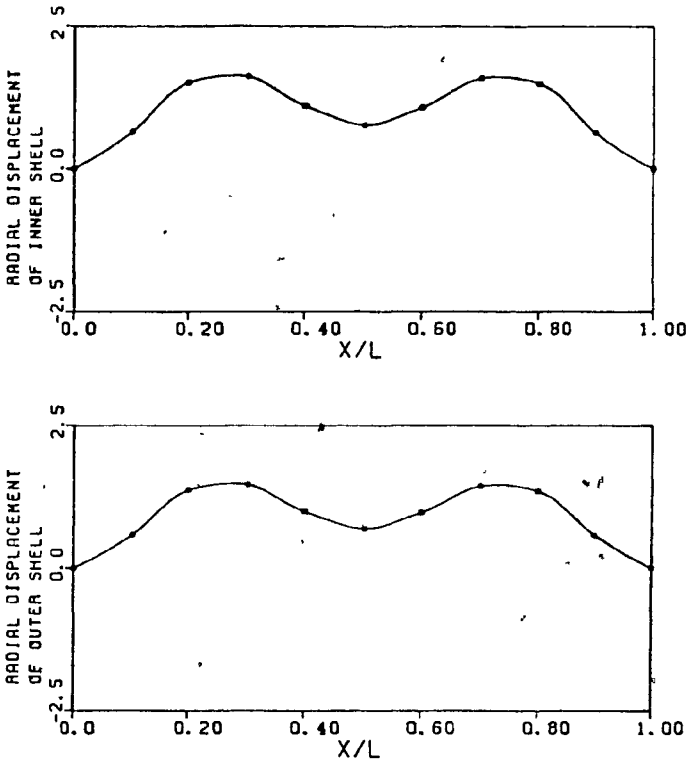

(a)

Fig. 0.26: Axial modal shapes of the inner and outer shells for the n=3, m=3, symmetric mode of the 1/10-gap steel-water system of Figure 18, at (a) $\bar{U}_o$ = 0.110 (shells have buckled).